SAN/1213-02 (PRIME)
SAN/1294-02 (SEC)



**Prepared for U.S. Department of Energy**

**August 1978**

Assistant Secretary for Conservation and Solar Applications
Division of Transportation Energy Conservation

# Near-Term Electric Vehicle Program





# Phase Mid-Term Summary Report

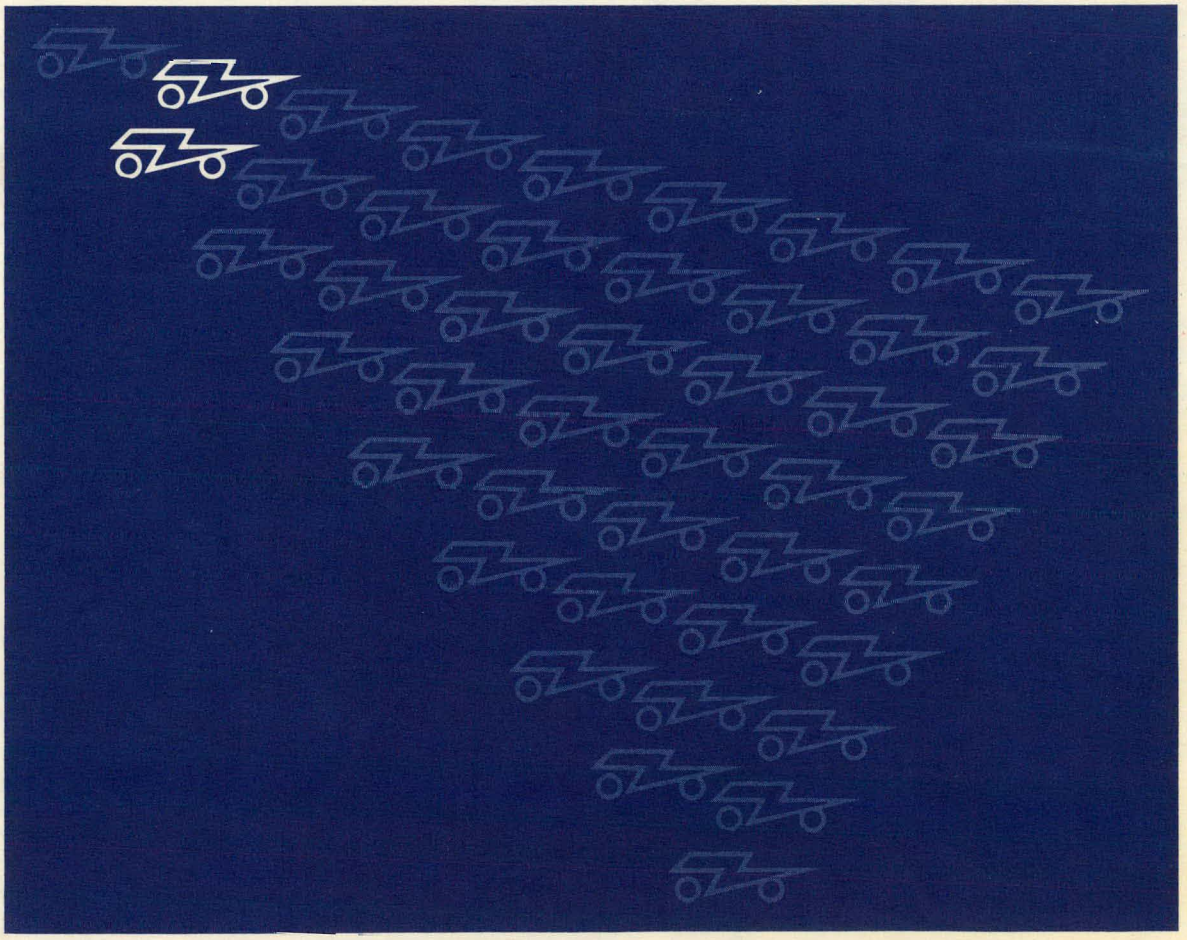

## DISCLAIMER

Available from:

National Technical Information Service (NTIS)
U.S. Department of Commerce
5285 Port Royal Road
Springfield, Virginia 22161

Price: Printed copy: $14.00
Microfiche: $3.00

**Prepared for the U.S. Department of Energy**

Assistant Secretary for Conservation and Solar Applications
Division of Transportation Energy Conservation
Washington, D.C. 20545

SAN/1213-02
SAN/1294-02

Distribution Category UC-96

# Near-Term Electric Vehicle Program

# Phase II
# Mid-Term Summary Report

**August 1978**

**Part 1 —**
Prepared by General Electric Company
Corporate Research and Development
Schenectady, New York 12301
Under Contract No. EY-76-C-03-1294

**Part 2 —**
Prepared by Garrett Corporation
Airesearch Manufacturing Co. of California
Torrance, California 90504
Under Contract No. EY-76-C-03-1213

For sale by the Superintendent of Documents, U.S. Government Printing Office
Washington, D.C. 20402

Stock No. 061-000-00169-0

# PREFACE

The Near Term Electric Vehicle (NTEV) Program is a constituent element of the overall national Electric and Hybrid Vehicle Program that is being implemented by the Department of Energy in accordance with the requirements of the Electric and Hybrid Vehicle Research, Development, and Demonstration Act of 1976. Phase II of the NTEV Program is focused on the detailed design and development, of complete electric integrated test vehicles that incorporate current and near-term technology, and meet specified DOE objectives.

The activities described in this Mid-Term Summary Report are being carried out by two contractor teams. The prime contractors for these contractor teams are the General Electric Company and the Garrett Corporation. This report is divided into two discrete parts. Part 1 (yellow pages) describes the progress of the General Electric team and Part 2 (pink pages) describes the progress of the Garrett team.

# Part 1

# General Electric Company
# Corporate Research And Development

Contract No. EY-76-C-03-1294

THIS PAGE

WAS INTENTIONALLY

LEFT BLANK

# ABSTRACT

The activities described in this Mid-Term Summary Report are being carried out by the General Electric Company and its subcontractors under Contract No. EY-76-C-03-1294 with the U.S. Department of Energy (DOE) as part of the Near-Term Electric Vehicle Program (Phase II). This report covers the period from April 1977 through April 1978.

The program described in this report will result in the development and delivery to DOE of two Integrated Test Vehicles incorporating technology improvements for energy-efficient operation. The vehicles will meet the DOE Near-Term Objectives shown in the report and will be designed for adaptation to future production requirements specified by Public Law 94-413.

The Mid-Term Summary Report covers developments in the areas of system analysis and design, subsystem analysis and design, and test and evaluation. Significant technical accomplishments which are described include aerodynamic design and testing to achieve an extremely low-drag body design and development of a lightweight vehicle structure which will satisfy the current Federal Motor Vehicle Safety Standards.

Achievements in the electrical drive subsystem include the design of a highly efficient dc drive motor, improvements in the motor controller technology, and the development of high-power, low-cost transistor power modules. An improved lead-acid traction battery has been designed, which promises to provide a 25% increase in energy density as compared with present commercially available batteries. By the proper integration of these technology advancements, it is predicted that the Integrated Test Vehicles will satisfy DOE's objectives for performance, safety, and producibility.

THIS PAGE

WAS INTENTIONALLY

LEFT BLANK

# TABLE OF CONTENTS

# TABLE OF CONTENTS (CONT'D)

# TABLE OF CONTENTS (CONT'D)

## TABLE OF CONTENTS (CONT'D)



## LIST OF ILLUSTRATIONS

# LIST OF ILLUSTRATIONS (CONT'D)

## LIST OF ILLUSTRATIONS (CONT'D)

## LIST OF ILLUSTRATIONS (CONT'D)

## LIST OF ILLUSTRATIONS (CONT'D)

## LIST OF ILLUSTRATIONS (CONT'D)

# LIST OF TABLES

## LIST OF TABLES (CONT'D)

# Section 1

# INTRODUCTION

## PROGRAM MANAGEMENT

The activities described in this report are being carried out by the General Electric Company and its subcontractors under a contract with the U.S. Department of Energy (DOE). This work is part of the Near-Term Electric Vehicle Program being administered by DOE in accordance with Public Law 94-413, the Electric and Hybrid Vehicle Research, Development and Demonstration Act of 1976. Management responsibility for the Near-Term Electric Vehicle Program is within the Division of Transportation Energy Conservation under the Assistant Secretary for Conservation and Solar Applications. Messrs. V.J. Esposito and P.J. Brown are the DOE Program Manager and Deputy Program Manager respectively of the overall national ELECTRIC & HYBRID VEHICLE PROGRAM of which this Near-Term Electric Vehicle Program is a major element.

R.S. Kirk and G.J. Walker are the DOE Program Director and Program Manager respectively of this Near-Term Electric Vehicle Program. General Electric's contract is administered by the San Francisco Operations Office of DOE; Mr. J. Hirahara is the responsible Contract Specialist. The organizational relationships within DOE are shown in Figure 1-1.

Technical management of the General Electric contract is the responsibility of the Jet Propulsion Laboratory (JPL) of Pasadena, California. Mr. Thomas A. Barber is Manager of the Electric and Hybrid Vehicle Systems Project at JPL. The Contract Technical Manager for General Electric's contract is Mr. T.A. Almaguer.

Within the General Electric Company, primary responsibility for the Near-Term Electric Vehicle Program has been assigned to Corporate Research and Development (CRD), at Schenectady, New York. Mr. E.A. Rowland is the Program Manager. The relationship of CRD to other elements of the General Electric Company is shown in Figure 1-2.

The General Electric program organization for the Near-Term Electric Vehicle Program is shown in Figure 1-3. Project leaders within GE/CRD are identified in this figure along with Project Managers for each major subcontractor. Also shown in Figure 1-3 are other departments of General Electric who are contributing to the design and development of the Integrated Test Vehicles (ITV). Table 1-1 provides an explanation of the roles performed by each contractor under this contract.

The Chrysler Corporation has a major role in the electric vehicle program, with responsibility for design and development

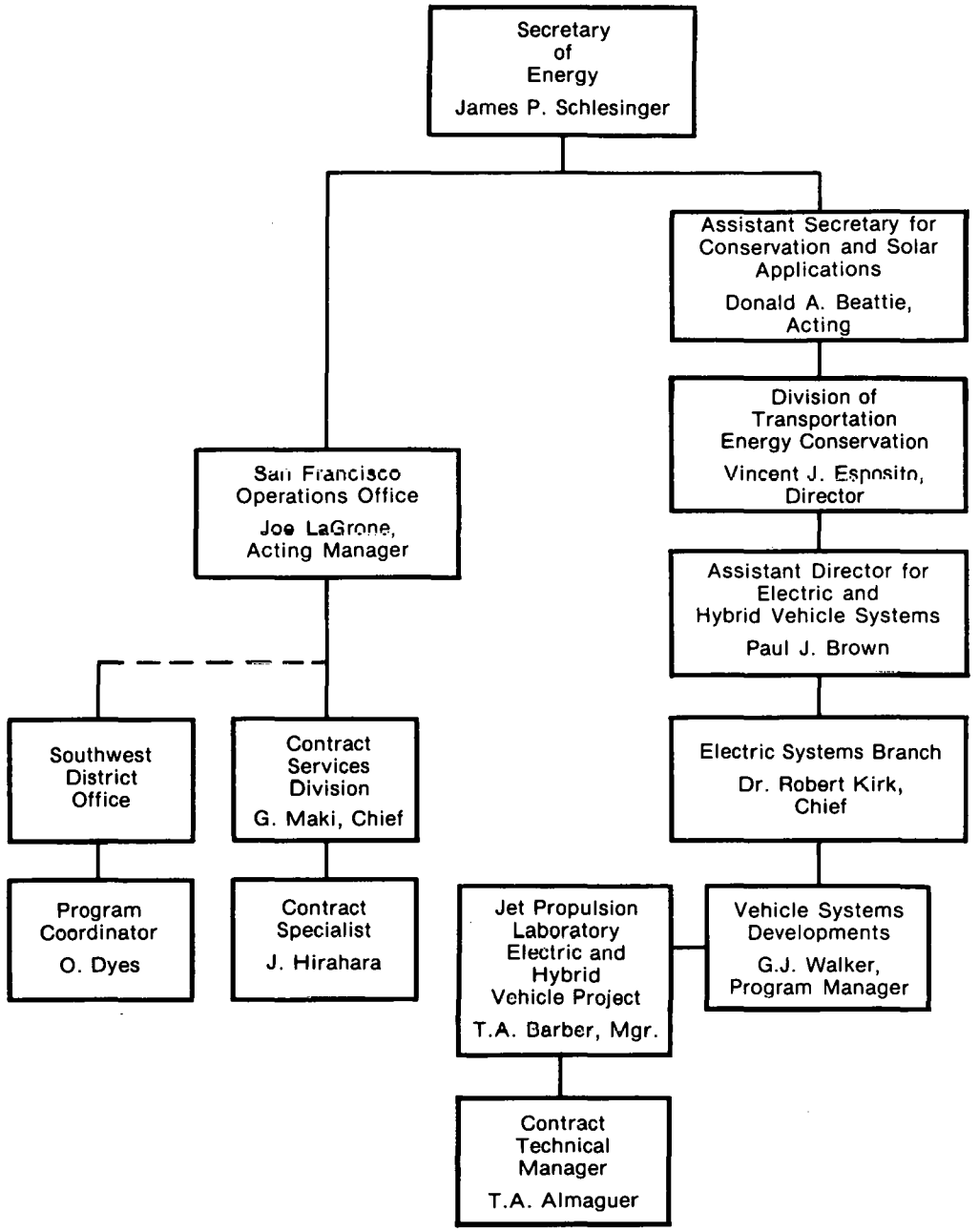


Figure 1-1. DOE Organizational Elements

of all vehicular systems, fabrication and assembly of the Integrated Test Vehicles, and performance of integrated vehicle tests. The key members of Chrysler's program staff are identified in Figure 1-4. Also identified in this figure is Chrysler's design and fabrication subcontractor, Modern Engineering Services of Detroit, Michigan.

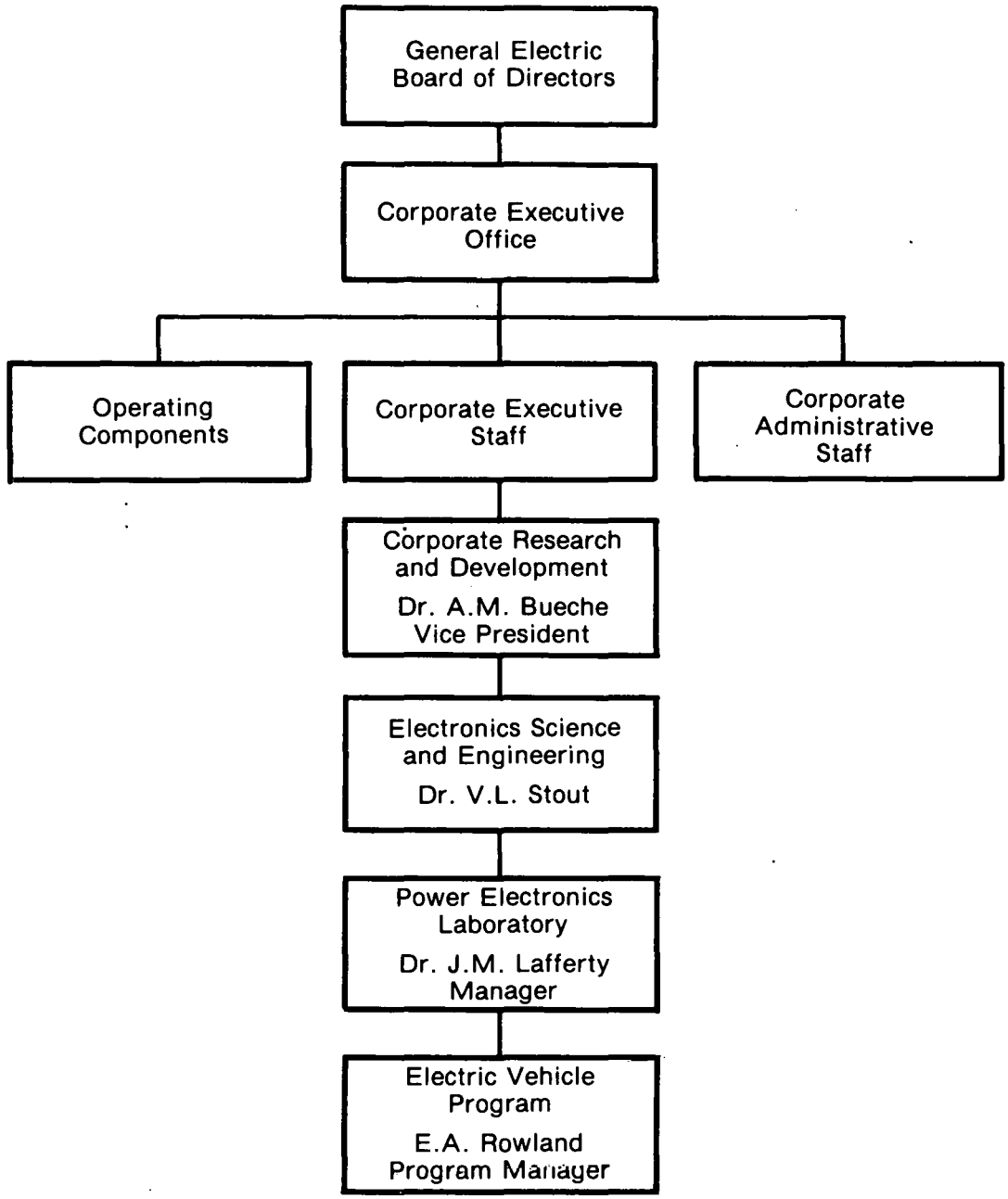


Figure 1-2. Relationship of General Electric Company to DOE Electric Vehicle Program

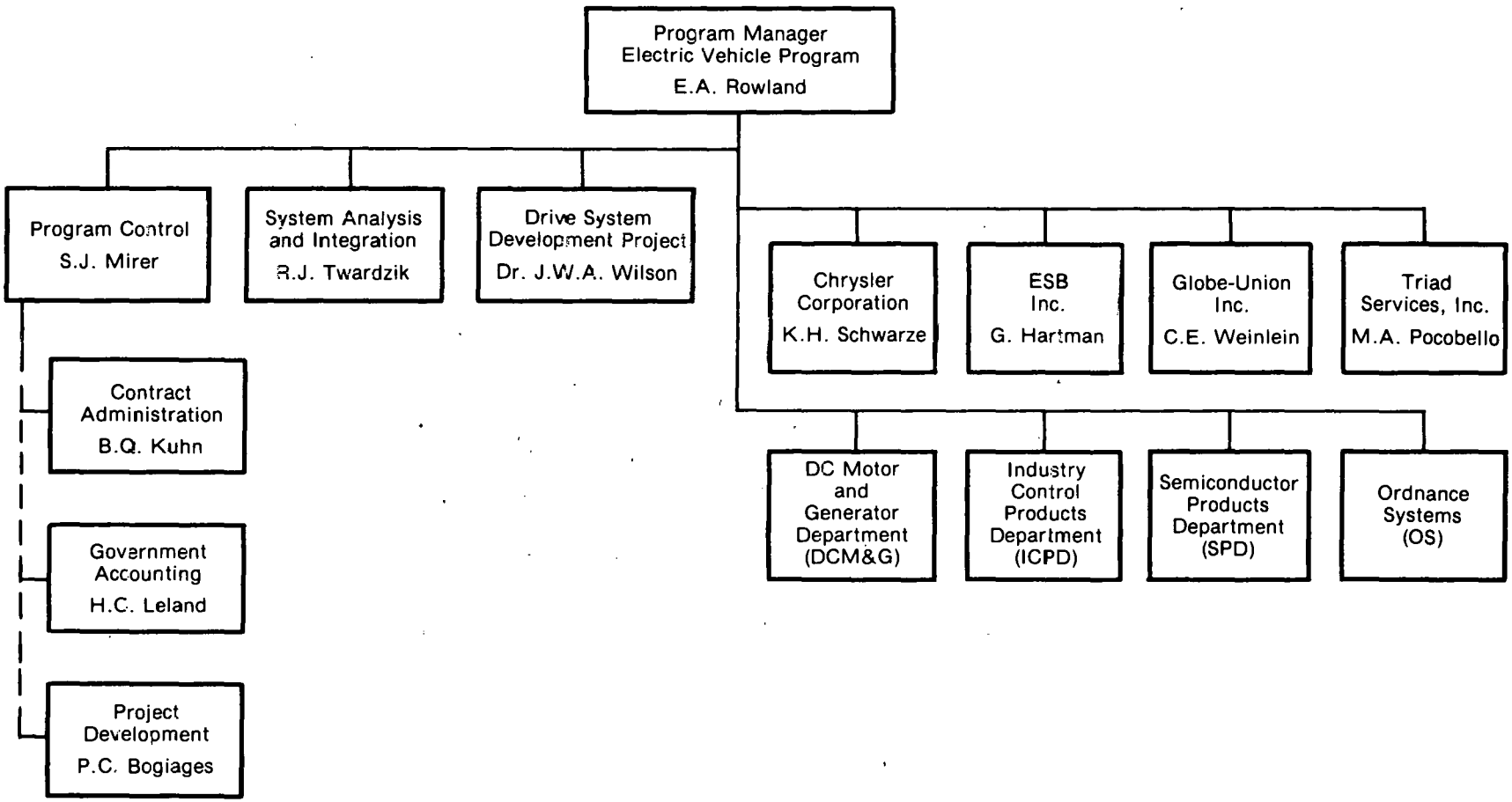


Figure 1-3. General Electric Electric Vehicle Program Organization

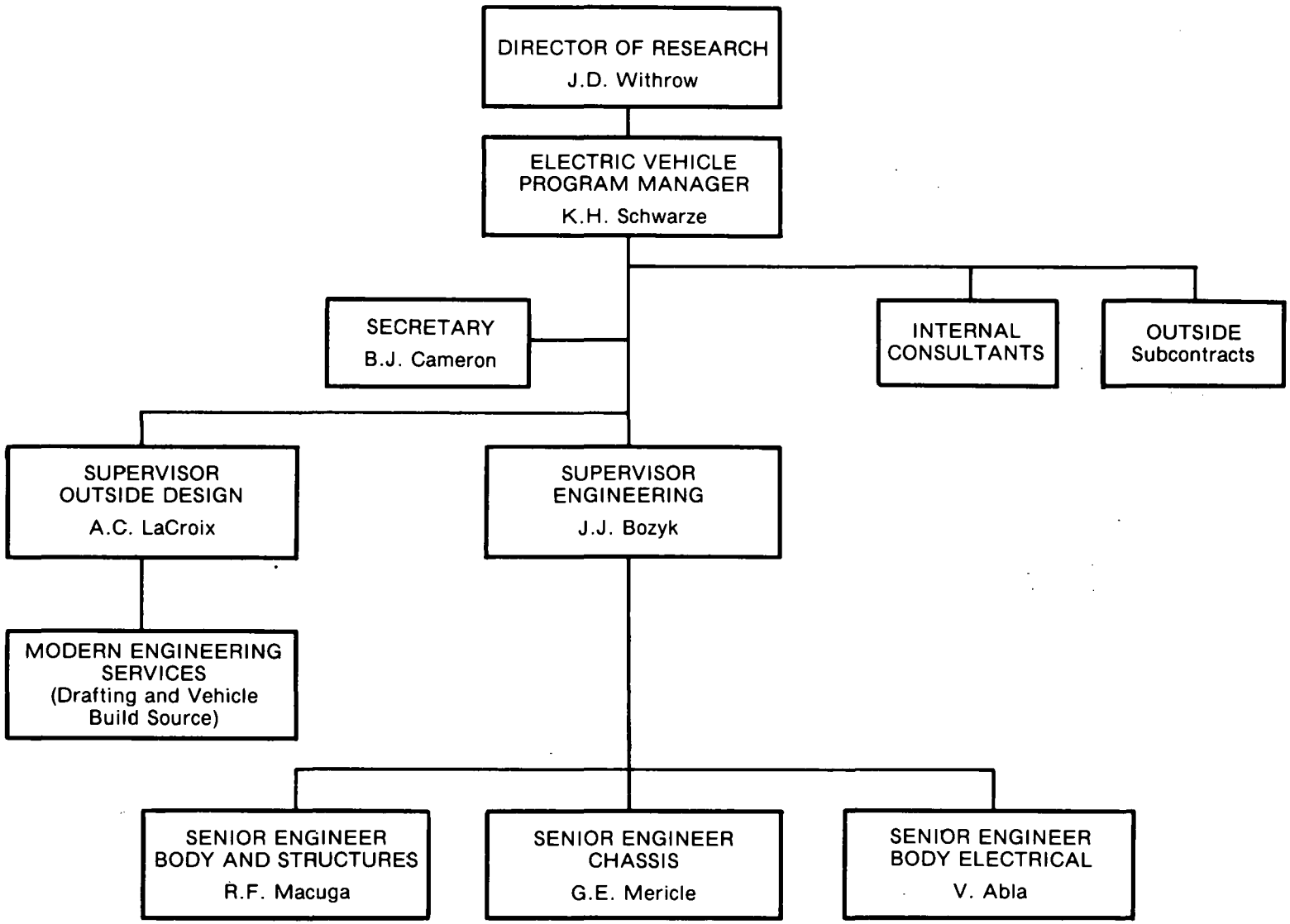


Figure 1-4. Chrysler Task Force Organization for the Near-Term Electric Vehicle Program -- Phase II

TABLE 1-1

CONTRACTOR RESPONSIBILITIES

| Contractor | Role in Program |
|---|---|
| General Electric/CRD | • Prime Contractor & System Integrator<br>• Development of Electrical Drive Subsystem<br>• Development of Power Transistor Modules |
| Chrysler Corporation | • Development of Vehicle Subsystem<br>• Vehicle Fabrication and Assembly<br>• Integrated Vehicle Testing |
| ESB, Inc. | • Consultant, Battery Modeling and Regenerative Braking |
| Globe-Union, Inc. | • Development of Lead-Acid Battery<br>• Battery Subsystem Integration<br>• Battery Fabrication and Testing |
| Triad Services, Inc. | • Phase I Vehicle Design<br>• Consulting, Phase II |
| General Electric/DCM&G | • Design of DC Drive Motor<br>• Drive Motor Fabrication & Testing |
| General Electric/ICPD | • DC Contractors & Controls<br>• Consulting, Motor Controllers |
| General Electric/OS | • Mechanical & Thermal Design<br>• Packaging of Drive System Electronics<br>• Environmental Testing |
| General Electric/SPD | • Power Transistor Fabrication |

## PROGRAM OBJECTIVES

The general objective of the Near-Term Electric Vehicle Program is to confirm

1. That, in fact, the complete spectrum of requirements placed on the automobile (e.g., safety, producibility, utility) can still be satisfied if electric power train concepts are incorporated in lieu of contemporary power train concepts, and

2. That the resultant set of vehicle characteristics are mutually compatible, technologically achievable, and economically achievable.

The approach to meeting this general objective is focused on the design, development, and fabrication of complete electric vehicles incorporating, where necessary, extensive technological advancement.

The program described in this report will result in the development and delivery to DOE of two Integrated Test Vehicles (ITVs) incorporating technology improvements for energy-efficient operation. The Integrated Test Vehicles will meet the DOE Near-Term Objectives shown in Table 1-2 and will be amenable to mass production in the early 1980s.

Specific DOE vehicle performance and characteristic objectives for this program are presented later in this section under "Technical Approach." These objectives define a four-passenger car similar in concept to today's subcompact vehicle, which is widely used for urban transportation and commuting service. The driving mission for this car is specified by means of the Society of Automotive Engineers J227a (Schedule D) driving cycle, which is representative of urban stop-and-go driving.

The electric car resulting from this program must be suitable for future production at a cost comparable to conventional (internal combustion engine) autos. When produced in quantities of 100,000 or more per year, the electric car should be available at a consumer price equivalent to $5000 in 1975 dollars. Life cycle cost must not exceed $0.15/mile, on the basis of a ten-year life-span and 10,000 miles of operation per year.

Performance objectives specified for the electric car include a range of 75 miles in simulated urban driving, acceleration from 0 to 30 mph in nine seconds, and a top speed of 60 mph. Hill-climbing capability on a one-mile-long grade will be sufficient to maintain 50 mph on a 5% grade. To meet these performance requirements an improved lead-acid battery which delivers an energy density of 17 Wh/lb must be used. Significant improvements in design and efficiency are required, to meet these performance objectives, as compared with present commercially available vehicles.

TABLE 1-2

DOE OBJECTIVES

| Parameter | Near-Term DOE Objectives |
|---|---|
| Minimum passenger capacity | 4 adults |
| Maximum curb weight, lbs | Open |
| Minimum urban range (J227D), miles | 75 |
| Maximum initial cost, projected, 1975 | 5000 |
| Minimum life, miles | 100,000 |
| Minimum life, years | 10 |
| Maximum life-cycle cost, projected in 1975 dollars/mile | 0.15 |
| Cost of energy in dollars/kWh | 0.05 |
| Maximum electric recharge energy in urban driving, kWh/mile | 0.5 |
| Maximum recharge time, hr (115 volts, 30 ampere service) | 6 |
| Minimum top passing speed, mph | 60 |
| Minimum top cruising speed, mph | 55 |
| Minimum accessories | Heater/defroster, on-board charger |
| Safety features | FMVSS requirements at time of contract |
| Minimum unserviced park duration, day | 7 |
| Maximum years till production ready | 5 |
| Maximum critical materials required | Few |
| Minimum acceleration (0-30 mph), sec | 9 |
| Minimum merging time (25-55 mph), sec | 18 |
| Sustained speed on 5% one-mile grade, mph | 50 |
| Maximum scheduled maintenance, dollars/mile | 0.02 |
| Minimum ambient temperature range, $^{o}F$ | -20 to +125 |
| Interior noise | Minimum |
| Turning and braking | No power assist required |

## TECHNICAL APPROACH

The specific technical approach to be implemented in the General Electric Integrated Test Vehicle includes the following design features which have been identified as key requirements by DOE:

- Regenerative Braking -- The vehicle will utilize regenerative braking to recover electrical energy during periods of deceleration.

- Integrated Propulsion Control/Charging -- Onboard electronics will be provided for battery charging, and the charger function will be integrated with propulsion control electronics to minimize size, weight, and production cost.
- Microprocessor Control -- A microprocessor will be utilized to provide on-line supervisory control of the electric propulsion system, including acceleration, cruise, and regenerative braking modes. In addition, the microprocessor will provide monitoring and control functions associated with operator displays, warning indicators, battery charging, and emergency overrides.
- Transistorized Controls -- DC chopper controls for the vehicle drive motor armature and field will be implemented with high power transistors selected or developed to meet the vehicle power requirements and operating environment. Packaging of power transistors will be accomplished in the manner that is more amenable to future low-cost production.
- Integrated Power Modules -- An objective of the General Electric design program is to furnish integrated power modules for both armature and field choppers. These modules will consist of high-current, low-cost transistors packaged and bonded directly to a heat sink for simple plug-in or bolt-down replacement.

## DESIGN GOALS

Specific design goals were established at the outset of this program for each subsystem of the Integrated Test Vehicle. These goals are summarized in Table 1-3.

## WORK BREAKDOWN STRUCTURE

The General Electric contract effort has been organized into manageable work packages as depicted in the Work Breakdown Structure (WBS) of Figure 1-5. The WBS provides a convenient method to define and assign responsibility for all major technical tasks under the contract. In general, the division of work has been planned so that a single organization has responsibility for each work package. Responsibility for the coordination of work packages within each major WBS element is assigned to one contractor, who is then responsible for delegating and supervising any subcontract work within his area of responsibility. A summary of the major contractor responsibilities, by WBS element, is shown in Table 1-4.

TABLE 1-3

DESIGN GOALS

| Subsystem | Critical Parameter | Design Goal |
|---|---|---|
| Vehicle Body/Structure | Aerodynamic Drag | $C_DA$ product $\leq$ 5.7 $ft^2$ |
| | Vehicle Curb Weight | $W_c \leq$ 3000 lb |
| Vehicle Chassis & Drive Train | Rolling Resistance | Drag force $\leq$ 9 lb/1000 lb |
| | Vehicle Curb Weight | $W_c \leq$ 3000 lb |
| | Regeneration Braking | Range increase $\geq$ 15% |
| | Transmission Efficiency | $\eta_T$ = 98% at 45 mph cruise |
| Electrical Drive Subsystem | Motor Speed Range | 2:1 with field control |
| | Motor Efficiency | 90% at full load |
| | Max. Armature Current | 400A for 5% grade @ 50 mph |
| | Armature Chopper Efficiency | 97% @ full load |
| | Field Chopper/Battery Charger Efficiency | >90% in both modes |
| | Size and Weight | 100 lb & 2.5 $ft^3$, max. |
| Battery Subsystem | Energy Density | 17 Wh/lb at 3 hour rate |
| | Power Density | 100 W/lb maximum |
| | Cycle Life | 500 cycles to 70% discharge |

TABLE 1-4

CONTRACTOR ASSIGNMENTS BY WBS

| Contractor | WBS Elements |
|---|---|
| General Electric | 1.0, 2.0, 3.2, 4.0, 5.0, 6.0 |
| Chrysler Corporation | 3.1, 4.3, 4.6, 5.2, 5.3, 6.0 (Inputs) |
| Globe-Union, Inc. | 3.3, 6.0 (Inputs) |

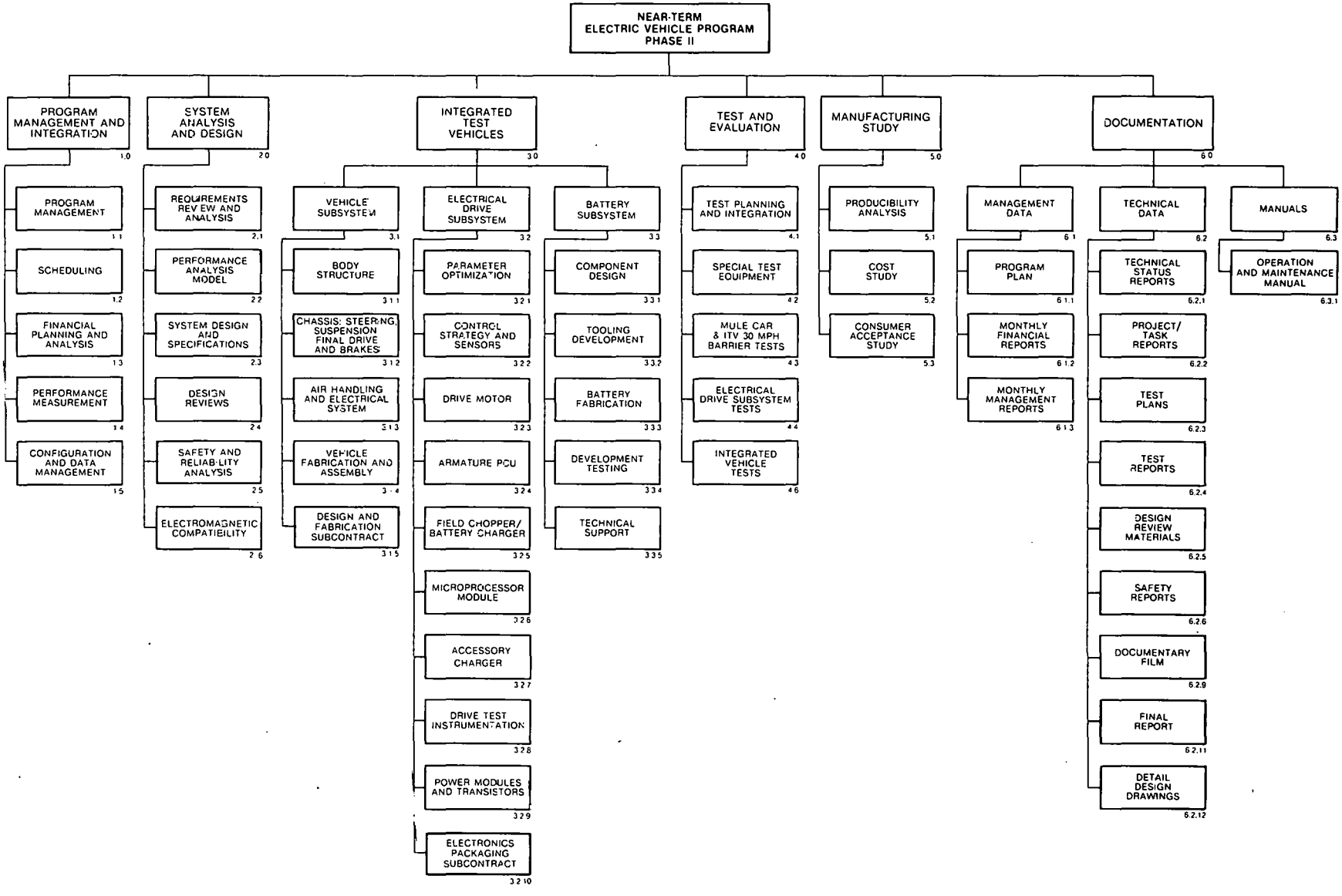


Figure 1-5. Contract Work Breakdown Structure (WBS)

## PROGRAM SCHEDULE

A summary schedule for the General Electric contract effort is shown in Figure 1-6. The 24-month contract started on April 28, 1977 and is scheduled for completion by April 28, 1979. Program milestones have been established for each WBS element; these milestones provide the basis for measuring technical progress versus plan, and this progress is reported monthly to DOE.

## PROGRAM STATUS

This section describes the status and findings of the General Electric contract one year after contract go-ahead. The systems engineering phase (conceptual design, trade-off studies, performance analyses, and specification development) has been completed. Performance goals and design criteria established during this early phase have been translated into design layouts, circuit designs, and working "breadboard" hardware. Detailed design and fabrication of subsystems are now underway, leading to the final assembly of test vehicles which will occur near the end of calendar year 1978. A brief summary of the technical progress in each WBS category is presented here; further details can be found in later sections of the report.

### System Analysis and Design

Based on a thorough analysis of the DOE Near-Term Objectives and Statement of Work requirements, design concepts were formulated for the Integrated Test Vehicle. Design studies carried out during the Phase I portion of this contract provided a starting point for the development of a compliant Phase II design.[1] Additional studies and tradeoffs were necessary, and these were performed with the aid of computer simulation programs developed by General Electric for the purpose of accurately predicting vehicle performance under the specific operating conditions set by DOE.

By reiterating the performance prediction programs while varying a number of vehicle design parameters, target performance values were selected for each vehicle subsystem. These performance targets were then documented in the form of system and subsystem specifications which control the total vehicle design. Separate specifications were developed for weight control and power loss control, to ensure a continuing emphasis on weight reduction and energy efficiency. System and subsystem performance specifications were issued early in the program and have been updated to reflect changes determined by subsequent analyses.

---

(1) "Near-Term Electric Vehicle Program, Phase I, Final Report," SAN/1294-1, General Electric Company, Corporate Research and Development, August 1977.

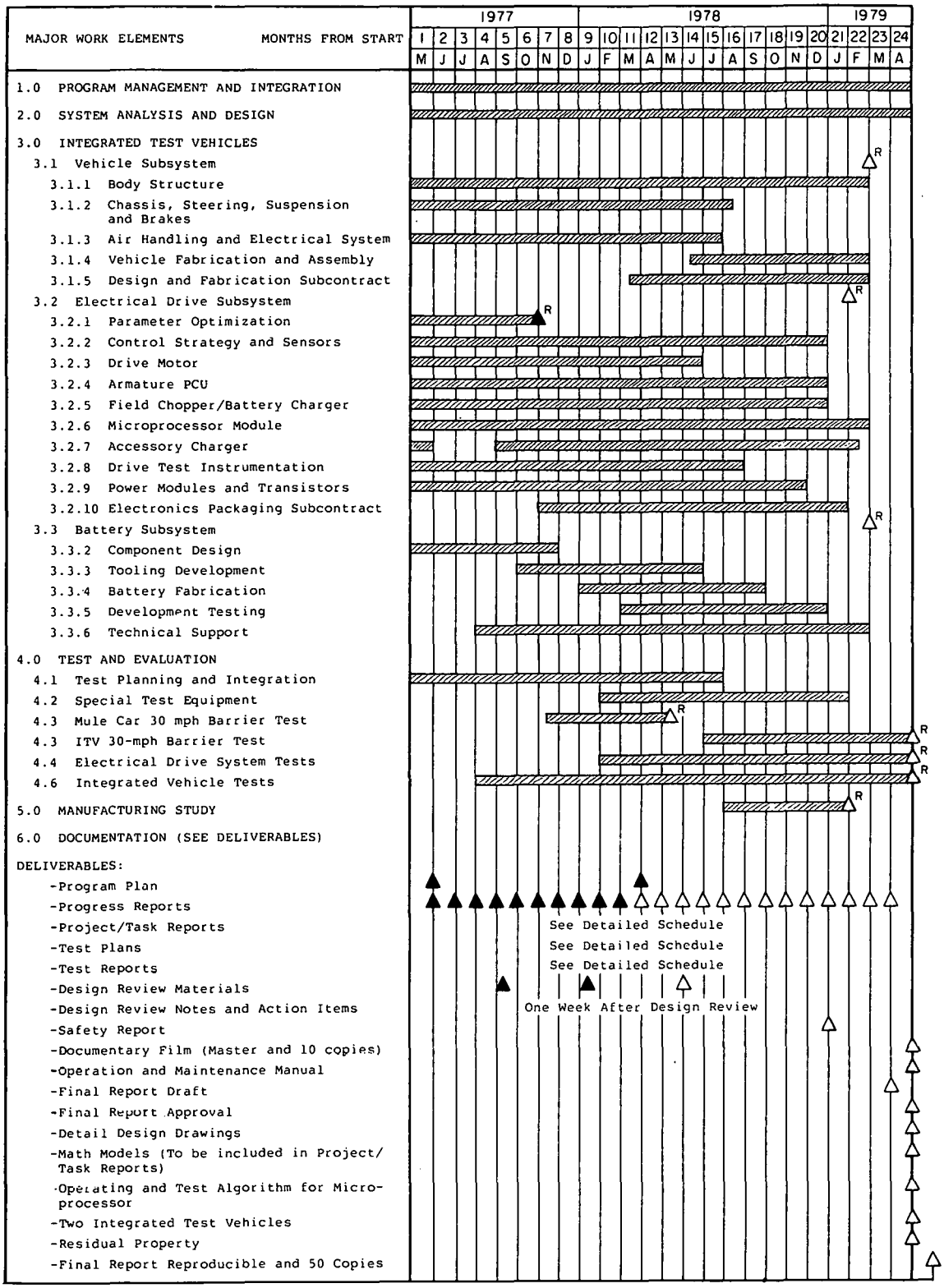


LEGEND:

△ = Scheduled Milestone

▲ = Completed Milestone

◇ = Modified Milestone

▨ = Time Span

$\triangle^{R}$ = WBS Reports

Figure 1-6. Electric Vehicle Program Schedule

Interface specifications have also been developed to assist in defining electrical, mechanical, thermal, and operational interfaces between major subsystems. When augmented by interface control drawings which are now being developed, these documents will completely define the interactions between subsystems.

Design reviews, conducted by the Jet Propulsion Laboratory, have been held to audit the work performed by General Electric and its subcontractors and to verify compliance of the emerging vehicle design with DOE requirements. A preliminary design review (PDR) was held on September 15 and 16, 1977. The PDR confirmed the early design concepts of the ITV and allowed detailed design work to begin on many of the electrical and vehicular subsystems. Because of special concerns expressed at the PDR, separate minireviews were scheduled on the Power Modules and Transistors project and the Battery Subsystem. These reviews were held on September 29 and October 7, 1977, respectively. Guidelines established at the minireviews provided direction for the detailed work on these important projects.

An Interim Design Review (IDR) was held on February 1, 2, and 3, 1978. Detailed design data and preliminary test results were presented to describe the technical progress achieved during nine months of contract effort. Approval was obtained from JPL to proceed with the final design activities leading to the generation of detailed drawings and prototype tools. A Critical Design Review (CDR) is scheduled for June 14 and 15, 1978. The CDR will serve as a final validation of the ITV design prior to the start of vehicle fabrication and assembly activities.

Other activities within the system analysis and design area include reliability and safety analyses and electromagnetic compatibility studies. These analyses are designed to ensure that the Integrated Test Vehicles will be free from catastrophic failure modes, safety hazards, and electromagnetic interference.

## Vehicle Subsystem

Based upon size, weight, and performance requirements of the ITV, the Chrysler "L Car" vehicle was selected as a baseline for development of the electric vehicle body structure and chassis. The L Car, which was unannounced at the start of this contract, is now known as the Plymouth Horizon and Dodge Omni. The L Car represents a modern lightweight design featuring front wheel drive, excellent seating accommodations, and full compliance with Federal Motor Vehicle Safety Standards (FMVSS). Selected components from the L Car were used to formulate a preliminary design layout of the ITV. Subsequent tradeoff studies have resulted in the modification or replacement of some production components to obtain the performance required for the ITV, but many L Car components have proved to be an excellent choice and were retained. Only by using proven production components wherever feasible is it possible to achieve a well-engineered vehicle within the 24-month schedule allocated for this program.

The first major design study undertaken on the vehicle subsystem was to determine the optimum means of packaging the propulsion batteries, along with four adult occupants, into the vehicle envelope. The result of this study was a battery tunnel which extends through the vehicle centerline and branches into a T-shape at the rear. This battery arrangement and other features of the vehicle packaging are illustrated in Figure 1-7. The batteries are carried in a tray which is raised into place by a hydraulic jack and bolted to the underside of the car. This arrangement was found to combine low weight, good accessibility, and excellent structural properties.

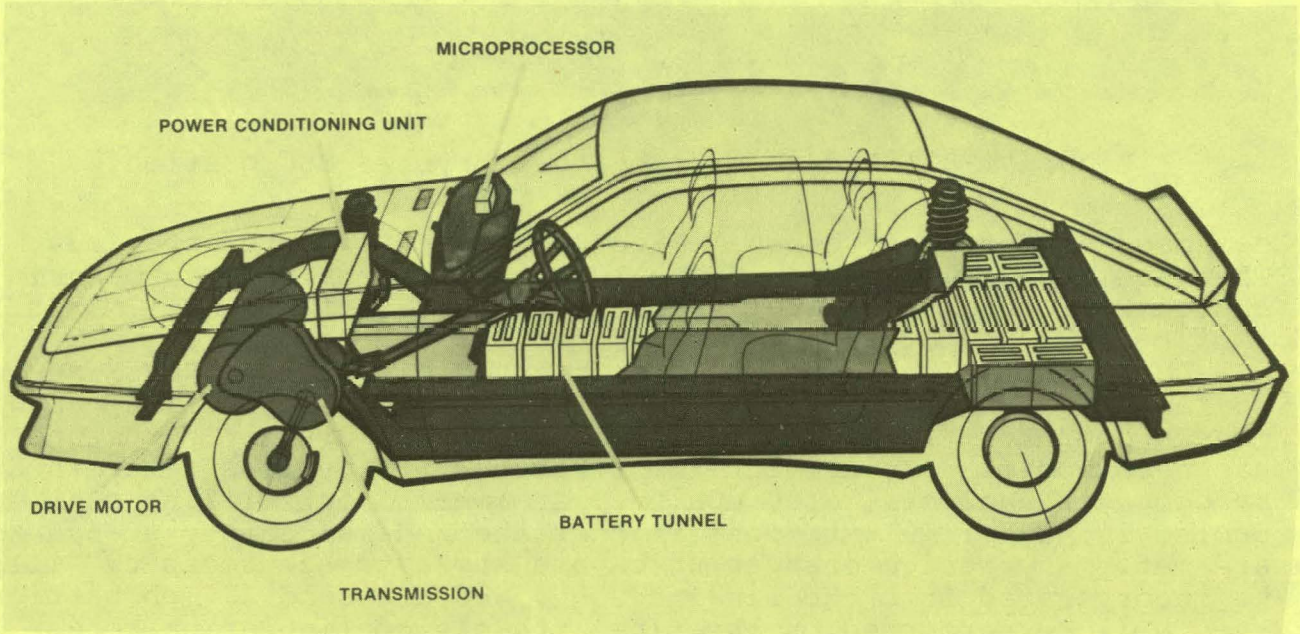


Figure 1-7. U.S. Department of Energy Near-Term Electric Vehicle Program -- GE/Chrysler Vehicle

After the preliminary vehicle packaging study was complete, a detailed styling and aerodynamic design effort was conducted by the Chrysler Corporation. The resultant body design is shown in Figure 1-8. This attractive fastback coupe exhibited an aerodynamic drag coefficient of 0.30 during wind tunnel tests, making it an extremely efficient design in terms of road losses.

To allow on-road development of suspension, steering, and brake systems for the ITV, a "Mule Car" was built and tested at the Chrysler Proving Grounds. The Mule Car consists of a modified Plymouth Horizon, which is fitted with a battery compartment and ballasted to duplicate the weight and balance properties of the ITV. Modified suspension and brake systems were fitted to the Mule Car, including a fully independent trailing arm rear suspension. After development testing, the Mule Car was evaluated for riding comfort and handling qualities by a "ride jury"

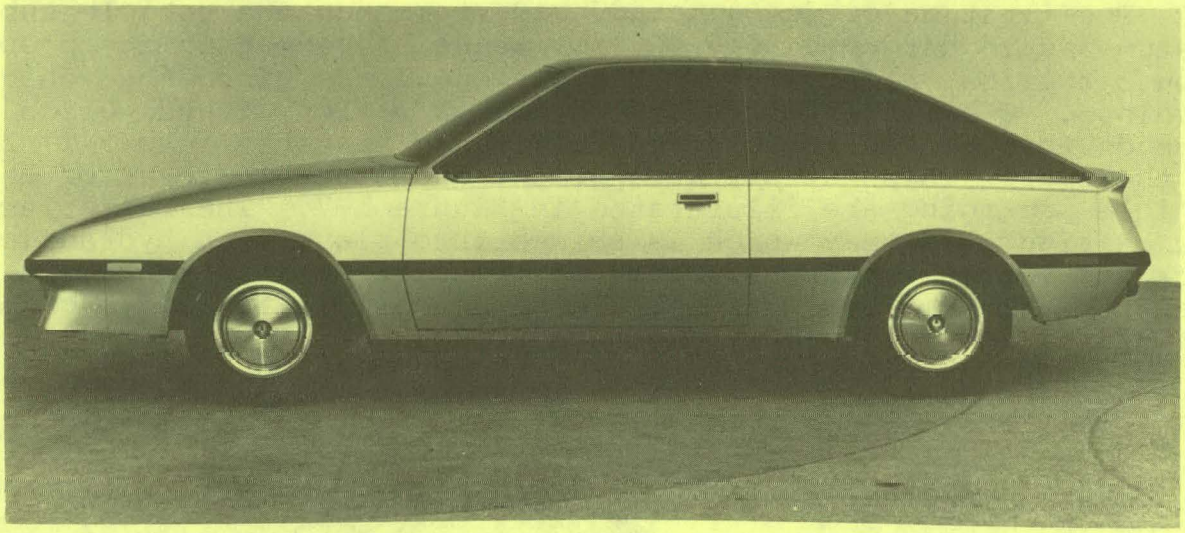

Figure 1-8. Body Design by the Chrysler Corporation

composed of Chrysler, General Electric, and JPL representatives. The Mule Car was judged to be fully satisfactory, and its chassis design will be carried over directly to the final ITV.

Structural design of the electric vehicle to meet FMVSS requirements has been carried out by the Chrysler Corporation, using modern computer-aided design techniques. The Mule Car structure has been modified to reflect the structural properties determined by computer analysis; a 30 mph barrier impact test will be conducted in May of 1978 to confirm that the Federal safety standards are met. Any design changes which are shown to be necessary will be incorporated into the final design, and a second 30 mph barrier test will be performed on the final vehicle configuration to establish FMVSS compliance.

Detailed drafting, tooling development, component fabrication, and final vehicle assembly will be performed by Modern Engineering Services under a subcontract with the Chrysler Corporation. The detailed design work is now in process, and vehicle fabrication and assembly work will be started soon after the Critical Design Review.

## Electrical Drive Subsystem

Studies conducted by General Electric during the Near-Term Electric Vehicle Phase I contract established a baseline configuration for the electrical drive subsystem (Ref. 1). This baseline design incorporated a separately excited dc motor with transistorized choppers to control both armature and field power. An onboard battery charger was to be integrated into the control electronics, to minimize size and weight. A microcomputer was conceived to provide efficient, flexible control of the drive system during all modes of driving and during battery charging.

Regenerative braking was specified as a means of energy recovery, to achieve greater range in urban driving. Integrated transistor power modules were to be used in both the armature and field modules, providing advantages in size, weight, energy efficiency, and production cost.

The Phase II contract to date has resulted in the design and breadboard testing of all critical elements of the electrical drive subsystem. Early simulation studies resulted in the selection of a custom-designed drive motor which provides high energy efficiency, excellent torque characteristics, and a field control speed range from 2500 to 5000 rpm. More than twenty motor designs were examined in arriving at the selected motor. A transistorized armature chopper has been designed and tested at full power. This chopper provides smooth control of the motor from 0 to 2500 rpm in both motoring and regenerative modes. Operating over a frequency range from 100 to 2000 Hz, the armature chopper achieves a full-load efficiency greater than 96%. A transistorized field chopper/charger has also been designed and tested. This circuit accomplishes dual-mode operation without switching relays or transformers, and achieves high efficiency for both field control and battery charging operations. Speed control of the drive motor from 2500 to 5000 rpm is provided by the field chopper. A compact solid-state logic power supply and a solid-state dc-to-dc converter to charge the 12 volt accessory battery from the 108 volt propulsion battery have also been designed and tested.

All of these power electronics modules are being packaged in a single Power Conditioning Unit (PCU) which provides efficient, forced-air cooling by means of an innovative cast aluminum heat exchanger. Thermal control, size and weight, and environmental control characteristics of the PCU are fully compliant with the design goals established for this program.

A microcomputer based on the Intel 8080A microprocessor family has been developed and tested. Software design and verification for the microcomputer is well underway and will be completed in time for integrated drive subsystem testing later this year. The microcomputer is a finite-state machine which provides fail-safe sequencing of the drive subsystem as well as closed-loop control of the drive motor speed and torque. Additional functions of the microcomputer are fuel gaging (battery charge indication), driver displays and warnings, and built-in self-test features.

An international survey of power transistors, to meet the demanding requirements of the electrical drive subsystem, revealed that only two manufacturers could provide transistors which would meet the electrical requirements and were suitable for power module packaging. One of these candidates was a power Darlington transistor developed by General Electric for low voltage (100 volt) applications. During the past year, this transistor has been redesigned and repackaged to create a 400 ampere, 300 volt power module which is uniquely suited to the power and frequency requirements of the electric vehicle. The specifications of the General

Electric power module, and a comparison with other competing devices in this power range, are shown in Figure 1-9.

**POWER TRANSISTORS AND INTEGRATED MODULE TECHNOLOGY**

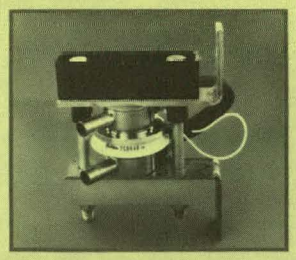

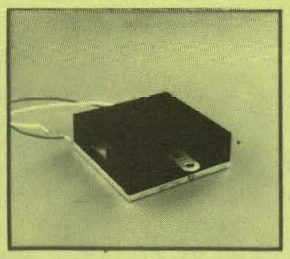

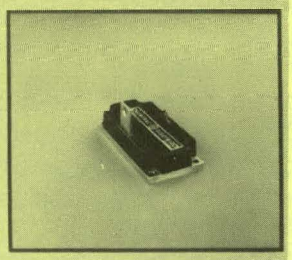

| | Toshiba "Giant Transistor" | Power Tech "Power Block" | General Electric Power Module |
|---|---|---|---|
| Volume | 318 cc (19.4 $in^3$) | 208 cc (12.7 $in^3$) | 115 cc (7 $in^3$) |
| Weight | 1.6 Kg (57 ozs) | 1.1 Kg (39 ozs) | 0.4 Kg (14 ozs) |
| Number of Transistors | 1 | 6 | 2 |
| Other Integrated Components | None | None | Power Diode |
| Current Rating (Gain≥100) | 400 A | 300 A | 400 A |
| Voltage Rating (BVceo) | 300 V | 325 V | 300 V |
| Max. Power Dissipation (25°C Case) | 2500 W | 1750 W | 1750 W |
| Present Unit Price (Quantity<100) | $338 | $944 | $90 (Includes $30 Power Diode) |
| Estimated Production Price (350,000/Year) | NA | $360 | $37 (Includes Power Diode) |

Figure 1-9. Power Transistors and Integrated Module Technology

## Battery Subsystem

The Globe Battery Division of Globe-Union, Inc. was selected by General Electric to furnish an improved lead-acid battery for the Integrated Test Vehicles. This battery will represent a significant improvement over currently available traction batteries. An energy density of 17 Wh/lb is predicted, at the three-hour discharge rate. Total battery capacity for the ITV will be approximately 18 kWh at 108 volts. A cycle life of 500 deep-discharge cycles has been specified for the battery. Several unique design features are used to obtain the improved energy density and long cycle life required for this program. One of these innovations consists of a modified container design which allows the battery plates to be rotated 90 degrees from their usual orientation; a high-rise cover is also used, allowing the battery plates to be somewhat larger in the vertical direction. The resultant grid size for the Globe-Union battery is much larger than a conventional golf-car battery, as illustrated in Figure 1-10. The

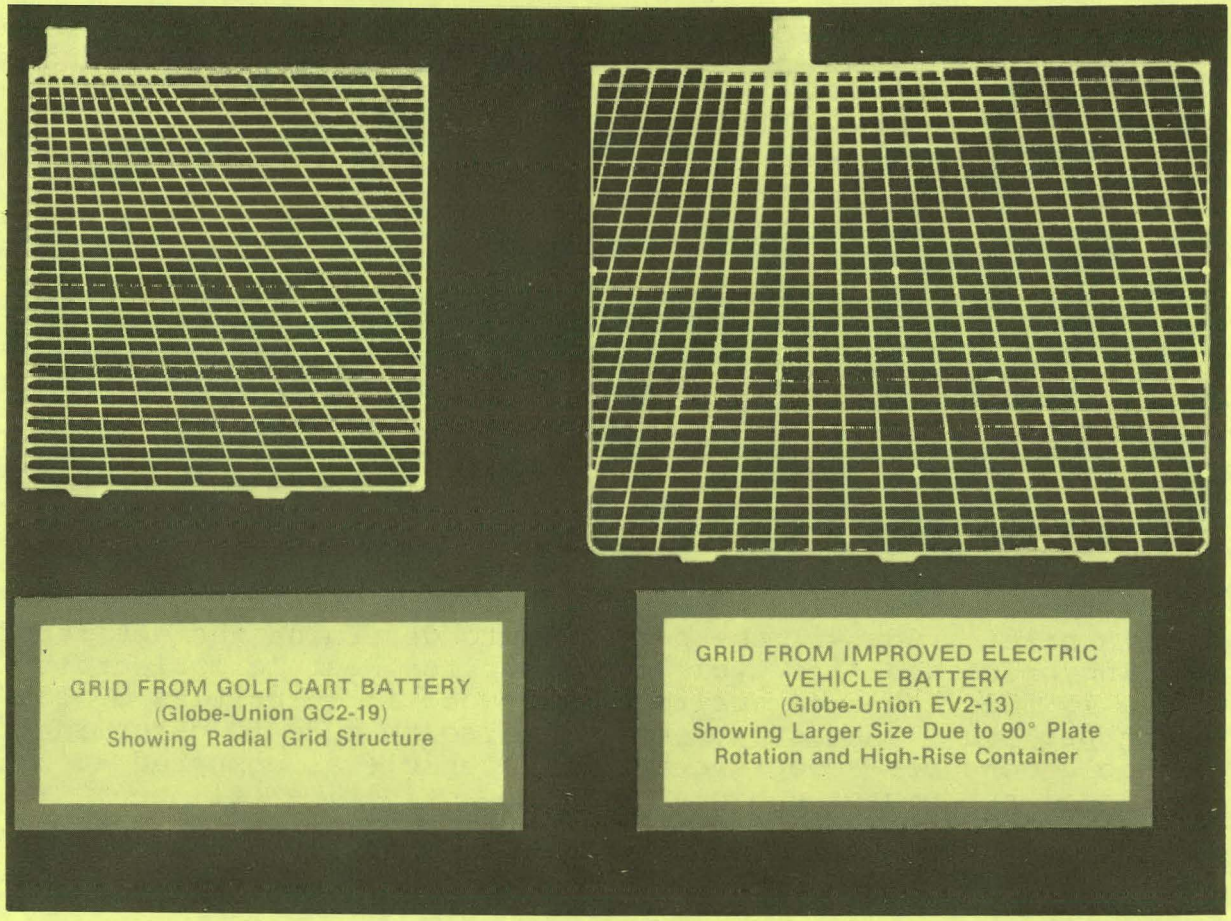


Figure 1-10. Grids from Golf Car (left) and EV2-13 Battery

large plate area, along with other design innovations, results in improved energy density and power density for the EV2-13 battery.

The EV2-13 battery design is complete and a few hand-pasted cells have been tested. These preliminary tests indicate that the design objectives for the battery will be met. Fabrication and testing of complete batteries are contingent on delivery of the container tooling, which is scheduled to be received in August of 1978.

## TEST AND EVALUATION

A comprehensive test program has been planned to validate the performance and safety aspects of the Integrated Test Vehicles. A master test plan was developed to establish the specific tests required for subsystem and system evaluation.

Categories of tests to be performed include development testing of major components; subsystem testing of the Mule Car, Electrical Drive Subsystem, and Battery Subsystem; and integrated

vehicle testing of the completed test vehicles. All specification requirements for speed, acceleration, driving range, and energy consumption will be verified by road tests. In addition, 30 mph barrier tests will be performed to verify crashworthiness. An electromagnetic compatibility test will be performed to ensure that the vehicle operates without internal failures due to electromagnetic radiation and does not radiate undesirable levels of interference into the environment.

Component-level testing has been performed to validate the design of all critical elements. Mule Car testing, as previously described, has also been completed. Preparations and test plans are nearly complete for the Mule Car 30-mph barrier test (scheduled in May 1978) and the Electrical Drive Subsystem integrated testing (to start in August 1978). Integrated Vehicle Testing will occur in the first quarter of calendar year 1979.

## MANUFACTURING STUDY

A brief study will be performed to determine the estimated selling price and life cycle costs for the Near-Term Electric Vehicle if this vehicle were to be produced in quantities of 100,000 units per year. An assessment will also be made to determine the probable consumer acceptance of this vehicle as compared to conventional subcompact vehicles. These activities will begin in August 1978 and are scheduled for completion by April 1979.

## Section 2

## SYSTEM ANALYSIS AND DESIGN

### WBS 2.1 REQUIREMENTS REVIEW AND ANALYSIS

The system design was initiated with a review of the Phase I design, the ERDA Near-Term Performance Objectives, and the Phase II Statement of Work requirements. The initial baseline system requirements are shown in Table 1-2.

A specification tree was developed which allocated system requirements to four major subsystems: Vehicle, Electrical Drive, Battery, and Support Equipment. The specification tree is depicted in Figure 2.1-1. As shown, each major subsystem is further broken down into major components or groups, with a specification sheet developed for each.

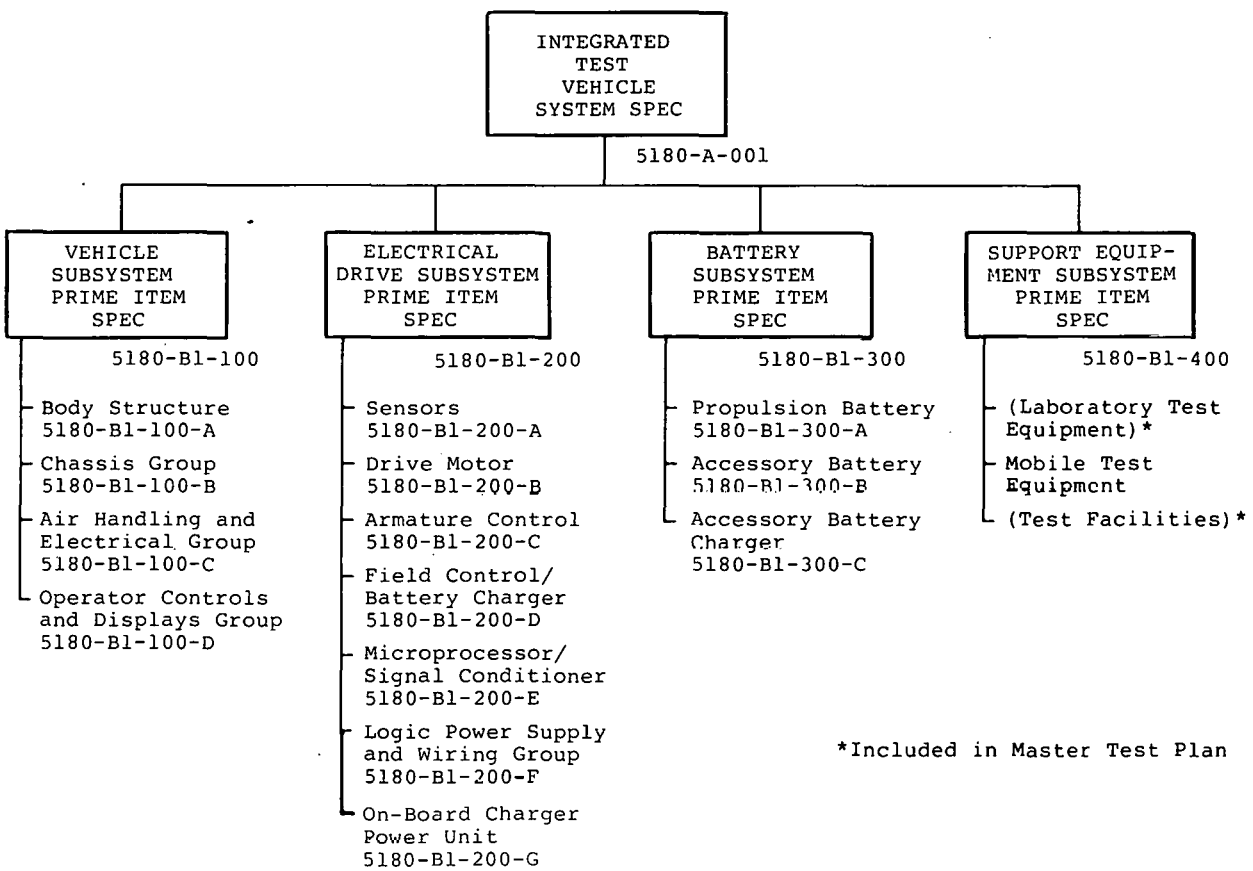


Figure 2.1-1. ITV Specification Tree

In addition to the above, an interface matrix was developed delineating major interface requirements between subsystems. This matrix resulted in the development of an interface specification tree and subsequent interface specifications. The interface specification tree is shown in Figure 2.1-2. A working group on vehicle design tradeoffs was initiated consisting of the Lead Systems Engineer and representatives from both Chrysler and Globe-Union. A Weight Control Specification and Power Loss Control Specification were generated and are used as a formal means of controlling these parameters and as a prime input for design tradeoff decisions.

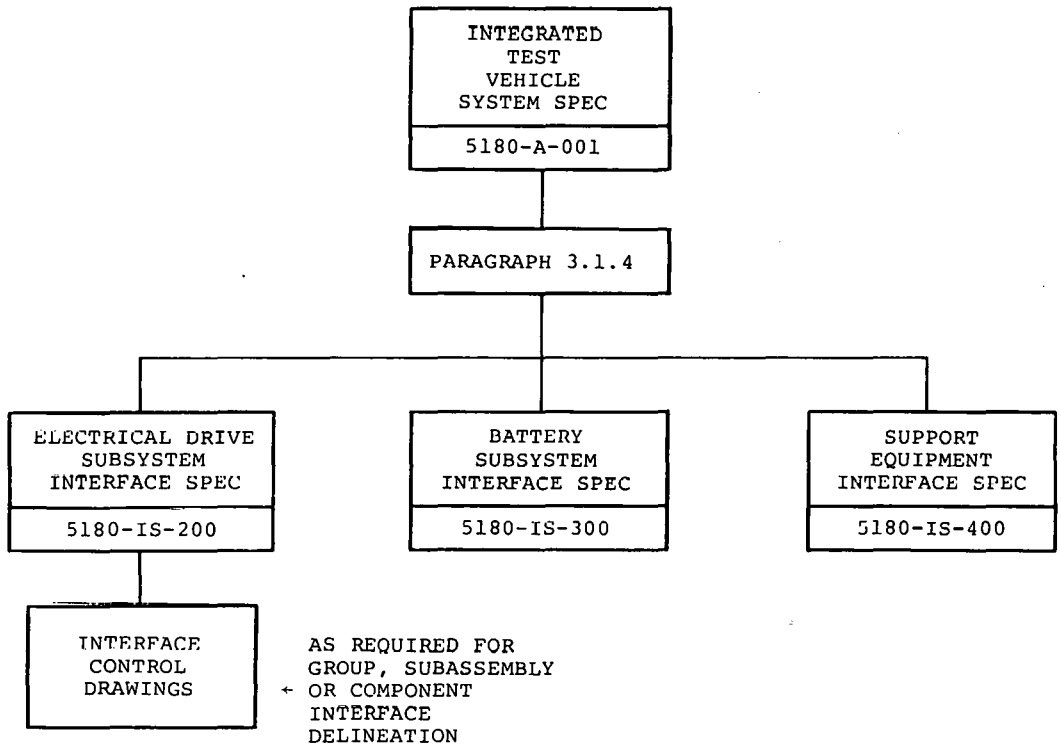


Figure 2.1-2. ITV Interface Specification/Document Tree

## WBS 2.2 SYSTEM MODELING AND PERFORMANCE PREDICTION

WBS 2.2.1 Description of Program

Programs are available for simulating a variety of performance tests, including SAE J227a driving cycles. Five basic types of simulations are possible:

1. Vehicle range on SAE J227a driving cycle. Schedules B, C, and D can be simulated.

2. Vehicle range at any constant velocity from 5 to 55 mph (or higher, if desired).

3. Time to accelerate from 0 to 30 mph or 0 to 60 mph. (Conversely, program will define power profile to achieve 0 to 30 mph in specified time.)

4. Time to accelerate from 25 to 55 mph, or other specified velocities. (Conversely, program will define power profiles to achieve 25 to 55 mph in specified time.)

5. Maximum speed achievable on a specified grade. (Conversely, program will define power profile to maintain a specified speed on a specified grade.)

A great deal of flexibility is available in the existing programs to accommodate a wide variety of vehicle parameters. The following parameters can be entered or changed independently:

- Vehicle test weight
- Wheel rolling radius
- Final drive ratio
- Aerodynamic drag coefficient ($C_D$) and frontal area ($A_F$)
- Number of transmission speed ranges (gears)
- Speed ratio for each gear
- Rolling resistance drag coefficients ($k_1$, $k_2$, $k_3$)
- Wheel inertia
- Transmission/final drive efficiency
- Motor design parameters (as defined by motor model)
- Battery design parameters (as defined by battery model)
- Electrical losses in drive train (as defined by armature and field chopper models)
- Auxiliary power losses (including logic power, accessories, and ventilating blowers)

A number of output (print) options are available for each simulation, depending upon the information desired. For example, when the J227a Schedule D range test is run, a single cycle print-out can be obtained which shows the calculated values of motor current and voltage, battery current and voltage, etc. at each second during the cycle. An alternate print mode displays snap-shots of each variable at specified points during each cycle, and records the number of cycles (as well as distance traveled) for one continuous driving mission. Since the main use of this program is design optimization, a record of vehicle losses is made during each simulation to account for the energy consumed by each system component.

Another feature of the program is that a regeneration mode can be simulated in the J227a cycle. The regeneration mode occurs during the coastdown phase of the cycle to provide internal combustion engine "feel," and during the braking phase to simulate both electrical and hydraulic braking. During regeneration, the motor acts as a generator with losses modeled in a fashion similar to the motoring phase.

## Modeling and Simulation Techniques

Vehicle performance during a simulated driving segment is determined by solving a series of equations which mathematically define the response of the vehicle subsystems to each calculated set of operating conditions. For example, to determine the vehicle range on the J227a Schedule D driving cycle, the computer program would step through the following calculations:

- Specify vehicle speed versus time according to stored Schedule D velocity-time coordinates.
- Compute vehicle propulsion loads for each time increment (aerodynamic drag, rolling resistance, etc.).
- Compute motor torque and speed required at each time increment to achieve the specified velocity or required acceleration.
- Computer drive subsystem voltages, currents, and power losses at each time increment.
- Compute instantaneous values of battery current and terminal voltage.
- Calculate from the battery discharge model the fraction of battery capacity consumed during each time interval.
- Repeat the above steps until the battery is completely discharged, calculating the total distance traveled during the mission.

The mathematical models which are used to represent the vehicle and drive subsystems are represented by blocks in the overall system model of Figure 2.2-1. A brief description of the individual models will be presented.

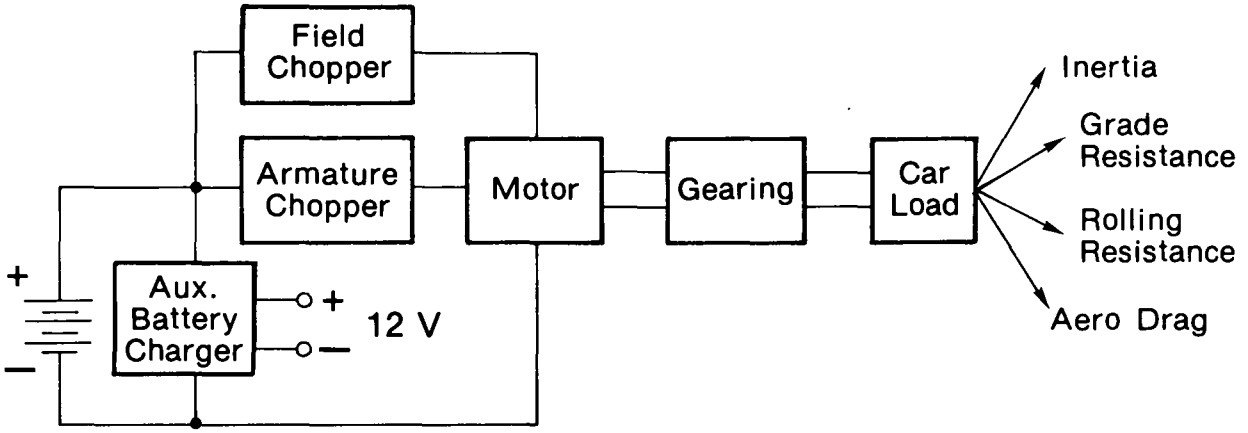


Figure 2.2-1. Overall System Model

The propulsion battery is modeled as shown in Figure 2.2-2. This is a very simple representation, whereas the equations which describe the battery behavior are quite complex. However, the figure does illustrate the basic concept. The battery consists of a voltage source ($E_B$) supplying current through a variable resistance (R). The value of R is determined by battery state-of-discharge, represented by S. During regeneration, current flow to the battery is reversed and the battery state-of-charge is increased (state of discharge, S, is decreased).

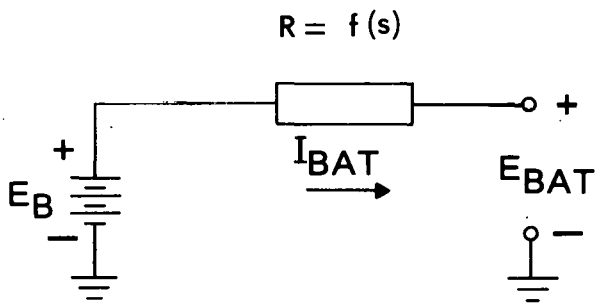


Figure 2.2-2. Propulsion Battery Model

Speed and torque of the electric vehicle drive motor are controlled by means of armature and field choppers. Each of these chopper devices is modeled as shown in Figure 2.2-3. Here the chopper is represented as a variable-ratio dc transformer which converts the battery voltage to a lower value as required to achieve proper motor excitation. Ignoring chopper losses, Power Out = Power In, so that $V_M \cdot I_M = E_{Battery} \cdot I_{Battery}$. In the actual armature chopper model, internal losses are accounted for by means of fourteen equations which are solved for each time step.

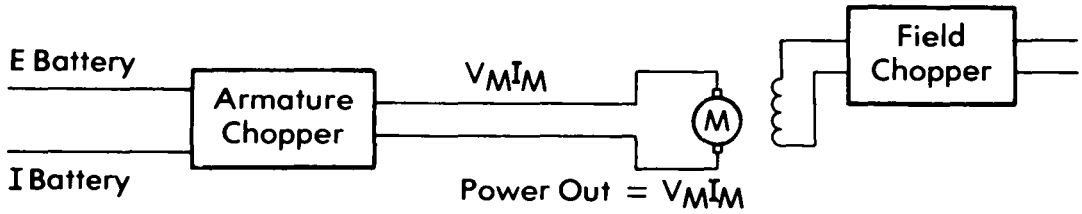


Figure 2.2-3. Chopper Model

Figure 2.2-4 illustrates the model used to represent a dc separately excited drive motor. The equations which define rotor speed, torque, and motor losses are shown; these equations constitute the actual model used by the computer to predict motor performance during each time interval.

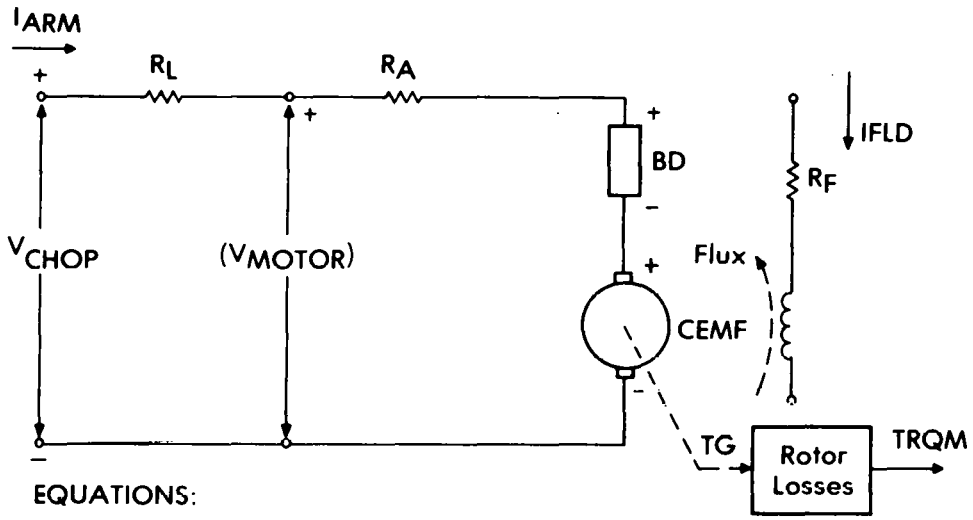


EQUATIONS:

Armature Loop: VCHOP = CEMF + BD + IARM (RA + RL)

CEMF = KV * RPM * FLUX

Rotor Power Loss:

Core Loss: WCL = WCL1 $(RPM/1000)^{1.5}$

Friction: WF = WF1 (RPM/1000)

Windage: WDG = WDG1 $(RPM/1000)^3$

Stray Load Loss: WLL = 1% of Power Out

Torque: TG = IARM * KT * FLUX

Figure 2.2-4. Motor Model

The remaining models for the electric vehicle are quite simple and do not merit a detailed description. Over a period of more than two years the accuracy of these models has been refined, and new components have been modeled as the need has been identified.

WBS 2.2.2 Summary of Results

The initial system-modeling mathematical model was developed for the Parameter Optimization Project and used to select the optimum dc drive motor design. Boundary values for key vehicle parameters (weight., $A_F$, $C_D$, $F_{RR}$), were selected and used to determine sensitivity of the motor design to variations in vehicle design. The results of this effort were presented at the Preliminary Design Review (PDR) and documented in Task Report SRD-77-160, WBS 3.2.1 - Parameter Optimization, dated 31 October 1977.

The initial Performance Predictions of the Near-Term Electric Vehicle were made using the EV-106 battery model and a regeneration technique that used no friction brake blending during the braking mode, resulting in very high armature currents. Armature currents of this magnitude result in high battery currents which, in turn, would adversely affect battery life.

The initial range performance results and vehicle parameters are summarized as follows:

| | |
|---|---|
| Range J227 D cycle | 61 miles |
| Range 25 mph cruise | 117 miles |
| Range 35 mph cruise | 131 miles |
| Range 45 mph cruise | 104 miles |
| $C_DA$ | 5.7 $ft^2$ |
| Rolling resistance | 0.009 lb/lb |

In response to a concern expressed at the PDR, a brief analysis of the performance tradeoffs associated with shifting transmissions was performed. The results indicated a potential range performance improvement of less than 1% on the J227a Schedule D cycle if realistic values of transmission efficiency are used. This analysis was documented in a letter report dated October 14, 1977.

Globe-Union provided an estimate of the performance of the improved EV2-13 battery, which was modeled analytically and incorporated into the program. The regeneration model was revised to incorporate regeneration during the coastdown phase of the J227a Schedule D cycle and electrical and hydraulic brake blending during the braking phase. The battery charging currents used during both phases were adjusted to acceptable values based on data provided

by Globe-Union. The new battery model also reflected full discharge to 1.3 volts per cell as the criterion for termination of the cycle. The effective frontal area ($C_DA$) was increased to 5.8 $ft^2$, based on scale-model wind tunnel tests.

The following additional modifications were made to the Performance Model:

- Updated and more detailed modeling of the armature chopper losses.
- Decrease in field chopper efficiency from 95 to 90 %.
- Improved drive motor performance based on design optimization.
- Inclusion of updated power requirements of the logic power supply, accessory charger, and armature and field contactors.
- Inclusion of transmission overall efficiency of 96 %.
- Optimized acceleration profile (constant $I_{BAT}$).

The range performance and vehicle parameters resulting from the above updates are summarized as follows:

| | |
|---|---|
| Range J227a Schedule D | 71 miles |
| Range 25 mph cruise | 129 miles |
| Range 35 mph cruise | 146 miles |
| Range 45 mph cruise | 124 miles |
| $C_CA$ | 5.8 $ft^2$ |
| $F_{RR}$ (rolling resistance) | 0.009 lb/lb |

Energy flow models were developed for the Integrated Test Vehicle (ITV) for the J227a Schedule D driving cycle and constant speeds of 25, 35, and 45 mph. These are shown as Figures 2.2-5 through 2.2-8.

As a result of an IDR Action Item, the acceleration segment of the J227a Schedule D driving cycle was modified to simulate a linear acceleration. Using this profile and restricting motor current to the present design limit resulted in a significant range decrease. A letter report dated February 23, 1978 was written detailing GE's position on establishing an arbitrary constraint on the velocity versus time profile during this acceleration segment. As a result, JPL requested that the acceleration profile in the performance model be simulated to provide a repeatable constant $I_{BAT}$ acceleration, cycle to cycle. This request has been implemented in the model.

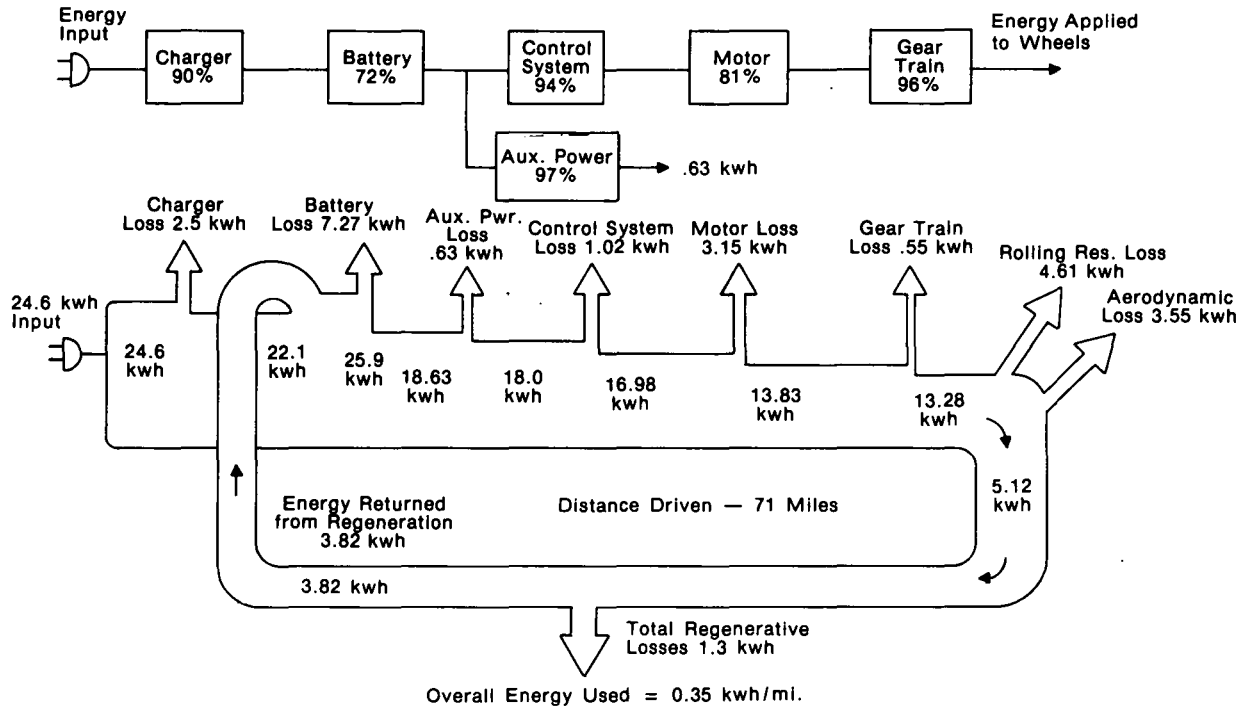


Figure 2.2-5. Energy Flow Model for GE-ITV on J227a Schedule D — Performance Prediction Model

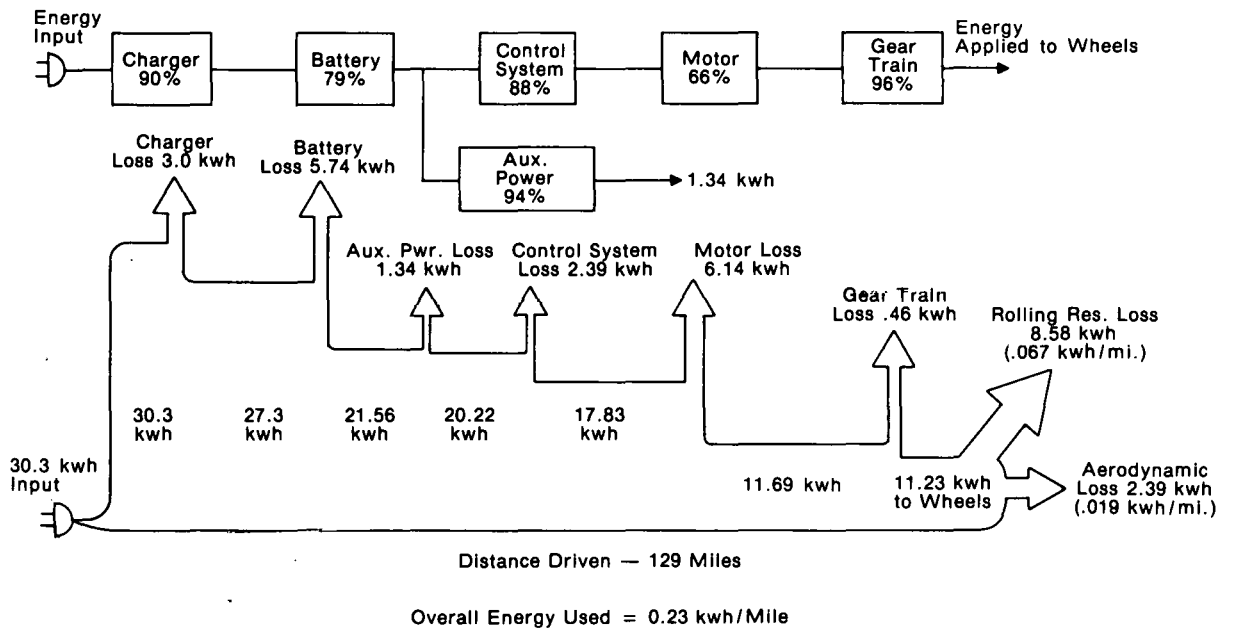


Figure 2.2-6. Energy Flow Model for GE-ITV at Constant 25 Mph — Performance Prediction Model

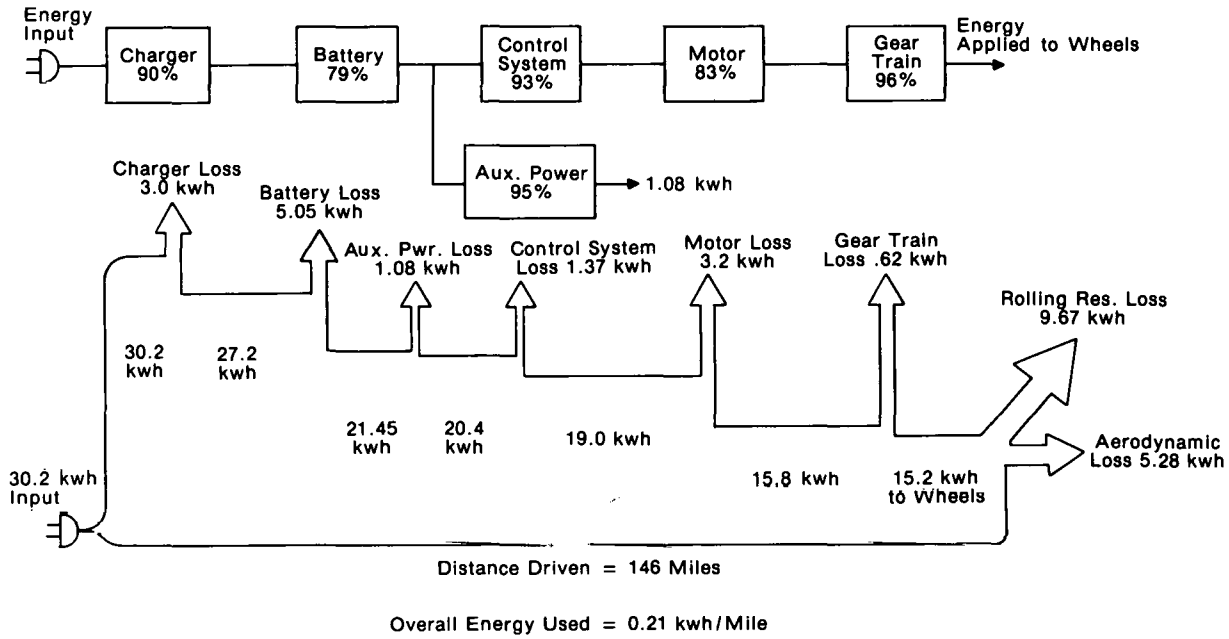


Figure 2.2-7. Energy Flow Model for GE-ITV at Constant 35 Mph – Performance Prediction Model

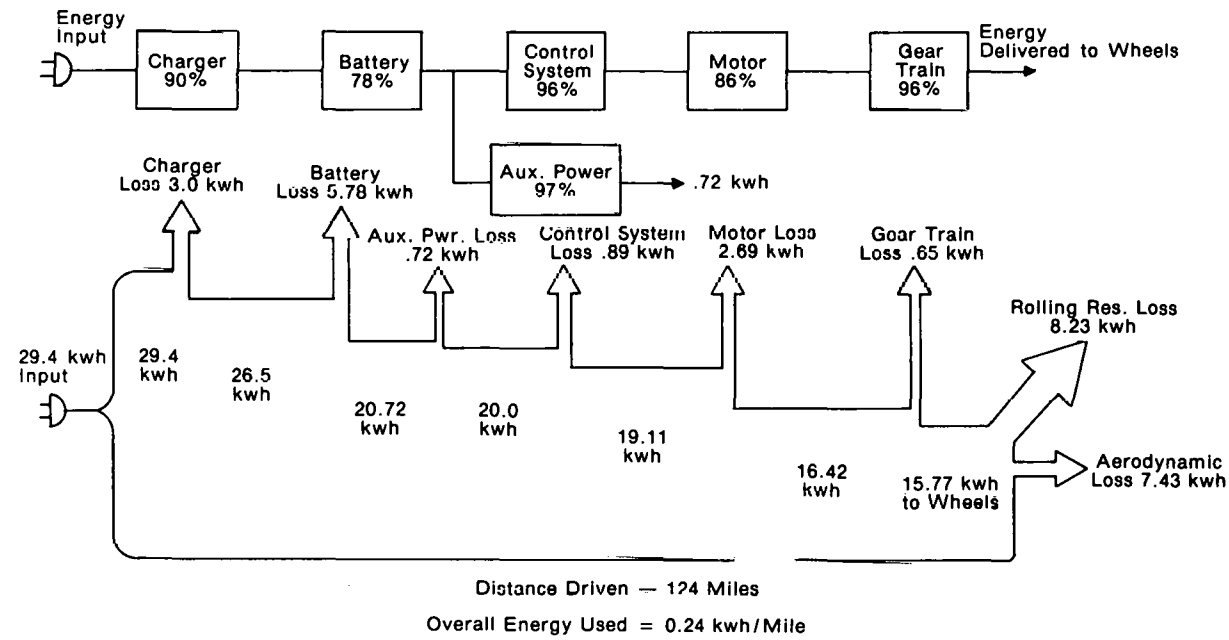


Figure 2.2-8. Energy Flow Model for GE-ITV at Constant 45 Mph – Performance Prediction Model

## WBS 2.3 SYSTEM DESIGN AND SPECIFICATION

### WBS 2.3.1 General System Description

The Integrated Test Vehicle is an all-electric subcompact vehicle designed to carry up to four passengers in a suburban driving environment. The ITV system block diagram is depicted in Figure 2.3-1.

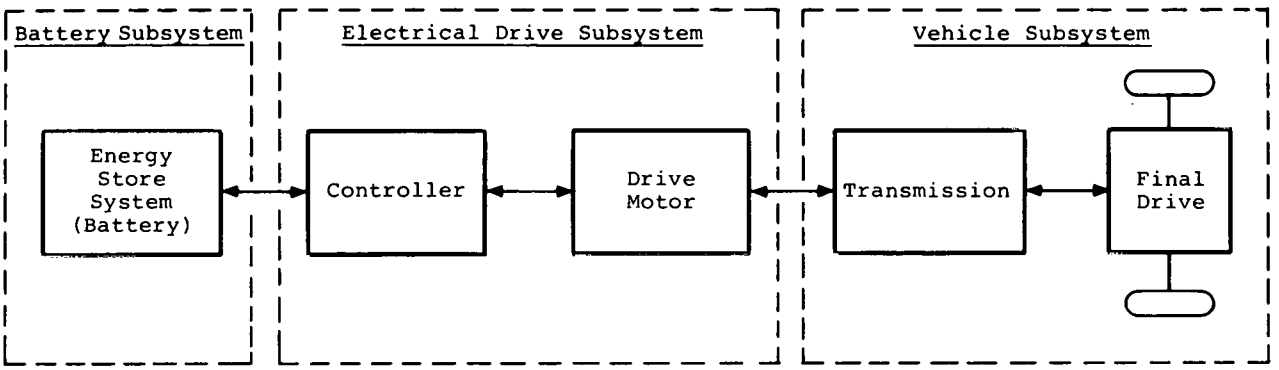


Figure 2.3-1. ITV System Block Diagram

The principal system elements are the Battery Subsystem, the Electrical Drive Subsystem, and the Vehicle Subsystem. The Battery Subsystem includes 18 propulsion batteries and their venting/watering system, propulsion battery wiring, the 12 volt accessory battery, and the accessory battery charger, which is physically located in the power conditioning unit (PCU). The Electrical Drive Subsystem includes the PCU, which contains the armature controller, field control/battery charger, logic power supply, and the accessory battery charger. The drive motor, microprocessor/signal conditioner, onboard charger power unit, and differential pressure transducer amplifier and exciter (part of the regenerative braking system) are also elements of the Electrical Drive Subsystem. The Vehicle Subsystem is composed of the body structure, chassis, and air handling and electrical groups. The ITV is designed to conform to applicable Federal Motor Vehicle Safety Standards (FMVSS). Other significant system parameters are delineated in the Integrated Test Vehicle System Specification, 5180-A-001.

### WBS 2.3.2 Summary of System and Subsystem Specifications

Figure 2.1-1 showed the five major equipment-related specifications of the Integrated Test Vehicle. The specifications were developed in general according to the MIL-STD-490 specification format. The top level specification is that for the system. The subsystem specifications have requirements allocated from the system specification. Specifications sheets which form a part of

the subsystem specifications define component requirements. In addition to the hardware-related specifications, a weight control specification and a power loss control specification have been developed. Performance against these specifications is tracked on a continual basis. The specifications are useful as a design tradeoff decision-making tool, since control of weight and power loss are the key factors affecting vehicle performance. These specifications were issued for the Preliminary Design review and revised for the Interim Design Review. The final revision, Revision 2, is in process and will be available for the Critical Design Review.

### WBS 2.3.3 Summary of Interface Specifications and Drawings

Section 2.1 (Figure 2.1-2) defined the interface control specification tree. The interface specifications are used to define principal functional interfaces between the Vehicle Subsystem and the Electrical Drive Subsystem, Battery Subsystem, and Mobile Test Equipment. These specifications also serve as an integration tool and are structured to define responsibilities and provide visibility of unassigned areas and responsibilities. Interface Control Drawings (ICDs) currently being documented contain most of the details of the interfaces. Drawings defining the vehicle power wiring, signal wiring, general safety interlock system, and battery safety quick-disconnect system are being prepared. A major revision to the interface specifications to include the ICDs is in process, with a goal of completion for the Critical Design Review.

### WBS 2.3.4 Special Studies

As part of the system analysis and design task, a number of special studies have been performed. The most significant ones are:

- Battery compartment heating, cooling, and venting
- Alternate designs to improve vehicle range
- Electrical drive subsystem cooling
- Battery emergency disconnect system
- Effects of battery life as a function of equalization charge
- Battery life above 100 $^{o}$F ambient temperature operation
- Implementation of a ground fault current interrupter
- Hydrogen safety during battery charging and motoring
- Electrical hazards

## WBS 2.4 SAFETY AND RELIABILITY ANALYSIS

### WBS 2.4.1 Safety Analysis

An electrical safety analysis was performed to document potential hazards and to provide guidance for elimination of these hazards. The ITV operator and passengers must be protected from two types of shock potential in addition to those associated with the 12 volt electrical system found in an internal combustion powered automobile.

The 108 volt propulsion system is the first source of possible electric shock. The 108 volt system has been isolated from the vehicle body and chassis. For a shock hazard to occur, therefore, there would have to be at least two electrical subsystem or component failures. An example is a motor insulation failure, resulting in the chassis being at approximately the same potential as the positive 108 volt supply, coupled with a failure which causes exposure of the 0 volt common in the microcomputer to the passenger or driver's "touch." The probability of two such failures occurring and resulting in a shock hazard is extremely low.

The second possibility of electrical shock is leakage current from the propulsion battery charging circuitry. The installation of a ground fault current interrupter (GFCI) in the vehicle to preclude the possibility of shock due to leakage current resulted from a study performed following the Interim Design Review. The results of this study were documented in a report dated March 6, 1978.

A study has been initiated to investigate the hazard potential of environmental electrical noise and strong radio frequency signals. Of prime concern are sudden or uncalled-for increases in acceleration or malfunctions that could cause the driver to lose vehicle control. The EMC susceptibility of the electrical drive subsystem is being examined to identify the most probable paths into the microcomputer system. In addition, an EMI/EMC test of the total vehicle is planned during the integrated vehicle testing program. A search is continuing for the required shielded room to permit RF radiation testing of the ITV.

An analysis was made of the requirements of the NHTSA Electric/Hybrid Vehicle Safety Standard draft, especially in the area of safety hazards not covered by existing standards. The following safety standards included in the draft have been implemented on the Integrated Test Vehicle:

- Propulsion system isolated from the vehicle chassis
- Transformerless onboard charger provided with a GFCI
- Battery charger receptacle interlock disconnecting charging power if the battery compartment is opened

- Interlock to prevent driving the vehicle while connected to the power source
- Warning light activitated if the motor overheats
- Positive ventilation of battery compartment during charging
- Flame arrestors utilized
- Battery mounts implemented to restrain the batteries from occupant compartment intrusion during collisions
- Auxiliaries on a separate circuit from the propulsion system
- Audible warning for reverse

In addition to the above, other interlocks have beem implemented to prevent electrical shock hazard.

WBS 2.4.2 Reliability Analysis

As a result of direction received at the Interim Design Review, the primary focus of the reliability task is to analyze critical failure modes of the electrical drive subsystem, with emphasis on vehicle/ personnel safety. The following failure categories to be used in the reliability analysis were defined:

- Category IA - A critical failure resulting in loss of vehicle control (allowable only if fall back mode exists)
- Category IB - a critical failure resulting in an electrical shock hazard (no such failures allowable)
- Category IC - a critical failure resulting in other forms of hazard (explosion, fire --no such failures allowable)
- Category II - a failure other than critical, resulting in total or major loss of vehicle function
- Category III - a minor failure resulting in no or slight impairment of vehicle function and for which corrective maintenance can be deferred until convenient to perform

The failure mode effects analysis of the armature chopper circuit has been completed. Analysis of potential malfunctions in the armature chopper circuit primarily indicate that they will cause either direct shutdown or subsequent commanded shutdown of the microcomputer, resulting in loss of vehicle power. Failures in this category, although listed as Category IA, are normally

recoverable since a fall-back mode exists (steering the vehicle to the side of the road and stopping).

The potential of a failure resulting in the vehicle's lurching when stopped in traffic under conditions of maximum field current and zero armature current has been identified. This failure mode will be further analyzed, and results of the analysis will be reported at the CDR.

Failure mode effects of the field chopper/charger circuit have been completed. Malfunctions in the charging circuit cause no critical failures. Malfunctions in the field chopper result in an increase in vehicle acceleration characteristics, power loss, or a commanded microcomputer shutdown. In all cases, a fall-back mode exists which allows recovery.

Efforts are underway to perform a failure mode effects analysis of the microcomputer.

## Section 3

## SUBSYSTEM ANALYSIS AND DESIGN

### WBS 3.1 VEHICLE SUBSYSTEM

Introduction

The Phase II Near-Term Electric Vehicle represents the state-of-the-art in automobile design. The sleek aerodynamic styling is attractive and contemporary in appearance and contributes significantly to the attainment of the range performance goals. The front air dam, contoured door glazing, "Coke bottle" body, side paneling, and rear spoiler are all functional features that were sculptured and refined in the Chrysler wind tunnel. These features are illustrated in Figures 3.1-1 and 3.1-2. The flush glazing, concealed headlamps, low drag rearview mirror, full-belly pan, and low frontal area combine with the other features to produce a low $C_DA$ of 5.8 $ft^2$. The vehicle comfortably seats four passengers and provides storage space behind the rear seat for groceries, luggage, or other cargo. Package comparisons are shown in Table 3.1-1.

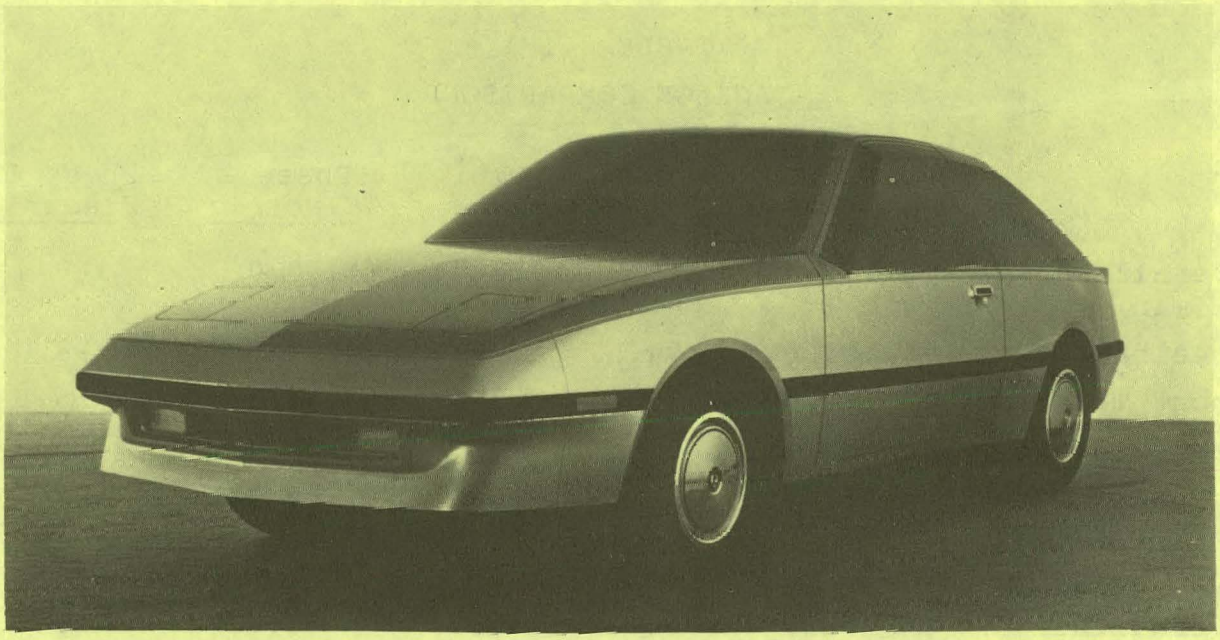

Figure 3.1-1. Phase II Near-Term Electric Vehicle

Chassis features include front-wheel drive, independent front and rear suspension, rack and pinion steering, and low rolling resistance steel-belted radial tires. Braking is provided by combining the regenerating electric drive at the front with a

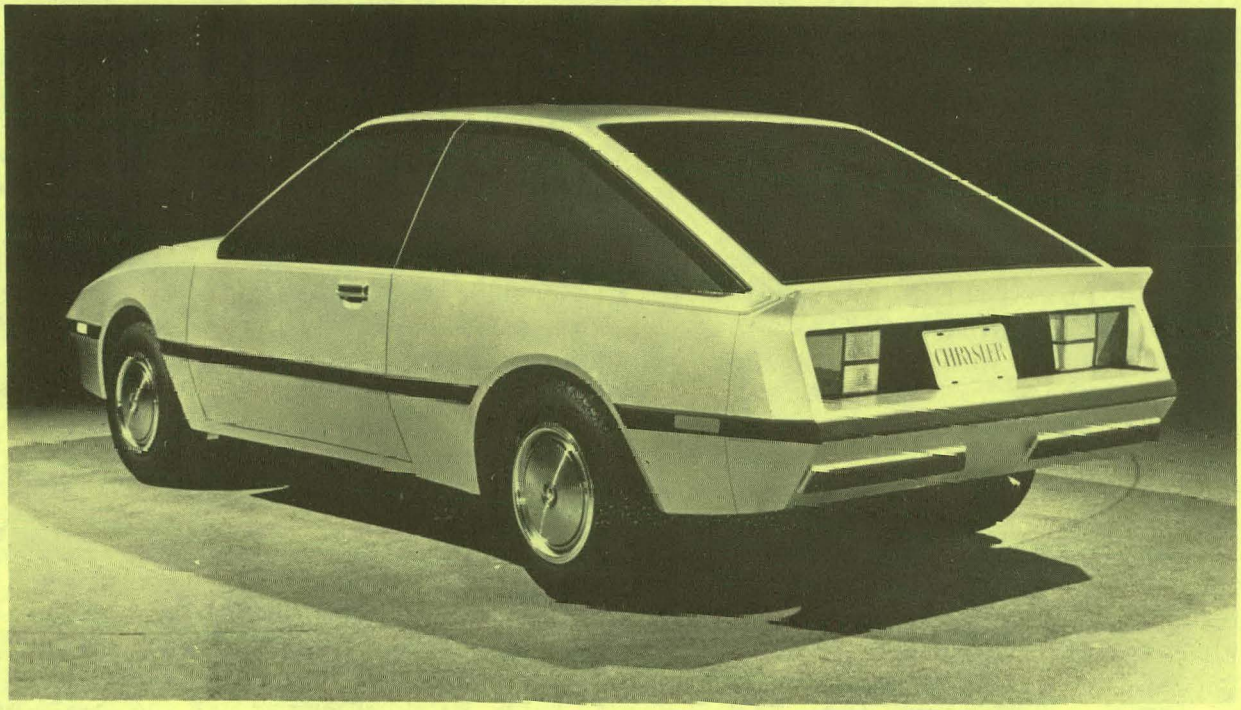

Figure 3.1-2. Phase II Near-Term Electric Vehicle

TABLE 3.1-1

PACKAGE COMPARISONS

| | Vega Coupe | Pinto Coupe | Omni Sedan | Phase I Electric | Phase II Electric |
|---|---|---|---|---|---|
| Overall Length (min) | 175.4 | 169.3 | 162.2 | 160.0 | 169.4 |
| Wheelbase | 97.0 | 94.5 | 99.2 | 92.0 | 98.0 |
| Front Track | 54.8 | 55.0 | 55.5 | 54.5 | 55.5 |
| Rear Track | 53.6 | 55.8 | 55.1 | 58.0 | 55.5 |
| Overall Width at B-Pillar | 65.4 | 69.5 | 66.1 | 66.12 | 65.7 |
| Curb Weight | 2533.0 | 2443.0 | 2098.0 | 2942(Est) | 3208(Est) |
| Overall Height | 50.0 | 50.6 | 53.7 | 53.62 | 51.6 |

four-wheel hydraulic system. Power from the motor is transmitted to the wheels through a two-stage chain drive transaxle.

Extensive use of lightweight materials, including aluminum, various plastics, and high-strength low-alloy steels, helps to offset the mass of lead-acid batteries used to power the vehicle.

In addition to all of the above, this car, unlike most electric vehicles now on the road, is designed to meet the requirements of all Federal Motor Vehicle Safety Standards (FMVSS). Particular attention has also been paid to minimizing those hazards that are peculiar to electric cars.

## WBS 3.1.1 Body Structure

### Basic Packaging

A thorough review of the Phase I design revealed several areas where repackaging could achieve significant improvement in aerodynamic drag, crashworthiness, and customer acceptance.

Placement of the batteries in a center tunnel is most appropriate for proper weight distribution and barrier crash performance. However, the double row arrangement in the Phase I car results in an unnecessarily wide, high frontal-area configuration. Rearranging this concept slightly to the T-shape shown in Figure 3.1.1-1 resulted in a low frontal area of 19.1 $ft^2$.

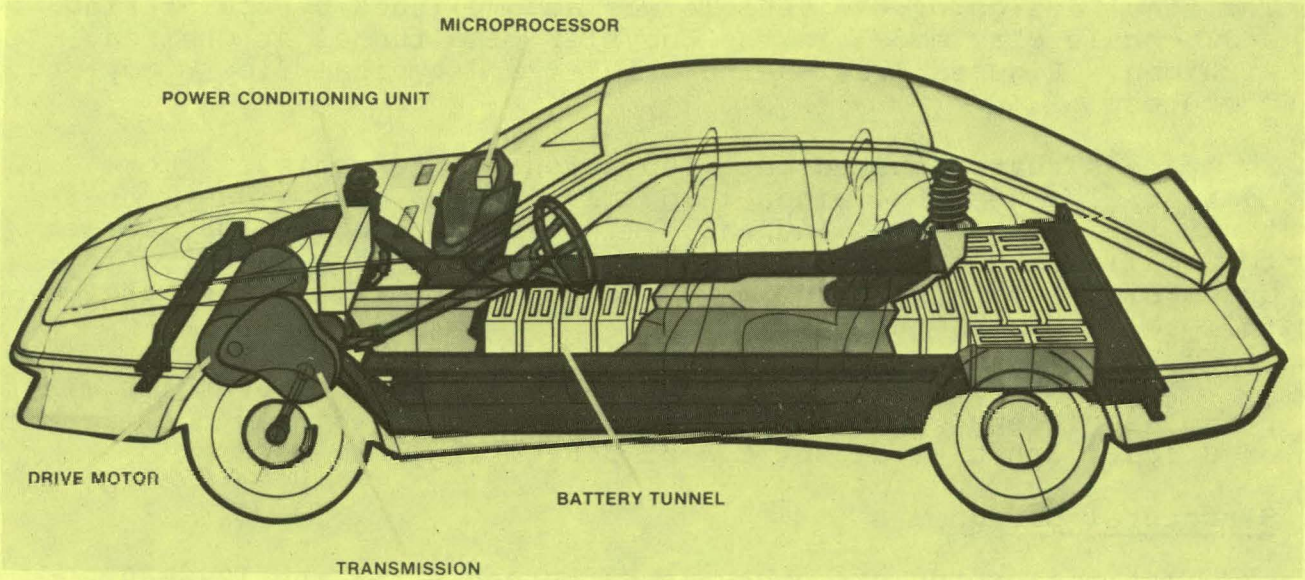


Figure 3.1.1-1. GE/Chrysler Phase II Electric Vehicle

The fore and aft positioning of the traction motor was found to be questionable for impact performance, since it does not provide adequate crush space and would be likely to protrude into the passenger compartment. Positioning the motor in a transverse configuration low in the motor compartment (Figure 3.1.1-1) results in a direct load path for the batteries into the barrier face and provides adequate crush space to absorb the energy of the vehicle. An additional benefit is realized by eliminating the need for a relatively high loss right-angle gear set, since the motor and drive axes are parallel.

The Phase I design used an unconventional seating arrangement with the rear passengers facing rearward. Since this arrangement was judged to be undesirable in terms of consumer acceptance, the seating package was rearranged to provide four forward facing seats. The vehicle comfortably seats two 95th percentile males in the front and two 50th percentile males in the rear. Another major change from the Phase I design is the lift-up, bolted-in-place battery pack (Figure 3.1.1-2). Alternate approaches, including the roll-in design of the Phase I car, resulted in weight penalties with no significant advantage in serviceability.

## Aerodynamic Development

Once the basic packaging task was completed, a number of styling themes were evaluated for esthetic value and aerodynamic drag. The final design selection involved aerodynamic studies of a square-back station wagon style and a modified fastback sedan. Although the basic station wagon design was slightly superior to the sedan for parallel flow, it deteriorated much more rapidly when subjected to a quartering or cross wind and did not respond as well as the sedan to the addition of the rear spoiler. The final design of the vehicle was accomplished by sculpturing a 3/8-scale clay model in the Chrysler wind tunnel at Chelsea, Michigan. Figures 3.1.1-3 and 3.1.1-4 are typical flow study pictures.

Areas that required detailed attention to achieve a more laminar flow were the windshield - A-pillar - door glass transition, the front fascia and air dam, wheel openings, side glass to C-pillar transition, and rear spoiler. Flush glazing contributes significantly to the drag reduction effort, as does the full-belly pan.

The final design, including windshield wipers, rearview mirrors, and license plates, yielded a yaw corrected drag coefficient of 0.303, with a resultant $C_DA$ of 5.8 $ft^2$.

## Structural Design

The basic body structure is patterned after the 1978-79 Chrysler Omni-Horizon vehicles, which use a unitized body construction. The main load-bearing members in these vehicles are two trusses consisting of the front and rear longitudinals, the side sills, roof rails, and A-, B- and C-pillars, which with the floor pan and crossmembers are integrated into a unitized body. The electric car has a third main structural member, the battery tunnel, which extends the full length of the passenger compartment and protrudes forward into the motor compartment. This member carries the weight of the batteries and distributes that load to the body truss system.

Structural analysis of the vehicle utilizes a NASTRAN computer model with the Omni-Horizon as the base of reference, as shown in Figure 3.1.1-5. A full-size "mule" vehicle, which was

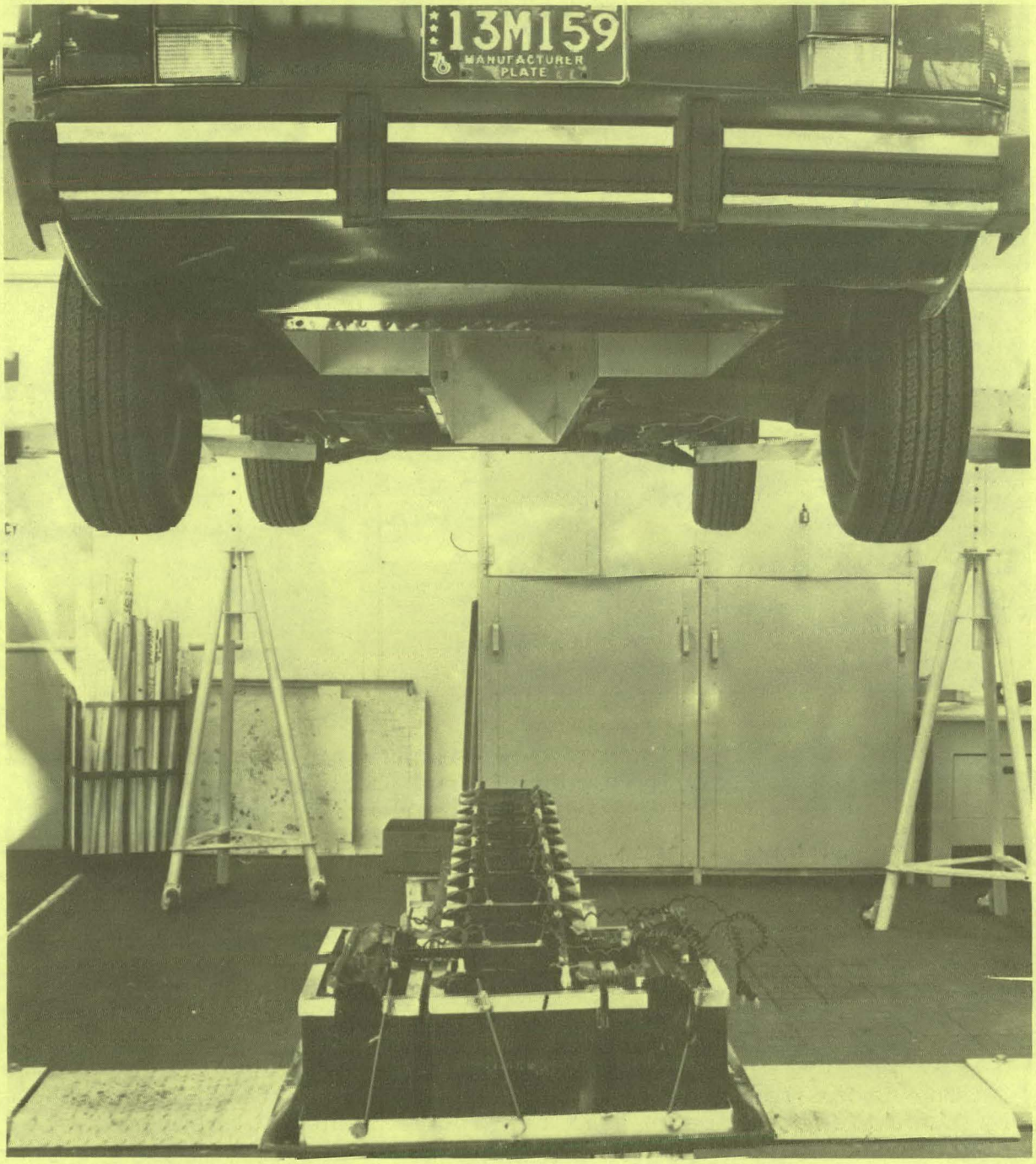


Figure 3.1.1-2. Mule Car Battery Pack

built primarily for development of the suspension system, incorporates a complete battery tunnel as well. This car is being used to confirm the computer model through static loading in beam and twist modes. The static test sequence is illustrated in Figures 3.1.1-6, -7, and -8.

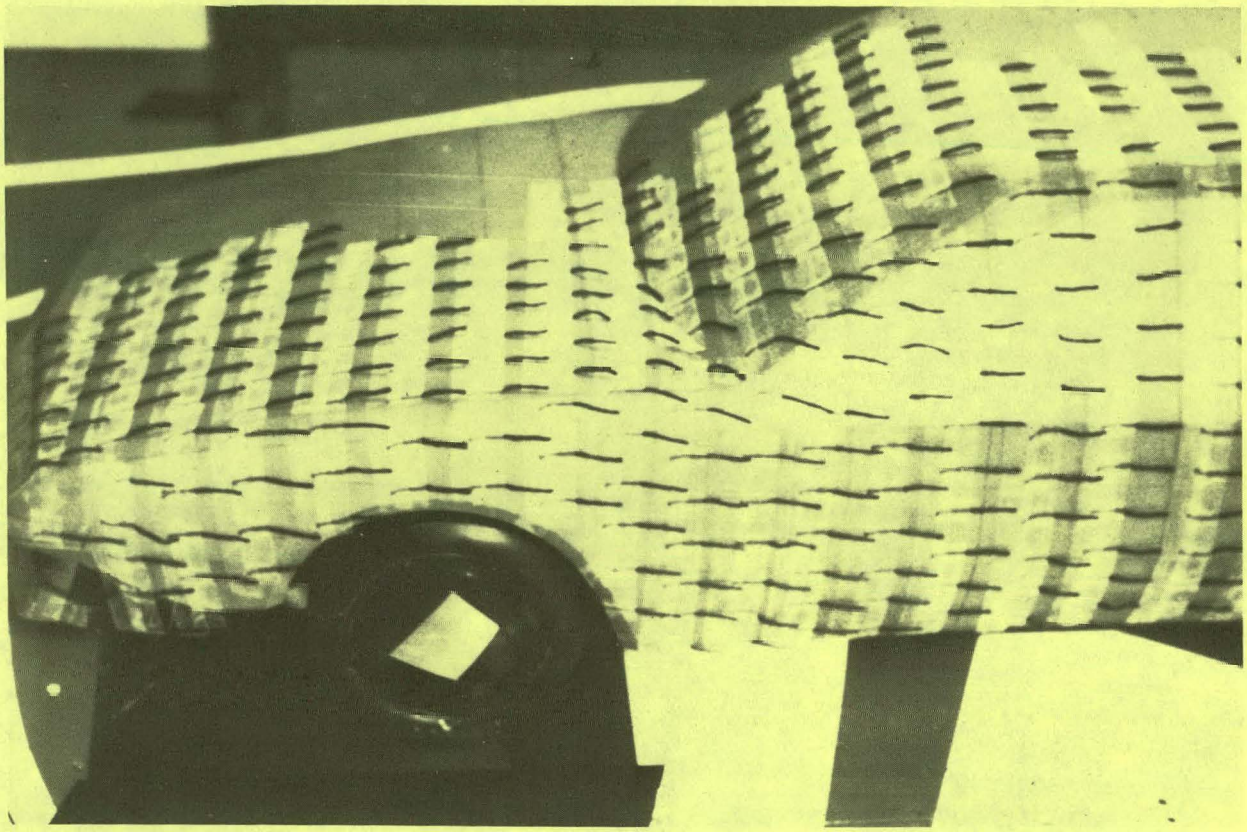

Figure 3.1.1-3. Clay Model Flow Visualization Study in Chelsea Proving Grounds Wind Tunnel

Design of the passenger compartment and "greenhouse" structure is also based on the Omni-Horizon. The proprietary computer programs listed in Table 3.1.1-1 were used to generate a set of minimum required sectional properties for 18 different areas of the vehicle. These section targets are being used to evaluate the various electric vehicle sections as the design progresses.

Frontal Impact Structure

The front longitudinals and the forward extension of the battery tunnel are the main load bearing and energy absorbing elements of the vehicle during frontal impact. These elements provide parallel load paths into the barrier face, with the tunnel extension absorbing the energy of the battery mass and the longitudinals and sills providing for the rest of the vehicle. A spring-mass model (Figure 3.1.1-9) was developed to represent the mule

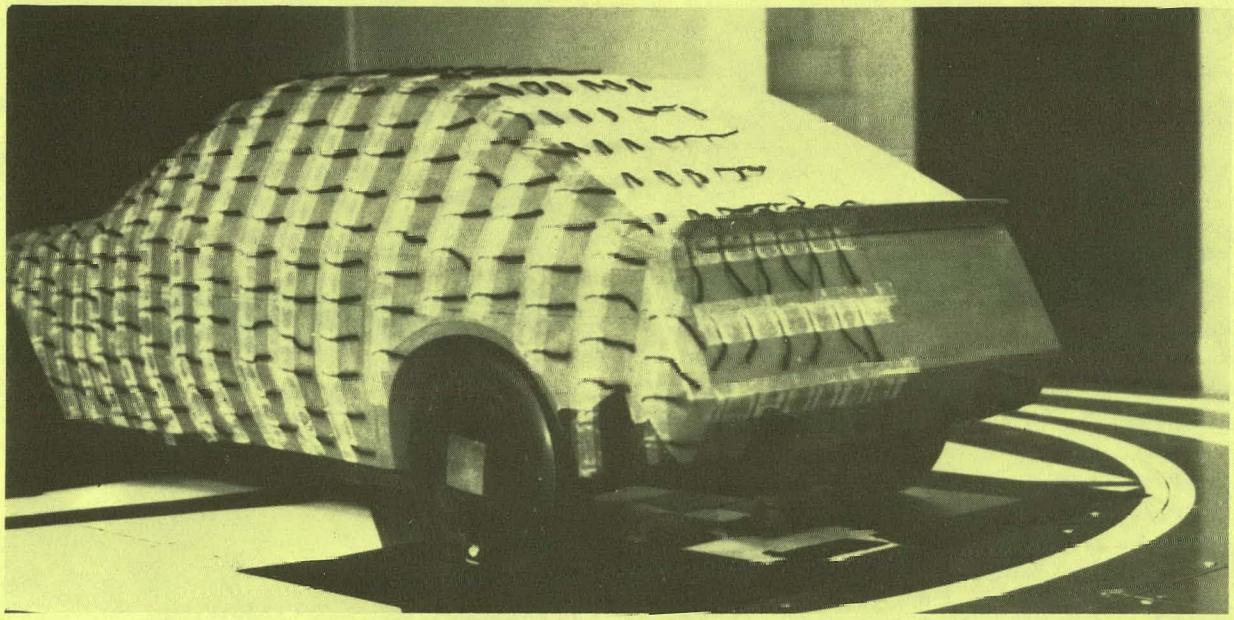

Figure 3.1.1-4. Clay Model Flow Visualization Study in Chelsea Proving Grounds Wind Tunnel

vehicle. An impact simulation computer program utilizing this mathematical model provided design guidelines for the impact structure as illustrated in Figure 3.1.1-10. The predicted vehicle response to a 30 mph barrier impact is plotted in Figure 3.1.1-11.

A full-scale 30 mph impact test of the mule vehicle is scheduled for mid-May to verify this concept and to provide specific input to the structural design of the electric car.

WBS 3.1.2 Chassis

Steering and Suspension

A four-wheel independent suspension system utilizing a MacPherson type iso-strut at the front and a trailing arm with

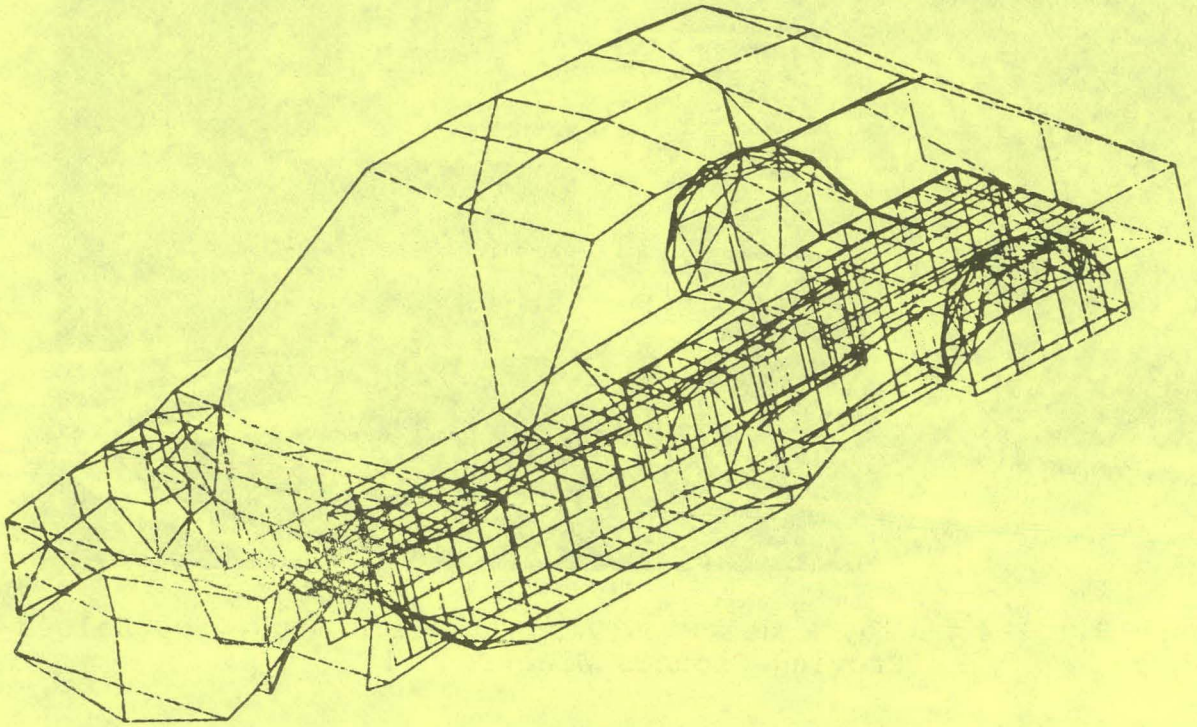

Figure 3.1.1-5. ITV Mule Car NASTRAN Model

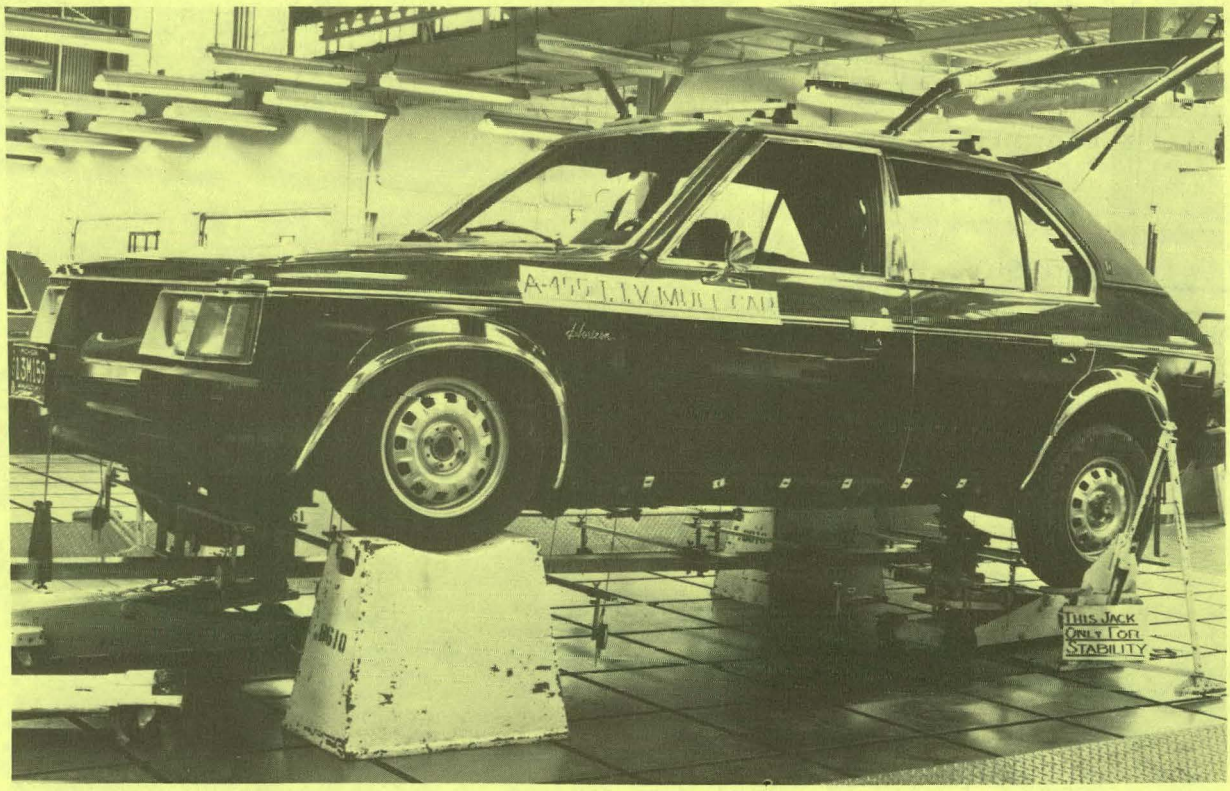


Figure 3.1.1-6. Mule Car Structural Twist Test

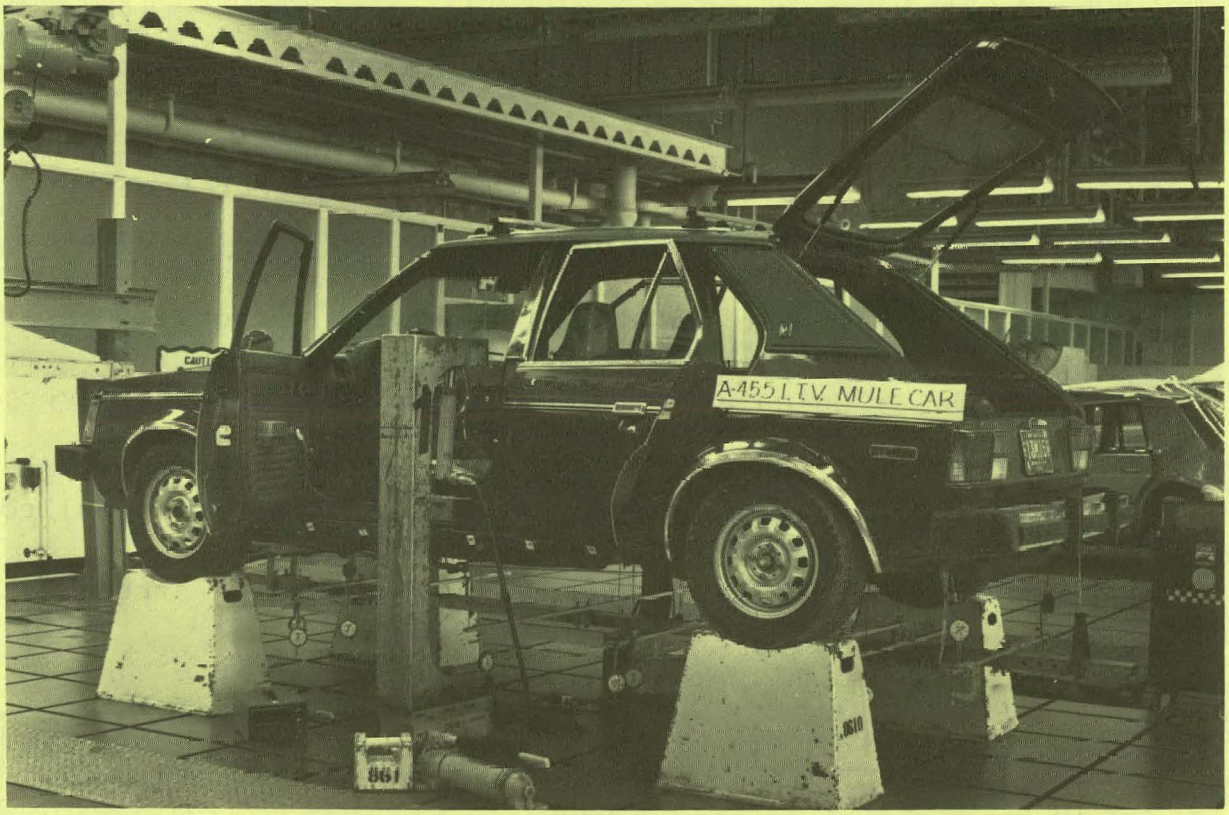


Figure 3.1.1-7. Mule Car Structural Beam Test


Figure 3.1.1-8. Mule Car Jacking Test

TABLE 3.1.1-1

COMPUTER PROGRAMS FOR STRUCTURAL ANALYSIS

- o SST - Calculates structural section targets from base parameters selected for each section
- o MINIBASH - Determines dynamic response of a structural system for impact loading
- o NASTRAN - Static and dynamic analysis of body structure by finite element method
- o SEPROP - Calculates section properties and optimizes gauges of thin-walled sections
- o SECRIP - Calculates allowable axial and allowable bending loads about two axes for thin-walled beam sections
- o DRBEAM - Calculates crippling and buckling strength of door side impact beams

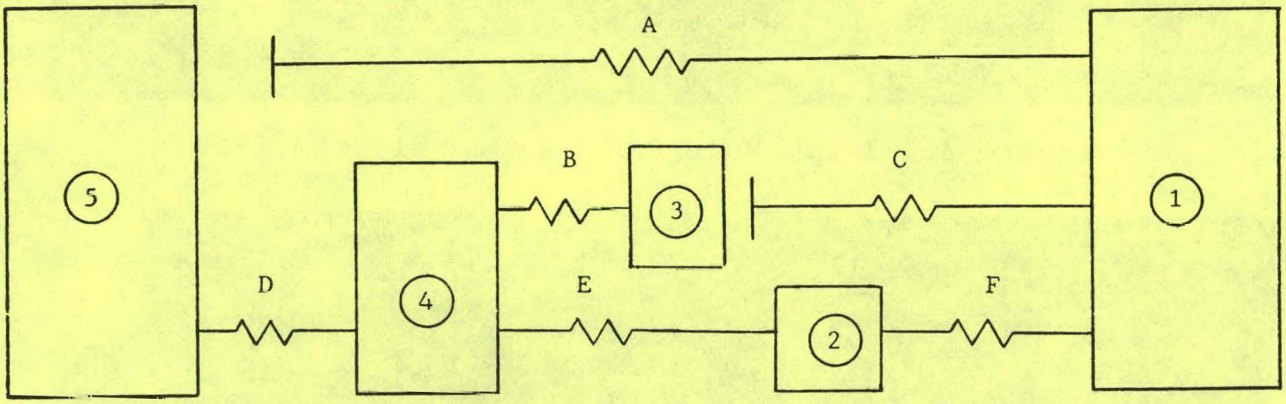


MASSES

1 Body
2 Crossmember & Suspension
3 Motor
4 Front Yoke & Bumper
5 Barrier

RESISTANCES

A Sheet Metal
B Front Motor Mount
C Impact Structure
D Bumper, Front End Sheet Metal
E Front Rails
F Rear Rails

Figure 3.1.1-9. MINIBASH Model - Mule Car 30 Mph Frontal Impact

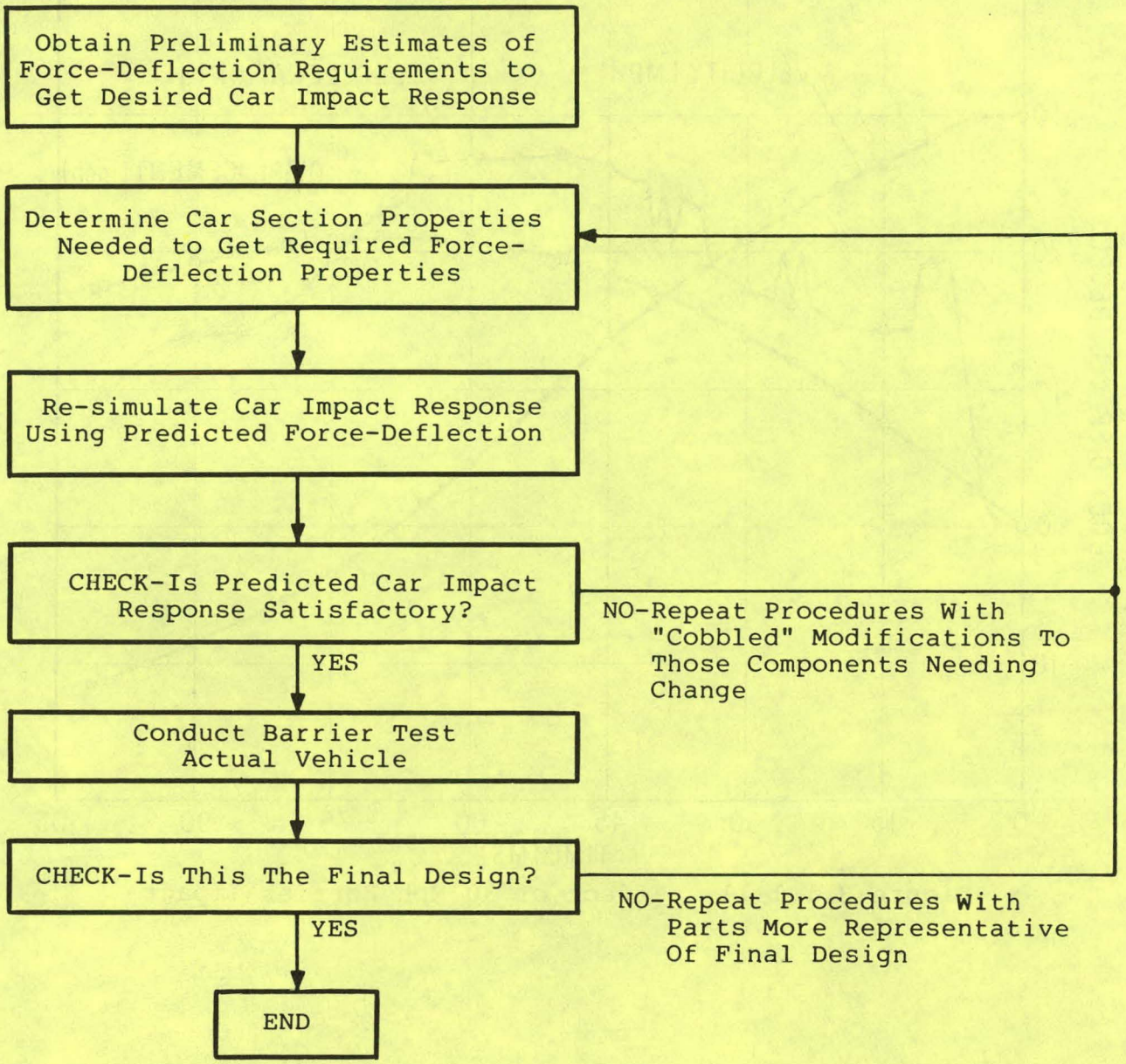


Figure 3.1.1.-10. Impact Simulation Process

strut at the rear was designed and developed on the mule car. The iso-strut is well suited to this vehicle size and facilitates the design of the front-wheel drive. The parts used are common to the 1978-79 Omni-Horizon cars as shown in Figure 3.1.2-1. The independent rear suspension was necessitated by the placement of the battery tray. The trailing arm arrangement (Figure 3.1.2-2) provides the proper geometry. Figure 3.1.2-3 illustrates a NASTRAN model of the trailing arm.

An anti-roll bar at the front of the vehicle completes the suspension system. Steering control is provided by a rack and pinion common to the Omni-Horizon.

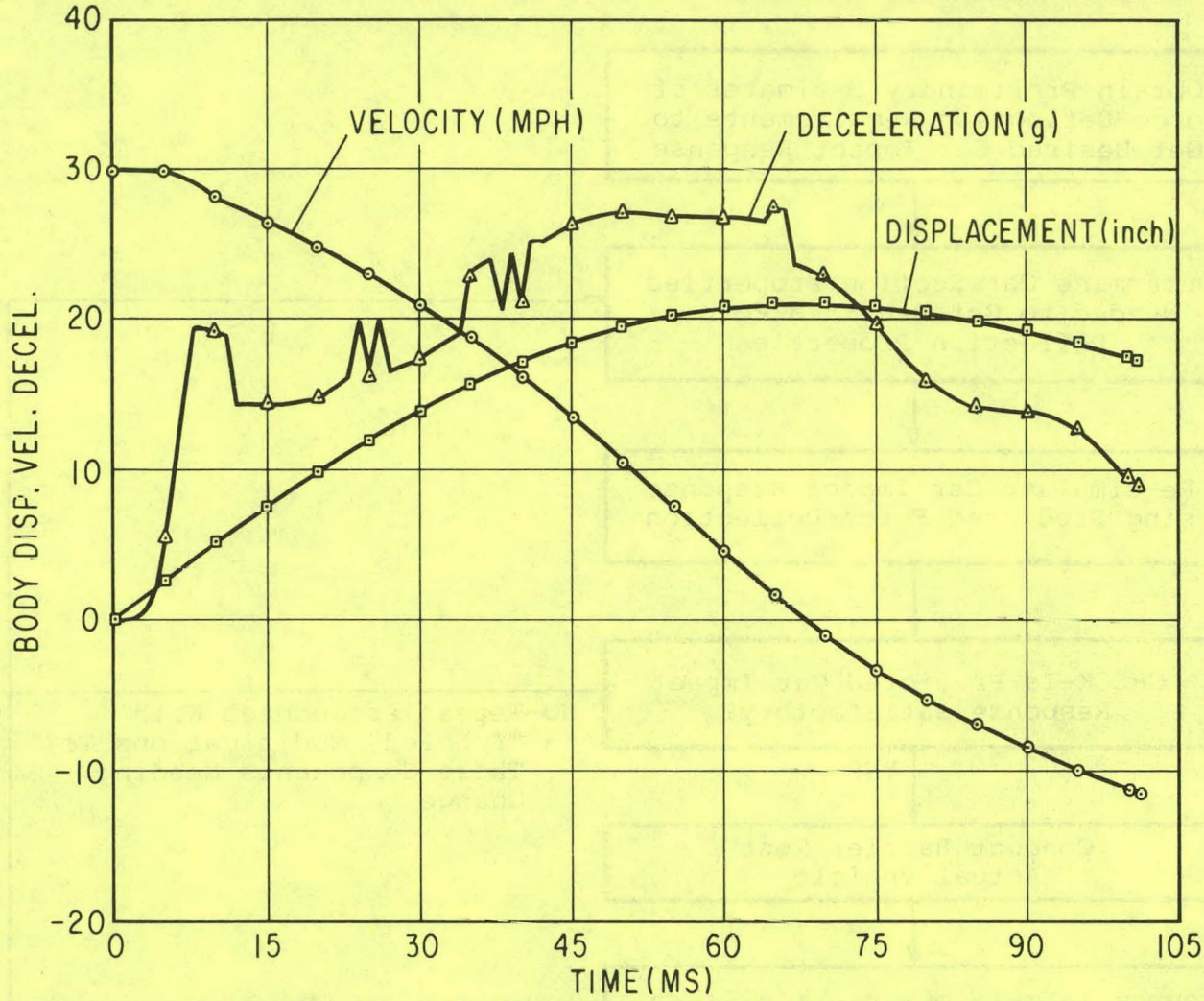


Figure 3.1.1-11. Effect of 30 Mph Barrier Impact

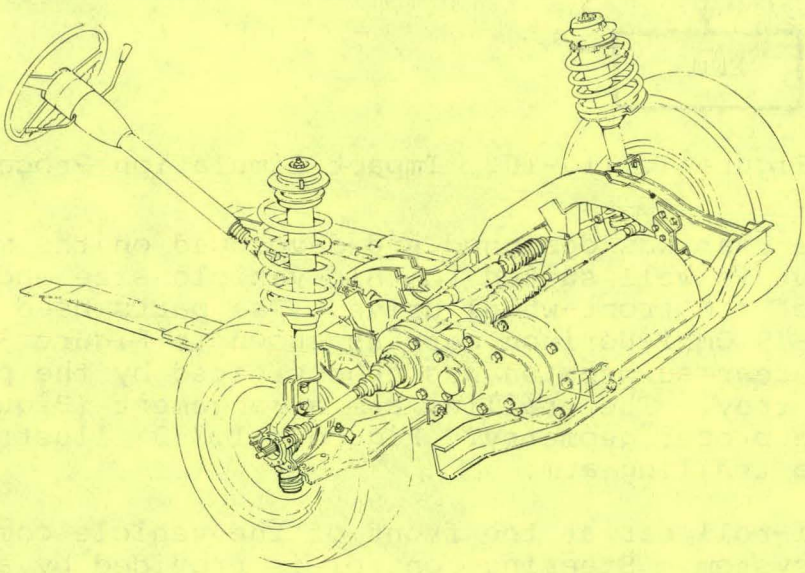

Figure 3.1.2-1. Front Suspension Schematic Diagram

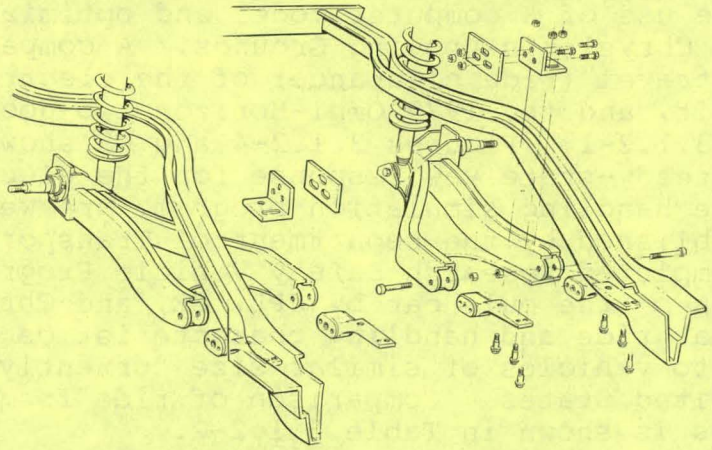

Figure 3.1.2-2. Mule Car Rear Suspension Schematic

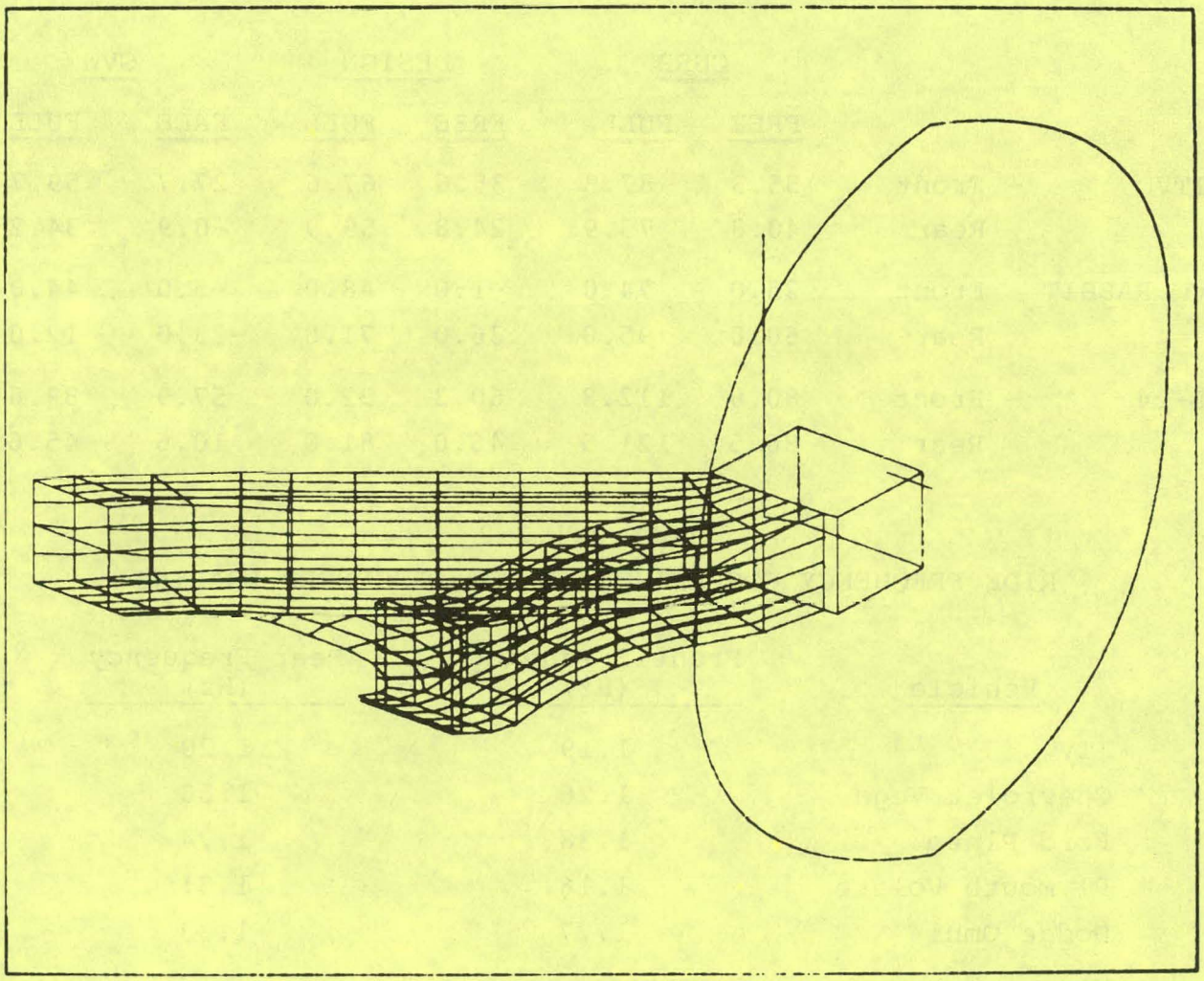

Figure 3.1.2-3. NASTRAN Model Rear Suspension

The suspension geometry and rates were determined analytically through the use of a computer model and optimized on the mule vehicle at Chrysler's Proving Grounds. A comparison of suspension jounce travel (ride clearance) of the electric car, the Volkswagen Rabbit, and the 1979 Omni-Horizon two-door model is shown in Table 3.1.2-1. Figures 3.1.2-4 and -5 show that the transient and steady-state yaw response for the electric car, as predicted by the handling simulation program, are well within the boundaries established by the Department of Transportation for the recently completed Research Safety Vehicle Program. Subjective evaluations of the mule car by JPL, GE, and Chrysler personnel verified that ride and handling characteristics of the vehicle are comparable to vehicles of similar size currently being marketed in the United States. Comparison of ride frequencies for various vehicles is shown in Table 3.1.2-2.

TABLE 3.1.2-1

JOUNCE TRAVELS - MM

| | | CURB | | DESIGN | | GVW | |
|---|---|---|---|---|---|---|---|
| | | FREE | FULL | FREE | FULL | FREE | FULL |
| ITV | - Front | 55.3 | 87.3 | 35.6 | 67.6 | 27.7 | 59.7 |
| | Rear | 40.8 | 75.9 | 24.8 | 59.9 | -0.9 | 34.2 |
| VW RABBIT | - Front | 25.0 | 74.0 | -1.0 | 48.0 | -5.0 | 44.0 |
| | Rear | 60.0 | 95.0 | 36.0 | 71.0 | -23.0 | 12.0 |
| L-24 | - Front | 80.8 | 112.8 | 60.3 | 92.0 | 57.9 | 89.6 |
| | Rear | 86.5 | 121.5 | 46.0 | 81.0 | 10.6 | 45.6 |

TABLE 3.1.2-2

RIDE FREQUENCY COMPARISON AT TWO-PASSENGER LOADING

| Vehicle | Front Frequency (Hz) | Rear Frequency (Hz) |
|---|---|---|
| ITV | 1.19 | 1.20 |
| Chevrolet Vega | 1.26 | 1.66 |
| Ford Pinto | 1.38 | 1.74 |
| Plymouth Volare | 1.16 | 1.31 |
| Dodge Omni | 1.27 | 1.33 |

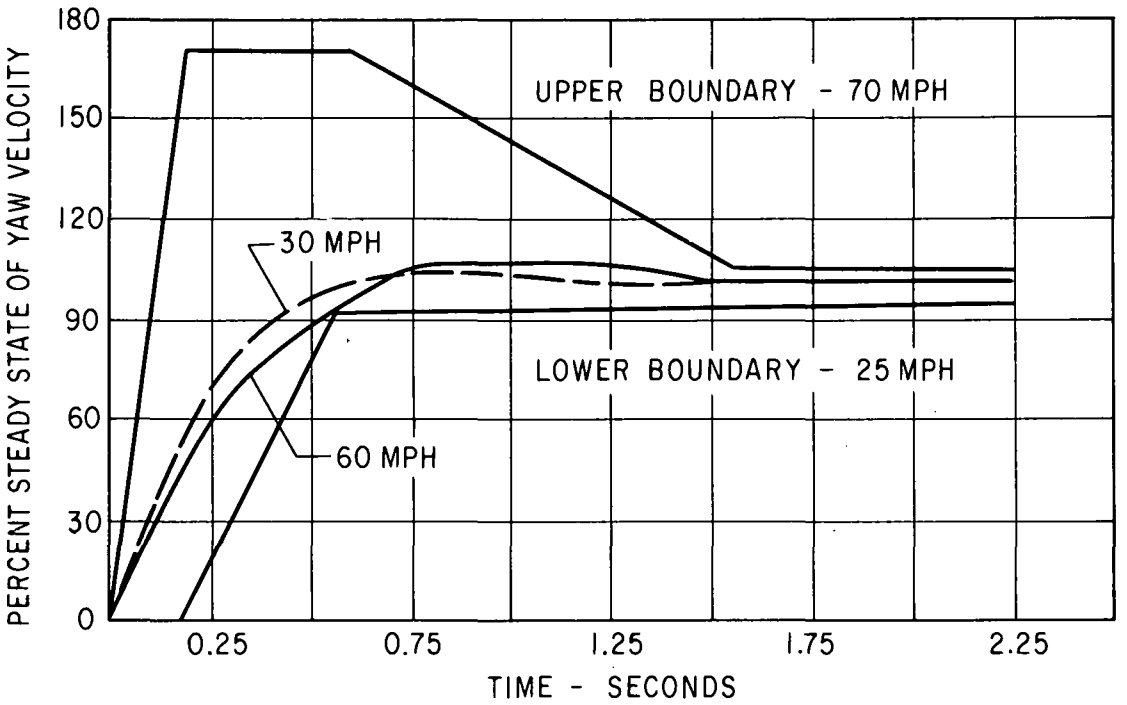


Figure 3.1.2-4. Transient Yaw Response

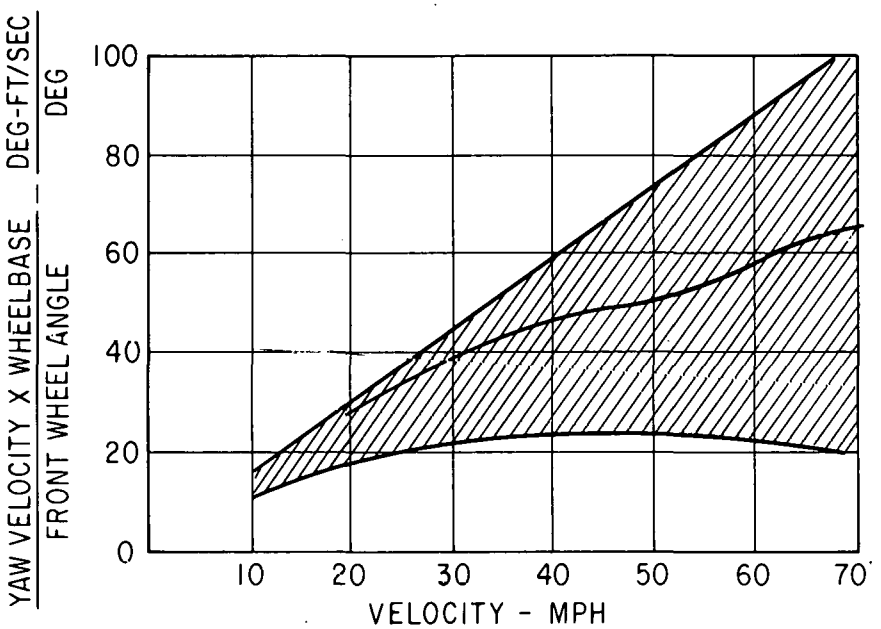


Figure 3.1.2-5. Steady-State Yaw Response at 0.4 g Lateral Acceleration

## Brakes

Vehicle braking will be accomplished through a dual mode system. A conventional hydraulic system will be combined with an electric system that uses the traction motor as a retarder. The resulting energy generated is used to recharge the propulsion batteries, extending the vehicle range.

The hydraulic system has been designed to meet the applicable portions of FMVSS 105(75) without utilizing any regenerative capability. The system features outboard-mounted front disk and rear drum brakes that are similar to those used on the Omni-Horizon. A separate hydraulic system for front- and rear-wheel brake actuation will used to accommodate the regenerative brake system. A proprietary computer model was used to analyze and predict the performance of the system.

The regenerative brake system, shown in schematic form in Figure 3.1.2-6, is designed to blend with the hydraulic system so that the driver will not be able to discern a change in mode during normal operation. Approximately 70% of the braking effort, up to a maximum deceleration rate of 6 ft/s/s, will be provided by the motor/generator; the remaining 30 % will be provided by the brakes at the rear wheels. Deceleration rates from 6 to 16 ft/s/s will be handled by a blending of regenerative and hydraulic braking with full hydraulic braking occurring at rates above 16 ft/s/s. This braking transition is accomplished by the use of a metering valve and a differential pressure transducer.

The metering valve controls the pressure to the front-wheel brake cylinder according to the curve shown in Figure 3.1.2-7. The microprocessor regulates the retarding torque of the motor in proportion to the output signal of the differential pressure transducer as shown in Figure 3.1.2-8. Point B on both curves corresponds to the 6 ft/s/s deceleration rate; point C corresponds to the 16 ft/s/s rate.

The regenerative function will also be activated whenever foot pressure is removed from the accelerator pedal to simulate the feel of engine compression braking in a conventional car.

The parking brake will consist of a pedal mechanism actuating a tension cable to the rear brakes. A similar system was successfully evaluated on the mule car chassis on a 32% grade in both uphill and downhill attitudes at the Chelsea Proving Grounds.

## Tires

The variety of tires evaluated for handling and rolling resistance on the mule car included one set with an experimental elliptical cross section configuration. The best tires to date for both characteristics are P175/75 R13 steel-belted radials inflated to 29 psi front and 41 psi rear. Coastdown testing conducted according to the EPA-approved procedure resulted in a rolling

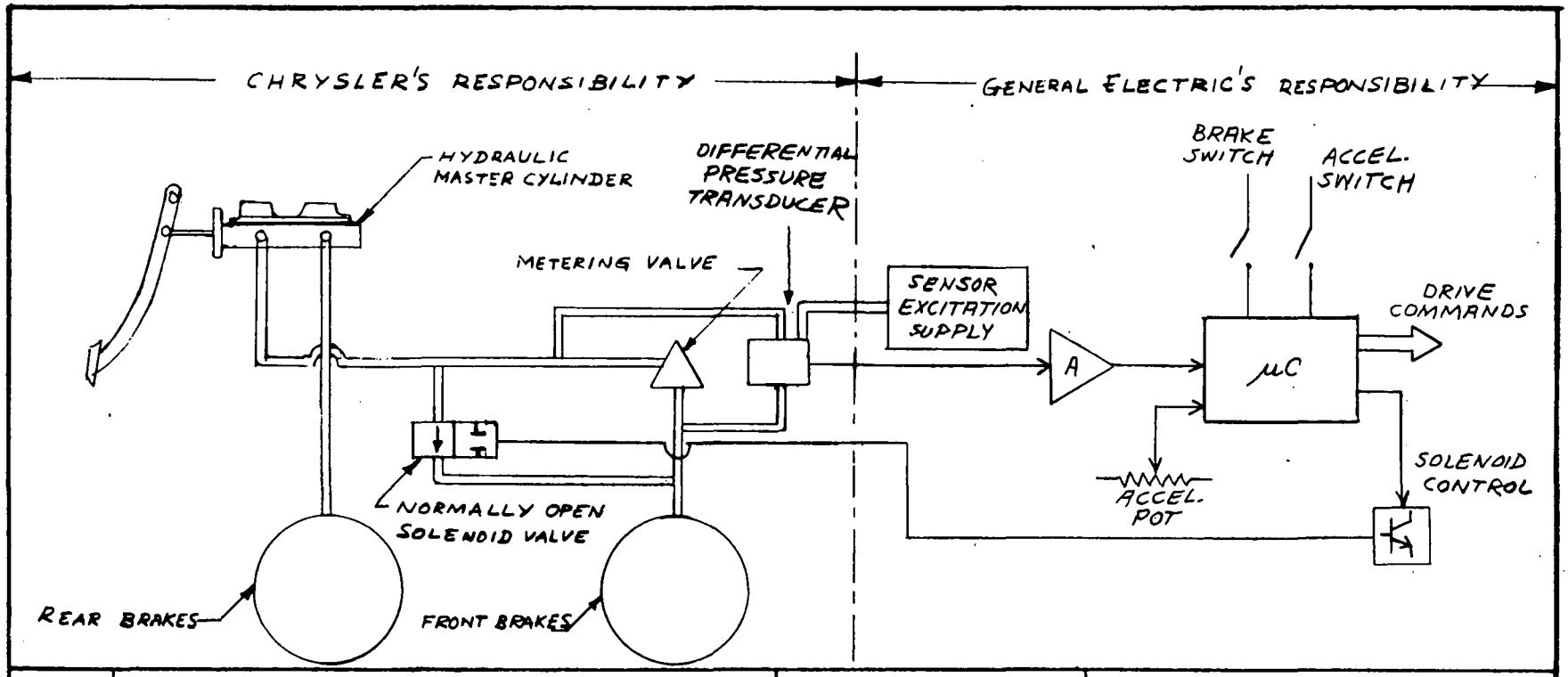


| CASE | PEDAL POSITION | SOLENOID VALVE | CONDITION |
|---|---|---|---|
| 1 | NEITHER ACCELERATOR OR BRAKE PEDAL APPLIED | OPEN | GET COAST 'DOWN REG. TORQUE |
| 2 | BRAKE PEDAL ON & ACCELERATOR PEDAL OFF | CLOSED | GET REGENERATIVE BRAKE TORQUE |
| 3 | BRAKE PEDAL OFF & ACCELERATOR PEDAL ON | OPEN | GET DRIVE TORQUE |
| 4 | BRAKE PEDAL ON & ACCELERATOR PEDAL ON | OPEN | GET DRIVE TORQUE BUT NO REGENERATIVE BRAKE TORQUE |





Figure 3.1.2-6. Regenerative/Hydraulic Brake Blending System

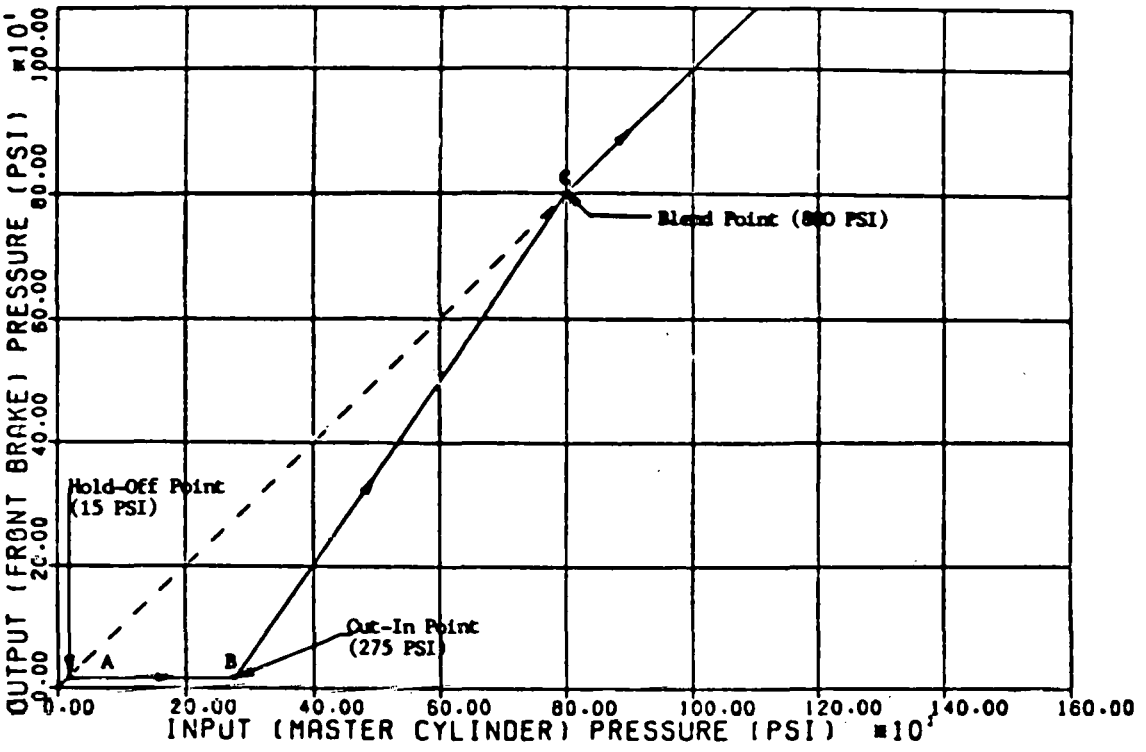


Figure 3.1.2-7. Metering Valve (Typical) Performance Curve

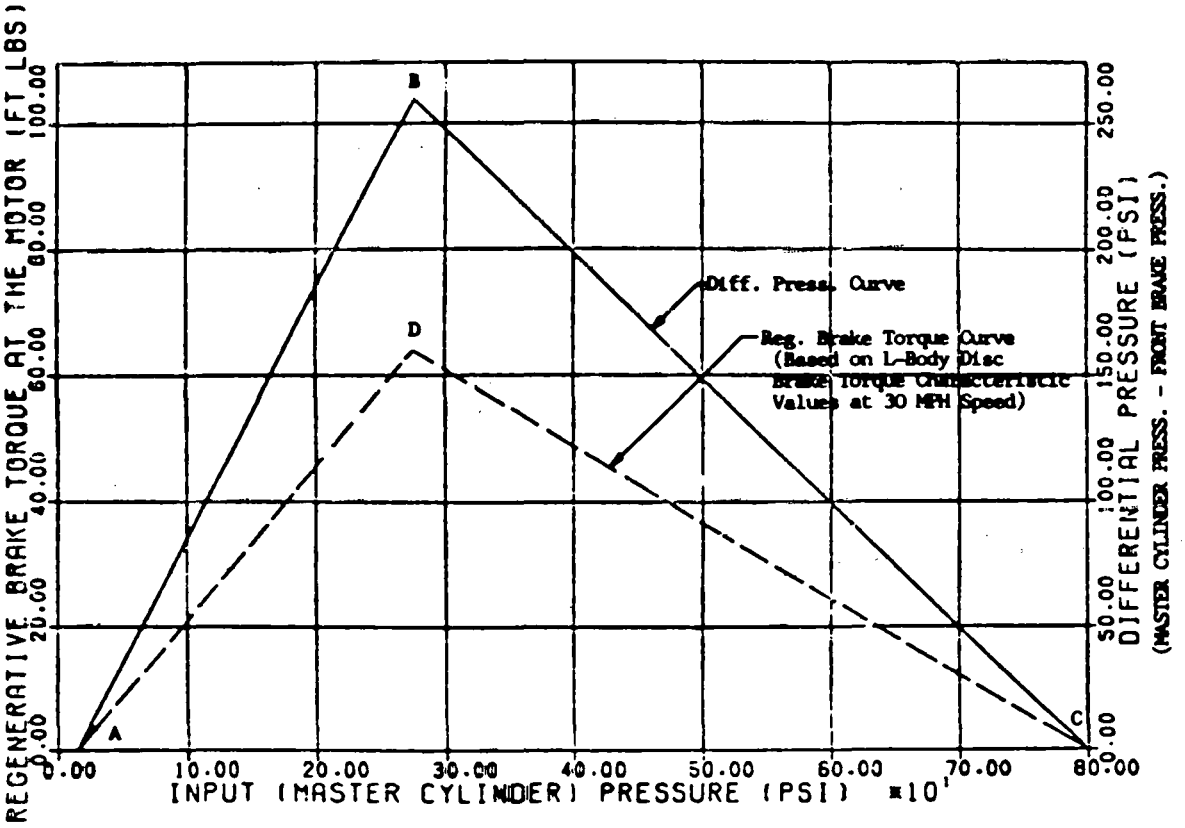


Figure 3.1.2-8. Regenerative Brake Torque/Differential Pressure vs Input Pressure Curves

resistance coefficient of 0.01114 lb/lb. This coastdown coefficient includes tires, bearings, differentials, and some of the transmission losses. Tire evaluation will continue as additional submissions by the tire companies become available.

Final Drive

Power is transmitted from the motor to the front wheels through a double-reduction chain-drive transaxle designed and built by Chrysler's New Process Gear Division. A modified Omni-Horizon differential is incorporated in the design. Each of the axle half shafts has two constant-velocity universal joints to allow normal articulation of the suspension and steering system. The speedometer drive is taken off the right axle at the transaxle housing. The transmission case, after rough machining at New Process Gear, is shown in Figure 3.1.2-9.

A dynamometer test of the transaxle to verify durability is scheduled for mid-July. Table 3.1.2-3 briefly describes the dynamometer test mode.

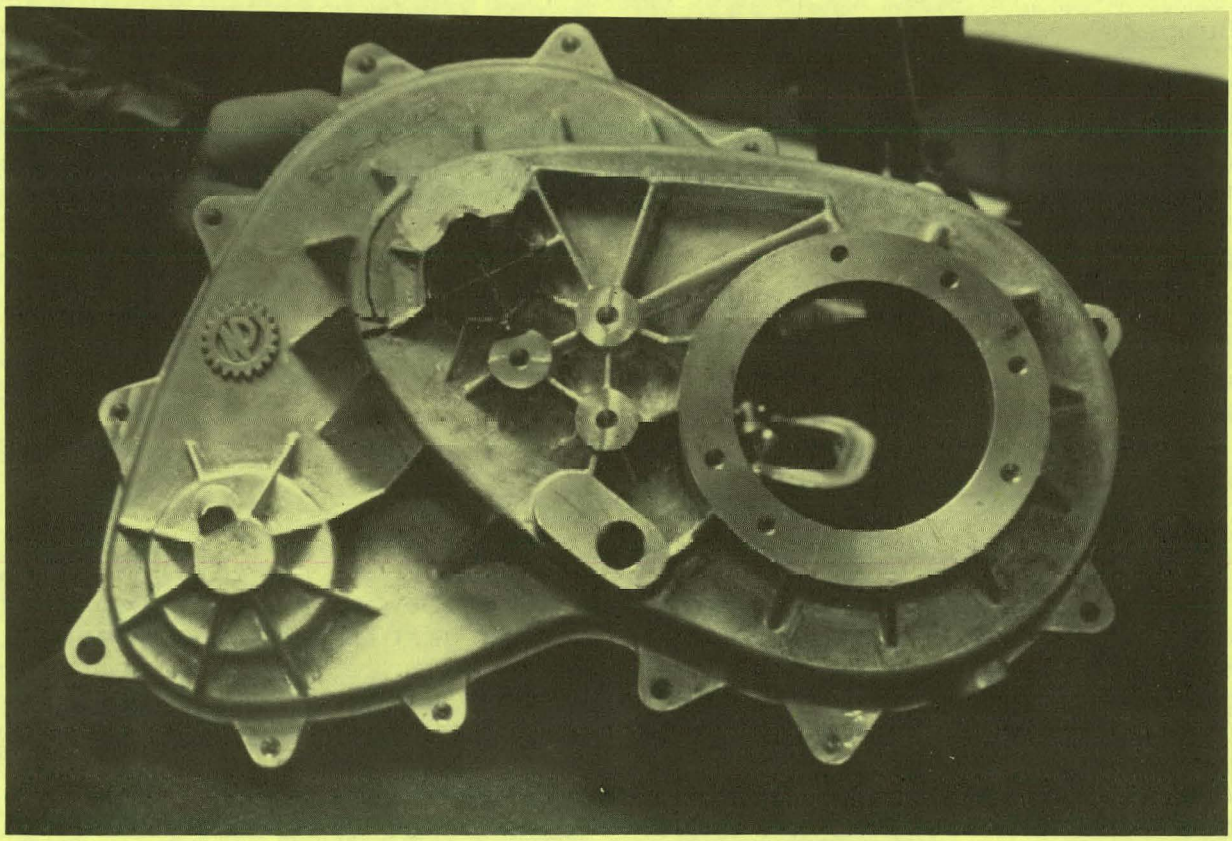

Figure 3.1.2-9. Transmission Case--Left Side Partially Machined

TABLE 3.1.2-3

ITV TRANSMISSION DYNAMOMETER TEST CYCLE

1. Wide open throttle acceleration to 60 mph.
2. Coast to 20 mph with regenerative braking to simulate engine braking.
3. Wide open throttle acceleration to 40 mph.
4. Regenerative brake to 5 mph using 130 ft-lbs torque.
5. Auxiliary brake to stop.
6. Hold @ (0) mph for five seconds.
7. Repeat steps one through six.

Bumpers

The bumper systems utilize a soft plastic fascia over a rigid beam attached to hydraulic energy absorbers to obtain the property protection requirements of FMVSS 215 without adversely affecting the aerodynamic performance of the vehicle. Because of timing and cost considerations this program will be limited to design and fabrication only; there will be no developmental or certification testing of these systems. This approach involves little risk, however, since the beams and absorbers are very similar to those used on the Omni-Horizon and the subcontractor chosen to supply the reaction injection molded (RIM) urethane fascias has considerable experience with similar parts.

WBS 3.1.3 Air Handling and Electrical Components

Heater and Defroster

The heater/defroster system is an air-water-air system that meets the requirements of FMVSS 103. A gasoline-fired burner, specifically sized for this vehicle and mounted in the motor compartment, is used to heat a water-glycol mixture that is circulated through a heat exchanger in the passenger compartment. All of the passenger compartment components, including the heat exchanger, blower, and heater/defroster distribution ducting, are derived from the Omni-Horizon. The water heating components are taken from a commercially available diesel engine preheater manufactured by Stewart-Warner.

Other systems were considered, including direct air-to-air exchangers, but none of them could provide the level of performance required by the Federal standards. The recirculating fluid

approach also provides a quiet system, since the burner is isolated from the passenger compartment and eliminates noxious fumes and odors in the vehicle.

A full-scale compliance test on an Omni-Horizon prototype was successfully conducted in January 1978. Figure 3.1.3-1 shows the sequential photographs of the time versus defrosting action results to confirm compliance to FMVSS 103.

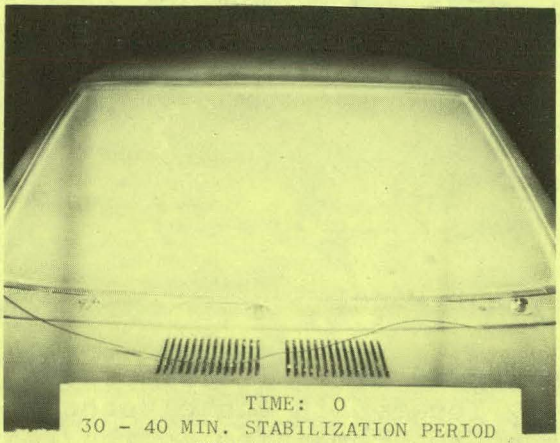


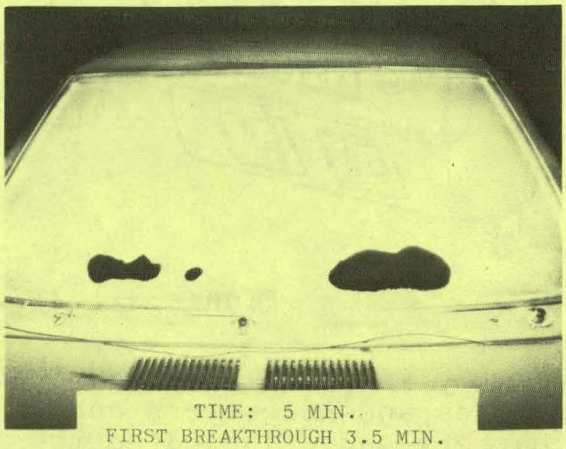


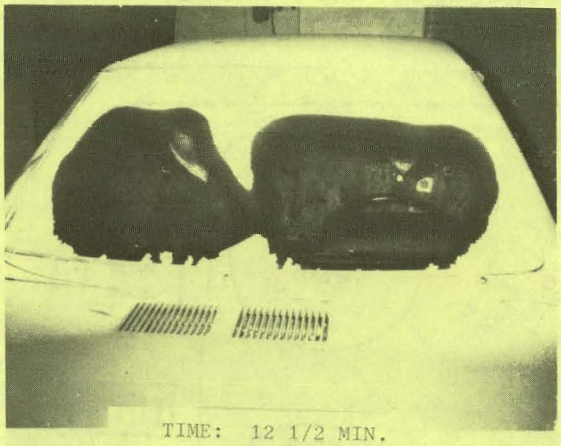



Figure 3.1.3-1. Time vs Defrosting Action Results to Confirm Compliance to FMVSS 103

## Windshield Wipers and Washers

The windshield wiper and washer system is common to the 1979 Omni-Horizon cars and complies with the requirement of FMVSS 104.

## Instrument Panel and Controls

The instrument panel shown in Figure 3.1.3-2 is a one-piece molded plastic unit with a separate instrument cluster located

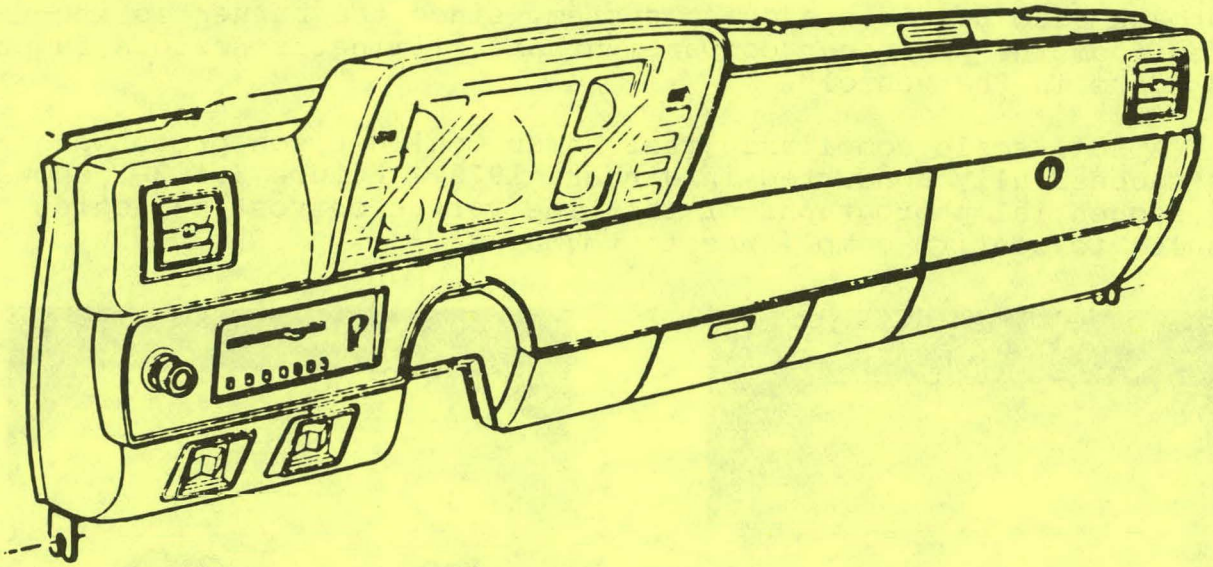

Figure 3.1.3-2. Instrument Panel

directly in front of the operator. The speedometer is calibrated in miles and kilometers and is centrally located in the cluster. A battery gauge indicates the level of energy remaining in the batteries. Other functions are monitored by warning or indicator lights, as shown in Figure 3.1.3-3. The cluster wiring is accomplished by means of a flexible printed circuit board, shown in Figure 3.1.3-4.

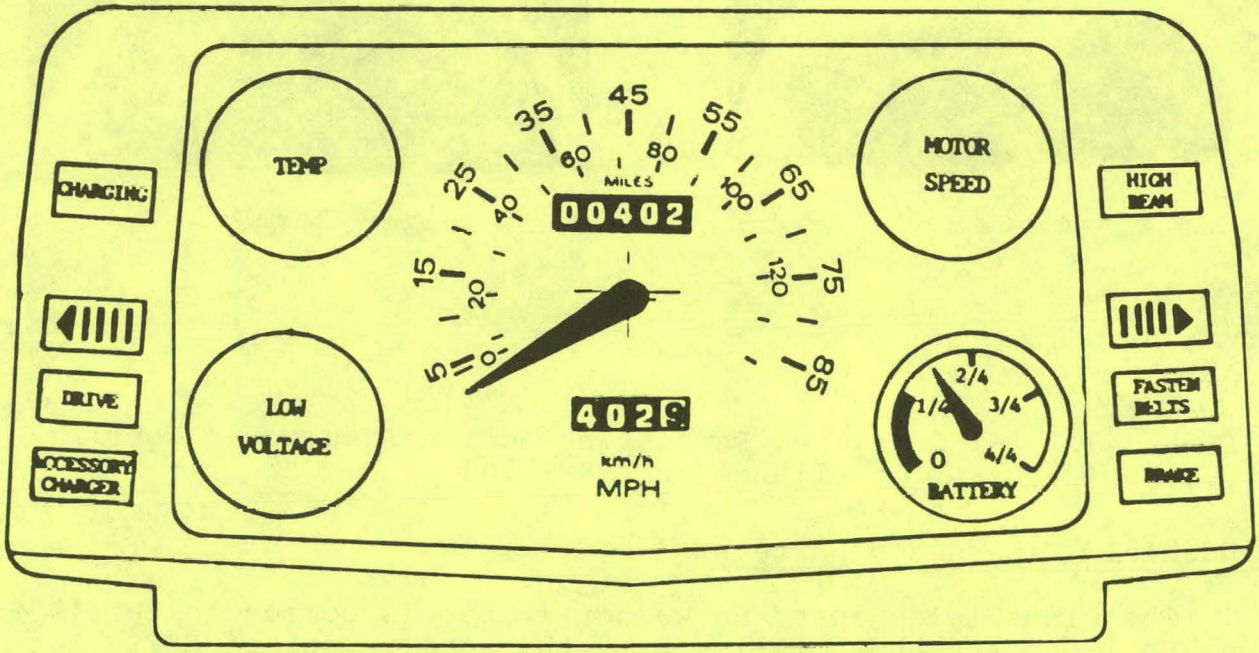


Figure 3.1.3-3. Instrument Cluster

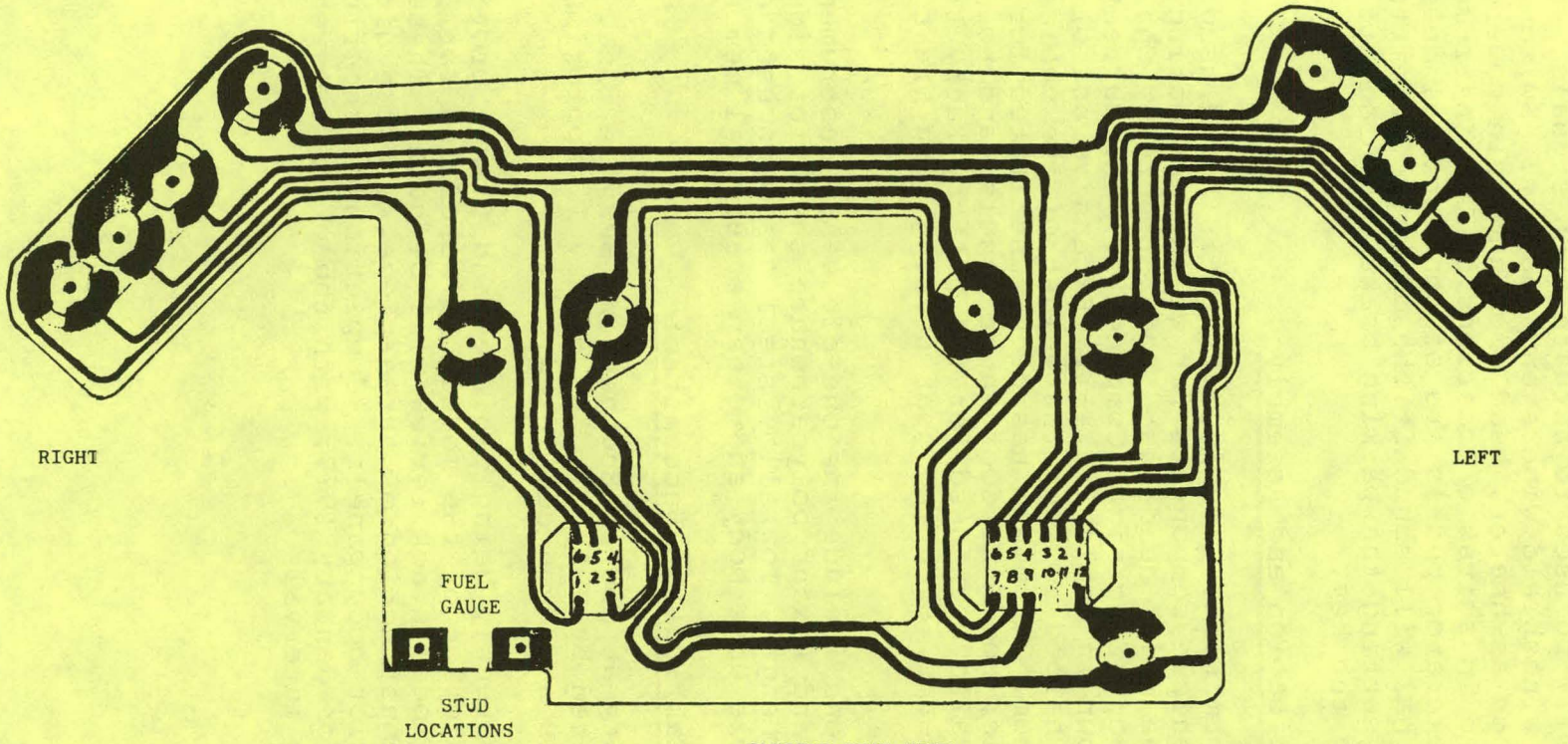


CLUSTER REAR VIEW

I/P WIRING HARNESS
6 WAY CONNECTOR

1 Brake Warning Lamp
2 Open
3 T/S Indicator Right
4 High Beam Indicator
5 Ignition Feed
6 Over Temp Warning Light

I/P WIRING HARNESS
12 WAY CONNECTOR

1 Ground
2 Accessory Charger Warning Light
3 Drive Energized Indicator
4 Over Speed Warning Light
5 Turn Signal Indicator Left
6 Main Battery Charging Indicator
7 Seat Belt Indicator Feed
8 Seat Belt Indicator Ground
9 Illumination Lamp Feed
10 Open
11 Open
12 Low Voltage Warning Light

Figure 3.1.3-4. Flexible Printe Circuit Board

A drive mode selector with forward, neutral, and reverse positions will be mounted on the battery tunnel. A steering-column-mounted stalk will be used to actuate turn signals, headlamp beam change, and windshield wipers and washers. Switches for other functions such as heater, headlamps and main power disconnect will be mounted in suitable locations on the instrument panel. Brake and accelerator pedals are of conventional design. An audible warning signal will sound if the operator attempts to leave the car without setting the parking brake, turning off the headlamps, or removing the key.

WBS 3.1.4 Vehicle Fabrication and Assembly

Chrysler's Uniform Parts Grouping system is being used to identify all of the vehicle components for weight estimating purposes. There are three major headings: Body Structure, Chassis, and Air Handling and Body Electrical Components. The current weight estimate is shown in Table 3.1.4-1. Extensive use of lightweight materials have helped to keep the weight of the vehicle subsystem to the minimum. Aluminum has been substituted for steel for all exterior panels, hood and door inner panels, and road wheels. Aluminum has also been used for the battery rack, transmission case, bumper beams, steering gear housing, and brake master cylinder.

Plastic applications include the one-piece ABS instrument panel, ABS belly pan, and Lexan® polycarbonate sheet for side and rear glazing. High strength, low alloy steel has been used extensively in the vehicle underbody and other structural members.

WBS 3.1.5 Design and Fabrication Subcontract

The design activity at Modern Engineering Service, Inc. is scheduled to be completed by July 31. As of May 1, approximately 25 % of the known tasks had been completed.

Die models are currently being finished and flange provisions are being added. Completion of the models is scheduled for June 10, at which time the die model stack review will be held. These models will be used for the construction of three-piece kirksite dies for the aluminum exterior body panels. Completion of the first vehicle is scheduled for January 1979, with the other two vehicles following at one-month intervals.

---

® Registered trademark of General Electric Company

# TABLE 3.1.4-1

## WEIGHT ESTIMATE (KG)

| WBS 3.1.1 Body Structure | | | WBS 3.1.2 Chassis | | | WBS 3.1.3 Air Handling | | |
|---|---|---|---|---|---|---|---|---|
| UPG No. | | Weight | UPG No. | | Weight | UPG No. | | Weight |
| 11A01 | Underbody | 87.0 | 31 | Final Drive | 42.0 | 12F | Windshield Wipers | 3.56 |
| 11A02 | Cowl-Dash | 30.0 | 32 | Fore Structure | 36.0 | 12G | Ventilation Components | 5.21 |
| 11A03 | Center Pillar | 26.0 | 33A | Front Suspension | 35.0 | 13 | Interior Lamps & Switches | 1.35 |
| 11A04 | Quarter | 19.0 | 33B | Rear Suspension | 29.0 | 21 | Instrument Panel | 7.27 |
| 11A05 | Deck Panels | 6.0 | 34A/B | Steering Gear & Linkage | 6.0 | 79 | Wiring | 5.15 |
| 11A06 | Roof | 16.0 | 34C/D | Steering Column & Wheel | 7.5 | 80 | Heater | 18.53 |
| 11A07 | Doors | 23.8 | 35 | Brakes | 35.0 | 85 | Windshield Washers | 1.51 |
| 11A09 | Liftgate | 0.5 | 36A | Wheels & Tires | 69.7 | 86A | Battery Cable Wiring | 3.26 |
| 11A10 | Front Fender | 5.0 | 36D | Parking Brake Controls | 2.8 | 86B | Male Battery Connectors | 0.90 |
| 11A11 | Hood | 8.4 | 36G | Fender Shields | 9.0 | 86C | Quick Disconnect Switch | 1.5 |
| 11A13 | Front Structure S/Metal | 6.0 | 36H | Bumpers | 39.0 | | | |
| 11A14 | Battery Tray | 20.0 | 36L | Tools | 4.0 | | | |
| 11D | Loose Panels | 1.2 | 35H | Regenerative Brake System | 2.8 | | | |
| 12 | Operating Hardware | 5.0 | | | | | | |
| 14 | Exterior Ornamentation | 6.0 | | | | | | |
| 15 | Trim | 40.6 | | | | | | |
| 16 | Seats | 39.0 | | | | | | |
| 17 | Sealers/W/Strip | 11.8 | | | | | | |
| 18 | Glass | 31.3 | | | | | | |
| 19 | Convenience Items | 8.3 | | | | | | |
| 20 | Interior Moldings | 2.7 | | | | | | |
| 22 | Paint | 4.0 | | | | | | |
| | Subtotal | 397.6 | | Subtotal | 317.8 | Subtotal | | 48.24 |

Total 763.64 kg (1683.0 lb)

## WBS 3.2 ELECTRICAL DRIVE SUBSYSTEM

### WBS 3.2.1 Parameter Optimization

The work effort was to evaluate all candidate motor designs submitted by the Direct Current Motor and Generator Department (DCM&G) for suitability on the electric vehicle. The motors have been examined for performance on the J227a Schedule D urban driving cycle and range at a constant 45 mph while also meeting the requirements of 0 to 30 mph accleration in 9 seconds, 25 to 55 mph acceleration in 18 seconds, and climbing a sustained 5 % grade of 1 mile at 50 mph.

The digital computer program which modeled the battery, drive, and vehicle was used to select the motor producing maximum range on the J227a Schedule D cycle. A model of the EV-106 battery was used because the model of the EV2-13 battery, being installed in the vehicle, was not available when this study was conducted.

Because the performance differences between the best performing motors were small, the choice was difficult. The motor selected gave the best performance on the J227a Schedule D urban cycle and remained a leading candidate for all sensitivity studies made for vehicle and battery changes.

The motor selected is designated as General Electric frame size 2366, armature design 2513. The motor is physically designed around the following set of preliminary design parameters:

- Continuous rating 20 hp, 96 volt, 2500/5000 rpm speed range
- Shunt wound, 4-pole with commutating poles
- Totally enclosed, blower ventilated
- Shunt field turns = 250
- Voltage constant = 0.050 volt/megaline-rpm
- Torque constant = 0.352 lb-ft/megaline-amperes
- Resistance - armature + commutator pole (hot) = 0.0405 ohm
- Resistance - shunt field (hot) = 5.67 ohms
- Approximate weight = 217 lb

Table 3.2.1-1 gives the results for all motors evaluated. For all motor/parameter sets the first step in the analysis was the determination of the optimum field flux to use during the acceleration/deceleration portion of the J227 cycle in the armature control region. This was determined by varying the flux level and noting the energy required for one J227 cycle.

Figure 3.2.1-1 shows the results for the selected motor presented in graphical form. The tests were repeated for an 80%

# TABLE 3.2.1-1

## SUMMARY OF EVALUATION RESULTS

| GE DCM&G | | Speed Range (RPM) | J227A-D | | Range @ 45 MPH (Miles) | Motor Wgt (lb) | ARMATURE CURRENT - AMPS | | | | | | | |
|---|---|---|---|---|---|---|---|---|---|---|---|---|---|---|
| | | | | | | | Fully Charged Battery | | | | 40% Discharged Battery | | | |
| Frame No. | Armature Design | | Cycles | Miles | | | SEGI J227 | 0/30 | 25/55 | 5% Grade | SEGI J227 | 0/30 | 25/55 | 5% Grade |
| 2366 | 2513 | 2500/5000 | 54 | 54.28 | 78.2 | 225 | 209 | 320 | 370 | 327 | 214 | 327 | 413 | 358 |
| 2369 | 4111 | 2500/5000 | 54 | 53.26 | 74.7 | 305 | 244 | 411 | 343 | 304 | 247 | 415 | 364 | 322 |
| 2369 | 2513 | 1250/5000 | 53 | 54.01 | 77.9 | 280 | 200 | 278 | 413 | 354 | 205 | 287 | Not enough torque | |
| 2366 | 3312 | 3750/5000 | 53 | 52.64 | 77.3 | 225 | 227 | 369 | 353 | 315 | 230 | 374 | 383 | 339 |
| 2368 | 4511 | 3000/5000 | 53 | 52.07 | 74.7 | 260 | 251 | 434 | 343 | 303 | 255 | 435 | 363 | 320 |
| 2378 | 2513 | 1250/5000 | 52 | 52.88 | 74.0 | 450 | 208 | 289 | 392 | 340 | 213 | 299 | 438 | 371 |
| 2368 | 2513 | 1750/5000 | 52 | 52.63 | 77.8 | 260 | 205 | 300 | 401 | 347 | 210 | 307 | 500 | 400 |
| 2368 | 5711 | 2500/5000 | 52 | 51.55 | 76.6 | 260 | 233 | 383 | 357 | 317 | 237 | 388 | 385 | 340 |
| 2364 | 2913 | 2500/5000 | 50 | 49.94 | 77.8 | 200 | 225 | 360 | 395 | 344 | 229 | 369 | 485 | N.G. |
| 2366 | 5711 | 3750/5000 | 50 | 49.09 | 74.3 | 225 | 255 | | | | 258 | | | |
| 2366 | 4911 | 3750/5000 | 50 | 48.88 | 72.2 | 225 | 271 | 480 | 348 | 301 | 273 | 480 | 366 | 319 |
| 2368 | 4111 | 3500/5000 | 50 | 48.73 | 70.5 | 260 | 291 | | | | 293 | | | |
| 2368 | 3711 | 3750/5000 | 47 | 45.74 | 70.5 | 260 | 319 | | | | 320 | | | |
| 2364 | 5711 | 3750/5000 | 43 | 41.82 | 70.5 | 200 | 336 | | | | 337 | | | |
| 2368 | 2511 | 5000/5000 | 42 | 40.85 | 69.0 | 260 | 470 | | | | 472 | | | |
| 2346 | 4911 | 5000/10,000 | 49 | 48.69 | 69.2 | 150 | 237 | | | | 240 | | | |
| 2346 | 4511 | 6000/10,000 | 48 | 47.48 | 68.4 | 150 | 247 | | | | 252 | | | |
| 2346 | 4111 | 6500/10,000 | 48 | 47.19 | 67.4 | 150 | 262 | | | | 265 | | | |
| 2346 | 3312 | 5000/10,000 | 47 | 47.51 | 69.7 | 150 | 218 | | | | 223 | | | |
| 2346 | 2912 | 5000/10,000 | 47 | 47.19 | 69.4 | 150 | 225 | | | | 231 | | | |
| 2346 | 3711 | 5500/10,000 | 46 | 45.32 | 65.0 | 150 | 283 | | | | 285 | | | |

(-) Data not calculated due to poor performance of candidate motor on J227 cycle

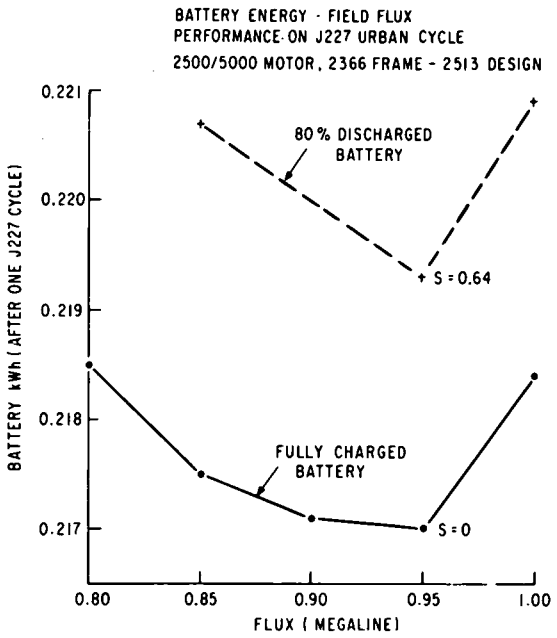


Figure 3.2.1-1. Battery Energy -- Field Flux Performance on J227a Urban Cycle

discharged battery to verify that there was not a shift in the optimum field flux as the battery lost charge. Figure 3.2.1-1 shows that a flux level of 0.95 megaline is optimum for the J227 cycle for both a fully charged and an 80 % discharged battery. The normal rated field flux for this machine is 0.72; thus the optimum flux represents a 32 % field flux forcing. This in turn represents approximately a 113 % field current forcing due to the machine's magnetic structure saturation.

## Vehicle Parameter Variations

In order to assure that the motor selected was suitable for the anticipated range of car parameters, test cases were run for the expected range of parameters. Four candidate motors were selected for this study and their performance calculated for the range of variables shown below.

### Aerodynamic Drag

$Fd = 2.151 * K_1 * A * D * V^2$ (lb)

A = Frontal area ($ft^2$)

D = Drag coefficient

V = Velocity (mph)

K = $\rho/2g = 1.19 * 10^{-3}$ at standard atmosphere

Rolling Resistance

$$FR = 1/K_2(W + W_m)(1 + 2.05 \times 10^{-3} \times V + 2.58 \times 10^{-5} \times V^2) \text{ (lb)}$$

where W = wgt of car + 300 lb passenger load

$W_m$ = wgt of motor

V = Velocity (mph)

The range of values for $1/K_2$, W, and A * D * K is shown below

| | Min. | Max. |
|---|---|---|
| $1/K_2$ | 0.0101 | 0.0138 |
| W | 2800 | 3100 |
| $2.151 * K_1 * A * D$ | 0.01359 | 0.01689 |

The results are shown on Figure 3.2.1-2. Within the range of vehicle parameters tested, the chosen motor design is either at the maximum range or within one cycle of the maximum.

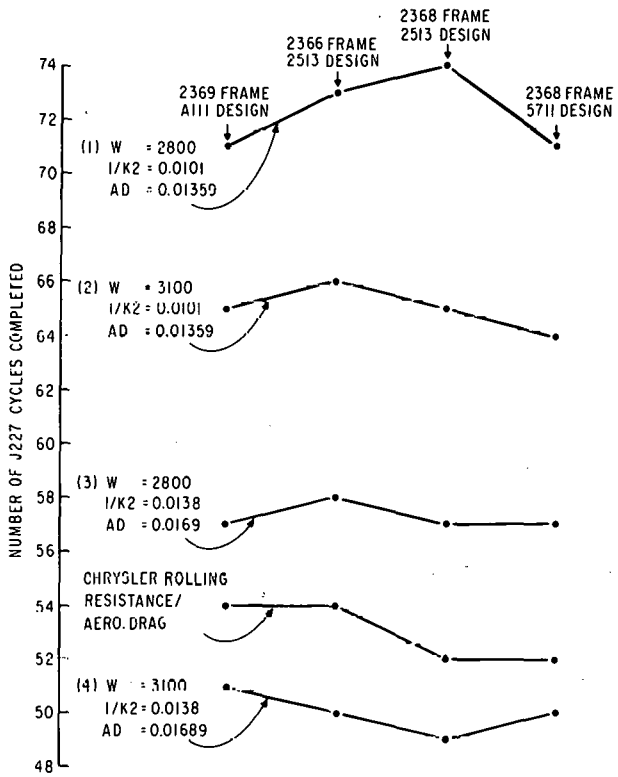


Figure 3.2.1-2. Vehicle Sensitivity Study

## WBS 3.2.2 Control Strategy and Sensors

This task includes strategy selection relating to (a) drive control methods, (b) rating philosophy, (c) fuel gauge principle, and (d) battery charging.

### Drive Control Methods

The regenerative braking drive requirement favors the selection of a dc, separately excited motor. Motor design evaluation studies conducted under WBS 3.2.1 have resulted in the selection of a motor which operates with armature voltage control from approximately 30 to 60 mph. In the armature control mode, the field current $I_f$ is held constant and $I_a$ is varied by adjusting armature voltage $V_a$. In the field control mode, $V_a$ is at full value and $I_a$ is adjusted by varying $I_f$.

The important points relating to this strategy are:

- $T_e \propto I_a$ in armature control (provided $I_f$ is fixed)
- $T_e \propto 1/N$ in field control (provided $V_a$ is fixed)
- $\partial T_e/\partial I_a$ is variable

To give the vehicle a constant accelerator pedal "feel" in the light of these points, a torque control scheme was selected. Figure 3.2.2-1 (a) and (b) shows two possible closed-loop torque control schemes using, respectively, a motor shaft torque transducer and a torque computation circuit. Figure 3.2.2-1 (c) shows an open-loop torque control system, the main feature of which is a nonlinear gain block that processes the armature current command, $I_a^*$, from the total torque reference. This gain block has an inverse law relationship, $I_a^* \propto 1/I_f$, neglecting saturation. The curve can be modified to include saturation, depending upon the detailed motor design.

The open-loop torque scheme was chosen over the closed-loop schemes on the basis of simplicity and the moderate torque accuracy required by this application.

The nonlinear gain block of Figure 3.2.2-1 (c) has since been found to be highly complex to implement using a microcomputer. The nonlinear block is at present being simplified and is replaced with a linear gain constant.

A control strategy block diagram is shown in Figure 3.2.2-2.

### Rating Philosophy

The ratings and torque envelope resulting from the selected control strategy are shown in Table 3.2.2-1 and Figure 3.2.2-3 respectively.

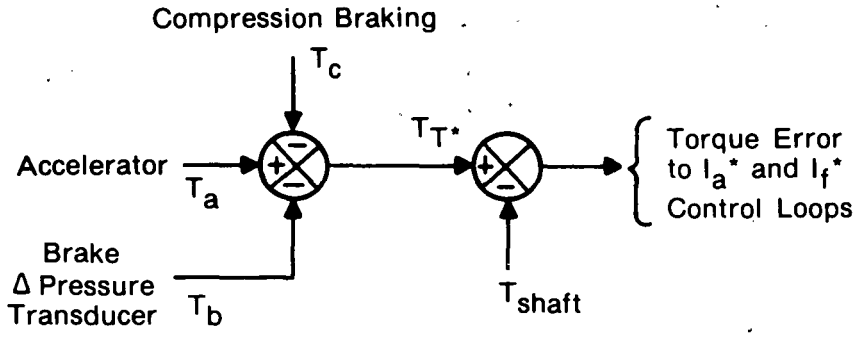


(a) Closed-Loop Scheme Using Shaft Torque Sensor

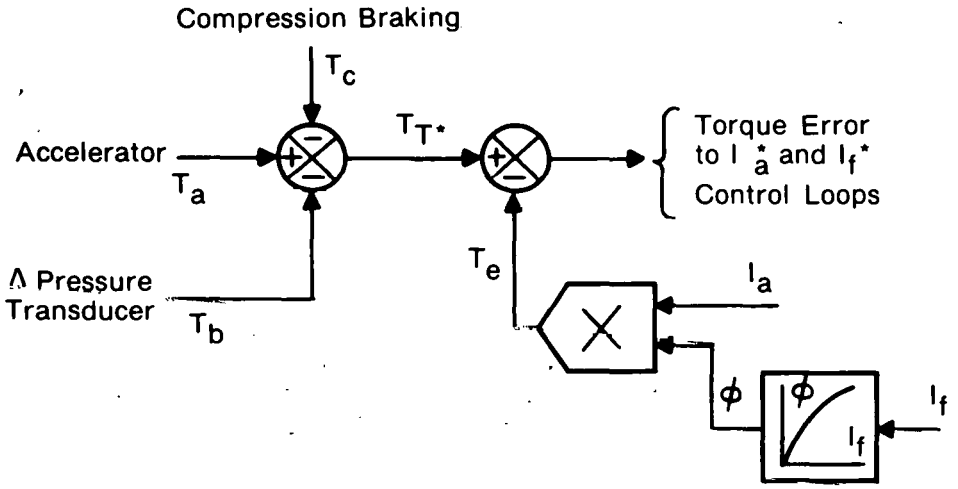


(b) Closed-Loop Scheme Using Computed Torque

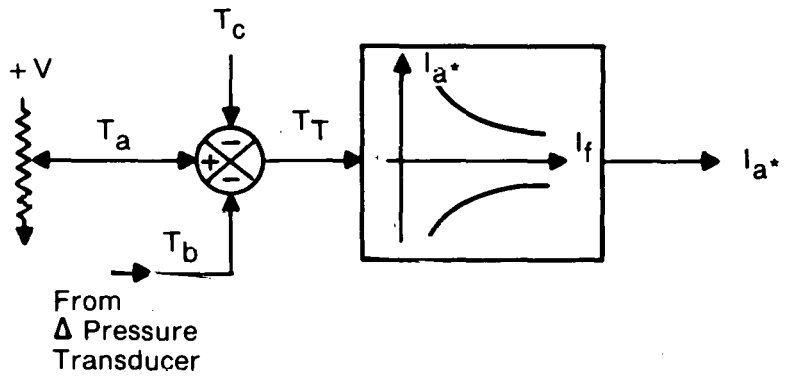


(c) Open Loop Torque Control

Figure 3.2.2-1. Torque Control Schemes

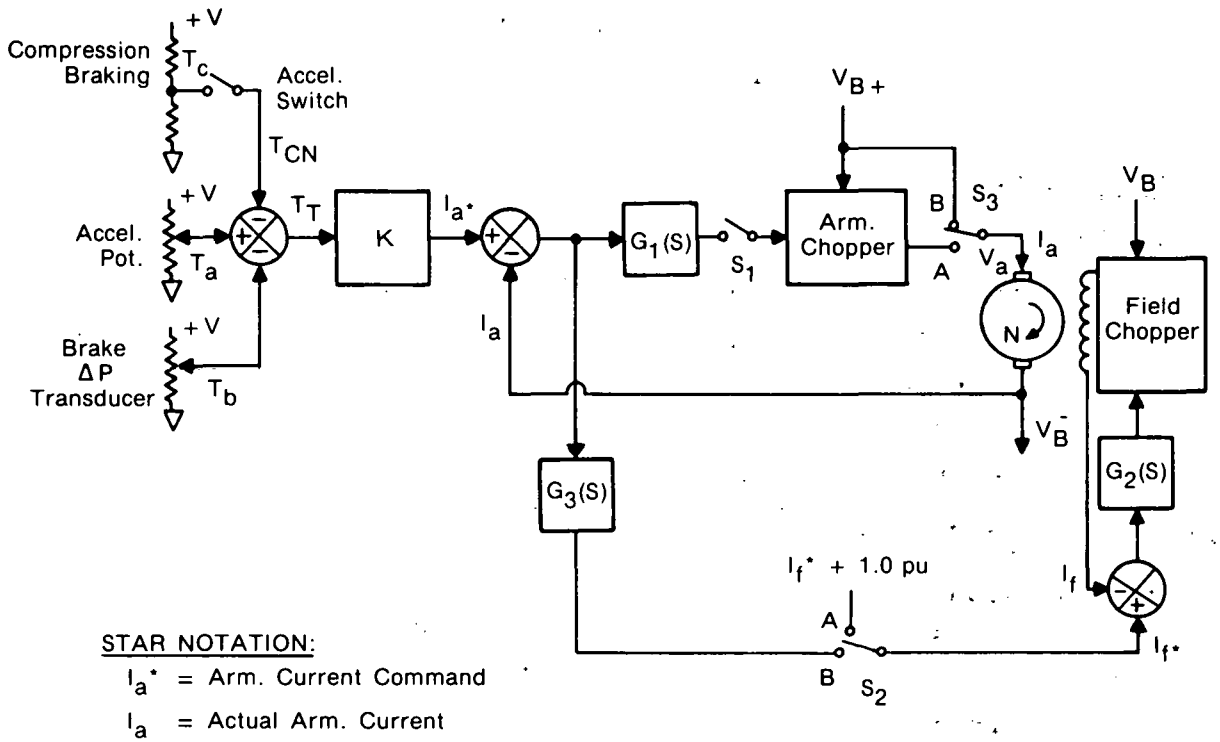


Figure 3.2.2-2. Overall Control Strategy Block Diagram

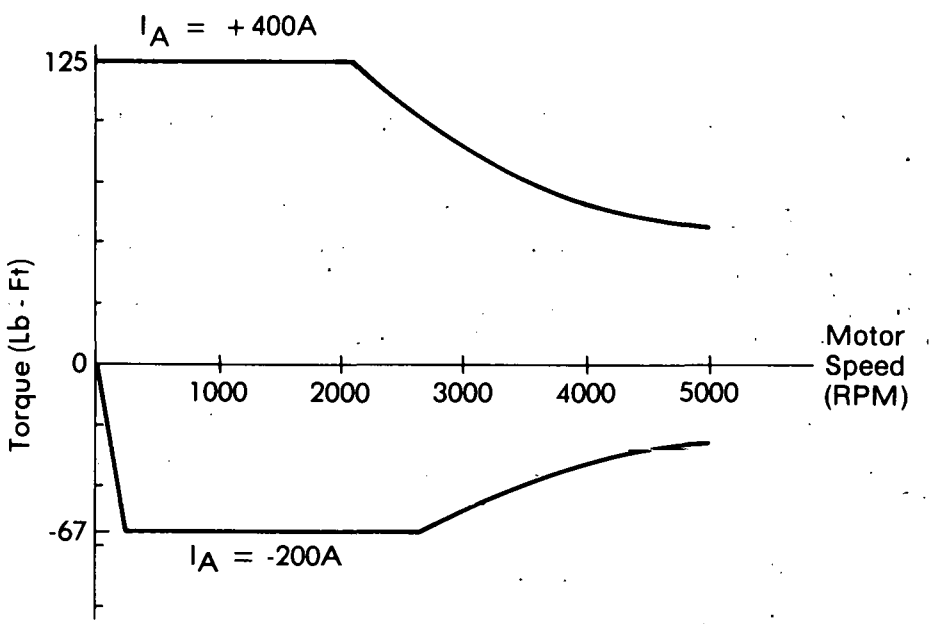


Figure 3.2.2-3. Torque Envelope

## Fuel Gauge

The fuel gauge principle, as it is formulated at the present time, consists of straight-line approximations to the state of

TABLE 3.2.2-1

DRIVE COMPONENT RATINGS

Armature Chopper

- Continuous Rating
  - Motoring: $I_A = +200$ A, $\tau = 50$ %
  - Generating: $I_A = -100$ A, $\tau = 50$ %
- Transient Rating
  - Motoring: $I_A = +400$ A, $\tau = 50$ %
  - Generating: $I_A = -200$ A, $\tau = 50$ %

Field Chopper/Charger

- Continuous Rating
  - Field Supply: $I_f = 10.6$ A, $V_f = 53$ V
    $\Phi NL = 0.95$ ML
  - Charging: $I_B = 24$ A, $V_B = 132$ V, $T_B = 80^{\circ}F$ (30 A line)
    $I_B = 8$ A, $V_B = 132$ V, $T_B = 80^{\circ}F$ (15 A line)

Motor

- Continuous Rating: $I_A = \pm 175$ A, $V_A = 96$ V, $P_{Sh} = 20$ hp

charge versus terminal voltage curves, one of which is shown in Figure 3.2.2-4.

The fuel gauge algorithm involves the use of a continuous memory within the microcomputer to transistion the fuel gauge indicated value between motoring and charging modes. When the delivered battery characteristics are known, this straight-line approximation method will be reexamined.

Battery Charging

The adopted charging method, as illustrated in Figure 3.2.2-5, is as follows:

Constant Current Portion

The constant current portion consists of injecting a preset value of current into the battery until the battery voltage reaches the maximum allowable value, $V_{B(max)}$. The preset current value is in the order of 24 A dc for a 115 V, 30 A line, and approximately 8 A dc for a 115 V, 15 A line.

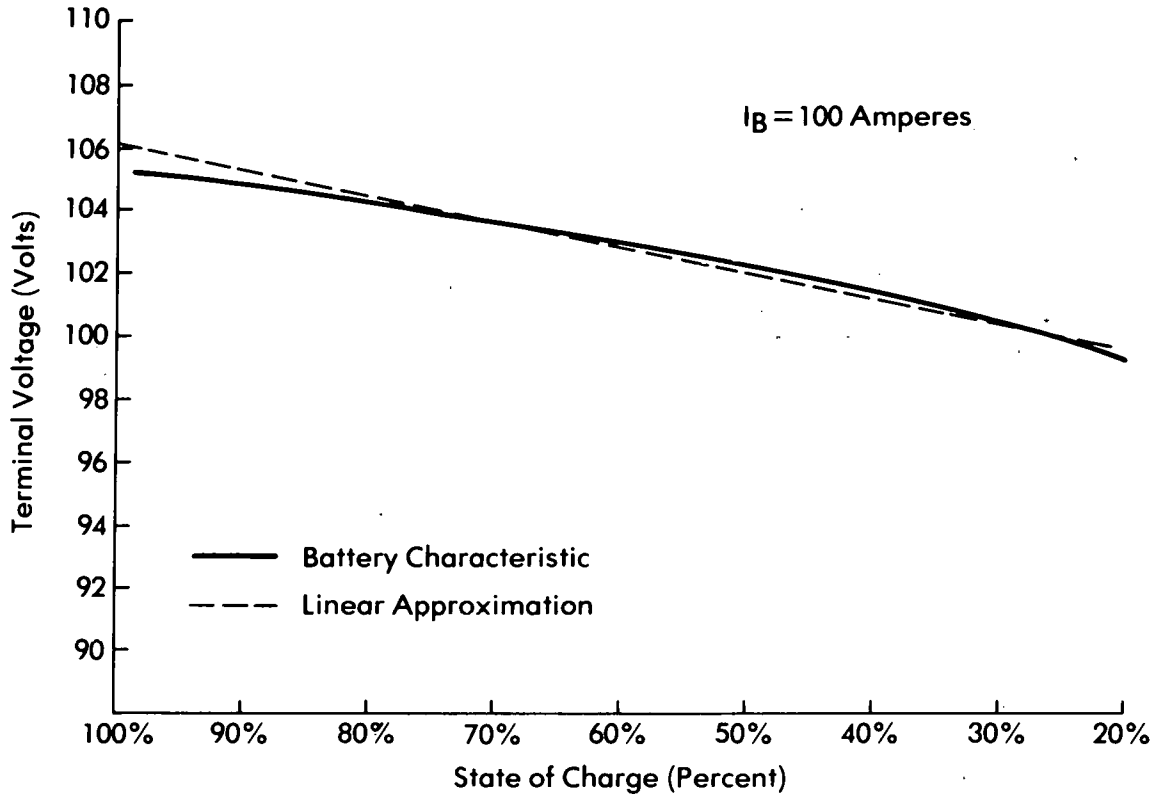


Figure 3.2.2-4. Fuel Gauge Principle

Voltage Measurement

The signal conditioning circuitry provides the microcomputer with an analog voltage, $V_{BA}$, which is related to the battery voltage, $V_B$, by the following equation:

$$V_{BA} = (V_B - 120)\ 0.25$$

This signal is resolved by the microcomputer to 1 part in 127. The maximum and minimum values of $V_B$ during the constant voltage portion of the charging method are 153.9 V and 122.6 V, corresponding to battery temperatures of -20 $^{o}$F and +125 $^{o}$F respectively.

Constant Voltage Portion

The constant voltage portion is described below, assuming an ambient temperature of 80 $^{o}$F for the purposes of illustration. At 80 $^{o}$F, $V_{B(max)}$ = 132.3V.

Method

1. Maintain constant charging current until $V_B = V_{B(max)} = 132.3$ V; $V_{BA} = 3.08$ V.

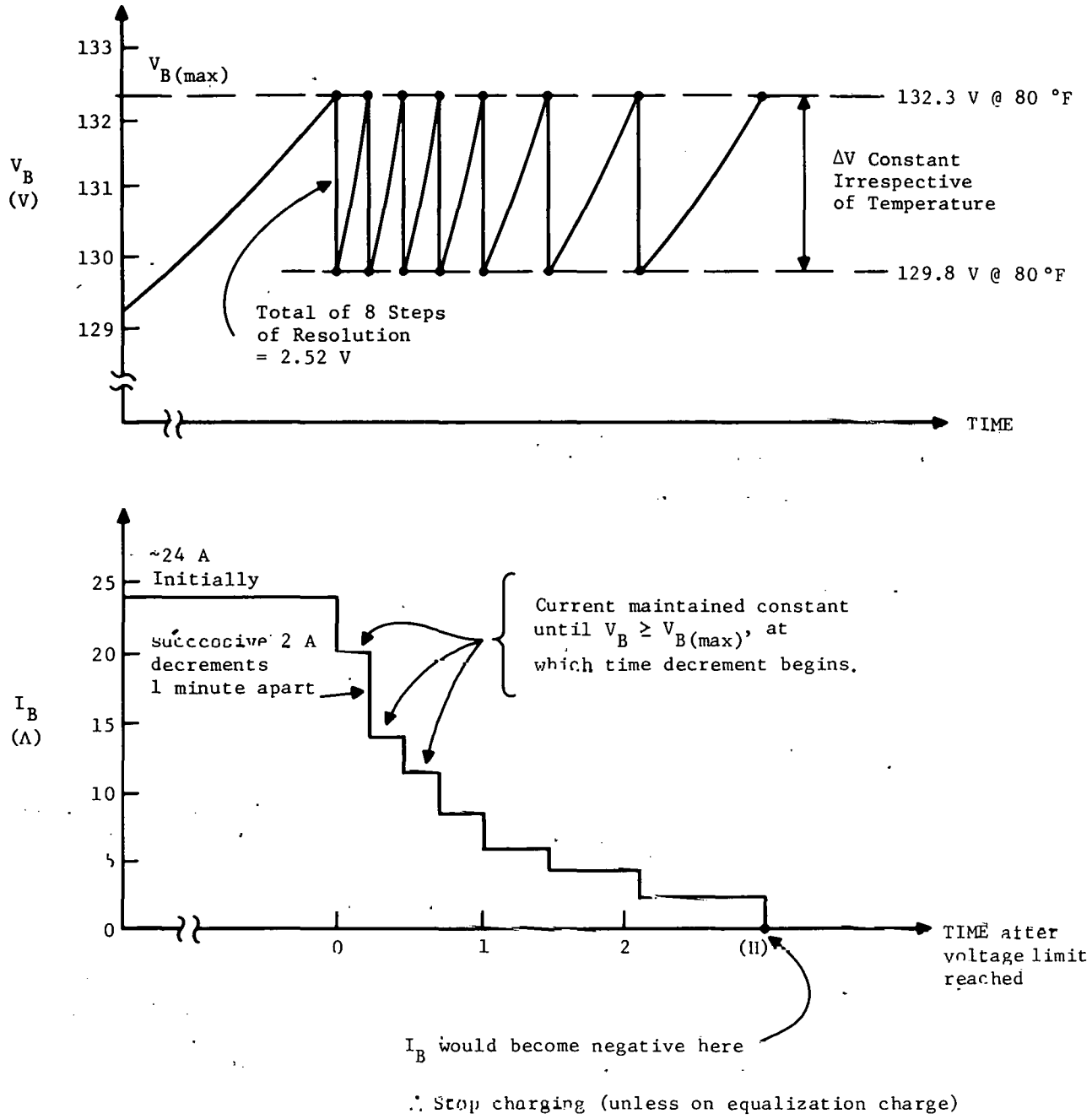


NOTE: Average battery voltage during "constant-voltage" portion is approximately $\frac{132.3 + 129.8}{2}$ = 131.1 V, instead of the 132.3 V of the "ideal" system.

Figure 3.2.2-5. Battery Charging Method -- Diagrammatic Summary

2. When $V_B$ = 132.3 V, decrement battery current $I_B$ by a succession of two-ampere steps until $V_{BA}$ is reduced by approximately 8* steps of resolution. [1 step = 0.31 battery volt; hence 8 steps = 2.52 battery volts, using Equation (1).]

3. The resulting $I_B$ value is maintained until $V_{B(max)}$ is again reached and step 2 is repeated.

4. If $I_B$, using the above method, would result in a zero (or negative) value, then charging is terminated, as the battery is now fully charged (regular charging).

5. When step 4 is reached, charging ceases for regular charging. If equalizing charge is required, $I_B$ is then set at 1.5 A and charging continues with no current decrement. The conditions for termination of equalizing charge have not been determined at this time.

Step Timing

It is expected that battery chemistry will demand a wait time between the successive 2.0 A decrements. A wait time of 45 to 60 seconds has been recommended by Globe-Union.

WBS 3.2.3 Drive Motor

A separately excited dc motor was chosen by CRD as described in WBS 3.2.1. Of foremost concern was the selection of the optimum degree of field weakening to be used to accommodate the various drive requirements. The required drive motor capabilities include: continuous, level vehicle operation at all speeds to 60 mph; start/stop service, repeated continuously in accordance with SAE J227a Schedule D; intermittent acceleration from 0 to 30 mph in 9 seconds; intermittent acceleration from 25 to 55 mph in 18 seconds; and a sustained speed of 50 mph on a one-mile 5 % grade. All of these requirements are to be satisfied with acceptable heating and commutation and at the minimum weight consistent with high efficiency.

A speed of 5000 rpm corresponding to 60 mph was selected initially. As the study progressed, designs were surveyed to confirm the wisdom of this choice. Consideration was also given to higher speed designs (10,000 rpm), as will be discussed.

A four-pole motor, incorporating a full complement of commutating poles, was given greatest attention. Such a motor affords

*The feasible number of resolution steps will depend upon battery voltage ripple, temperature drift effects, etc. The exact number of steps will be determined by experiment with the delivered batteries.

greatest design flexibility and provides suitable high power density, commutation margin, and thermal capability -- particularly at overloads.

Analyses of other dc drive motor types will be discussed later. These include: permanent magnet motor designs, motors having larger and smaller numbers of main poles, and 10,000-rpm designs.

Results

Details regarding the design which has been selected for prototype manufacture are given in Table 3.2.3-1. (Design parameters have been modified slightly from preliminary values cited in subsection 3.2.1.)

TABLE 3.2.3-1

MOTOR DATA

NP Rating: 20 Hp, 2500/5000 Rpm, 96 V, 175 A Cont., Separately Excited at 4.9 A

Force-Ventilated: 125 Cfm (1 In. $H_2O$)

Winding Resistance: 25 $^{o}C$

| | |
|---|---|
| Armature | 0.0189 Ω |
| Commutator Field | 0.0054 Ω |
| Shunt Field | 4.3 Ω |

Shunt Field: 330 Turns/Pole

Winding Inductances:

| | Unsat. | Sat. ($\overline{FFF}$ @ 3600 A.T.) |
|---|---|---|
| Armature + CF | 0.52 mH | 0.16 mH |
| Shunt Field | 2.3 H | 0.21 H |

$K_T$ = 0.352 lb-ft/A Megaline

$K_V$ = 0.050 V/rpm Megaline

$WK^2$ = 2.2 lb-$ft^2$

The selection of the proposed prototype design was the result of careful consideration of more than 20 candidate designs (of various diameters, stackings, and windings) all of which fulfilled the five drive requirements with varying degrees of margin and with varying weights and efficiencies. The design selected provides the maximum range in fulfilling the J227a Schedule D duty using the best vehicle and battery information available at the time, and promises to be close to the optimum design, as these

duty requirements undergo modification as the result of varying battery and vehicle characteristics.

The speed-torque characteristic of the motor is shown as curve $\overline{FFF}$ in Figure 3.2.3-1 under forced full field conditions which will provide more torque per battery ampere during brief periods of acceleration. The corresponding armature current is shown as curve $\overline{I_{FFF}}$ (scale at right margin). Operating point A (60 mph level) is achieved by field weakening, providing the speed-torque characteristic $\overline{WF}$. Line $\overline{CC}$ is a locus of operating points at constant armature current as field strength is varied. The motor current at point A is 150 A, the current $\overline{I_{FFF}}$ corresponding to the intersection of the constant current locus $\overline{CC}$ and the forced full field excitation line $\overline{FFF}$.

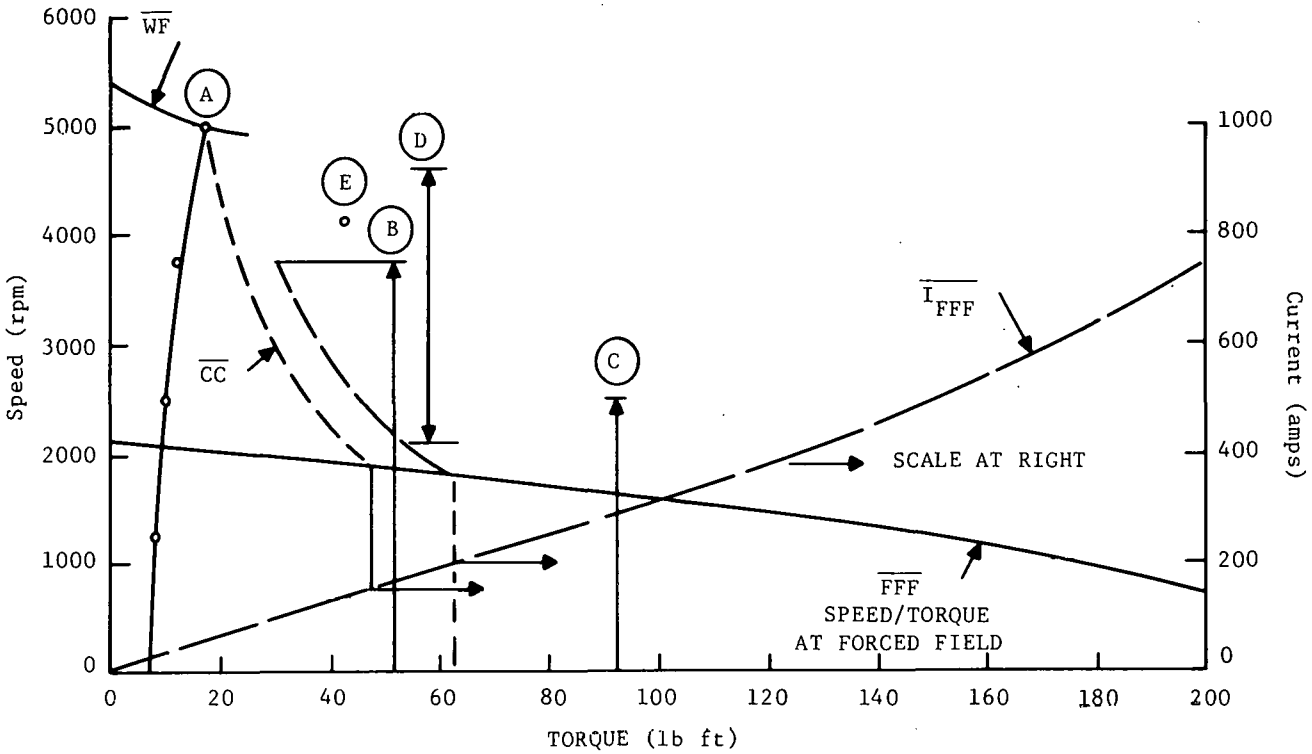


Figure 3.2.3-1. Motor Capabilities and Current Requirements

The current requirements of operating duties B, C, D, and E were found similarly. For example, the J227 acceleration duty (B) is seen to require about 200 amperes and is accomplished at forced full field to 1800 rpm followed by field weakening to 3750 rpm. The throughway merging duty (D) is accomplished entirely with weakened field, requiring about 390 amperes.

By this process the capacity of the various designs examined to fulfill the duty requirements was determined. Some of the early designs were discarded because they were incapable of fulfilling the duty requirements. In these cases, it was found that

the constant armature current locus $\overline{CC}$ corresponding to some of the operating duty requirements did not intersect the forced field line $\overline{FFF}$.

The various designs chosen for evaluation by CRD were selected from those which were shown to be capable of the duty requirements. Generally the performance characteristics and the current requirements found during the screening process agreed closely with those resulting from the later analysis.

## Variety of Designs Developed for Evaluation

Designs were considered in three different armature diameters; however, most attention was given to designs having an armature diameter of 5-3/4 in. The axial length, or stacking, of the designs in this diameter was varied more than 2:1. A range of armature turns was considered, resulting in a spectrum of full field speeds between the limits of 1250 rpm (4:1 field weakening) and 5000 rpm (no field weakening). In general, as the full field speed was reduced, the motor size was required to be increased to meet the duty requirements. For a given full field speed, as the motor size was increased beyond the minimum size capable of satisfying duty requirements, efficiency was somewhat improved; however, when the motor size greatly exceeded the minimum required size, by a factor of about 2:1, the vehicle range was reduced as a result of the increased vehicle weight.

The results of computer runs show maximum vehicle range on the J227a Schedule D duty with a nominal full field speed of 2500 rpm. With field forcing, the speed is lowered to about 1800 rpm. The motor design limits are primarily the torque required for the 0 to 30 mph in 9 seconds acceleration and for the 50 mph, 5 % grade. Because of this, the selected motor will exhibit a very moderate temperature rise on the J227a Schedule D urban cycle. Because the design is of ample proportions, commutation duty will not be severe.

Computer runs show that a machine having a higher full field speed, although it can be built in a smaller size, is capable of a more limited J227 duty range -- even if made oversized. It is pointed out, however, that these relations are not highly sensitive. A spread of ±15 % as applied to the optimum motor size and optimum full field speed results in a variation in vehicle range of only a few cycles of J227 duty.

## Appraisal of Other Motor Design Types

### Number of Main Poles

Motor designs built with greater and fewer numbers of main poles were considered. Two-pole designs were substantially heavier and do not offer performance advantages of such significance as to offset the weight penalty. The primary advantages of six-pole designs, as compared with four-pole designs, is a weight

reduction of about 15 lb and an armature circuit resistance reduction of about 10 %. Disadvantages include: increased core loss; a poorer stator space factor, resulting from the larger number of poles and coils; and an inherently lower armature circuit inductance, resulting in greater current ripple when operated from a pulse power supply and/or requiring a heavier smooth reactor. Reduced armature reaction per pole allows the use of a smaller air gap, tending to offset the need for more field copper because of the increased number of poles.

Six-pole designs afford less flexibility as to armature winding. In particular, a gap exists between the ratings which can be met with parallel-lap and series-wave winding types. The rating under consideration borders on the unavailable range. It is quite possible that the optimization process described above for the four-pole designs considered would result in an acceptable six-pole design; however, it is likely that further investigation would uncover an "optimum" degree of field weakening for a six-pole motor, which is impractical because of the intrinsic gap in this winding type. For this reason, and because of the near equality of four- and six-pole winding types, a four-pole drive motor was selected for development.

High Speed Motors

Higher speed motor designs were considered but were not judged suitable for maximum range battery operated vehicular application. In particular, five motor designs providing a top speed of 10,000 rpm were evaluated and judged inferior to the 5000 rpm designs described above.

Friction, windage, and core losses of such motors are inherently higher, and, whereas the armature windings can be shrouded and streamlined, the increased machine losses more than offset the advantage afforded by the weight reduction. The vehicle weight can be reduced about 60 lb by the use of a motor rated 20 hp, 6000/10,000 rpm. Not included in this figure are the increased weight and decreased efficiency likely to be involved in the doubling of the speed-changer ratio.

Permanent Magnet Motors

Permanent magnet excitation of the drive motor offers the obvious advantage of elimination of excitation power. Significant size and weight reductions can be foreseen, particularly with the use of the new cobalt-rare earth magnetic materials which are now available. A motor design using such magnets developed by the General Electric Company under the trade name Gecor was developed for evaluation by CRD. The machine designed uses approximately 16 lb of permanent magnet material. Two serious shortcomings are evident.

First, whereas a permanent-magnet-excited machine using Gecor can be designed for reasonably high airgap flux densities as re-

quired for acceptable motor losses during level vehicular operation, a significant flux decrease at severe overloads cannot be avoided -- as compared with the flux increase achieved by field forcing with the separately exicted machines discussed above. Increased armature current provides the required torque results.

A second shortcoming is the increased motor current associated with peak loading when all of the speed control range is achieved by armature voltage control. Motor currents in the range of 700 A are required, as compared with a maximum current of less than 400 A when using the design selected for prototype manufacture.

Fabrication

Four motors are now being fabricated with the parameters shown in Table 3.2.3-1. Fabrication is expected to be completed during May 1978.

WBS 3.2.4 Armature Chopper

Circuit Selection

Both single-phase and multiphase choppers were considered for the armature chopper design. Also considered was a bidirectional chopper arrangement in which electric braking is accomplished by the use of a voltage stepup chopper, which is separate from the motoring chopper. Consideration was also given to a single armature chopper with reversing contactors to accomplish the braking function (in this approach, the field must also be reversed to accomplish braking).

The single-phase bidirectional chopper was selected for the following reasons:

- Lowest weight
- Simpler control
- Fewer base drive circuits
- Faster transition time from motoring to braking
- Greater efficiency (no armature motoring/braking contactor or series SCR)

Power Transistor Evaluation

Several types of power transistors were evaluated under actual circuit conditions in the breadboard armature chopper shown in Figure 3.2.4-1. Devices obtained from Power Tech, Inc.; EVC, Inc.; Westcode; and Toshiba were considered as well as the developmental GE power Darlington. The GE power Darlington was selected for use in the armature chopper on the basis of its superior switching speed and its adaptability to low-cost power module fabrication techniques. Two GE power Darlingtons in parallel along with a

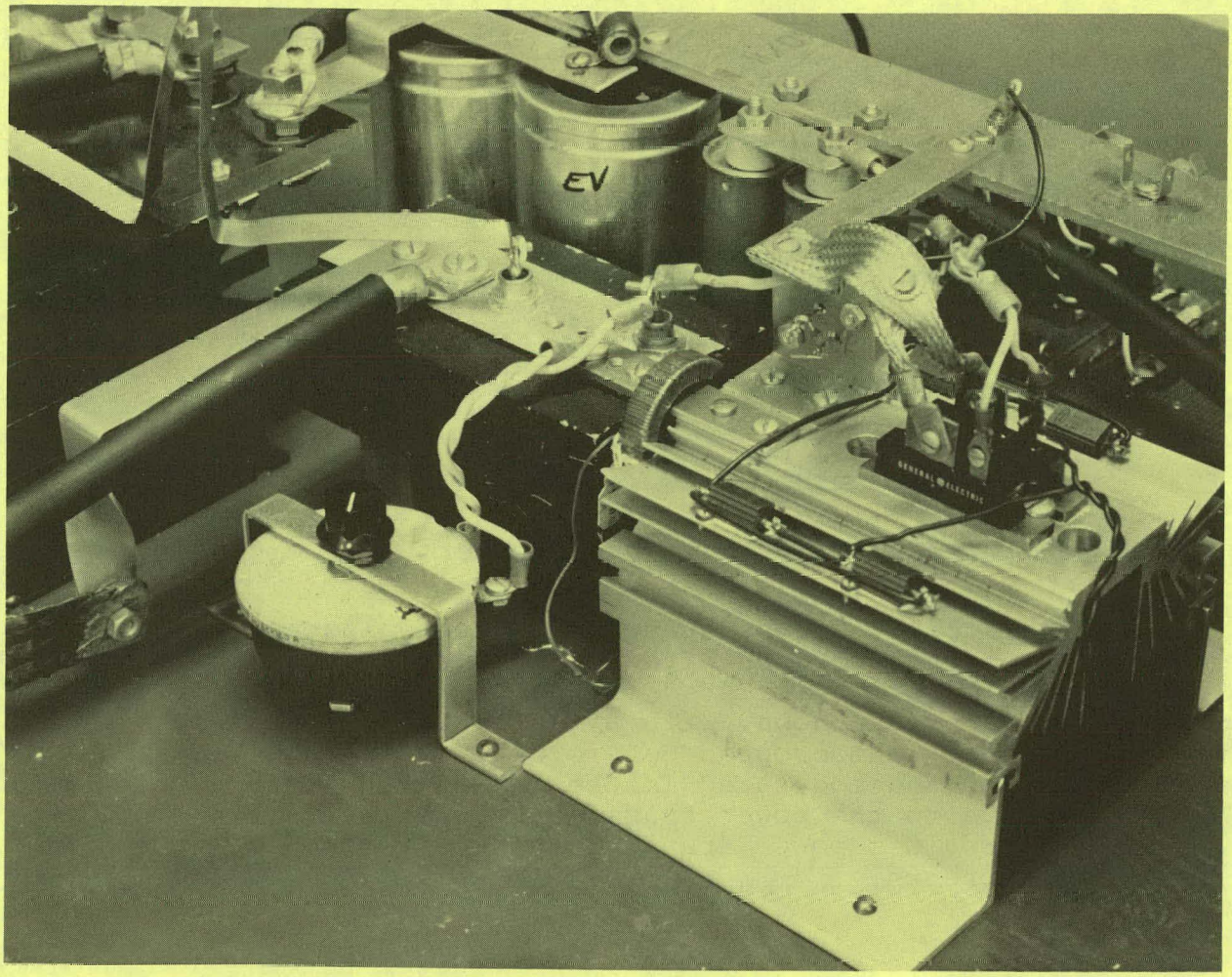

Figure 3.2.4-1. Breadboard Armature Chopper

feedback diode form a single module capable of turning off the required 270 A peak current in less than 1 μs.

Armature Chopper Design

Figure 3.2.4-2 is a simplified schematic diagram of the armature chopper. Since the peak motoring requirements (400 A) are twice the peak braking requirements (200 A), two modules are used in parallel for the motoring transistors (Q1 and Q2), while only a single module is needed for the braking chopper (Q3). There are two GE power Darlingtons in parallel per module. A capacitor bank (≃1200 μF) supplies the high frequency currents required by the chopper. The resistor/capacitor/diode networks across each module provide turnoff stress reduction for the power transistors while L1 and its associated diode and resistor provide turnon stress reduction for the power transistors. Transformer T1 forces dynamic current sharing between Q1 and Q2. The use of magnetoresistive sensors to sense the armature current eliminates the power loss normally associated with current shunts and provides electrical isolation.

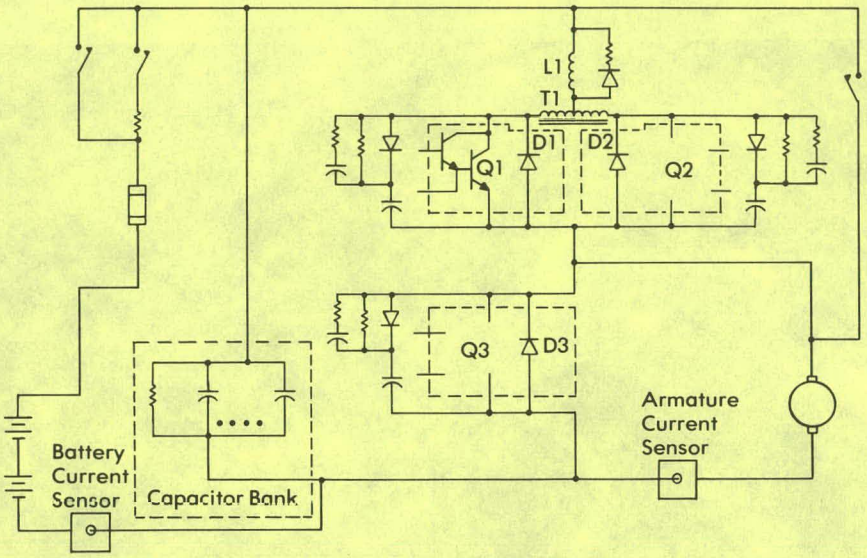


Figure 3.2.4-2. Armature Chopper Power Circuit

Figure 3.2.4-3 illustrates the control electronics which interface the microprocessor with the chopper power transistors. The malfunction signals listed in Figure 3.2.4-3, if positive, result in system shutdown, with a fault signal being sent to the microprocessor. The chopper duty cycle, $\tau$, is received from the microprocessor and modulated in the interface electronics to provide the drive to the power transistors. A fast acting local current limit provides power transistor protection in the event of rapid overcurrents.

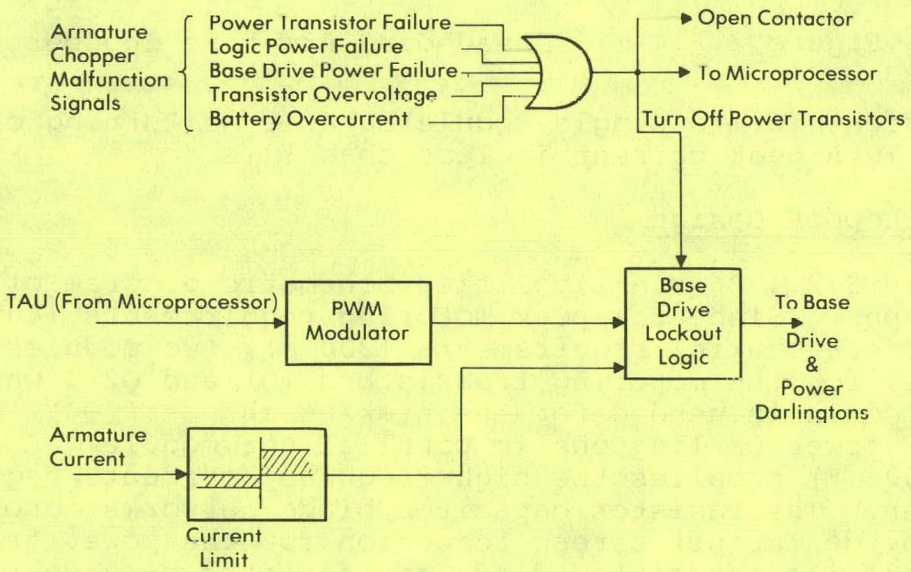


Figure 3.2.4-3. Interface Electronics

Figure 3.2.4-4 shows the armature chopper power loss computed from measured quantities obtained from the breadboard chopper. The switching frequency varies parabolically as a function of percent of time (duty cycle) as determined by the PWM modulator. This constant ripple current control results in the minimum switching frequency (minimum switching losses) being used for a given load condition while keeping the peak-to-peak ripple current at an acceptable constant value.

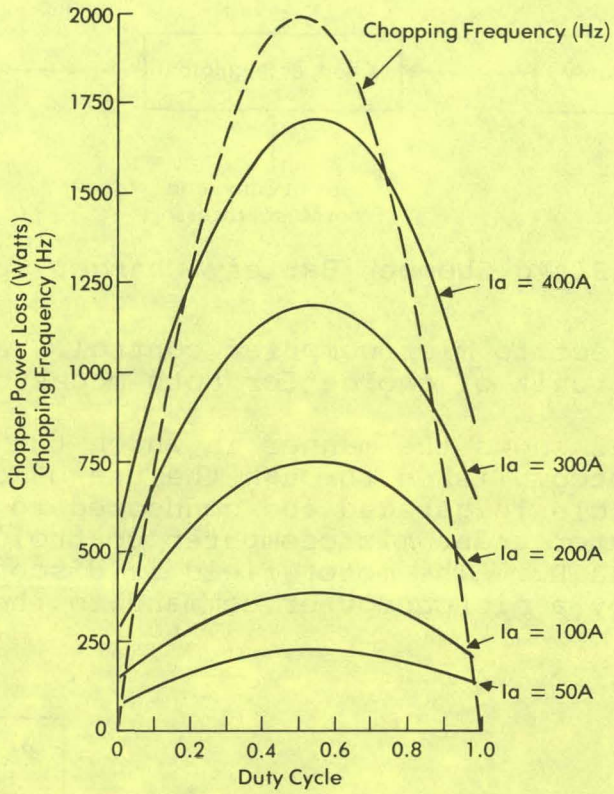


Figure 3.2.4-4. Armature Chopper Power Loss

## WBS 3.2.5 Field Chopper/Battery Charger

The field chopper/battery charger (FC/BC) circuit is required to perform the dual functions of providing the appropriate electronic interface between the household power source and the vehicle propulsion battery and providing appropriate motor field excitation under microcomputer control when the vehicle is in motion.

### Power Circuit

The block diagram of Figure 3.2.5-1 shows the two operational modes of the FC/BC circuitry. When connected to a 115 V service outlet, the circuitry is arranged to provide propulsion battery charging under microcomputer control. When the vehicle is in motion, the circuitry controls the propulsion motor's field current,

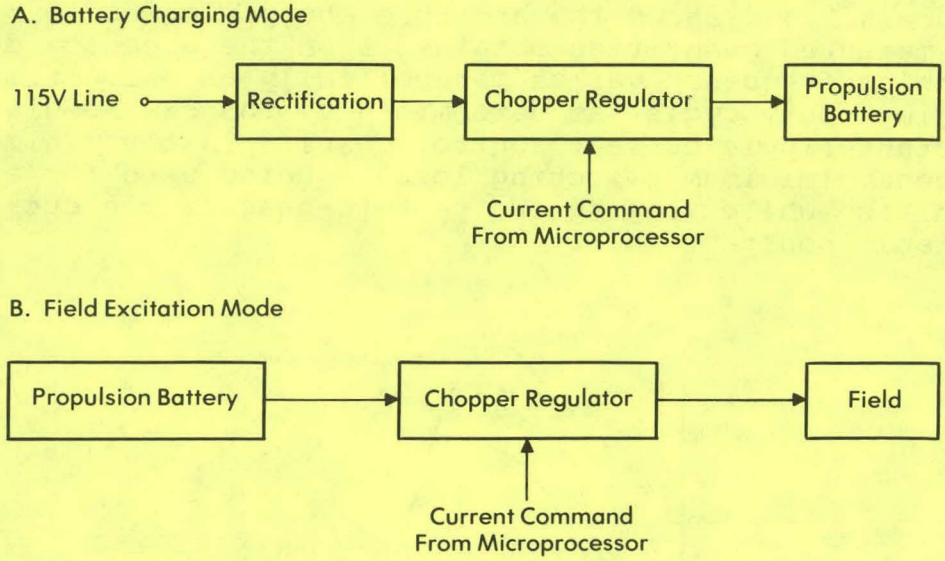


Figure 3.2.5-1. Field Chopper/Battery Charger Operational Modes

which is also subject to microcomputer control. A transistor down-chopper was the circuit of choice for both modes of operation.

Figure 3.2.5-2 shows the manner in which the dual-mode circuit function is accomplished through the use of diodes $D_2$ and $D_3$. When the vehicle is garaged and connected to the 115 V line, the chopper regulator under microcomputer control charges the propulsion battery via $D_3$. The motor field is disconnected in this operational mode by a microcomputer command to the field relays.

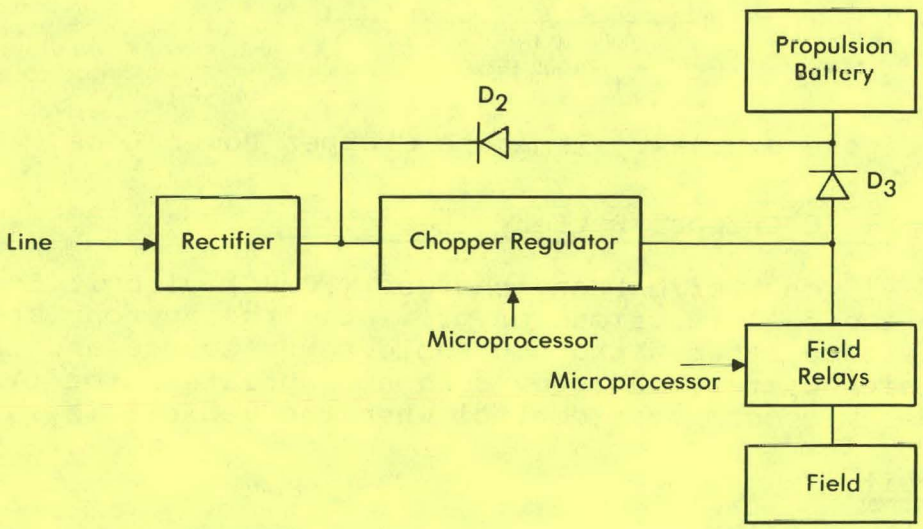


Figure 3.2.5-2. Field Chopper/Battery Charger Block Diagram -- Power Circuit

Charging occurs whenever the full-wave rectified line voltage is instantaneously greater than the battery voltage, a condition which reverse-biases $D_2$. During time intervals when the battery voltage is greater than the rectified line, the "rectifier" prevents reverse battery current. When the vehicle is in motion, the microcomputer commands the field relay to connect the field (forward or reverse, as appropriate) and the propulsion battery supplies the chopper regulator through diode $D_2$. Diode $D_3$ is back-biased in this operational mode, since the field voltage is less than the battery voltage.

The interconnections of the principal components of the FC/BC power circuit are shown in Figure 3.2.5-3. Additional components of significance are the coasting inductance, $L_1$, which provides the necessary energy storage for the battery charging mode; the coasting diode, $D_2$, which is included with the power switch transistors, $Q_1$ (in modular form); and the location of the current sensors which provide both instantaneous and average current signals to the control logic that feeds the base drive circuitry.

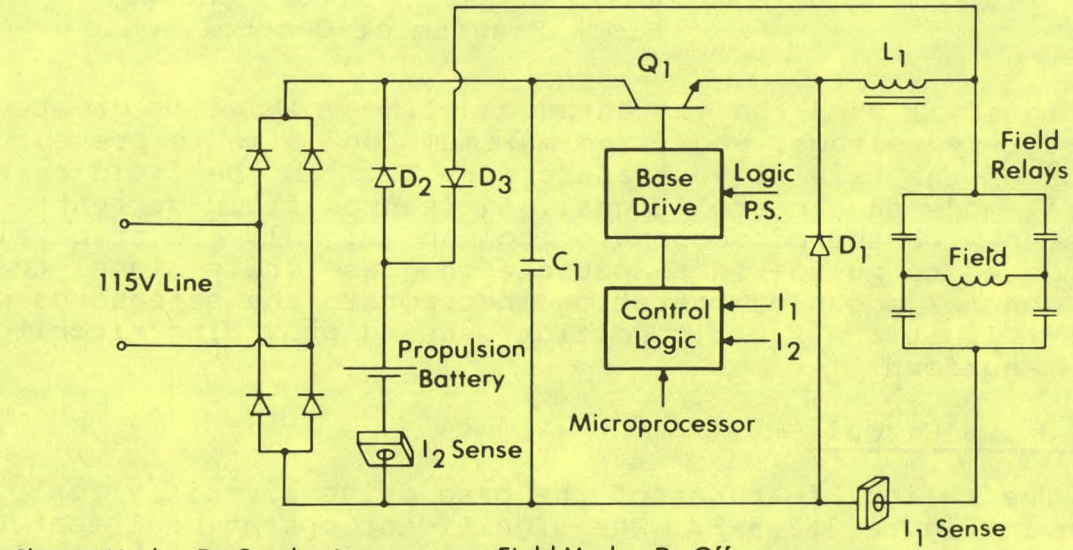


Figure 3.2.5-3. Field Chopper/Battery Charger -- Power Circuit

## Control Logic Circuit

A block diagram of the control circuitry is shown in Figure 3.2.5-4. In the battery charge mode of opeation, the amplified ($I_1$) signal (sensed battery current) is used to control the "on" time of the power switch transistor $Q_1$. Features of this circuitry include peak current control for fast circuit response during the

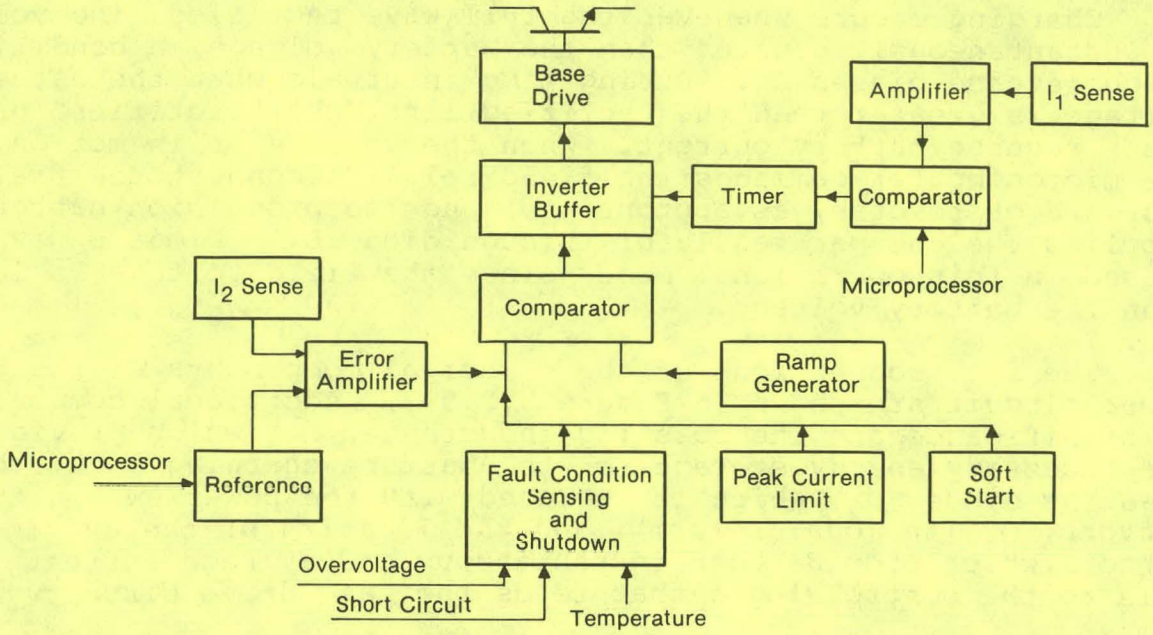


Figure 3.2.5-4. Field Chopper/Battery Charger -- Block Diagram of Control Logic

time interval when the instantaneous line voltage is greater than the battery voltage, and fixed maximum "on" time to prevent saturation of the base drive transformer, $T_1$. In the field current control mode the control signal, $I_2$ (sensed field current), is compared with the microcomputer command signal, the error signal being used to pulse-width-modulate the base drive signal to $Q_1$. Both control modes of operation incorporate the safeguards of peak current limit and fault condition sensing providing circuit operation shutdown.

## Base Drive Circuit

The salient features of the base drive circuitry for $Q_1$ are shown in Figure 3.2.5-5. The significant operational features provided by this circuitry are fast transistor switching times, regenerative self-driving of $Q_1$, and a low control signal power requirement. The high frequency of operation (10 to 20 kHz) permits the use of relatively small sized magnetic components in the power circuitry.

## Circuit Breadboards

The base drive circuitry has been breadboarded (Figure 3.2.5-6) and exercised. Snubbers (circuit components to protect $Q_1$, not shown in figures) have been designed appropriate to the breadboard circuit layout. The initial design for the coasting inductance, $L_1$, has been modified for minimum leakage flux to permit mounting in a small space. The logic circuitry has been breadboarded and exercised in an open-loop mode. All circuit designs have been transitioned to GE Ordnance Systems for packaging and circuit board design.

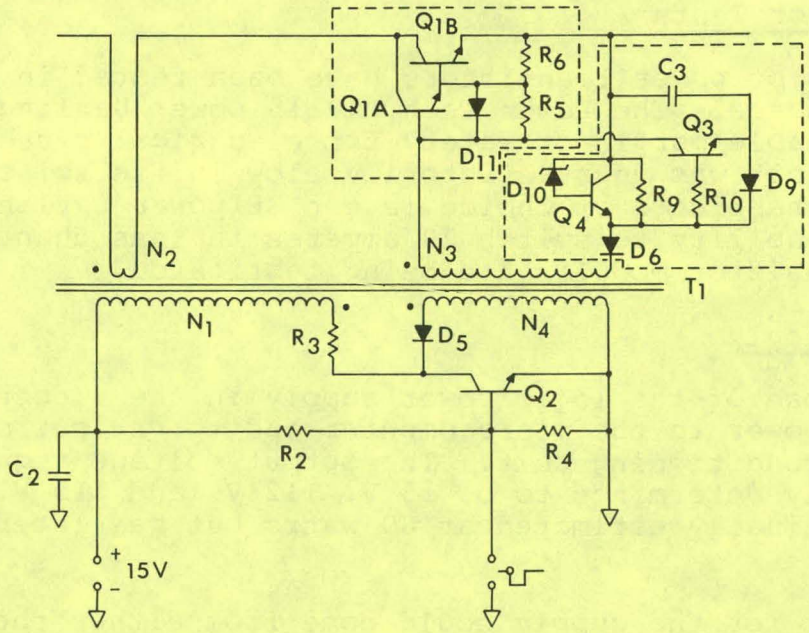


Figure 3.2.5-5. Field Chopper/Battery Charger -- Base Drive Circuitry

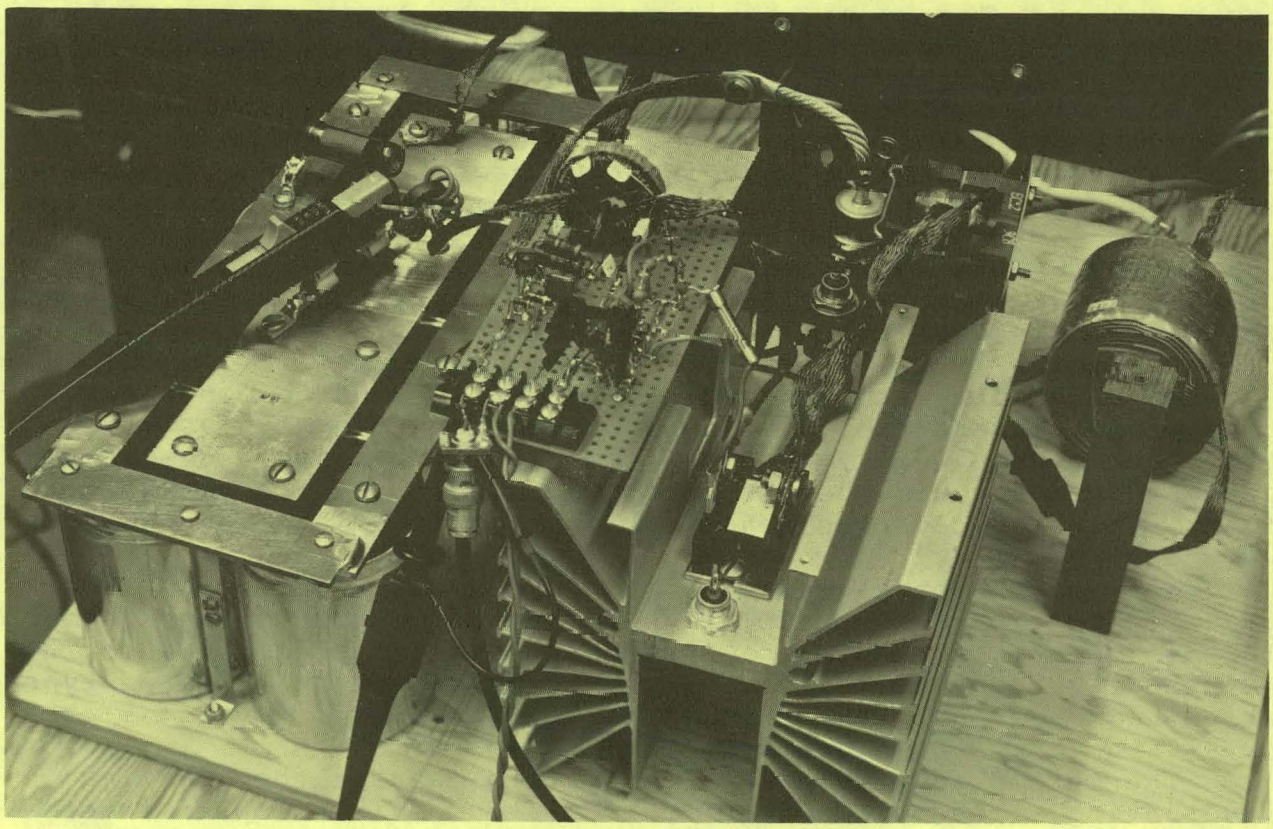

Figure 3.2.5-6. Breadboard Circuit Layout

## Power Transistor Tests

Two types of power transistors have been tested in the power circuit breadboard. The Power Tech MT1115 power Darlington provided a reasonable margin of safety for electrical stress (voltage, current) but was unsatisfactorily slow in its switching behavior. The transistor of choice is the GE power Darlington, which displayed the ability to switch 70 amperes in less than 500 nanoseconds. Transistor modules are being fabricated.

## Logic Power Supply

The purpose of the logic power supply in the electric vehicle is to supply power to the microcomputer and to various circuits in the power conditioning unit. The output voltage requirements were originally determined to be +5 V, +12 V, and ±15 V. Output power was originally estimated at 80 watts but was later increased to 160 watts.

The power for the supply could come from either the auxiliary 12 volt battery or the main 108 volt propulsion battery. The 12 V battery maintains a more stable output voltage but is likely to be less reliable than the 108 V system. Consequently, the 108 V system was chosen as the power source for the supply.

The 108 V system actually has an output that fluctuates between 60 V at complete discharge and 160 V when the vehicle is regenerating. The major requirement for the logic power supply is the capability of accepting this wide voltage swing.

Since the purchase of an off-the-shelf unit was preferable to designing a unit, a search was conducted for a power supply capable of accepting the wide input voltage swings and supplying the five required output voltages. Furthermore, the supply would have to meet the temperature specifications for the vehicle, which are more severe than the standard 0 to 70 °C commercial temperature specifications. Unfortunately, no single supply could be found which met all three requirements.

An alternative considered was to design a dc-dc converter that would convert the varying input voltage to a standard military bus voltage (e.g., 48 V). Commercially available dc-dc converter modules would then be used to produce the five output voltages. This approach was rejected for reasons of size and weight.

Work had already been done within General Electric on a supply with multiple output voltages and a wide input voltage range. The design approach used for that supply was adopted, because it met the requirements and had already been proven in the prototype stage.

The method adopted uses a chopper to convert the incoming fluctuating voltage to a tightly regulated dc level on an intermediate bus. Energy storage for the system is carried out by a

filter capacitor on this bus. The required output voltages are produced by a high frequency, square-wave inverter and a multi-winding transformer. Since the output waveform is a high frequency square wave, output filtering requirements are modest.

The circuit used in the GE study was redesigned to meet the voltage and current requirements of the present application. All components were checked to ensure that they would operate over the required temperature range. Additional protective circuitry was incorporated in the supply and a warning system was added to monitor system voltages and warn the microcomputer of fault conditions in the logic power supply.

During the design phase, a requirement for a source of base drive power for the armature chopper was defined. Rather than build another power supply for the base drive, it was decided to use the logic power supply. Therefore, a 36 V ac winding was added to the output transformer. This 36 V ac at 25 kHz is converted to 5 V dc within the armature chopper by a transformer, rectifier, and filter. This new requirement raised the output power of the supply to 160 W, as previously mentioned. A block diagram of the logic power supply is shown as Figure 3.2.5-7.

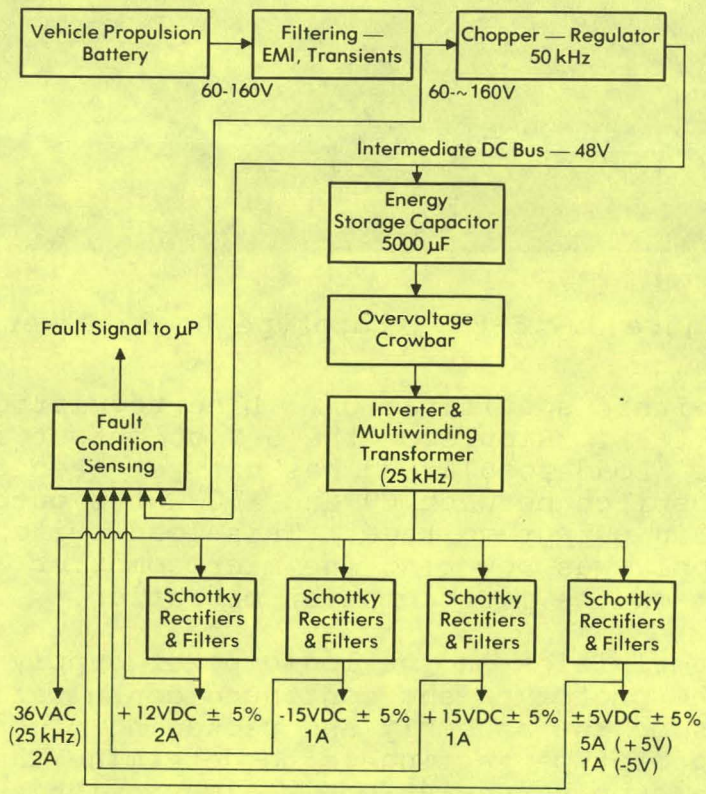


Figure 3.2.5-7. Logic Power Supply -- Block Diagram

A complete prototype logic power supply (Figure 3.2.5-8) has been built at CRD to allow the supply to be tested with the microcomputer and other loads. Initial tests on this prototype show

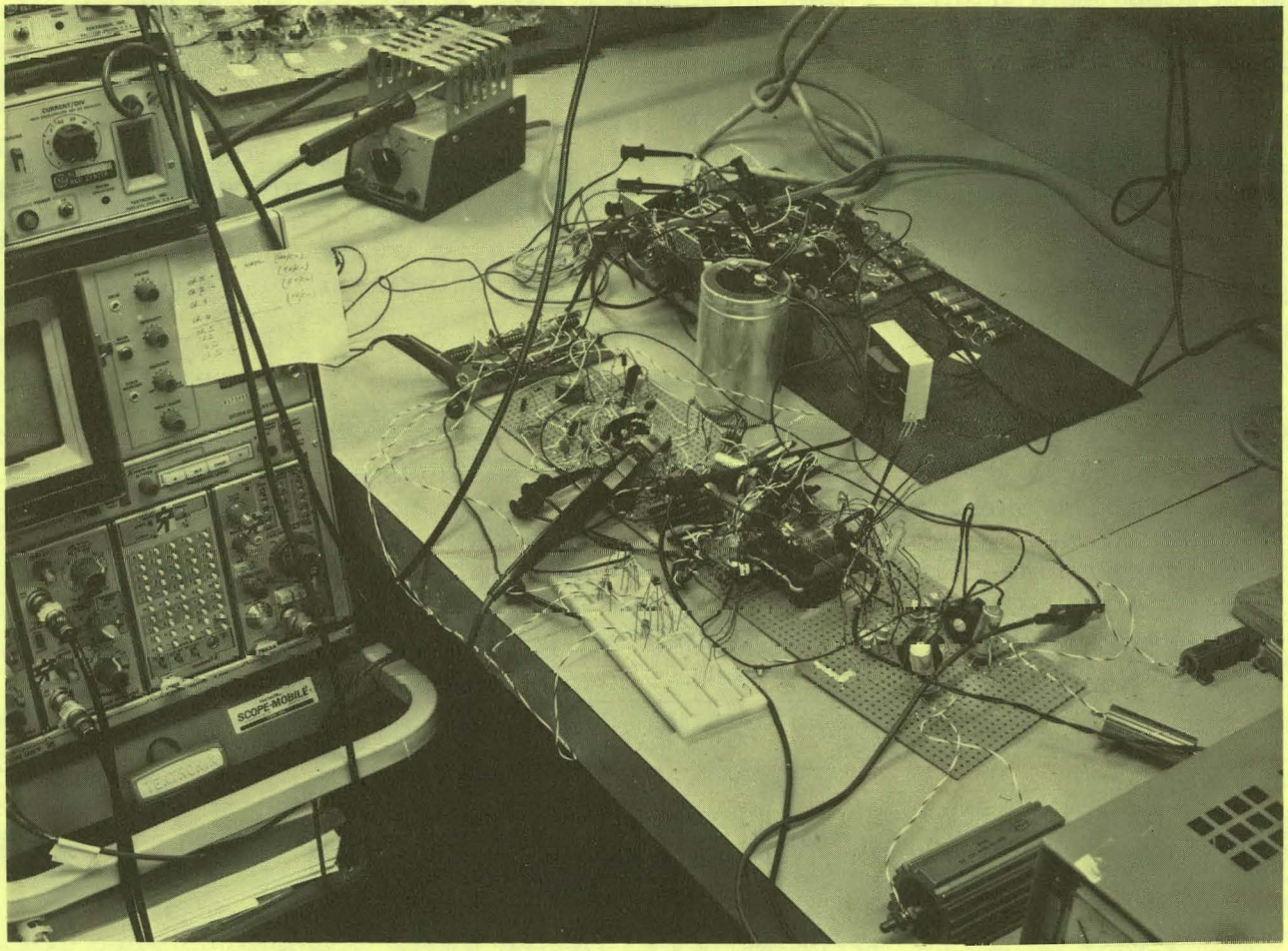


Figure 3.2.5-8. Prototype Logic Power Supply

performance within specification. Line regulation is very tight (better than 1 %). Ripple on the 5 V dc output is about 100 mV, peak to peak. Load regulation has not yet been completely determined, but a switch between 60 and 160 watts output resulted in a 5 % change in output voltage. This load switching was performed while the supply was powering the microcomputer. The switching had no effect on the microcomputer operation.

Future activities on the logic power supply include further testing of the prototype and continued consultation with GE Ordnance Systems on the assembly and packaging of the supply. One goal of the prototype testing is to determine the supply regulation. If the supply regulation is always within ± 5 % for the vehicle loads and load changes, it may be possible to eliminate some of the regulators currently included for critical analog circuits and tight voltage-tolerance digital components.

## WBS 3.2.6 Microprocessor Module

### System Analysis and Simulation

The electric vehicle will have an Intel 8080 microprocessor based control system which will perform the functions of propulsion control, sequencing, fuel gauging computation and display, and programmed battery charging.

In propulsion control, the armature current will be controlled in both the chopping and field weakening modes, as shown in Figure 3.2.6-1. The feedback control loops in the above modes have been analyzed by Bode diagrams, and suitable gain and compensator parameters have been determined. The drive subsystem is then simulated on the hybrid computer, to verify the digital control algorithm and sampling period and to study subsystem stability conditions.

The prototype control software resident in the developmental system (MDS-800) (Figure 3.2.6-2) has been interfaced with the real-time simulation of the drive subsystem on the hybrid computer. Static and dynamic performances have been evaluated.

A simplified vehicle sequencing diagram is shown in Figure 3.2.6-3. There are 18 sequential states corresponding to five principal operating modes. For example, the forward operating modes consist of motoring, regeneration, and coasting states corresponding to chopping and field weakening control modes. Responding as to a set of driver commands, control transfers from one state to another. A precise set of actions is performed during the transition.

Battery charging and equalization strategies have been formulated and flow charts drawn. Preliminary formulation of the fuel gauging strategy has been completed.

### Microprocessor Software Development

Functional specifications for the software have been defined and were presented at the IDR. The software architecture has a top-down hierarchical structure with an executive program at the top. The software development has been partitioned into modular subroutines in order to provide unit testing of each module.

The system, as shown in Figure 3.2.6-4, has been partitioned into five major subsystems: multitask executive (Real Time Scheduler), motor control, sequential control, tachometer calculations, and monitoring subsystem. In addition, a limited set of diagnostics is provided for monitoring and testing the microcomputer system. All subsystems except the monitoring subsystem have been implemented and tested on the INTEL microprocessor development system. Once the monitoring subsystem is completed, the system will be integrated and tested on the prototype hardware in the laboratory.

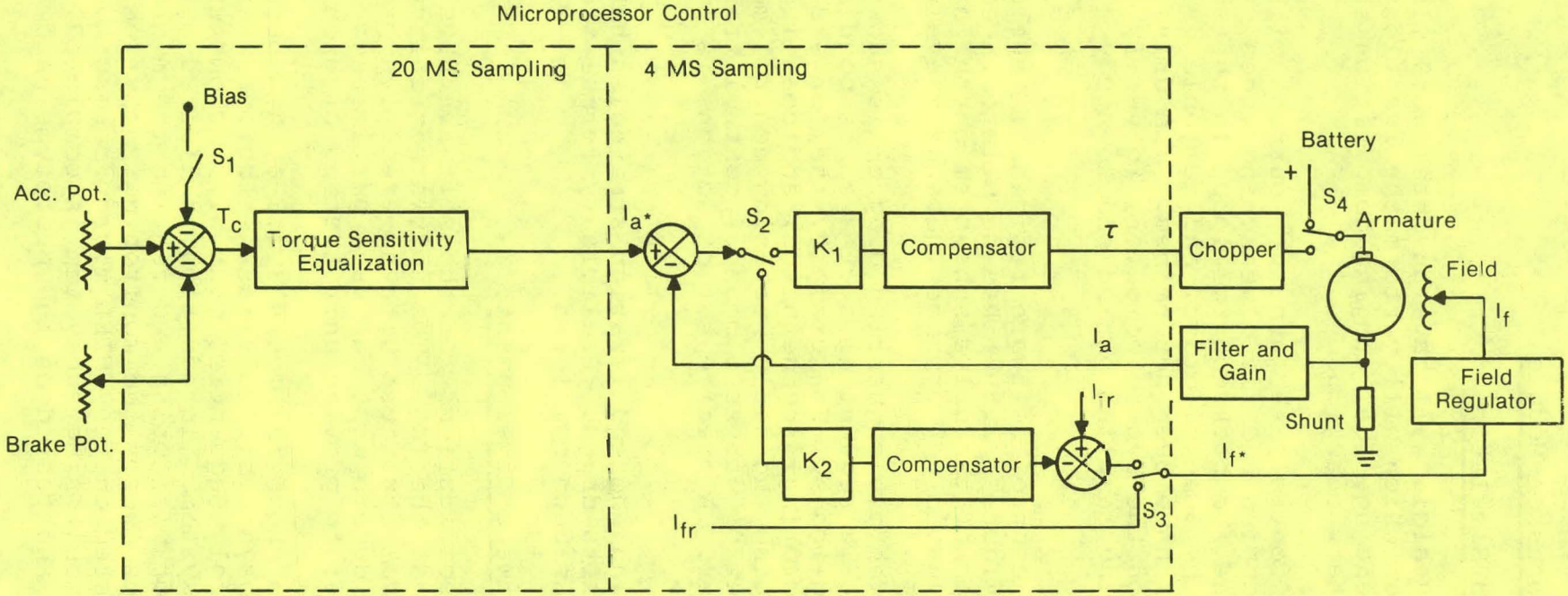


Figure 3.2.6-1. Control System -- Block Diagram

Figure 3.2.6-2. Microcomputer Developmental System

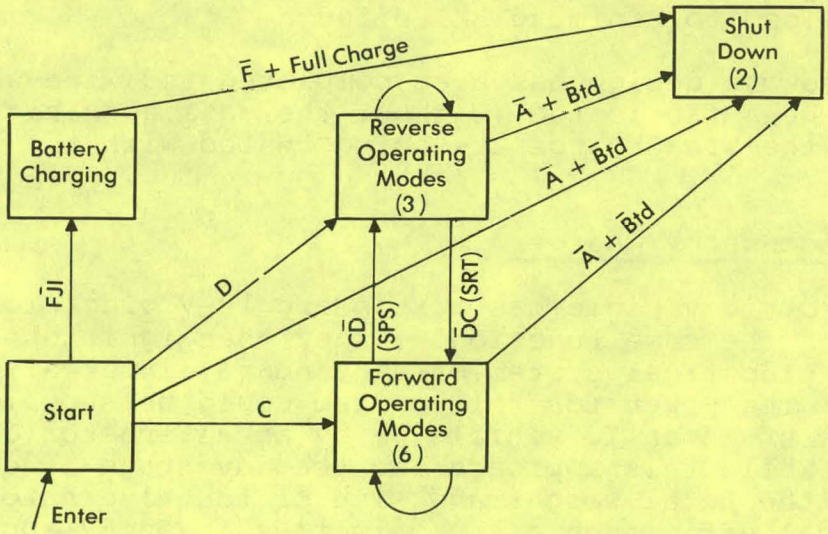


Figure 3.2.6-3. Simplified State Sequencing Diagram

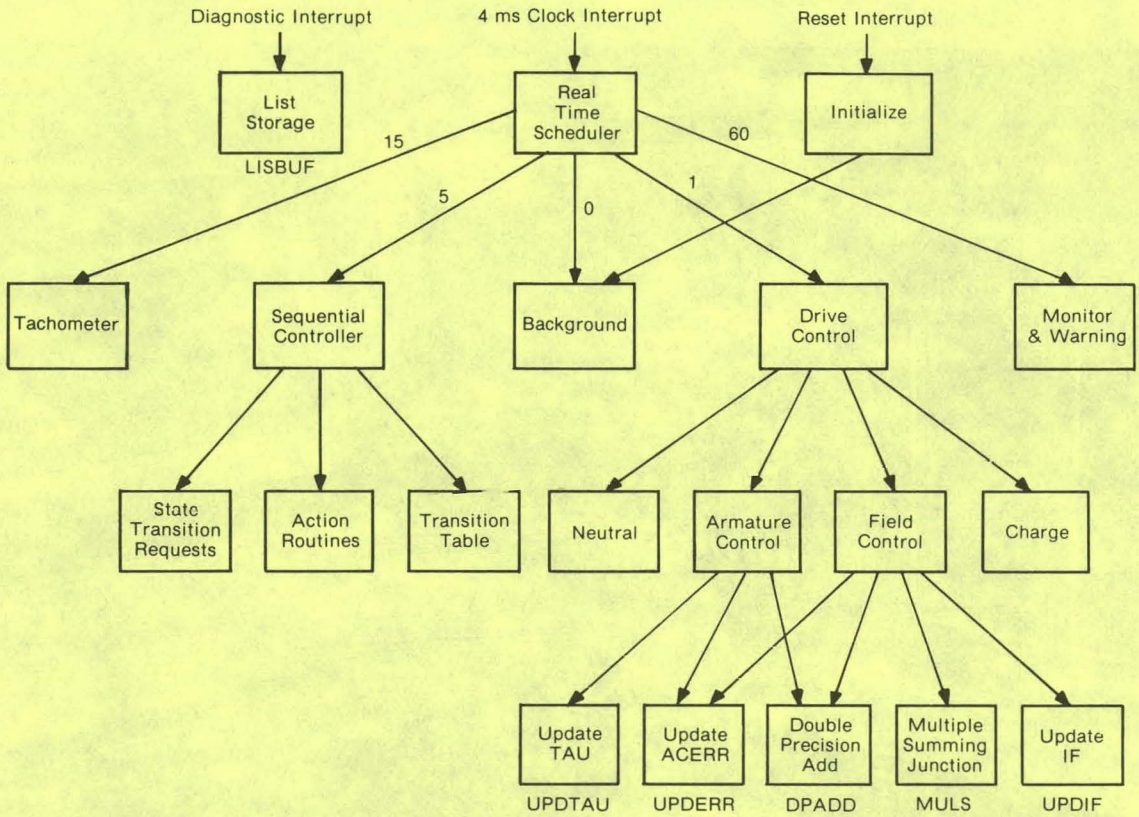


Figure 3.2.6-4. Structure Chart of Present EV Software

## Hardware Design and Test

The hardware of the microcomputer has been custom-designed, mainly with the use of MIL-SPEC components. The modular data acquisition and output systems, programmable interrupt controller, and interval counter minimize the amount of hardware. The design includes diagnostic hardware, and adequate decoupling and shielding are provided to minimize EMI effects.

The hardware design has been completed and wire-wrapped breadboards have been fabricated (without the data acquisition system). At present, the breadboards are being tested with the in-circuit emulator.

## WBS 3.2.7 Accessory Charger

The electric vehicle has a standard 12 V electrical system that performs the same functions (other than ignition and starting) as the electrical system of a standard, internal-combustion-engine car. The power for this system could be supplied in the same fashion as in an IC vehicle -- by an alternator driven by the motor. While this approach has the advantage of using proven technology, the total weight and size of the alternator and its low electrical efficiency are prohibitive in an EV application.

An alternative solution is to use a dc-dc converter to supply the 12 V power from the vehicle propulsion battery. A small 12 V battery is used to allow accessories to operate for a time even if the propulsion battery is discharged. The auxiliary battery also allows the 12 V system to handle peak loads above the capacity of the dc-dc converter. Dc-dc converters are light and small and represent a relatively mature technology. Therefore, this approach was chosen to power the vehicle 12 V system.

The dc-dc converter for the system, called the accessory charger, has the following characteristics:

- When the accessory battery voltage is below its gassing voltage, the converter operates in a current limited mode, supplying 36 amperes to the 12 V circuit.
- When the accessory battery charges up to its gassing voltage (indicative of full charge), the charger enters a voltage limiting mode in which the voltage is held constant and current is allowed to vary.
- When the temperature of the accessory battery changes, the temperature-sensitive charger changes the threshold between the current and voltage limiting modes.

The first design approach for the accessory charger was to scale up the logic power supply circuit to the 500 W output level required and make appropriate changes in the control circuitry to allow the circuit to run in the modes described above. Next, however, in order to simplify the packaging and assembly efforts of Ordnance Systems, a simpler design was sought. A flyback type of converter, containing only one power transistor, proved to be the most cost-effective while still allowing an efficiency of over 80 %.

Detailed design of the power and control circuit began in early 1978. Particular attention was paid to making the charger as rugged as possible, since the 12 V system in an automobile is traditionally subject to owner tinkering. The flyback circuit has transformer isolation between the propulsion battery, and the 12 V system and is inherently short-circuit-proof. Open-circuit protection is provided by the large filter capacitors in the output of the supply, which limit the rate of rise of voltage, and by the voltage limit circuit, which acts to keep the average voltage below 15 V. A reversed diode across the output terminals in conjuction with a fuse protects the charger from reversed battery polarity. Both the input and output of the converter are fused. The accessory battery-charger circuit is illustrated in Figure 3.2.7-1.

The system was breadboarded, as shown in Figure 3.2.7-2, during Feburary and March of 1978. After some work on removing noise in the control logic and improving the base drive to the power transistor, the charger performed as specified. It handled

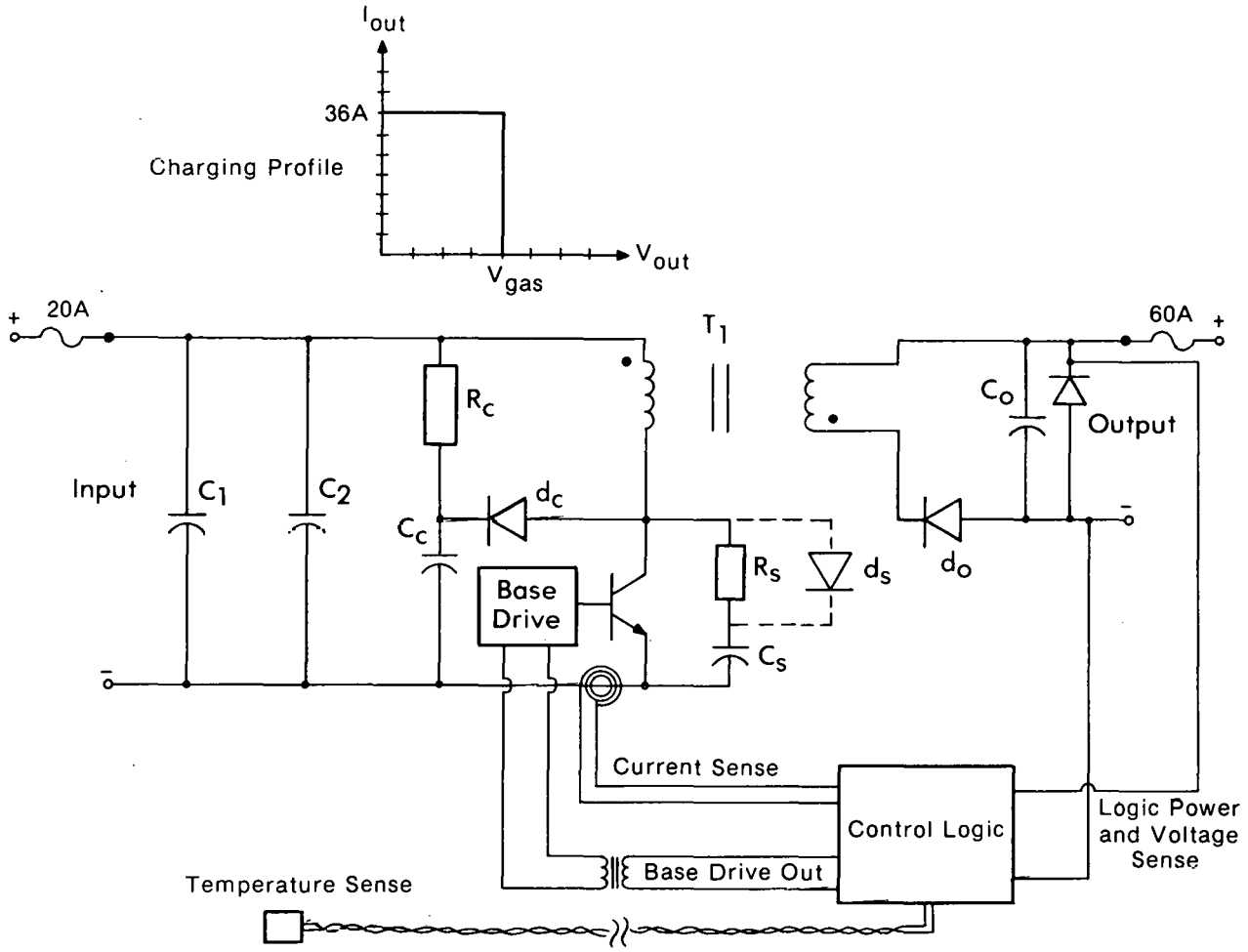


Figure 3.2.7-1. Accessory Battery-Charger Circuit

open- and short-circuit conditions and passed properly from current limit to voltage limit modes. The output current drops to about 30 A when the propulsion battery voltage drops below 70 V. This is not a serious problem, since the propulsion battery drops below 70 V only on extreme discharge, which rarely occurs under normal conditions.

When the circuit design was provided to Ordnance Systems in March for assembly and packaging, it was found that the accessory charger could be packaged in the power conditioning unit, resulting in weight and space saving.

Future plans for the accessory charger include further testing and continued consultation with Ordnance Systems on the assembly and packaging. The testing is primarily to accurately determine the efficiency of the converter. A quick test indicated that the efficiency was somewhat below the 80 % originally estimated, but the accuracy of the instruments used is questionable when operating on non-standard waveshapes.

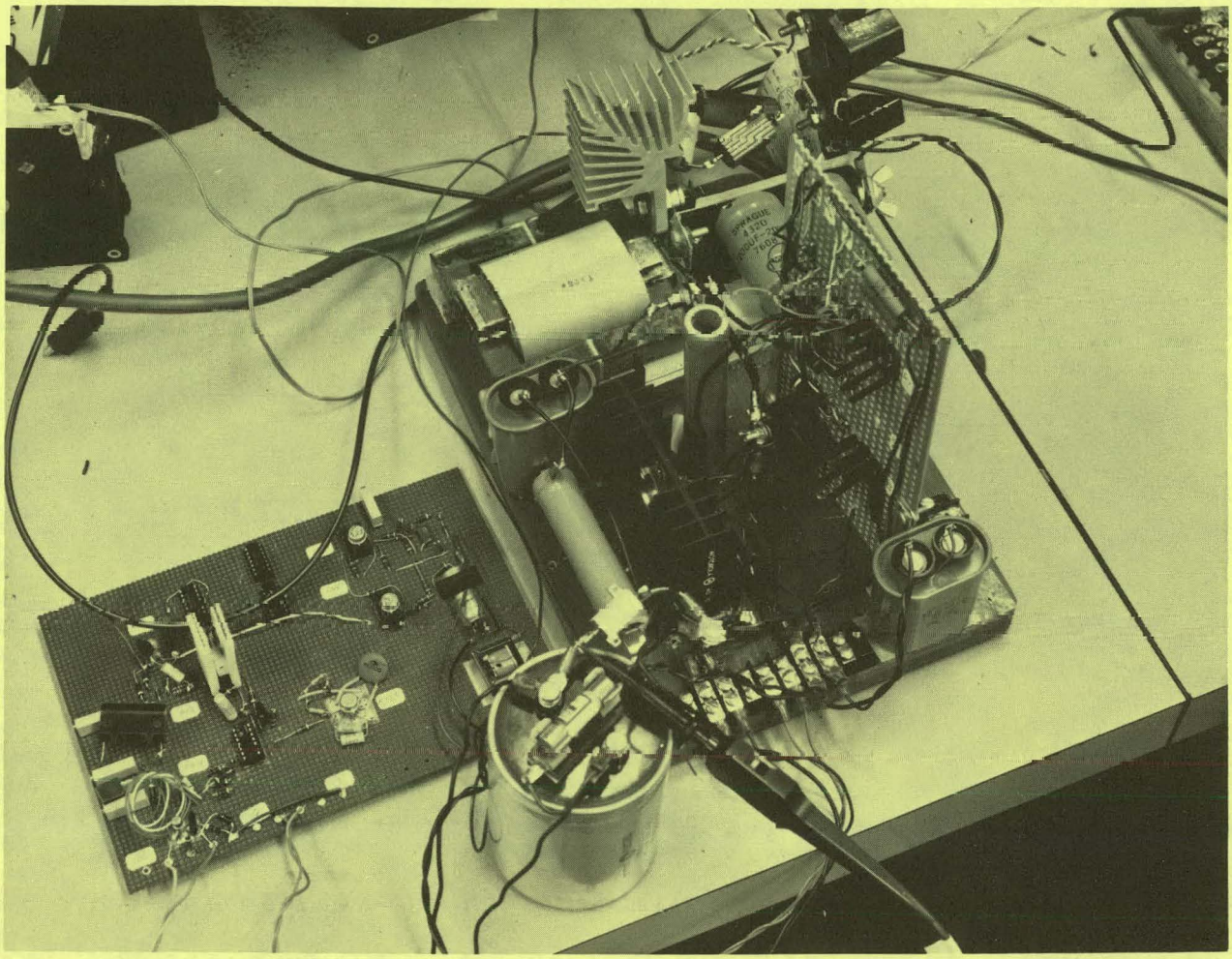

Figure 3.2.7-2. Accessory Charger Breadboard

If the efficiency is really less than 80 %, some adjustment of snubbers and clamp circuits will have to be performed to raise the efficiency.

WBS 3.2.8 Drive Test Instrumentation

The objective of this GE-funded task is to construct a drive test facility for evaluation of the Electrical Drive Subsystem prior to its installation in the vehicle.

A sketch of the facility, now under construction, is shown in Figure 3.2.8-1. It consists of the following:

- A load generator, used in conjunction with a resistor load bank and field controller to simulate the aerodynamic drag and rolling resistance of the vehicle. The system also simulates the force of gravity if the negative gravitational thrust is less than the forward positive thrust of the drive subsystem. An example

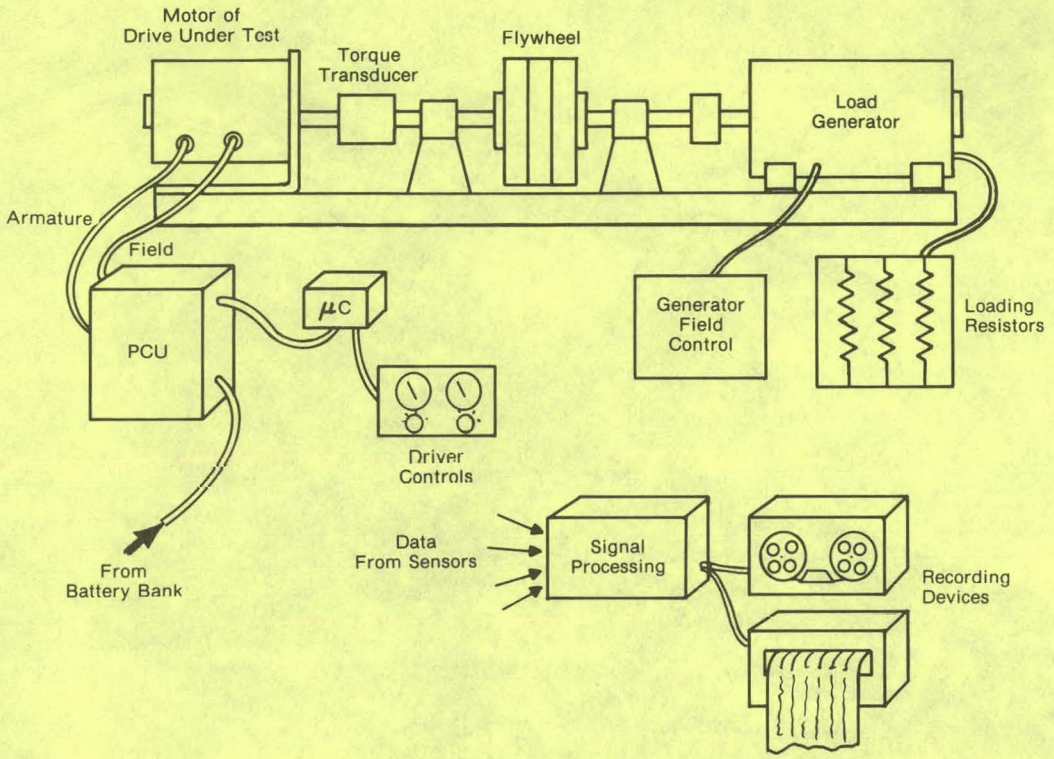


Figure 3.2.8-1. Drive Test Facility with Drive Under Test

of this is hill-climbing when the vehicle is always moving forward.

- A flywheel which is used to simulate vehicle mass.
- A torque transducer, used to provide a torque signal for the recording equipment.
- A bracket to which the motor of the drive under test is mounted.
- Signal processing circuitry to amplify, attenuate, filter, average, and isolate (in various combinations) the input signals.
- Sensors (not shown in Figure 3.2.8-1 except for the torque transducer) to measure quantities such as battery current and voltage, motor armature current and voltage, motor field current and voltage, and PCU and motor temperatures.
- Recording devices, such as an instrumentation tape recorder or a chart recorder.

Construction of this facility is underway and is scheduled to be operational by mid-July 1978.

## WBS 3.2.9 Power Modules and Transistors

### Armature Chopper

In May 1977, letters were sent to and information solicited from both foreign and domestic vendors of power transistors and rectifiers with products that might be suitable for the needs of the armature and field choppers. The devices evaluated in the armature circuit are listed in Table 3.2.9-1. Based on the requirements of the armature chopper, and a need for the transistors and diodes to be compatible with integrated power module technology, it became evident that the only suitable candidate transistors were the Power Tech PT4502 and the GE monolithic power Darlington transistors. Furthermore, it was seen that the GE transistor had significantly higher current handling capability and current gain than the PT4502, and was therefore selected for the module design.

TABLE 3.2.9-1

DEVICES EVALUATED IN CHOPPER CIRCUIT

| DEVICE | MANUFACTURER | MANUFACTURER'S RATINGS $I_{C\ DC}$ (A) | MANUFACTURER'S RATINGS $I_{C\ PK}$ (A) | MANUFACTURER'S RATINGS $V_{CEO}$ (V) | MAX, $I_{C\ PK}$ TESTED | CASE |
|---|---|---|---|---|---|---|
| PT 7511 | Power Tech | 50 | 90 | 200 | 110 | T063 |
| PT 4502 | Power Tech | 60 | 110 | 325 | 100 | T0114 |
| PT 4500 | Power Tech | 100 | 150 | 200 | 100 | T0114 |
| Experimental Low Voltage Power Darlington | GE | | | $\leq$200** | 180 | Flat Base Module |
| Experimental High Voltage Power Darlington | GE | | | $\geq$300** | 200 | Flat Base Module |
| RSD-751 | EVC | 100 | 300 | 450 | 160 | Flat Base Module |
| WT GEX | Westcode | 120 | | 450* | 150 | Flat Base |
| 2SD648 | Toshiba | 400 | | 300 | 400 | Press Pak |

*$V_{CER}$

**Approximate Voltage Capability of Devices Tested

The Power Tech transistor would provide the alternative choice, should later tests prove its superiority. As the GE device had not been designed specifically for the electric vehicle application nor packaged in a form suitable for module integration, substantial modifications of the semiconductor chip design, metallization, and assembly were necessary.

The original chip had been designed to operate from a 56 V battery source; hence, its blocking voltage $BV_{CEO}$ ranged from 100 to 200 volts. This was considerably lower than the 300 to 400 volts needed for the armature. The low voltage device had the dc parameters listed in Table 3.2.9-2. The higher voltage capability was achieved by the design of a "guard ring" located 8 μm from the collector base junction. This guard ring structure reduces the high-intensity electric field at the junction, thereby raising the threshold voltage for avalanche breakdown.

TABLE 3.2.9-2

DC TRANSISTOR PARAMETERS

| Device No. | $V_{CE}$(sat) (200 A/0.2 A) | $h_{FE}$ (200 A/2.5 $V_{CE}$) | $BV_{CEO}$ (100 μA) | $BV_{CEO}$(sus) (100 μA) |
|---|---|---|---|---|
| 1 | 1.42 | 3570 | 130 | 180 |
| 2 | 1.44 | 3570 | 190 | 204 |
| 3 | 1.32 | 3640 | 140 | 166 |
| 4 | 1.41 | 4880 | 140 | 164 |
| 5 | 1.31 | 4000 | 150 | 160 |
| 6 | 1.41 | 5400 | 190 | 200 |

This modified version of the Darlington is operating in the armature chopper and has a $BV_{CEO}$ range from 300 to 400 volts. Early tests of the Darlington in the chopper showed an anomalous behavior in the fall time characteristic. As seen in Figure 3.2.9-1 (a) and (b), the removal of the snubber capacitance results in an increase in the fall time of the collector current from 1 to 16 μs. This effect is contrary to what is expected from transistor theory. The reason for this anomaly can be explained by Figure 3.2.9-2.

Where the snubber is present, the collector voltage rises slowly as the collector-to-emitter current decays; therefore, the displacement current is negligible. In the absence of the snubber, the dv/dt and corresponding base displacement current in the given example is still only 50 mA, but the high gain (2000) of the Darlington requires an emitter (and collector) current of 100 A, which is almost as much as the load current that is being turned off. Reducing the gain of the transistor should therefore remove this displacement current effect; this is, in fact, what happens in Figure 3.2.9-3 (a) and (b). The Darlington chip was, therefore, not only designed to meet the higher voltage requirements, but processed to significantly reduce its current gain.

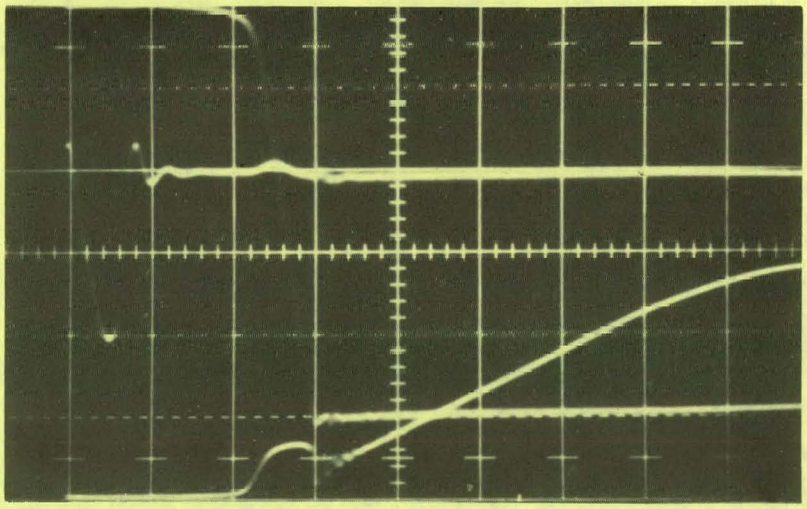

Figure 3.2.9-1(a). High Gain Darlington (≈2000) With Snubber. $I_B$ = 1 A/cm, $I_C$ = 20 A/cm, $V_{CE}$ = 50 V/cm $t^B$= 1 μs/cm, $C^C$= 4 μF.

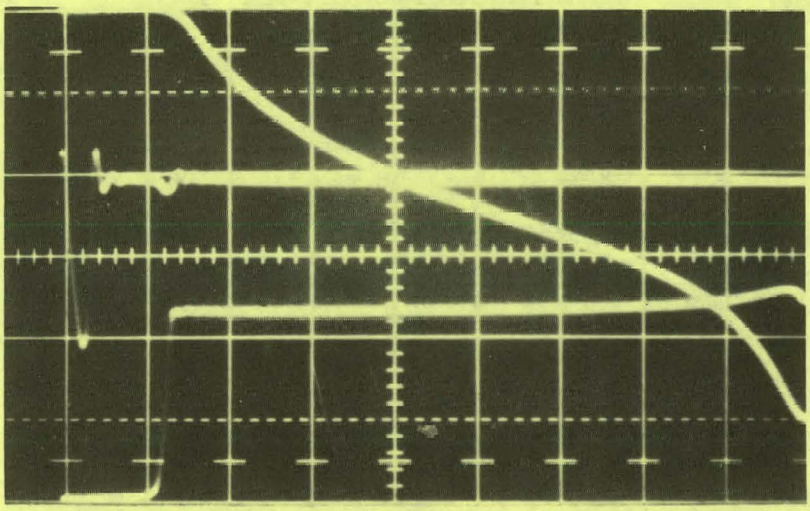

Figure 3.2.9-1(b). High Gain Darlington (≈2000) Without Snubber. $I_B$ = 1 A/cm, $I_C$ = 20 A/cm, $V_{CE}$ = 50 V/cm $t^B$= 2 μs/cm.

Transistor Packaging

The packaging and assembly for this transistor required innovations to maximize its power dissipation, to provide electrical isolation between the collector and the copper substrate (heat sink), and to be consistent with hybrid integration techniques that utilize solder reflow mountdown. Analytical studies of stress in a multilayer structure that may consist of silicon, solder, copper, BeO, and/or moly indicated that a low-stress combination of materials that can provide efficient cooling and electrical isolation was indeed possible. Furthermore, it was felt that this

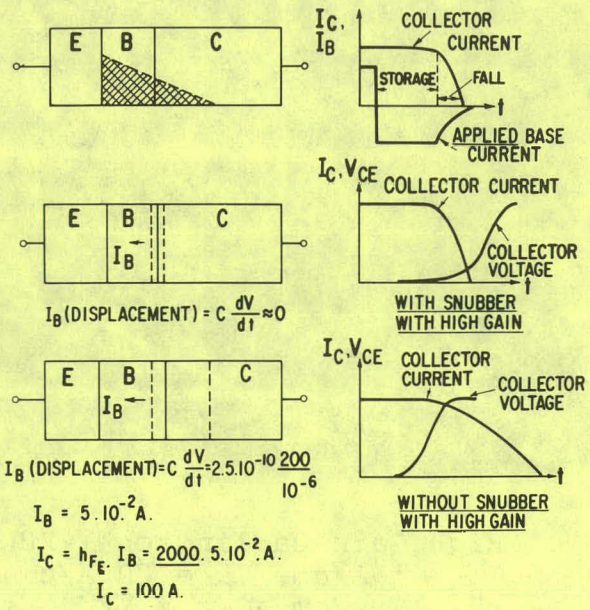


Figure 3.2.9-2. Effect of High Current Gain on Fall Time in Inductive Circuits

assembly could be applied to a single transistor chip as in the "Power Pak" or, in an integrated form, in the power module.

Two processes developed by General Electric earlier were applied to this program. The first consisted of directly bonding copper to the ceramic (BeO). This allows for a relatively void-free bond with very effective heat transfer capabilities. Comparative performance tests on the direct-bonded copper and silver pastes (on BeO) in temperature cycling (-50 to +125 °C) showed that the silver paste assembly deteriorated completely by the 75th cycle, while the chip on direct-bonded copper shoed only a 30 % degradation in gain after 275 cycles.

Another unique feature in the packaging of the Darlington transistor was the use of a "structured copper" plate that is bonded to the emitter silicon surface. The individual strands of copper wire are pressed together to have 90 % of the density of the bulk material. This allows for stress relief when an expansion or contraction of the silicon chip takes place. Moreover, the structured material has nearly the same excellent thermal and electrical conductivity as the bulk material.

The objective of using structured copper is threefold:

- To provide for uniform current conduction over the entire emitter surface.
- To replace several wire bonds with one plate to connect the chip's base and emitter pads to the package.
- To provide an additional path for the transfer of heat from junction to case.

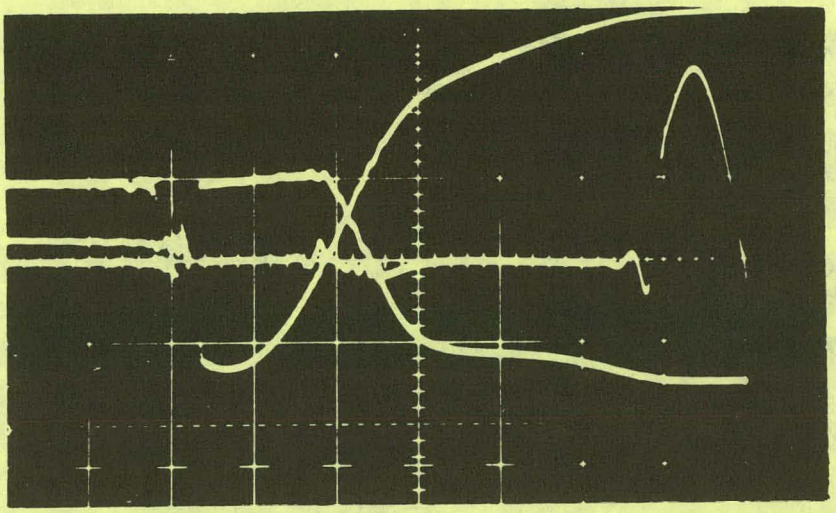

Figure 3.2.9-3(a). Low Gain Darlington (≈200) With Snubber. $I_B$ = 1 A/cm, $I_C$ = 50 A/cm, $V_{CE}$ = 50 V/cm t = 1 μs/cm, C = 1 μF.

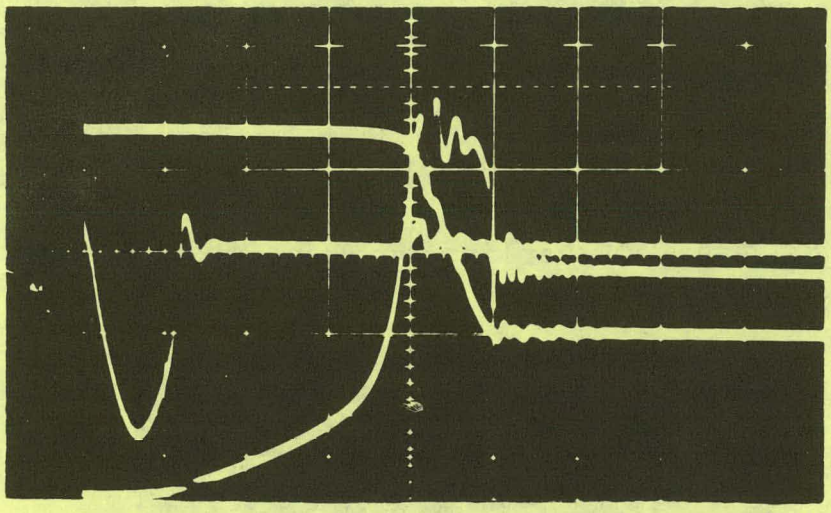

Figure 3.2.9-3(b). Low Gain Darlington (≈200) Without Snubber. $I_B$ = 1 A/cm, $I_C$ = 50 A/cm, $V_{CE}$ = 50 V/cm.

It was found that the bonding of the chip to BeO and structured copper can be carried out in one solder reflow operation. The resultant Subscrete® transistor assembly shown in Figure 3.2.9-4 can be tested for dc gain, saturation voltage, etc. This is very useful in selecting and matching devices and will be discussed later.

The electrical performance of the individual GE Darlington transistor in the armature breadboard circuit switching 200 A of collector current is shown in Figure 3.2.9-5. It will be seen from this figure that the collector current remains unchanged

®Registered trademark of General Electric Company.

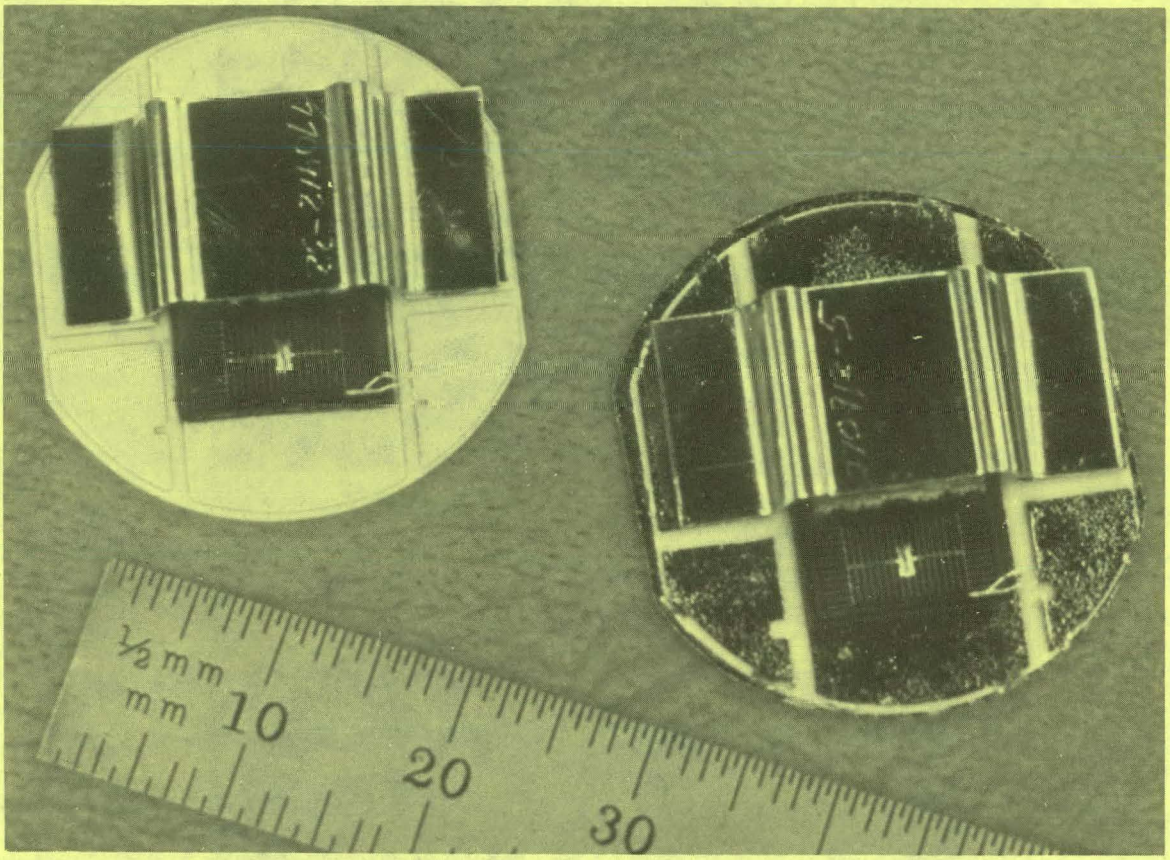


Figure 3.2.9-4. GE/Darlington Transistor as a Subscrete

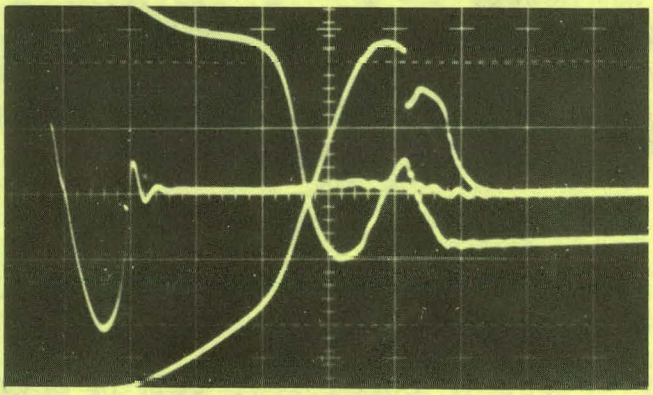

Figure 3.2.9-5. Turnoff Characteristics of High Voltage ($BV_{CEO}$ = 310 V) Darlington Transistor: $I_C$ = 50 A/cm, $I_B$ = 1 A/cm, $V_{CE}$ = 50 V/cm, $C_C$ = 1 μF, t = 1 μs/cm.

even after the base current has dwindled to perhaps a few miliamperes. Such a storage effect is quite unusual for transistors in a Darlington configuration, where the output stage is never in saturation.

A reasonable explanation of this phenomenon is illustrated by Figure 3.2.9-6. In the "conventional" Darlington shown in the figure, the saturation of the input stage sets up a voltage whose polarity reverse-biases the base collector junction region. In the high voltage version of the Darlington, the bulk resistance of the output stage collector may, in fact, drop the saturation voltage of the input transistor. In this event, the base-collector junction of the output would be forward-biased, and injected charge would build up in both the base and collector regions. This charge would be removed to some extent by the resistor across the emitter-base junction of the driver (corresponding to about 50 mA of base current in this case). However, some portion of the stored charge would disappear by hole-electron recombination, with a time constant that is directly related to the lifetime of the material.

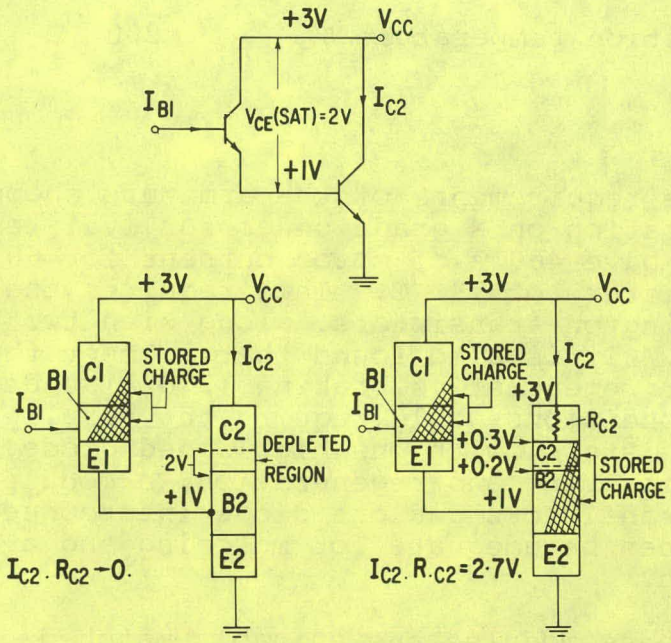


Figure 3.2.9-6. Comparison of Saturation Points in Low Voltage (Conventional), at Left, and High Voltage Darlington Transistors

The thermal impedance of the Power Pak assembly has been measured, using the emitter-base diode as the temperature sensor. Preliminary indications suggest a junction to case thermal resistance that is in the range of 0.15 to 0.25 °C/W, depending upon the temperature, time, and ambient of the solder reflow mountdown process.

Tentative ratings for the GE Darlington transistor for use in the armature chopper of the electric vehicle are as follows:

| | |
|---|---|
| $BV_{CEO}$ at $I_{CEO}$ < 5 mA | 300-400 V |
| $h_{FE}$ at $I_C$ = 100 A, $V_{CE}$ = 2.5 V | 100 (min.), 400 (typical) |
| $h_{FE}$ at $I_C$ = 200 A, $V_{CE}$ = 2.4 V | 200 (typical) |
| Storage time $t_s$*, $I_C$ = 200 A, $V_{CE}$ = 300 V | 2-4 μs |
| Fall time $t_F$*, $I_C$ = 200 A, $V_{CE}$ = 300 V | 1 μs (typical) |
| $V_{CE}$ (SAT)* at $I_C$ = 200 A, $I_B$ = 4 A | < 2 V |
| $R_{\theta j-c}$ | 0.15-0.25 °C/W |
| Maximum junction temperature $T_j$ | 200 °C |

Modules

To meet the requirements of the armature chopper under conditions of acceleration on a grade under survival temperatures, it is necessary to have 400 A of motor current for 60 seconds, at a heat sink temperature of 78 °C. This requires the paralleling of four GE Darlington transistors, along with two high speed freewheeling diodes. It is also found that to meet the maximum current demands for regenerative braking (270 A) under equally severe environmental conditions would require the paralleling of two GE Darlington transistors, with one high speed diode. To meet the needs for both motoring and regeneration, a module was chosen having two GE transistors and one diode interconnected. Two such modules would then be adequate for motoring and a single module for regeneration.

Provided these modules are suitably matched, they are interchangeable and would make a cost-effective manufacturing scheme. As there is no industry standard for the paralleling of transistors much less for Darlingtons (even though the matching of $V_{BE}$ is often used), an attempt was made to match the dc gain ($h_{FE}$) at the highest level of collector current. In Figure 3.2.9-7 the dc current characteristics of two unmatched transistors is shown.

The dynamic performance of these two devices operating in parallel in the armature chopper is shown in Figure 3.2.9-8. Clearly there is an unequal distribution of collector current in the two transistors. When two devices are matched in current gain, as in Figure 3.2.9-9, they are seen to share the load current during switching (Figure 3.2.9-10). In the motoring area of the armature chopper, there are two modules operating in parallel, each module consisting of two Darlington transistors.

*As measured in the armature breadboard circuit

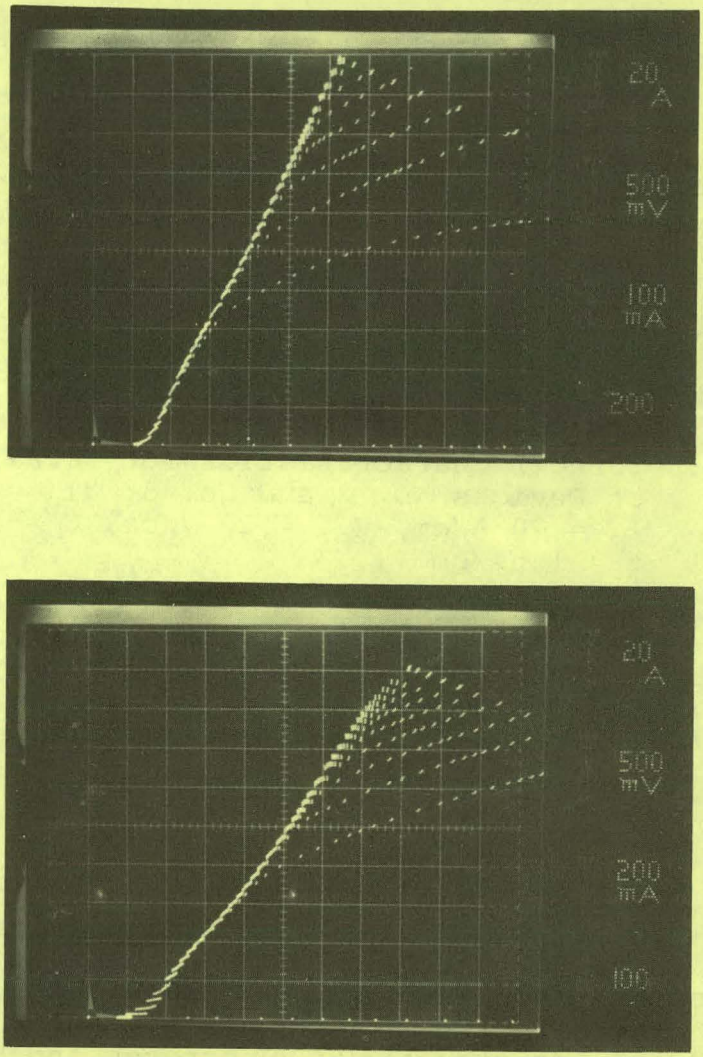


Figure 3.2.9-7. Current Gain Characteristics for Darlington Devices No. 2 (top) and No. 3

It follows from the earlier argument that the two modules, or four transistors, must be matched in dc gain for optimum performance in the circuit. It should be pointed out that the requirement to parallel four GE Darlington transistors does not come about from the requirement for 400 A of motoring current but from the survival heat sink temperature of 78 °C, which may raise the temperature of the copper substrate of the module to 110 °C.

Recognizing that the plastic epoxy package is not capable of temperature excursion much above 150 °C, the modules must dissipate 270 watts without raising the transistor junction temperature by more than 40 °C. This corresponds to a requirement for the thermal impedance from junction to copper heat sink of

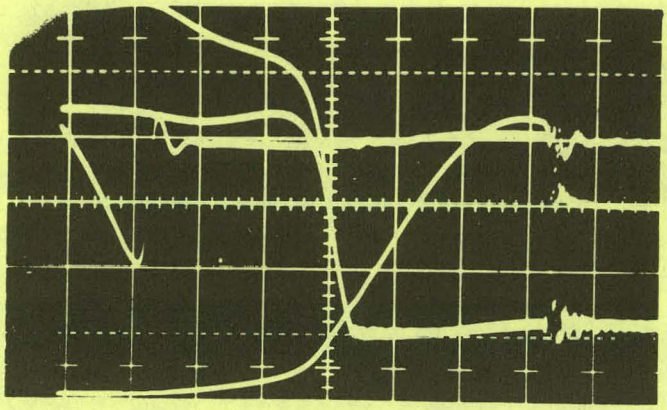

Figure 3.2.9-8. Turnoff Characteristics for Parallel Operation of Devices No. 2 and No. 3: $I_B$ = 1 A/cm, $I_C$ = 20 A/cm, $V_{CE}$ = 20 V/cm, $C^B$= 1 μF, t = 1 μs/cm

0.14 °C/W for each module. This value translates to maximum permissible thermal impedance of 0.28 °C/W for a single chip. The values measured for the GE Darlington and listed in its ratings indicate the device and module should meet the needs of the system under extreme and severe conditions.

Module Assembly

The scheme for the assembly of the module is an extension of the Power Pak idea. Subscretes are packaged with the chip mounted on BeO, with the structured copper plate on the emitter surface. The subscrete is tested for voltage, gain, and saturation $V_{CE}$(sat) characteristics and matched for paralleling in the module. The module consists of two subscretes and one diode connected internally in parallel with the necessary electrical isolation. The assembly is covered with silicone rubber and encapsulated in epoxy resin. The silicone is used to provide a stress buffer between the epoxy and the rigid lead terminals of the semiconductor devices. The epoxy is then cured at an appropriate temperature. A schematic diagram of the various component elements in the power module and the assembly sequence is shown in Figure 3.2.9-11.

To date, three power modules have been given a variety of tests in the armature chopper; these will be described later. Because of the small number of modules that have been studied, it is too early to develop a rating sheet; this will come about when more comprehensive data are generated. To date, little information has been generated on the performance of these modules under a variety of environmental conditions. Studies of the effects of thermal cycling on thermal impedance and electrical behavior, temperature stress on the epoxy encapsulation, and extended power cycling on these modules are planned, and in some cases have commenced.

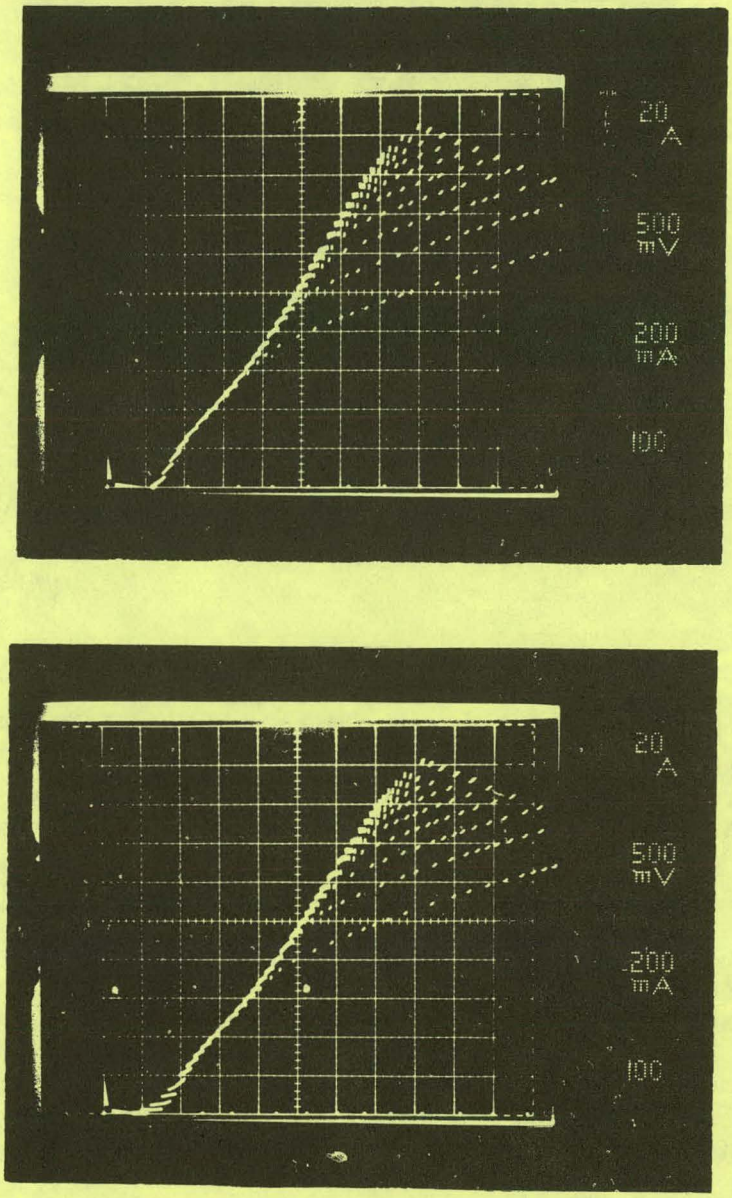


Figure 3.2.9-9. Current Gain Characteristics for Darlington Devices No. 1 (top) and No. 3

Each power module is tested in the armature breadboard circuit under conditions that simulate motoring and regeneration. The performance of a module switching a motor current of 200 A at 60 Hz is shown in Figure 3.2.9-12. These tests were performed over a case temperature range of -40 to +100 $^{o}$C. A test was also performed at 2 kHz under the very severe regeneration conditions, which require a module current of 250 A at a 60 % duty cycle for 1 minute. These are two tests that the power modules will be required to pass before they can be selected for the drive subsystem. An additional test will be the parallel operation of two modules with a motor load current of 450 A.

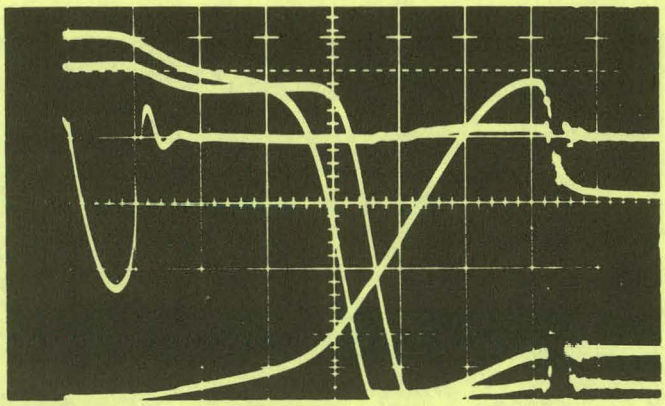

Figure 3.2.9-10. Turnoff Characteristics for Parallel Operation of Devices No. 1 and No. 3: $I_B$ = 1 A/cm, $I_C$ = 20 A/cm, $V_{CE}$ = 50 V/cm, $C^B$= 1 μF, $t^C$= 1 μs/cm

Field Chopper

The search for a transistor to fill the needs of the field chopper and once again be compatible with power module assembly techniques singled out the Power Tech PT3523. This is a 400 V, 90 A device capable of switching in 1 microsecond. However, when the PT3523 was compared with the GE power Darlington transistor in the field chopper breadboard, as shown in Figure 3.2.9-13, the latter device showed better switching behavior (<200 ns).

In the battery charging mode, this circuit is required to perform at frequencies ranging from 10 to 20 kHz. Higher speed transistors are therefore necessary. Moreover, it was found that using the GE Darlington chip would replace two PT3523's (for a Darlington connection) along with two resistors and a turnoff diode. The field chopper module consists of a GE Darlington transistor in parallel with a freewheeling diode.

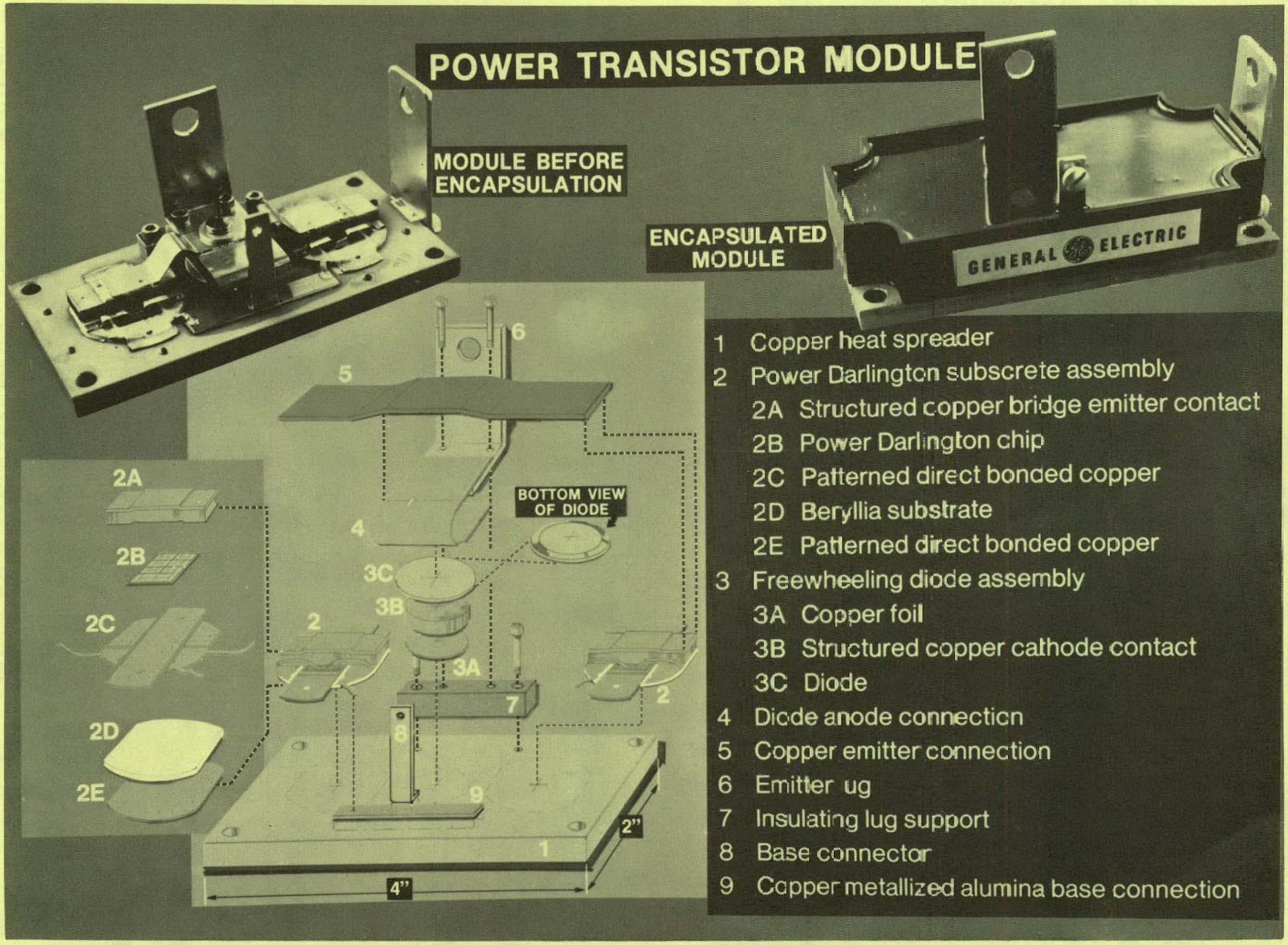


Figure 3.2.9-11. Power Transistor Module

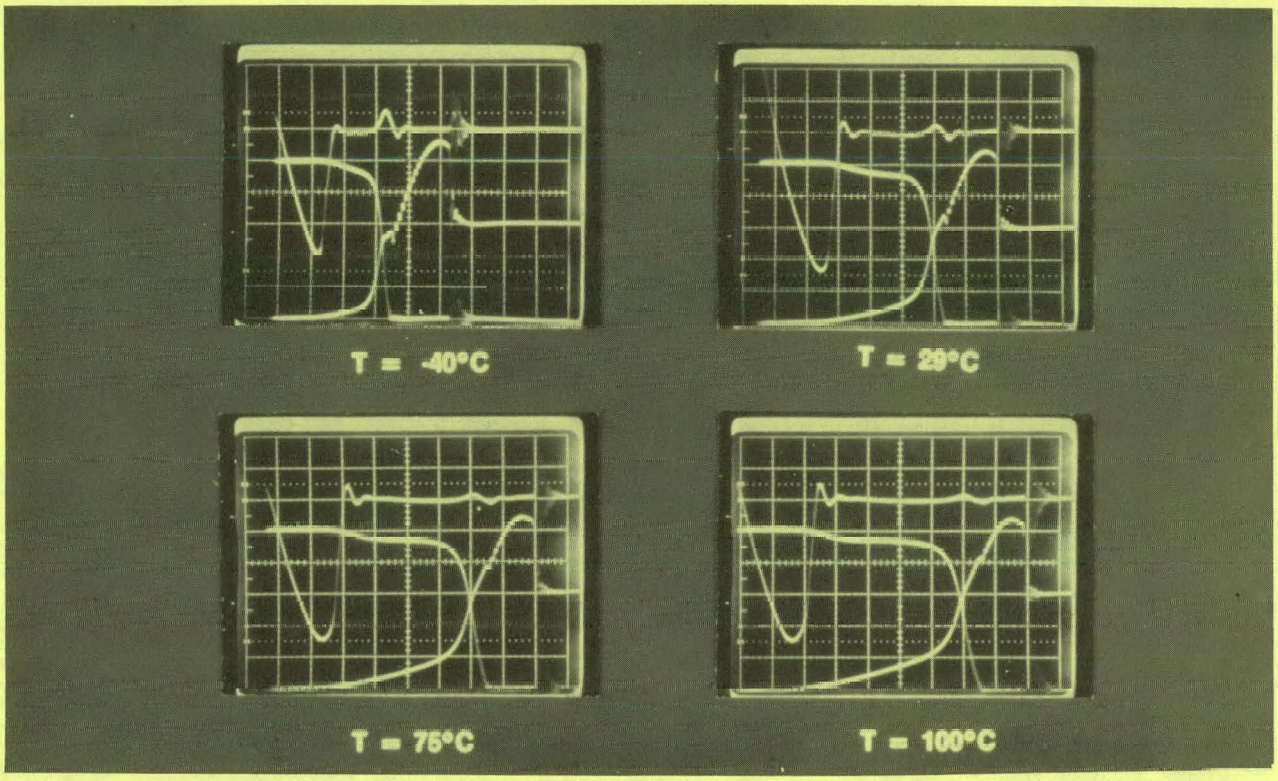


Figure 3.2.9-12. Operation of Power Module in Armature Chopper: $I_C$ = 40 A/cm, $I_B$ = A/cm, $V_{CE}$ = 50 V/cm, $t_C$ = 1 µs/cm, C = 1 µF (Snubber)

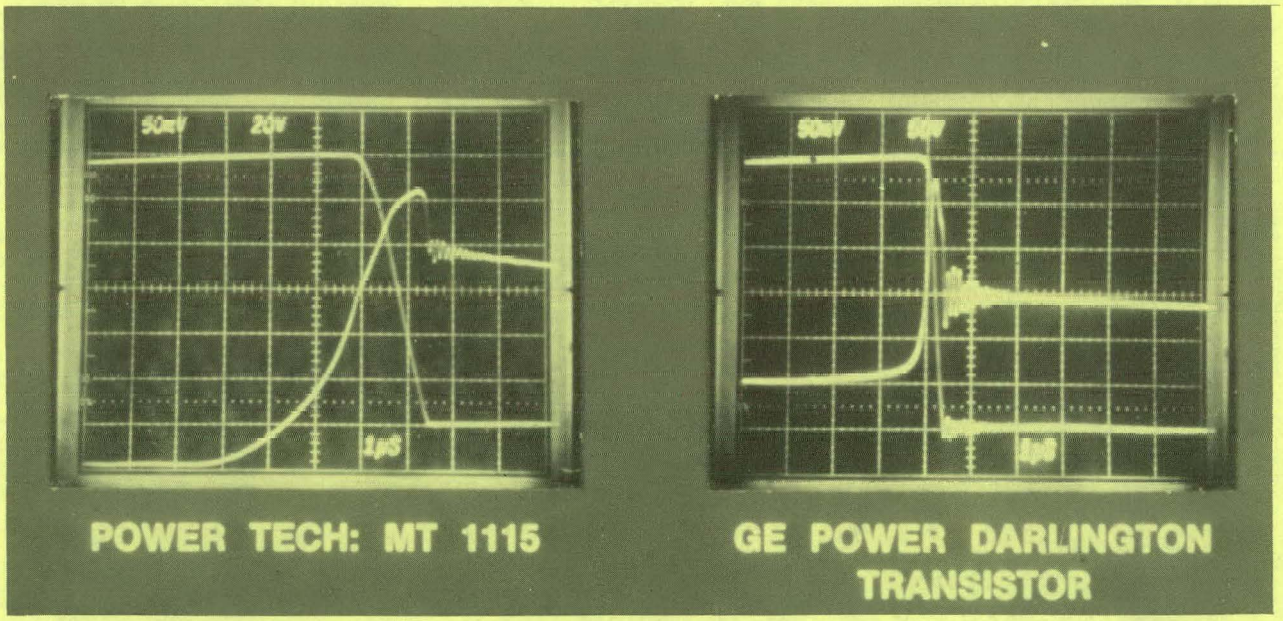


Figure 3.2.9-13. Field Chopper/Battery Charger: $I_C$ = 10 A/cm, $I_B$ = 1 A/cm, $V_{CE}$ = 50 V/cm, t = 1 µs/cm

WBS 3.2.10 Electronics Packaging Subcontract

The electronics packaging subcontract is being performed by General Electric Ordnance Systems, located in Pittsfield, Massachusetts. The objective of the project is to design the mechanical and thermal aspects of the drive subsystem electronics and to fabricate four packaged sets of hardware.

The power conditioning unit (PCU) contains an armature chopper, field chopper/battery charger, logic power supply, and accessory charger. A separate package will contain the microcomputer control unit.

Ordnance Systems has been furnished with schematic circuit diagrams, electrical components, parts lists, environmental specifications, layout constraints, circuit dissipation estimates, and technical guidance as required.

The PCU will have an outward appearance as shown in Figure 3.2.10-1.

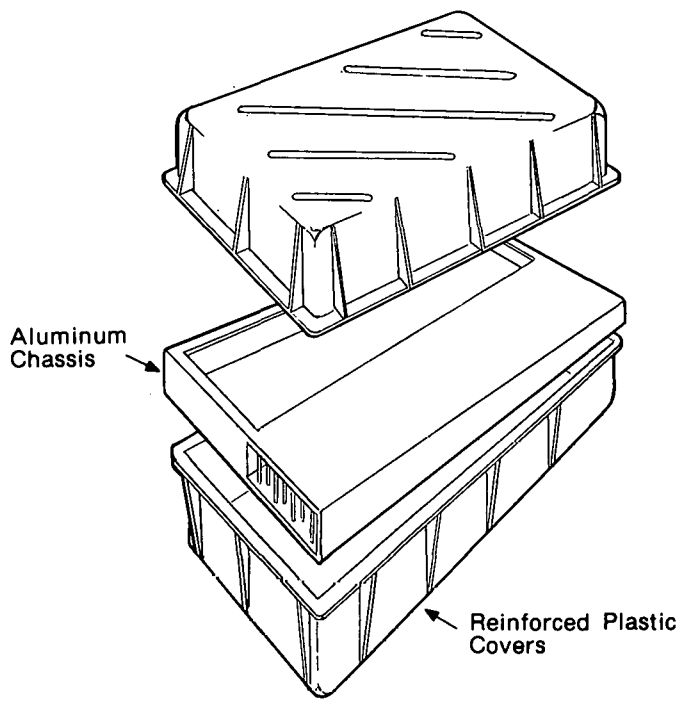


Figure 3.2.10-1. Power Conditioning Unit (PCU)

The unit consists of an aluminum chassis and two reinforced plastic covers. The aluminum chassis is essentially an integral forced-air heat exchanger with a calculated thermal resistance from sink to ambient of 0.024 $^{o}C/W$ at a forced-air condition of 125 $ft^3/min$ having a 1.08 inch $H_2O$ pressure drop. Tables 3.2.10-1 and 3.2.10-2 show these calculations.

# TABLE 3.2.10-1

## HEAT EXCHANGER PRESSURE DROP

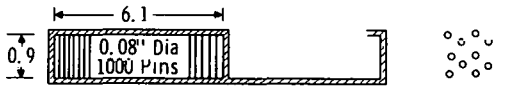


A. TEMPERATURE RISE OF COOLING AIR:

$$T'_{a_R} - T'_{a_R} = q/m\ Cp = 951\ W/125\ \frac{ft^3}{min} \times 0.068\ \frac{lb}{ft^3} \times 7.6\ \frac{W\text{-}min}{lb\text{-}^oC}$$

$$= \boxed{14.72^oC'}$$

B. AIR VELOCITY:

$$V = \frac{Ql}{v} = \frac{125\ ft^3/min \times 1.88\ ft}{0.068\ ft^3} = \boxed{3327\ ft/min}$$

C. REYNOLDS NUMBER:

$$N_R = \frac{V\ D_{e^o}}{u} = \frac{199,620\ ft/hr \times 0.131\ ft \times 0.068\ lb/ft^3}{0.0475\ lb/ft\text{-}hr}$$

$$= \boxed{37,436}$$

D. PRESSURE DROP:

$$H_L = \frac{fLV^2}{D2g} = \frac{12 \times 0.025 \times 9.34\ ft \times (55.45\ ft/sec)^2 \times 0.068\ lb/ft^3}{0.131\ ft\ (64.4\ ft/sec^2) \times 64.2\ lb/ft^3}$$

$$= \boxed{1.08\ in.\ H_2O}$$

WHERE:

$T_{a_R}$ = RAM AIR TEMPERATURE
$D_e$ = EFFECTIVE HYDRAULIC DIAMETER
f = FRICTION FACTOR(DEVELOPED FROM MOODY DIAGRAM)

# TABLE 3.2.10-2

## HEAT EXCHANGER THERMAL RESISTANCE

A. CONDITIONS:

1. 1000 Pins, 0.08"D x 0.9"L
2. AIR FLOW @ 125 cfm (6.1" x 0.9" Duct)
3. Film Temperature = 68.5°C

B. MASS FLOW

$$G = \frac{Q_o}{Ac} = \frac{125 \times 0.064 \times 60}{0.038} = 12,631\ \frac{lb}{hr\text{-}ft^2}$$

C. HEAT TRANSFER COEFFICIENT: (KRAUS)

$$h = 1.4\ \frac{k}{d}\left(\frac{aG}{\mu}\right)^{.28}\left(\frac{Cp\mu}{k}\right)^{.33}$$

$$= \frac{1.4 \times .0172}{0.00067}\left(\frac{0.0067 \times 12,631}{0.049}\right)^{.28}\left(\frac{0.241 \times 0.049}{0.0172}\right)^{.33}$$

$$= \boxed{0939\ \frac{W}{in.^2\text{-}^oC}}$$

D. EFFICIENCY:

$mb = .075\sqrt{4h/kd}$

$\eta$ = 82.5% (KRAUSS; CYLINDRICAL SPINE EFFICIENCY)

E. THERMAL RESISTANCE:

$$\theta = \frac{1}{h\eta S} = \frac{1}{0.0939 \times 0.825 \times 541} = \boxed{0.024\ ^oC/W}$$

The layout of the components mounted on the aluminum casting has been completed. Wire types and wire routing options are now being engineered. Figure 3.2.10-2 shows the PCU casting layout.

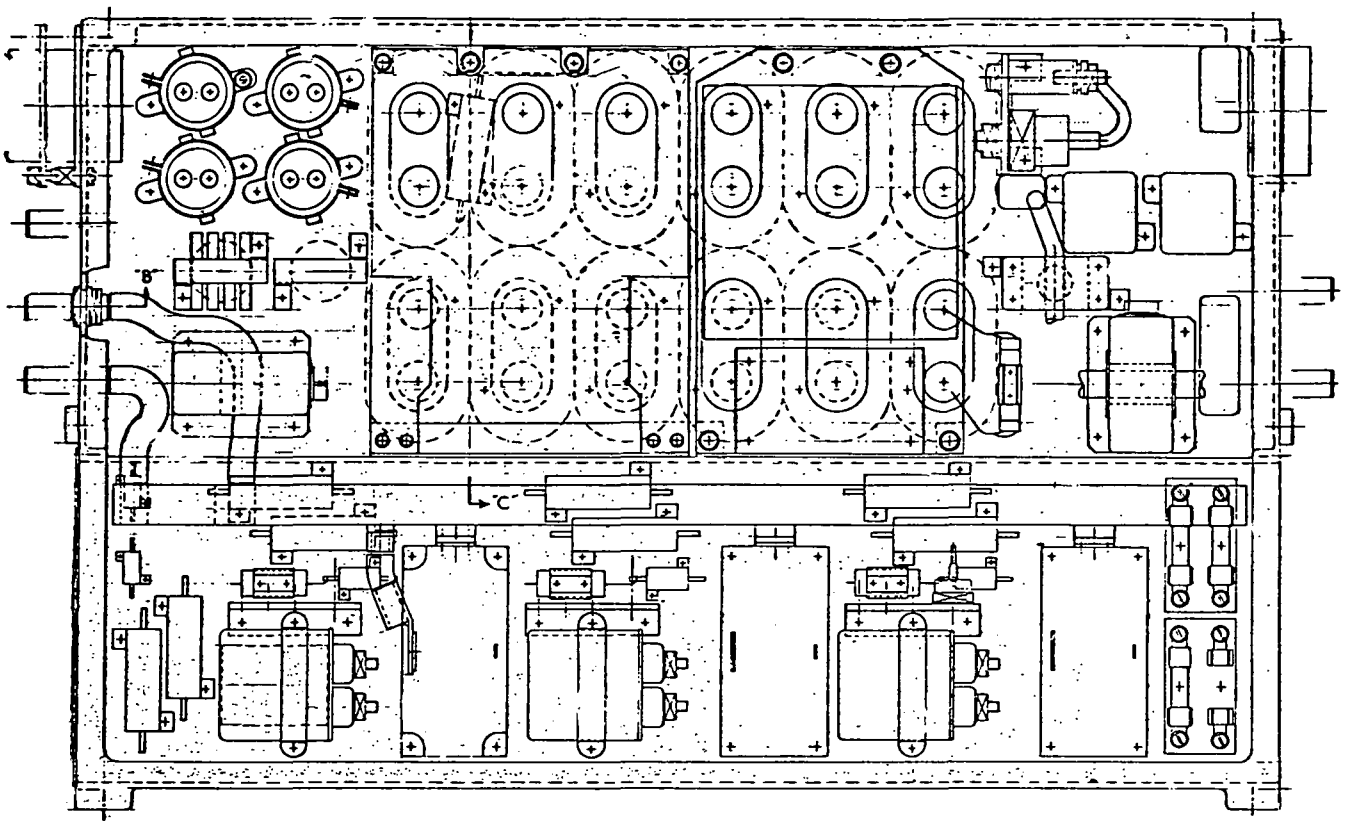

**PRELIMINARY**

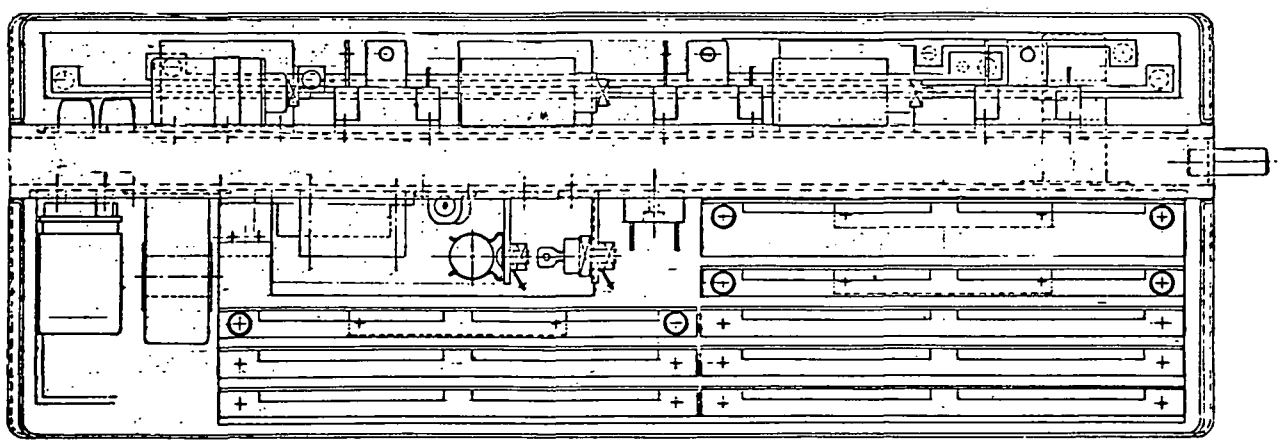

Figure 3.2.10-2. Power Conditioning Unit Layout

Printed circuit board layout work has resulted in the design of nine 5 in x 9 in stack-mounted boards and four smaller casting-mounted boards. The card stack is mounted within the PCU.

All the printed circuit boards for the PCU are scheduled to be completed by the end of June, 1978. Target date for the delivery of the first PCU is July 1978.

The circuit design for the microcomputer will be provided to GE Ordnance Systems in June 1978. Delivery of the first microcomputer is expected by October 1978.

## WBS 3.3 BATTERY SUBSYSTEM

### WBS 3.3.1 Battery Component Design

The design goals and specifications of the propulsion battery, designated EV2-13, are summarized in the Subcontract Statement of Work (SOW) and in Table 3.3.1-1.

TABLE 3.3.1-1

PROPULSION BATTERY GOALS AND SPECIFICATIONS

| Performance | Minimum | Goal |
|---|---|---|
| Performance at 3 h Rate, 5.25 V Cutoff | | |
| Usable Energy (Wh) | 970 | 1031 |
| Weight Energy Density (Wh/lb) | 16 | 17 |
| Volume Energy Density ($Wh/in^3$) | 1.5 | |
| Peak Power Density at Full Charge (W/lb) | 100 | |
| Cycle Life - 70% Depth of Discharge at 3 h Rate (number of cycles) | 500 | |
| **Size** | **Maximum** | |
| Length (in.) | 10-3/8 | |
| Width (in.) | 7-3/16 | |
| Height (in.) | 11-1/8 (but lower at sides of tunnel) | |

The battery had to be designed within the external length and-width dimensional constraints of a standard golf car battery (BCI group size GC2). The height dimension was limited by the tunnel design, which allowed for potential additional height (over that of a standard golf car battery) except near the sides of the tunnel. The battery was to be nominally 6 volts. Eighteen batteries would be connected in series to provide a 108 V battery pack. The battery was also to incorporate a semiautomatic, single-point watering system.

Globe investigated two general approaches to maximizing the performance of the lead-acid system within the golf car envelope. The first approach encompassed computer-assisted optimization of the battery design within the existing golf-car battery cell configuration and orientation. The optimization program included:

- Grid and top lead efficiency through establishment of minimum weights with ideal lead distribution.

- Positive-to-negative active material ratios and total weights.
- Electrolyte to active material ratios.
- Active material and electrolyte distribution within the cell.

The second approach involved not only a complete optimization program but also an effort to minimize the plate design restrictions imposed by the conventional golf-car battery cell configuration. From previous work on computerized electric vehicle battery design optimization, Globe has determined that there are ideal basic plate design characteristics. These characteristics include ranges of plate apparent surface area and ranges of width-to-height aspect ratio. Existing golf car battery plates are significantly below the desired ranges in both area and aspect ratio. Ideal aspect ratios and surface areas cannot be achieved within the golf car battery envelope, but improvements in each can be made if the cells are rotated 90° from their normal orientation.

Rotation of the cells by 90° dictated a new terminal location and a 90° rotation of the vent strip which is used in this battery for both the venting and watering (water top-off) functions. The relocation of the vent strip has definite advantages for the selected tunnel configuration, which provides for a side-by-side battery layout as shown in Figure 3.3.1-1.

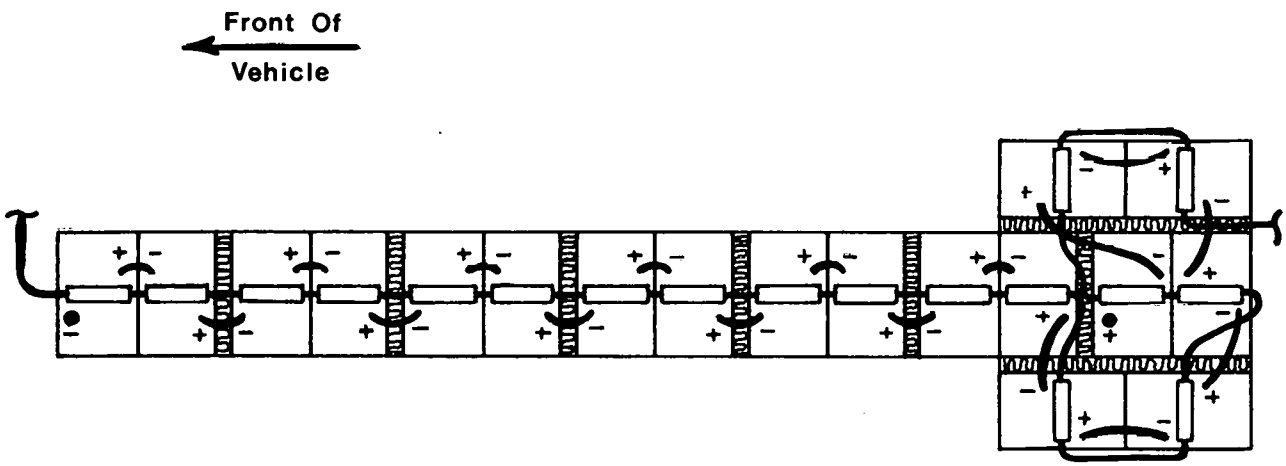


Figure 3.3.1-1. Battery Pack Layout

The 90° rotated design was chosen over the conventional layout for two reasons:

- Lighter weight for equivalent performance
- Simplified and lighter plumbing for the watering/vent system

A cutaway view of the EV2-13 is shown in Figure 3.3.1-2. A high-profile cover design was chosen to accommodate increased volumes of active material and electrolyte, which provide additional energy storage capacity. The stepped cover design shown in Figure 3.3.1-2 was necessary in order to provide a high-profile cover which would fit in the battery tunnel.

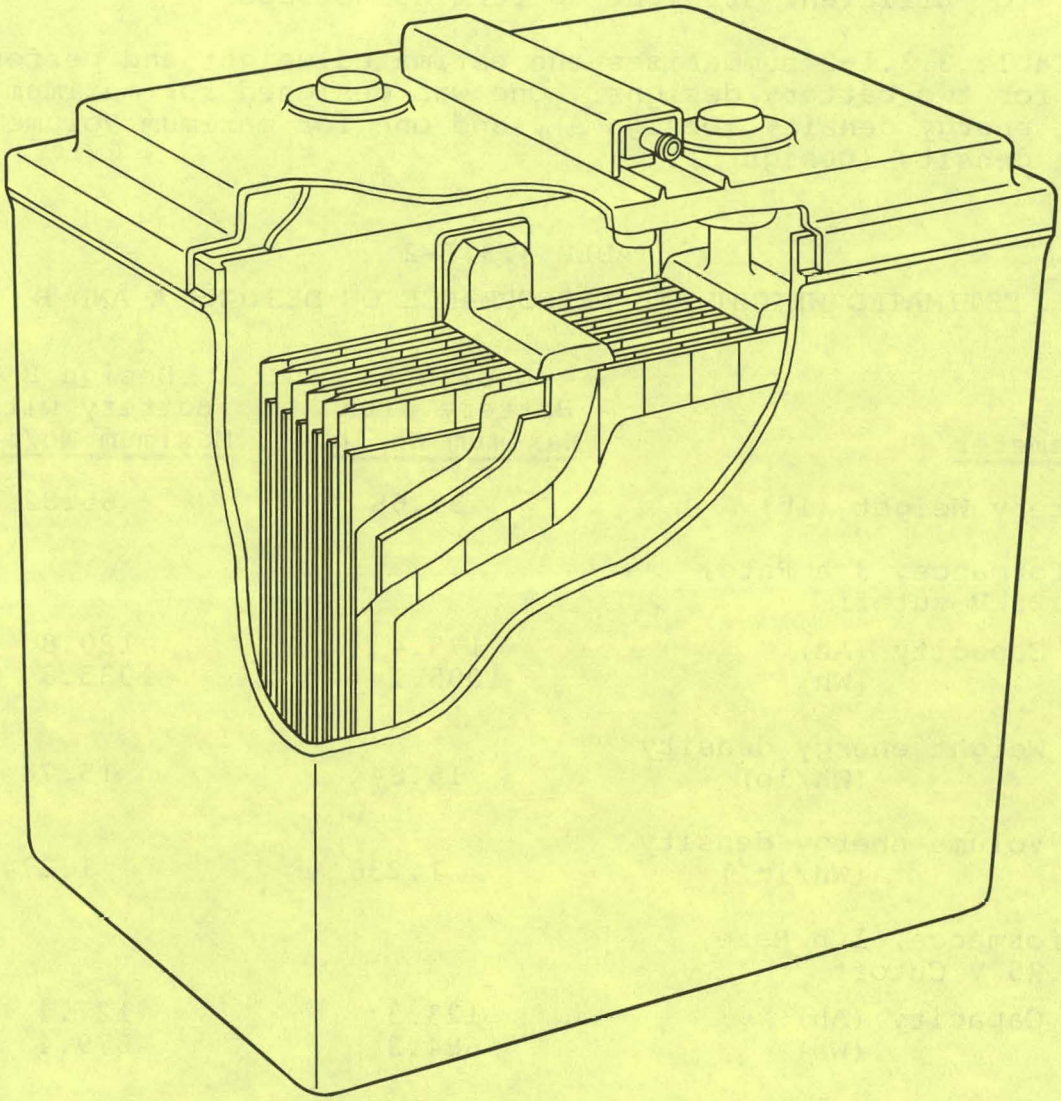

Figure 3.3.1-2. Cutaway View of EV2-13 Propulsion Battery

Other features of the battery can be seen in Figure 3.3.1-2:

- Thin-walled, heat-sealed polypropylene container
- Low-resistance, through-the-partition intercell welds
- Removable vent cap with semiautomatic watering design

- Different sized positive and negative terminals
- Designed so that acid will not leave cell unless battery is inclined more than 30°
- Low-resistance, radial-design grids with near-center lugs
- Envelope-type separators with glass mat for long battery life
- Efficient straight-up terminal straps

Table 3.3.1-2 summarizes the estimated weight and performance for two battery designs. One was designed for maximum weight energy density (Design A), and one for maximum volume energy density (Design B).

TABLE 3.3.1-2

ESTIMATED WEIGHT AND PERFORMANCE OF DESIGNS A AND B

| Parameter | Design A Battery with Maximum Wh/lb | Design B Battery with Maximum $Wh/in^3$ |
|---|---|---|
| Battery Weight (lb) | 59.68 | 65.82 |
| Performance, 3 h Rate, 5.25 V cutoff | | |
| Capacity (Ah) | 175.4 | 180.8 |
| (Wh) | 1005.1 | 1035.8 |
| Weight energy density (Wh/lb) | 16.84 | 15.74 |
| Volume energy density ($Wh/in^3$) | 1.236 | 1.274 |
| Performance, 1 h Rate, 5.25 V Cutoff | | |
| Capacity (Ah) | 123.3 | 127.4 |
| (Wh) | 684.3 | 679.4 |
| Weight energy density (Wh/lb) | 11.47 | 10.32 |
| Volume energy density ($Wh/in^3$) | 0.842 | 0.836 |

Figures 3.3.1-3, -4, and -5 show additional estimated performance characteristics for the two designs. Based on this estimated data, General Electric selected Design A, which was designed under the maximum weight-energy-density philosophy. The advantages of Design A are:

- o Lower weight and higher weight energy density (Table 3.3.1-2)
- o Better performance at high rates (Figure 3.3.1-4)
- o Increased resistance to electrolyte freezing at low temperatures (Figure 3.3.1-5)

Table 3.3.1-3 summarizes the estimated battery weight and performance and compares the estimates with the SOW specifications. The values are close to those for Design A, discussed previously. The differences are due to a design refinement and

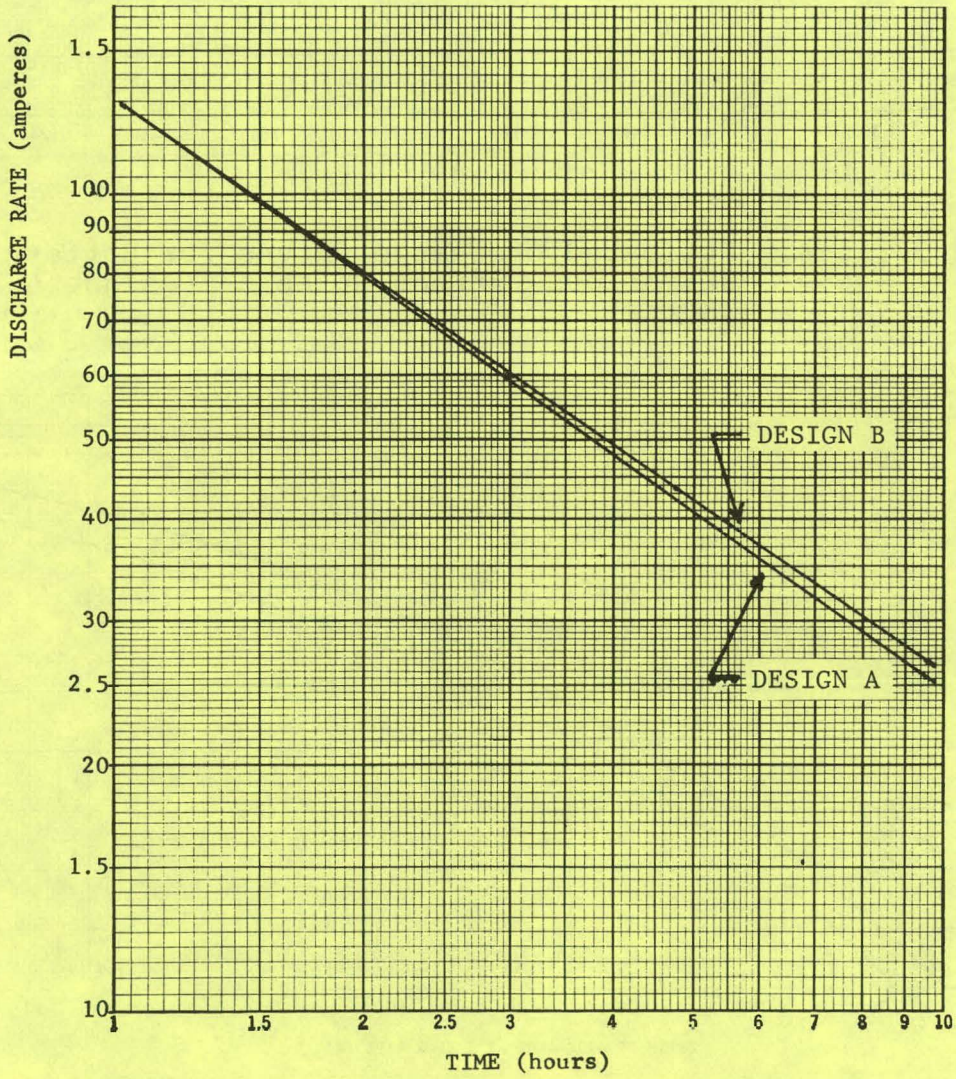


Figure 3.3.1-3. Estimated Peukert Curves for Battery Designs A and B (80 °F)

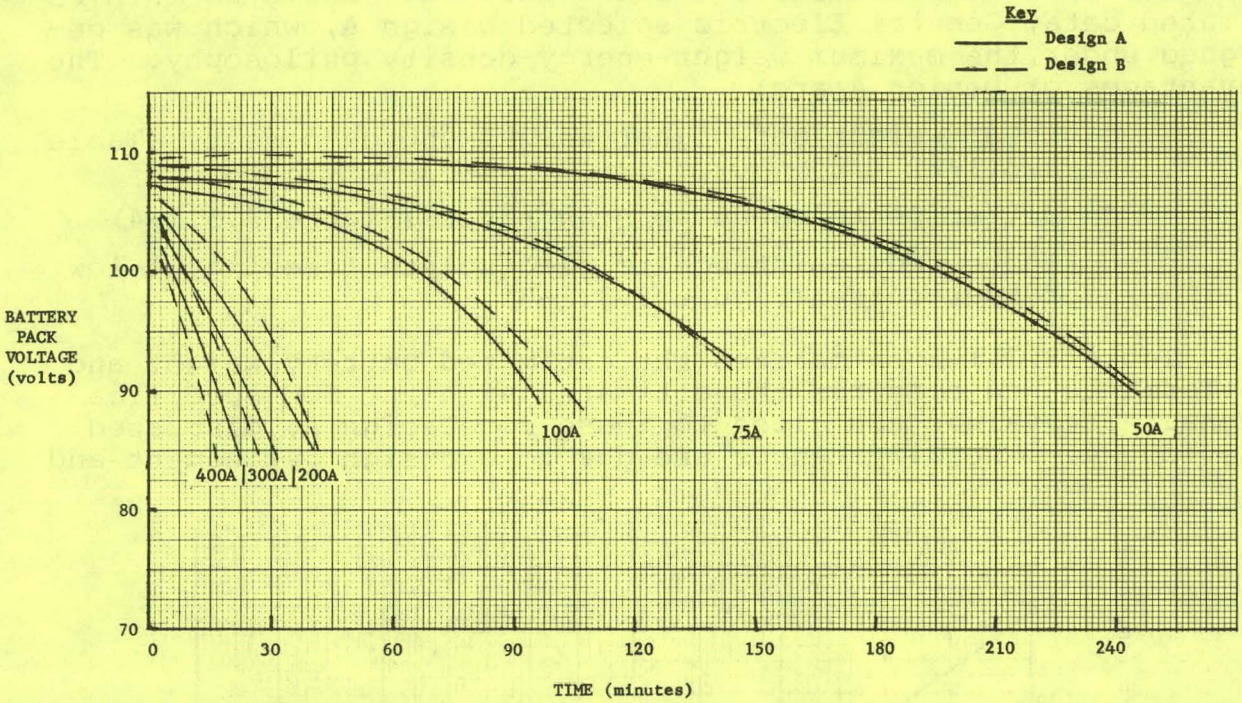


Figure 3.3.1-4. Estimated Discharge Curves for Battery Pack at Various Current Rates -- Designs A and B (80 °F)

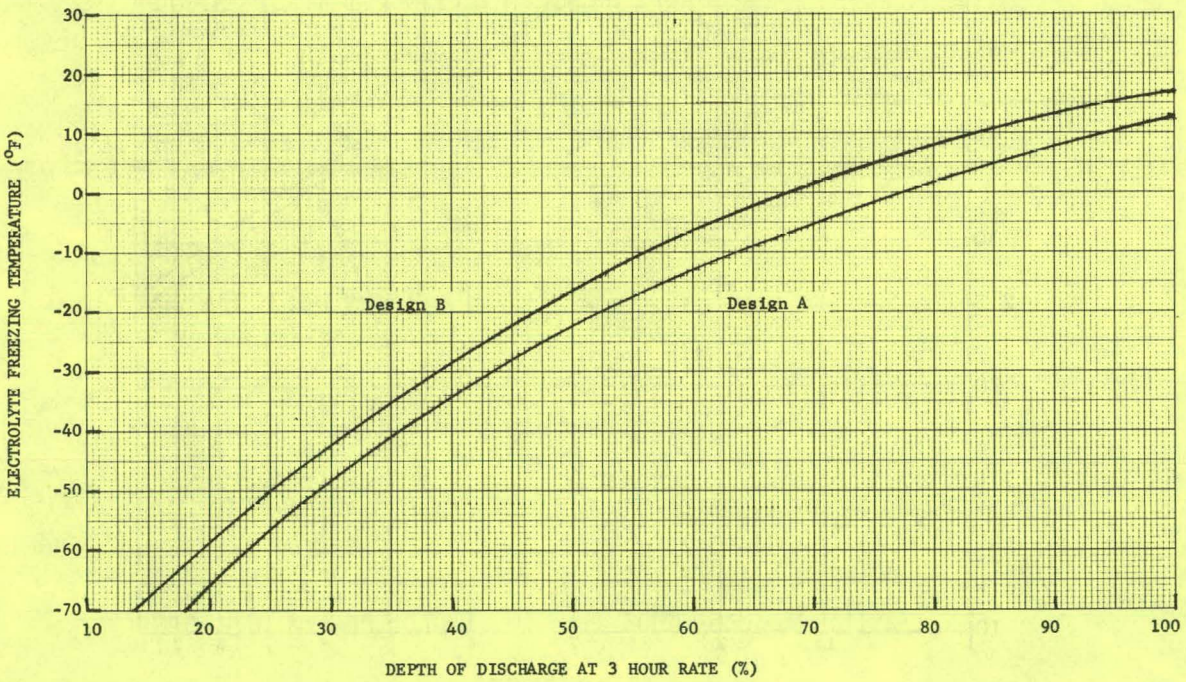


Figure 3.3.1-5. Estimated Electrolyte Freezing Temperature as a Function of Depth of Discharge -- Designs A and B

TABLE 3.3.1-3

ESTIMATED EV2-13 WEIGHT AND PERFORMANCE
VERSUS SOW SPECIFICATIONS

| Parameter | Estimate | Specification (Minimum) |
|---|---|---|
| Battery Weight (lb) | 60.65 | |
| Performance, 3 h Rate, 5.25 V Cutoff | | |
| Capacity (Ah) | 174.1 | |
| (Wh) | 997.5 | 970 |
| Weight energy density (Wh/lb) | 16.45 | 16 |
| Volume energy density (Wh/in$^3$) | 1.35 | 1.5 |
| Performance, 1 h Rate, 5.25 V Cutoff | | |
| Capacity (Ah) | 133.1 | |
| (Wh) | 738.8 | |
| Weight energy density | 12.18 | |
| Volume energy density | 1.00 | |
| Peak Power Density (W/lb) | 100 | 100 |
| Cycle Life, 70% Depth of Discharge at 3 h Rate (number of cycles) | 500 | 500 |

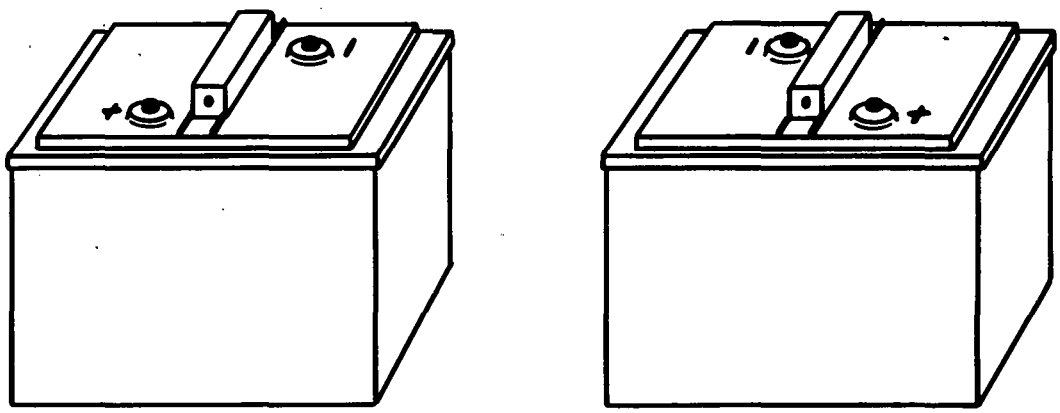


Figure 3.3.1-6. Propulsion Battery (EV2-13) -- External View of Two Types

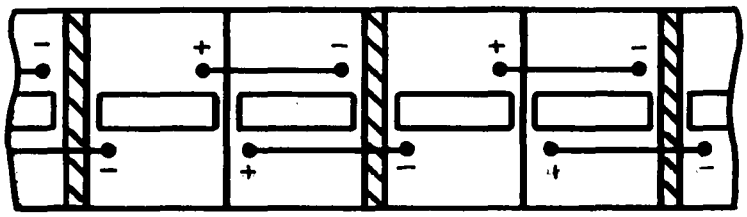

Cabling With One Battery Type

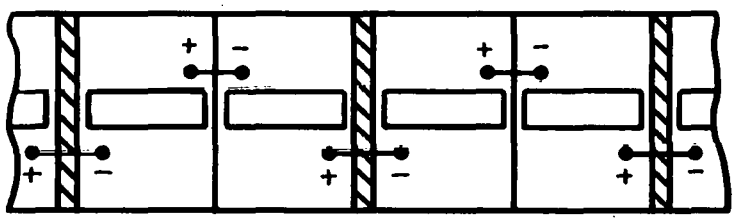

Cabling With Two Battery Types (9 of each)

Figure 3.3.1-7. Advantages of Having Two Battery Types: Less Cable Is Required, Resulting in: (1) Lower Cable Weight (-2 lb) and (2) Lower Circuit Resistance and Inductance

a more accurate estimate of component weights. As shown in Table 3.3.1-3, it is estimated that all of the SOW specifications will be met or exceeded with the exception of the volume energy density. This is because the specified value was established without consideration for the extra battery volume associated with the semiautomatic watering/venting system.

The 18-battery pack will contain nine LHF and nine RHF batteries, as shown in Figure 3.3.1-6. The advantages of having two battery types are illustrated in Figure 3.3.1-7. Table 3.3.1-4 is a complete list of the drawings which comprise the EV2-13 product drawing package.

The battery design was completed about 1-1/2 months behind the original schedule, because of the alternative approaches investigated and a slight delay in receipt of the contract. A greater number of approaches were considered than had been originally planned.

TABLE 3.3.1-4

LIST OF EV2-13 PRODUCT DRAWINGS -- FEBRUARY 27, 1978

| Drawing No. | Title | Dwg. Date | Last Revision |
|---|---|---|---|
| 77173-D | Positive Grid | 10-27-77 | None |
| 77161-D, Sh 3 | GE Positive Grid Mold | 11-01-77 | None |
| 77172-D | Inside Negative Grid | 10-26-77 | None |
| 77159-D, Sh 3 | Inside Neg. Grid - Wire & Frame | 10-21-77 | None |
| 77171-D | Outside Negative Grid | 10-26-77 | None |
| 77160-D, Sh 3 | Outside Neg. Grid - Wire & Frame | 10-21-77 | None |
| 77-175-B | Envelope Separator Blank | 10-11-77 | None |
| 77174-C | Internal Post & Strap | 10-11-77 | 1-3-78 |
| 77167-D | Container | 10-07-77 | None |
| 77168-D | Cover | 10-07-77 | 2-7-78 |
| 77169-D | Vent & Watering Cap | 10-12-77 | 2-13-78 |
| 77170-C, Sh 1 | Cover - Vent & Watering Cap | 10-12-77 | 2-14-78 |
| 77170-B, Sh 2 | Cover - Top View, Vent & Watering Cap | 12-28-77 | None |
| 77166-D | GE Battery Assembly | 10-10-77 | None |
| 77188-D | EV Battery | 11-16-77 | None |
| 77180-D | Battery Connection & Water Flow | 11-07-77 | None |
| 77179-B | Terminal Connecting Strap | 11-02-77 | 11-28-77 |
| 77195-A | Terminal Post - GE, EV | 11-28-77 | None |
| 77196-A | Terminal Post & Strap Assembly | 11-28-77 | None |
| 77202-B | Connector Shield | 12-15-77 | None |

WBS 3.3.2 Tooling Development

The status of tooling and equipment modifications is summarized in Table 3.3.2-1.

TABLE 3.3.2-1

STATUS OF EV2-13 TOOLING - APRIL 28, 1978

| Item | Design Complete | Fabrication in Progress | Estimated Completion Date |
|---|---|---|---|
| Container Mold Modifications | x | x | 8-11-78 |
| Cover Mold | x | x | 6-26-78 |
| Watering/Vent Mold | x | x | 5-17-78 |
| Watering/Vent Heat Seal Tooling | | | |
| Platen | x | | Complete |
| Backup plate | x | | Complete |
| Spacers | | | As Required |
| Grid Molds | x | | Complete |
| Grid Trim Tooling | x | | Complete |
| COS Modifications | | | |
| Molds | x | | Complete |
| Other | x | x | 5-12-78 |
| Container Punch Tooling | x | | Complete |
| Cover Heat Seal Platen | x | | Complete |
| Heat Seal Cover Backup Plate | x | | Complete |
| Post Burn Tooling | x | x | 5-15-78 |
| Paster Tooling | | | |
| Orifice plate | x | | Complete |
| Feeder modifications | x | x | 5-3-78 |
| Separator Enveloper | x | x | 5-3-78 |

The main item of concern is the estimated delivery date for the container injection mold tooling. This date has been extended past the original estimate because of the extension of the product design phase and a delay encountered in processing the ordering paperwork by the supplier.

WBS 3.3.3 Battery Fabrication

The acid, separators, lead materials, and 40 special cell containers required for cell construction are on hand. All of the grids have been cast, trimmed, and allowed to age-harden. The cells were completed by mid-May.

Two preliminary test cells have been completed. These cells contain grids slightly out of specification, which were cast before the grid molds were corrected. The plates were hand pasted in the laboratory and the straps were hand burned to the plates. These two cells were used for preliminary testing.

Delivery of the first set of batteries has been changed from June 1, 1978 to mid-August 1978 at the earliest. The critical item affecting the delivery date of this first set of EV2-13 batteries is the container injection mold tooling. The first battery set will consist of 22 batteries and the associated cabling hardware.

The two battery sets for the integrated test vehicles will consist of 22 batteries per set plus all of the associated watering/venting system and cabling system hardware. Delivery is scheduled for October 1, 1978 at the latest.

Two sets of spare batteries, consisting of 22 batteries per set plus the cabling system hardware, will be delivered by December 1, 1978. These spares will be used during the vehicle testing phase, to minimize the loss of time due to recharging of batteries.

WBS 3.3.4 Development Testing

The primary purpose of the testing performed under this task is to determine if the EV2-13 batteries comply with the performance specifications in the Statement of Work. Additional testing related to battery charging, fuel gauge, mathematical battery modeling, etc., will be performed under WBS 3.3.5 "Technical Support." Much testing related to these items has already been performed on standard Globe golf car batteries.

Testing of EV2-13 cells began in April 1978. Test results for the two preliminary EV2-13 test cells are summarized in Table 3.3.4-1. These two cells have slightly out-of-specification grids and hand-pasted plates. The test results are within 2 % of the previously estimated values.

TABLE 3.3.4-1

TEST RESULTS FOR TWO PRELIMINARY EV2-13 TEST CELLS

| | Cell Results | Cell Estimates |
|---|---|---|
| Performance, 3 h Rate, 1.75 V Cutoff | | |
| Capacity (Ah) | 172.5[1] | 174.1 |
| (Wh) | 335.7[1] | 332.5 |
| Weight energy density (Wh/lb) | 16.51[1] | 16.45 |
| Performance, 1 h Rate, 1.75 V Cutoff | | |
| Capacity (Ah) | 130.2[2] | 133.1 |
| (Wh) | 245.9[2] | 246.3 |
| Weight energy density (Wh/lb) | 12.10[2] | 12.18 |

Notes: (1) Average for two cells (test cycles 11 and 13)
(2) Average for two cells (test cycles 12 and 21)

Testing of EV2-13 batteries will commence in August or September 1978. A report detailing the results of the battery testing will be submitted to General Electric by November 1, 1978. Cycle life testing will not be completed in time for the report; the test results will be reported separately to General Electric after the testing is completed.

The development of the Battery Subsystem Test Plan is in progress. The plan will describe in detail the testing necessary to determine compliance with the Statement of Work specifications. A statistical multiple sampling plan, described in MIL-STD-105D will be used. Three tests will be performed as briefly described below. All of the specified performance characteristics can be calculated from the resulting test data. The term "unit" below refers to a cell or a battery. Batteries will be tested as soon as they are available.

Discharge Test at 3 Hour Rate

- Sample -- 9 units
- Test Procedure -- After rate is established, conditioned unit is discharged at the constant-current 3 hour rate at 80 °F. The time required to reach 1.75 and 1.3 V/cell will be recorded.

Peak Power Test

- Sample -- 9 units
- Test Procedure -- Conditioned unit is discharged at a high rate (to be determined) at 80 °F. Current and voltage are recorded as a function of

time. Power is equal to the product of voltage and current at any time. Peak power is the maximum power observed during the test. It is likely to be observed at less than one second after the start of the test.

Cycle Life Test

- Sample -- 12 units
- Test Procedure -- Conditioned unit is discharged at the constant-current 3 hour rate at 80 °F for 2.1 hours (70% depth of discharge), then recharged. Repeated until voltage after discharge is less than 1.75 V/cell. At this point, unit is considered to have failed; it can no longer supply 70 % of its original ampere-hour capacity at the 3 hour rate. Record number of cycles to failure.

WBS 3.3.5 Technical Support

Work performed and reported under the Technical Support task covers studies directed by the General Electric Company.

Charging

Globe's initial propulsion-battery charging recommendation was to limit the maximum charging voltage to a temperature-corrected value, to be specified after EV2-13 cell testing. It was estimated that this value would be close to 2.45 V/cell at 80 °F. Globe recommended that this voltage limit be corrected by 0.004 V/cell/°F. For every degree above 80 °F, the maximum cell charging voltage should be 0.004 volt less than the value specified for 80 °F; and for every degree below 80 °F, the maximum cell charging voltage should be 0.004 volt greater than the value specified for 80 °F. These recommendations were based on Globe testing performed prior to the contract. Charging voltages in excess of the specified maximum would be harmful to the batteries, resulting in decreased capacity and cycle life.

All of the charging experiments described below were performed on standard Globe golf car batteries (type GC2-19). Additional testing will be required when EV2-13 cells are available.

The first charging experiments provided typical battery voltage and current profiles during charging. A constant-voltage charging scheme with a current limit was used. A battery which was 80 % discharged at the three hour rate was charged at 80 °F with a current limit of 15 amperes. Similar tests were conducted using current limits of 20, 25, and 30 amperes. Figure 3.3.5-1 is typical of the data which resulted from this testing.

For minimum charging time a constant-voltage, current-limited scheme was recommended. It was pointed out that, as the current limit is reduced as a result of electrical service limitation,

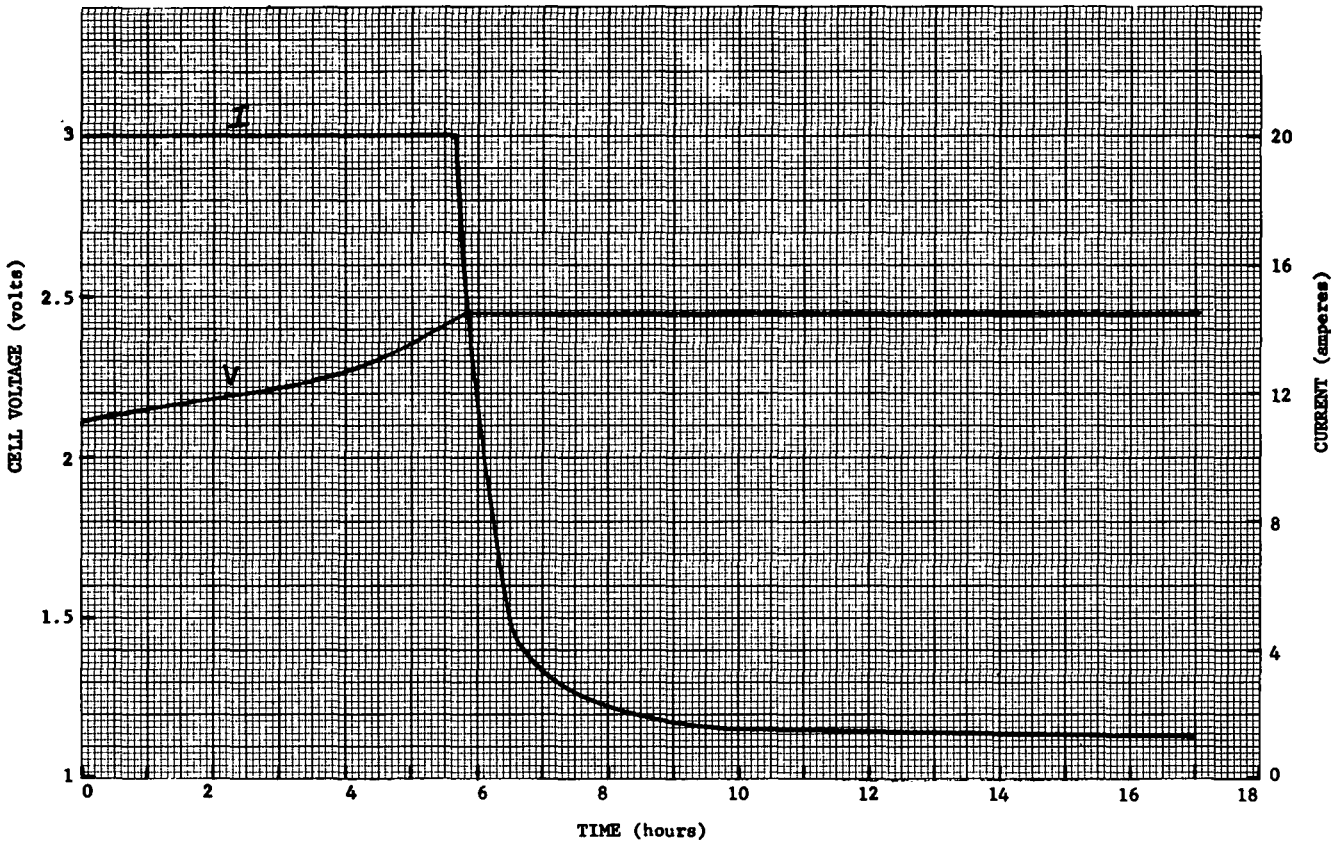


Figure 3.3.5-1. Voltage and Current Profile During Constant-Voltage, 20 A Current-Limited Charge of a GC2-19 Battery at 80 °F (Prior Discharge - 80 % at 3 h Rate)

the time required for charging must be extended. Globe recommended, for maximum battery life, daily charge of the batteries only up to the 96 to 98 % state of charge, and an equalization charge once every two weeks. Original time estimates for the daily charge ranged from 4.1 to 8.5 hours, and for the equalization charge from 20 to 28 hours.

Because implementation of a constant-voltage, current-limited scheme would be difficult, a number of stepped-current charging schemes were investigated. The initial currents of 24 A and 8 A correspond to estimates of the maximum charging current available from 110 V household circuits of 30 A and 15 A respectively.

Table 3.3.5-1 summarizes the results of the studies. The chosen charging scheme, $V_{limit} - V_{min}$, is essentially a modification of the 24-12-6-3-1.5 ampere stepped-current scheme. It is estimated that the daily charge would bring the pack up to the 96.5 % state of charge (basis: 3 h rate). The equalization charge (once every two weeks) should bring the pack up to 100 % state of charge while also producing the chemical effects that are necessary to keep the battery in good condition. Figure 3.3.5-2 shows

TABLE 3.3.5-1

CHARGING TIME ESTIMATES FOR GC2-19 BATTERIES
DISCHARGED 80 % AT THE 3 HOUR RATE

| Temperature ($^{o}$F) | Charging Scheme | Estimated Charging Time (h) Regular | Equalization |
|---|---|---|---|
| 80 | Constant-Voltage, 48 A Limit | 6-7 | 13-16 |
| | Constant-Voltage, 24 A Limit | 8.7-9.2 | 18.5-19 |
| | Stepped-Current 24-20-16-12-8-6-4-3-2 A | 9.5-10 | |
| | $V_{Limit} - V_{Min}$, 24 A Limit | 9.5-10 | |
| | Stepped-Current 24-12-6-3-1.5 A | 10.5-11* | 22.5-23 |
| | Stepped-Current 8-4-2-1.5 A | 19-21 | 31-33 |
| 35 | Stepped-Current 24-12-6-3-1.5 A | 11.5-12 | |
| 0 | Stepped-Current 24-12-6-3-1.5 A | 15-15.5 | |

*If batteries are only 40 % discharged, charge will take 1 to 2 hours less time.

the estimated state of charge of the pack as a function of charging time for the 24-12-6-3-1.5 A scheme at 80 $^{o}$F, assuming an 80 % discharged pack of GC2-19 batteries at the start of charging. This graph can be used to estimate the state of charge of the pack if the charging cycle is not allowed to go to completion.

Two other observations can be made from Table 3.3.5-1:

- Low temperatures have an adverse effect on charging time. Preliminary tests at -15$^{o}$ indicate that charging will be extremely inefficient and the charging times will be long. The inefficiency is due to the fact that a much greater portion of the energy input is wasted on electrolysis of water. There are not sufficient data at this time to estimate charging times.
- There is a definite time advantage in having a charging circuit capable of supplying higher currents (48 A vs 24 A or 8 A).

Battery Temperature Control

Figure 3.3.5-3 provides an overview of the effect of temperature on battery performance. The temperature at which the elec-

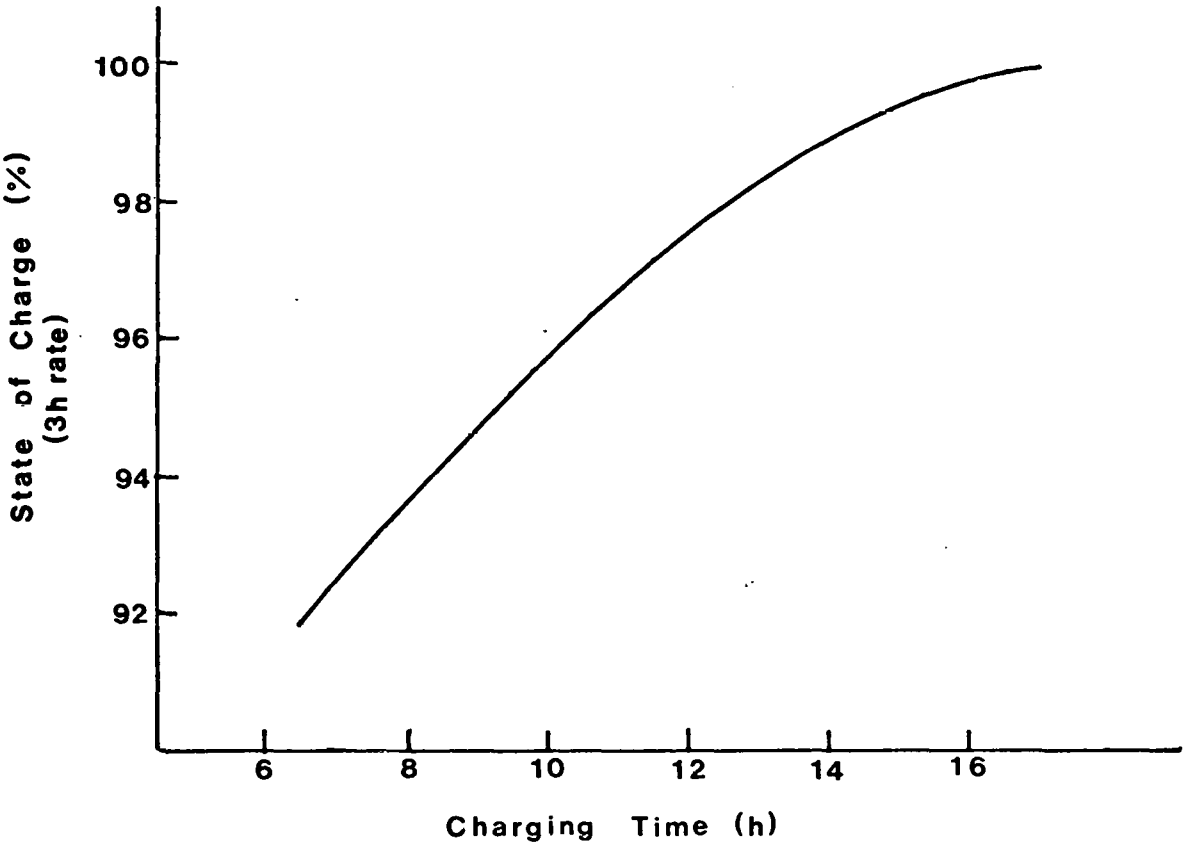


Figure 3.3.5-2. Final State of Charge vs Charging Time (Note: 80 % Discharged Pack, 24-12-6-3-1.5 A Scheme, GC2-19, 80 $^{o}$F)

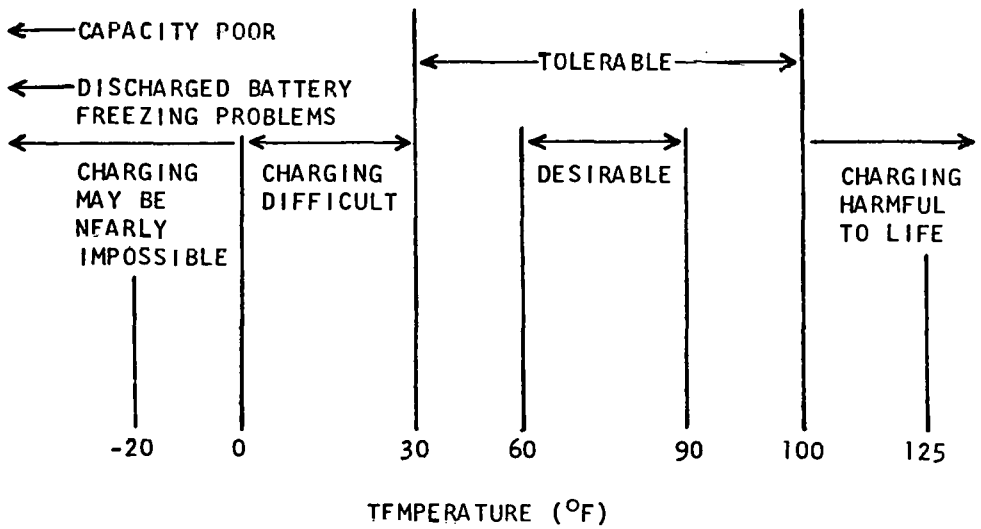


Figure 3.3.5-3. Overview of Effect of Temperature

trolyte of the EV2-13 will freeze is a function of the concentration of the electrolyte, which is a function of the depth of discharge; the higher the depth of discharge, the higher the freezing temperature. The curve for Design A in Figure 3.3.1-5, which was previously discussed, provides a good estimate of the freezing temperature of the electrolyte as a function of depth of discharge. As shown, electrolyte freezing becomes a concern below 20 °F if the battery is fully discharged at the 3 hour rate.

The effect of temperature on the capacity of the EV2-13 battery can be estimated by referring to Figure 3.3.5-4, which was prepared specifically for Design A. As an example, it is estimated that the battery at 0 °F will be able to deliver 60 % of the capacity it could deliver at 80 °F at the one hour rate.

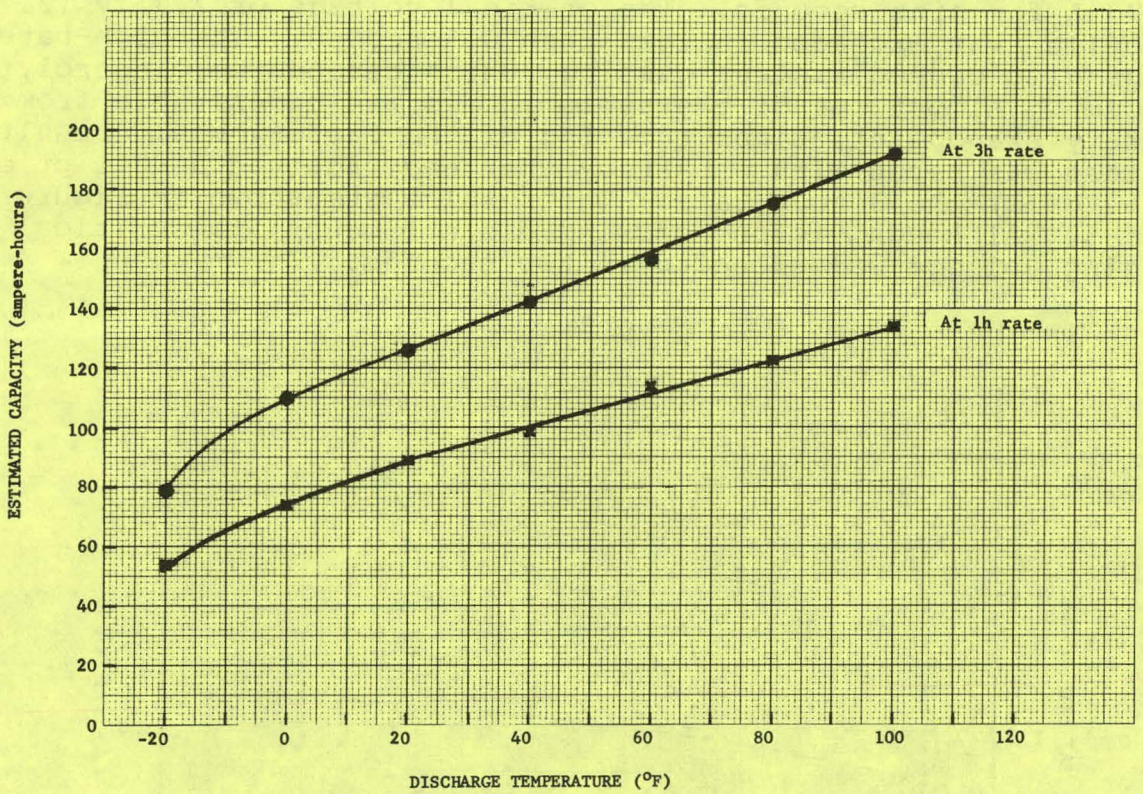


Figure 3.3.5-4. Effect of Temperature on Capacity of GE EV Battery - Design A

Temperatures in excess of 100 °F, especially during charging, will shorten the cycle life of the battery. Elevated temperatures have a number of adverse effects on battery life. It is believed that the worst effect is that positive grid corrosion, which is one of the failure modes for lead-acid batteries, is

greatly accelerated at elevated temperatures. For example, in laboratory tests the grid corrosion rate was found to increase an order of magnitude with a temperature increase from 90 to 120 °F. The corrosion rate jumped another order of magnitude with a temperature increase from 120 to 150 °F.

On the basis of tradeoff studies by General Electric, it was decided not to employ active battery temperature control in the Near-Term Electric Vehicle. The battery compartment will be insulated to limit temperature excursions.

## Regenerative Braking

Globe's voltage limit recommendation for regenerative braking is the same as the charging recommendation: 2.45 V/cell at 80 °F, which will be verified by EV2-13 cell testing.

A battery which was only slightly discharged was subjected to 400 A for nine seconds. The critical voltage of 7.35 V (2.45 x 3 cells) was exceeded in less than 0.5 second. The high-rate charge also caused violent gassing, which caused the electrolyte to foam up almost out of the cells. This was undesirable from a safety standpoint, since shorting of the battery could result. The test was rerun with a battery that had received a 40 % prior discharge at the 3 hour rate. The results are shown in Figure 3.3.5-5. Although violent gassing did not occur, the critical charging voltage was exceeded in two seconds.

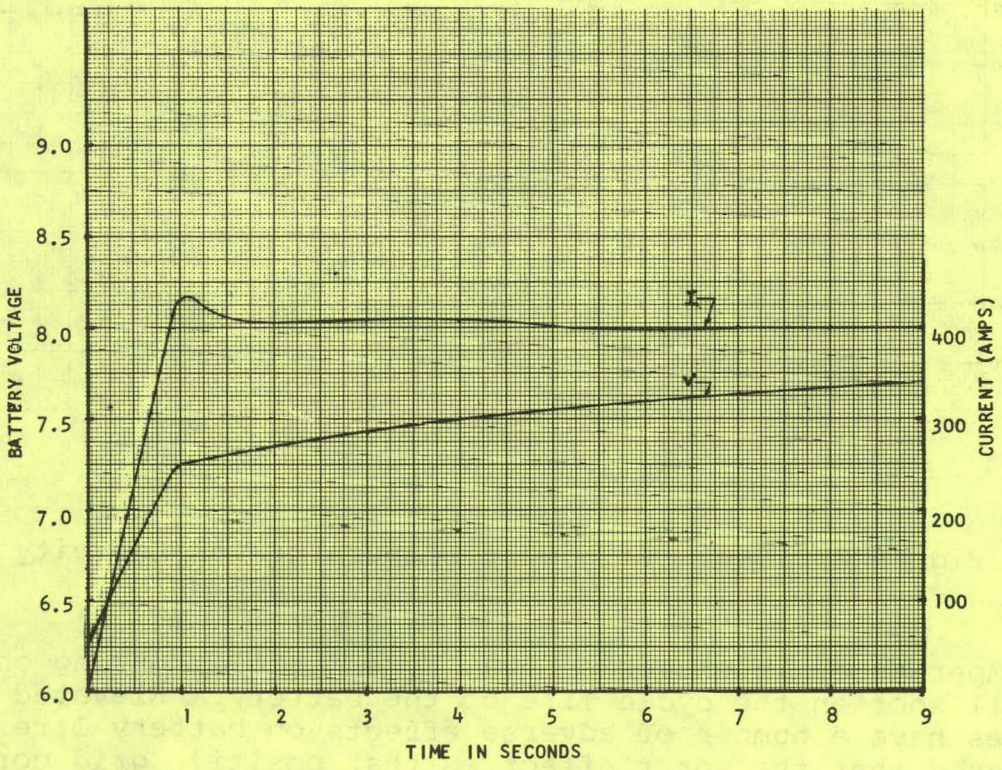


Figure 3.3.5-5. 400 A Charge of GC2-19 Battery -- Prior Discharge, 40 % at 3 Hour Rate, 80 °F

Curves similar to Figure 3.3.5-5 were obtained for all of the specified combinations of current and state of charge. The results of the tests, conducted at 80 °F, are summarized in Table 3.3.5-2. As shown by the stepped line in the table, the current that the battery will accept without exceeding the critical voltage is a function of the state of charge of the battery. Table 3.3.5-3 shows the results of similar tests performed at 3 °F.

TABLE 3.3.5-2

REGENERATIVE BRAKING - BATTERY DATA (80 °F, GC2-19)
Globe-Union, Inc., October 24, 1977

| Prior Discharge | State of Charge | Battery Voltage After 9 Second Charge (volts) Charge Rate (amperes) 400 | 300 | 250 | 200 | 150 | 130 | 100 | 75 | 50 | 25 |
|---|---|---|---|---|---|---|---|---|---|---|---|
| 136 A for 30 seconds just prior to charge to simulate 0-45 mph acceleration of J227a (Case 1) | Slightly less than 100 % | - | 9.08 | 8.84 | 8.63 | 8.30 | - | 7.58 | 7.03 | 6.68 | 6.50 |
| 10 % at 3 h rate | 90 % | 9.80 | 8.95 | 8.54 | 7.32 | 7.04 | - | 6.80 | - | 6.60 | - |
| 20 % at 3 h rate | 80 % | - | 7.73 | 7.44 | 7.24 | 6.97 | - | 6.76 | - | 6.56 | - |
| 40 % at 3 h rate | 60 % | 7.73 | 7.61 | 7.38 | 7.02 | 6.85 | - | 6.63 | - | - | - |
| 60 % at 3 h rate | 40 % | - | 7.59 | 7.35 | 7.19 | - | 6.93 | 6.72 | - | 6.50 | - |

NOTE: Critical battery voltage = 7.35 volts.

TABLE 3.3.5-3

REGENERATIVE BRAKING - BATTERY DATA (3 °F, GC2-19)

| Prior Discharge | State of Charge | Battery Voltage After 9 Second Charge (volts) Charge Rate (amperes) 300 | 250 | 200 | 150 | 100 | 50 |
|---|---|---|---|---|---|---|---|
| 10% at 3 h rate | 90 % | 9.70 | 9.43 | 9.08 | 8.76 | 8.40 (7.9s) | 8.02 |

NOTE: Critical battery voltage = 8.27 volts.

Comparison of Tables 3.3.5-2 and -3 indicates that lower temperatures have an adverse effect on battery acceptance of the regenerative braking currents. At the 90 % state of charge a battery at 80 °F will accept 200 amperes for 9 seconds without exceeding the maximum allowable voltage. However, at 3 °F the battery will only accept something less than 100 A, even through the temperature-corrected critical voltage is much higher.

## Fuel Gauge

Figure 3.3.5-6 relates the open-circuit voltage (OCV) of the battery pack at 80 °F to the state of charge based on the 3 hour rate. The state of charge in Figure 3.3.5-6 is equivalent to the percentage of the 3 hour ampere-hour capacity that remains. It is estimated that for every degree below 80 °F, the battery pack OCV will be 0.01 V lower than it is at 80 °F for the same state of charge; and for every degree above 80 °F, it will be 0.01 V higher. Testing of EV2-13 cells will be required to firmly establish the effect of temperature.

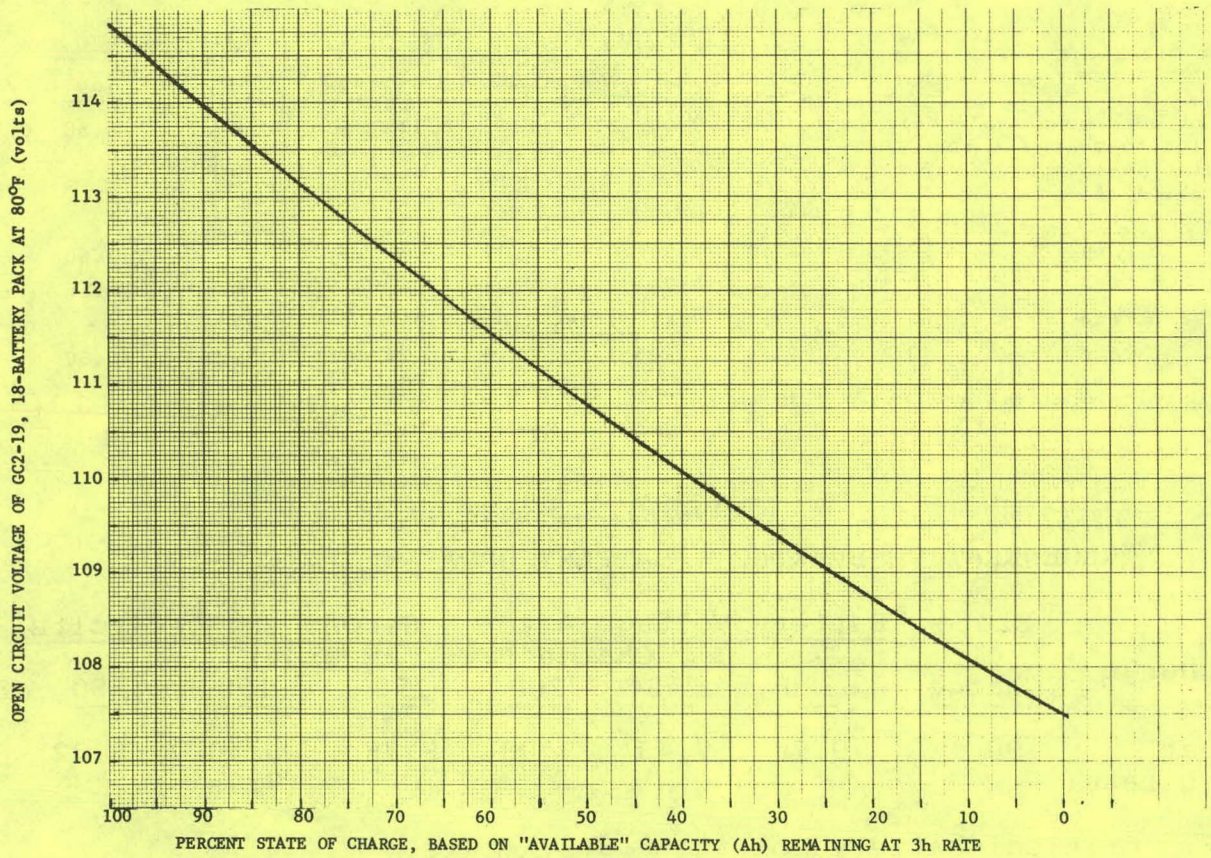


Figure 3.3.5-6. Battery Pack Open-Circuit Voltage vs State of Charge (80 °F)

Figure 3.3.5-7 relates the battery pack voltages that were observed during a constant-current discharge at the specified rate of 80 °F to state of charge values. The state of charge values were calculated by taking the ratio of the ampere-hour capacity remaining (at the specified rate and temperture) to the initial ampere-hour capacity (assuming 1.75 V/cell cutoff and no rest periods).

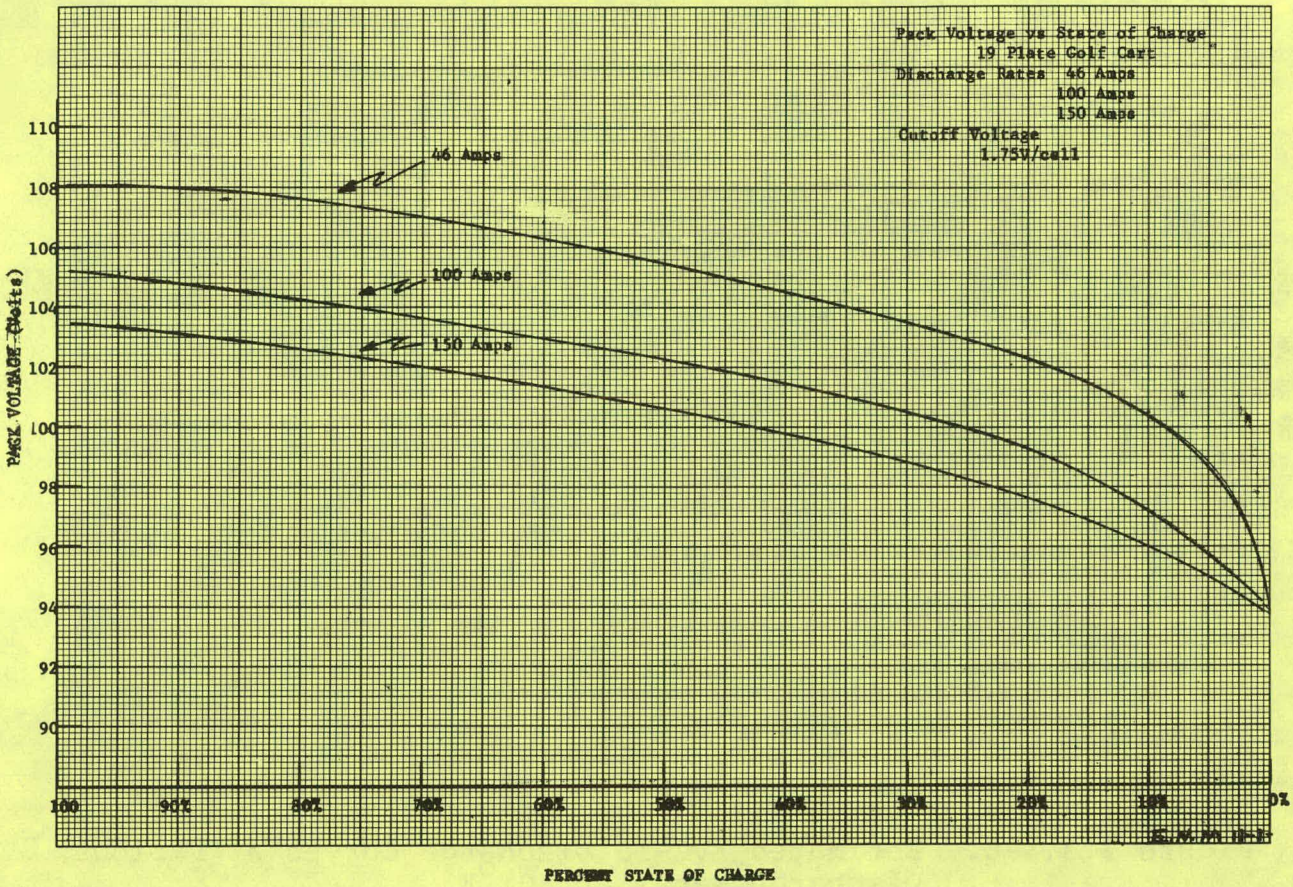


Figure 3.3.5-7. Battery Pack Voltage During Constant-Current Discharges at 3 Rates at 80 °F vs State of Charge

## Battery Mathematical Model

Figure 3.3.5-8 indicates estimated EV2-13 voltage-versus-time discharge curves for constant-current discharge rates of 400, 300, 200, 100, 75, and 50 amperes. Estimated Peukert curves for three different cutoff voltages are shown in Figure 3.3.5-9.

## Hydrogen Gas Generation

Figure 3.3.5-10 shows the estimated cumulative amount of hydrogen generated during the charging of an 18-battery pack of standard Globe GC2-19 golf car batteries at 80 °F. The gas was collected on one cell by a water-displacement method during the charging of a battery, and this value was multiplied by 3 cells/battery and 18 batteries/pack. The data illustrate six separate experiments as described in the key. The solid lines on the graph are based on data and the dashed lines are based on calculations. The calculations assumed the worst possible case, where 100 % of the current (1.5 A in these cases) is used for electrolysis of water.

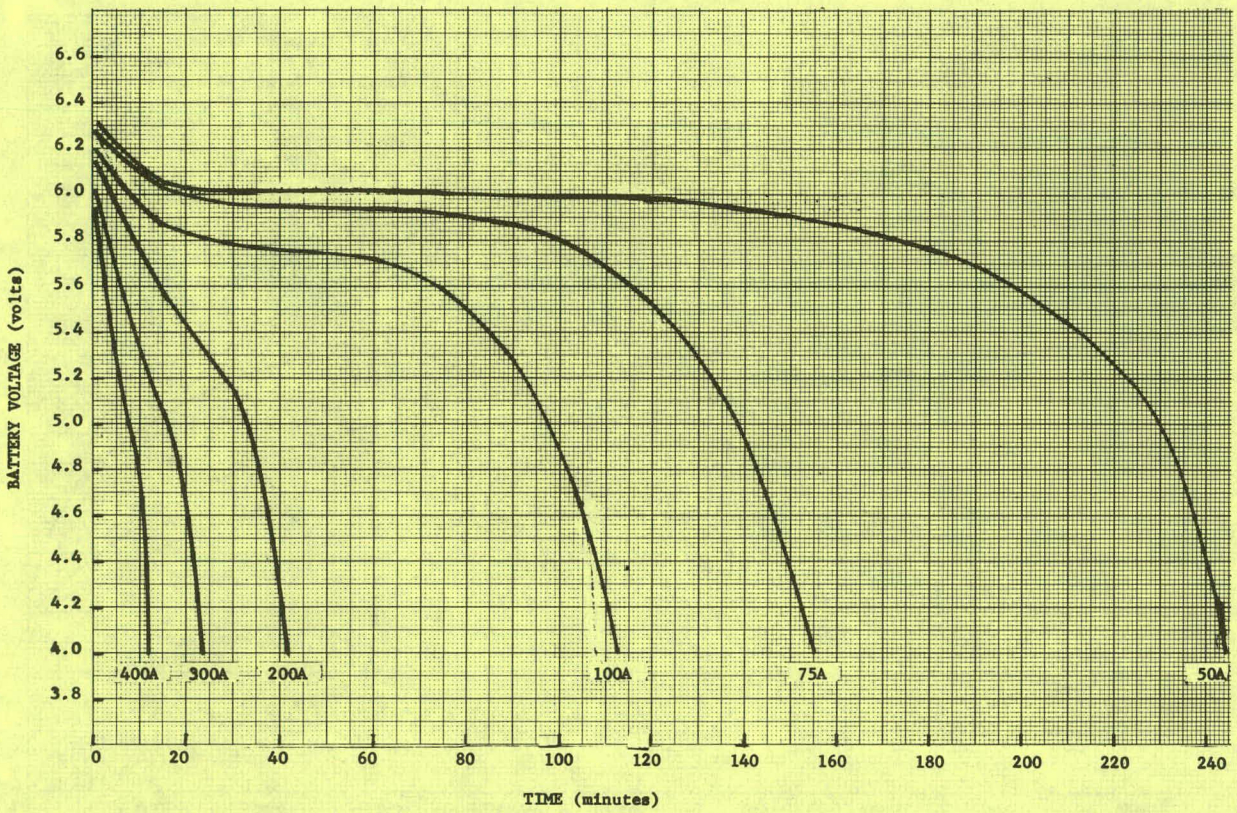


Figure 3.3.5-8. Estimated EV2-13 Discharge Curves at Various Discharge Rates at 80 $^{o}$F

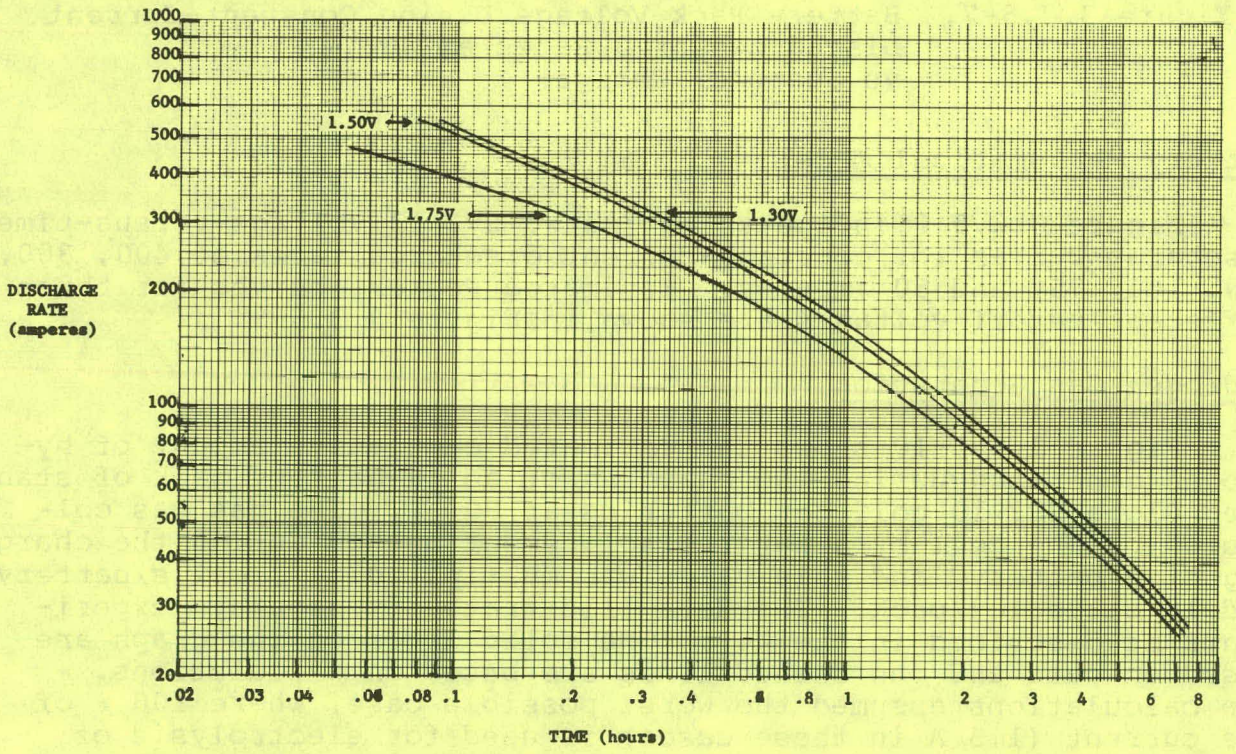


Figure 3.3.5-9. Estimated Peukert Curves for EV2-13 at 80 $^{o}$F (3 Cell Cutoff Voltages)

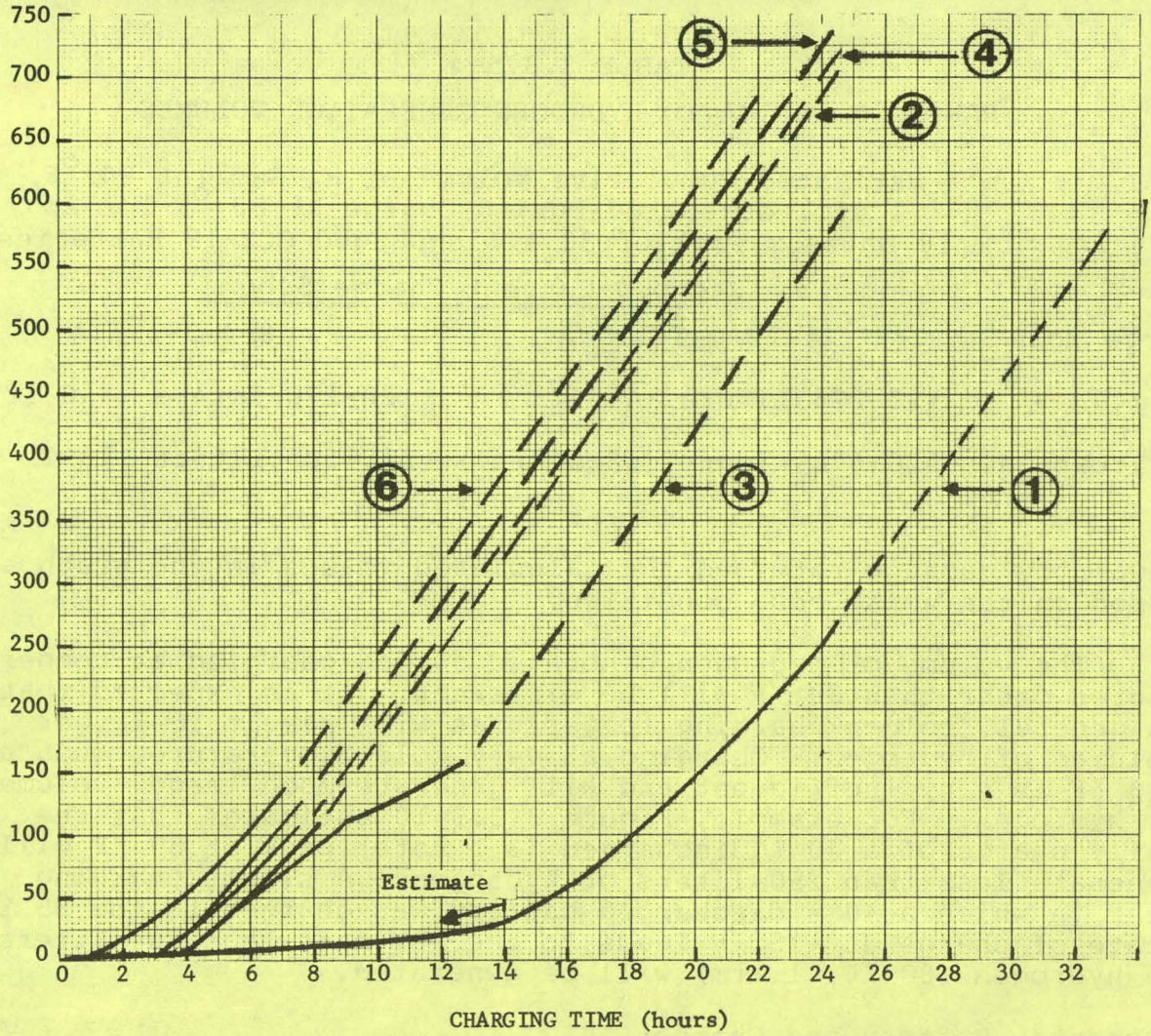


NOTE: Solid lines = Actual Data
Dashed lines = Calculated. The calculation assumed the worst possible case where 100% of current is used for electrolysis of water.

| | CURVE | PRIOR DISCHARGE | CHARGE SCHEME (A) | EST. CHARGE TIME REQ'D (h) DAILY | EQUALIZATION |
|---|---|---|---|---|---|
| KEY: | #1 | 80% | 8-4-2 1.5 | 19-21 | 31-33 |
| | #2 | 80 | 24-12-6-3-1.5 | 10.5-11 | 22.5-23 |
| | #3 | 80 | 24-12-6-3-1.5 | 10.5-11 | 22.5-23 |
| | #4 | 80 | 24-12-6-3-1.5 | 10.5-11 | 22.5-23 |
| | #5 | 77.2 | 24-12-6-3-1.5 | 10.5-11 | 22.5-23 |
| | #6 | 40 | 24-12-6-3-1.5 | 8.5-10 | 20.5-22 |

Figure 3.3.5-10. Hydrogen Gas Generation During Charging

The plotted curves, in conjunction with the estimated recharge times shown in the key in Figure 3.3.5-10, provided the values shown in Table 3.3.5-4, which is a convenient summary of the data.

It is anticipated that the EV2-13 battery will generate lower hydrogen volumes than those shown in Figure 3.3.5-10 and Table 3.3.5-4, because the lead-alloy system which will be employed should

TABLE 3.3.5-4

RANGE OF ESTIMATED HYDROGEN GENERATION VOLUMES

Estimated Cumulative Volume of $H_2$ Gas (at 80 °F, 1 atm) Generated During Charge at 80 °F for an 18-Battery Pack of 80 % Discharged GC2-19 Batteries

| | Stepped-Current Charge Scheme | |
|---|---|---|
| Charge Mode | 24-12-6-3-1.5 A | 8-4-2-1.5 A |
| Daily | 125-225 Liters (4-8 $ft^3$) | 120-170 Liters (4-6 $ft^3$) |
| Equalization | 520-670 Liters (18-24 $ft^3$) | 510-585 Liters (18-21 $ft^3$) |

lower the gassing rate and the calculated values in the graph are based on the worst-case condition.

The volume of hydrogen generated during charging at temperatures other than 80 °F will be different. It is expected that, in general, colder charging tempertures will result in larger volumes of hydrogen. Charging at very cold temperatures such as -15 °F is very inefficient and will generate much larger volumes of hydrogen. For example, Figure 3.3.5-10 estimates that the daily charge of a 40 % discharged (3 h rate) pack at 80 °F will generate less than 250 liters of hydrogen. A single charging test in which a 40 % discharged battery was charged to the 85 % state of charge at -15 °F leads to the estimate that 864 liters of hydrogen (80 °F, 1 atm) will be generated.

Accessory Battery and Charger

Globe's U1-9AD52-81 electric vehicle battery, which weighs 21 pounds has a capacity of 22 ampere-hours at the 3 hour rate, will be used for the accessory battery. Based on anticipated accessory loads, a charging voltage of 2.35 V/cell at 80 °F with a temperature-correction factor of 0.002 V/°F/cell is recommended. The recommended charging voltage is lowered 0.002 V/cell for every degree above 80 °F and raised 0.002 V/cell for every degree below 80 °F. Any change in the accessory load or in the accessory battery charger output might result in a change of charging recommendations by Globe.

Maintenance Schedule

- Watering -- A semiautomatic, single-fill-point watering system will be provided with each battery pack. It is currently estimated that watering with distilled water should be performed once every two months. Charging should not be performed during or immediately after watering. The watering procedure should not be restarted after filling is complete.

- o Cleaning -- Cleaning of the battery package will be placed on a schedule similar to lubrication and general maintenance of the vehicle. Once every six months should be adequate if the pack is reasonably well isolated from road dirt. The pack will be removed from the vehicle and the battery connectors checked for corrosion or damage. Removal of dirt and other debris can be accomplished by washing with water.
- o Checking Specific Gravity of Electrolyte -- Specific gravity will be monitored at least once every six months by sensing the open-circuit voltage (OCV) of each battery. A temperature-dependent linear relationship exists between specific gravity and OCV. The OCV should not be measured immediately after charging, since a capacitive surface charge is stored by the battery. Before the measurement is made, the batteries should be discharged a few seconds and allowed to recover for 5 to 10 minutes. An alternative procedure is to wait 12 to 18 hours after charging ends.

Connectors, Connector Shields, and Cabling

Connectors used to electrically connect the batteries will be burned on the battery terminal posts, because burned connections offer the lowest resistance and best reliability. The lead connectors have been designed and are shown schematically in Figures 3.3.5-11 and -12.

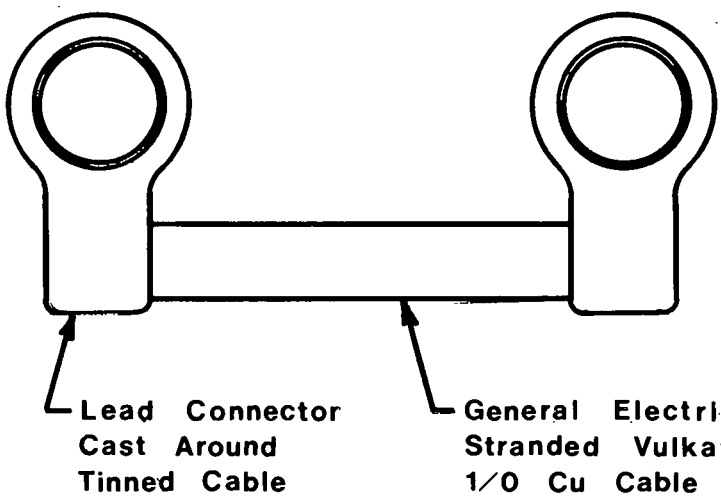


Figure 3.3.5-11. Connector and Cable Top View

Stranded Vulkaflex® cable has been selected for interbattery and battery-motor connections. It is a 1/0 cable with a conductor diameter of 0.374 inch, an overall diameter of 0.65 inch, a weight of 0.45 lb/ft, and a resistance of 0.128 ohm/1000 ft at 100 °C.

®Registered trademark of the General Electric Company.

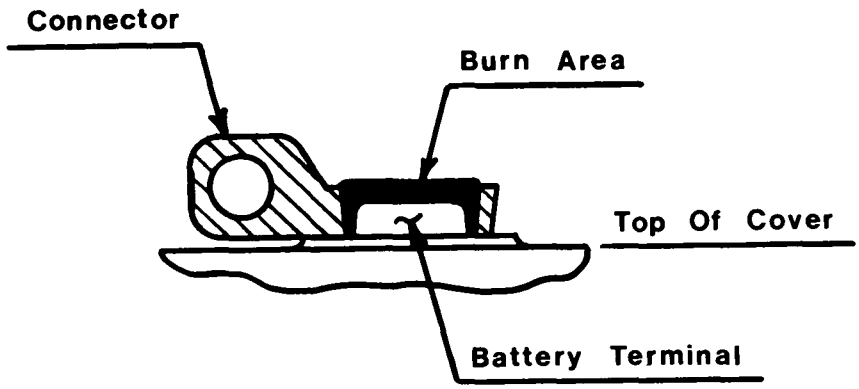


Figure 3.3.5-12. Section View of Connector on Battery Terminal

The special high-temperature cable has 133 copper strands, each of which is tin plated.

The estimated weight of the cabling system between batteries (which does not include cable to motor or controller) is 12.9 lb. This 12.9 lb can be broken down into 9.6 lb for the 36 lead connectors and 3.3 lb for the 7.3 feet of copper cable.

Globe designed a connector shield to provide electrical protection for service personnel when the battery pack has been removed from the vehicle. Each lead connector will be capped with a connector shield which snaps onto the cable. The connector shields will be hand cast by Globe by a rubber mold process. The materials currently being studied are epoxy and fiberglass-reinforced epoxy.

External (to the battery) Watering/Venting System

The external watering/venting system includes all of the watering/venting system apparatus except for the 18 watering/venting caps which fit on the eighteen EV2-13 batteries. Figure 3.3.1-1, discussed previously, shows the interbattery plumbing arrangement of the system. The eighteen batteries are connected in series by plastic tubing.

Figure 3.3.5-13 is a schematic diagram of the watering/venting system. Globe is working with Chrysler to assure that the rear safety vent port, or some part of the tubing leading to it, is higher in elevation than the water level of the fill bottle; this will eliminate the need for valves.

Globe will supply the tubing, water fill and collection containers, and the safety vent ports. The safety vent port is a flame-arresting device which provides for the safe venting of hydrogen from the battery pack to the atmosphere. Globe has recently designed and successfully tested a hand-fabricated safety vent port suitable for use on the vehicle. Globe recommends that two

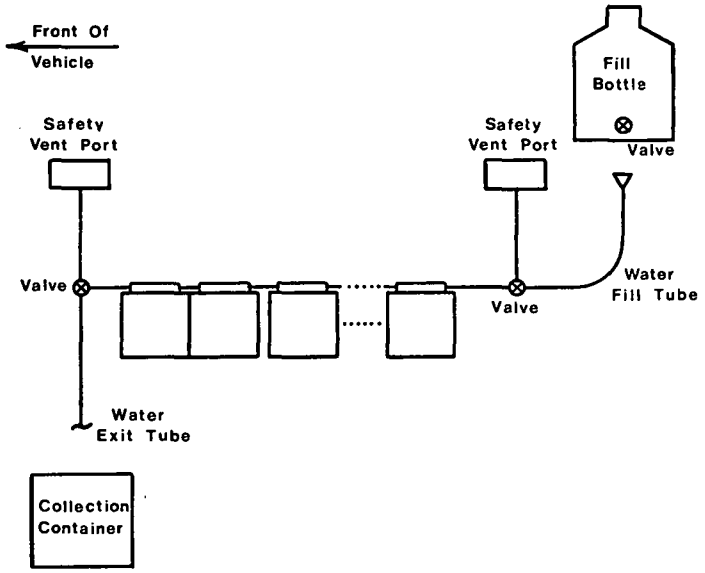


Figure 3.3.5-13. Venting/Watering System Schematic

safety vent ports be installed on each vehicle -- one located near the front of the vehicle, and one near the rear. It is important that the vent ports be located away from any areas where a pocket of hydrogen could accumulate, such as a fender well.

## Evaluation of EV-106 Battery Performance with Regenerative Braking

Computer simulations performed using the EV-106 battery model, described in Task Report WBS 3.2.1 "Parameter Optimization," predicted a range improvement with regeneration of 15 % on the J227a Schedule D driving cycle. The improvement due to regeneration is predicted, based on calculation of the incremental charge returned to the battery on each cycle by means of electrical regeneration. An ampere-hour efficiency of 100 % during the charge interval is assumed in the battery model.

In an effort to confirm or refine the simulation results, a series of tests were undertaken at the ESB Technology Center. The results of these tests show that the method of battery modeling developed for the program gives conservative results in predicting battery capacity on a stop-and-go driving cycle. The test results further demonstrate that an increase up to 34 % in vehicle range on the J227a Schedule D test cycle (Figure 3.3.5-14).

### Test Preparation

Battery power profiles corresponding to the J227a Schedule D cycle were generated by means of performance prediction programs operating on the H-6000 time-sharing computer system. The power profile with regenerative braking is shown in Figure 3.3.5-15(a); a similar profile but without regenerative braking is shown in

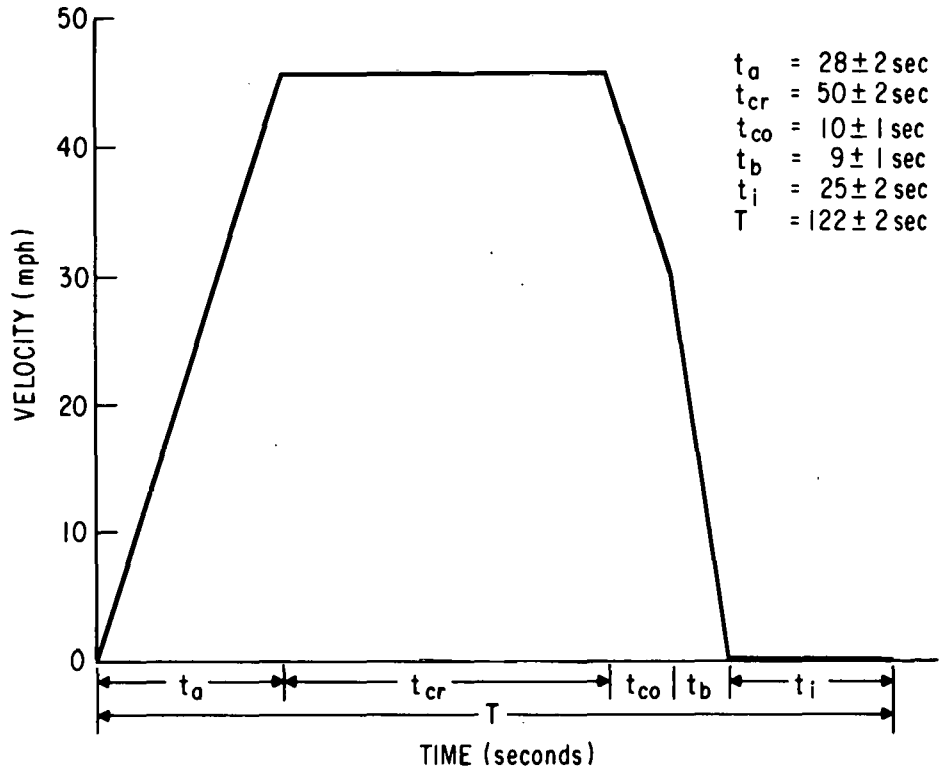


Figure 3.3.5-14. J227a Schedule D Test Cycle

Figure 3.3.5-15(b). The braking strategy represented in Figure 3.3.5-15(a) corresponds to a mild regenerative torque during the "coastdown" segment of the test cycle, followed by a higher torque value which is applied during the braking segment. Average vehicle deceleration is approximately 1.5 mph/s during the "coastdown" segment, where all braking effort is obtained electrically. During the braking segment, a deceleration of 3.3 mph/s is obtained by using a combination of electrical and friction braking. Approximately 70 % of the total braking effort during the braking segment is obtained electrically. Vehicle parameters for the simulation are shown in Table 3.3.5-5.

From the simulated power profiles of Figure 3.3.5-15, a minicomputer was programmed to operate an automatic battery tester capable of accurately duplicating the power variations. A block diagram of this battery tester is shown in Figure 3.3.5-16. The test equipment and computer program were thoroughly checked out prior to the running of recorded tests.

Battery Selection and Charging Procedures

The EV-106 battery selected for these tests was taken at random from a group of eight standard golf car batteries manufactured during the summer of 1977. The batteries were delivered to the ESB Technology Center and used in a Citicar electric vehicle

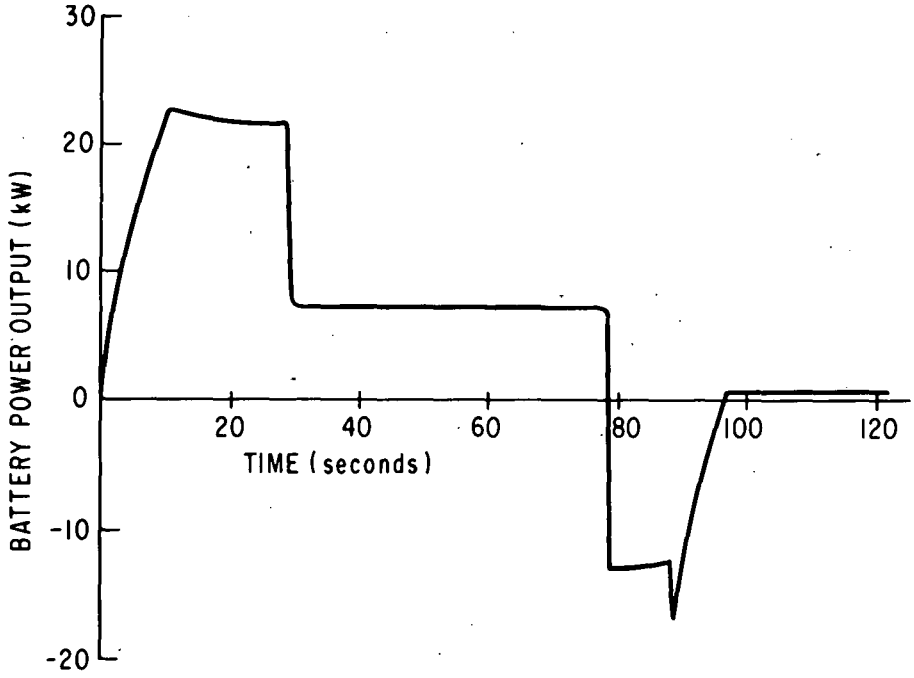


Figure 3.3.5-15(a). Power Profile with Regenerative Braking

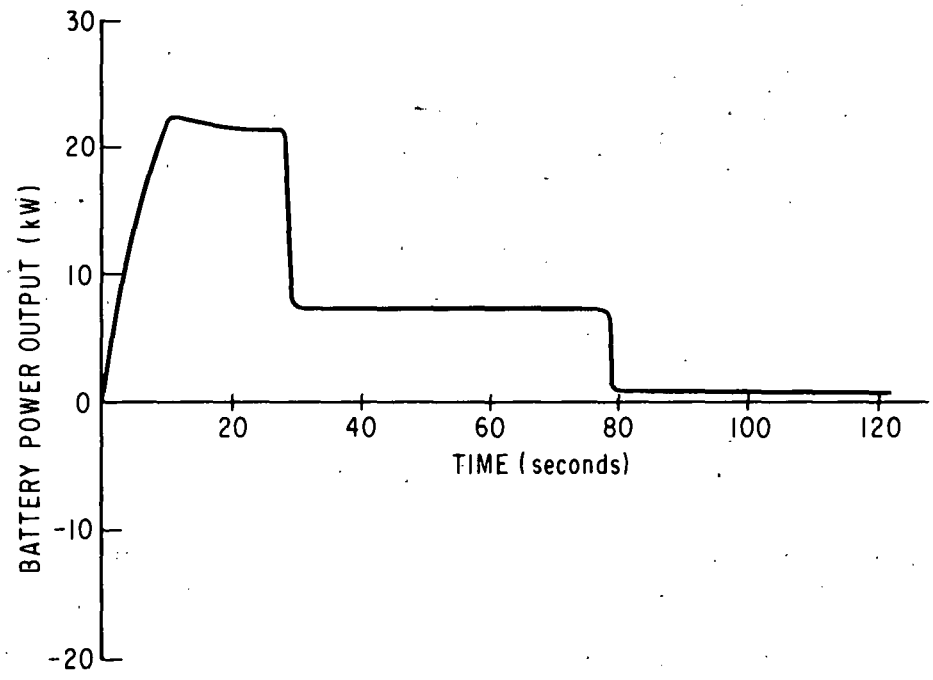


Figure 3.3.5-15(b). Power Profile Without Regenerative Braking

TABLE 3.3.5-5

VEHICLE DESIGN CHARACTERISTICS

| | |
|---|---|
| Gross Weight | = 3700 Lb (1678 kg) |
| Frontal Area | = 19.2 $Ft^2$ (1.78 $M^2$) |
| Aerodynamic Drag Coefficient | = 0.30 |
| Static Rolling Resistance | = 0.009 Lb/lbm |
| Wheel Rolling Resistance | = 0.921 Ft (0.28 M) |
| Overall Gear Ratio | = 5.48:1 |
| Overall Drive System Efficiency (on J227a Schedule cycle) | = 52.6 % |

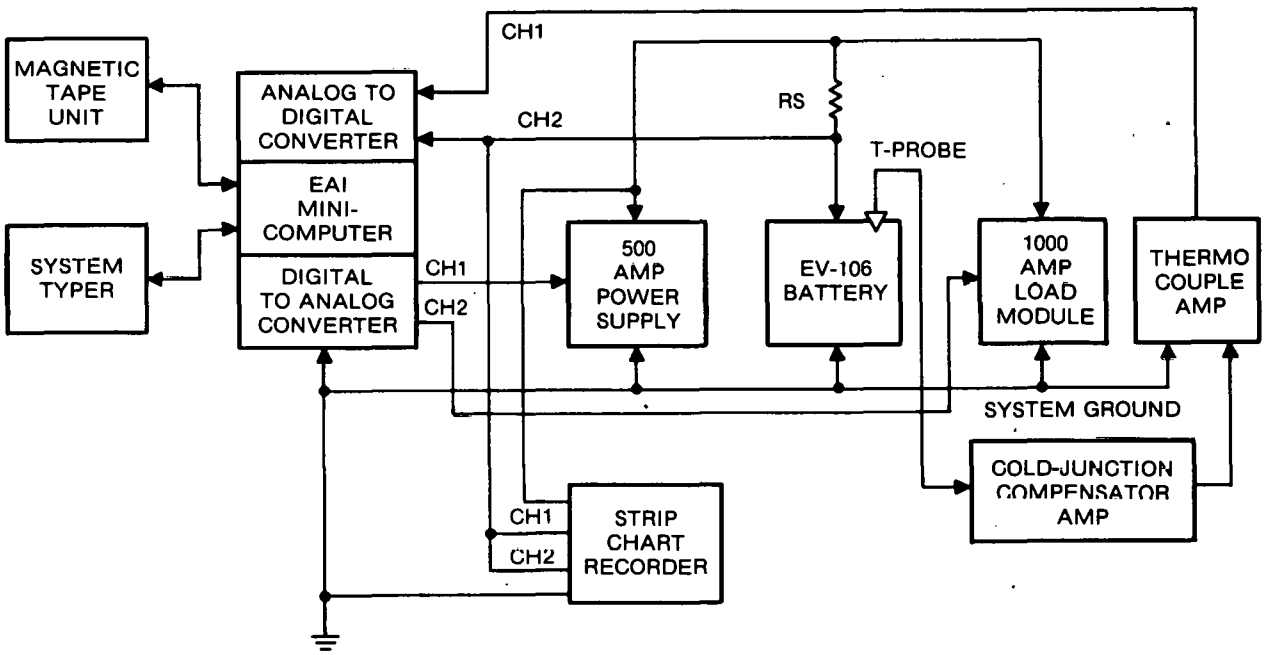


Figure 3.3.5-16. Battery Test System

for approximately 20 cycles. During use, they were cycled to about 80 % depth of discharge and recharged by a commercial Lester charger. The batteries were not used for a period of four months prior to testing but did receive an occasional topping charge.

The same battery was used for all tests. Prior to each test, the battery was charged by a modified constant potential procedure. The voltage limit was set at 2.4 V/cell and the initial current limited to 15 A. When the voltage limit was reached, the charge current would gradually decrease to a value of 5 A. The

final current value was maintained at 5 A until the specific gravity remained at the same value for three consecutive readings (±0.005) taken at one-hour intervals. The battery was then allowed to stand for a minimum of four hours prior to the start of each test. The total time during charge was approximately 18 hours.

Test Procedure

The EV-106 battery was charged to a specific gravity of 1.280 and cycled according to the power profile of Figure 3.3.5-15(a) until a cutoff voltage of 1.3 V/cell was reached under peak current conditions. This cutoff condition was found to correspond to 80 % discharge as defined by computer simulations. The test was then repeated without regenerative braking, using the power profile of Figure -15(b). Battery current and voltage were recorded at one-second intervals during each test, and computed values of output (input) power, output (input) energy, and output (input) charge were logged during each second of discharge (charge) operation. Values of average voltage, averge current, watt-seconds output, watt-seconds input, ampere-seconds output, and ampere-seconds input were calculated for each driving cycle and summarized for each complete test.

Battery temperature was measured at five-minute intervals during each test, and gas was collected continuously from the center cell. Specific gravity was recorded before and after the test.

After completion of the J227 driving cycle tests, the battery was recharged to 1.280 specific gravity and then discharged continuously at a dc rate determined from the nonregenerative cycle as follows:

$$\text{average dc rate} = \frac{\text{total ampere-seconds (discharge)}}{\text{total test time in seconds}}$$

This test was used as a benchmark to determine the ratio of energy delivered under simulated driving conditions to the energy delivered during a dc discharge at the same average current. It was hoped that the test data might provide a simple means of predicting vehicle range on the Schedule D cycle from published curves of discharge time versus dc current. Another purpose of the dc discharge test was to determine the performance of the particular battery selected for test, as compared with average results for a number of standard production units.

Test Results

The results of tests performed during March 1978 are summarized in Table 3.3.5-6. The predicted vehicle range obtained from the computer simulation studies is also shown in this table for comparison with equivalent ranges obtained by testing. Several observations can be made from these results:

TABLE 3.3.5-6

TEST RESULTS

| Test Type | J227 Schedule D with Regenerative Braking | Predicted Range from Computer Simulation | J227 Schedule D with No Regenerative Braking | Predicted Range from Computer Simulation | Constant Current - 76.5 A |
|---|---|---|---|---|---|
| Cycles Completed (equiv. miles) | 71 (68.6) | 55 | 53 (51.2) | 48 | NA |
| Total Ampere-Hours Charge | 30.56 | | 0 | | 0 |
| Total Ampere-Hours Discharge | 185.17 | | 138.79 | | 153.70 |
| Net Ampere-Hours Discharge | 154.61 | | 138.79 | | 153.70 |
| Total Watthours Charge | 198.21 | | 0 | | 0 |
| Total Watthours Discharge | 1012.91 | | 763.05 | | 878.02 |
| Net Watthours Discharge | 814.70 | | 763.05 | | 878.02 |
| Total Time of Test | 145 Min., 1.63 Sec. | | 108 Min., 0.03 Sec. | | 120 Min., 37.43 Sec. |
| Specific Gravity* Cell 1 (start end) | 1.280 1.132 | | Not Measured | | 1.287 1.155 |
| Gas Evolved (one cell) | 620 cc | | 227 cc | | 282 cc |
| Temperature (start/end) | 75 °F/98 °F | | 76 °F/92 °F | | 71 °F/83 °F |

*Room Temperature

- Predicted range from computer simulations agrees very closely with equivalent range as determined by the battery discharge test for the case without regenerative braking.
- Equivalent range with regenerative braking is significantly greater than predicted, and cannot be accounted for simply by computing the amount of energy in charge returned to the battery.
- The application of regenerative braking appears to offer a dramatic increase in vehicle range under the regenerative charge-discharge mode of operation obtained in the SAE J227 Schedule D driving cycle.

## Conclusions

This sequence of tests was carried out on only one EV-106 battery. There was no attempt to select a battery with optimum performance; however, when the constant-current discharges are compared with the average performance for an EV-106 battery (Figure 3.3.5-17), the discharge time at 76.5 A is 25.6 % greater than average. This fact would explain the higher than predicted range without regenerative braking.

In comparison of the tests with and without regenerative braking, it was found that regenerative braking extended the apparent vehicle range by 34 % (71 cycles vs 53 cycles). The net discharge capacity of the battery was increased from 138.79 Ah to 154.61 Ah, an improvement of 11.4 % (on an energy basis, the improvement is 6.8 %). These improvements are over and above the direct gains of 30.56 Ah and 198.21 Wh which are achieved by

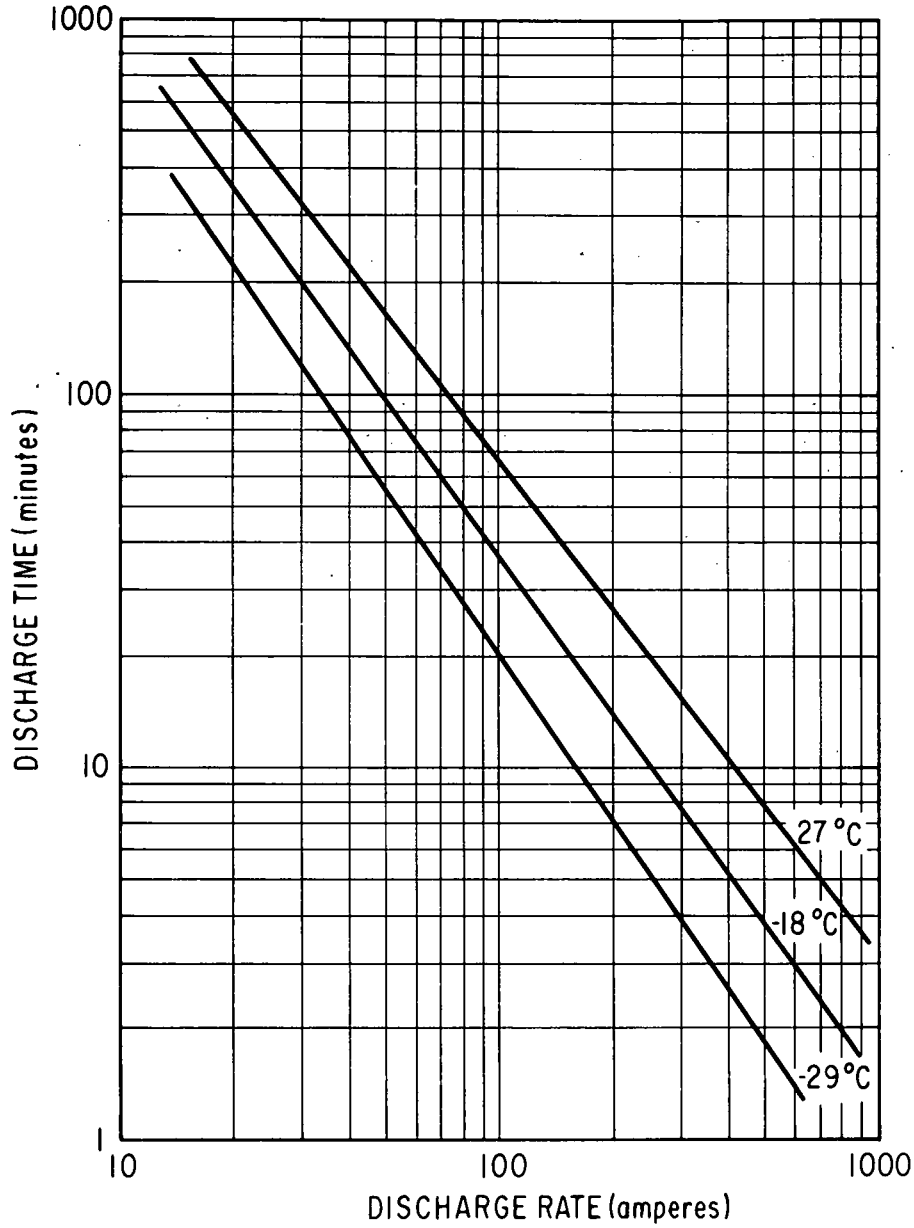


Figure 3.3.5-17. EV-106 Battery Discharge Rate vs Discharge Time at Various Temperatures

returning braking energy to the battery. If one attempts to account for this behavior in the battery model previously discussed, a regenerative charging efficiency factor greater than unity is obtained.

The maximum voltage reached during regenerative braking was 7.57 V. This voltage remained above the normal charging voltage of 7.2 V for only 6 seconds of the braking portion of the cycle. During the second cycle, the voltage reached a peak value of 7.34 V and remained above the normal charging voltage for 2 seconds. All subsequent cycles were less than 7.2 V. There is no indication

at this time that this higher voltage for such a short duration would be detrimental to the battery in terms of life or performance.

The total gas evolved was greater with than without regenerative braking by 393 $cm^3$ for the cell measured. This is probably due to a combination of local action and removal of residual gas. Additional experiments are required, to define this more precisely.

Comparison of the test without regenerative braking and the constant-current test at 76.5 amperes shows an overall decrease of 14.91 Ah (9.70 %) or 114.97 Wh (13.09 %) for the start-stop cycle compared with a constant discharge. This reduction in capacity is less than generally predicted, and demonstrates that the repetitive use of moderate pulse currents (less than 300 A) does not deplete the battery quickly, so long as the driving cycle allows time between pulses for recuperation to occur.

# Section 4

# TEST AND EVALUATION

## WBS 4.1 SYNOPSIS OF MASTER TEST PLAN

The Master Test Plan was issued in January 1978 and has been approved by the Jet Propulsion Laboratory.

The objective of the Master Test Plan is to describe and define the comprehensive testing program required for the successful development of the Integrated Test Vehicle and to determine how well the vehicle performance conforms to DOE objectives. The test planning and integration activity provides overall planning coordination and control of the comprehensive test program. The test plans provide the approval interface with DOE's technical contract manager at JPL. Testing will verify calculations and predictions and will permit the characterization of components and subsystems required for verification of tradeoffs. The tests will serve to evaluate the ITV before delivery to DOE. Testing and evaluation will be performed on a continuing basis with appropriate changes and redirection as determined by engineering, and in turn approved by DOE.

Specific DOE design objectives for this program define a four-passenger car similar in concept to today's subcompact vehicle which is widely used for urban transportation and commuting service. The driving mission for this car is specified by means of the SAE J227a Schedule D driving cycle, which is representative of urban stop-and-go driving.

In addition to the ITV system test, there are three subsystems which will be tested. These are:

- o Vehicle Subsystem (WBS Element 3.1)
- o Electrical Drive Subsystem (WBS Element 3.2)
- o Battery Subsystem (WBS Element 3.3)

There are two barrier tests under WBS Element 4.3. These are:

- o Mule Car 30-mph Barrier Test
- o ITV 30-mph Barrier Test

Component tests will be performed and documented but are not included in the Master Test Plan.

Integrated Vehicle Tests

The objective of the Integrated Vehicle tests is to determine the degree to which the DOE goals have been met. Before the Integrated Vehicle tests are begun, the vehicle is to be examined for

completeness and condition. The vehicle will be tested in its normal configuration with all normal appendages, such as mirrors, bumpers, and hubcaps.

The vehicle will be tested at the rated gross vehicle weight. Tire pressures will be set at the design pressure and, initially, new tires will be used. Lights, brakes, and safety equipment will be checked for proper operation. Any instrumentation included in the vehicle will be checked to see that it has been calibrated. The battery will be fully charged for vehicle range, maximum speed, acceleration, and gradability tests. Weight of the vehicle with the driver, all test equipment, and ballast weight will be recorded. The fifth wheel will be up so that it is included as part of the test equipment weight for those tests requiring the fifth wheel.

Ambient temperatures during ITV testing will be those existing at the selected test site in conformance to the environmental conditions stated in SAE J227a.

## Structural Safety Tests

The objective of the structural safety tests is to demonstrate compliance with current applicable industry-developed and federal mandated standards and to obtain extensive test data for analysis of vehicle impact performance.

Two structural tests are planned: a mule car 30 mph barrier test, and an ITV 30 mph barrier test.

The mule car test vehicle will be modified to accept the battery tunnel configuration and rear suspension attachments as well as the sheet metal modifications. Components simulating the electrical drive subsystem, transmission, air handling system, battery subsystem, accessory battery and tray, and other modified components will be used to provide as much data as possible resulting from the 30 mph barrier test.

## Vehicle Subsystem Tests

No subsystem tests will be conducted for the body structure. Chrysler will run one dynamometer durability test of the transmission.

Air handling tests will be run to verify compliance with FMVSS 103, "Windshield Defrosting and Defogging Systems," and to ensure various performance levels to satisfy customer acceptance criteria.

Customer acceptance tests for heating and ventilation will cover:

- Temperature control and response linearity tests
- Air flow and distribution tests

- Maximum performance warmup tests
- Stratification tests
- Jury evaluations

Defroster compliance tests will be performed in accordance with Compliance Procedure CP152 and established Chrysler Laboratory procedures and performance evaluation tests. The tests will measure velocity profiles over the windshield.

Performance tests will be conducted on laboratory bucks and roadable bucks, in wind tunnels and cold rooms, and under actual road conditions, with suitable instrumentation to establish compliance with FMVSS 103 and other customer acceptance specifications.

Electrical Drive Subsystem Tests

The objective of the Electrical Drive Subsystem Tests is to provide an evaluation of the electrical drive subsystem prior to its installation in the vehicle. Tests of the electrical drive subsystem are intended to measure energy flow rates, determine light load losses, measure efficiency of energy transfer, and verify design calculations.

Electrical signals obtained from the laboratory operation of the electrical drive subsystem will be read and recorded. Temperature monitoring at specific points on each subsystem component will be included, in order to verify the thermal design. The drive motor and associated controls will be set up in the laboratory. The drive motor will be operated by power from the battery and will be controlled with respect to output torque and speed. The drive motor will also be operated as a generator and will return energy to the battery.

The electrical drive subsystem tests will verify the ability of the drive to perform the following:

- Accelerate from 0 to 30 mph in 9 seconds
- Accelerate from 0 to 45 mph in 28 seconds
- Accelerate from 25 to 55 mph in 18 seconds
- Sustain a speed of 50 mph on a 5 % grade
- Obtain minimum passing speed of 60 mph
- Obtain minimum cruising speed of 55 mph

Battery Subsystem Tests

The objective of the propulsion battery electrical test program is to provide a standard procedure to confirm the overall design specification and to ensure that the manufactured product will perform as required. Globe-Union development facilities will be used for the proposed work.

Tests will be performed at 26.6 °C to determine the rated capacity of the battery at the 1-, 3-, and 6-hour rates. During the course of these tests, parameters to be measured and recorded will include the following:

- Half-cell potentials vs $Hg/Hg_2SO_4$ reference electrode
- Electrolyte temperature
- Specific gravity
- Initial (minimum) volts vs current
- Connector drop (IR)

Life cycling tests will utilize batteries which are first subjected to a conditioning cycle. The batteries will be placed on a life cycle unit and automatically charged and discharged. When the battery falls below the specified minimum, the test will be terminated and the total number of cycles recorded.

For peak power tests, the peak power capability of the battery will be measured at 26.6 °C.

Support and Special Test Equipment

The objective in providing special test equipment is to permit measurement of significant performance parameters of the completed vehicle, which in turn permits evaluation of the vehicle design.

Electrical and mechanical quantities of interest can be measured with a variety of devices such as shunts and load cells. To be useful to the engineer or technician performing tests, the outputs of these devices must be converted, using power sources available on the vehicle, into a format suitable for recording or display in engineering (SI) units.

The special test equipment must connect to the vehicle in an easy manner so that all equipment other than the transducers can be removed. Following completion of the special test equipment package, a complete laboratory test will be conducted and documented.

Each integrated test vehicle will be equipped with a set of transducers, augmented by necessary interface circuits, to allow onboard display of certain parameters. Provision will also be made on the vehicle for the recording of data for subsequent manual analysis.

Documentation

Reports presenting test results and conclusions will be prepared and submitted to DOE for the following tests:

- Integrated Vehicle Test
- Mule Car 30 Mph Barrier Test

- o ITV 30 Mph Barrier Test
- o Electrical Drive Subsystem Tests
- o Battery Subsystem Tests

## WBS 4.2 SPECIAL TEST EQUIPMENT AND FACILITIES

A draft of the Integrated Vehicle Test Plan (WBS 4.6) was prepared during April 1978. The plan specified the system variables to be measured by the mobile test equipment.

Preliminary studies indicate the probable use of the following equipment:

- o 8-channel chart recorder
- o Signal conditioning circuitry
- o Sensors (including 5th wheel)
- o 12 VDC - 115 VAC, 500VA or 1000VA inverter
- o 12 V lead-acid batteries
- o NASA/Lewis cycle timer

Additional effort in defining the test equipment configuration for integrated vehicle testing will resume after the CDR, when the test plan has been finalized.

## WBS 4.3 MULE CAR 30 Mph BARRIER TEST

The chassis mule vehicle described in Section 3 will be barrier-impact-tested at 30 mph to verify the front structure design concept and to obtain additional design guidelines for the final near-term vehicle. Body modifications made to the mule vehicle are as follows:

- o Front floor pan assembly modified to accept new tunnel configuration
- o Rear floor pan assembly modified to accept new tunnel configuration and rear suspension attachments
- o Front impact structure installed at centerline of vehicle with a hexcel energy absorber for the battery mass (see Figure 4.3-1)
- o Heat-treated 6009 series aluminum alloy fenders installed
- o Heat-treated 6009 series aluminum alloy hood assembly installed
- o Yoke panel assembly modified to accommodate spare tire retention system

The following items were installed on the mule vehicle to make it representative of the final car:

- Modified electric motor with final ITV mounts and impact target (Figure 4.3-1)
- Simulated transmission housing (Figure 4.3-1)
- Simulated power conditioning unit (PCU) and supporting structure (Figure 4.3-2)
- Simulated air handling system
- Modified front crossmember
- Front suspension complete with rack and pinion
- New rear suspension
- Steering column assembly
- Complete carryover bumper system
- Battery tray and battery retaining rings
- 18 Globe-Union golf car batteries filled with noncorrosive liquid to simulate active batteries
- Modified front seats
- Accessory battery and tray
- Spare tire assembly with retention system
- Windshield glass
- Instrument panel assembly
- Tires and wheels
- Two fiftieth percentile noninstrumented male dummies seated in front seats and restrained with unibelts

The mule car impact test was scheduled for May 10, 1978.

Barrier Test Instrumentation

The following test and recording equipment will be used:

- Photographic reference tubes--Fixed, accurately marked measuring devices used to indicate distance from the barrier surface. The tubes are mounted on the road surface perpendicular to the barrier face and straddling the test vehicle. Mountings are designed to permit removal and reinstallation of the tubes without changing the position in space of the markings relative to the barrier face.
- Photoelectric trap timer--With its known distance between sensing elements, provides the means for measuring vehicle speed. The timer is located to measure test vehicle velocity within 10 feet of the barrier.

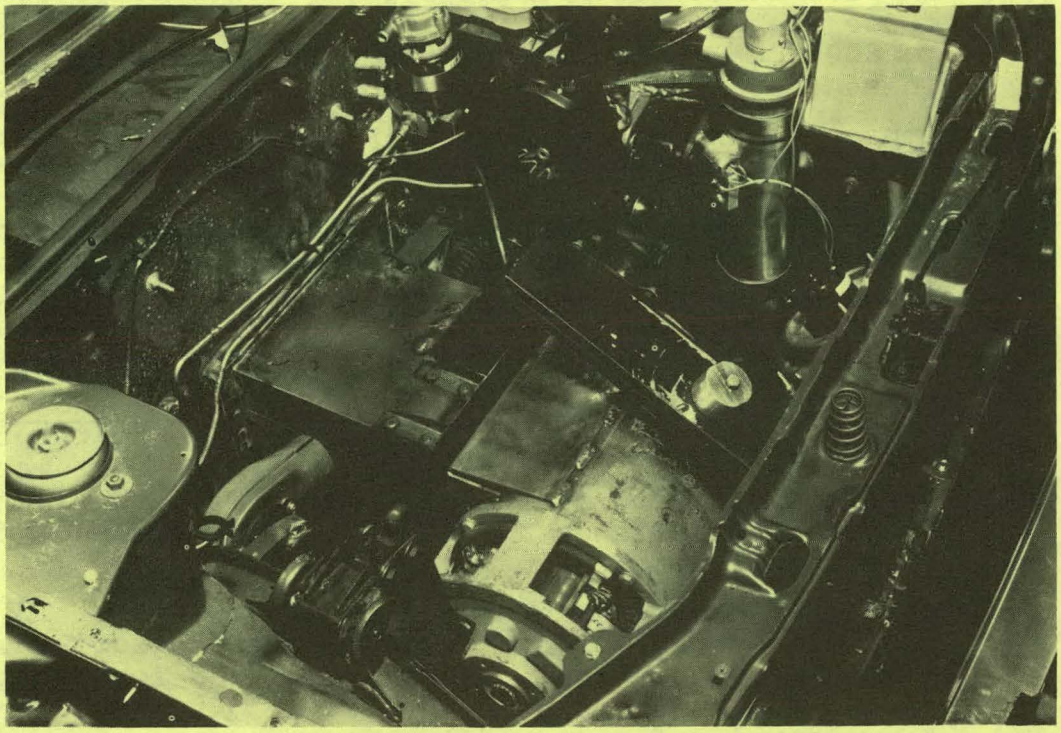

Figure 4.3-1. Mule Car Motor Compartment Without PCU Mockup and Spare Tire

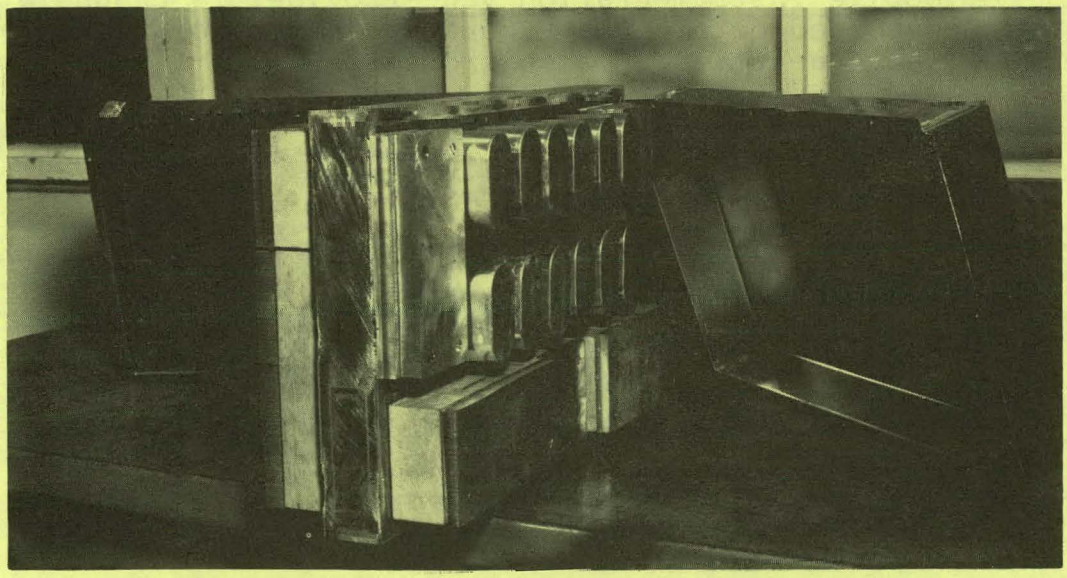

Figure 4.3-2. Mule Car PCU Mockup for Impact Test

- o Barrier force measurement system--Consists of five force plates, each capable of force measurements up to 300,000 lb, mounted on the steel barrier face. These force plates are covered with 3/4 inch plywood.
- o Impact timing marker switch--A contact switch mounted on the face of the barrier at the first point of contact with the test vehicle. Closing this switch energizes an electrical circuit, containing a lamp or neon tube, in each high speed camera; the resultant light produces a streak along one edge of the film. The beginning of the streak on the film identifies the moment of barrier impact.
- o Pulse generator with 1000 Hz serial output and BCD (binary code--digital) timing system--Marks the film for timing identification. This permits correlation of film data with different cameras or with electronic data and establishes an accurate time reference for film and/or electronic data analysis.
- o High speed motion picture cameras--Minimum of 10, to provide coverage of the vehicle, steering column, and dummy kinematics. See Figure 4.3-3 for location of the film targets used to provide visual references for analysis of impact films.
- o One stop-action camera--Records the impact event in a series of 8 to 10 sequential pictures.
- o Mobile instrumentation van--Provides 13 channels of recorded data. See Figure 4.3-4 for location, types, and quantities of accelerometers.

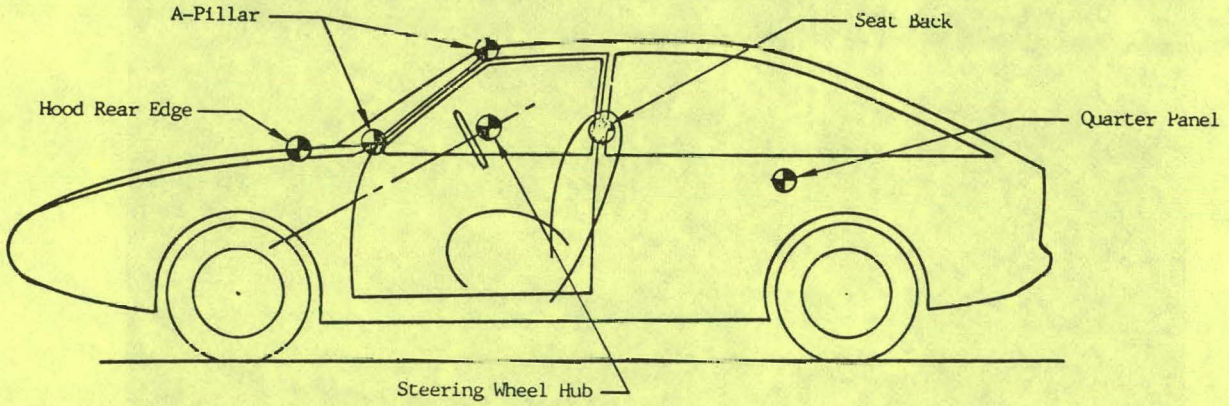


Figure 4.3-3. ITV Mule Car Barrier Test--Preliminary Film Target Location

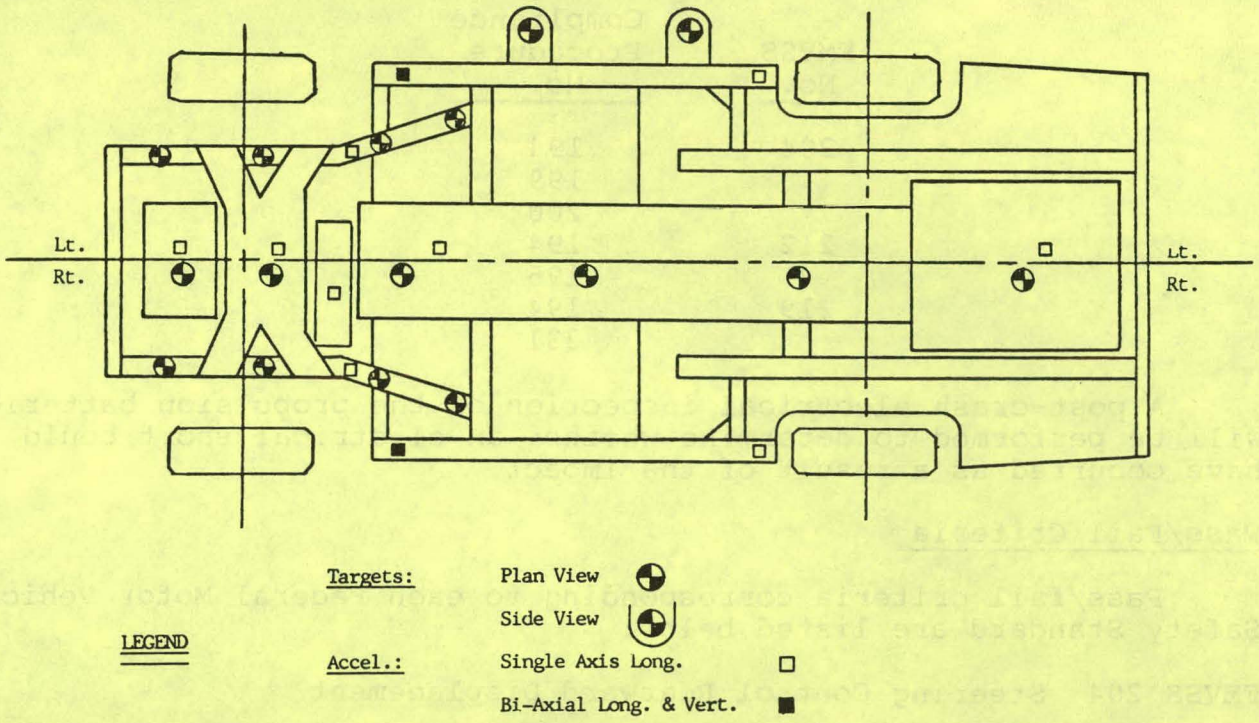


Figure 4.3-4. ITV Mule Car Barrier Test--Target and Instrumentation Location

## Support Requirements and Facilities

The Chrysler Proving Grounds are located 60 miles west of Detroit, at Chelsea, Michigan. The covered barrier at Chelsea is a facility used to create vehicle-to-barrier impacts, vehicle-to-vehicle crashes, and vehicle rollover tests. The building is 100 feet wide by 150 feet long. It houses a 265 ton barrier, a 5000 pound force winch to propel the test vehicle, two photographic pits, a photographic catwalk 37 1/2 feet above the test floor, and a lighting system that consumes 1,300,000 watts to produce 20,000 foot-candles of illumination. The approach runway is 1000 feet long.

Impact testing and development engineers (Proving Grounds personnel), who are responsible for the conformance of Chrysler Corporation cars to internal and various Federal and state standards relating to vehicle impacts or crashes, will conduct the barrier impact tests.

## Test Procedure and Recording Equipment

Evaluation of the mule car impact vehicle will be done in accordance with Chrysler Safety Documentation Compliance Procedures applicable to the 1978 model year vehicles. Correlation of Compliance Procedures to applicable FMVS Standards is as follows:

| FMVSS No. | Compliance Procedure No. |
|---|---|
| 204 | 194 |
| | 199 |
| | 200 |
| 212 | 194 |
| | 195 |
| 219 | 194 |
| | 231 |

A post-crash electrical inspection of the propulsion batteries will be performed to determine whether an electrical short could have occurred as a result of the impact.

Pass/Fail Criteria

Pass/fail criteria corresponding to each Federal Motor Vehicle Safety Standard are listed below:

FMVSS 204 Steering Control Rearward Displacement

Specifies requirements limiting rearward displacement of the steering control into the passenger compartment to 5 inches during a 30 mph frontal impact. (Initially effective January 1, 1968.)

FMVSS 212 Windshield Mounting

Specifies requirements for retention of the windshield in a 30 mph frontal barrier collision test. (Initially effective January 1, 1970.)

FMVSS 219 Windshield Zone Intrusion

Limits the intrusion of vehicle components into a prescribed zone ahead of the windshield in a frontal barrier crash at speeds up to and including 30 mph. (Initially effective September 1, 1976.)

## WBS 4.4 ELECTRICAL DRIVE SUBSYSTEM PERFORMANCE TESTS

The drive subsystem testing is scheduled to begin during July 1978. In preparation for testing, an Electrical Drive Subsystem Test Plan has been issued, subject to JPL review.

The main elements of the electrical drive subsystem assembled for testing will be:

- o DC Drive Motor
- o Power Conditioning Unit
- o Microprocessor and Controls

- o Propulsion Battery Pack
- o DC Motor/Generator
- o Mechanical Flywheel

The first four items constitute the drive subsystem undergoing test. The last two items are test equipment and are not installed in the vehicle. Figure 4.4-1 is a block diagram of the Electrical Drive Subsystem test configuration.

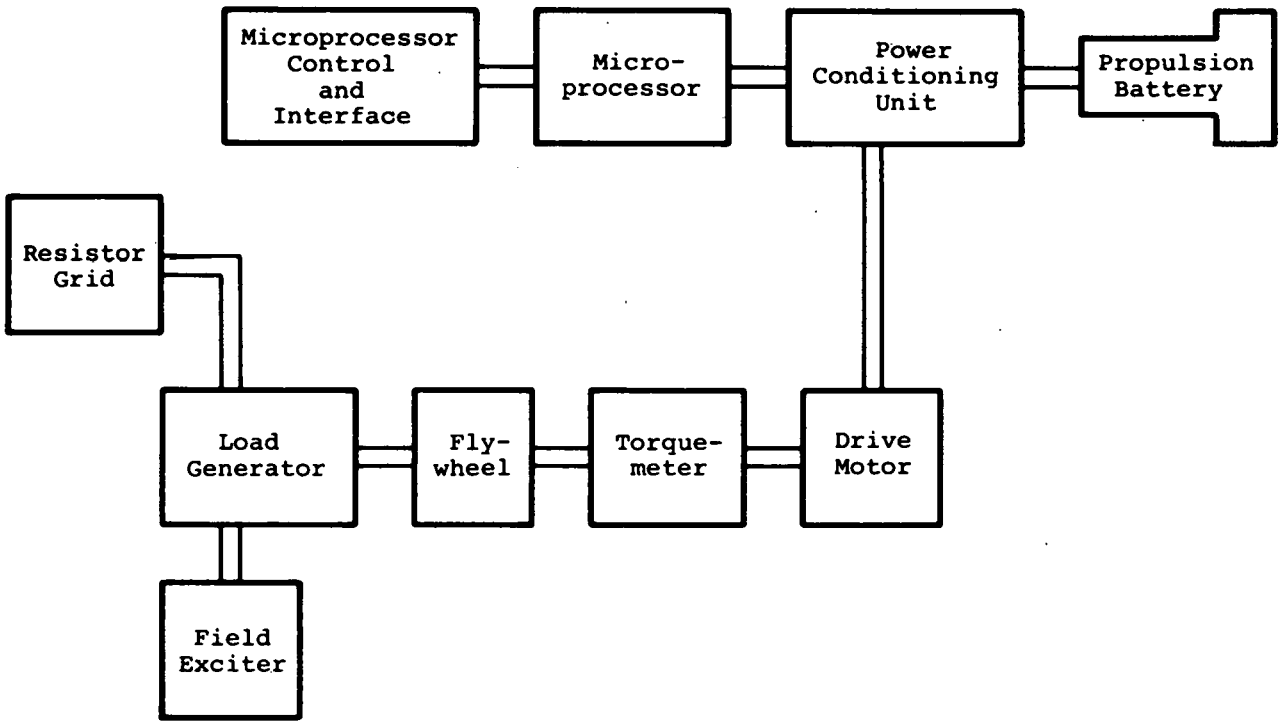


Figure 4.4-1. Electrical Drive Subsystem Test Configuration

Instrumentation

Measurements taken of the performance of the electrical drive subsystem will be monitored and recorded by the following instrumentation:

- o Honeywell 5600E analog tape deck, capable of recording up to 14 different input parameters. This recorder is able to record and play back any combination of channels with suitable data electronics cards.
- o Honeywell Accudata 113-3, which performs as a signal conditioning unit. This instrument is a 3-channel input/output and channel-to-channel isolated amplifier.
- o Himmelstein MCRT torquemeter with usable range of 0 to 4000 lb-in. This instrument will measure the torque generated by the drive motor.

- Fluke Digital Thermometer 2100A-06, to measure the temperature of the battery pack, motor, and power conditioning unit (PCU) components. It is capable of displaying information from six different types of thermocouples.
- Fluke Model 2150A-20 thermocouple switching unit. This unit is capable of switching up to 20 separate thermocouples.
- Current Integrator (the Curtiss Model SHR-C3 current integrator is under consideration).

Facilities

The Electrical Drive Subsystem (EDS) will be tested in an independent, General Electric-funded electric vehicle propulsion system test facility. This facility will include a propulsion battery, drive motor, load motor, mechanical flywheel and control, and metering equipment. The drive motor, the load motor, and the mechanical flywheel will be mounted on a steel railbed, which will be bolted to the floor. This will ensure ease in handling of the larger components, isolation of those sensitive to mechanical vibrations, and the stability necessary for high-speed testing.

J227a Schedule D Driving Test

The J227a Schedule D cycle tests will be run with a cycle timer acquired from the NASA-Lewis Research Center, located in Cleveland, Ohio. It was designed to assist a driver in following SAE Schedules B, C, and D. The SAE schedule to be driven is permanently stored on a Programmable Read-Only Memory (PROM).

The profile of the SAE schedule is continuously reproduced on one needle of a dual-movement analog meter. The second needle is normally connected to the output of a fifth wheel. The driver "matches needles" to accurately drive the programmed schedule. The laboratory tests will not include a fifth wheel; therefore, the output of an rpm detector will be inputted to the cycle timer and the output matched to the programmed profile displayed on the first meter. EDS performance will be measured at battery discharge levels of 0, 40, and 60 %.

Gradability Test

Gradability will be measured by subjecting the drive motor to a retarding force from the load generator, the magnitude of the torque being proportional to the load placed across the generator. The percentage grade will be proportional to the generator load. Through variation in the generator load, simulation of any percentage grade can be made on the EDS.

Acceleration Tests

Acceleration tests will be conducted by controlling the output of an acceleration potentiometer. The tests will be repeated for

battery discharge levels of 0, 40, and 60 %. The time required to reach the following conditions will be recorded:

- o Maximum acceleration and maximum speed
- o 0 to 30 mph at maximum acceleration
- o 25 to 55 mph at maximum acceleration

Range tests will be run on the EDS at rpm rates corresponding to speeds of 25, 35, and 45 mph. The test will be terminated when the EDS is unable to maintain 95 % of the required test speed. The range at a given speed will be recorded. Each test will begin with the battery fully charged.

Braking Test

Regenerative braking will be tested by accelerating the EDS to a predetermined speed and then switching to the regenerative mode. A signal to initiate regenerative braking, which simulates the signal to be sent from the brake blending system, will be sent to the microprocessor. In this mode, the mechanical energy available in the flywheel will be converted to electrical energy by operating the drive motor as a generator.

The current charging the propulsion battery will be measured by inserting a T-connection in the power conditioning unit and microprocessor cabling. The time it takes the EDS to come to rest after converting to the generating mode will be recorded. The charging current and voltage will be recorded for tests performed at battery discharge levels of 0, 40, and 60 %.

Temperature Measurements

Temperature measurements will also be conducted. The temperature sensor for the drive motor was built in during motor fabrication. This sensor will furnish information about the operating environment of the drive motor. When its operating temperature reaches a predetermined value, the drive motor will be cooled by a fan drawing air through the PCU and the motor and then exhausting it to the outside. The fan can also be activated by sensors mounted in the PCU.

Sensors mounted in the inlet and outlet of the cooling duct will measure the temperature change in the air as it is being drawn through the duct. This cooling system will be similar to that used in the electric vehicle. The sensor output will be connected to a multichannel temperature recorder during performance tests of the EDS.

Battery temperature will be measured by a temperature sensor, a linear thermistor network (LTN), built into the battery. The temperature of the battery will be recorded before and after all tests.

Electromagnetic Compatibility and Electromagnetic Interference Test

Electromagnetic compatibility (EMC) and electromagnetic interference (EMI) tests will be conducted in the following areas:

- o 115 V ac battery charging harmonic currents
- o Radio noise present in power line emissions below 30 MHz

The EMC/EMI tests will be conducted when the battery has a state of charge of 20 % (determined from measurements of specific gravity and/or open-circuit voltage) and when its state of charge is in a range of 90 to 95 %.

## WBS 4.6 INTEGRATED VEHICLE TESTING

Early in the program, preliminary planning was initiated for the Integrated Vehicle Tests to be performed at the Chrysler Chelsea Proving Ground. This early planning was incorporated into the initial Master Test Plan - Draft, issued on September 20, 1977. This draft defined the scope of the testing, the instrumentation requirements, data to be recorded, and descriptions of the performance tests that would be performed on the two vehicles. The performance directly relates to the near-term vehicle SOW requirements.

As a result of the PDR, a series of EMI radiation and susceptibility tests were also planned for one of the vehicles. A preliminary plan for these tests was included in the Master Test Plan, and a draft update was developed for the Interim Design Review. This testing was further refined and included in the Integrated Vehicle Test section of the Master Test Plan update dated January 16, 1978.

During this period, it was decided that instrumentation requirements and special test equipment requirements for the Integrated Vehicle Tests would be integrated with the requirements of the Electrical Drive Subsystem Test to be performed under WBS 4.4. This would not only provide good correlation between both test programs but would also be more cost-effective.

A preliminary version of the Integrated Vehicle Test Plan was developed during the months of March and April. The baseline for these tests was the Master Test Plan. The concept of performing two groups of tests, one for each vehicle, was developed. The Group 1 tests would be performed on the first available vehicle. These tests are basically the tests to determine vehicle performance characteristics to satisfy the DOE goals.

The tests planned for Group 1 are as follows:

- o Range on SAE J227a Schedule D Driving Cycle
- o Range at Constant Speed

- Maximum Level Speed
- Acceleration (0 to 30 mph and 25 to 55 mph)
- Sustained Speed at 5 % grade
- Gradability
- Recharge Capability
- EMC/EMI

Where applicable, tests will be performed at battery discharge levels of 0, 40, and 60 %.

Group 2 tests will be performed on Vehicle 2. Some Group 1 tests will be repeated to obtain additional test data, but testing will concentrate primarily on vehicle subsystem evaluation. Group 2 tests are:

- Range on SAE J227a Schedule D Driving Cycle
- Maximum Level Speed
- Acceleration (0 to 30 mph and 25 to 55 mph)
- Sustained Speed at 5 % grade
- Rolling Resistance
- Aerodynamic Drag
- Environmental (humidity, water splash, etc.)
- Heater/Defroster
- Limited Endurance
- Braking
- Other tests to be defined by Chrysler

Copies of the preliminary draft of the Integrated Vehicle Test Plan have been distributed to GE, Chrysler, and JPL for review and further development. The next update is schedule for August 1, 1978, prior to issuance on September 1, 1978.

## Section 5

# COST AND CONSUMER ACCEPTANCE STUDIES

## SELLING PRICE

The objective of this activity is to determine an estimate of the selling price of an electric vehicle, similar to the Integrated Test Vehicles, for a quantity of 100,000 units per year. This estimate will provide a preliminary indication of the feasibility of meeting DOE's cost goal for a near-term electric passenger car of $5000 in 1975 dollars.

Cost determination will be accomplished by adding the cost of electrical vehicle components to, and eliminating the cost of internal-combustion-engine vehicle components from, the 1978 Omni/Horizon subcompact baseline vehicle. The Chrysler Corporation will integrate the differential costs and estimate the selling price of the electric vehicle.

Representative internal-combustion-engine components which will be deleted in the study are the engine, transmission, radiator, fuel tank, rear suspension, and steel body panels.

Components pertaining solely to the electric vehicle include the motor, power conditioning unit, microprocessor, onboard charger power unit, batteries, battery tunnel, rear suspension, transmission, gasoline heater, and aluminum panels.

The planned approach for obtaining production costs for the electric vehicle indigenous components is to request each of the manufacturing sources to perform a brief producibility analysis to determine optimum production techniques. Consultations will be held with the General Electric Direct Current Motor & Generator Department on the electric motor; with the Industry Control Products Department on optimizing the packaging and assembly of the power conditioning unit, microprocessor, and onboard charger power unit; and with the Semiconductor Products Department on the production of power modules.

Globe-Union, Inc. will provide the cost of the traction batteries. Chrysler will develop costs for all unique vehicle components, including the transmission and gasoline heater. Included in Chrysler's effort will be a limited producibility analysis to determine how best to apply automated fabrication and assembly techniques to production of the electric vehicle.

## LIFE CYCLE COST (See Tables 5-1 and 5-2)

A life cycle operating cost estimate has been prepared using a methodology essentially the same as in the Department of Transportation study report, "Advisability of Regulating Electric Vehicles for Energy Conservation," of August 1976.

TABLE 5-1

VEHICLE CHARACTERISTICS

| | |
|---|---|
| Vehicle Life (years) | 10 |
| Annual Vehicle Utilization (mi/yr) | 10,000 |
| Total Vehicle Travel (mi) | 100,000 |
| Battery Life (cycles) | 800 |
| Battery Life (yr) | 4.8 |
| Batteries/Vehicle (over vehicle life) | 2.1 |
| Base Vehicle Price ($) | $4076 |
| Battery Price ($) (0.84/lb) | $ 924 |
| Battery Replacement Cost | $ 869 |
| Vehicle Acquisition Price (1975 dollars) | $5000 |

TABLE 5-2

LIFE CYCLE OPERATION COSTS (¢/MI)

| | |
|---|---|
| Capital Recovery (vehicle) ($CR_F$ X cost/mi/yr) (3 %) | 4.8 |
| Capital Recovery (batteries) (3 %) | 2.0 |
| Registration, Title, Sales Tax | .8 |
| SUBTOTAL, CAPITAL SENSITIVE COSTS | 7.6 |
| Repairs and Maintenance | 2.0 |
| Insurance | 1.5 |
| Garage, Parking, Tolls, etc. | 2.1 |
| SUBTOTAL, NONFUEL OPERATING COSTS | 13.2 |
| Cost of Fuel @ $.032/kWh (.35 kWh/mile) | 1.1 |
| TOTAL OPERATING COSTS | 14.3 |

A battery life of 4.8 years was obtained by assuming an average range of 60 miles per recharge and a projected cycle life of 800 cycles for production batteries, which is the ISOA objective. The battery price was assumed to be $0.84/lb with a salvage value of $0.05/lb. Later analysis will use cycle life estimates for production versions of the EV2-13 battery.

Capital Sensitive Costs are depreciation and interest on the base vehicle and batteries plus annual taxes and fees. A 4 % sales tax, a 4 % title fee, and a $30/year registration fee were used for determining the costs. Capital Recovery Costs (depreciation plus interest) are a function of vehicle utilization and useful life. The interest value used is lower than current quoted commercial interest rates, since present rates have to provide for the devaluation of currency due to inflation. The annual payments thus include a correction factor for an annual inflation rate of 6 %, giving an effective interest rate of 3 %.

The repairs and maintenance estimate is assumed to be $0.02/mile, which is the maximum specified DOE objective. As more data are accumulated, it is anticipated that this figure will decrease. Insurance, parking, tolls, and other related costs used are based on those found in "Cost of Owning and Operating an Automobile - 1976," DOT.

The cost of fuel used was 3.2¢/kWh, which is lower than the 5¢/kWh in the Statement of Work. This figure is based on the national average retail price of electricity in 1975 (Edison Electric Institute). The energy consumption used was 0.35 kW/mile, obtained from the Energy Flow Model for the GE-ITV on the J227a Schedule D driving cycle.

## CONSUMER ACCEPTANCE

It is important to judge consumer acceptance of the near-term electric vehicle to determine whether or not a well designed car with improved performance and styling will be well accepted by the public. To date, consumer acceptance of electric vehicles has been limited, because of poor styling, poor performance, and the high cost of present offerings.

Normally, for a new vehicle of this nature a complete and thorough marketing analysis would be undertaken. However, time and money considerations make this approach impractical. To obtain an answer in the available time, the expertise of the Chrysler Styling and Design Office will be employed to determine consumer acceptance.

Experienced stylists and human engineering specialists from Chrysler will analyze the vehicle, comparing it with Chrysler and industry standards for appearance, seating comfort, visibility, and ease of operation.

Results of all the studies will be incorporated in a Task Report for WBS 5.0, "Cost and Consumer Acceptance Studies."

# Part 2

# Garrett Corporation
# Airesearch Manufacturing Company
# Of California

Contract No. EY-76-C-03-1213

THIS PAGE

WAS INTENTIONALLY

LEFT BLANK

CONTENTS

CONTENTS (Continued)

CONTENTS (Continued)

ILLUSTRATIONS

ILLUSTRATIONS (Continued)

ILLUSTRATIONS (Continued)

ILLUSTRATIONS (Continued)

TABLES

TABLES (Continued)

# SECTION 1

# INTRODUCTION AND SUMMARY

# SECTION 1

# INTRODUCTION AND SUMMARY

## INTRODUCTION

This document was prepared by AiResearch Manufacturing Company, a division of The Garrett Corporation, under Contract EY-76-C-03-1213 for the Department of Energy (DOE). It presents the mid-term review summary for Phase II of the Near-Term Electric Vehicle (NTEV) program.

Phase II of the Near-Term Electric Vehicle program is a continuation of the Phase I Preliminary Design Study previously conducted, and is based on the multi-phase development plan that was developed during the Phase I work.

The general objective of the Near-Term Electric Vehicle Program is to confirm (1) that, in fact, the complete spectrum of requirements placed on the automobile (e.g., safety, producibility, utility, etc.) can still be satisfied if electric power train concepts are incorporated in lieu of contemporary power train concepts, and (2) that the resultant set of vehicle characteristics are mutually compatible, technologically achievable, and economically achievable. The focus of the approach to meeting this general objective involves the design, development, and fabrication of complete electric vehicles incorporating, where necessary, extensive technological advancements.

The work described in this report is supported by several major subcontracts. The vehicle design was created by The Brubaker Group. The vehicle structural design, detail design, and fabrication are being done by the Budd Company. The scale-model crash test program to verify the crashworthiness of the all-plastic structure also is being done by the Budd Company at the Fort Washington Technical Center. The advanced lead-acid battery, which is being especially designed to match the new vehicle and power system, is being developed by Eagle-Picher Industries. Much of the safety and handling analyses of the vehicle design were conducted by Dynamic Sciences, Inc., who also will conduct the crashworthiness testing of the full-scale crash test vehicle at a later date. All American Racers participated in the design analysis and selection of the various components of the suspension, steering, and brake systems and also will assist during vehicle testing.

## VEHICLE DESIGN CONCEPT

The vehicle being developed is an all new design, highly optimized for the particular requirements of a small, four-passenger, electric-powered urban/suburban car. The power system is a new and unique design that uses flywheel energy to supplement battery power during peak demands and incorporates a regenerative braking feature to convert vehicle kinetic energy into retrievable flywheel energy during deceleration and braking. The process of energy storage and conversion to propulsive power is accomplished by a unique arrangement of the flywheel, two motor/generator units, and a power drive connected through a differential planetary gear set that functions as a fully

automatic, infinitely variable transmission. The result is a highly efficient electric vehicle that requires a minimum of batteries while providing acceptable performance and driving characteristics that are similar to those of conventional internal combustion engine powered compact cars.

## REPORT ORGANIZATION

Section 2, Program Management, describes the DOE and AiResearch management organizations and their relationship for the NTEV program.

Section 3, Program Description, summarizes the objectives of the DOE Near-Term Electric Vehicle program. The scope of the Phase II effort is given and the technical approach, based on the conclusions of the Phase I study, is described in detail.

Section 4, System Integration and Performance, briefly describes the overall vehicle characteristics that were included in the analytical studies used to predict the overall performance of the vehicle. A description of the Eagle-Picher tubular lead-acid battery and its predicted performance are included, as is a discussion of the analytical modeling used for the performance evaluations. Sensitivity studies that have been used to evaluate some of the more critical aspects also are discussed.

Section 5, Power System, presents a detailed description of the unique power system and its operation. The design of the laminar composite flywheel is described, and endurance test results are included. The high-vacuum system, which uses a molecular pump, is described and test verification of its design is given. The design of the two identical dc motor/generator units is described in detail. The electronic control system, which includes the two field controls and the battery current supply, is described and detail schematic diagrams are presented.

Section 6, Vehicle Design, describes the lighweight vehicle design, which is based on the use of fiber-reinforced plastic for the unitized frame and body. The simplicity of the parts breakdown and assembly is shown. The various material selections also are described.

Section 7, Suspension, Brakes, and Steering, describes the vehicle suspension, steering, and braking systems. Most of the components are adaptations of components from the BMW 320i automobile. The various geometric characteristics of the resulting design such as steering diagrams and braking weight distribution are shown.

Section 8, Scale-Model Testing, describes the scale model crash test program conducted by the Budd Company, which has verified the structural concept. Tests results are included showing the crush and energy absorption characteristics of the lead-acid batteries.

Section 9, Structural Analysis, describes the structural analysis conducted to support the detail design. Computer modeled crashworthiness studies and finite-element structural analyses are presented.

Section 10, Vehicle Dynamics Analysis, describes the analysis of the gyroscopic forces caused by the flywheel, the transient handling analysis, the ride quality analysis, and an analysis of the expected noise characteristics. The flywheel gyroscopic moments are shown to have a stabilizing effect during all yaw rates and vehicle speeds. The handling analysis, which includes the combined effects of weight distribution, suspension geometry, and the transient effect of the gyroscopic moments, shows that the characteristics are all well within the acceptable ranges.

# SECTION 2

# PROGRAM MANAGEMENT

# SECTION 2

# PROGRAM MANAGEMENT

## DEPARTMENT OF ENERGY MANAGEMENT

The activities described in this report are being carried out by the AiResearch Manufacturing Company and its subcontractors under a contract with the U.S. Department of Energy (DOE). This work is part of the Near-Term Electric Vehicle Program being administered by DOE in accordance with Public Law 94-413, the Electric and Hybrid Vehicle Research, Development and Demonstration Act of 1976. Management responsibility for the Near-Term Electric Vehicle (NTEV) Program is within the Division of Transportation Energy Conservation under the Assistant Secretary for Conservation and Solar Applications.

V. J. Esposito and P. J. Brown are the DOE Program Manager and Deputy Program Manager, respectively, of the overall National Electric and Hybrid Vehicle Program of which this Near Term Electric Vehicle Program is a major element. R. S. Kirk and G. J. Walker are the DOE Program Director and Program Manager, respectively, of this Near Term Electric Vehicle Program. AiResearch's contract is administered by the San Francisco Operations Office of DOE; Mr. J. Hirahara is the responsible Contract Specialist. The organizational relationships within DOE are shown in Figure 1.

The technical Management of the AiResearch contract is the responsibility of the Jet Propulsion Laboratory (JPL) of Pasadena, California. Mr. Thomas A. Barber is Manager of the Electric and Hybrid Vehicle Systems Project at JPL. The Contract Technical Manager for AiResearch's contract is Mr. R. Y. Yoshida.

## AIRESEARCH MANAGEMENT

Within AiResearch, the work is being directed by the engineering department of the Mechanical Power Systems Product Line, one of five major product lines which are part of a matrix that combines product lines with functional departments. The relationship of the NTEV program to AiResearch management is shown in Figure 2.

Program tasks are assigned as indicated in the NTEV program chart of Figure 3.

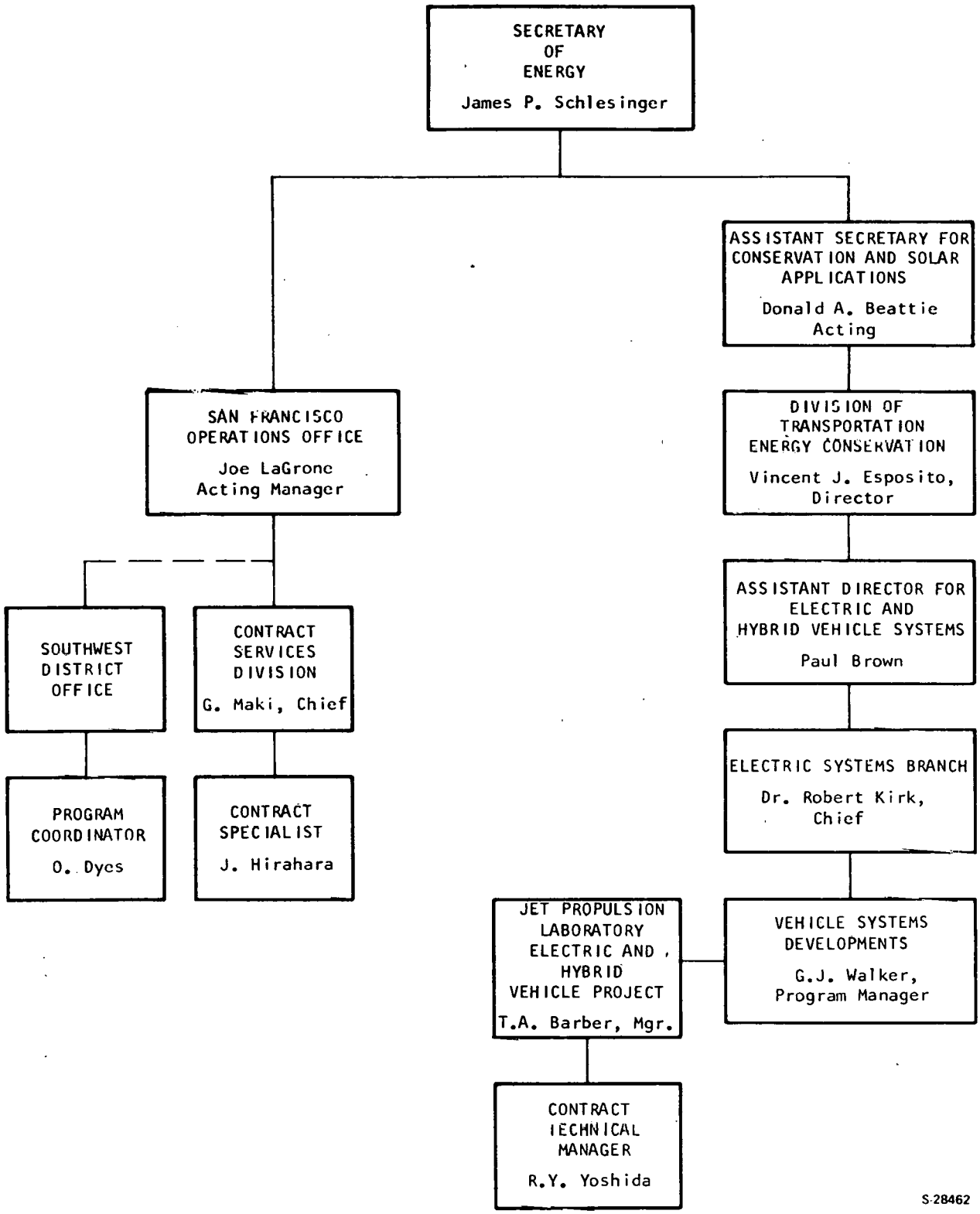


Figure 1. DOE Organizational Elements

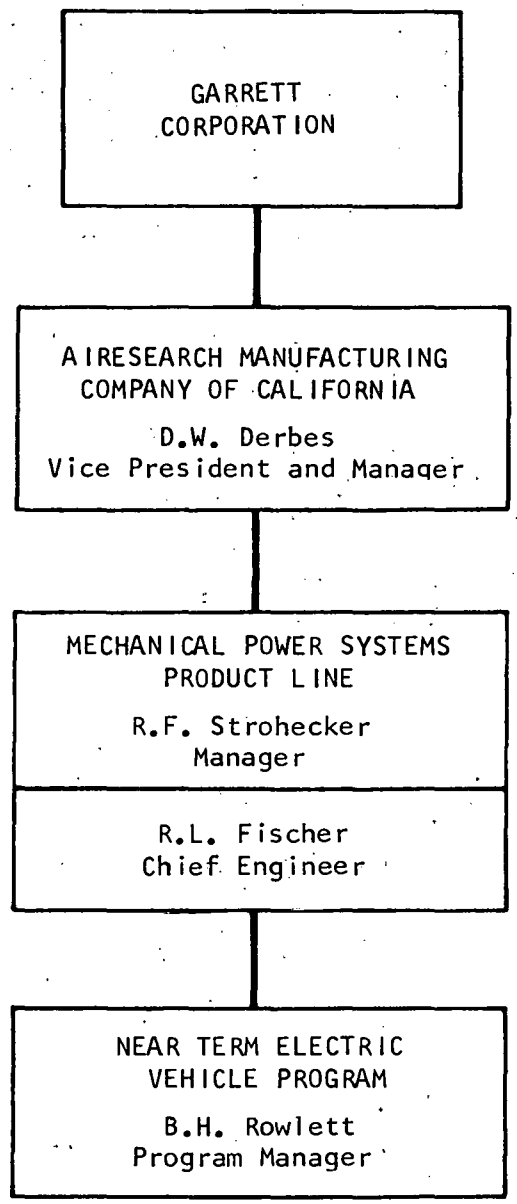


Figure 2. Relationship of Near-Term Electric Vehicle Program to AiResearch Management

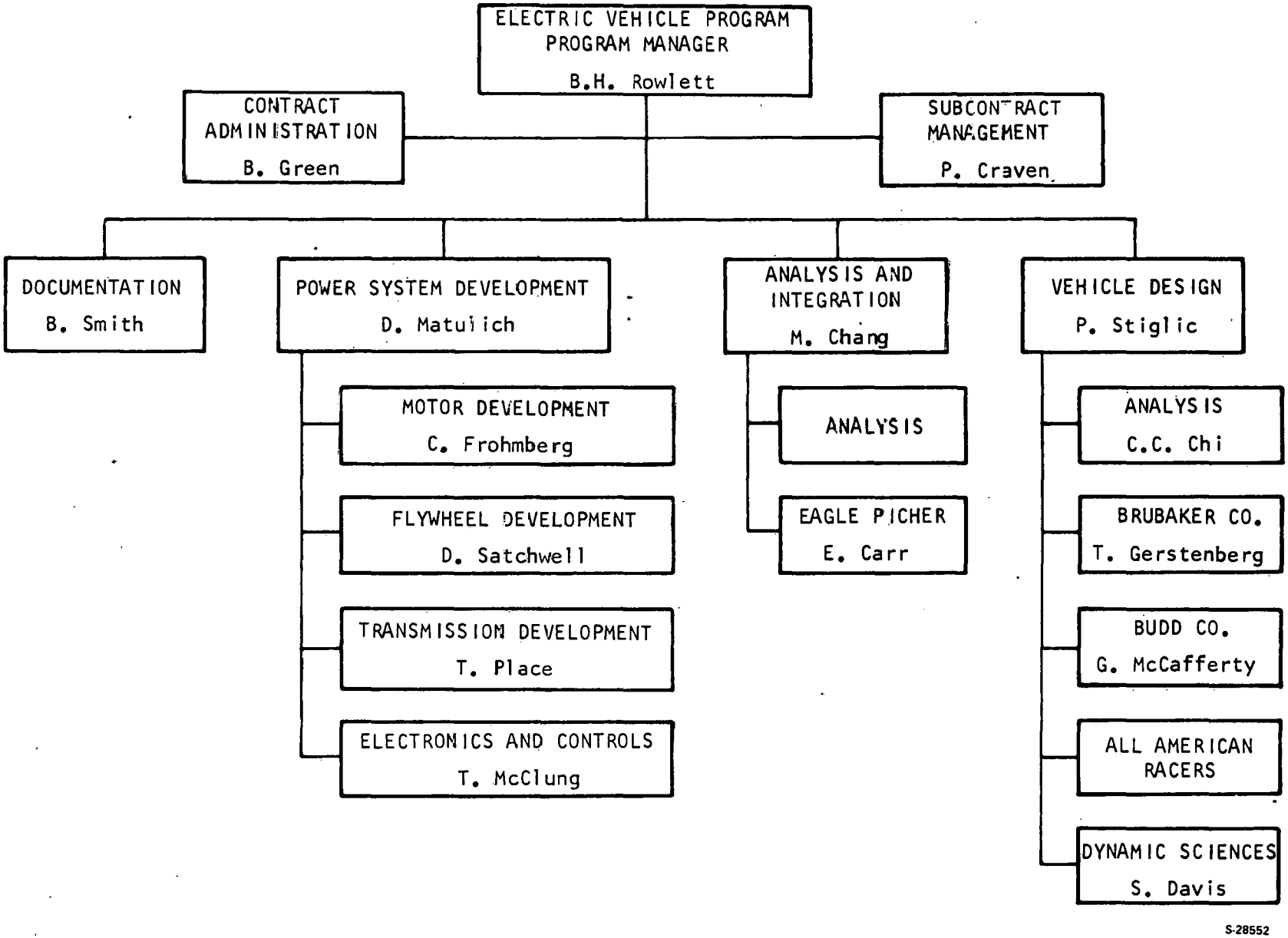


Figure 3. AiResearch Near-Term Electric Vehicle Organization

# SECTION 3

# PROGRAM DESCRIPTION

# SECTION 3

# PROGRAM DESCRIPTION

## PROGRAM OBJECTIVES

The specific objective of this Phase II program effort is to proceed from the Phase I preliminary design through a proof-of-concept test vehicle demonstration. This requires a 24-month development program, resulting in the completion, in-depth test and analysis, and the delivery of two integrated test vehicles that meet the DOE electric vehicle near-term objectives shown in Table 1.

## SCOPE OF WORK

The scope of work is based on the continuation of the vehicle design that resulted from the Phase I preliminary design study and essentially follows the development plan for Phase II, which was submitted during Phase I under Task 4. Briefly, the work includes:

(a) Program planning and management

(b) Analysis of the Phase I preliminary design

(c) Detail design

(d) Scale model crush and crash safety test program

(e) Restraint system design and test confirmation

(f) Fabrication and delivery of two integrated test vehicles

(g) Fabrication and crash testing of one crash-test vehicle

(h) Development and development testing at the component, subsystem, and vehicle levels

(i) Specified documentation

(j) Program reviews

## TECHNICAL APPROACH

The proposed plan concentrates on needed technological improvements that eventually can be mass produced at competitive costs. This is a challenging task, requiring a multiplicity of talents, experience, and facilities.

The Phase I preliminary design studies provided insight into major problems that have prevented development of an economically viable and acceptable electric passenger car. The studies demonstrated that, with sufficient emphasis and with new (but available) technology, the major problems can be solved, and an acceptable, economical car can be developed.

TABLE 1

DOE ELECTRIC VEHICLE PROGRAM NEAR-TERM OBJECTIVES

| Parameter | Near-Term DOE Objectives |
|---|---|
| Minimum passenger capacity | 4 adults |
| Maximum curb weight, lb | Open |
| Minimum urban range (J227A (D)), mi | 75 |
| Maximum initial cost, projected, 1975 dollars | 5000 |
| Minimum life, mi | 100,000 |
| Minimum life, yr | 10 |
| Maximum life-cycle cost, projected in 1975 dollars/mi | 0.15 |
| Cost of energy in dollars/kw-hr | 0.05 |
| Maximum electric recharge energy in urban driving, kw-hr/mi | 0.5 |
| Maximum recharge time, hr (115-vac, 30-amp service) | 6 |
| Minimum top passing speed, mph | 60 |
| Minimum top cruising speed, mph | 55 |
| Minimum accessories | Heater/defroster, onboard charger |
| Safety features | FMVSS* requirements at time of contract |
| Minimum unserviced park duration, days | 7 |
| Maximum years until production ready | 5 |
| Maximum critical materials required | Few |
| Minimum acceleration (0 to 30 mph), sec | 9 |
| Maximum merging time (25 to 55 mph), sec | 18 |
| Sustained speed on 5-percent one-mile grade, mph | 50 |
| Maximum scheduled maintenance cost, ¢/mi | 2 |
| Minimum ambient temperature range, °F | -20 to +125 |
| Interior noise | Minimum |
| Turning and braking | No power assist required |

*Federal motor vehicle safety standards

Major problem areas, because of their importance in the program, are:

(a) Development of an energy-efficient regenerative power system

(b) Design and development of a lightweight vehicle structure

(c) Fabrication of batteries with increased energy density

(d) Meeting federal motor vehicle safety standards

(e) Meeting the cost goals

The following paragraphs briefly discuss the approach to solving these problems.

Power System

The most critical technological need is for a more efficient power-and-battery system. The various possible batteries, including advanced batteries, are currently under intensive development, through DOE sponsorship. AiResearch is closely monitoring these developments. The principal thrust in this program is to develop the most efficient power system possible for a given battery technology.

It has been shown in the Phase I study (and other sources) that the battery capacity and life and the vehicle range and acceleration performance can be increased by an efficient regenerative power system with load-leveling capability. A power system using an energy-storage flywheel will significantly increase both acceleration and range; however, it has been shown that the obtainable performance goals are very sensitive to component efficiencies, and to components matching and integration into the system. Furthermore, careful analysis, followed by test confirmations, will be required to determine the type of adaptive controller schedule that is best for all types of driving cycles.

Each of the power system component designs is based on design work accomplished in Phase I. The components will be fabricated and checked out in the component laboratory before installation in a power system test setup. The system test setup will be used throughout the program for correlation with all vehicle testing.

Lightweight Vehicle Structure

The primary structure and body must be lightweight to minimize power losses and avoid excessive battery weight. Designing and developing a lightweight structure involves several technical problems. The lightweight structure must be strong to protect the occupants and also must retain the batteries during a collision. The battery-retention method must allow the batteries to absorb a major share of the impact energy. Finally, the lightweight, high-strength structure must be producible at a low cost.

The structure, as specified during the Phase I preliminary design, will be made predominantly of reinforced plastic, and will be based on previous work conducted by the Budd Company on the use of plastics in automotive structural design. Consequently, the major portion of this work, including the detail design, scale model testing, and fabrication of the vehicle bodies, has been subcontracted to the Budd Company. The Brubaker Group will continue to be responsible for the automotive design and styling, and All American Racers has been subcontracted portions of the suspension design and fabrication work.

## Improved Lead-Acid Batteries

Current production traction (deep discharge) batteries, characterized by golf-cart batteries, have an energy density of about 12 w-hr/lb and an average life of less than 500 deep discharge cycles. These batteries have been in production for many years and, although it is possible to build better vehicle batteries today, production has not yet been justified from the present marketing or economic aspects.

The objectives of the DOE Near-Term Electric Vehicle Program can be met with a battery energy density of approximately 18 w-hr/lb, which is within the presently known technology; such a battery could be put into production if justified by realistic near-term marketing goals. Accordingly, Eagle-Picher Industries has been awarded a major subcontract to provide the improved batteries for this program.

The Eagle-Picher battery will be a tubular positive plate construction which will ensure a long cycle life during deep-discharge vehicular service. The new battery will also be antimony-free, which will improve the battery performance over the extended life cycle and also minimize or eliminate the water servicing requirements.

## Production Costs

Current studies indicate that the cost of the electric passenger vehicle, in its present form, would be excessive, even in high-volume production. This is specifically due to the high battery weight, which affects cost by requiring a heavy frame and body, and the cost of the power system, including the batteries. Although the cost of the motors and the electronics could be reduced somewhat with higher production quantities, the more fundamental problem is to reduce the total weight of the vehicle to that which can be produced for the required cost. This will be a difficult task until smaller and lighter batteries are available. The objective of this program is, therefore, to minimize battery weight by designing an optimally efficient vehicle that will require the lowest possible battery power--one with a lightweight frame and body and an efficient power system. Both of these features must be achieved with low-cost materials and with producibility inherent in the design.

The Phase I study of manufacturing costs established the feasibility of achieving the cost goals. This estimate was based on studies by plastics manufacturers of their new materials and processes specifically developed to compete with steel automotive parts. Also, it was shown that costs of some parts, currently in low-volume production (such as the traction motors and the electronics), must be extrapolated into lower estimates for higher production rates.

## Safety Standard

The design must comply with all federal motor vehicle safety standards as of the date of the contract. This includes all existing crashworthiness requirements, which impose a severe challenge with respect to the light weight plastic structure that also must accommodate the 1000 lb of batteries required by the vehicle. The design concept will be verified by scale model testing as the design proceeds.

Other government safety standards that must be met include material specifications, nonflammability, operational requirements, braking, restraint system integrity, and accident avoidance handling. Some of these requirements will be demonstrated by actual testing. Dynamic Sciences, Inc., has been subcontracted to perform consulting services in many of these areas and to conduct the required safety testing.

## SUMMARY SCHEDULE

A summary program schedule for the 24-month program (Figure 4) shows start and stop dates for all major segments of program activity such as analysis, design, testing, fabrication, and component development.

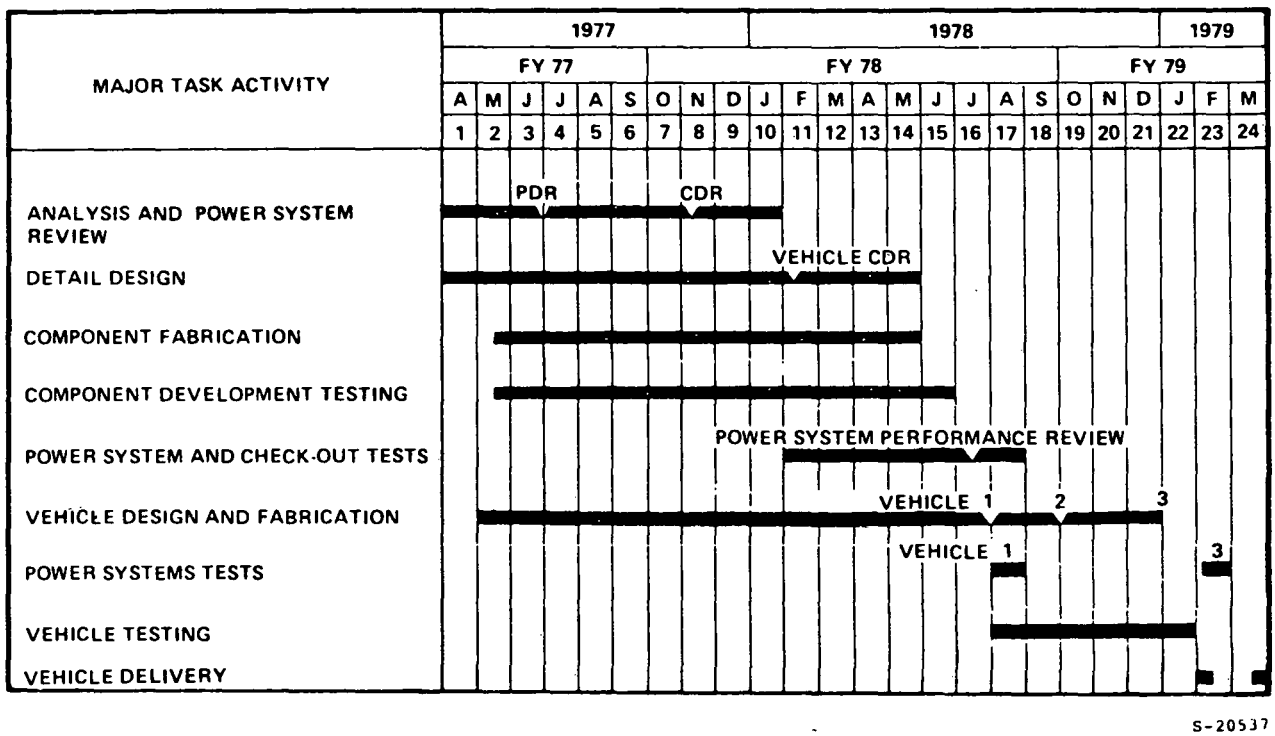


S-20537 A

Figure 4. Near-Term Electric Vehicle Program Schedule, Phase II

# SECTION 4

# SYSTEM INTEGRATION AND PERFORMANCE

# SECTION 4

# SYSTEM INTEGRATION AND PERFORMANCE

## VEHICLE PERFORMANCE

Dynamic performance of a vehicle can be categorized into several areas: driving range, acceleration power, hill-climbing capacity, braking power, and handling and ride characteristics. An acceptable vehicle should yield good performance in all of these areas, but emphasis was placed on the acceleration power and driving range during the study and design phases of the program. Basically, the design goals of the electric vehicle are for hill-climbing capacity, braking power, handling, and ride quality to be comparable to that of the conventional internal combustion engine car. A relatively modest acceleration standard of 20 sec from standstill to 55 mph was chosen as the acceleration design goal. The vehicle was then optimized to yield the maximum driving range per battery charge while still preserving the other design goals.

Several digital computer simulation programs (discussed in more detail later in this section) were developed during Phase I to evaluate the dynamic performance of the vehicle. As detailed design continued in the Phase II development program, more accurate assessments of each component's performance, or losses, were possible, and the computer simulation programs were updated accordingly.

A summary of the current performance projection of the Phase II design, based on the updated simulation programs, is presented in Table 2 along with the near-term DOE goals. The dynamic performance of the present design of the vehicle meets the near-term DOE goals in each category.

In general, the projected vehicle performance of the Phase II design is lower than that projected in the Phase I study. The Phase I projection was based on the state of the art for a final production version of the design, whereas projections for the Phase II design are based on the prototypes under development. Because of some of the relatively new and unique concepts involved, some overdesign was advisable for the prototypes in several critical areas to ensure success at first build. In addition, limited development time and resources restricted the selection of several noncritical items, such as electrical contactors and sensors, to commercially available items, rather than specially built items which would be selected for production versions. Hence, performance of the future production unit should exceed these projections.

Detailed discussions of the vehicle dynamic performance are presented in the following paragraphs and in Section 5.

TABLE 2

SUMMARY OF VEHICLE PERFORMANCE

| | Near-Term DOE Objectives | Projection for Phase II Design | |
|---|---|---|---|
| | | 4 Passengers | 1 Passenger |
| Urban range, mi | | | |
| SAE J227A (D) cycle | 75 | 79 | 88 |
| Federal urban driving schedule | Not specified | 78 | 92 |
| Acceleration time, sec | | | |
| 0 - 30 mph | 9 | 9 | 8 |
| 25 - 55 mph | 18 | 13 | 11 |
| 0 - 60 mph | Not specified | 23 | 20 |
| Top cruising speed, mph | 55 | 68 | 68 |
| Sustained speed on 5% grade, mph | 50 for 1 mi | 50 for 1.3 mi | 50 for 1.5 mi |
| Energy consumption, kw-hr/mi (from city power line) | 0.50 | 0.39 | 0.36 |

SAE J227A (D) Driving Cycle

The SAE J227A (D) driving cycle has been used for most of the computer simulation studies to optimize the system and its components. The final design of this vehicle has a projected range of 79 mi while being subjected to this driving cycle. The system performance over this cycle is summarized in Figure 5.

The upper portion of the figure summarizes the energy losses for each group of components during each segment of the cycle; the middle portion tabulates the energy levels stored in the flywheel (vehicle internal energy) and in the vehicle (vehicle kinetic energy) at the end of each segment, as well as the battery energy which is required to overcome the system losses (battery energy into p.s.).

The unique load-leveling feature of this electric propulsion system is clearly shown in Figure 6. During the acceleration segment of the SAE cycle, the instantaneous power required to overcome vehicle losses and supply the vehicle kinetic energy is several times greater than the power required during the constant-speed cruise segment. This peak power requirement is supplied by using the flywheel kinetic energy to supplement battery power to propel the vehicle.

SUMMARY OF ENERGY LOSSES FOR DRIVING CYCLE IN WT-HR

| TIME | ROAD LOAD | PLNTY DFRNTL | CARRIER MOTOR GEAR | RING MOTOR GEAR | FINAL DRIVE DFRNTL | FLYWHEEL LOSSES | CARRIER MOTOR ARMATURE | CARRIER MOTOR FIELD | RING MOTOR ARMATURE | RING MOTOR FIELD | CNTRLR AND CHOPPER | FAN | TOTAL LOSSES |
|---|---|---|---|---|---|---|---|---|---|---|---|---|---|
| 0.- 28. | 15.45 | 4.75 | .95 | 1.11 | 4.42 | 2.93 | 13.99 | 3.74 | 7.42 | .97 | 1.41 | 1.13 | 58.27 |
| 28.- 78. | 81.12 | 4.33 | .96 | .08 | 3.73 | 4.53 | 9.95 | .88 | 4.14 | 4.17 | 1.49 | 1.94 | 117.32 |
| 78.- 88. | 11.27 | 1.81 | .23 | .54 | .91 | .94 | 2.29 | .31 | 4.44 | .41 | .29 | .39 | 23.83 |
| 88.- 97. | 2.45 | 1.60 | .34 | .46 | 1.70 | .90 | 6.54 | 1.76 | 10.77 | .09 | .52 | .35 | 27.48 |
| 97.- 122. | .00 | 3.06 | .00 | .68 | .00 | 2.58 | .00 | .00 | 4.98 | .36 | .55 | .97 | 13.18 |
| TOTALS | 110.29 | 15.55 | 2.48 | 2.87 | 10.76 | 11.88 | 32.77 | 6.69 | 31.74 | 6.00 | 4.26 | 4.78 | 240.07 |

ENERGY STORAGE SYSTEM SUMMARY IN WT-HR

| TIME | VEHICLE INTERNAL ENERGY | VEHICLE KINETIC ENERGY | BATTERY ENERGY INTO P.S. | ENERGY CONSUMPTION |
|---|---|---|---|---|
| .0 | 743.02 | .00 | .00 | |
| | | | | 56.16 |
| 28.0 | 641.15 | 95.57 | 49.87 | |
| | | | | 117.20 |
| 78.0 | 630.87 | 95.57 | 156.79 | |
| | | | | 21.57 |
| 88.0 | 677.30 | 48.30 | 177.52 | |
| | | | | 30.60 |
| 97.0 | 708.37 | .00 | 190.89 | |
| | | | | 13.16 |
| 122.0 | 742.74 | .00 | 238.42 | |
| | | | | 238.70 (TOTAL) |

ENERGY INPUT TO POWER SYSTEM/MILE = 252.18 WATT-HOURS

ENERGY INPUT TO BATTERY/MILE = 333.31 WATT-HOURS (75.66 PERCENT BATTERY WATT HOUR EFFICIENCY)

ENERGY INPUT TO BATTERY CHARGER/MILE = 392.13 WATT-HOURS (85.00 PERCENT CHARGER EFFICIENCY)

RANGE = 76.1 MILES (1040.0 LBS. OF BATTERIES) + 3.2 MILES (1.0 KW-HR OF FLYWHEEL)

= 79.3 MILES PER BATTERY CHARGE

Figure 5. System Performance Over J227A (D) Driving Cycle

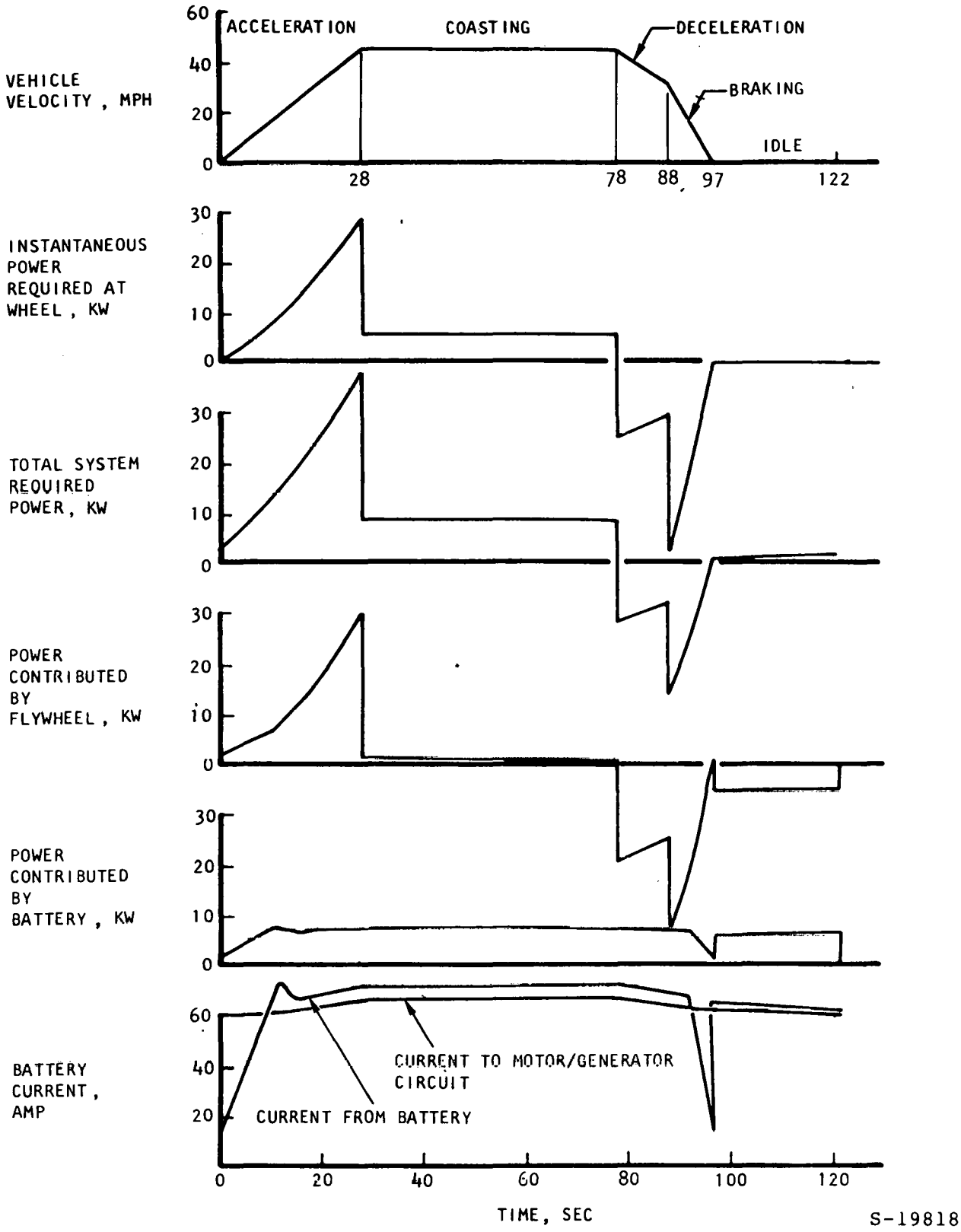


Figure 6. System Power Flow Paths For J227A (D) Driving Cycle

During the coasting and braking segments of the cycle, the prescribed time rate of change in vehicle kinetic energy is greater than the power required to overcome vehicle losses. Over the braking interval, this extra energy is recovered by the system and used to recharge the flywheel. Battery current is drawn during the coasting, braking, and idling periods to recharge the flywheel back to its initial kinetic energy level. The flywheel system's ability to maintain a nearly constant battery current despite the wide variation of power requirements as the vehicle proceeds through the driving cycle, combined with the flywheel's regenerative ability during braking, are the key features that result in the increased range during stop-and-go driving.

Several vehicle characteristics such as tire rolling resistance, vehicle body aerodynamic drag, and drive train efficiency influence the dynamic performance of the vehicle. The variation of vehicle range, over the J227A (D) cycle as a function of the best and worst-case variation in the pertinent vehicle-design parameters, is summarized in Figure 7. The range differences between the worst and best-case projections reflect the cumulative effects of possible inaccuracies in calculating the various losses such as drive train efficiency, vehicle size, and tire characteristics. Table 3 shows the losses used to compute the curves of Figure 7. The current estimate is based on the latest detailed analysis of vehicle design results. This figure demonstrates the importance of meeting the system design weights.

TABLE 3

SUMMARY OF LOSSES USED IN THE SENSITIVITY ANALYSIS

| Parameter | Optimistic Estimate | Best-Case Estimate | Worst-Case Estimate |
|---|---|---|---|
| Rolling resistance, lb/lb | 0.0054 | 0.0060 | 0.0072 |
| Aerodynamic drag area, CA, ft | 7.2 | 8.0 | 9.6 |
| All gear losses, w | 840 | 933 | 1120 |
| Flywheel assembly losses, w | 316 | 351 | 421 |
| Control and miscellaneous losses, w | 235 | 262 | 314 |
| Motor/generator peak efficiency, percent | 89 | 89 | 87 |

The range is directly proportional to battery energy density, hence the significance of the battery can not be overemphasized. The computer simulation studies in Phase II were based on a battery with a nominal energy density of 40 w-hr/kg at a 3-hr discharge rate. This energy density is the DOE near-term objective for the electric-vehicle application of the improved state-of-the-art lead-acid battery. In this case, it is a projection based on the modification of an existing state-of-the-art lead-acid battery.

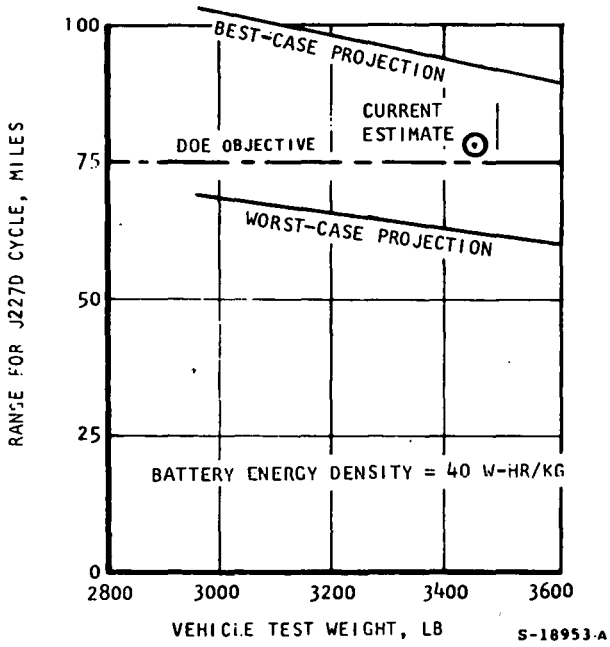


a. VEHICLE WEIGHT SENSITIVITY

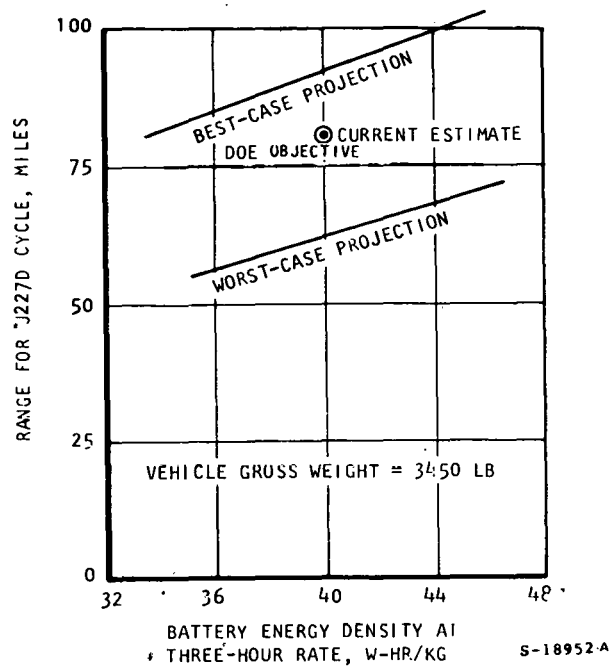


b. BATTERY ENERGY DENSITY SENSITIVITY

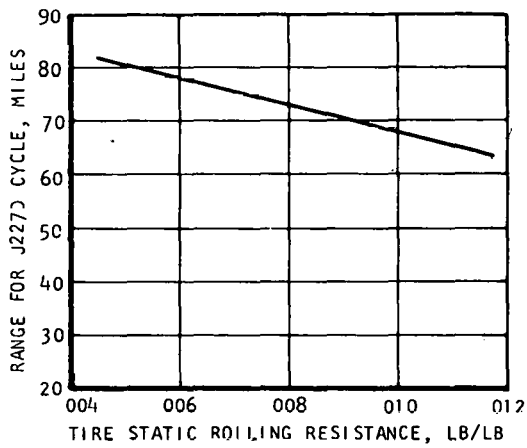


c. TIRE ROLLING RESISTANCE SENSITIVITY

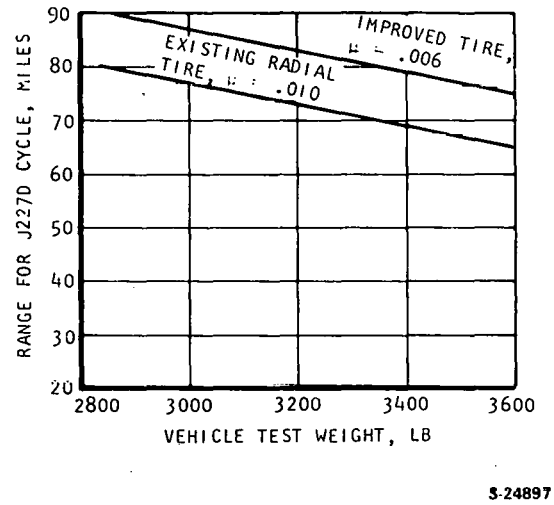


d. TIRE CONFIGURATION AND TEST WEIGHT SENSITIVITY

Figure 7. Sensitivity of Vehicle Range to Various Vehicle Parameters

Because of the load-leveling feature of this flywheel power system, high power density or a high battery discharge rate are not required. Hence a golf-cart battery with 27 w-hr/kg can be redesigned to yield 40 w-hr/kg as discussed in detail later in this section. In the future, redesigning this battery to achieve 50 w-hr/kg is feasible, and improved state-of-the-art batteries are being developed through DOE effort.

Federal Urban Driving Schedule

Computer simulation studies also were conducted for the Federal Urban Driving Schedule (FUDS). In contrast to the SAE J227A (D) cycle, this pattern reflects a variety of intracity conditions, derived from actual driving records. The velocity-time distribution, shown at the top of Figure 8, includes segments representative of freeway, surface street, and congested urban driving. The cycle covers a total distance of 7.5 mi, at an average speed of 19.6 mph, with an average of 2.4 stops per mile.

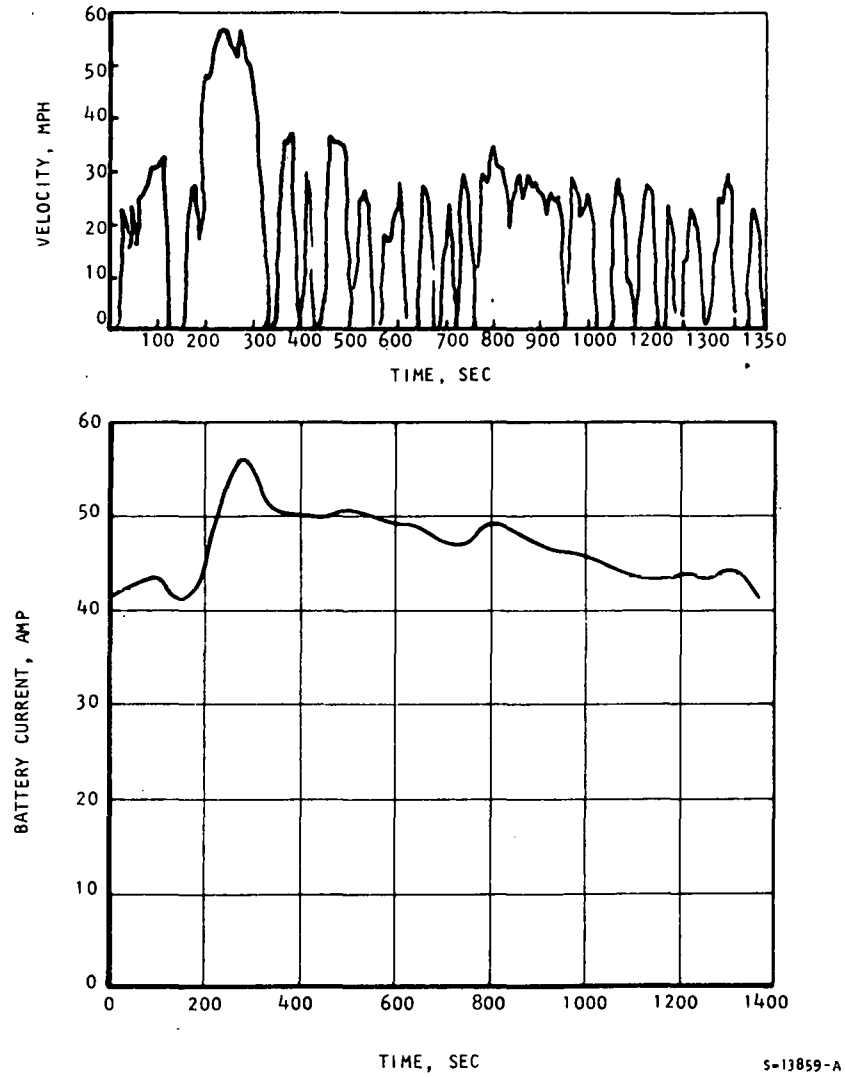


Figure 8. Power System Load Leveling, Federal Urban Driving Schedule

The battery discharge current computed for this cycle is shown at the bottom of Figure 8. The battery output adjusts to changes in the average power requirement over successive segments of the cycle, while the additional power demand for acceleration is provided by the flywheel and the power regenerated during braking is absorbed by the flywheel. The maximum battery power is 5.2 kw in contrast to the peak power system output of 36.4 kw. The regenerative braking capability (discussed later in this section) is adequate to meet the deceleration requirements over the entire cycle. The load-leveled duty cycle permits the near-optimum use of battery energy. The battery discharge time for the 78-mi range, at an average speed of 19.6 mph, is 4.0 hr.

Constant-Speed Cruise

The motive power for constant-speed cruising over sustained intervals is provided entirely by the battery. While cruising, the flywheel is maintained at operational speed by drawing additional power from the battery, and does not supply any portion of the tractive power. The variation of vehicle range with cruise speed is shown in Figure 9. The range exceeds 120 mi for a constant 40 mph.

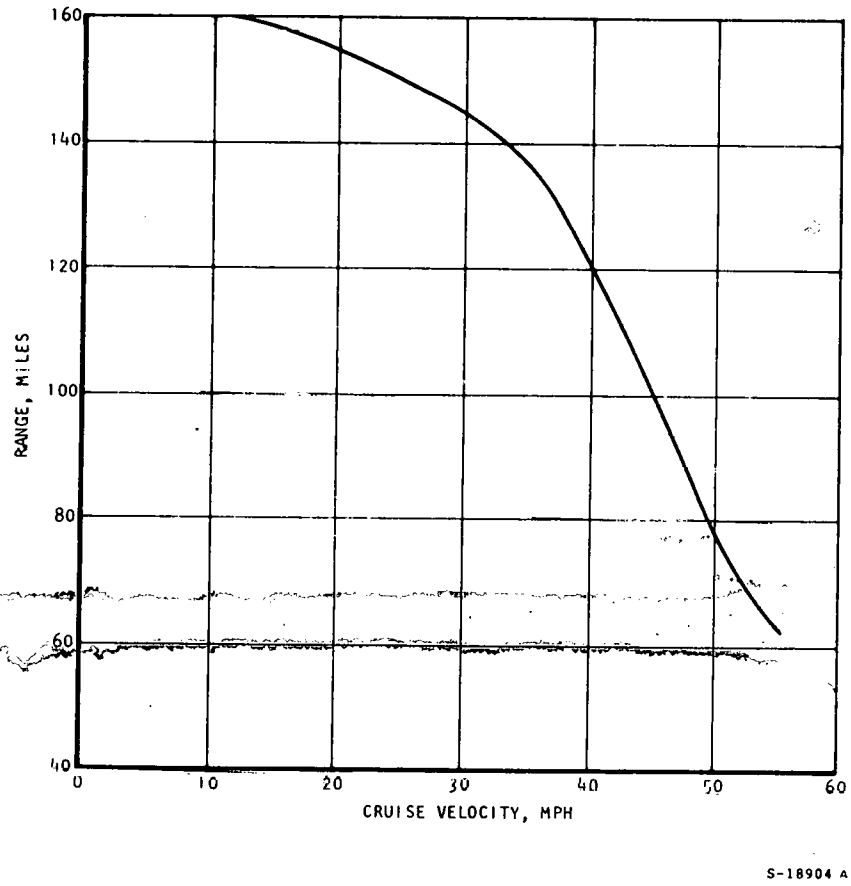


Figure 9. Vehicle Range at Constant Speed

## Acceleration Power

In addition to leveling the battery load demand, the flywheel in this power system provides excellent acceleration and passing power. The acceleration capability, shown in Figure 10, is adequate for meeting the normal requirements of both urban and suburban traffic patterns, such as FUDS. The elapsed time from zero to 60 mph is 23 sec, with a maximum acceleration of 3.7 mph/sec. The acceleration time from zero to 30 mph is 9 sec and the 25- to 55-mph merging maneuver requires 11 sec. The maximum vehicle speed is 68 mph, which is limited by the maximum speed of the traction motor, instead of by the available power.

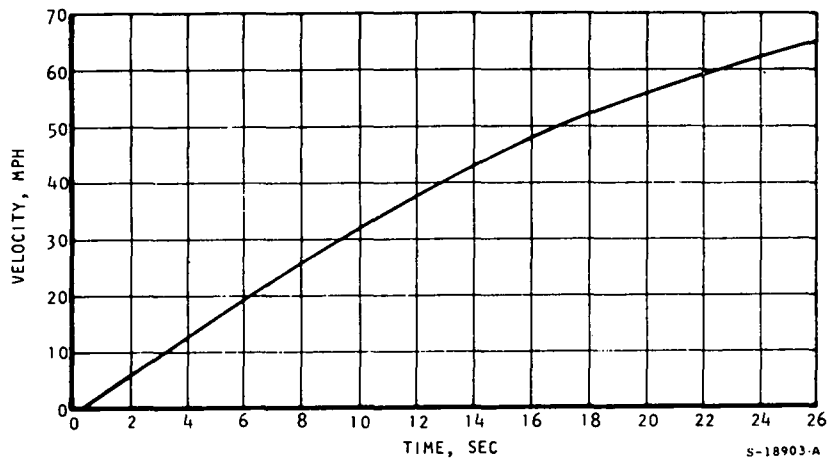


Figure 10. Maximum Acceleration, Flywheel Powered, Full Throttle

## Hill Climbing

The high power required for hill climbing, at highway speed, can be delivered by the flywheel without approaching the peak-power capability of the traction motor. The hill-climbing profile for a 5-percent grade at 50 mph (presented in Figure 11) shows the power split between the flywheel and battery, as a function of the total climbing distance. During the initial 1.35 mi of the climb, the flywheel provides approximately 70 percent of the required power.

The fluctuation of battery power demonstrates the effect of the battery current controller. The battery output climbs to a maximum of 11.5 kw at 120 amp as more and more energy is drawn from the flywheel. The battery output then begins to drop as the generator falls below base speed, thus dropping the system line voltage. The traction motor armature current must increase to maintain system output as the line voltage decreases. This current is limited to a maximum of 200 amp by restricting the battery output. The power-system output falls below 5 kw when the flywheel approaches minimum speed and the generator slows to the point where it can no longer produce the required current. The system switches to simple battery power when this output reaches a level within the 18-kw capability of the traction motor alone. This transition occurs over a distance of 0.05 mi.

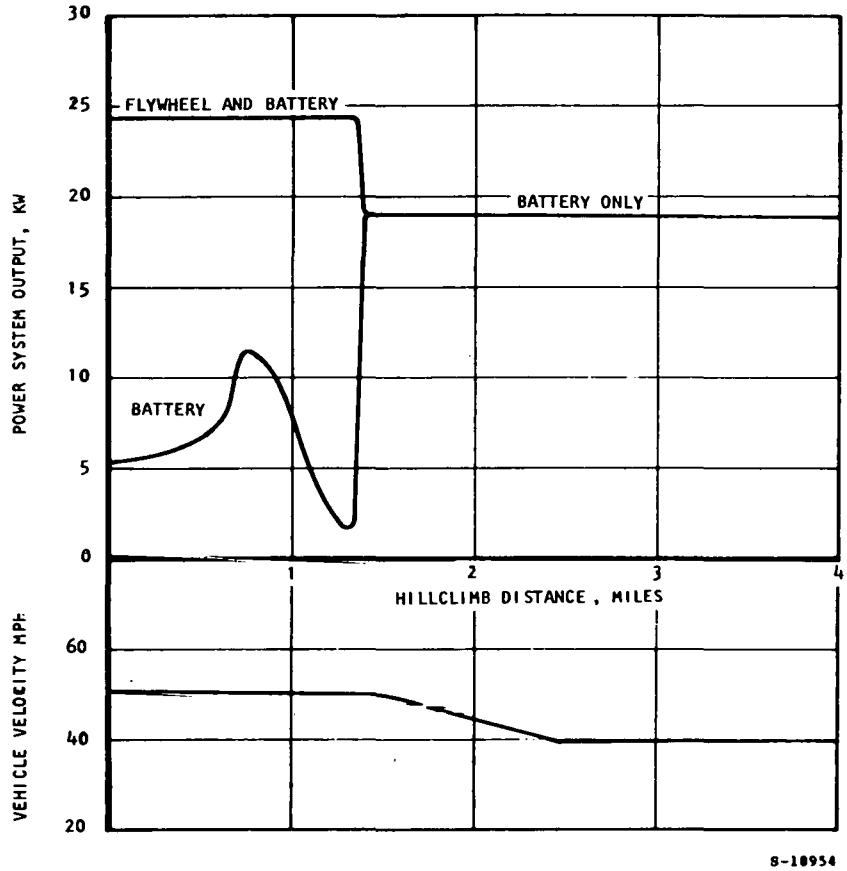


Figure 11. Flywheel-Powered Hill Climb on 5-Percent Grade

The traction motor is capable of sustaining 40.5 mph on the 5-percent grade. The transition to this speed occurs over the succeeding mile, as shown in Figure 11. The hill-climbing range, in this battery mode, is limited to two to three miles by the thermal capacity of the traction motor. A thermal override will then begin limiting armature current, so that the vehicle can continue at reduced speed. The steady-state capability on a 5-percent grade is 26 mph.

## Braking

The vehicle braking system currently is being designed to meet the Federal Motor Vehicle Safety Standards summarized in Section 6. The maximum braking rate specified for the combined friction and electrical braking system is 13.6 mph/sec. The friction brake system will complement the performance of the electrical, regenerative brakes, which are discussed below.

Full-power regenerative braking provides strong braking power at high system efficiency. The full-power braking rates over the vehicle speed range are shown in Figure 12. Friction brakes are needed below 2 mph and for braking rates greater than 3.5 mph/sec. Regenerative braking provides sufficient power to meet the braking requirements associated with normal driving, which are generally less than 3.5 mph/sec. The power system efficiency during a full-power braking cycle from maximum speed is 90 percent. Of the 201 w-hr of vehicle kinetic energy at 68 mph, 21.2 w-hr are used to overcome tire losses and aerodynamic drag while 152.8 w-hr are recovered in flywheel kinetic energy.

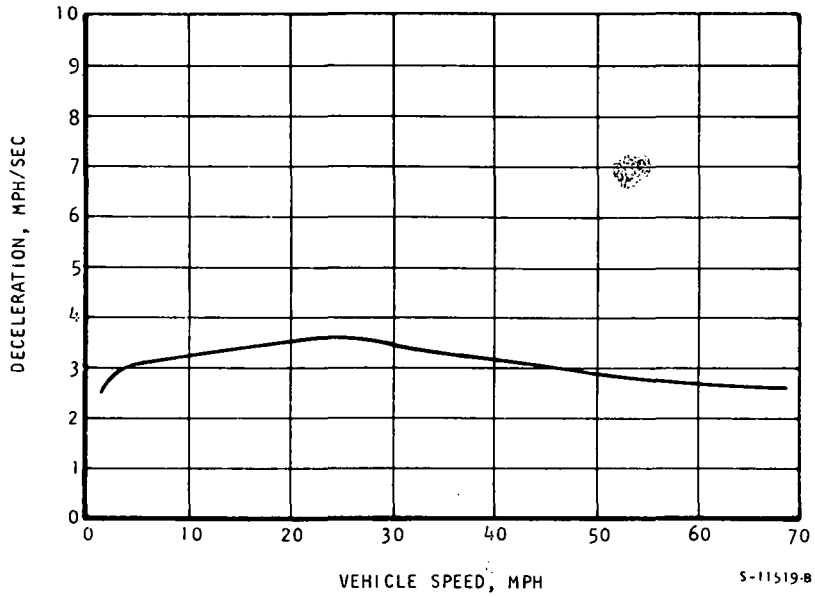


Figure 12. Regenerative Braking, Deceleration

Low-Temperature Operation

Performance of battery-powered vehicles has always been limited by the reduced electrochemical activity of the battery at low temperature. Also, the increased viscosity of the lubricants in the transmission and bearings at low temperatures further reduces system performance. Performance of the two motors is, however, enhanced by low temperature due to the reduction of the electrical resistance.

Vehicle system performance has been analyzed for the case of a -20°F soak temperature. Acceleration capability (time to speed) is reduced by approximately 10 percent and the range capability, calculated for the SAE J227A (D) cycle, is reduced to 38 mi; however, the battery would warm up during this driving, so the range computed with actual transient temperatures would be increased.

At present it is not planned to insulate or heat the battery compartment or the power system compartment. During cold weather operation, the normal daily driving and overnight recharging cycle will tend to maintain the batteries and the power unit at temperatures well above a low soak temperature. Detailed thermal transient studies would be needed to determine the need for insulation and electrical heating, or the use of an onboard fuel heater.

## VEHICLE WEIGHT

The gross vehicle weight, with four 150-lb passengers, is currently estimated to be 3449 lb, and forms the basis for the vehicle performance described in this report. A vehicle weight summary is given in Table 4.

TABLE 4

VEHICLE WEIGHT SUMMARY

| Part Name | Weight, lb |
|---|---|
| Body assembly, final | 498.6 |
| Operating hardware | 53.7 |
| Lamps/switches, instrument panel controls | 7.2 |
| Exterior ornaments | 16.3 |
| Trim panels | 7.0 |
| Seats | 65.0 |
| Seals, w/strip, insulation | 5.5 |
| Glazing | 82.6 |
| Convenience items | 17.8 |
| Interior molding and ornaments | 0.5 |
| Instrument panel and console | 13.5 |
| Paint | 10.0 |
| Power system | 606.4 |
| Batteries | 1040.0 |
| Final drive | 26.0 |
| Suspension | 143.4 |
| Steering | 16.7 |
| Brakes | 86.1 |
| General chassis, complete | 128.0 |
| Chassis Indirect material | 2.5 |
| Heater | 13.0 |
| Accessory equipment | 9.2 |
| Vehicle total weight, lb | 2849.0 |

The weight of the power system is based on complete detail drawings and on detailed listings of the major parts, including an allowance for wiring and miscellaneous parts. The power system weight summary is shown in Table 5.

TABLE 5

POWER SYSTEM WEIGHT SUMMARY

| Description | Weight, lb |
|---|---|
| Power Unit | |
| Flywheel and housing assembly | 156.05 |
| Transmission and housing assembly | 89.72 |
| Motors | 229.58 |
| Mounting brackets and shims | 3.0 |
| Controls and Electronics | |
| Controller | 9.0 |
| Power electronics | 41.5 |
| Data recorder | 6.2 |
| Fuses (6) | 1.5 |
| Contactors (4) | 23.8 |
| Reverser | 0.8 |
| Sensors (5) | 6.2 |
| Electrical wires, cables, and fuse box | 14.0 |
| Charger assembly | 11.0 |
| Miscellaneous Mechanical Parts | |
| Cooling Fan | 5.1 |
| Air supply ducts (2) | 3.4 |
| Supports, cables, ducts, and clamps | 5.6 |
| Power system total weight, lb | 606.45 |

The vehicle body-weight breakdown (Table 4) is based on less complete detail drawings, but it includes specific calculations for the structural parts that have been defined and are now being detailed.

The estimated weight of the body assembly is based on current estimates of the Phase II design, and does not represent the minimum weight believed achievable when the weight-savings benefits of the plastic construction are fully realized. Even with the presently predicted weight, however, a considerable weight reduction over conventional steel construction will be realized.

## VEHICLE COST

During Phase I, economic studies were made of the potential production cost of the new design concept. The objectives of these studies were to verify that the concept could be mass produced for a selling price of $5,000 (1975 dollars) and that the overall (10-year) life-cycle cost would be no more than 15 cents per mile. Based on the preliminary design definition of the various components, the conclusion of the cost study was that these objectives could be achieved.

In the current Phase II period, the primary objective is to demonstrate that the new concept can meet the performance goals of the program. The cost objectives, while not applicable to the two experimental vehicles, must be maintained for the projected production versions. Hence, the primary cost objective for Phase II is to maintain the simplicity of the original component designs, and to avoid undue complexity that would result in increased production costs or life-cycle costs.

At the completion of the detail-design task, all of the detail drawings will be used for careful studies of component costs. Concurrently, producibility studies will be conducted to further improve the production potential, based on the development and test experience gained during the test program. The final report will contain the results of the Phase II production and life-cycle cost estimates.

## VEHICLE OPERATION

From the driver's point of view, the operation of the vehicle is very similar to that of an internal combustion engine (ICE) vehicle with an automatic transmission. The driver selects the desired mode of operation, either drive, neutral, reverse, or park, as in the ICE vehicle. The rates of acceleration and braking are controlled by the throttle and brake in a similar manner. The vehicle regenerative braking capability is used to simulate the feel of compression braking, when both the brake and throttle are off.

The principal differences are in vehicle startup and battery recharging. Recharging is accomplished by plugging the retractable cord from the onboard charger into a 30-amp, 110-vac power source for several hours. To begin vehicle operation, the flywheel must first be brought up to a minimum speed. The driver begins the flywheel-charging sequence by switching the key to the on position, with the gear selector in park. If the charger is plugged in, the flywheel-charging power is delivered from the wall socket; otherwise battery power is used. Once the flywheel reaches minimum speed, which normally requires from one to two minutes, the vehicle is ready to drive.

PERFORMANCE SIMULATION MODELS

Detailed mathematical equations and loss models were derived for each component, and were presented in AiResearch Document No. 76-13465, Final Report, Electric-powered Passenger Vehicle Design Study Program, and in SAE Technical Paper No. 780217, Computer Simulation of an Advanced Hybrid Electric-Powered Vehicle. The component models and the driving cycle velocity profile were integrated into a performance simulation computer program, according to the logic diagram shown in Figure 13. In this program, an ideal driver and controller are assumed to close the loop. In other words, the vehicle power required at any instant during a driving cycle is assumed to be matched ideally by the driver's exact positioning of the throttle or brake pedal, and by the controller's instant response. With this assumption, the vehicle velocity and acceleration follow the specified driving cycle exactly at all times, so that an objective study can be made.

In addition, three system models were developed to provide the required flexibility in simulating system operation over a given driving condition: (a) SUBURB, (b) ACCEL, and (c) UPHILL.

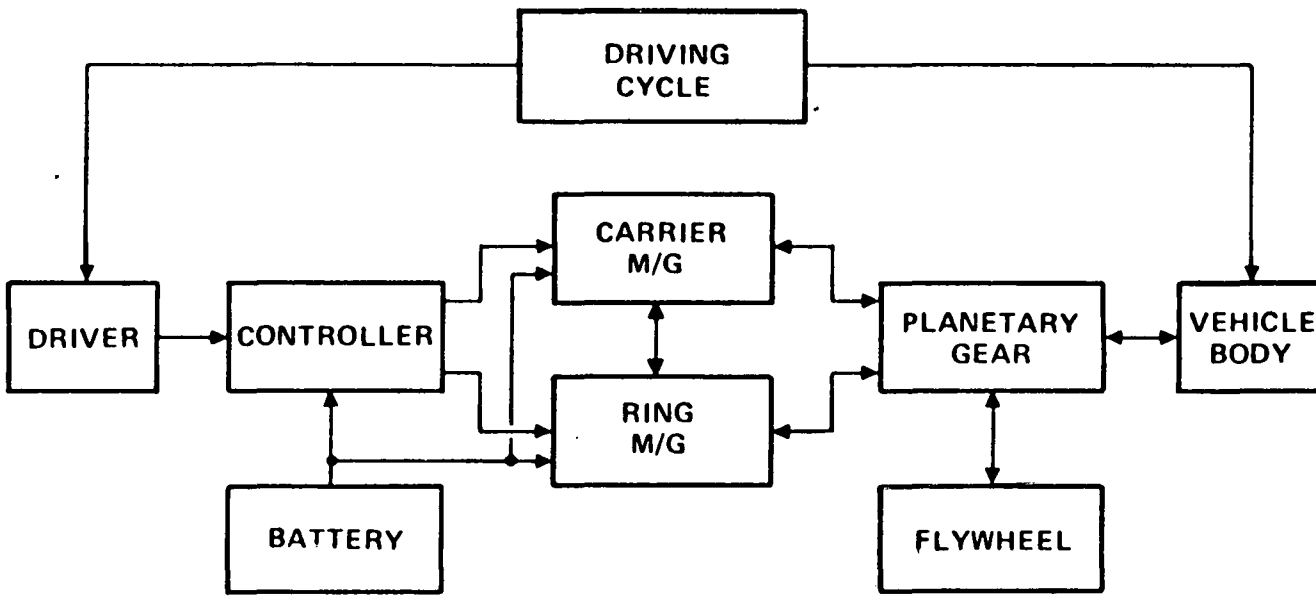


Figure 13. Vehicle Performance Simulation Program

Simulation Program SUBURB

SUBURB simulates vehicle operation over any arbitrary driving cycle comprising any number of specified segments. It is presently set up to simulate the five segments of the SAE J227A (D) suburban driving cycle. The power requirement is determined by the vehicle speed and acceleration prescribed in the driving cycle.

Simulation program SUBURB is used to (1) compute the range of the vehicle from the total summation of the energy requirements for the cycle,

(2) examine the individual losses in the system, and (3) show the sensitivity of the resultant range to each of the component losses.

SUBURB has been modified to simulate other driving cycles, in addition to the SAE J227A (D). Similar range and loss studies have been conducted using FUDS. The increased time duration (1370 sec) and the wide range of actual traffic conditions covered in this cycle make it well suited for the investigation of battery control schedules.

Simulation Program ACCEL

The second program, ACCEL, simulates maximum system performance during full-throttle acceleration to a given maximum speed, followed by full-power-regenerative braking.

Complete system and component performance is calculated for each time interval (usually 1 sec) throughout the entire operation, and includes all component speeds and accelerations, torque forces, and system losses. In addition, the computer provides plots of some of the major variables during acceleration and deceleration to facilitate comparison and evaluation of predicted performance.

Simulation program ACCEL is used to study maximum system power capability, as a function of the component sizes and efficiencies. The output shows the effect of the gear ratios used; the relation between the selected generator, flywheel, and motor speeds; and the resulting vehicle acceleration and deceleration performance. Also shown are the overall efficiency and the split between mechanically and electrically transmitted power.

Simulation Program UPHILL

The third program, UPHILL, simulates the operation of climbing up a grade at a given speed. This program logic is the same as SUBURB. In use, three segments are simulated: (1) level-ground acceleration to a given speed, (2) a short transition to the specified grade, and (3) vehicle steady-state speed up the grade, powered by the energy from both the flywheel and the generator, which is terminated when the generator no longer maintains a sufficient voltage speed, signifying that about 75 percent of the total energy stored in the flywheel has been extracted. The peak power of the battery is less than 10 kw, supplying less than 25 percent of the energy required for the hill climb.

BATTERY SUBSYSTEM

The performance of the electric-powered passenger vehicle is limited primarily by the energy-storage capacity of its batteries. High energy density, high specific power, capability for a large number of deep-discharge cycles, minimum maintenance, and reasonable initial cost are criteria for the selection of the candidate battery. At present, there is no off-the-shelf battery suitable for the electric vehicle application. The energy density of the best available golf-cart battery is only about 70 percent of the minimum acceptable requirement. Several advanced batteries such as nickel-zinc and nickel-iron show promise, but most are still in the laboratory development

stage. Improved state-of-the-art lead-acid batteries are the only feasible candidates within the development time frame of this program.

The specific power and specific energy of a battery are usually related in an inverse manner: a battery with high specific power normally has a low specific energy, and vice-versa. Batteries for high discharge rate (high specific power) applications must be designed differently from batteries for moderate or low-rate use. The most obvious difference is that batteries for high-rate service require significantly more plate area in each cell. This is accomplished by using a relatively large number of very thin plates (typical thicknesses are 1 to 3 mm). A battery designed in this manner has a very high specific power, but cycle life is sacrificed, since thin plates do not perform well in deep-cycling use. An example is the standard automotive battery. This type of battery is capable of supplying very high discharge currents, but can only deliver approximately 100 deep-discharge cycles.

An ideal battery (one with high specific power and high specific energy, long cycle life, and 100-percent use of active materials) cannot be made. The battery developer must make a compromise among these factors. Alternatively, the electric vehicle design engineer can consider hybrid battery systems to optimize electric vehicle performance. Thus, a battery with high specific power (to give higher speeds) can be used along with a battery with high specific energy (to give better range).

The unique feature of the AiResearch flywheel-regenerative power system is to create a load-leveled duty cycle for the battery. The elimination of the high-specific-power requirement makes the design emphasis on specific energy and on cycle life possible. The load-leveled duty cycle allows greater use of the active battery materials, and use of long-life, tubular-positive-plate construction. Compared to the golf-cart batteries, the active material is reduced by 20 to 25 percent, corresponding to a specific-energy improvement of approximately 4 w-hr/kg. In addition, the low current demand allows a significant reduction in the weight of the current-carrying parts. The weight of the current conductors for the load-leveled battery can be reduced by 45 percent compared to those for golf-cart batteries. This reduction corresponds to a specific-energy improvement of approximately 6 w-hr/kg.

## Battery Description

A tubular plate battery, proposed by Eagle-Picher Industries, was selected for this electric vehicle application. This battery features positive-tubular-electrode design, and grids with no antimony content for both the positive and the negative plates. Tubular plates retain the active materials, prevent shedding, and provide long cycle life. Eliminating antimony from the grid design prevents antimony contamination of the negative plate, thereby providing long wet-life, improved charge retention, and reduced maintenance.

Figure 14 shows the construction of the tubular plate battery cell. The component parts for the complete 6-volt module are shown in Figure 15. The 6-volt module dimensions and battery pack characteristics are shown in Figure 16. Preliminary performance characteristics are shown in Figures 17 and 18.

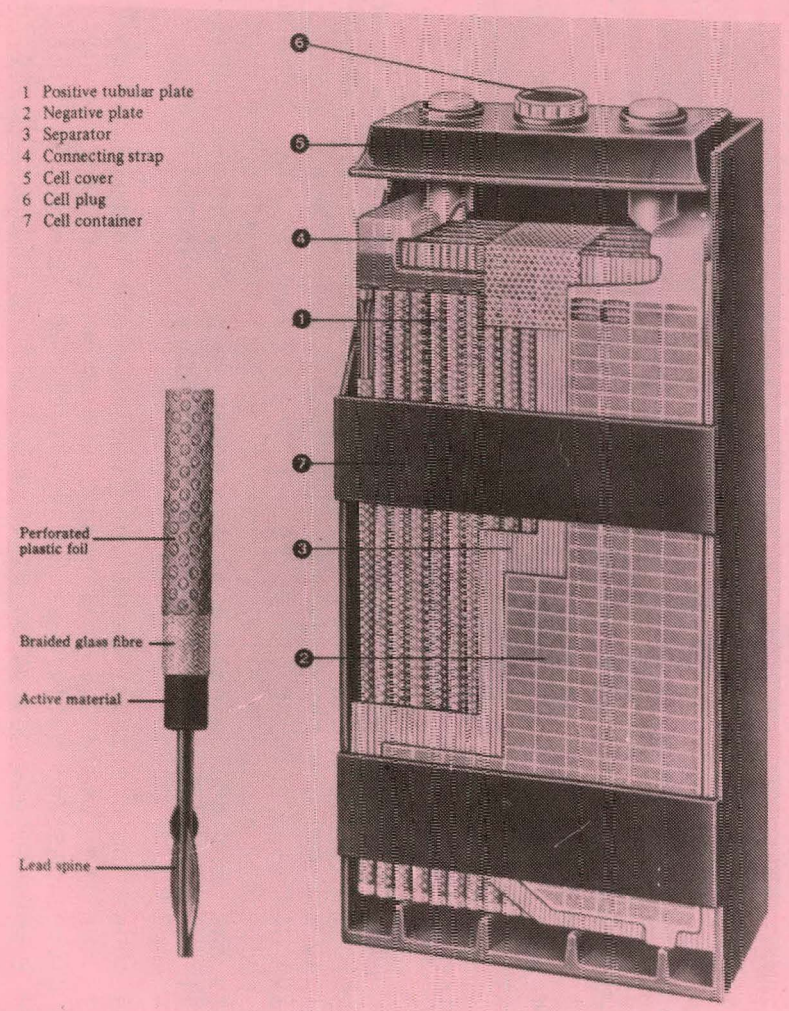


Figure 14. Tubular-Plate Battery Construction

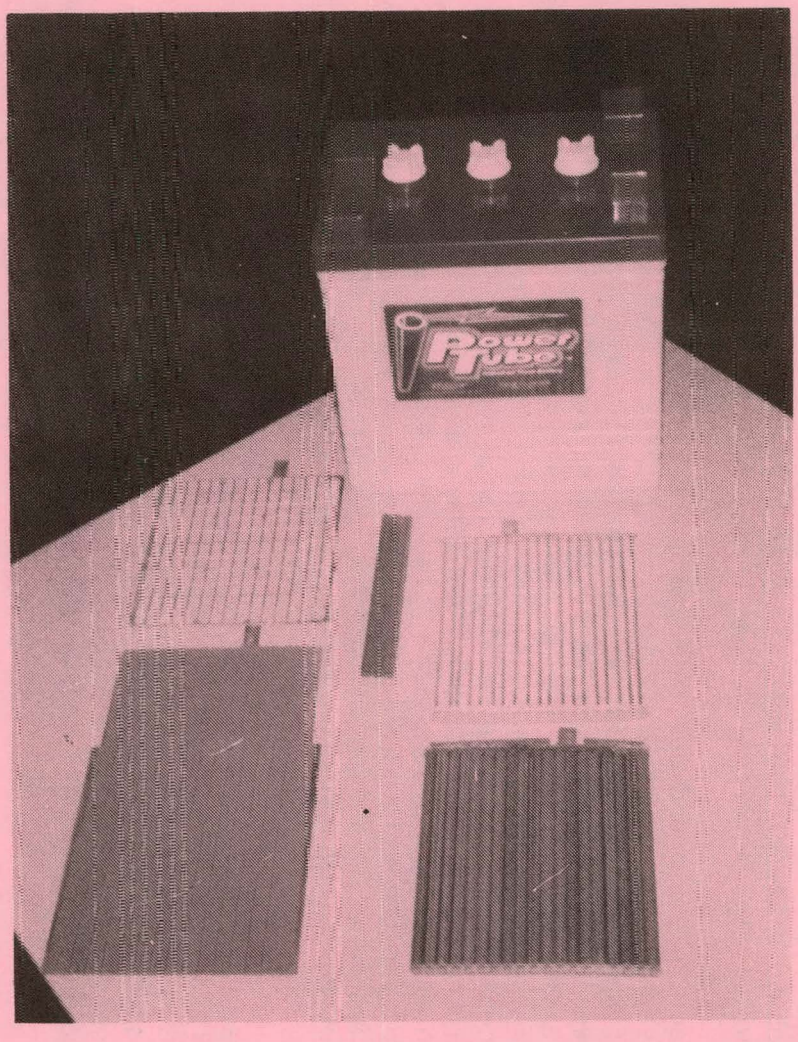


S-28475

Figure 15. Tubular-Plate Battery Componerts

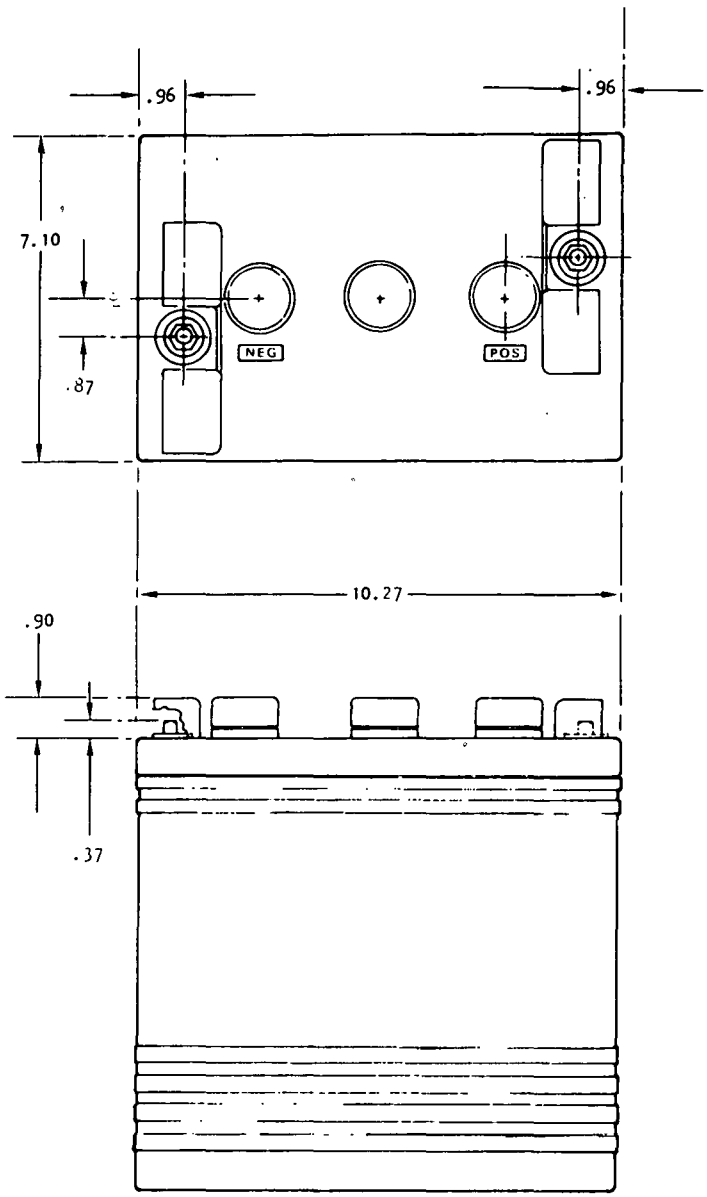


BATTERY PACK CHARACTERISTICS

| | | |
|---|---|---|
| NUMBER OF 6-VOLT UNITS | 18 | |
| WEIGHT OF ONE 6-VOLT UNIT | 57.8 LB. | |
| WEIGHT OF BATTERY PACK | 1040 LB. | |
| CAPACITY, 6-VOLT UNIT | | |
| 3-HR RATE | 187A-HR | 1040 W-HR |
| 5-HR RATE | 212A-HR | 1185 W-HR |
| TOTAL CAPACITY, 3-HR RATE | | 18.72 KW-HR |
| SPECIFIC ENERGY, 3-HR RATE | | 18 W-HR/LB |

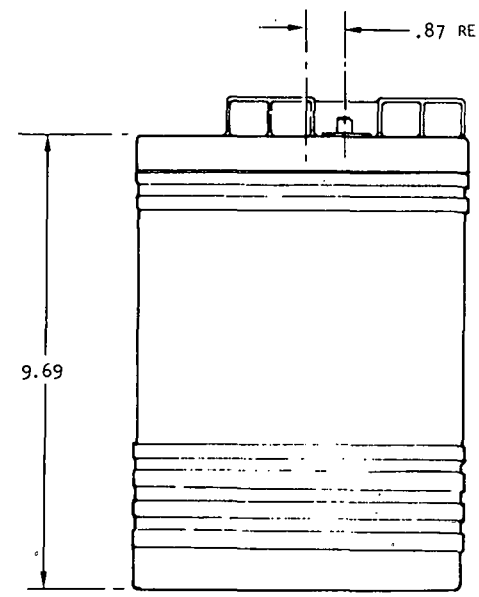


S-28583

Figure 16. Battery Outline Dimensions and Battery Pack Characteristics

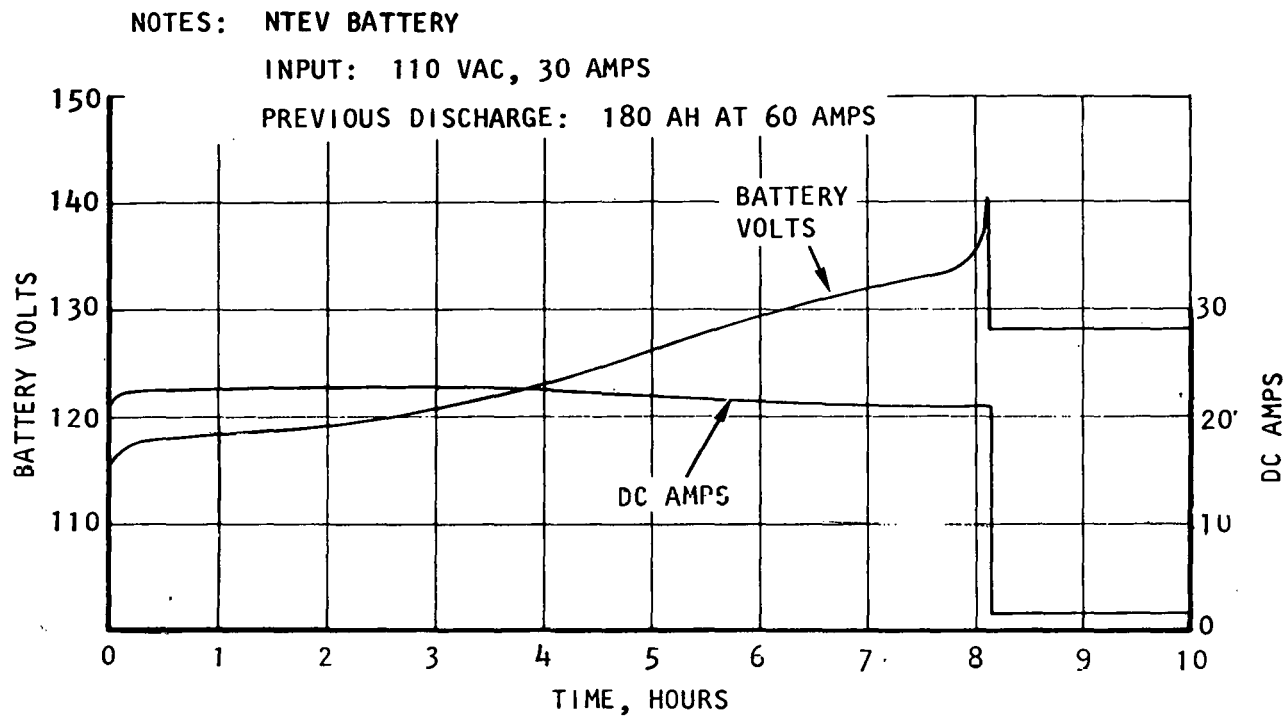


Figure 17. Battery Typical Charging Characteristics

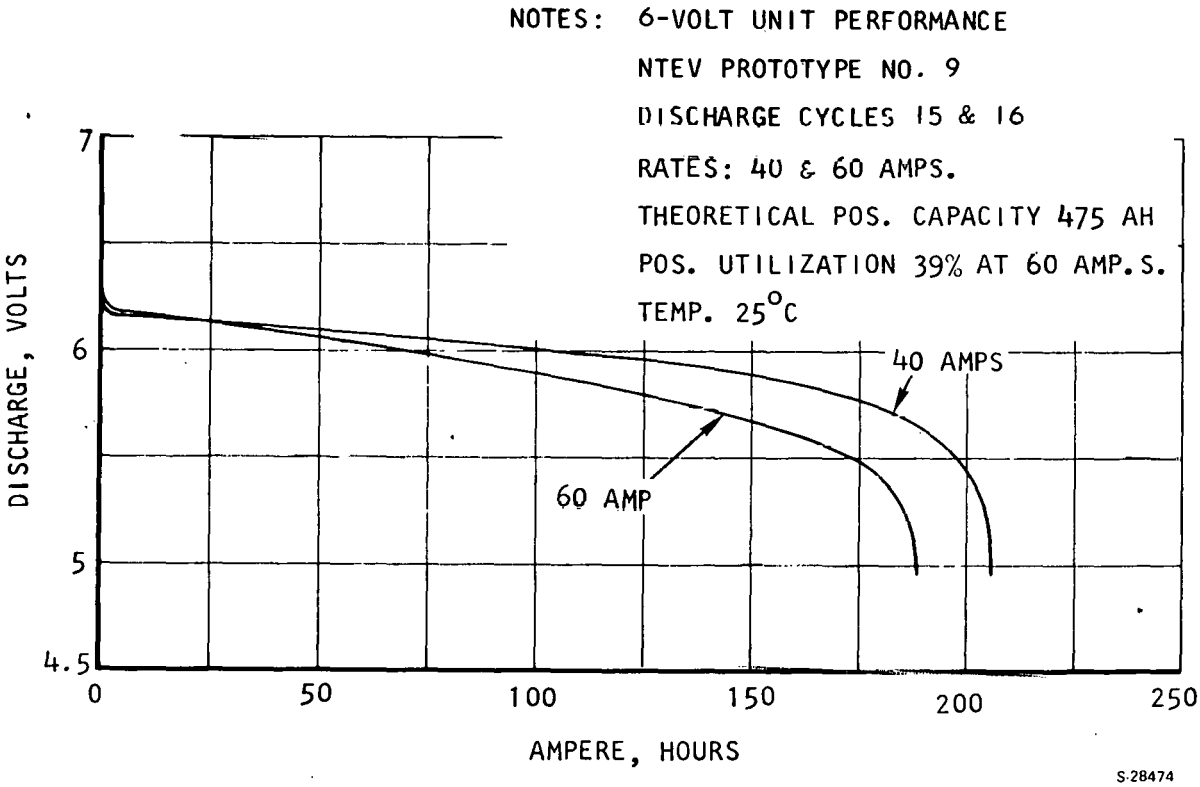


Figure 18. Battery Discharging Characteristics (based on initial test results)

## Battery Performance

The projected performance of the Eagle-Picher Model EP200AH tubular lead-acid battery is discussed in the following paragraphs.

The voltage of a battery cell depends upon the potentials of the positive and negative plates with respect to the electrolyte solution. The potentials vary with the concentration of the electrolyte (at a fixed discharge rate and temperature), which in turn is a function of the discharge time. Hence, as the battery discharges, the voltage at the terminals falls gradually from its open-circuit value, until the end of the discharge is approached, when it begins to fall much more rapidly. Figure 19 shows the typical discharge curves for the EP200AH battery at 77°F.

Low temperatures increase the resistivity and the viscosity of the electrolyte, reducing conductivity and impairing its circulation in the pores of the plates. This effect of temperature on battery voltage is shown in Figure 20.

The most commonly used method of rating battery capacity is in terms of ampere-hours for a specified rate of discharge and end voltage. Figure 21 shows the typical variations in the ampere-hour capacity of the EP200AH battery, as a function of discharge rate and temperature.

Another commonly used battery-performance indication is the relation between energy density and power, shown for the EP200AH battery in Figure 22.

The battery cycle life depends on a number of factors. If the battery has been operated and maintained properly, the cycle life becomes a function of environmental temperatures and the depth of discharges, as shown in Figure 23. The recommendation is made, therefore, to limit the environmental temperature to 100°F, and the depth-of-discharge to 80 percent during normal operation.

The effect of the battery cycle life on the total mileage available over the life of the battery pack is examined in Figure 24 for the 77°F ambient temperature case. Maximum utilization of battery stored energy is achieved by regular cycling to 50-percent depth of discharge.

## Battery Model

A series of digital computer simulation programs was developed to predict both the steady-state and the dynamic performance of the EP200AH battery. The results are described in the following paragraphs.

## Steady-State Performance

Computer Program EP200 was developed by Eagle-Picher to predict the battery cycle life and its steady-state performance, such as capacity, voltage profile, etc. Inputs are current-discharge rates (amperes), ambient temperatures, depths of discharge, and the age of the battery in terms of the charge-discharge cycles.

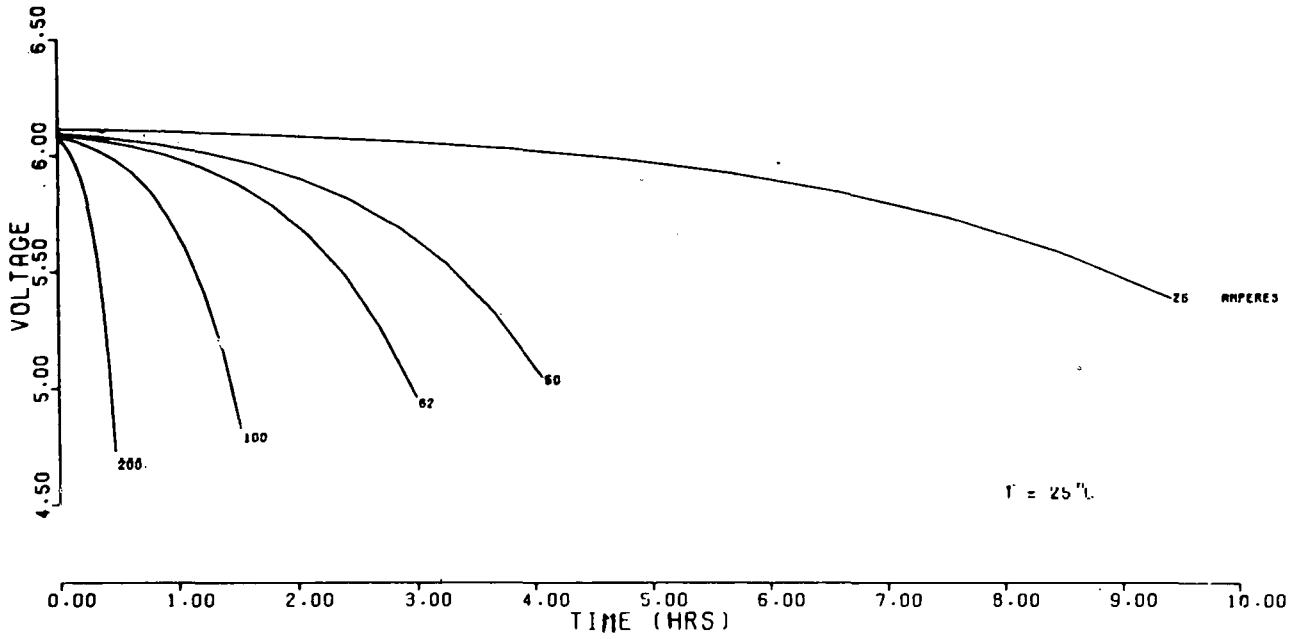


Figure 19. Effects of Discharge Rate on Battery Voltage Profile

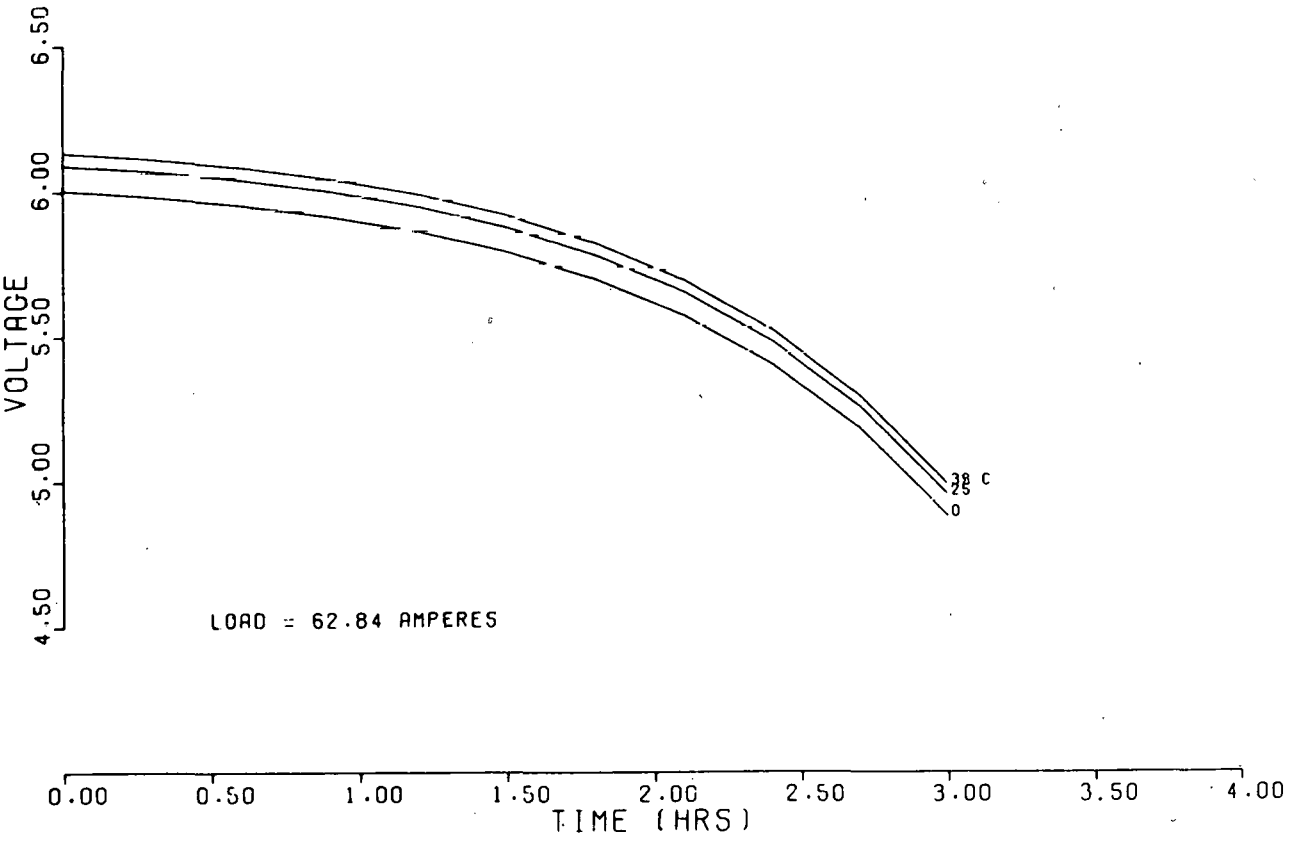


Figure 20. Effect of Temperature on Battery Voltage Profile

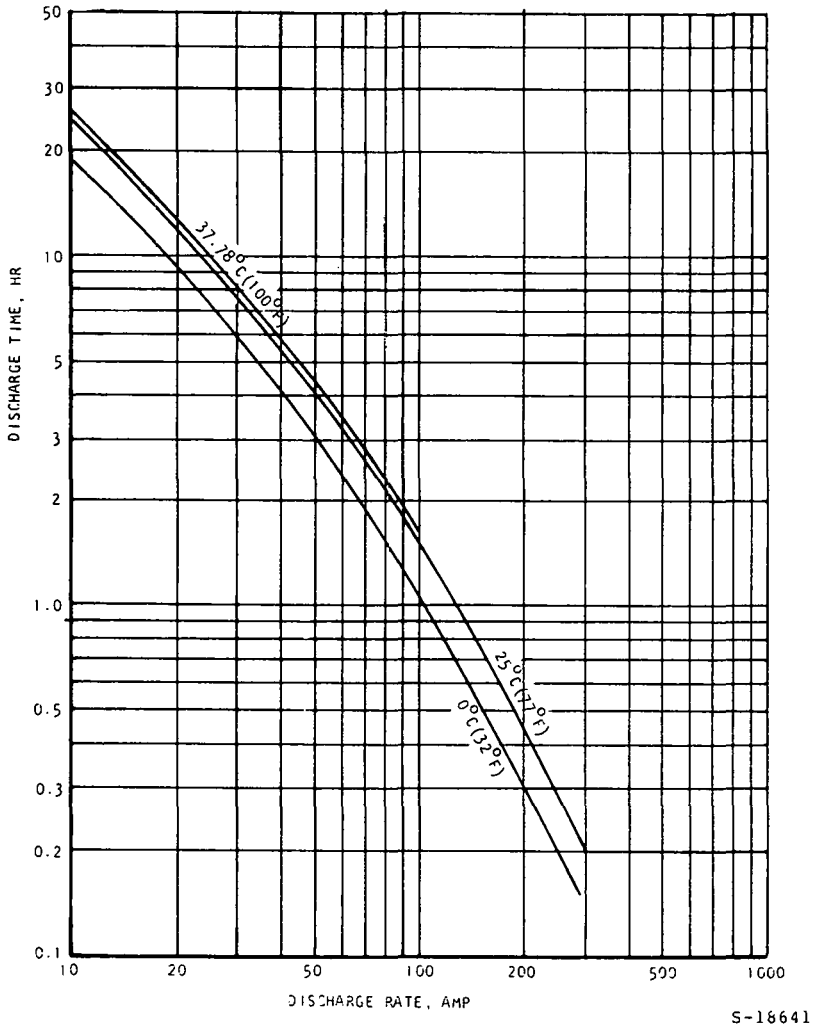


Figure 21. EP200AH Battery Discharge Time vs Discharge Rate at Various Temperatures

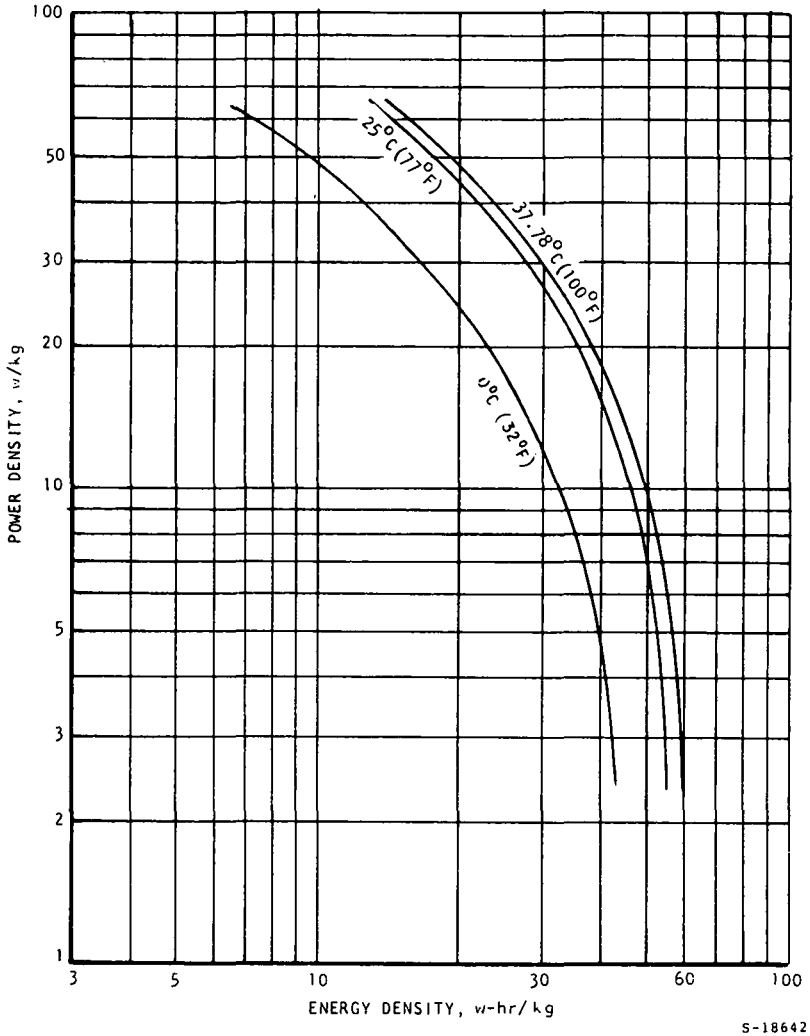


Figure 22. EP200AH Battery Energy Density vs Power Density at Various Temperatures

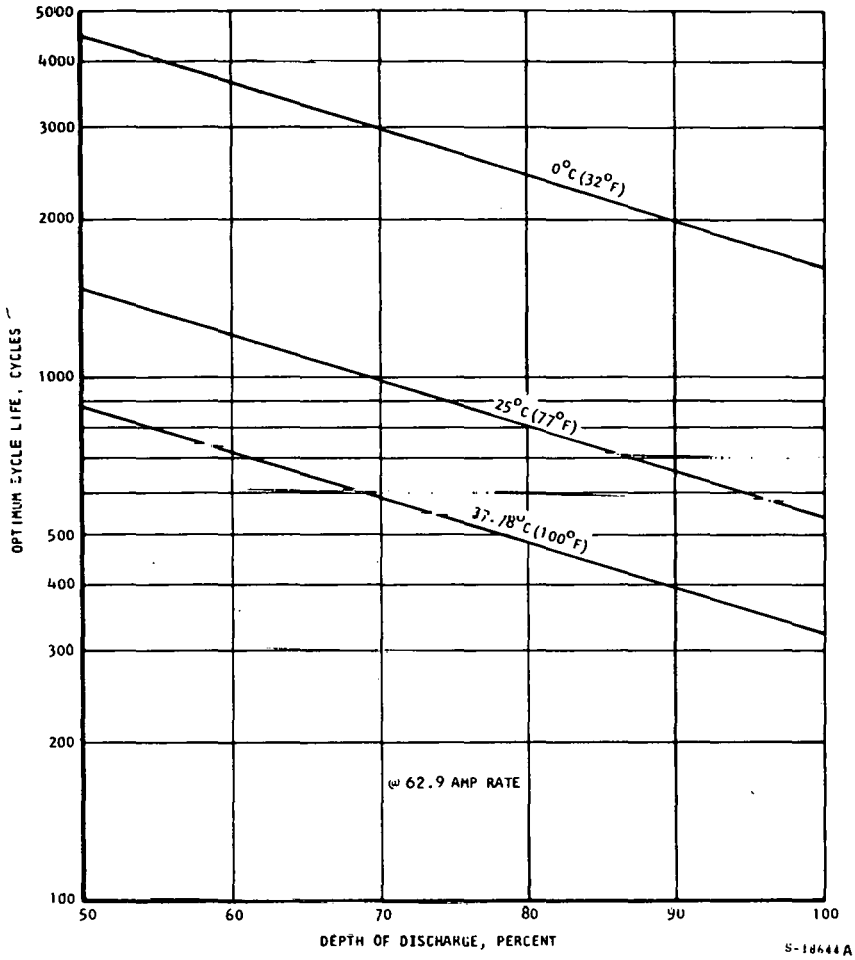


Figure 23. Optimum Cycle Life vs Depth of Discharge at Various Temperatures

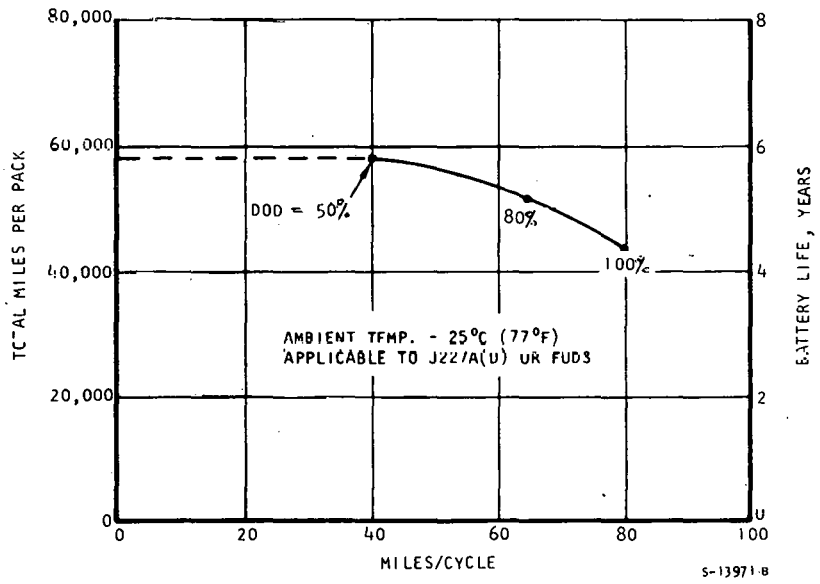


Figure 24. Total Battery Pack Miles vs Nominal Miles per Charging Cycle

The program predicts (a) the expected cycle life, which is a function of depth-of-discharge and ambient temperature; (b) the theoretically available capacity, which is a function of discharge rate; (c) the actual capacity, which is the available capacity modified by the cycling and temperature effects; (d) the actual voltage profile, which is a function of the discharge rate and is modified by the temperature effect; and (e) the discharge watt-hours, which is the actual capacity multiplied by the average voltage. It also predicts the electrolyte-concentration profile, the thermal-neutral-voltage profile, the thermal-neutral watt-hours, the total heat liberated, and the discharge temperature rise, as depicted in the program logic sequence (Figure 25). A printout of this program is shown in Table 6.

## Battery Dynamic Performance Computer Programs

While the electric vehicle is subjected to various driving cycles, the current demanded of the battery varies unavoidably with the power demand, even though the flywheel power system provides a load-leveling effect. As shown in Figures 6 and 7a, the current variations are substantially lower than those of conventional electric vehicles, but the influence on voltage and range predictions should be considered, nevertheless. Two digital computer programs were developed to predict the dynamic performance of the battery while it is being subjected to variable current demands and variable ambient temperatures.

### Program No. 1

Program No. 1 evolved from the previously described steady-state performance program, developed by Eagle-Picher, and from the fractional-utilization method. With the steady-state performance program, the battery capacity and its voltage profile can be calculated for any current-discharge demand at an ambient temperature. The fraction of capacity used, in any segment of time, is the ampere-hours used during that time, divided by the ampere-hour capacity at that power level or discharge rate. By tracking the fraction of capacity used and that remaining, one can determine the battery voltage on the voltage profile. The program logic sequence is shown in Figure 26.

The range of the vehicle can be evaluated by dividing the travel-distance-per-driving-cycle by the fraction of capacity used during the driving cycle. This calculation is easily performed by a subroutine of the vehicle system simulation program to yield a conservative result. Because it is conservative, it has been chosen and used throughout this program to predict the battery performance and the vehicle driving range.

### Program No. 2

The theory behind the fractional-utilization method is that the fraction of capacity used in any segment of time is the energy used during that segment of time divided by the energy capacity at that power level or discharge rate. The drawback of this theory is that it does not take into proper account the variation in the energy capacity if the remaining portion is used at a different rate.

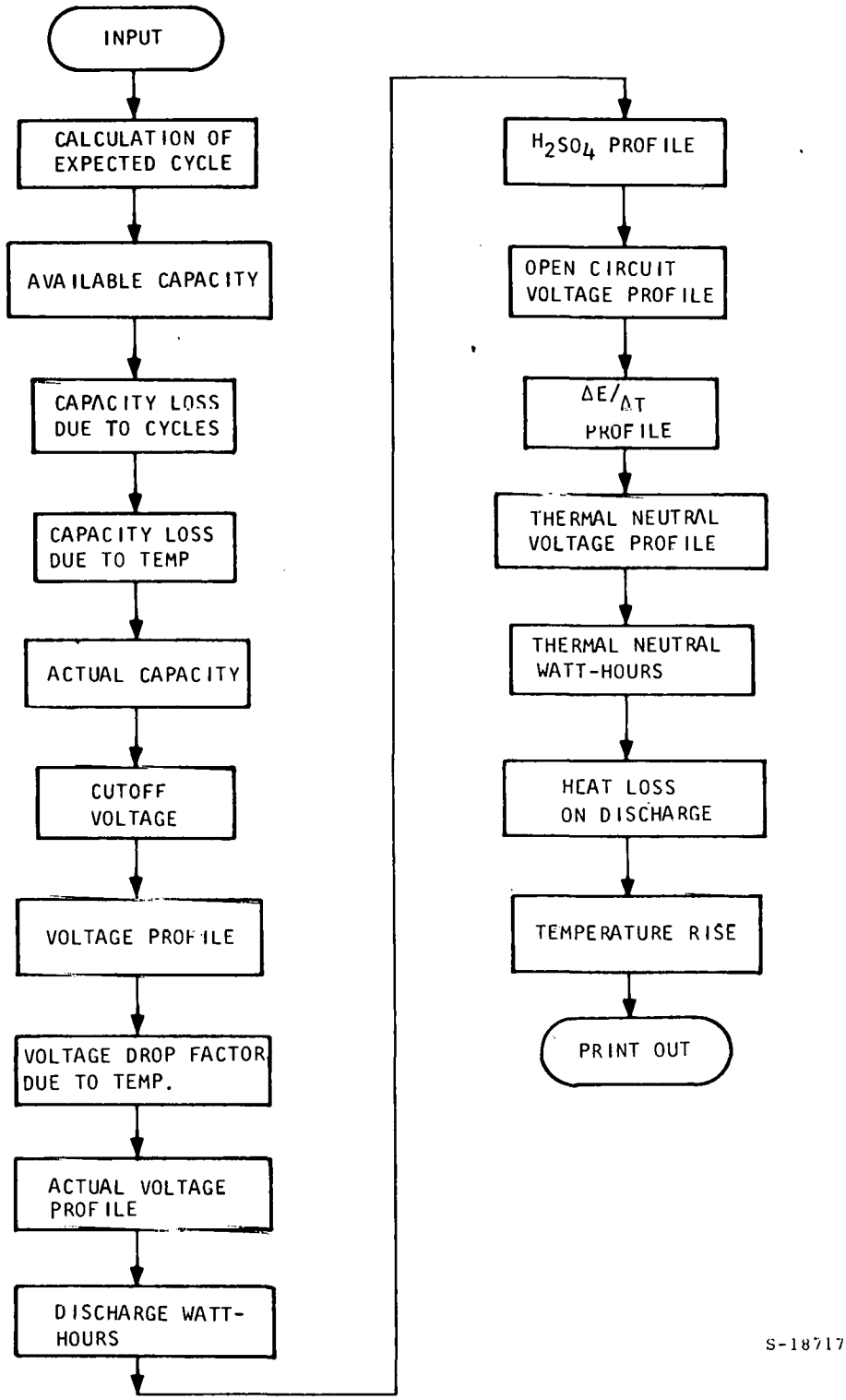


Figure 25. Steady-State Battery Performance Model, Program Logic Sequence

TABLE 6

STATE-OF-THE-ART ANALYSIS FOR EP200AH
TUBULAR LEAD-ACID BATTERY

SIMULATION OF CYCLE 200.. AT 62.9 AMP RATE
BATTERY REGIME= 80.0 D.O.D. AT FAHRENHEIT 77.0

OPTIMUM CYCLES AT THIS REGIME IS 800.

AVAILABLE CAPACITY (AH)= 188.506

REDUCTION FOR CYCLES 1.000
REDUCTION FOR TEMP. 1.000

ACTUAL CAPACITY (AH)= 188.506

VOLTAGE REDUCTION (TEMP) 1.000

VOLTAGE PROFILE

| PCT.DIS. | VOLT. |
|---|---|
| 0. | 2.030 |
| 10. | 2.023 |
| 20. | 2.013 |
| 30. | 2.000 |
| 40. | 1.982 |
| 50. | 1.958 |
| 60. | 1.926 |
| 70. | 1.884 |
| 80. | 1.827 |
| 90. | 1.751 |
| 100. | 1.650 |

DISCHARGE WATT HOURS 362.2

THERMAL NEUTRAL VOLTAGE AND PERCENT H2SO4 PROFILE

| PCT.DIS. | PCT.H2SO4 | VOLT. |
|---|---|---|
| 0 | 42.1 | 2.1316 |
| 10 | 40.3 | 2.1038 |
| 20 | 38.5 | 2.0776 |
| 30 | 36.5 | 2.0532 |
| 40 | 34.5 | 2.0304 |
| 50 | 32.4 | 2.0092 |
| 60 | 30.2 | 1.9894 |
| 70 | 27.9 | 1.9709 |
| 80 | 25.4 | 1.9535 |
| 90 | 22.9 | 1.9367 |
| 100 | 20.2 | 1.9200 |

THERMAL NEUTRAL WATT HOURS 378.3

WATT HOURS LIBERATED ON DISCHARGE 16.1

DISCHARGE TEMPERATURE RISE 10.83 F

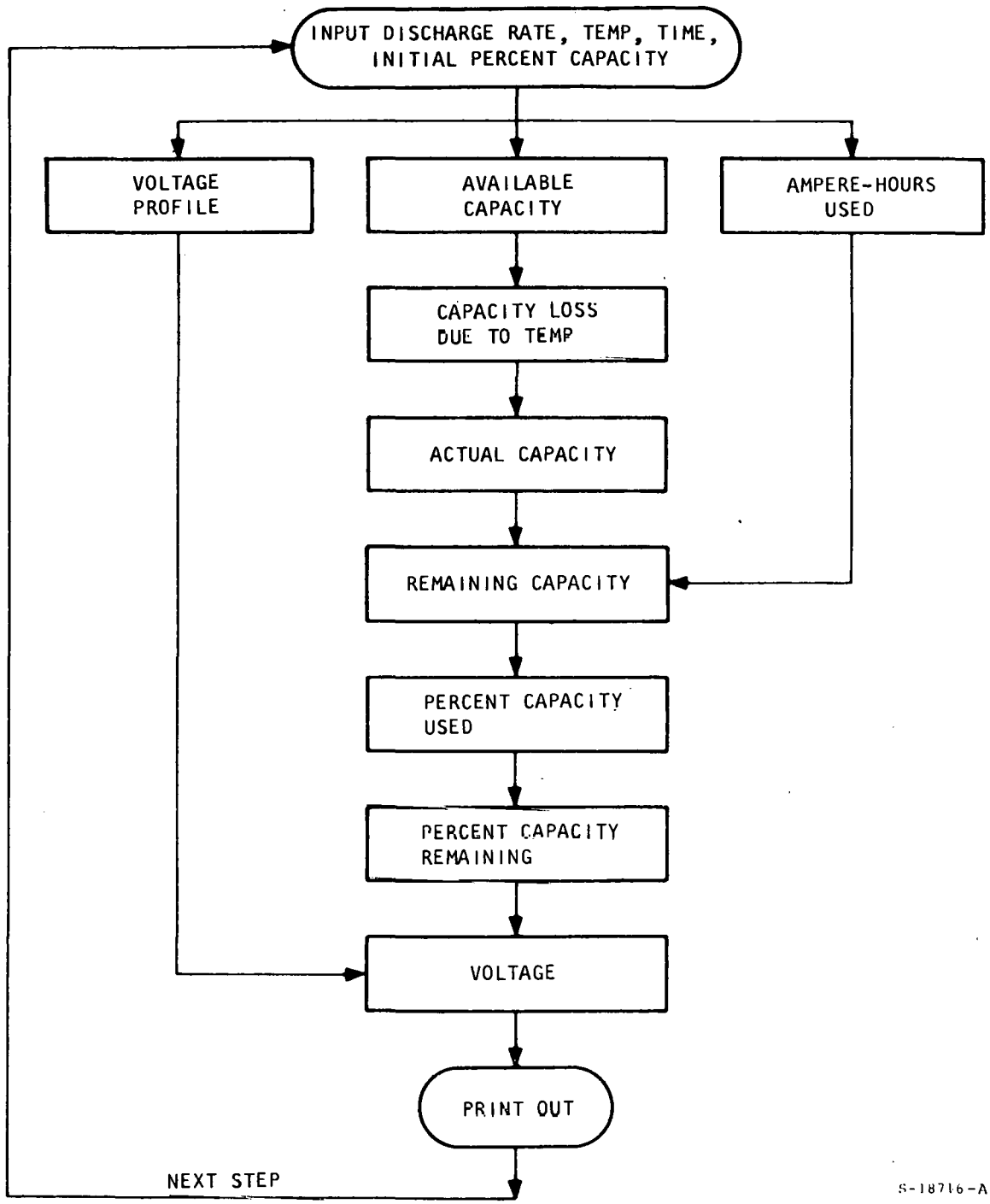


Figure 26. Dynamic Battery Performance Model No. 1, Program Logic Sequence

As the battery load varies, the percent of capacity used can no longer reflect its true remaining capacity. For example if a subsequent discharge rate is lower than that of the previous rate, the remaining capacity should be considered greater than that which would remain if the battery were subjected to the same discharge rate used previously, and vice-versa. The fractional-utilization method, of course, does not take into account the familiar "recuperation effect" of the battery.

A novel approach, aimed at these deficiencies of the fractional-utilization method, employs the steady-state performance program. As with Program No. 1, the actual battery capacity and its voltage profile are calculated for any current-discharge demand and for any ambient temperature. In contrast to Program No. 1, where the capacity used-and-remaining is a function of the past history of the current demand only (accumulated fraction of capacity used), the battery capacity used-and-remaining is a function of the past history (accumulated ampere-hours used and average past discharge rate), and a function of its relationship to the present demand (rate of average discharge rate to instantaneous rate), as expressed in the following equation:

$$\text{Percent of capacity used} = Ah/Ah_t \times R_a + Ah/Ah_a \times (1 - R_a)$$

where Ah is the accumulated ampere-hour capacity used, $Ah_t$ is the capacity based on the instantaneous discharge rate, $R_a$ is the ratio of present discharge rate to average discharge rate or its inverse, whichever is smaller, and $Ah_a$ is the capacity based on the past, average discharge rate.

By knowing the voltage profile and the percent of capacity used, one can determine the battery voltage. When the battery voltage drops below a specified cut-off voltage, it is considered exhausted. The program logic sequence is shown in Figure 27.

Program No. 2 can be adapted to other lead-acid batteries with known steady-state performances by replacing the steady-state performance program, developed by Eagle-Picher, with the Shepherd Equation and its associated constants. The validity of the program was shown by obtaining an exceptionally good match between the results calculated with this method and the actual laboratory simulation tests conducted by JPL. (Refer to JPL Publication 77-29, Evaluation of Battery Model for Prediction of Electric Vehicle Range.) The laboratory simulation results on the J227A Driving Cycle, schedules B, C and D, are 369, 184, and 49 cycles, while the results calculated using this method with EV106 data are 361, 184, and 52 cycles, respectively.

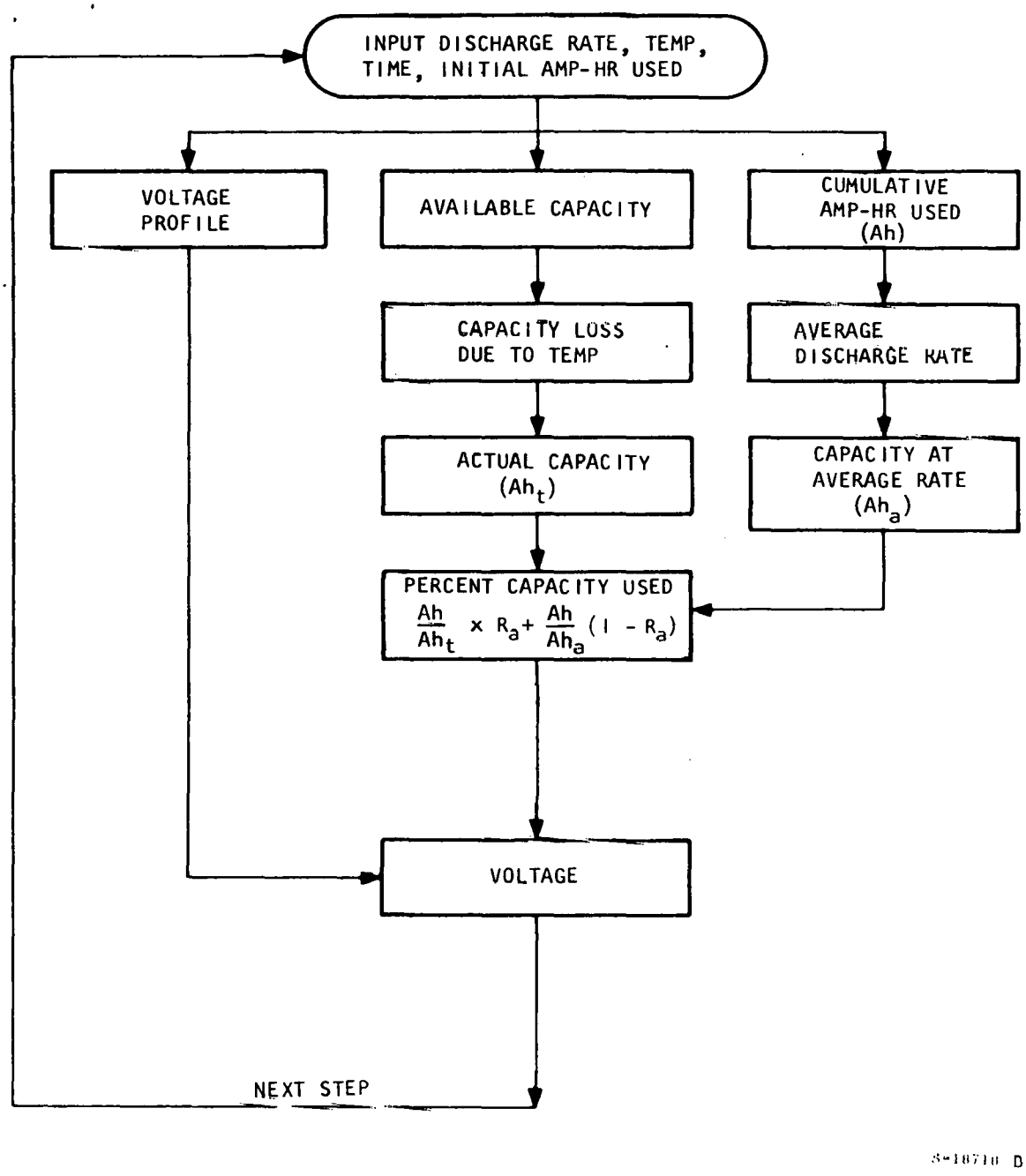


Figure 27. Dynamic Battery Performance Model No. 2, Program Logic Sequence

# SECTION 5

# POWER SYSTEM

SECTION 5

POWER SYSTEM

## SYSTEM DESCRIPTION

The power system for the Garrett Near-Term Electric Vehicle combines an energy storage flywheel with an electric motor/battery pack in a highly efficient arrangement as shown in Figure 28.

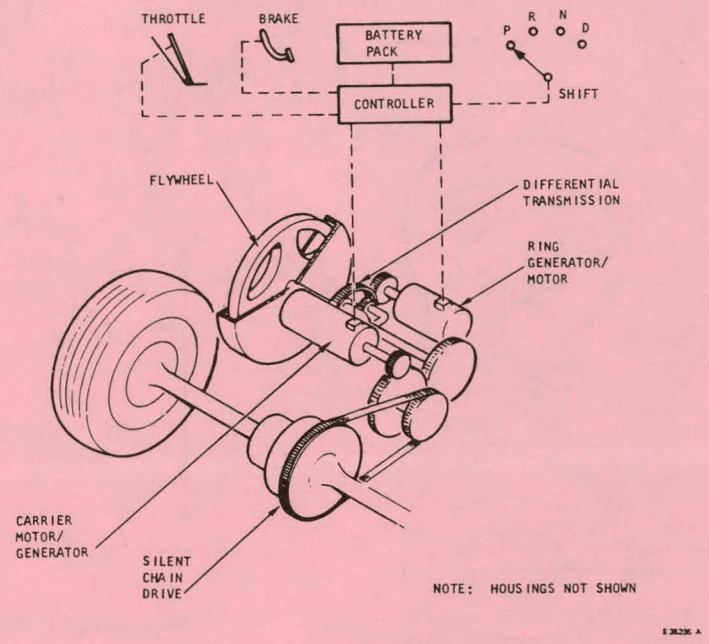


Figure 28. Power System Concept

The power system consists of a flywheel, a differential planetary transmission, a ring generator/motor, a carrier motor/generator, a battery pack, and various electronic control components. The flywheel, the ring generator/motor, and carrier motor/generator are linked mechanically through the three power paths of the planetary gear set and function together as an infinitely variable electromechanical transmission. The ring generator/motor and carrier motor/generator are identical units capable of operation as either a motor or a generator. In the discussions that follow, the two units are identified as generator or motor, according to their function, where helpful in describing the system.

Operator controls and displays are similar to those of conventional automatic transmission vehicles and allow a new driver to operate the electric vehicle with little or no instruction.

Power Flow and Control

The two principal features of the system, regenerative braking and load leveling of the battery current, greatly increase the driving range available from the battery. Their implementation hinges on proper transfer of power from the battery to the rear axle through the electromechanical drive arrangement shown pictorially in Figure 29.

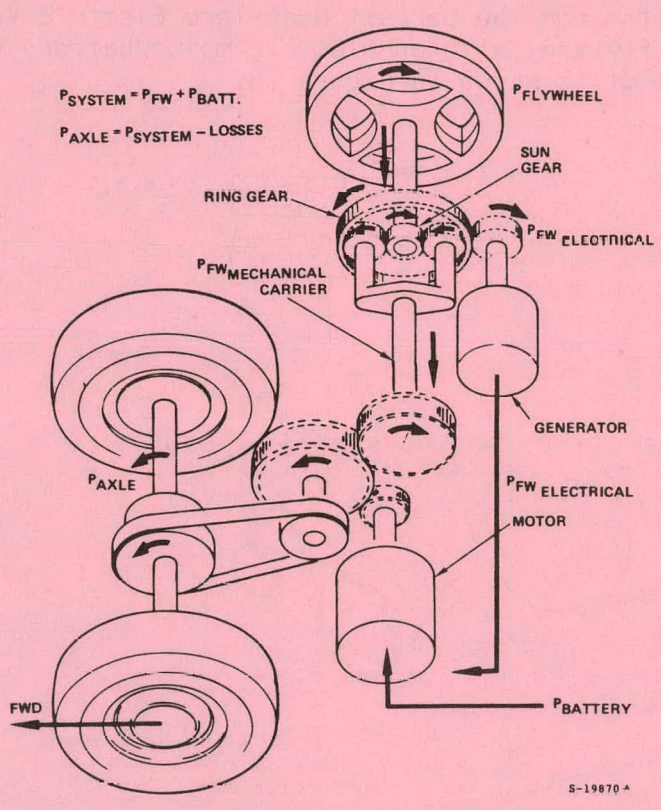


Figure 29. Power Unit--Power Flow Diagram

The flow of energy into and out of the flywheel is controlled by the generator. The flywheel speed reacts to the torque applied by the generator at the planetary ring gear. The generator torque is transmitted as mechanical power through the planetary output shaft, and as electrical power through the generator and motor armature circuit. The effective efficiency of the power transmitted exceeds the product of the motor and generator efficiencies, because of the highly efficient mechanical traction. The magnitude and direction of the power flow in the transmission is determined by the controller logic, in response to the operator commands.

The armatures of the two motor/generator units are electrically connected as shown in Figure 30. All control is accomplished by the motor and generator field circuits; varying the current in the two field circuits determines the magnitude and direction of the armature current. To provide transient power for acceleration and hillclimb, a generator torque, which slows down the ring gear, is applied by increasing the field current. The reaction at the sun gear

slows down the flywheel, extracting the required energy from the flywheel. Vehicle kinetic energy is recovered during braking by reversing the flow of power in the transmission. The carrier motor/generator now operates as a generator, and provides electrical braking power while the ring generator/motor now operates as a motor, speeding up the ring gear. The resulting action on the sun gear drives the flywheel to higher speeds, thereby restoring energy for future power demands.

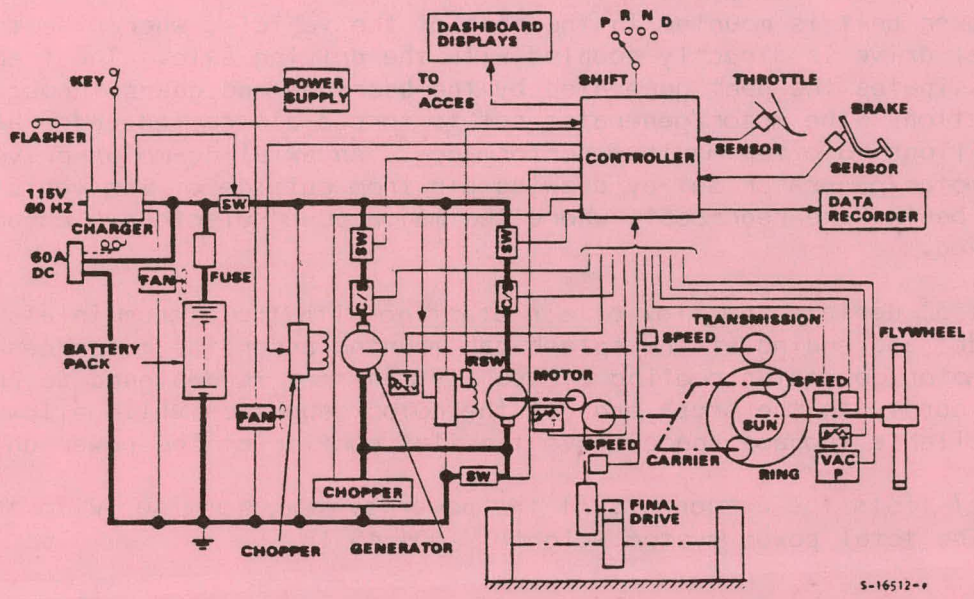


Figure 30. Power System Schematic

The battery pack is connected to the armature circuit, and current is determined by the armature voltage. The time-averaged power required for a driving cycle is provided by the battery pack. The flywheel fulfills transient, above-average power demands, enabling the battery to discharge at a near-optimum, load-leveled rate. When power demand is below the cycle average, such as during moderate-speed cruising or during short-term idling, the excess battery power is used to recharge the flywheel. During this recharging, the ring generator/motor operates as a motor powered by the battery.

As shown in Figure 30, power system control is provided by a solid-state digital electronic controller. The controller responds to operational demands by sensing the operating state of the vehicle, by switching to the appropriate mode of control, and then by modulating the flow of power between the flywheel, generator, motor and battery.

The controller programs smooth control mode transitions so as to eliminate acceleration jerks and large current transients to enhance driving confort and the service life of the power system switch gear.

In addition to the electronic controller and power electronics, the vehicl electrical subsystem includes: an onboard battery charger to provide local overnight battery recharge from 115-vac 60-Hz residential electrical service, a digital cassette data recroder to record vehicle performance parameters during field test trials, and accessory power supplies to convert the 108-vdc battery voltage to 12-vdc automobile power so that conventional autmotive electrical components can be utilized.

## Installation and Weight

The power unit is mounted in the rear of the vehicle, where the transmission's final drive is directly coupled with the driving axle. The transmission housing dissipates the heat generated by the bearings and gears through natural free convection. The motor/generator set is forced-air cooled under all operating conditions to offer maximum performance. An axial dc-motor-driven fan cools the motor/generator set by drawing air from outside of the vehicle into the plenum behind the rear seat, where the major power electronic components are installed.

Figure 31 depicts the flow of air starting with the plenum inlets (one on each side) and ending at the splash pan mounted under the motor/generator set. The motor/generator cooling air supply manifold is designed to provide proper air supply to the brush ends of the motor/generator while allowing maximum available luggage space above the flat portion of the power unit.

Table 7 lists the components of the power system, together with their weights. The total power system weight is 606.45 lb.

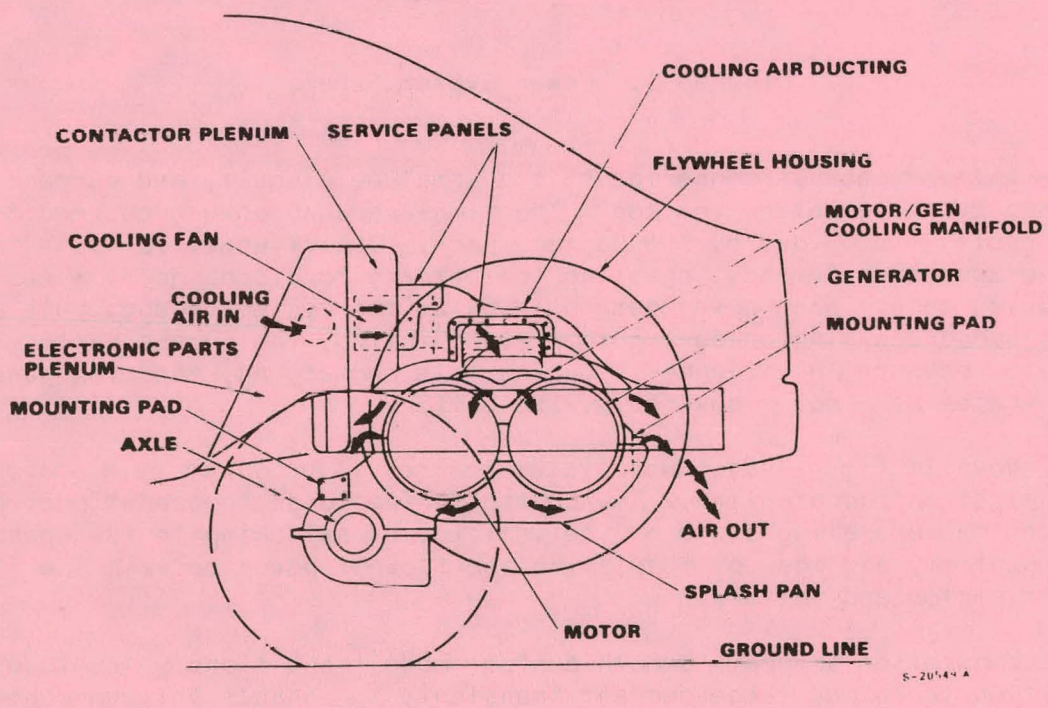


Figure 31. Power System Installation

TABLE 7

POWER SYSTEM WEIGHT

| Description | Qty | Weight, lb | |
|---|---|---|---|
| | | Component | Total |
| Power unit | 1 | | 478.35 |
| Flywheel and housing assembly | 1 | 156.05 | |
| Transmission and housing assembly | 1 | 89.72 | |
| Motor/generator | 2 | 229.58 | |
| Mounting brackets, shims | - | 3.0 | |
| Controls and electronics | | | 114.0 |
| Controller | 1 | 9.0 | |
| Power conversion unit | 1 | 41.5 | |
| Data recorder | 1 | 6.2 | |
| Fuses | 6 | 1.5 | |
| Contactors | 4 | 23.8 | |
| Reverser | 1 | 0.8 | |
| Current sensors | 3 | 5.7 | |
| Electrical wires, cables, fuse boxes | - | 14.0 | |
| Brake and throttle sensors | 2 | 0.5 | |
| Battery charger | 1 | 11.0 | |
| Miscellaneous mechanical parts | | | 14.1 |
| Cooling fan | 1 | 5.1 | |
| Air supply ducts | 2 | 3.4 | |
| Supports, clamps, etc. | - | 5.6 | |
| Power system total weight, lb | | | 606.45 |

## PERFORMANCE

The general characteristics of the vehicle power system during startup, acceleration, deceleration, and cruise are described in the following paragraphs. Power unit major characteristics and power dissipation during operation also are discussed.

### Startup

Startup is accomplished by accelerating the flywheel to operational speed using the generator as a motor, powered by the battery, while the motor connected to the output wheels is held stationary. During normal operation, before starting the first trip of the day, the flywheel is accelerated to full speed, using power provided by the battery, a cycle requiring approximately 5 min. Alternatively, the flywheel can be accelerated using power provided by the battery charger. While this option offers a more economical approach, the cycle time is approximately 40 min because the charging energy is limited by the 30-amp current limit of the residential electrical circuit.

During daily use, which includes parking events of short duration, the vehicle can be operated without the need for additional flywheel startup cycles. The flywheel is normally at operational speed (85 to 92 percent of maximum) when the vehicle is first parked. If the driver resumes operation within two hours, the flywheel will still contain sufficient energy to provide acceleration power for the initial vehicle acceleration. The flywheel is then accelerated back to operational speed during the subsequent 5 to 10 min of driving, using battery power.

An additional flywheel startup cycle will occur following a parking event of sustained duration; e.g., the all-day parking typical of commuter driving. The battery provides the startup power during parking-lot recharge. The cycle draws 140 to 200 amp from the battery, and reaches full operational speed in in approximately 5 min; however, the driver can begin driving, at reduced performance, after only 1 min of the charging cycle has elapsed. This reduced performance, with its associated range penalty, is presented in Figure 32 as a function of the initial charge time. For the minimum 1-min charge, the range penalty is 3.3 mi, and the acceleration time to 30 mph is increased by 50 percent to 11.3 sec. Following an initial 1-min startup, the flywheel would reach full load-leveling capacity after 5 to 10 min of driving.

### Acceleration

During acceleration, the generator supplies most of the armature current and the battery supplies a low current, depending on the speed of the flywheel. The flywheel decelerates, reacting to the torque applied by the generator at the ring gear. The generator torque is transmitted as mechanical power through the planetary output shaft and as electrical power through the generator/motor armature circuit. The overall efficiency of the combined power transmission exceeds the product of the motor and generator efficiencies because of the higher efficiency of the mechanically transmitted portion of the power. Maximum acceleration is achieved (when the throttle is fully depressed) by automatically switching the battery current off. This increases the generator current to its maximum value, which increases the energy extraction from the flywheel.

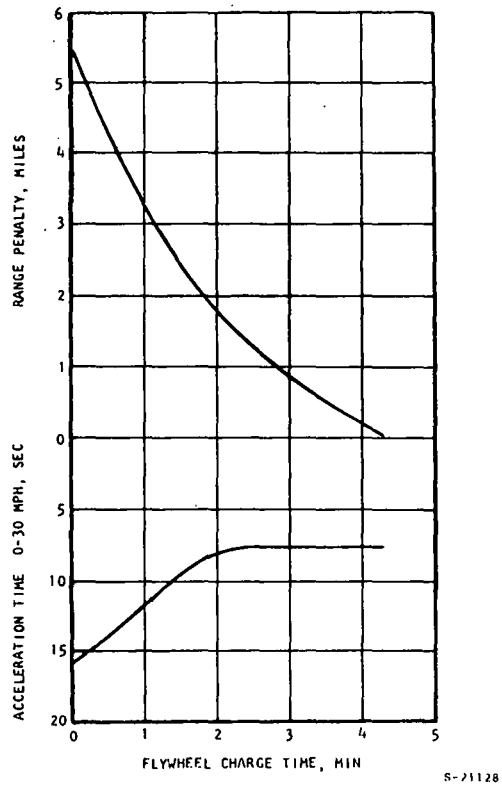


Figure 32. Range and Acceleration Penalty as a Function Of Flywheel Charging Time

The maximum acceleration requires maximum input power provided by the energy stored in the flywheel, as shown in Figure 33, where the power unit input and output and motor output power are plotted as a function of vehicle velocity.

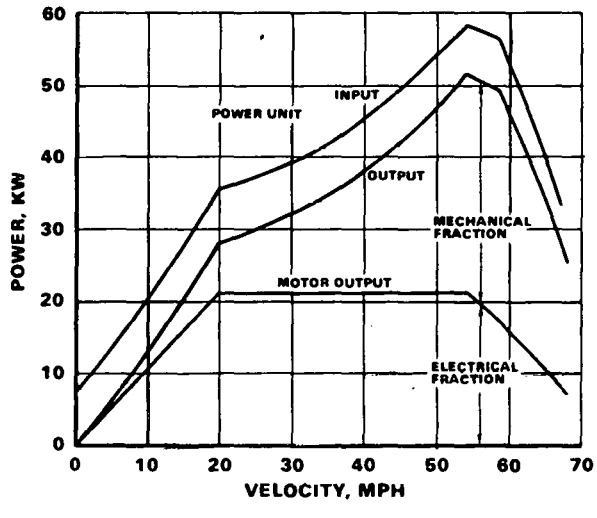


Figure 33. Power System Full-Throttle Output

The electrical and mechanical fractions of the power system output result in a power output profile that increases with vehicle velocity. The maximum power developed by the system at 228 amp maximum armature current is 52 kw at 54 mph. The drop in power above 56 mph can be explained by examining the individual motor/generator torque curves discussed subsequently. The generator drops below base speed as the velocity increases above 54 mph. The generator then operates with full field flux, and maintains a constant-torque output. As generator speed continues to decrease, the output power decreases.

Deceleration and Braking

Regenerative electrical braking is used to decelerate the vehicle and recover a substantial portion of the vehicle kinetic energy. Deceleration is the reverse of the acceleration mode. The armature current is reversed by the controller, which adjusts the motor and generator fields. The motor, acting as the generator, supplies current to the generator; the generator, acting as a motor, accelerates the flywheel.

A small amount of deceleration is initiated when throttle pressure is removed, thus simulating the normal compression braking of piston-powered vehicles. Brake pressure then increases the electrical braking up to a maximum beyond which the friction brakes will be blended in. The electrical braking will be sufficient for all normal driving speeds.

Cruise

Constant-speed cruise operation is similar to that of the conventional traction motor battery-powered system; all of the energy must be supplied by the battery except for the initial acceleration requirement.

Power Unit Major Characteristics

Major operating and performance characteristics of the power unit are tabulated in Table 8.

Power Dissipation During J227A (D) Driving Cycle

The estimated power dissipation associated with each of the mechanical and electrical components of the power system is based on the average losses for each over the SAE J227A (D) driving cycle (Table 9).

Power Dissipation for Electronic and Electrical Components

The estimated total power losses generated by the electronic and electrical components are summarized in Table 10. Estimates are based on minimum and maximum use of the components.

TABLE 8

POWER UNIT MAJOR CHARACTERISTICS

| | |
|---|---|
| **Flywheel** | |
| Total energy, w-hr | 1000 |
| Available energy, w-hr | 750 |
| Maximum speed, rpm | 25,000 |
| Loss at maximum speed, w | 380 |
| **Motor/Generator (per unit)** | |
| Peak power, hp | 28.1 |
| Rated power, hp | 13.7 |
| Rated speed, rpm | 11,650 |
| Nominal efficiency, percent | 88.7 |

TABLE 9

VEHICLE POWER DISSIPATION (J227A (D) CYCLE)

| | | |
|---|---|---|
| Power Unit, w | | 2862 |
| Flywheel rotor windage, bearings, seals, pumps | 351 | |
| Transmission and jackshaft | 559 | |
| Final drive | 205 | |
| Motor bearing and gear | 71 | |
| Generator bearing end gear | 83 | |
| Motor armature and field | 768 | |
| Generator armature and field | 825 | |
| Controller | | 25 |
| Power Electronic Unit | | 227 |
| Chopper and power supply | 86 | |
| Fan | 141 | |
| Displays and Sensors | | 5 |
| Data Recorder | | 0 |
| Contactors (X4) | | 28 |
| Reverser | | 0 |
| Wiring | | 22 |
| Charger | | 10 |
| Battery and Ventilation Fan | | 0 |
| Total power consumption, w | | 3179 |

TABLE 10

POWER DISSIPATION--CONTROLS AND ELECTRONICS

| | |
|---|---|
| Accessory power supply (internal and external load), w | |
| Peak Loss | 692 |
| Minimum Loss | 67 |
| Wiring Losses | 33 |
| Cooling Fan | 140 |
| Vacuum Pump | 117 |
| Lubrication Pump | 90 |
| Total, Peak, w | 1,072 |
| Total, Minimum, w | 447 |

SYSTEM CONTROLS

The system controls function to: integrate the power system with the vehicle controls; monitor and process vehicle operating conditions and driver inputs; and perform computations to generate commands for the power unit, switchgear, and dashboard indicators. System controls effectively utilize stored battery and flywheel energy to maximize the vehicle range.

The main elements of the system controls are shown in Figure 34. The digital processor receives flywheel speed, vehicle speed, throttle, brake, and shift position inputs, and schedules these inputs to develop motor and generator armature current commands. Armature currents are controlled by modulating either the armature chopper (to control motor voltage) or field choppers (to control field excitation current). Compensated, integrating-control loops are used to achieve proper stability and desired response. In addition, protective limit controls are incorporated to prevent equipment damage. These controls and the limits they set are:

(a) Motor/generator thermal limit control (328°F)

(b) Motor/generator overspeed control (11,650 rpm)

(c) Flywheel overspeed control (25,000 rpm)

(d) Armature current control (limit set at 228 amp from 0 to 10,000 rpm and reduced to 110 amp at maximum motor speed)

(e) Maximum battery current (200 amp)

(f) Maximum armature chopper current (120 amp)

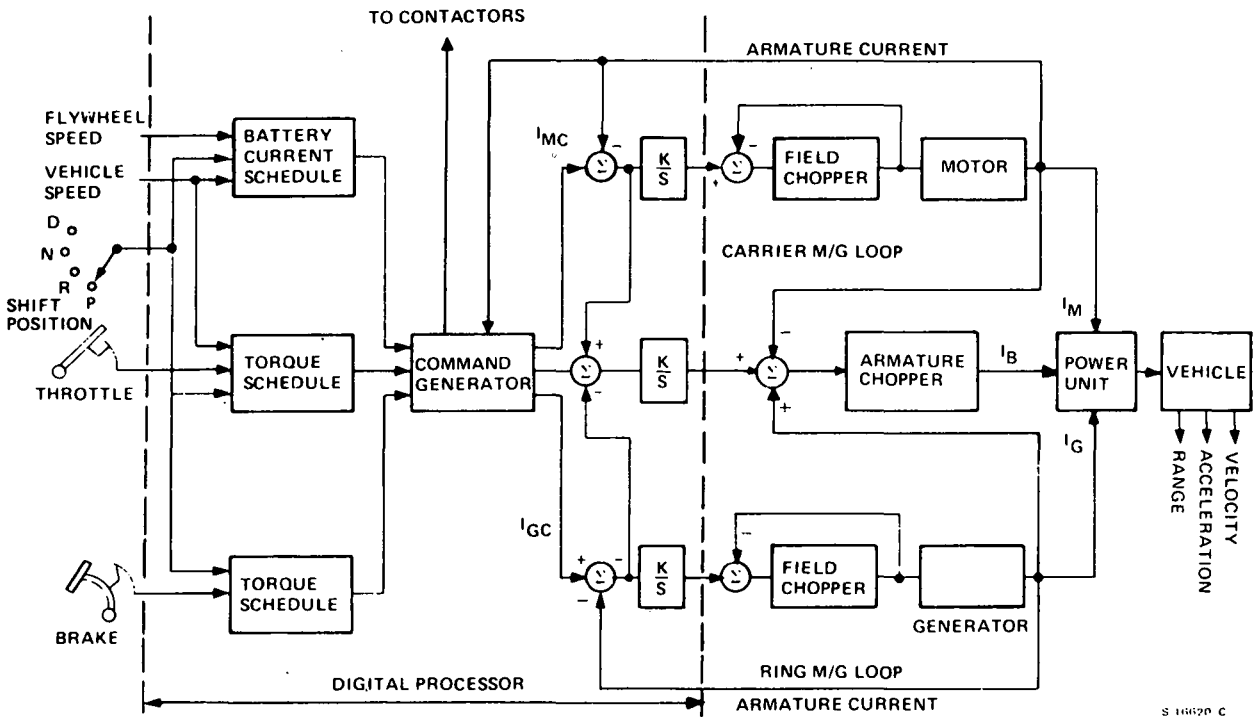


Figure 34. System Control Concept

## Battery Current Schedule

Battery current is programmed according to the operational control mode. There are three different battery current schedules: prestart, reverse, and operational.

During vehicle prestart, the battery is used to charge the flywheel to full capacity and battery current is programmed according to the prestart battery schedule shown in Figure 35.

During vehicle reverse, motive power is developed solely by the carrier motor with battery-supplied armature current programmed as a function of throttle pedal position as shown in the reverse battery schedule Figure 36.

During forward driving modes, the battery current to the motor armature is regulated according to the operational battery schedule shown in Figure 37. This schedule programs battery current so that the average road power requirement is provided by the battery, while the higher power transients required for hill-climbing and acceleration are provided by the flywheel.

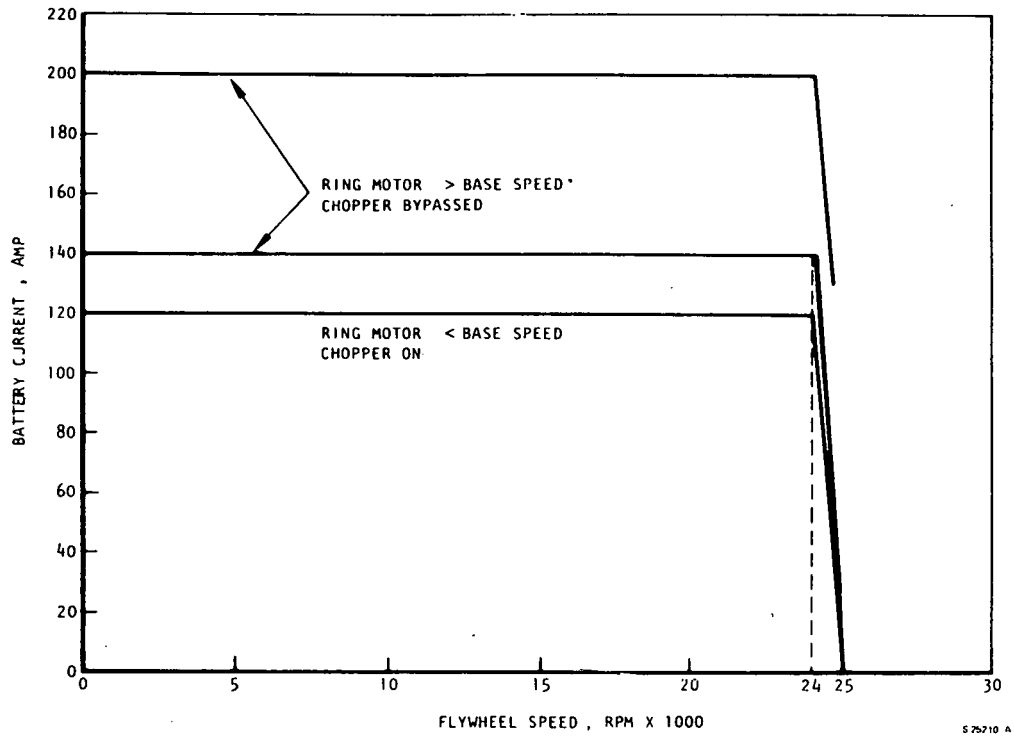


Figure 35. Prestart Battery Schedule

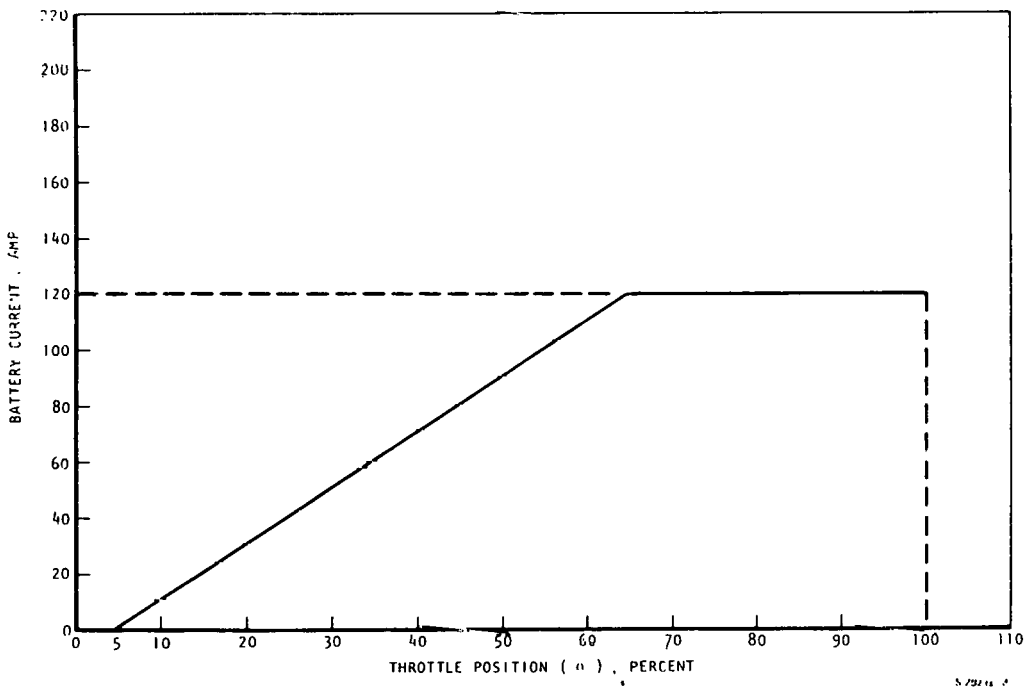


Figure 36. Reverse Battery Schedule

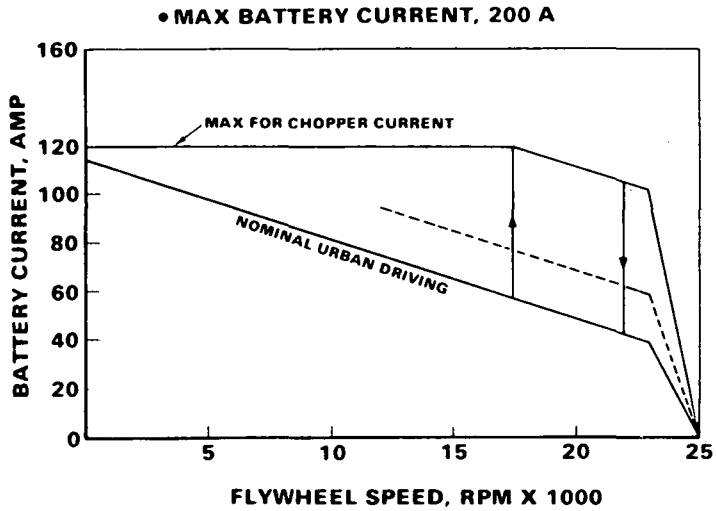


Figure 37. Operational Battery Schedule

The scheduled power from the battery ranges from 3 to 4 kw, required for congested urban traffic, to 13 kw, required for highway cruise. The battery-current control monitors the average vehicle power requirement by tracking the flywheel kinetic energy. The power system extracts energy from the flywheel when the power scheduled from the battery is not adequate to satisfy the throttle command from the driver. Over a sustained interval, the battery control must adjust the output from the battery to maintain the required flywheel speed.

The operational battery schedule (Figure 37) delivers the 4 to 5 kw average power normally required for urban driving. When the flywheel is operating between 50- and 92-percent capacity, the battery output responds to a decrease in flywheel speed by increasing battery current in discrete increments.

When the average power demand causes the flywheel to decrease below 50 percent of flywheel capacity, for a nominal duration of one minute, the controller shifts the battery current control schedule upward. This increment is determined by the difference between the scheduled current and the current at the 50 percent level, which is 60 amp. Each additional time interval below 50 percent results in another current increment, until the maximum current of 120 amp is reached.

This current-increment technique effectively controls the flywheel to between 50 and 100 percent of capacity during all duty cycles which require less than 13-kw average power (120 amp). Each added increment, while the flywheel is operating below 50-percent capacity, remains unchanged until the flywheel has been recharged to above 88-percent capacity. When the elapsed time above 88-percent capacity exceeds one minute, this current level is incrementally reduced.

If the flywheel rotational speed drops below the minimum flywheel capacity necessary to cover transient driving conditions, the control system will override the basic battery control current schedule.

## Throttle Torque Schedule

Vehicle acceleration is a function of engine torque delivered at the axle, road load, and vehicle weight. However, the maximum acceleration capability and smooth vehicle response depend on the control concept, computation, and quality of their implementation. Figure 38 shows the envelope of the required throttle torque command as a function of throttle position for various vehicle speeds.

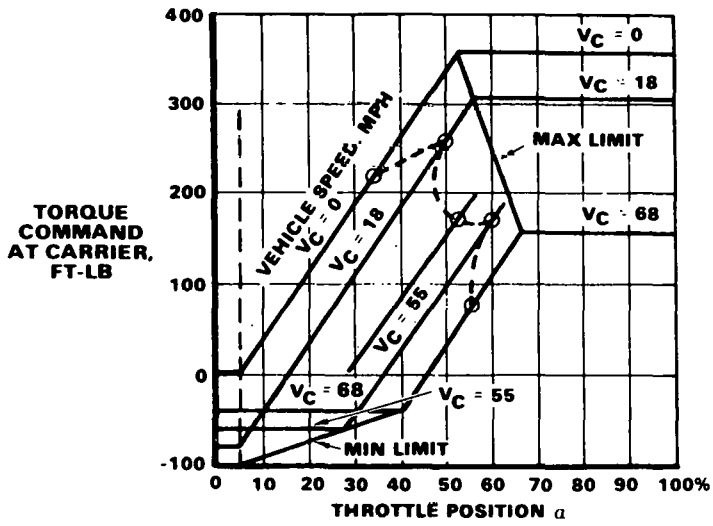


- **TORQUE COMMAND** = $-4.3\ V_C + 7.5\ (\alpha - 5)$ **AT** $\alpha \geq 5$
  $= -4.3\ V_C$ **AT** $\alpha \leq 5$
- **MAX LIMIT** = $355 + -2.79\ V_C$ **AT ANY SPEED**
- **MIN LIMIT** = $1.28\ V_C - 130$ **AT** $V_C > 23.2$ **MPH**
- **DASHED LINE SHOWS MAX POWER SYSTEM ACCELERATION TORQUE CAPABILITY**

Figure 38. Throttle Torque Schedule

## Braking Torque Schedule

Vehicle braking is implemented with regenerative (electrical) and friction (hydraulic) brakes. Regenerative braking is caused by the power unit final drive action on the rear axle (Figure 39). The power for regenerative braking is stored in the vehicle flywheel during the time when the drive motor functions as a generator, providing electrical energy to power the flywheel. If the flywheel is saturated when electrical energy is being generated, the excess energy is used to charge the batteries. The braking torque schedule, implemented by the processor under various pedal positions and vehicle speeds, is shown in Figure 40.

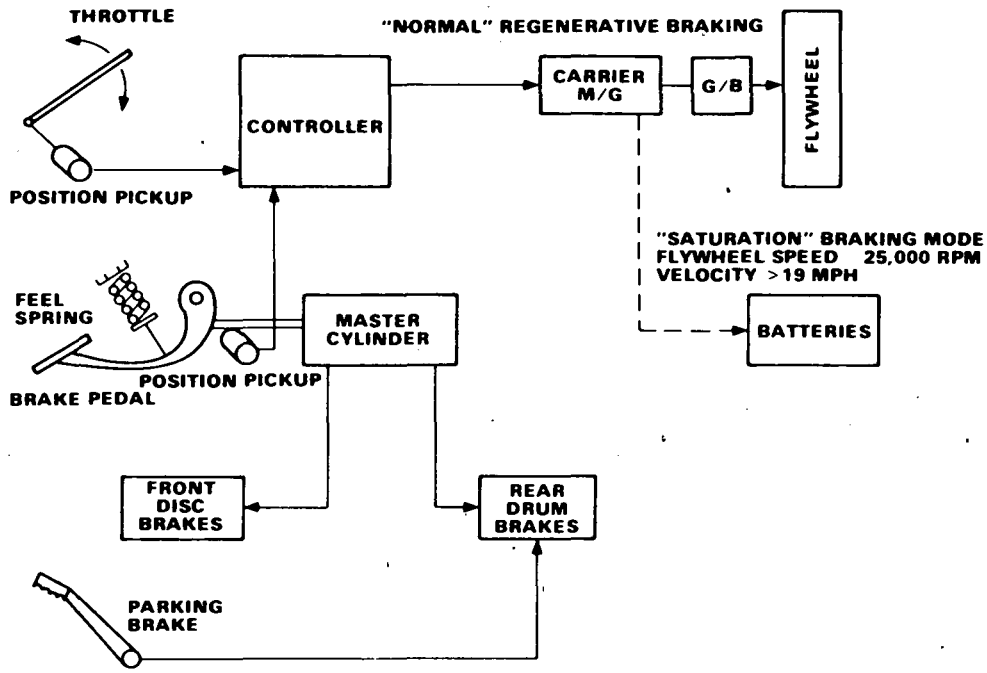


Figure 39. Brake System

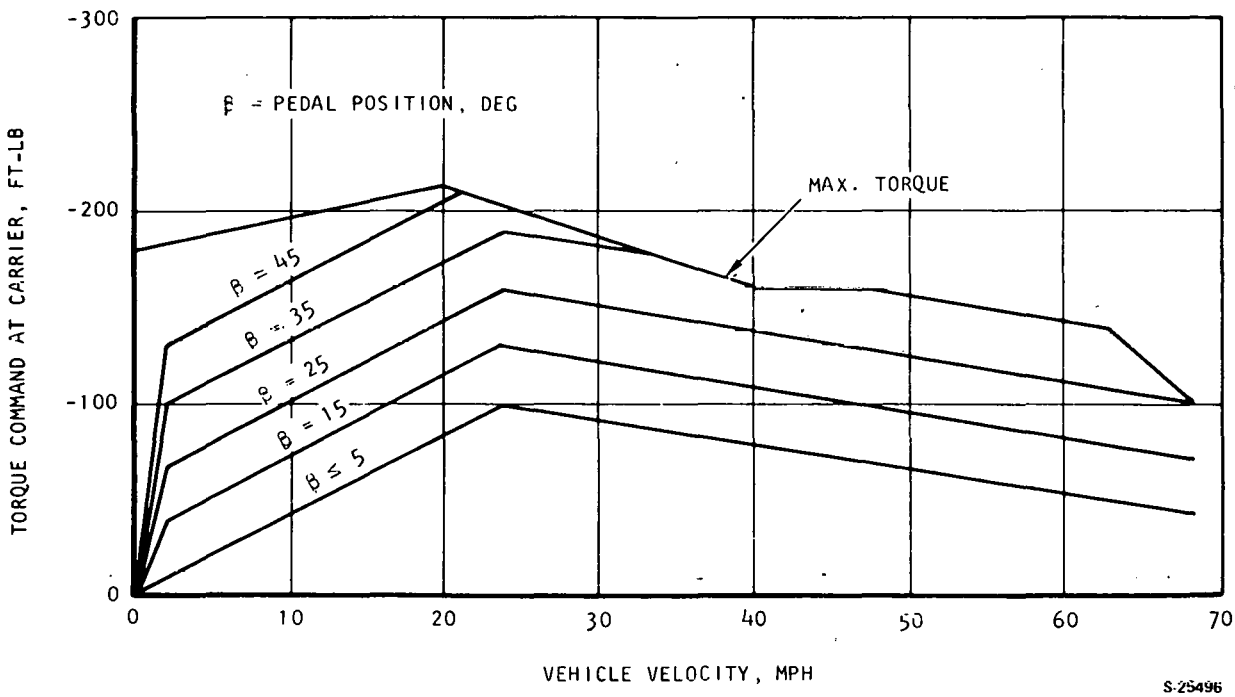


Figure 40. Electrical Braking Torque Schedule

Whenever the vehicle is in a driving mode, the regenerative braking is activated; its magnitude is a function of vehicle speed and pedal position. Even in an "off pedal" driving mode, compression braking feel is available. Only in the neutral shift position is the regenerative braking disconnected.

## SYSTEM OPERATION AND CONTROL MODES

### Battery Charging

With the vehicle deenergized (key in OFF position), the operator may at any time connect the vehicle battery charger to residential 115-vac, 60-Hz power. When the vehicle charger is connected to residential power, the charging current is controlled by the charger current-control circuits, since the vehicle controller is inactive. The vehicle range indicator acts as a voltmeter, giving an approximate indication of battery state-of-charge. If the operator turns the key to ON with the gearshift selector in PARK, the range indicator receives its information from the vehicle controller to provide its computed state-of-charge indication in terms of range available. With the key ON and the gearshift in PARK, the flywheel spins up, the battery and generator contactors close, and the motor and battery line chopper contactors remain open. (The system also provides a separate electrical circuit, permitting vehicle battery charging by use of a 220-vac 60-Hz charger separate from the vehicle. This provides a faster battery charge rate.)

### Startup

When the key is turned ON, the battery contactor closes, providing electrical power to the controller central processor. The 12-v, key-switch supply is activated, closing the battery-contactor relay, which applies 108-v battery power to the battery-contactor solenoid. The gearshift selection then determines the operational mode of the electrical subsystem. In the PARK position, with the charger connected to residential power, the controller monitors, the key, charger, and gearshift positions to inhibit any drive-mode command by the driver. The inhibit is removed when the driver disconnects the battery charger from the residential power source.

### Control Modes

The power system startup mode and the battery charging mode (when the battery remaining charge is unusable) are prerequisites to any driving control mode that can follow. Once these modes are completed, vehicle operation based on the driver's input commands is automatically controlled. There are 26 control modes necessary for vehicle operation. These modes of operation were mechanized for translation into system operation.

A simplified system schematic (Figure 41) shows the configuration of the battery, ring generator/motor, ring switch (RS), carrier motor/generator, carrier switch (CS), battery chopper, chopper bypass switch (CBPS), planetary differential transmission, and flywheel.

The operational state of the power system is determined by the vehicle and the flywheel energy level. In combination with the shift, throttle, and brake

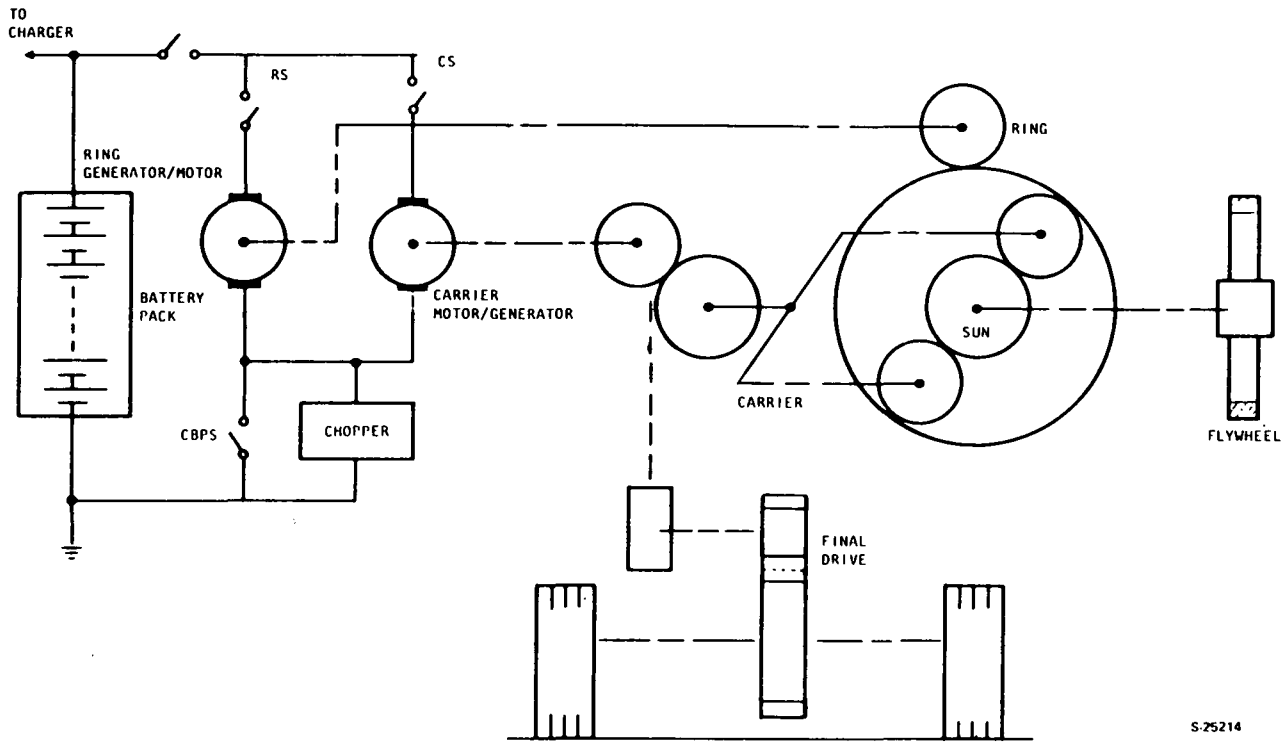


Figure 41. Power System Simplified Schematic Diagram

commands, this operational state effectively defines the speed relationship between the motor and generator, and thus the mode of control required.

The implementation of all control modes is automatic. The following paragraphs describe the 26 control modes necessary for vehicle operation. (All references are to Figure 41).

1. Flywheel Prestart

Charging the flywheel to operational speed prior to vehicle operation requires the delivery of power from the battery pack. The operator designates the prestart mode by switching the ignition ON, by shifting the gear selector to PARK. The carrier motor is held stationary by a mechanical parking interlock.

Flywheel Prestart Mode 1--Initially, the ring motor is below base speed, and the battery chopper is used to control the armature current, as required by the prestart battery schedule. This action is enabled by opening CBPS and CS and by closing RS.

Flywheel Prestart Mode 2--The ring motor reaches base speed at a flywheel speed of 8000 rpm. CBPS is then closed, and the chopper is switched off. The armature current is then controlled by weakening the field of the ring motor.

2. Vehicle Reverse

The vehicle operates exclusively on battery power in the reverse mode, using only the carrier motor to produce the motive torque. The operator activates reverse by shifting the gear selector to REVERSE and depressing the throttle. The armature chopper is used to control the carrier motor armature current, as required by the demand from the throttle. Vehicle speed is limited to less than 19 mph, so that the carrier motor is always operating below base speed and at full flux. The mode is enabled by opening CBPS, by closing CS, and by opening RS. The ring motor flux is set to zero, so that the flywheel loses speed only because of windage and bearing friction.

3. Vehicle Idle

During vehicle idle, the flywheel is charged by battery power. The power delivered to the flywheel during idle provides recharge power to the flywheel, making up a fundamental segment of the load-leveling cycle. The operator specifies this mode by shifting the gear selector to NEUTRAL or FORWARD with the ignition ON. Two modes are required to satisfy the system idling requirements.

> Vehicle Idle Mode 1--At flywheel speeds below 8000 rpm, the armature chopper is used to control ring motor armature current to the value prescribed by the operational battery schedule. This is enabled by opening CBPS, CS, and by closing RS.
>
> Vehicle Idle Mode 2--Above 8000 rpm, the field weakening of the ring motor is used to control motor armature current. This requires that CBPS be closed and that the armature chopper be turned off.

4. Vehicle Acceleration

The operator designates the acceleration mode with the key on, by shifting the gear selector to FORWARD, then depressing the throttle. The controllor responds to operator throttle demands by selecting one of 13 power system acceleration modes. Depending on the throttle setting and on the state of the system, acceleration power will be supplied by the flywheel, the battery, or a combination of both sources.

a. Vehicle Acceleration Below Carrier Motor Base Speed

For vehicle speeds of less than 19 mph, corresponding to below-base-speed operation of the carrier motor, six modes of operation are required, depending on the flywheel speed and the throttle setting.

> Mode 1--During the most frequently implemented of these acceleration modes, the ring generator is above base speed, and the command from the throttle for acceleration current exceeds the current prescribed by the operational battery schedule (OBS). The armature chopper is used to control the battery current to the carrier armature, required by the OBS. The carrier motor, adjusted to full flux in the field, fixes the lowest voltage in the circuit. The voltage drop between

the carrier and the ring generator determines the amount of acceleration current developed. The terminal voltage of the ring generator is modulated by adjusting the generator field current. Thus, an increase in throttle setting will result in increased generator field current. This mode is enabled by opening CBPS and by closing RS and CS.

Mode 2--For small throttle settings, the demand for acceleration current is exceeded by the battery current required by the OBS. The battery output is then split between the carrier and ring motors, so that power is delivered to both the flywheel and to the vehicle axle. This split is determined by the voltage drop between the two motors. The carrier motor field is adjusted to full flux. The ring motor field is modulated to achieve the required power split. The armature chopper is used to control the battery current to the carrier and ring armatures, as required by the OBS. This mode is enabled by opening CBPS and by closing RS and CS.

Modes 3 and 4--When the flywheel is nearly discharged, the ring generator can be required to operate below base speed. For the case when the command from the throttle for acceleration current exceeds the current prescribed by the OBS, the voltage drop between the carrier motor and the ring generator determines the amount of acceleration current developed. The carrier motor field is set to full flux, and the ring generator field is used to control the voltage drop when the generator speed exceeds the motor speed. When this motor speed exceeds the generator speed, the generator field is set to full flux, and the motor field is used to control the voltage drop. In both cases, the armature chopper is used to control the battery current to the motor armature, as required by the OBS. These two modes are enabled by opening CBPS and by closing RS and CS.

Mode 5--When the flywheel is fully discharged, the ring generator drops to a fraction of its base speed, so that the power system now effectively operates on battery power alone. The generator is switched out of the circuit by opening RS; the generator field current is set to zero. The CBPS is open and the CS is closed, the carrier motor field is set to full flux, and armature current is controlled by modulating the armature chopper.

Mode 6--To obtain maximum vehicle acceleration when the throttle is fully depressed, the motor and generator armature current is adjusted to the maximum allowable, and the battery output is switched out of the circuit. The armature current is controlled to 228 amp by setting full flux in the carrier motor field, and then by using the field current of the ring generator to regulate the voltage drop between the two machines. Eliminating the battery output from the circuit increases the allowable current, and therefore, the torque output of the generator. This mode is enabled by switching the armature chopper off, by opening CBPS, and by closing RS and CS.

b. Vehicle Acceleration Above Carrier Motor Base Speed

For vehicle speeds greater than 19 mph, corresponding to above base-speed operation of the carrier motor, seven modes of operation are required, depending on the flywheel speed and the throttle setting.

Mode 1--During the most frequently implemented of these acceleration modes, the ring generator is above base speed, and the command from the throttle for accelerator current exceeds the current prescribed by the OBS. The battery output is then controlled by adjusting the voltage drop between the battery and the carrier motor terminal. This control is accomplished by modulating the current in the carrier motor field. The developed acceleration current is modulated by adjusting the generator field current. This mode is enabled by switching the armature chopper off, and by closing CBPS, RS, and CS.

Mode 2--For small throttle settings, the demand for acceleration current is exceeded by the battery current required by the OBS. The battery output is then split between the carrier and ring motors. The battery output is controlled by modulating the current in the carrier motor field, as in the previous mode. The battery power split is determined by the voltage drop between the carrier and ring motors. The ring motor field is modulated to achieve the required split. This mode is enabled by switching the armature chopper off, and by closing CBPS, RS, and CS.

Mode 3--When the flywheel is below normal operational speed, or when the vehicle is near maximum speed, the ring generator can be required to operate below base speed. For the case when the command from the throttle for acceleration current exceeds the current prescribed by the OBS, the voltage drop between the carrier motor and the ring generator determines the amount of acceleration current developed. The ring generator field is set to full flux, and the carrier motor field is used to control the voltage drop. The battery current to the motor armature is controlled to the OBS requirement by using the armature chopper.

Mode 4--When the ring motor is below base speed, and when the throttle setting is so small that the demand for acceleration current is exceeded by the battery current required by the OBS, the battery output is split between the carrier and ring motors. This split is determined by the voltage drop between the two motors. The ring motor is set to full flux, and the carrier motor is used to control the voltage drop. The armature chopper is used to control the battery current to the motor armature circuit, as required by the OBS. This mode is enabled by opening CBPS and by closing RS and CS.

Mode 5--When the flywheel is fully discharged, the ring generator drops to a fraction of its base speed, so that the power system now effectively operates on battery power alone. The generator is switched out of the circuit by opening RS; the generator field current is set to zero. The chopper is switched off and the CBPS and CS

are closed. Battery output is then controlled by modulating the voltage drop between the battery terminal and the carrier motor. The motor field current is thus adjusted in response to the throttle command.

Modes 6 and 7--To obtain maximum vehicle acceleration when the throttle is fully depressed, the motor and generator armature current is controlled to 228 amp. The battery output also is switched out of the armature circuit by switching the chopper off, by opening CBPS, and by closing RS and CS. When the generator is above its base speed, the carrier motor field current is adjusted to maintain full line voltage at the motor terminals, and the ring generator field current is modulated to obtain the desired armature current. As the flywheel discharges, and the generator drops below its base speed, the generator field is increased to full flux, and the motor field current is then decreased to maintain the desired armature current.

5. Vehicle Coasting

During vehicle coasting, regenerative braking is switched off and the flywheel is recharged, using the battery output prescribed by the OBS. The operator designates the coasting mode by switching the gear selector to NEUTRAL, and by leaving the foot brake off. The system overrides all throttle commands, and controls to the current requirement established by the OBS.

Whenever the vehicle is in a driving mode, the regenerative braking is activated; its magnitude is a function of vehicle speed and pedal position. Even in an "off pedal" driving mode, compression braking feel is available. Only in the neutral shift position is the regenerative braking disconnected.

6. Vehicle Deceleration

The operator designates the deceleration mode by depressing the brake pedal when the ignition is ON, and when the gear selector is in FORWARD or NEUTRAL. The controller responds to operator braking demands by selecting one of five power system deceleration modes. During each of these modes, the carrier motor is operating as a generator, and the direction of current is into the ring motor, which recharges the flywheel. For braking demands exceeding 0.14 g, the vehicle friction brakes are used to augment electrical braking.

a. Vehicle Deceleration Below Carrier Motor Base Speed

For vehicle speeds of less than 19 mph, corresponding to below base speed operation of the carrier motor, three modes of operation are required, depending on the flywheel speed. Each mode uses the armature chopper to maintain the battery current to the ring motor armature, as prescribed by the OBS. These modes are enabled by opening CBPS and by closing RS and CS.

Mode 1--When the flywheel is at operational speeds, the ring motor is above base speed. Full field current is applied to the carrier generator; the ring motor, which controls the magnitude of the armature current, is adjusted by modulating the generator field current in response to the braking demand. This mode is enabled by opening CBPS and by closing RC and CS.

Modes 2 and 3--When the flywheel is nearly discharged, the ring motor can be required to operate below base speed. For the case when the ring motor exceeds the carrier generator speed, the system operation is identical to the base speed case explained in mode 1. When the carrier generator exceeds the ring motor speed, however, the ring motor field is increased to maximum current, and the carrier generator field current is modulated in response to the braking demand.

b. Vehicle Deceleration Above Carrier Motor Base Speed

For vehicle speeds greater than 19 mph, two modes of operation are required, depending on the flywheel speed.

Mode 1--When the ring motor is above base speed, the motor field current is modulated to maintain the armature current prescribed by the OBS. The field current of the carrier generator is adjusted to obtain the desired armature current in response to the braking demand. The armature chopper is switched off, and CBPS, RS, and CS are closed.

Mode 2--When the ring motor drops below base speed, the field current is increased to full flux, and the battery chopper is used to control the battery armature current, as required by the OBS. The field current of the carrier generator is adjusted to obtain the desired armature current. This mode is enabled by switching the armature chopper on, by opening CBPS, and by closing RS and CS.

COMPONENT DESCRIPTIONS

Power Unit

The heart of the electric vehicle propulsion system is its power unit. The unit comprises the transmission assembly (including the final drive), the flywheel assembly, and the motor/generator set, consisting of two identical motor/generator units, one geared to the planetary ring gear, and the other geared to the planetary carrier. Both motor/generator units are used alternately in the generator mode and in the motor mode.

The power unit is installed on four mounting pads in the rear of the vehicle, by means of four mounting brackets which are integral with the unit and provide for accurate mounting interface. Only the motor/generator set must be cooled by forced-air convection; therefore the inlet air cooled manifold and an outlet splash pan will be coupled with the motor/generator set.

The outline drawing (Figure 42) depicts the installation characteristics and defines the transmission, flywheel, and motor/generator subassemblies.

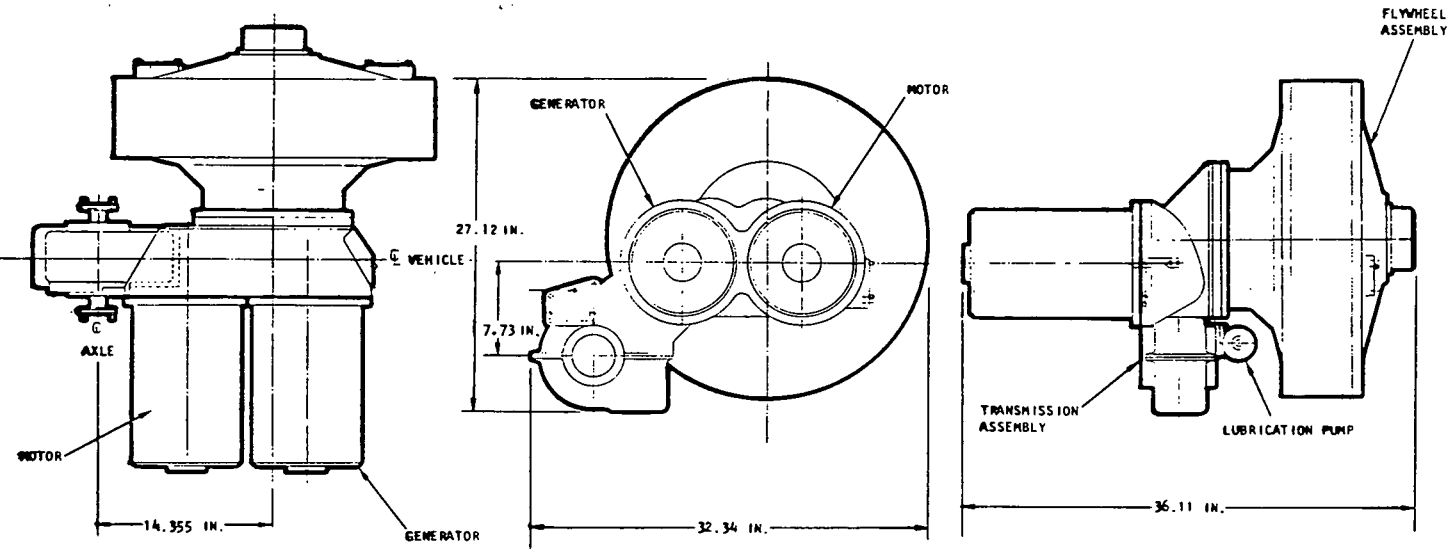


Figure 42. Power Unit

## 1. Performance

The full-throttle torque-speed characteristics shown in Figure 43 represent the power unit maximum performance. The graph shows the electrical torque fraction contributed by the motor and the total torque which combines the electrical fraction with the mechanical torque generated by the flywheel. The unit's peak power output of 52 kw, occurs at 54 mph. The maximum vehicle speed of 68 mph is limited by the maximum motor speed of 11,650 rpm. The generator torque increases with the increase in vehicle velocity. Since the generator is being driven by the flywheel, its speed is decreasing while it is developing greater and greater torque.

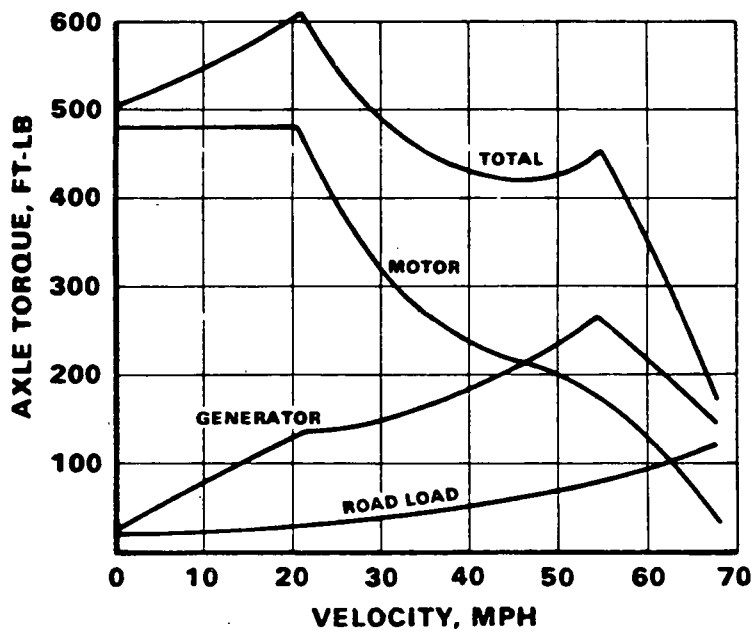


Figure 43. Full-Throttle Torque-Speed Characteristics

## 2. Design Duty Cycle

All power unit components that are speed dependent have their design and life predictions based on the duty cycle. The life cycle chosen for design is based on the number of (a) start-stops, (b) slow and rapid EPA (or Federal Urban) driving cycles, and (c) J227A (D) driving cycles. A combination of these modes of operation is used to evaluate component fatigue in order to satisfy the 4000-hr life design goal.

The most critical part of the power system is the flywheel. Its life expectancy, expressed in terms of number of cycles as shown in Table 11, is based on analysis and tests.

TABLE 11

DESIGN DUTY CYCLE

| Flywheel Speed Range | | No. of Cycles | Cycles Description |
|---|---|---|---|
| Percent | rpm | | |
| 0 to 90 | 0 to 21,250 | 6,460 | Start-stop (90%) |
| 50 to 100 | 12,500 to 25,000 | 1,000 | Start-stop (100%) |
| 64 to 85 | 16,000 to 21,500 | 5,000 | EPA (LA-4) slow |
| 75 to 80 | 18,750 to 20,000 | 96,400 | EPA (LA-4) rapid |
| 82 to 90 | 20,500 to 22,500 | 5,000 | J227A (D) |
| Total Number of Cycles | | 113,860 | |

## 3. Loads

The flywheel generates a gyroscopic moment that exerts a load on all power unit components. Analytically determined load values for design, limit, and crash modes are presented in Figure 44.

The flywheel rotor shaft assembly was analyzed at the maximum flywheel operating speed of 25,000 rpm. The critical loading condition for the flywheel rotor assembly was the yaw maneuver at the maximum operating flywheel speed. The flywheel and its support will not fail under crash loads which are considered as ultimate loads; deformation up to the point of fracture was permitted.

## 4. Structural Resonance Analysis

An interference analysis was conducted to predict and control structural resonances.

| | X G's | Y G's | Z G's | ROLL RAD/SEC | PITCH RAD/SEC | YAW RAD/SEC |
|---|---|---|---|---|---|---|
| DESIGN | 1.0 | 0.7 | 2.0 | 0.3 | 0.3 | 0.5 |
| LIMIT | 6.0 | 2.5 | 3.0 | 0.6 | 0.6 | 1.47 |
| CRASH | 10. | 10. | 10. | 6.0 | - | 6.0 |

NOTE: 1. ALL LOADS AND RATES ASSUMED TO BE APPLIED INDEPENDENTLY FOR PRELIMINARY ANALYSIS.
2. AN ADDITIONAL 1G VERTICAL, DOWNWARD, STATIC LOAD APPLIED SIMULTANEOUS IN ALL OF THE ABOVE CASES.
3. $M_{GYRO}$ = 2030 ft-lb

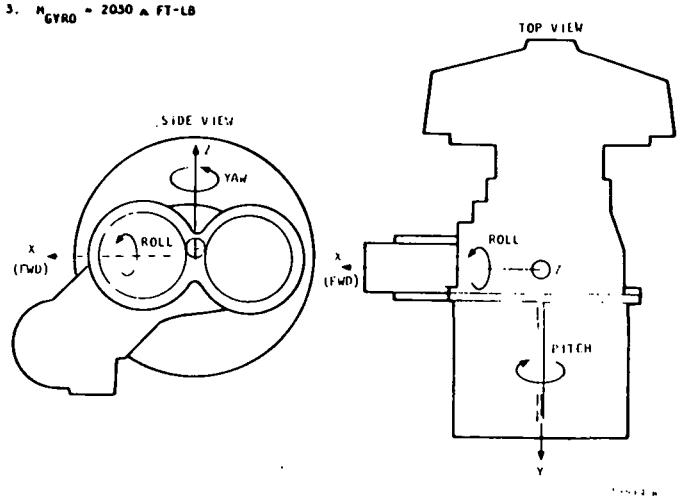


Figure 44. Design Loads

## 5. Transmission Assembly

The function of the transmission is to mechanically connect the various drive elements (axle, motor, generator, and flywheel) and provide speed ratios required of the drive. The principal speed ratio, key to the maximum power transfer, is between the flywheel and the axle. These are connected by means of a split power-train differential planetary gear set, a concept that provides an infinitely variable gear ratio from standstill to maximum speed.

Figure 45 illustrates the transmission drive configuration, the main gear ratios, and the kinematic relationship between the generator flywheel and motor speeds.

The sun gear of the planetary set is mounted on the flywheel shaft and rotates at flywheel speed. The planet gear carrier shaft is coupled to the drive axle(s) through a fixed-ratio drive mechanism (gear, belt). The electric motor also is coupled to the planetary shaft through a fixed-ratio drive. The ring gear is attached to the generator through a fixed-ratio drive, but the independently controlled generator speed provides for an infinitely variable ratio within the design limits of the ring gear speed, and consequently of the differential planetary drive ratio.

### a. Weight Breakdown

Table 12 lists the major elements of the transmission assembly and their respective weights.

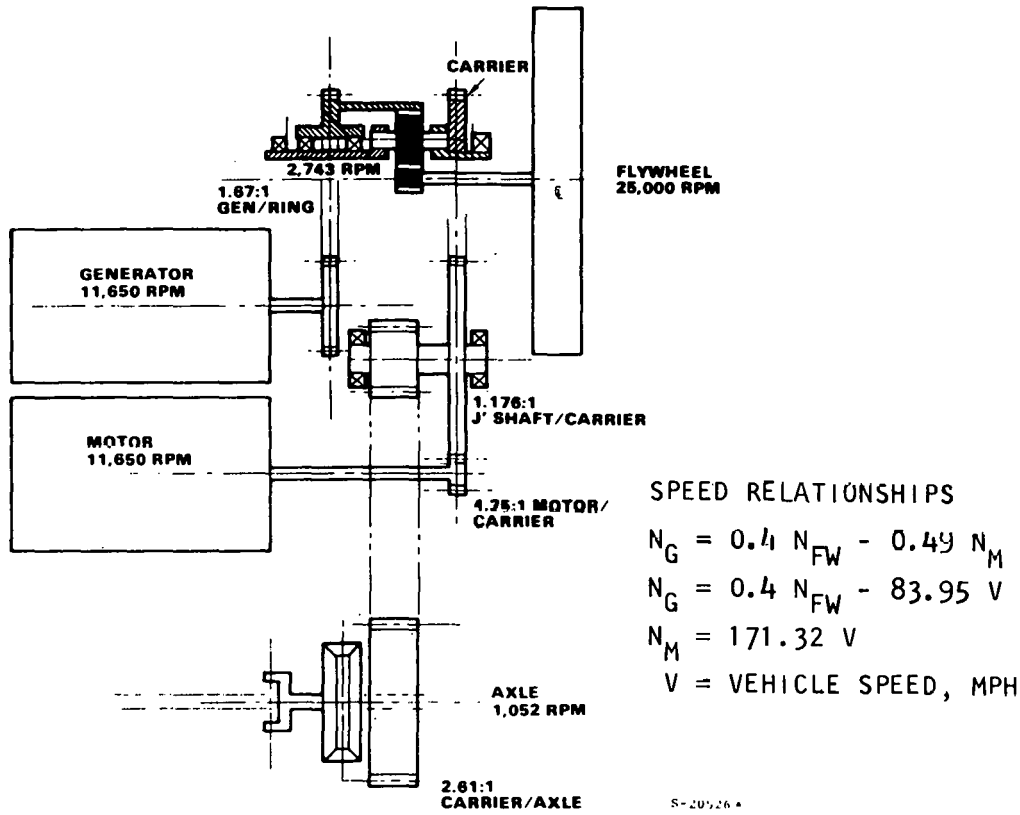


Figure 45. Transmission Drive Configuration

TABLE 12

TRANSMISSION ASSEMBLY WEIGHT BREAKDOWN

| | |
|---|---|
| Gears | 8.63 |
| Bulkhead | 3.64 |
| Housing | 19.36 |
| Carrier and differential | 8.13 |
| Lubrication pump | 3.40 |
| Housing differential | 5.83 |
| Chain and sprockets | 13.98 |
| Nuts, bolts, shafts, bearings, etc. | 18.55 |
| Fore pump | 8.20 |
| Total, lb | 89.72 |

b. Construction

The entire transmission assembly is enclosed by an aluminum housing that provides the interconnecting and mounting structure for the various power train elements. The motor, generator, and flywheel are attached by bolted flanges to the transmission case. Other minor elements, such as the lube/vacuum pump assembly, oil filter, etc., also are mounted on the transmission housing. The housing consists of a structural shell and a bearing bulkhead, which also forms the dividing wall between the transmission and the flywheel cavity.

The transmission housing structure dissipates all internal and external loads between the attached components (such as the motor/generators and the flywheel assembly) to the power unit mounts. The housing gear supports hold relative gear misalignment due to load deflection to a tolerable minimum; the loads are carried through basically cone-shaped elements to the dissipation points. Aluminum alloy A356-T6 is used as a casting material. It is well known for its high purity, strength, ductility, and vibration fatigue resistance. The gear bearings are supported by pressed-in, pin-retained steel sleeves for long life.

c. Efficiency

The power is extracted from the flywheel and transmitted through a quill shaft to the planet gear, which functions as a differential power-splitting device. The sun gear, integral with the quill shaft, drives the planet gears, which are connected through the planet carrier and related gears to the final drive. The planet gears, in turn, drive the ring gear, which is engaged with the generator drive. The drive motor engages a gear on the chain sprocket shaft and is part of the final drive. High efficiency of power transfer is fundamental to the transmission design concept.

The gear efficiency was optimized by using data from recognized gear authorities. To control the coefficient of friction, which is a major contributor to losses, the pitch-line velocity and load factors (k) were designed to be in a favorable range. The load factor was designed in the 200 to 400 range, while the pitch-line velocity functioned in the 2000 to 6000 ft/min range. The resulting coefficient of friction should be 0.03 to 0.04.

Bearings were selected for maximum efficiency. Roller or ball bearings were selected which have an inherent low power loss value by virtue of the rolling friction. Each bearing was selected for the minimum mean diameter to carry the load and to provide the 4000-hr B10 life. In this way, both the hydrostatic losses and the load losses were minimized.

d. Noise Considerations

Transmission noise has been minimized by three design steps. First, where possible, the gears are helical. In this way, tooth-to-tooth contact ratio is greater than one, thereby producing quiet gear-tooth engagement. Second, the tips of the gears have been relieved to minimize noise on initial contact. The critical tolerances for the gears have been selected as the best obtainable for an automotive application. The noise is controlled through accuracy of profile error, tooth-to-tooth spacing, pitch-line runout, and lateral runout.

General transmission design was guided by automotive practices. The case-hardened (carburized) material was selected to provide a controlled Rc 58 minimum surface hardness and a 35 to 38 core hardness for maximizing fatigue strength.

e. Lubrication

The transmission lubrication is accomplished in the simplest possible way, with an effort to keep churning losses and gear oil squeeze losses to a minimum. Jet lubrication is restricted to the planetary gear and the flywheel bearings; all other areas are splash lubricated.

The lubrication pump is a Gerotor pump delivering 1.5 gpm at 100 psig, with a power requirement of less than 100 w. The pump unit remains in operation as long as the flywheel is rotating.

The lubrication is designed to reduce friction-resulting losses and, therefore, to keep each section within the required temperature limits. The temperature of the oil has been set at 200°F on entering, and 220°F on existing each component. MIL-L-23699 lubrication oil was selected as the lubricant for prototype evaluation.

f. Stress

To calculate its stress levels, the housing structure section of the gearbox was idealized by an equivalent conical section. The four rubber mounts were idealized by two equivalent ring springs of infinite rigidity at the motor/generator and flywheel ends. In the actual installation, the mounts spring rates will be 2,000 and 4,600 lb/in. at the flywheel and motor/generator ends, respectively.

In addition to the inertia and gyroscopic loads shown in Figure 44, the housing is operated at a near vacuum; thus there is an equivalent external pressure of 14.7 psi acting on the housing.

The short-time stress design criterion for the housing is that the housing has a plastic yield if subjected to crash loads, but it should not rupture, and it should not have any yielding when subjected to limit loads. The long-time stress criterion specifies that the housing shall experience the normal, steady, operating stresses and the alternating stresses, without any fatigue failures.

The stresses produced by a roll-crash load of 14.7 psi external pressure, = 6.0 radians/sec, and 150°F operating temperature, were calculated and the margin of safety, based on crash-ultimate loads, is 1.25. The limit loads are 0.1 to 0.24 times the crash loads. Since the tensile yield is close to the tensile ultimate (about 83 percent), the margin of safety based on limit-yield loads will be ample, because it will be much higher than the crash loads.

The alternating stresses produced by the design loads are 1/12 to 1/20 of the crash-ultimate loads. Thus, the maximum alternating stress will be less than $\pm$1.03 ksi, which is well below the endurance limit of the 6061-T6 aluminum.

## 6. Flywheel Assembly

As illustrated in Figure 46, the flywheel is mounted in an aluminum housing that supports the bearings, seals, fore pump, molecular pump, and self-contained lubrication for the outboard bearing, and provides an evacuated enclosure. The housing is made of 6061 aluminum and has thin walls of low weight, but provides adequate stiffness to prevent collapse. The housing plate surface is free of porosity to prevent air from bleeding into the evacuated chamber molecular pump area. A 1/4-in.-thick steel ring affords safe flywheel containment. As indicated by Figure 46 the fore pump and molecular pump work together to provide the required vacuum for the flywheel.

### a. Weight

Table 13 lists the major flywheel assembly elements and their respective weights.

TABLE 13

FLYWHEEL ASSEMBLY WEIGHT BREAKDOWN

| | |
|---|---|
| Rotor | 60.47 lb |
| Outer cover | 15.69 |
| Inboard housing | 17.94 |
| Stator (molecular pump) | 5.22 |
| Containment ring | 44.63 |
| Nuts, bolts, bearings, seals, etc. | 12.10 |
| Total | 156.05 lb |

### b. Flywheel Construction

Figure 47 depicts the flywheel made of three components--the hub and two identical rims that mount on the hub. The hub is a single pancake forging of 7075 T3652 aluminum, which is stabilized by liquid nitrogen after it is bandsawed from the pancake and again before final machining. The hub is contoured so that it operates at uniform stress throughout its total volume except for the hub ends of each of the four spokes. In this manner, all of the material is working, and the weight is held to a minimum. The spoke hub ends provide a sufficient surface area so that the operational radial stresses on the rim from the spoke are below the allowable stresses for the rim. To further distribute the load on the rim at the spoke, thin pads of Melamine (epoxy glass) are bonded to each spoke tip, and thin pads of polyurethane are bonded to each Melamine pad. The rim is not bonded to the polyurethane.

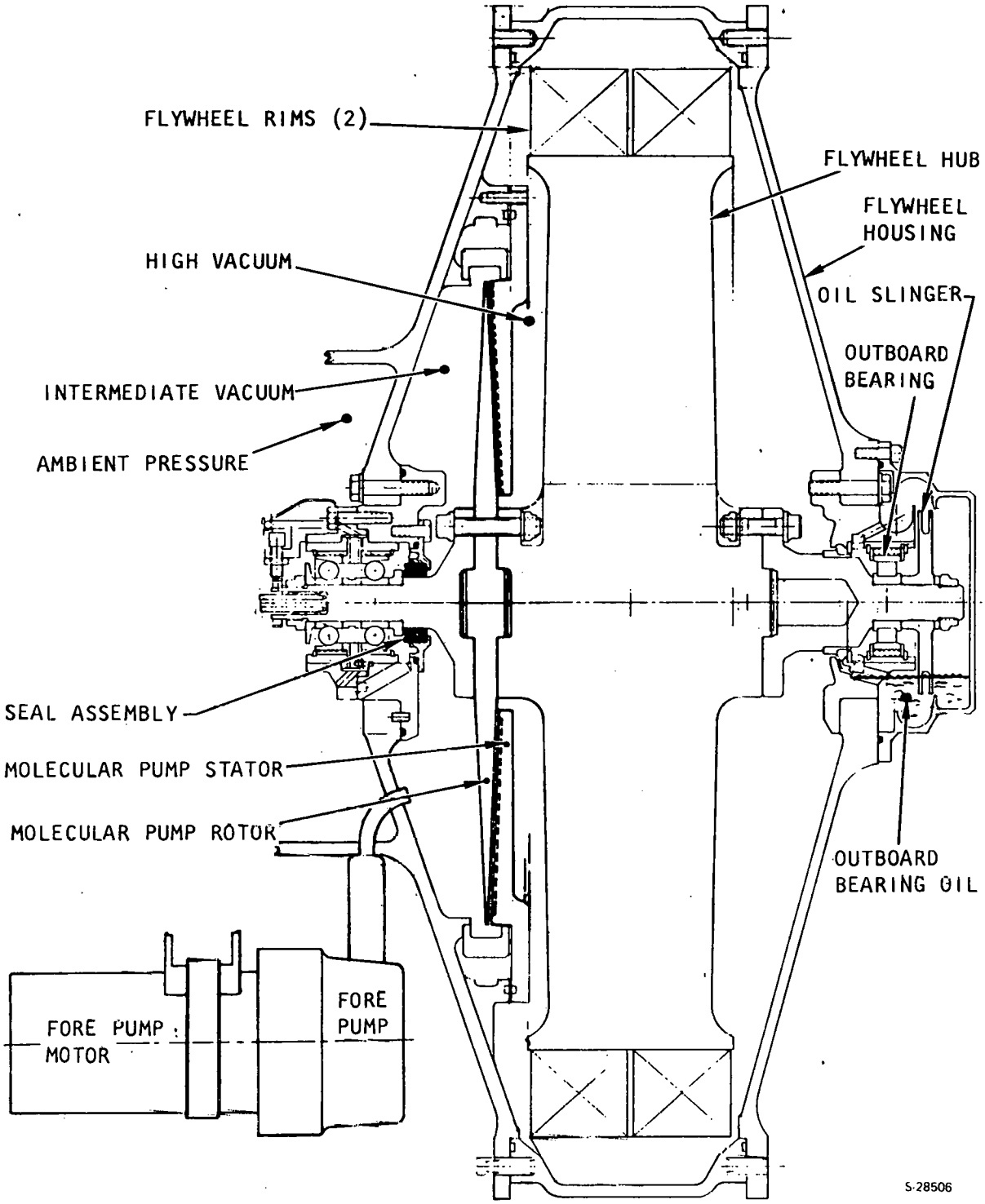


Figure 46. Flywheel Assembly and Housing

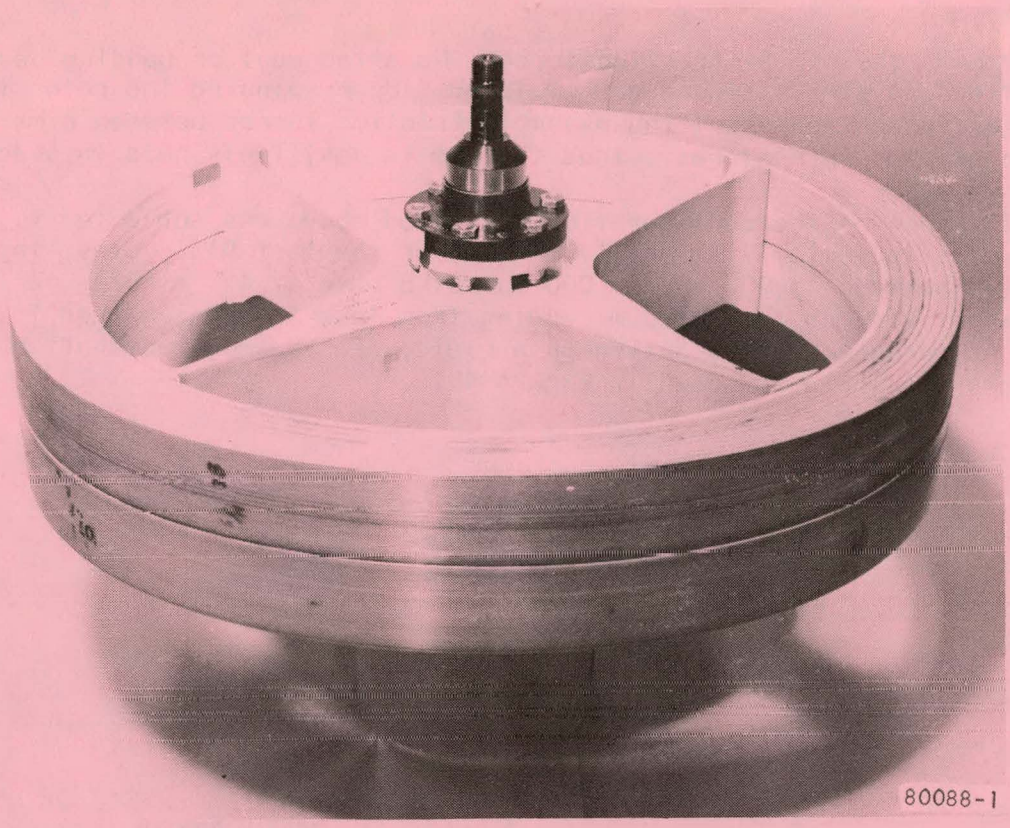


Figure 47. Composite Flywheel

Two rims are assembled onto each hub. Each rim consists of nine separate radially stacked rings. Each ring is 2.1 in. wide and either 0.240 in. or 0.184 in. thick. Each rim consists of rings of this construction. The first ring is an S-2 fiberglass/epoxy composite. This ring is 0.240 in. thick. All composites in the rims use the four-part elastomerized epoxy consisting of Dow DER 7818 epoxy resin, DER 7575.02 epoxy resin (the elastomerized component), ERL 4206 diluent, and TONOX 60-40 hardener. Rings 2 through 4 are made of Kevlar 29/epoxy composite. Rings 5 through 9 are made of Kevlar 49/epoxy composite. The first ring is wound on the mandrel and cured. A mold release agent is placed over the first ring so that the second ring will be permanently separated from it. Each ring is subsequently wound upon and permanently separated from the previous ring by the mold release agent.

This set of nine nested rings has a low radial stress when subjected to the radially graduated centrifugal force field. The low radial stress is necessary to prevent cracking and delamination in the epoxy composite transverse direction. Each ring works independently in the radial direction, and as a unit in unaxial hoop tension, taking best advantage of the filament-wound composite materials properties.

The two rims are mounted on the hub, separated from each other by an axial register. The rims are distorted to a subcircular shape to the amount that the hub diameter exceeds the inside diameter of the rims. Thus only the spring force in the rim from its attempt to return to its round free state

holds it onto the rim by friction force. No attachment or bonding devices and their attendant stress risers are employed. Upon spinning the rotor to speed, the radial forces and resulting assembly friction forces between rims and hub are even greater than at rest, thus the rim is positively held in place.

A flywheel of the configuration described above was subjected to 1000 speed cycles to verify its tensile life. For the last 933 cycles, the speed was varied between 13,000 and 25,000 rpm at a rate of 4.5 minutes per cycle. The flywheel was run in a vacuum ranging from less than one micron to 10 microns of mercury and was driven on a rigid, bearing-mounted shaft by a dynamometer test rig as shown in Figure 48.

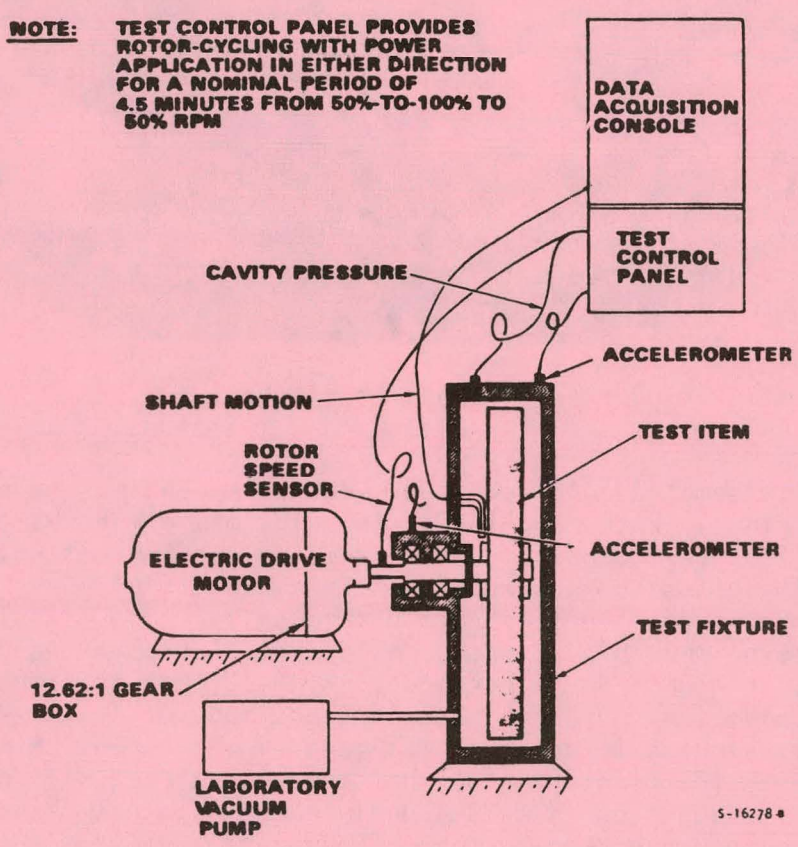


Figure 48. Flywheel Cycle Test Setup

There was no detectable change in rotor balance conditions in the 13,000 to 25,000 rpm range as indicated by the accelerometer data. The test was terminated at 1,000 cycles, with all indications that the rotor was performing normally.

Inspection after the cycle test was completed showed that one roving had parted around the whole circumference, and lay as loose fiber in the bottom of the test chamber. This roving parting did not propagate. There was a 0.042 in. average gap between the first and second rings of the rim. The gap had reduced to 0.03 in. 168 hrs after the test.

This testing is equivalent to 7,000 cycles from zero to 90 percent speed for tensile life. These 7,000 cycles represent essentially all of the damage fraction, since other less rigorous conditions do not add materially to the damage fraction.

c. Flywheel Design Characteristics

The flywheel design characteristics are as follows:

| | |
|---|---|
| Total energy | 1.0 kw-hr |
| Rim OD | 23.0 in. |
| Rim ID | 19.24 in. |
| Design speed, maximum | 26,250 rpm |
| Operating speed, maximum | 25,000 rpm |
| Rim weight (2 rims) | 27.7 lb |
| Spoke radial force | 5300 lb (3500 psi) |
| Ambient pressure at 25,000 rpm | 1 μHgA |
| Materials: | |
| Inner ring (1) | 0.24 in. S-2 fiberglass/epoxy |
| Mid-rings (3) | 0.24 in. Kevlar 29 |
| Outer rings (5) | 0.184 in. Kevlar 49 |
| Total wt (rim, hub and shaft) | 60.47 lb |

d. Bearings

The flywheel rotor is supported by two bearing assemblies, one on either side of the rotor. The inboard bearing group consists of a matched pair of angular contact ball bearings that provide accurate axial positioning of the flywheel rotor. The bearings axial location must be as close to the molecular pump as possible to minimize any variation in pump face clearance due to rotor thermal expansion.

The outboard bearing employs a roller bearing, which permits the rotor to expand axially. Since this bearing is located in the flywheel cavity and is exposed to a one-micron absolute pressure, a special lubrication design concept has been developed. The inboard bearings are separated from the flywheel cavity vacuum by a carbon face seal. These bearings are jet lubricated by the transmission lubrication pump. A self-contained 5-cu in. reservoir is charged with Coray 100 oil. A liquid pump disc attached to the flywheel shaft transports the oil from the reservoir to a splash shield, providing adequate lubrication and cooling for the bearing. The size of the disc and the quantity of oil used for lubrication are determined by tests, to minimize the power consumption. The results displayed in Figure 49 show that the power consumption will be less than 80 w.

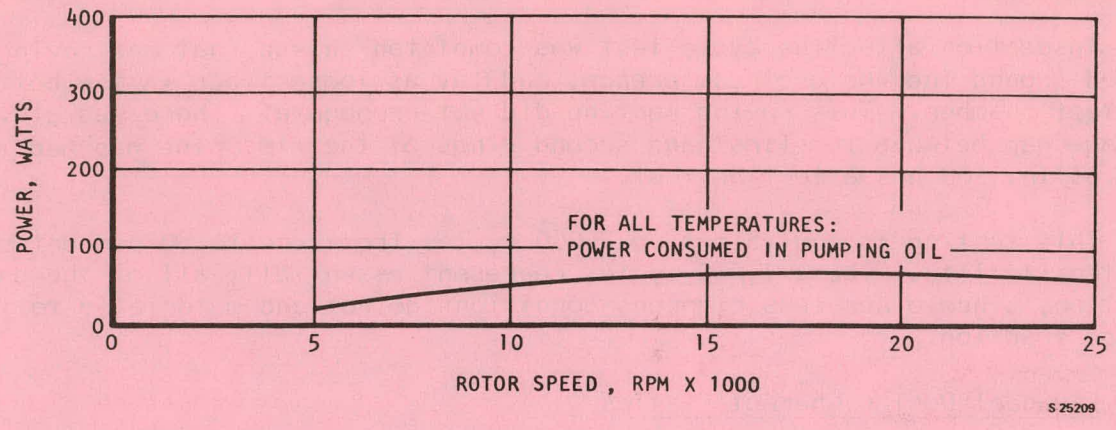


Figure 49. Outboard Bearing Lubrication Performance

e. Vacuum System

The vacuum system consists of two major components, a roughing or fore pump and a molecular pump, designed to maintain a vacuum in the flywheel cavity so that the windage friction does not create excessive flywheel surface temperatures. (See arrangement in Figure 46.)

The roughing or fore pump is a vane type of pump, capable of reducing flywheel cavity pressure to 1 torr. It is driven by an electric motor, which is energized whenever the flywheel is rotating and the cavity pressure rises above 1 torr.

The molecular pump is a mechanical drag type of pump consisting of a smooth-surface disc attached to the flywheel rotor and a stator with spiral grooves cut to accommodate the induced flow of air molecules. The stator is kept at an average of 0.020 in. clearance from the rotor disc and the spiral grooves shown in Figure 50 are curved in the direction of the disc rotation, allowing the disc to propell the molecules in an outward direction.

For evaluation purposes, the molecular pump performance tests were conducted by varying the fore pump pressure from 0.5 to 2 torr (molecular pump outlet pressure) and the face clearance from 0.012 to 0.02 in. The pump inlet pressure (or cavity pressure) was measured as a function of pump rotational speed as shown in Figure 51. Pressure ratios in excess of 20,000 were obtained.

The demonstrated capability of maintaining low cavity pressure enhances the overall design aim of low flywheel losses. In addition, the capability is required to generate quickly low pressure during the flywheel startup. The transient heat loss causes the flywheel surface temperature to rise until adequate vacuum is generated. Figure 52 combines the tested startup cavity pressure transient response with the flywheel surface temperature transient analysis. The fore pump and motor are sized to generate a volumetric pump-down rate of approximately 2500 cu in./min, a minimum necessary to prevent excessive flywheel temperature overshoot during the startup.

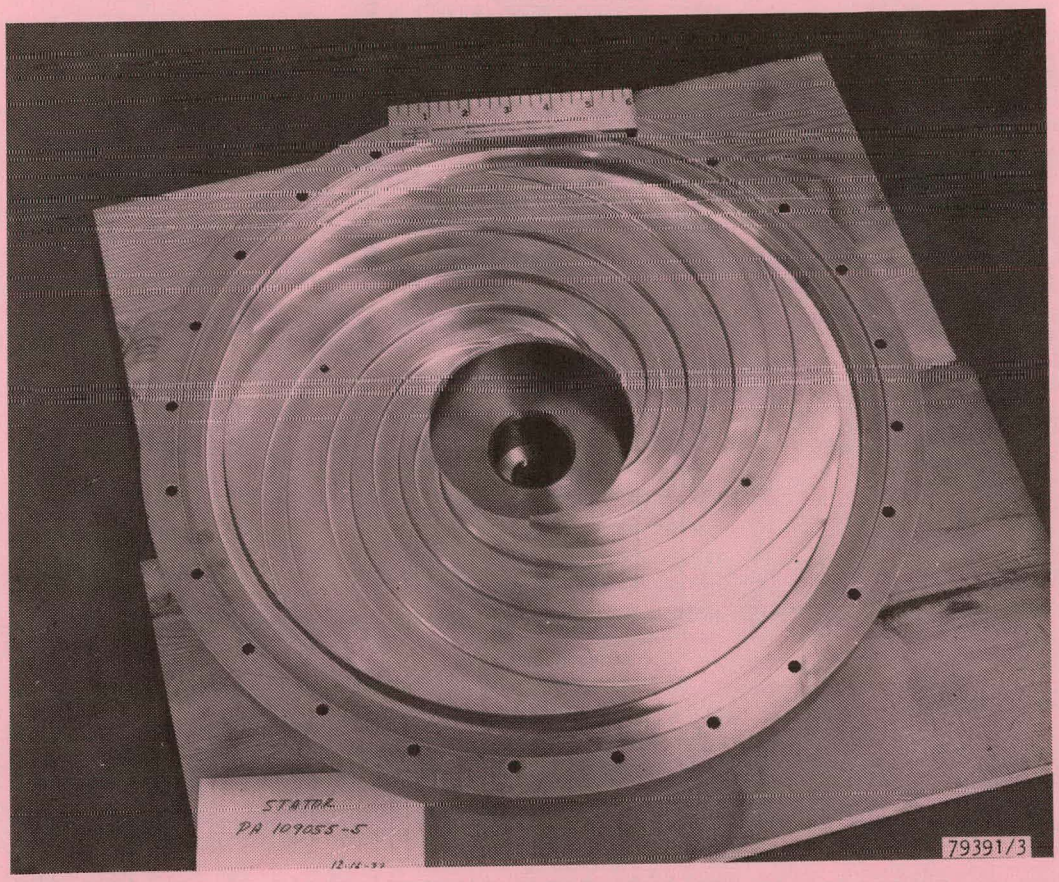


Figure 50. Molecular Pump Stator

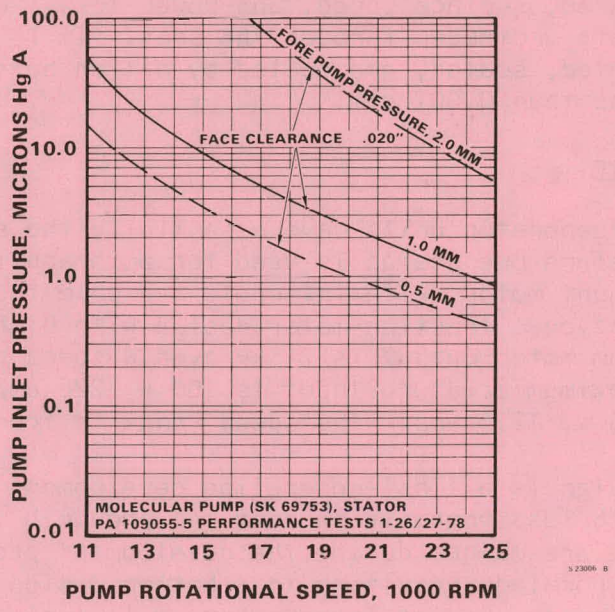


Figure 51. Molecular Pump Performance Characteristics

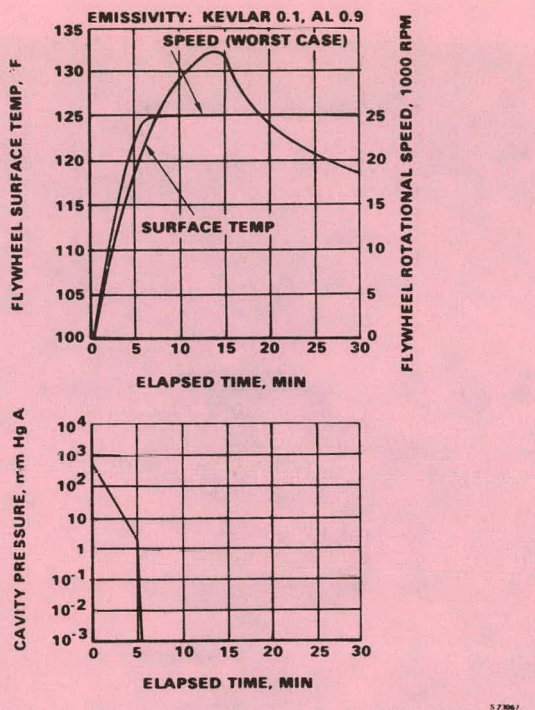


Figure 52. Flywheel Surface Temperature Response

f. Seal

A seal is located on the high-speed flywheel shaft to separate the flywheel cavity from the transmission cavity. It is subjected to an operational pressure differential of 14.7 psi, and is designed for the smallest practicable diameter to reduce sealing area, surface speed, and power loss. Only the small-diameter torque-carrying shaft protrudes through the seal. It is a carbon-faced seal, and is well lubricated, sealed, and cooled by oil on both sides. The tested leakage rate is less than 0.001 cfm.

7. Motor/Generator

The two motor/generator units have essentially the same power and thermal requirements, therefore one design is used for both applications. This design is a 4-pole, dc, shunt motor, with interpole and pole-face windings, and is similar to a conventional traction-motor design with high efficiency and low weight. The maximum motor output is 21 kw over a speed range of 3,000 to 10,000 rpm. The maximum armature input is 106 v, 228 amp. The control field maximum input is 80 v, 12.5 amp. The speed range is from zero to 11,650 rpm.

This motor design is a first-generation development unit of high efficiency and low weight, with less emphasis on cost and producibility. As operating data and experience are gained during the development program, design improvements will be incorporated, resulting in a better design from the standpoints of both weight and cost. Design improvements will include brush material changes

and overall size and winding changes (resulting from pole-face/interpole trade-offs). The current design provides the starting point for a high output-to-weight motor/generator with high efficiency.

The motor design is based on the operating requirements for a typical traction motor application; however, the design deviates from conventional motors of this rating, in order to minimize weight without lowering motor efficiency. The main differences in approach are as follows:

(a) Aluminum castings are used instead of steel for end bells to save weight.

(b) Pole-face windings are used to improve control of armature reaction magnetomotive force (mmf), thus permitting operation at smaller main field air gaps. This results in a net improvement in efficiency by reducing the main field losses.

(c) The field frame is made of low-carbon steel tubing and serves the dual purpose of being a structural member and providing a low-reluctance flux path between the poles.

(d) Commutator design parameters such as tip velocity, brush current density, and interior stresses are the maximum allowable values in order to save weight.

The significant dimensions of the motor are shown in a cross-sectional view (Figure 53). Weights of significant parts of the motor assembly are given in Table 14. Design characteristics are presented in Table 15.

TABLE 14

MOTOR/GENERATOR WEIGHT BREAKDOWN

| | |
|---|---|
| Armature laminations | 13.14 lb |
| Armature winding | 7.78 |
| Commutator | 13.60 |
| Shaft and bearings | 6.71 |
| Main field and pole laminations | 11.36 |
| Interpole laminations | 5.34 |
| Housing (field frame) | 23.19 |
| Pole face winding | 4.48 |
| Main field winding | 6.93 |
| Interpole winding | 3.97 |
| Insulation | 2.30 |
| Brush holder assembly and brushes | 2.54 |
| End bells (2) | 11.35 |
| Miscellaneous hardware | 2.06 |
| Total weight | 114.79 lb |

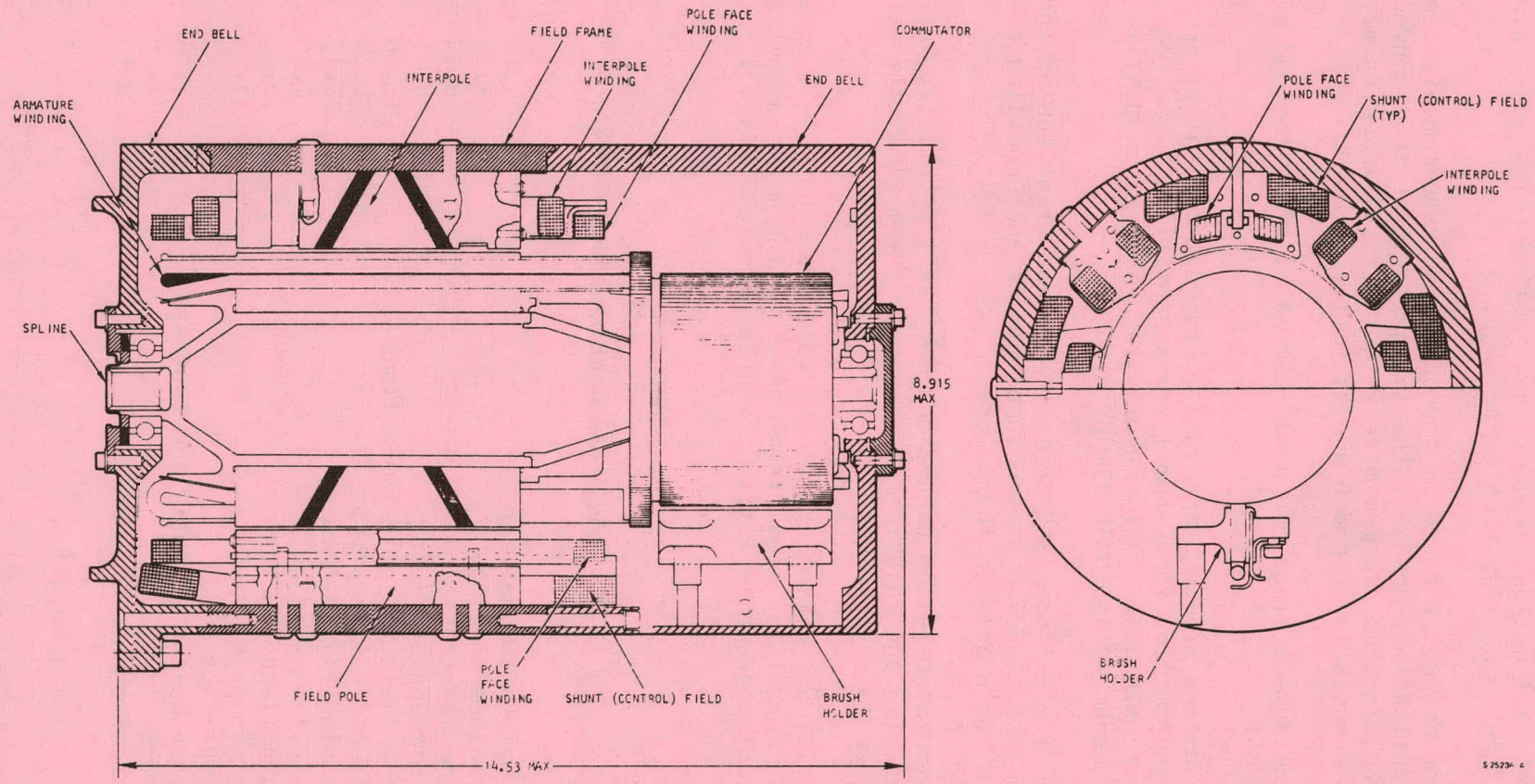


Figure 53. Motor/Generator Assembly Cross-Sectional View

TABLE 15

MOTOR/GENERATOR DESIGN PARAMETERS

Ratings

| | |
|---|---|
| Power, kw | 21 max. at 3000 to 10,000 rpm |
| Speed range, rpm | 0 to 11,650 |
| Power source voltage, v | 108 |
| Power source current, amp | 228 max |

Dimensions, in.

| | |
|---|---|
| Diameter | 8.915 |
| Length | 14.53 |

Circuit Resistance at 20°C, ohms

| | |
|---|---|
| Armature winding | 0.0205 |
| Shunt (control) winding | 3.81 |
| Interpole winding | 0.0059 |
| Pole face winding | 0.0093 |

Circuit Inductances, mh

| | |
|---|---|
| Armature winding | 0.097 |
| Shunt (control) winding | 81.9 to 409.6 |
| Interpole winding | 0.125 |
| Pole face winding | 0.0469 |

Electrical Loading, amp

| | |
|---|---|
| Maximum armature current | 228.0 |
| Maximum shunt field current | 12.5 |

Winding Descriptions

| | |
|---|---|
| Armature: | 75-bar commutator, 25 slots, 6 conductors/slot, wave winding, rectangular wire of 0.0138 sq in. |
| Shunt field: | 144 turns No. 16 AWG wire |
| Interpole: | 5 turns rectangular wire, 0.052 sq in. |
| Pole face: | 5 turns rectangular wire, 0.0304 sq in. |

Materials

| | |
|---|---|
| Housing | AISI 1010 steel |
| Wire | Annealed copper, Kapton wrapped |
| Shunt poles | Silicon steel |
| Armature laminations | M-19 steel |
| Interpoles | Silicon steel |
| Commutator | Silver bearing copper |
| Brushes | Electrographitic |
| End bells | Aluminum |

a. Performance

The maximum envelope of motor performance is shown in Figure 54. The motor will perform satisfactorily, although not necessarily continuously, at any point within this envelope. Operation at any point is determined by the shunt field current, the armature voltage, and the load torque. For any combination of armature current and field current, a motor-speed-torque curve is determined. Steady-state operation occurs at the point where the load-speed-torque intersects the motor curve. Acceleration occurs when the motor torque exceeds the torque required by the load, at any given speed.

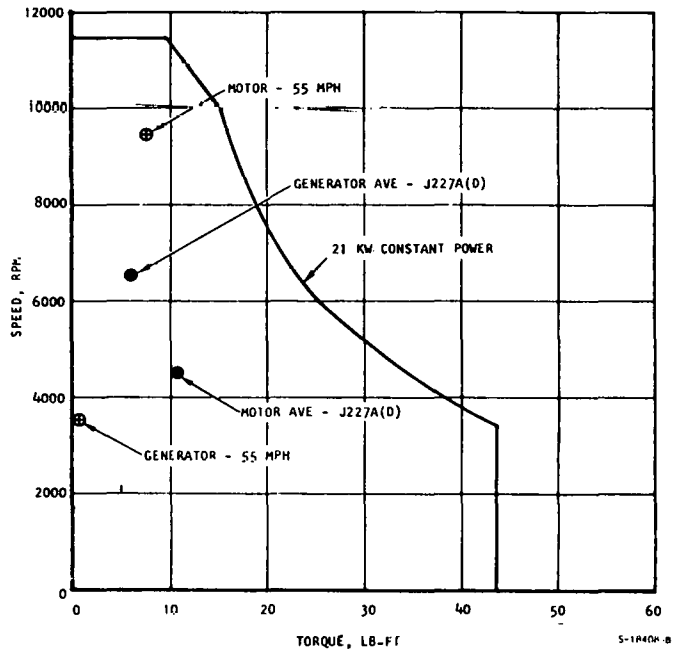


Figure 54. Performance Envelope

b. Physical and Operating Characteristics

There are four openings in the rear end bell, with one opening over each brush. The openings are covered by a shroud. The opening permits easy inspection and servicing of the brushes. Cooling air, at a volumetric rate of approximately 50 cfm, is ducted into the motor at the rear end, then directed over the commutator, along the armature and field structure, and finally exhausted through holes in the drive end bell. Armature leads enter through a strain relief near one of the brushes, and terminate inside the motor, one on a brush box and the other directly on the interpole winding. This minimizes the number of junctions required and improves reliability. Similarly, control field leads enter through a strain relief and terminate on the shunt field coil winding.

Two additional leads come from a thermal sensor located on the pole-face winding, across from the armature hot-spot. A shaft seal is incorporated at the drive end of the motor to prevent oil and contaminants from entering the motor. It is a positive-contact, lip-type wiping seal.

The armature, commutator and brushes, interpole and pole-face winding, and control field are discussed in the following paragraphs.

(1) Armature

The armature winding is a one-turn-per-coil, three-coils-per-slot, retrogressive-wave winding, with four poles and four brushes. The lamination has 25 slots, and the commutator has 75 bars. The three coils are formed and taped as a group. To reduce stress at the hairpin turn, each turn consists of two rectangular wires. Each wire is insulated with 3-mil Kapton tape, plus one layer of 4-mil glass tape. Armature coils terminate in slots in the commutator riser, and are welded into place. A large-diameter, hollow shaft is used for maximum stiffness with minimum weight.

The diametral interference between the shaft and the laminations will maintain load capability under all operating conditions. Angular alignment of the laminations and the commutator is achieved by tooling during assembly. The thermal analysis, under a variety of load conditions, showed that the armature hot-spot is on the conductor at the hairpin curve. At this point, the cooling air is the hottest, and there is no surrounding lamination material to act as a heat sink. To sense this temperature, without placing sensors on the rotating armature, a temperature sensor is located on the pole-face winding directly opposite the armature hot-spot.

(2) Commutator and Brushes

The commutator is characterized by an "arch-bound" design with silver-bearing copper segments and mica insulation. Because of the high axial width of the brushes, two brushes side-by-side are used in each holder. The shunts are joined in a common lug, so that they can be inserted and removed as a pair. One brush is wider than the other. When inserted into the brush holder, they are staggered, so that the individual brush-wear paths on the commutator overlap and produce a more even commutator wear.

Thermal analyses, under a variety of worst-case conditions of ambient temperature, cooling air temperature, and load cycle, showed that commutator temperatures are within the design maximum of 350°F.

(3) Interpole and Pole-Face Winding

Pole-face windings and interpoles are required to facilitate commutation, because the motor is required to operate over a wide range of speed and armature current. Armature-reaction flux, produced by the current-carrying armature conductors, produces cross-magnetizing and demagnetizing fields. Speed affects commutation time, and the magnitude of the reactance voltage. The pole-face windings are designed to counteract the magnetomotive force of the armature winding that is producing the armature reaction. The interpoles produce a flux that opposes the cross-magnetizing flux; they also tend to induce a voltage to counteract the reactance voltage.

Since the armature reaction is a function of armature current, both the pole-face winding and the interpole windings are connected in series with the

armature, and carry armature current. A final adjustment of interpole strength is made during testing. This adjustment consists of varying the reluctance of the interpole circuit by using a combination of magnetic and nonmagnetic shims between the pole and the field frame.

(4) Control Field

The main field of the motor is a separately excited shunt field; in conjunction with armature voltage, it is used to control the motor. Four field coils, connected in series, are designed to produce full-field capability with 80 v, minimum. The coils are layer-wound with 16-gauge, ML-insulated wire. Interlayer insulation is 0.003-in. Nomex. The entire coil is then wrapped with glass tape and Kapton tape.

c. Thermal Characteristics

The motor/generator insulation is rated at 428°F. Under a variety of steady-state and transient conditions, the armature, pole face, and interpole winding temperatures remain below this value. The typical transient thermal condition experienced during a hill climb is illustrated in Figure 55. A temperature-limiting control sensor measures the pole-face winding temperature, which is limited to a maximum of 350°F. At the same time, the armature winding is protected by limiting its temperature to 428°F. This control method permits a maximum utilization of motor power up to 21 kw. The elapsed time at peak power is only a function of ambient conditions and driving characteristics.

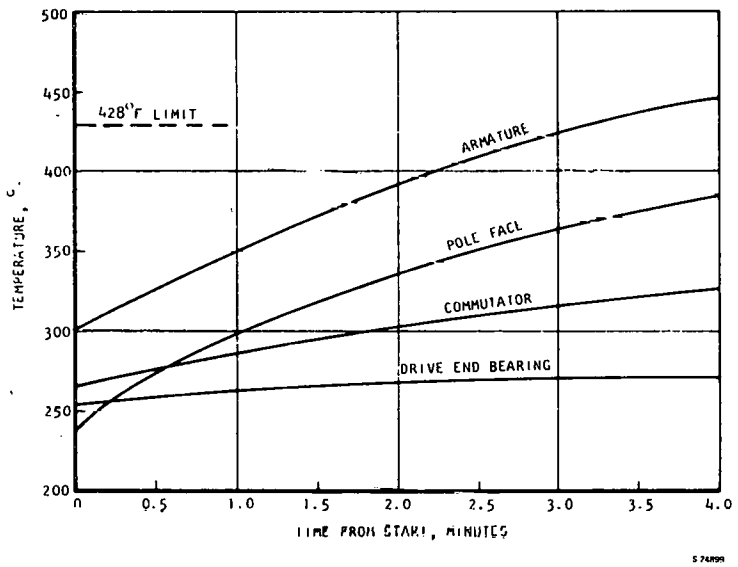


Figure 55. Transient Temperature Response in Hill-Climb Mode

## Controls and Electronics

The vehicle electrical system, through its interconnecting cabling and wiring, integrates all power system components, and interfaces the power system with the vehicle controls, displays, and accessories. The power system electrical schematic (Figure 56) defines the electrical interface among the following controls and electronic components: controller, power conversion unit, battery charger, data recorder, switchgear, fans, and driver controls and displays. The locations of these components in the vehicle are shown in Figure 57.

The controller, battery charger, and data recorder are installed in the vehicle front compartment, while the power conversion unit and the switchgear are installed in the rear compartment. The battery power outlet is adjacent to the power conversion unit to minimize cabling and provide maximum protection. The battery high-voltage circuits are located in the rear of the vehicle, except for the charger interface, which is located in the front compartment (under the hood) for convenient access. All dashboard controls and displays and vehicle accessories are powered by a solid-state, 12-vdc power supply for maximum safety--consistent with current automotive design practices.

Complex electric and electronic systems require design consideration as potential sources of electromagnetic interference (EMI). Precautions are taken to minimize radiated noise and prevent interference with other electrical/electronic devices. Also, the power system must be free of EMI susceptibility to ensure safe operation and efficient performance under all operating conditions.

The power conversion unit incorporates four choppers which are a source of electrical noise. The dc motor commutators and contactors also generate electromagnetic noise which must be suppressed. The design is based on the following;

(a) Metallizing nonmetallic vehicle body parts for noise containment (Figure 58); i.e. power conversion and switchgear enclosures, and adjacent ducting

(b) Suppressing dc motor commutators with capacitors in the motor housings (motor/generator and cooling fan)

(c) Shielding all 108-vdc cables (braided insulation)

(d) Filtering all auxiliary 108-vdc motor power supplies

(e) Filtering all 12-vdc power supply outputs

(f) Separating all control cabling and power supply cabling from other cabling; shielding and grounding them as appropriate

(g) Isolating the 108-vdc power circuits from the 12-vdc, $\pm$12-vdc, and 5-vdc circuits.

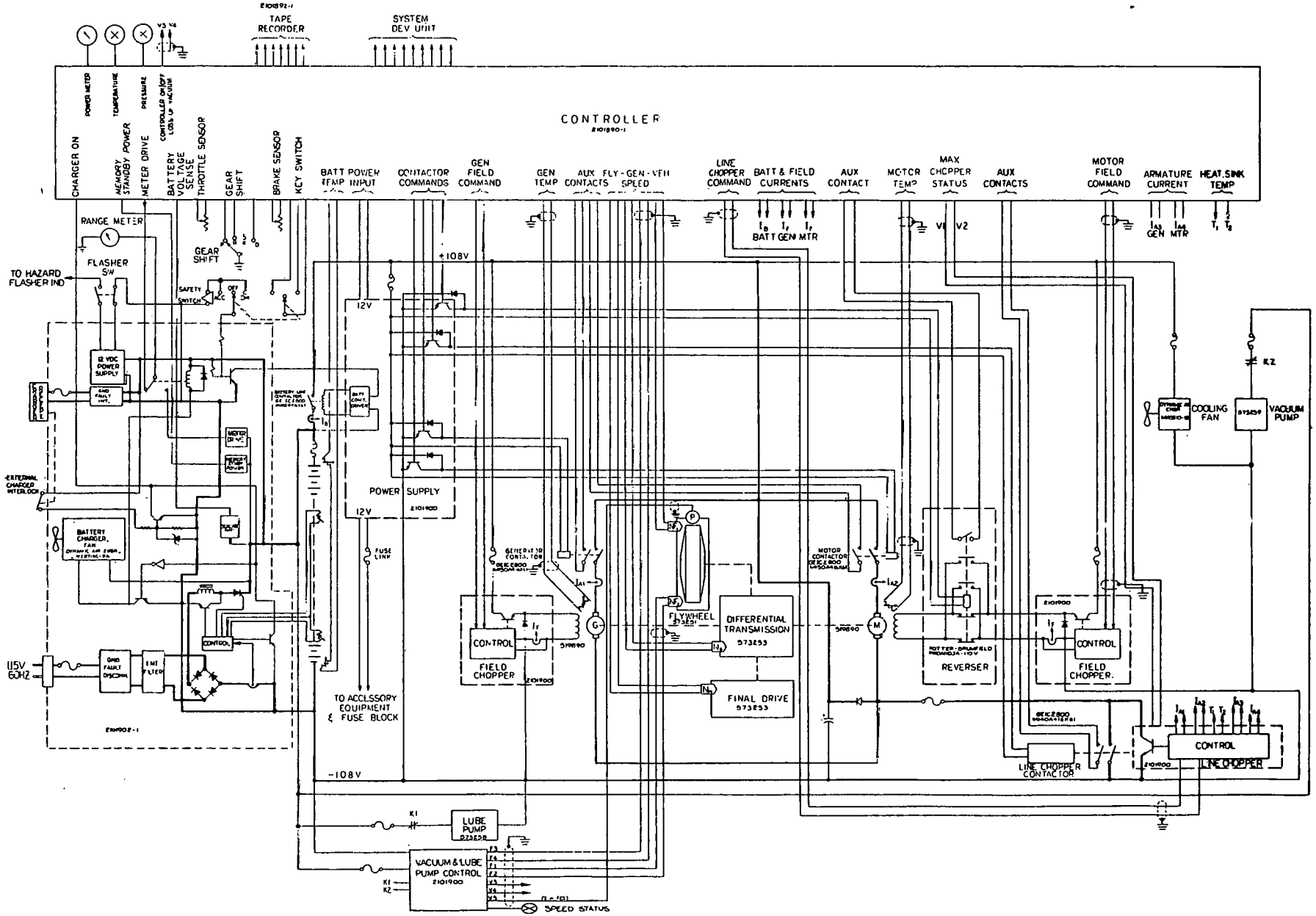


Figure 56. Power System Electrical Schematic

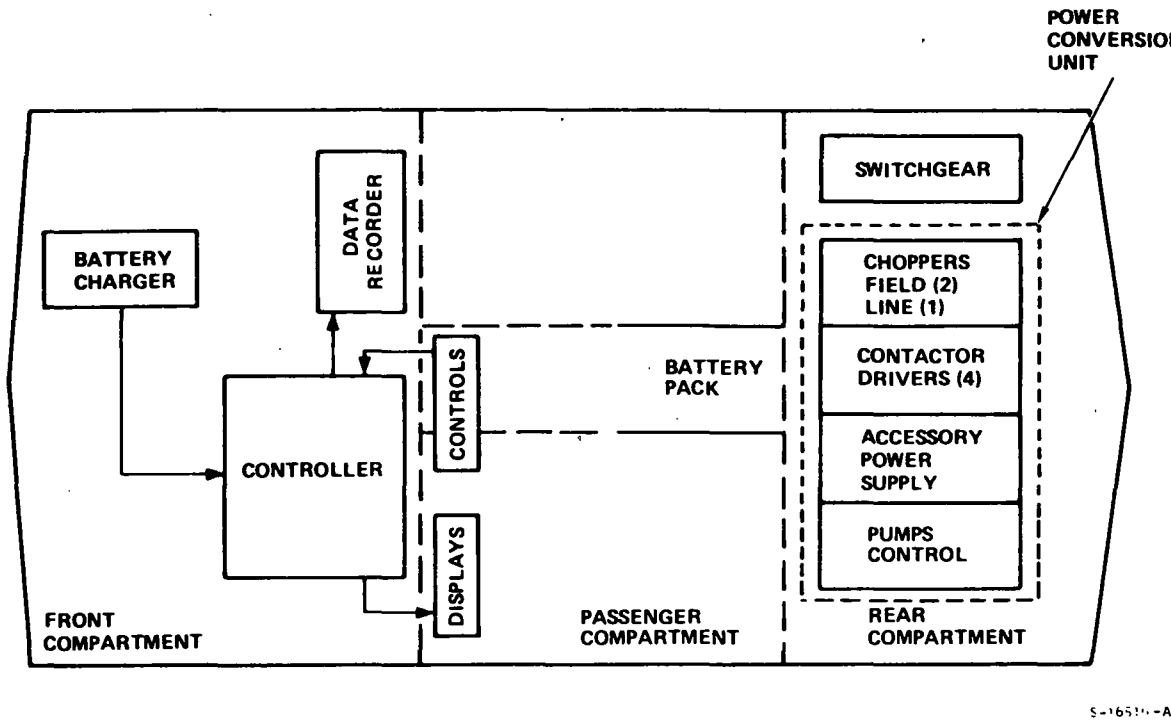


Figure 57. Electrical/Electronic Component Arrangement

BASIC PHILOSOPHY:

- FILTERS ON WIRES PENETRATING SHIELDS
- LARGER DC MOTORS COMMUTATION FILTERED WITHIN MOTOR CASE
- NONMETALLIC COMPARTMENTS METALLIZED WITH 0.001 IN. THICK LAYER OF COPPER

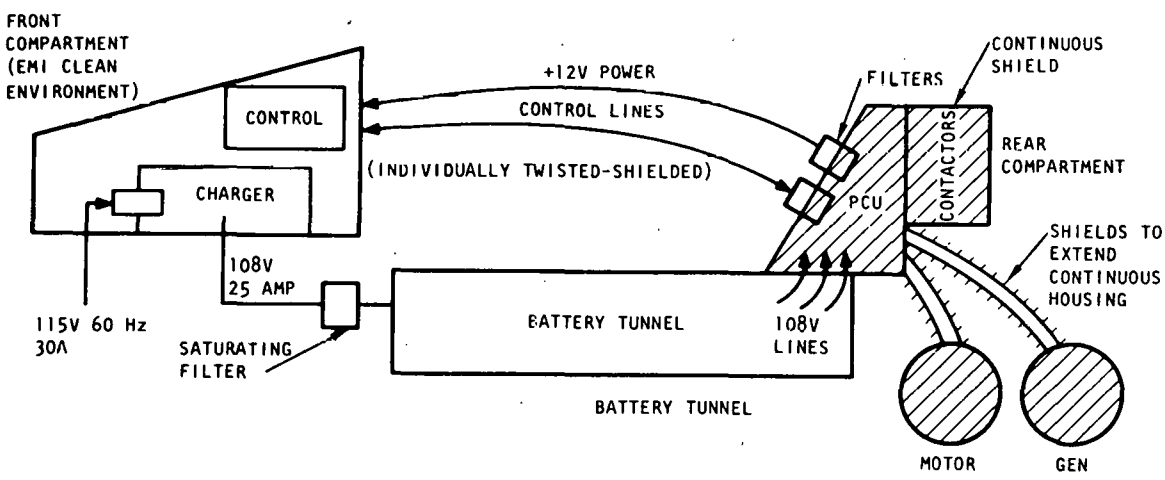


Figure 58. EMC/EMI Overview

(h) Circuit layout shielding and detail design to provide adequate EMI protection and suppression of internally generated EMI noise.

## 1. Controller

The controller functions to examine the instantaneous state of the vehicle and to issue appropriate commands to the control interfaces in response to operator (driver) input commands. The interfaces form the buffers between the controller and the control variables. The controller monitors the sensor inputs, decides which data are to be stored, and then does all of the data computation and control functions.

The controller is implemented by the use of a high-speed, microprocessor-based digital computer. The large number of control modes required by the vehicle are readily accommodated as software instructions stored in computer memory, rather than discrete analog hardware circuitry. This increases overall controller reliability. In addition, a high level of system design flexibility is achieved, since most basic control logic modifications, or additional control features desired to improve vehicle performance based on field trial data, can be accommodated by simple replacement of software instruction memory devices.

The controller receives commands exercised by the driver for acceleration (throttle position) or braking (brake position) and generates the corresponding torque commands. These commands are modified depending upon the vehicle operational mode (shift position), vehicle velocity, and the flywheel speed for optimum control. As depicted in the functional block diagram, Figure 59, the controller logic and dynamics computation is based on these modified commands as compared to the actual feedback information provided by current, voltage, and speed sensors. Various switches, contactors, and chopper circuits are controlled continuously to satisfy the driver commands.

The controller block diagram, Figure 60, shows the controller's major elements and circuit boards. The circuit mechanization of the control functions, data processing, and receiving and transmittal to various subsystems is illustrated in Figure 61. The corresponding software functions are presented in Figure 62.

The controller has four plug-in boards--a signal conditioning board, an input/output control board, a central processor unit (CPU), and a memory board--and an electrical interconnect board (motherboard).

### a. Signal Conditioning Board

The signal conditioning board processes the sensing of the battery current, carrier motor/generator armature current, and ring generator/motor armature current, using Hall-effect sensors. Field current feedback for carrier and ring motor/generators is sensed by measuring voltage drop across precision resistors. Additional input sensors include the throttle (accelerator) sensor, and brake sensor. The signal conditioning board conditions the sensor inputs to interface with a single analog-to-digital (A/D) converter (12 bits).

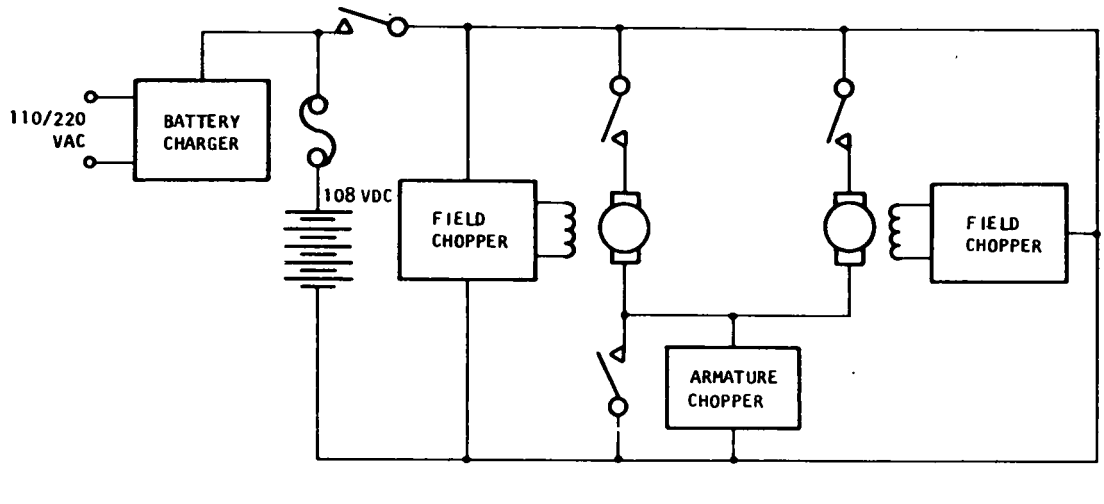


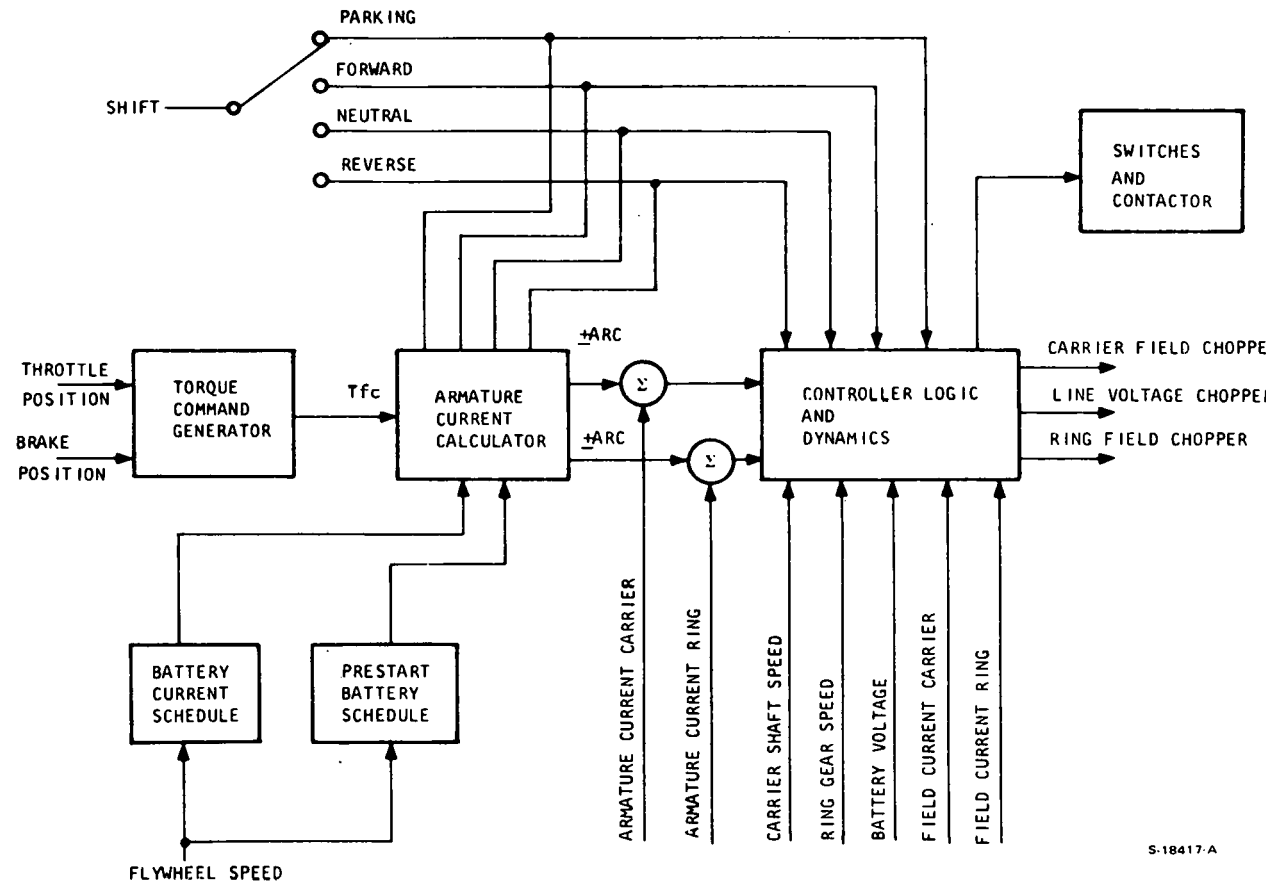


Figure 59. Functional Block Diagram.

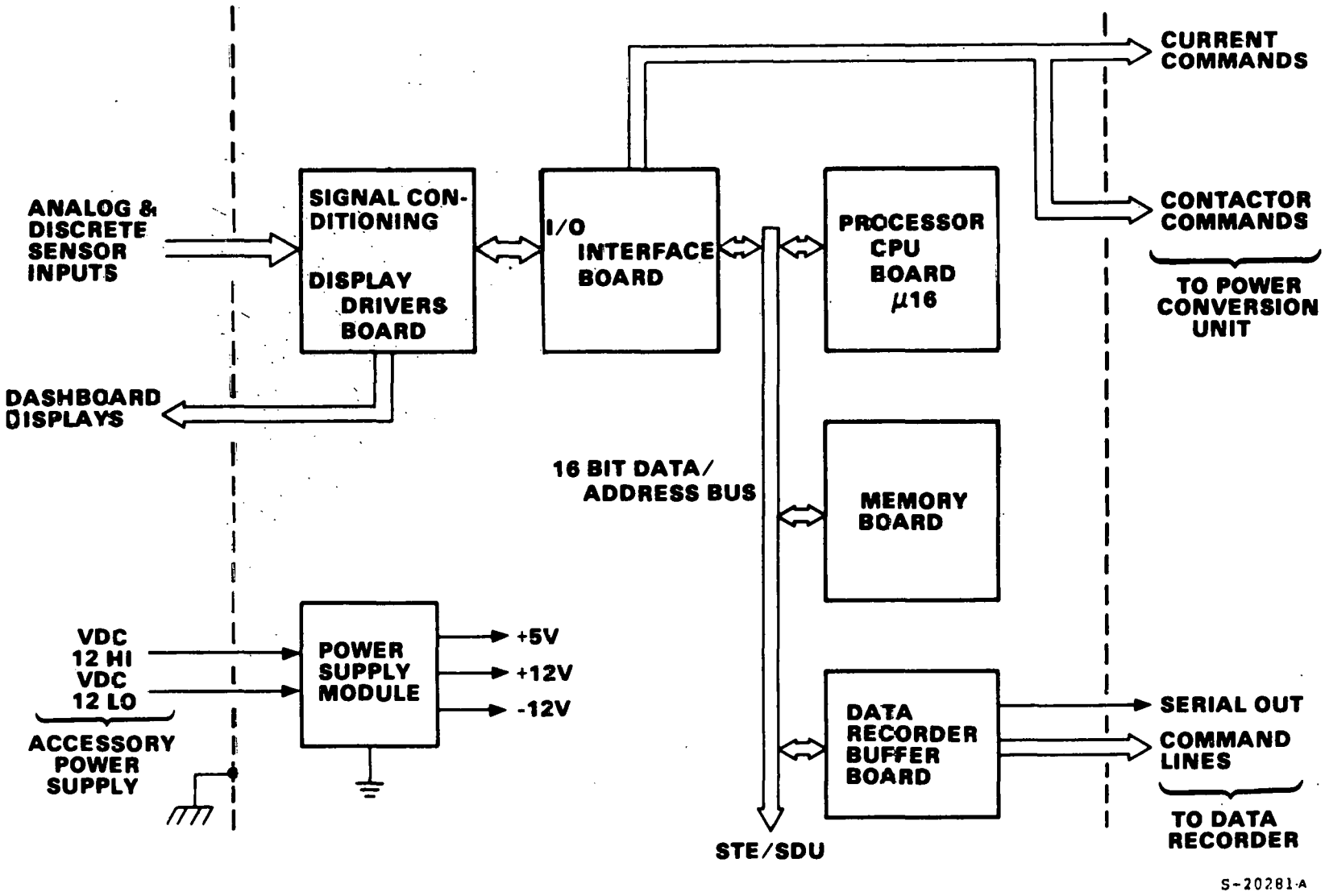


Figure 60. Controller Block Diagram

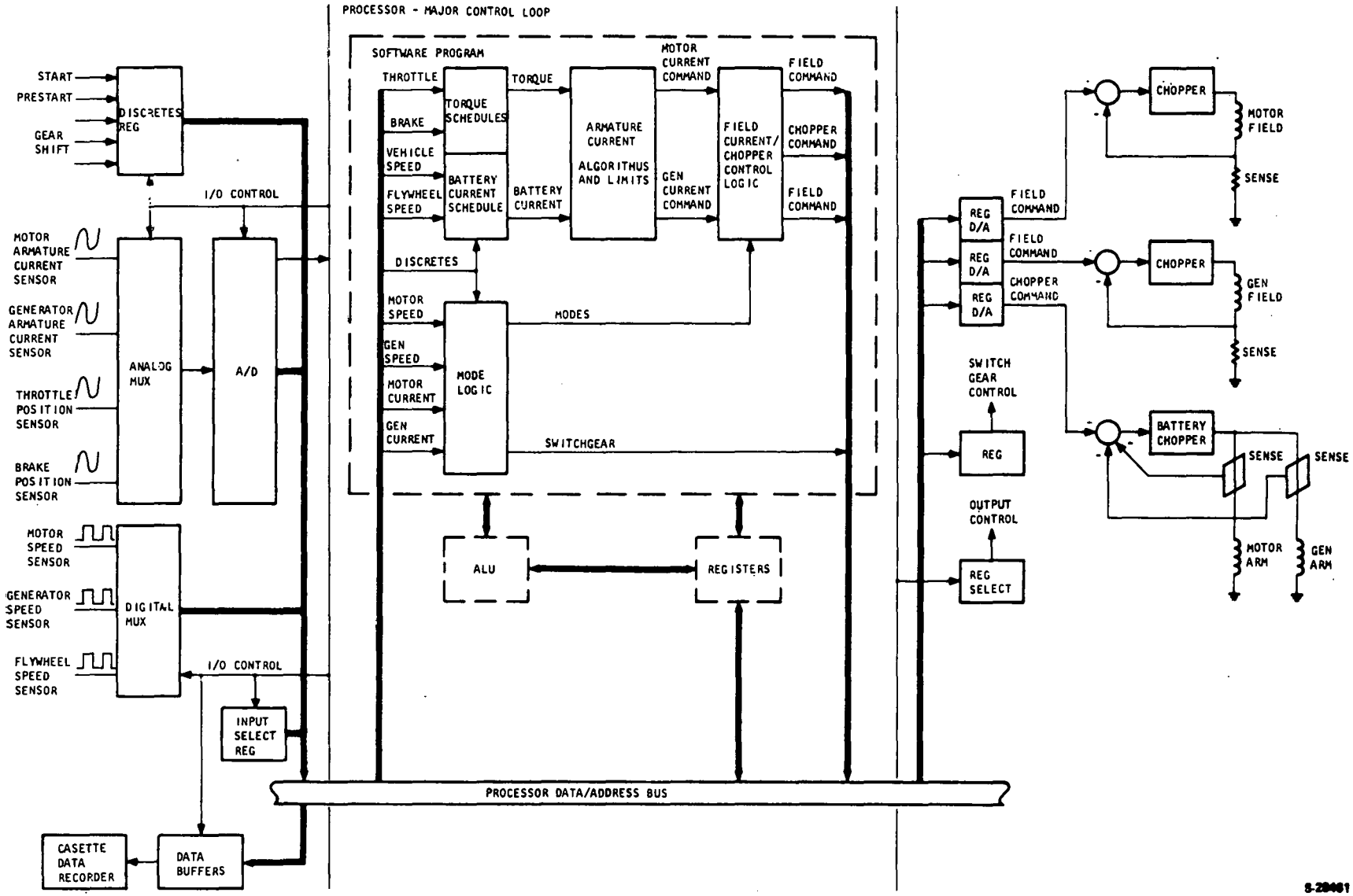


Figure 61. Controller Circuit Block Diagram

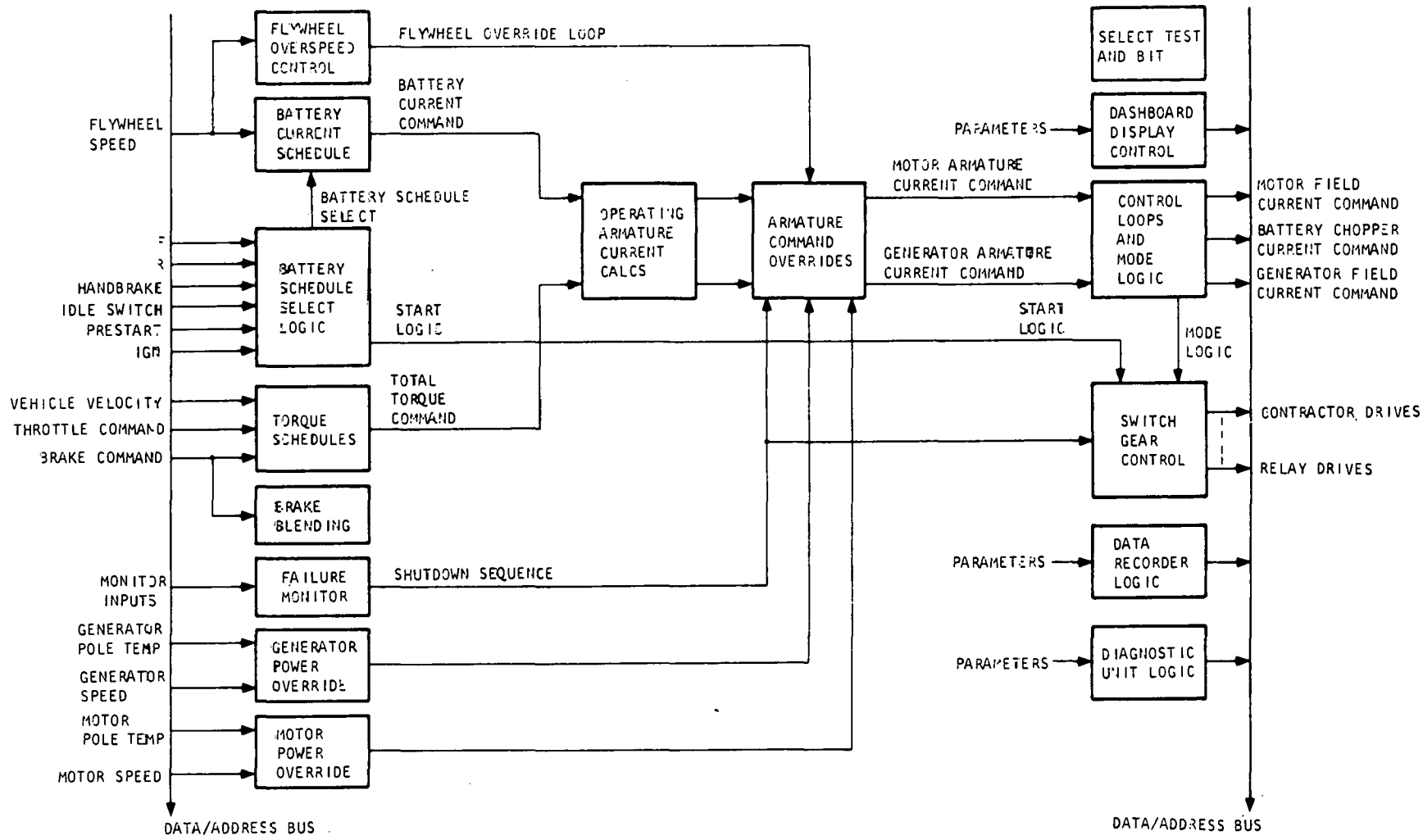


Figure 62. Software Control Functions Block Diagram

Carrier motor/generator speed, ring motor/generator speed, and flywheel speed are sensed by variable-reluctance monopoles, providing a frequency output that is proportional to speed. The input conditioning board receives the monopole signal and shapes the raw signal to be compatible with the digital processor. A discrete signal for sensing bidirectional rotation for the carrier motor/generator also is processed on this board.

b. Input/Output (I/O) Control Board

The I/O control board is organized into several I/O ports, and each port is assigned a number for the instruction to reference. This circuit decodes the data bus for the specific port address. If a match is found, the CPU control lines are decoded to the input and output states. If an input instruction is found, the transfer buffer connected to the data bus is opened. If an output instruction is detected, the external latch is enabled to retain the content of the data bus.

The system clock, generated by the CPU and the control lines, performs the system timing. Transfer of addresses and data takes place across the full-word parallel-data transfer bus. All analog voltages are transmitted through an analog multiplexer, an A/D converter, and a data buffer before entering the data bus. All speed signals are transmitted through a digital multiplexer, and are processed by use of a fixed time base and a counter.

c. CPU Board

The Micro-16 computer is a third-generation CPU design, based on more than seven years of development, testing, and production of a general-purpose processor. It is an engineer-oriented processor for medium-sized, dedicated processor applications, based upon contemporary LSI (microprocessor) device technology. The heart of the processor is its arithmetic-logic unit (ALU). The ALU of the Micro-16 is incorporated on microprocessor-slice chips. It provides for logical operations, summation, and shifting of data words. Each device includes four bits of the ALU; the devices cascade to provide full-word, arithmetic-data-processing capability.

Like most modern processors, the Micro-16 uses a general register file for working accumulators and index registers. Arithmetic, logic, and data-transfer instructions can operate, using these registers as data sources, saving substantial time over similar memory-referenced instructions.

Control over the selection and processing of data is provided within the processor by the microprogram control section. Processor data-bus interfaces are fully microprogram controlled.

Input-output is controlled, with three separate control lines, to indicate (1) presence on the processor bus of a peripheral address, (2) presence on the processor bus of data being output to a peripheral, and (3) availability of the processor bus for data input from the last-previously addressed peripheral. Finally, the processor provides an external test line, available to the input-output system, which can be used as a peripheral bus and tested under software control. This last feature enables the programmer to ensure that the addressed peripheral is ready to accomplish the intended input-output transfer function.

d. Memory Board

The major characteristics of the memory board are:

Storage capability of 8000 word x 16-bit EPROM (expandable in 1000-word modules); 1000 word x 16-bit N-Channel RAM; and 512 word x 16 BIT CMOS RAM

Provision for nonvolatile CMOS RAM operation

Power switching on EPROM memory for minimum power dissipation

Designed for 1.5- sec operation time (read or write)

External memory enabled by single control line

e. Motherboard

The motherboard forms the base for the four plug-in boards and for the interconnects to the control box connector.

f. Controller Power Drain

The controller power drain consists of the following losses:

| | |
|---|---|
| CPU board | 7.6 w |
| Memory board | 6.0 |
| I/O control board | 6.5 |
| Signal conditioning board | 4.0 |
| Miscellaneous interfaces | 1.0 |
| | 25.0 w |

g. Controller Weight and Size

The total weight of the controller is 9 lb, and its size is 3-1/2 by 8-1/2 by 17 in.

2. Power Conversion Unit

The power conversion unit consists of six subunits: armature chopper; carrier motor/generator field chopper; ring generator/motor field chopper; the contactor economizer drivers; the accessory power supply; and vacuum/lube pump controls. The various subunits comprising the power conversion units are interconnected as shown in the power conversion unit functional diagram (Figure 63).

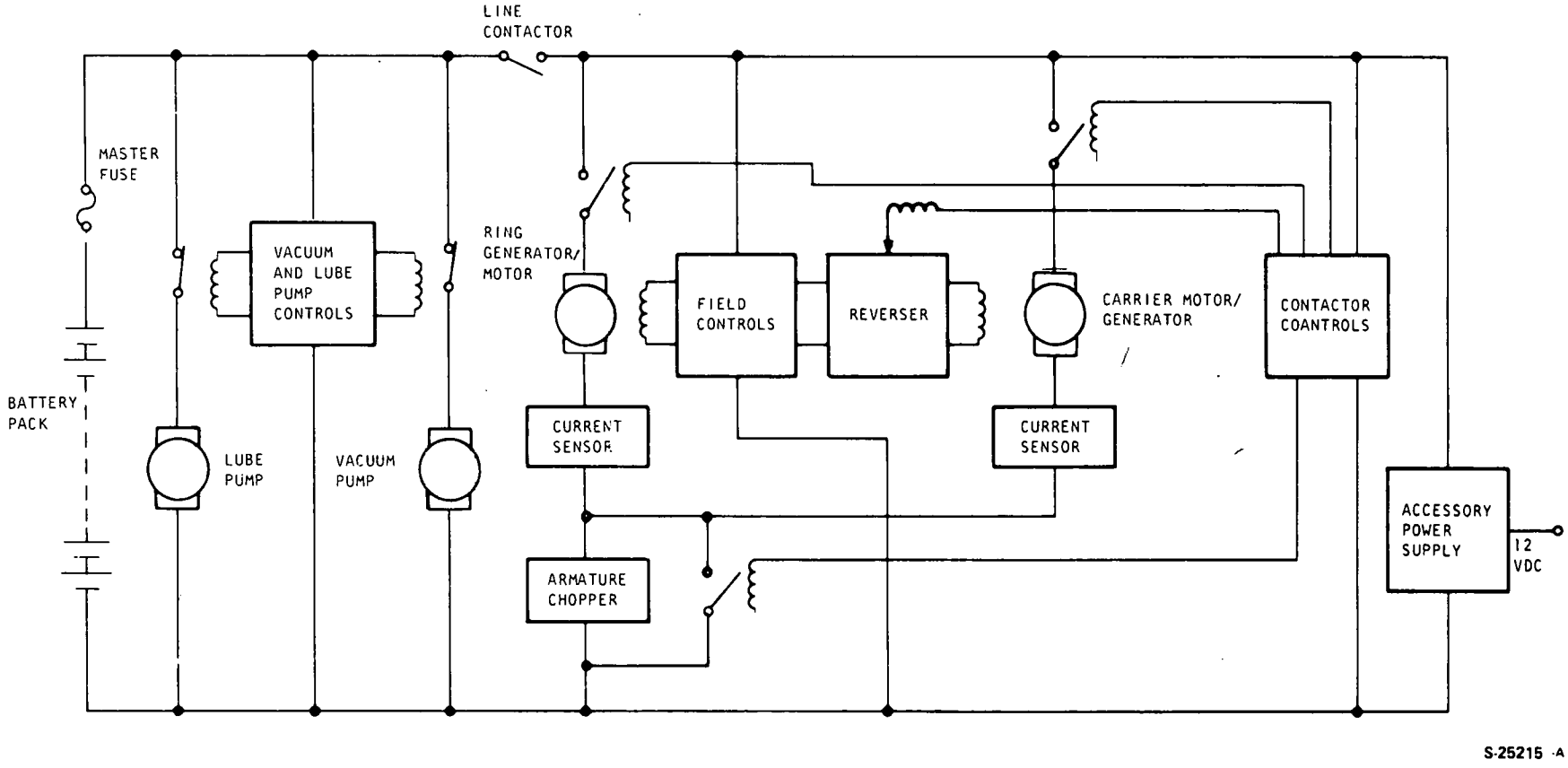


Figure 63. Conversion Unit Functional Diagram

The power conversion unit is designed to be installed in an electronics compartment behind the vehicle rear seat support structure as shown in Figure 64. The unit is contained in a shielded enclosure, which contains any generated electromagnetic interference.

The power electronics subunit mechanizations, loads, and power requirements, are described in the following paragraphs.

a. Armature Chopper

The armature chopper converts the 108-v battery voltage to a lower average voltage, via a pulse-width-modulation/regulation scheme. Its functional diagram is shown in Figure 65.

The chopper output drive is rated at a current of 120 amp. This is achieved by operating four matched lower-rated transistors in parallel.

A single comparator is used to generate a 2000-Hz reference signal and clock. The error signal, generated as the difference between the armature chopper current command and the current feedback signals is compared to a reference signal to generate a duty-cycle control, while a clock and logic steer the drive signals to the proper transistor. An inhibit signal turns off both drive signals in an overcurrent condition.

Depending on the levels of back emf in the motor and generator, the armature chopper will dissipate from 240 to 350 w at rated current. At a normal operating current of 50 amp, these power levels would drop to 100 to 125 w.

b. Field Choppers

The carrier motor/generator and ring generator/motor use identical field choppers, with a rated operating current of 15 amp. The field chopper (Figure 66) is a self-oscillating current regulator. Both frequency and duty cycle vary as a function of input command, load variations, and supply voltage.

Current feedback is supplied via a 10-milliohm ground-leg shunt. The feedback is scaled and is compared to the input command at a summing integating amplifier. Accompanying transistors form a bang-bang switch with hysteresis. Driven by the integrator output, this switch performs the necessary regulation functions with the field current following the input command. At rated current, the field-chopper loss will be approximately 24 w.

c. Contactor Drivers

The contactor drivers receive a discrete command from the controller. In response to this command, the circuit applies a starting pulse to the contactor coil and, after a fixed period of time, the current/voltage is dropped to a lower average value to reduce power dissipation.

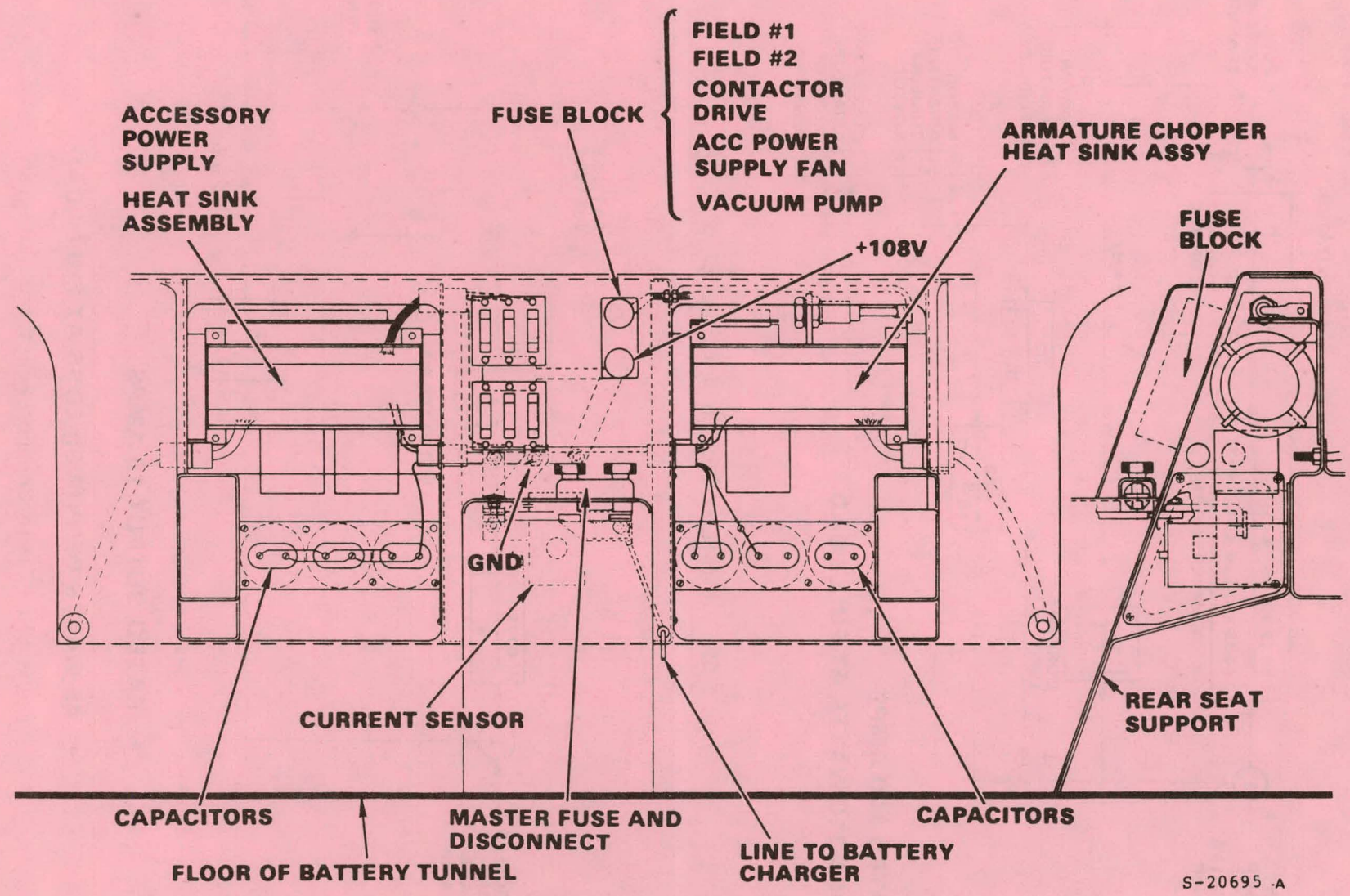


Figure 64. Power Electronics Compartment Arrangement

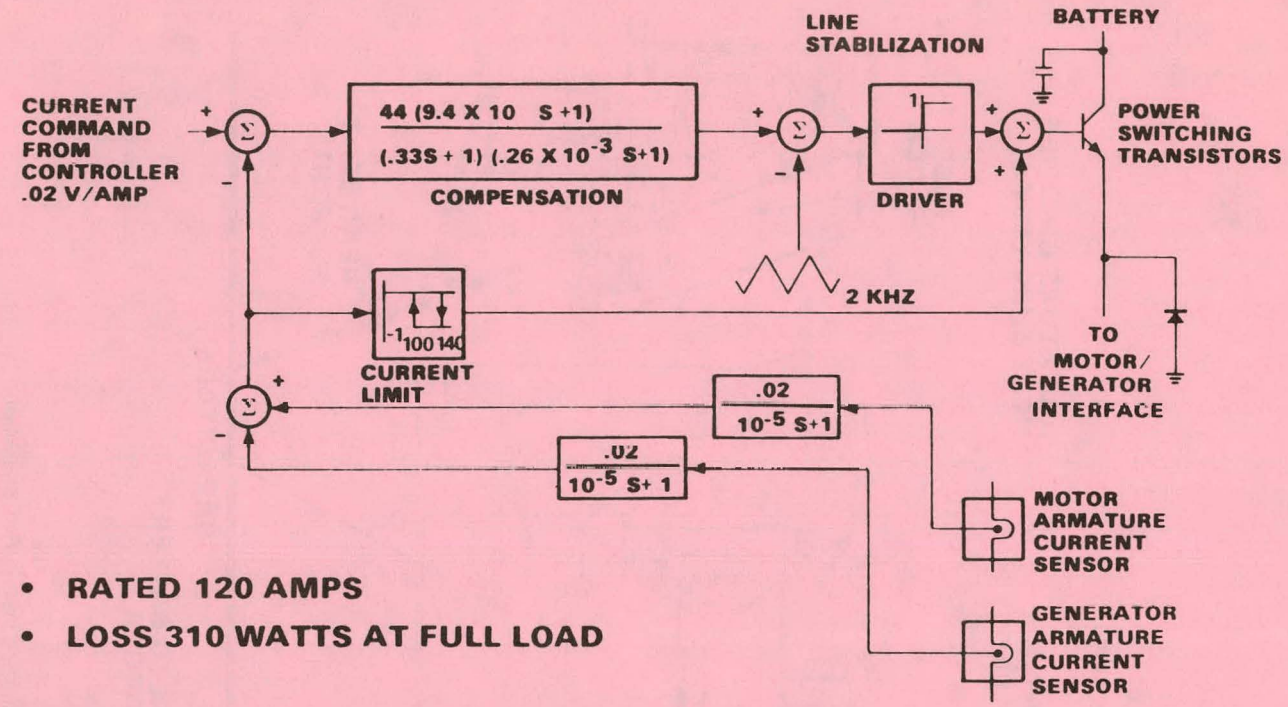


Figure 65. Armature Chopper Functional Diagram

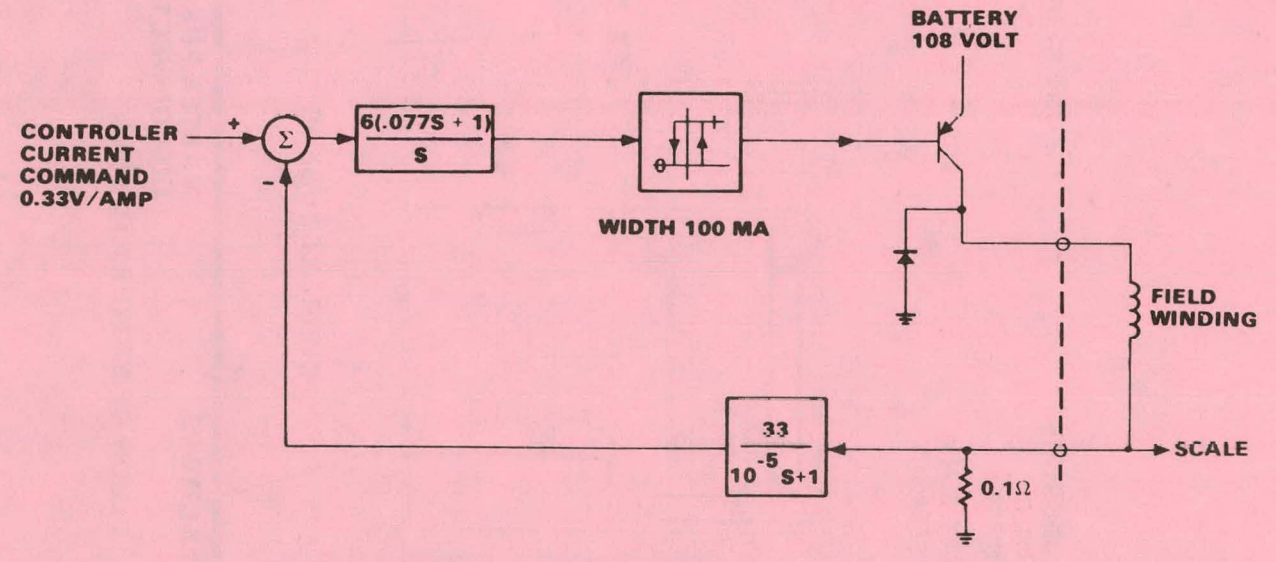


Figure 66. Field Chopper Functional Diagram

The contactor drive circuit, Figure 67, employs a one-shot, 0.25-sec pulse to provide the initial starting pulse; thereafter, the lower current/voltage is maintained by pulse-width frequency modulation, with the drive transistors using a current-bandwidth-regulating loop.

d. Accessory Power Supply

The accessory power supply is a lightweight, high-efficiency dc-to-dc converter which converts the 108-vdc battery power into 12-vdc power used by the vehicle accessory loads tabulated in Table 16. This supply is capable of providing 517 w continuously with 625 w for peak intermittent loads. Its circuit scheme is shown in Figure 68.

TABLE 16

ACCESSORY POWER SUPPLY DESIGN LOAD (WATTS)

| Item | Load |
|---|---|
| Controller | 30 w |
| Data recorder | 25 |
| Wiper | 75 |
| Radio | 5 |
| Annunciator | 20 |
| G-sensor | 20 |
| Defog fan | 90 |
| Headlights | 180 |
| Markers | 32 |
| Tail lights | 8 |
| Dome lights | 3 |
| Panel lights | 9 |
| Turn signal | 27 |
| Windshield washer | 40 |
| Back-up light | 54 |
| Brake light | 54 |
| Horn | 10 |
| Wiring | 5 |

Design conditions: min. continuous load: 60 w
max. continuous load: 517 w
peak intermittent load: 625 w

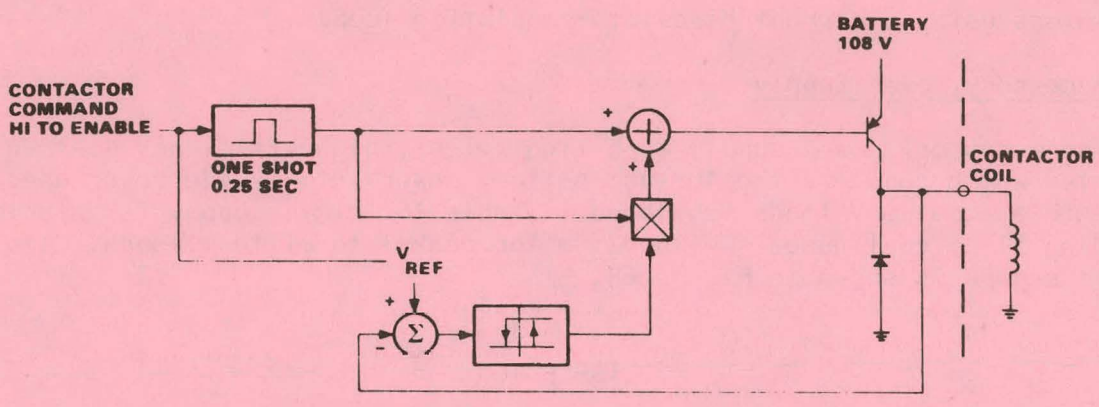


- **ECONOMIZER CIRCUIT - FULL LINE VOLTAGE FOR 0.25 SEC, 800 mA PULL IN, 0.12 AMP HOLDING CURRENT (14 VOLT)**
- **HOLDING LOSS 1.7 WATT**

Figure 67. Contactor Drivers Functional Diagram (Four Drivers per Unit)

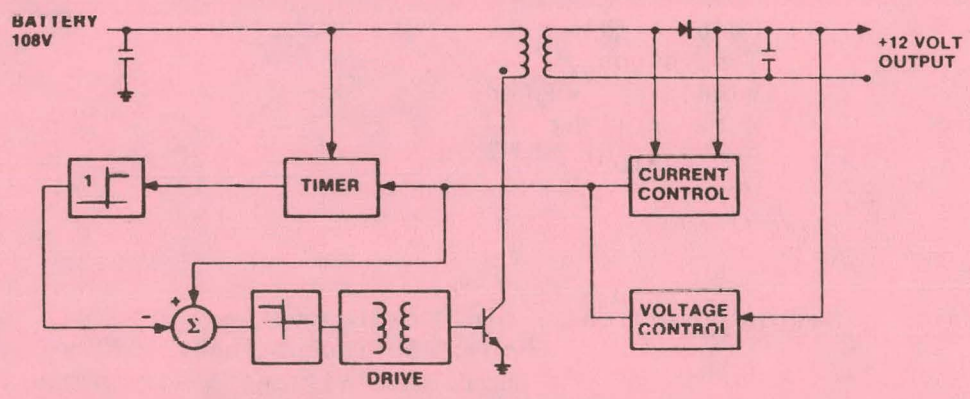


- RATED OUTPUT +12V, 47 AMP, 625 WATTS (PEAK), 517 WATTS (USE CONTINUOUS)
- POWER LOSS 70 WATT AT FULL LOAD, 89% EFFICIENCY

Figure 68. Accessory Power Supply Functional Diagram

e. Vacuum and Lube Pump Controls

The vacuum and lube pump controls operate independently of the electronic controller, since flywheel vacuum and system lubrication must be maintained whenever the flywheel is above 5000 rpm. As shown in the block diagram (Figure 69), the oil pump motor is energized whenever the control system is operating, and is not deenergized until flywheel speed drops below a safe minimum speed, even if the main controller fails or is shut down. The cavity fore pump is also armed whenever the control system is operating or the flywheel is above minimum speed. The cavity pressure switch energizes and deenergizes the fore pump motor in order to provide bang-bang control of cavity pressure to 1.0 torr.

3. Data Recorder

A digital cassette tape deck with read/write electronics is used for the data recorder. The tape deck provides storage means for recording vehicle performance data during test periods, and the cassette format simplifies data transmittal to a computer center for subsequent evaluation.

The system controller contains a tape deck control interface used to format data for storage and to generate hand-shake signals between the tape deck and the controller. The controller samples 41 system parameters (14 analog and 27 discrete) every second and stores this information in a 64-word, 16-bit buffer memory. This buffer memory is filled and then dumped onto the tape cassette every 3 sec.

The data recorder parameter list, storage capacity, and recorder specifications are summarized in Table 17.

4. Battery Charger

An onboard battery charger is provided to allow local overnight recharging of the vehicle battery pack. The charger will operate from either 15- or 30-amp rms, 115-vac household service, which is switch selectable at the charger. Provision is made in the unit to accept an external connection to a 60-amp dc remote charger for rapid recharge. Cooling is provided by a fan mounted on the charger; the same fan is used to provide battery tunnel ventilation.

Included with the charger is a small 12-vdc power supply derived directly from the 108-v battery, which is used to power the vehicle emergency flasher lights when all other electronics are inactivated.

Test results on a charger are shown in Figure 70 and 71.

5. Switch Gear

The battery-line contactor and the chopper contactor are part of the main power loop, and are required to carry 200 amp for several minutes, a current which is treated as a continuous-rating requirement. The selected contactors have a capability of interrupting fault currents in excess of 1200 amp. These contactors have blow-outs and arc-shutes, and are rated at 72 vdc at 0.62 amp, closing and holding at 20 percent of rated voltage.

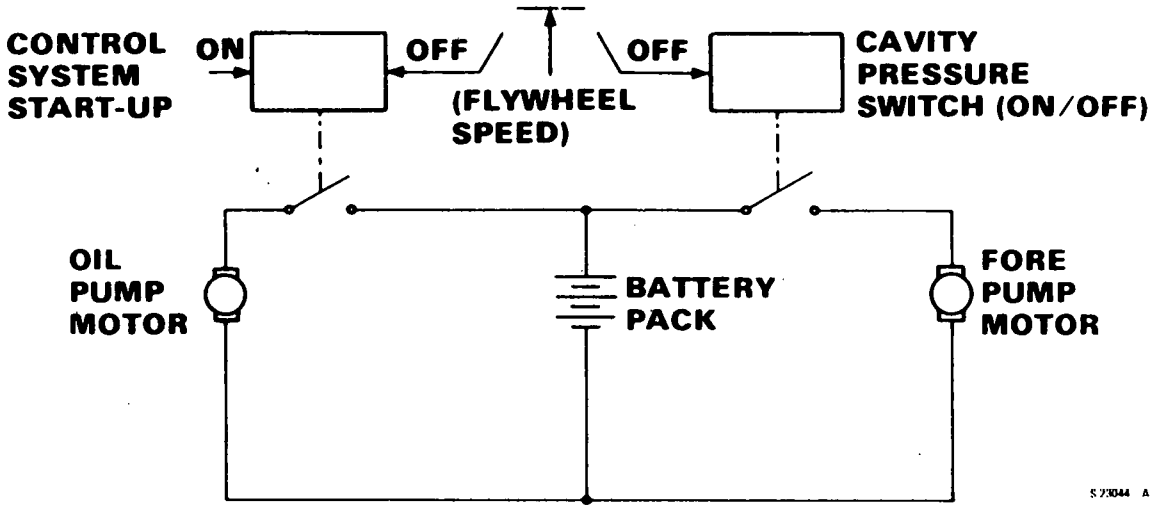


Figure 69. Vacuum and Lubrication Pumps Control

TABLE 17

DATA RECORDER

Parameter List

- Flywheel speed
- Motor speed
- Generator speed
- Motor armature current
- Gen armature current
- Motor field current
- Gen field current
- Battery current
- Brake sensor
- Throttle sensor
- Motor temperature
- Generator temperature
- Battery voltage
- Battery temperature
- Any CPU computed parameter

Storage Capacity

- 64-word buffer in controller
- 300 ft cassette tape, 7.5 ips
- Recording time 90 min., 20 words/sec

Recorder Specifications

- TEAC MT-609
- Dimensions: 7.5 by 7.5 by 5.5 in.
- Serial input, phase encoding
- Power requirement: +12 v at 2.1 amp
  -12 v at 0.1 amp
  +5 v at 1.8 amp

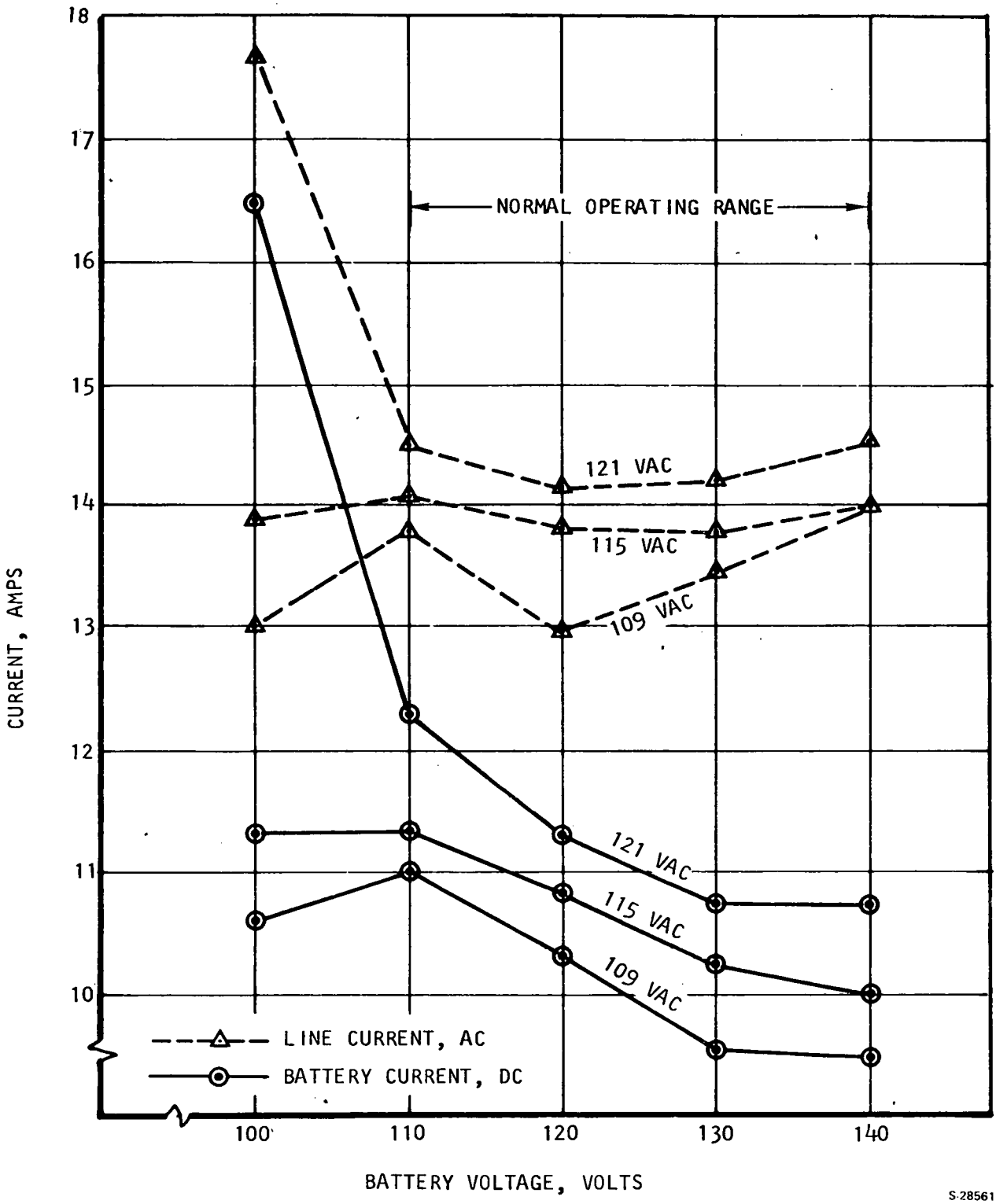


Figure 70. Battery Charger Characteristics - Operation on 15 Amp Household Circuit

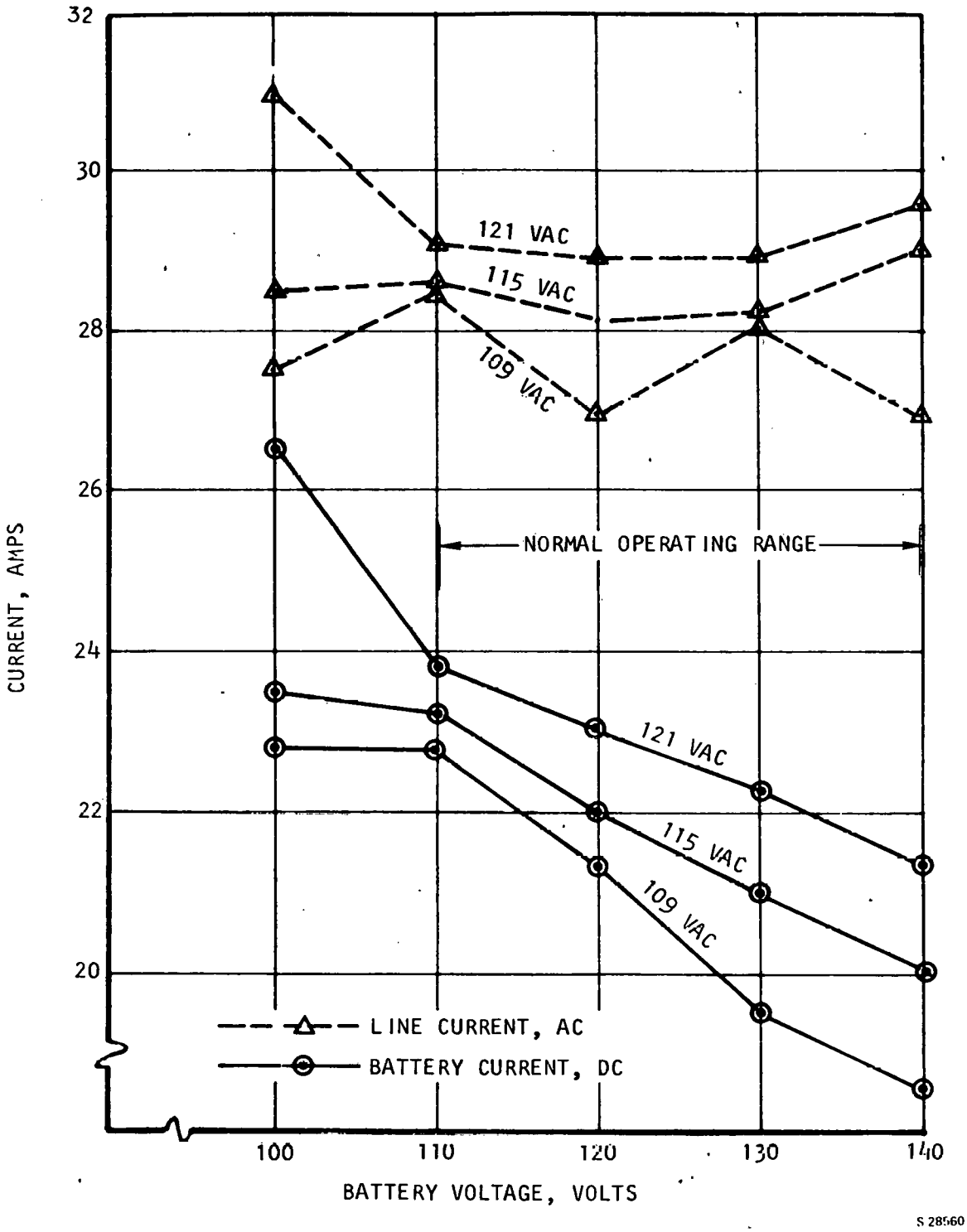


Figure 71. Battery Charger Characteristics - Operation on 30 Amp Household Circuit

The motor/generator contactors are similar units, but with a higher continuous-rating requirement of 228 amp, and allow current to flow in either direction. Their interrupt capability is in excess of 1800 amp, and when interrupting rated currents, arcing will be contained within the shutes.

The reverser switch carries a nominal 15-amp, and makes and breaks at 0 amp. In the interest of reliability and safety, the unit has load-braking capability, with magnetic blow-outs, but with no arc shutes. Its coil requires 2 w, closing and holding. Its auxiliary contacts are SPDT, and operate the backup lights.

The start-run relay is at the heart of the on-off control for the vehicle, supplying coil power to the battery contactor. This relay is a Siemens unit, weighing 12 ounces, and carrying 12 vdc, 7 w closing and holding. The range-meter relay is SPDT at relatively low current levels, with coil power of 2.2 w, and operates from the battery contactor at 108 vdc.

All fuses of the power circuits are 250 v, rated to ensure clearing of transients. Current sensors in the main power loop will accept fault-current transients of 2000 amp, recovering without loss of accuracy in microseconds.

6. Vehicle Cabling

The minimum selected wire size, for reasons of mechanical integrity at joints, is No. 18 AWG wire. Smaller size wires are used at some terminals in potted connectors, and at strain-relieved connections. A further consideration for selecting No. 18 wire was to minimize wiring power losses which would occur with smaller size wire. The ground wire is No. 10 for accessories and the 15- to 30-amp circuits to the charger. Power cables for the battery circuit and those for the motor-circuit use No. 1 wires. In the rear compartment, wiring insulation is rated for 300 v at 125°C, while in the forward areas 90°C insulation is used.

Cabling weights for the two sections of the electrical subsystem are as follows:

| | Length, ft | Weight, lb |
|---|---|---|
| Shielded twin pair | 100 | 2.2 |
| Twin pair | 210 | 3.4 |
| No. 4 cable | 5 | 0.6 |
| No. 1 cable | 20 | 5.8 |
| No. 18 wire, lb | 100 | 11.0 |
| Total weight | | 14.0 |

Power dissipation is as follows:

No. 18 Wire = 6.35/1000 x 1 x wire length (in feet)

No. 1 Wire = 1/5900 x wire length in feet

7. Cooling Fans

The cooling fans are standard, commercial items: one is used for ventilating the passenger compartment and windshield defrosting; it operates directly from the battery line on 108 vdc. An identical fan is part of the power electronics unit, and is used to cool the electronic unit, the generator, and motor units connected farther downstream; it operates directly from the battey 108-vdc line.

A smaller fan, attached to the charger installed in front of the vehicle, cools the charger electronics, and simultaneously ventilates the battery tunnel during the battery-charging mode.

8. Drive Controls and Displays

Every effort has been made to select and arrange the driver's controls and displays so that they will appear similar to those in conventional cars and thus will permit a new driver to operate the vehicle with little or no instruction. The functional diagram of the controls and displays is shown in Figure 72, and a preliminary layout of the instrument panel is shown in Figure 73.

a. Controls

Only two foot pedals are required--the brake pedal and the accelerator pedal. The planetary gear arrangement eliminates the need for a clutch, thus the car operates like one with an automatic transmission. The brake and accelerator pedals are both equipped with electrical position pickups for communication with the controller. A shift selector identical to an automatic transmission selector is used to select the operating modes:

PARK - Mechanically locks the power unit (hence the rear wheels)

REVERSE - Conventional reverse operation

NEUTRAL - Permits free-wheeling operation

DRIVE - Conventional drive operation

b. Displays

Three round-dial-type instruments are arranged into a center cluster together with various indicator lights.

SPEEDOMETER/ODOMETER--a Stewart-Warner electric instrument driven from the system electronic controller.

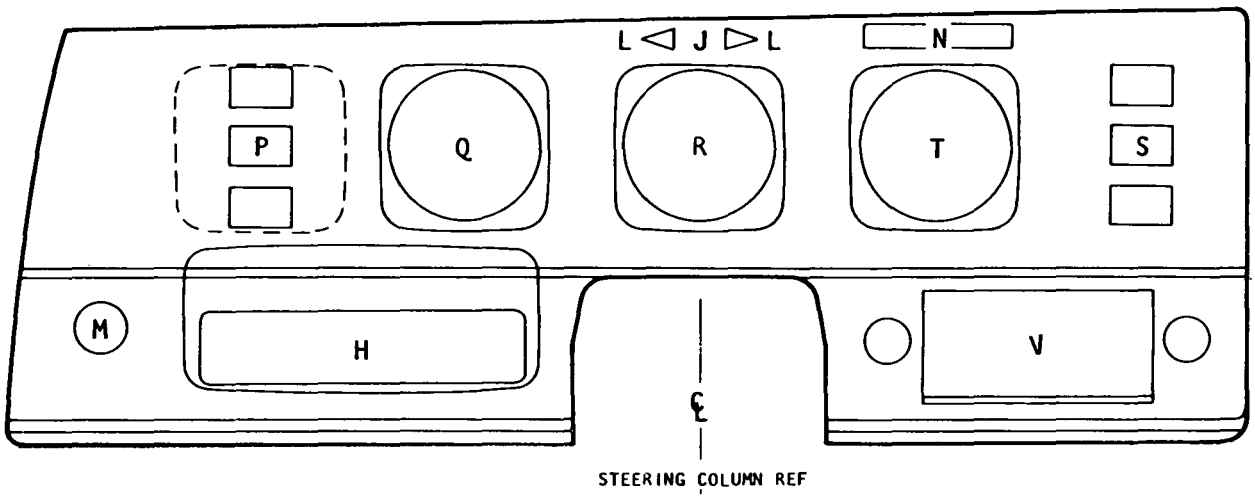


LOCATION KEY, INSTRUMENTS/CONTROL

P - INDICATOR LIGHTS, EMERGENCY, BRAKE FAILURE AND SEAT BELTS
Q - SPEEDOMETER
R - POWER METER
T - BATTERY CHARGE METER
S - INDICATOR LIGHTS, TEMPERATURE, PRESSURE AND BATTERY FAILURE
V - RADIO AM/FM
H - HEATER/DEFROST CONTROLS, RECIRC./FRESH AIR, HOT/COLD, FAN HI/LO
M - HEAT LIGHT SWITCH
L - INDICATOR LIGHTS. DIRECTIONAL SIGNAL
W - DIGITAL VOLTMETER. MILES REMAINING (FUTURE)
J - INDICATOR LIGHT, HI/LO BEAM HEADLIGHTS

S 28380

Figure 72. Controls and Displays

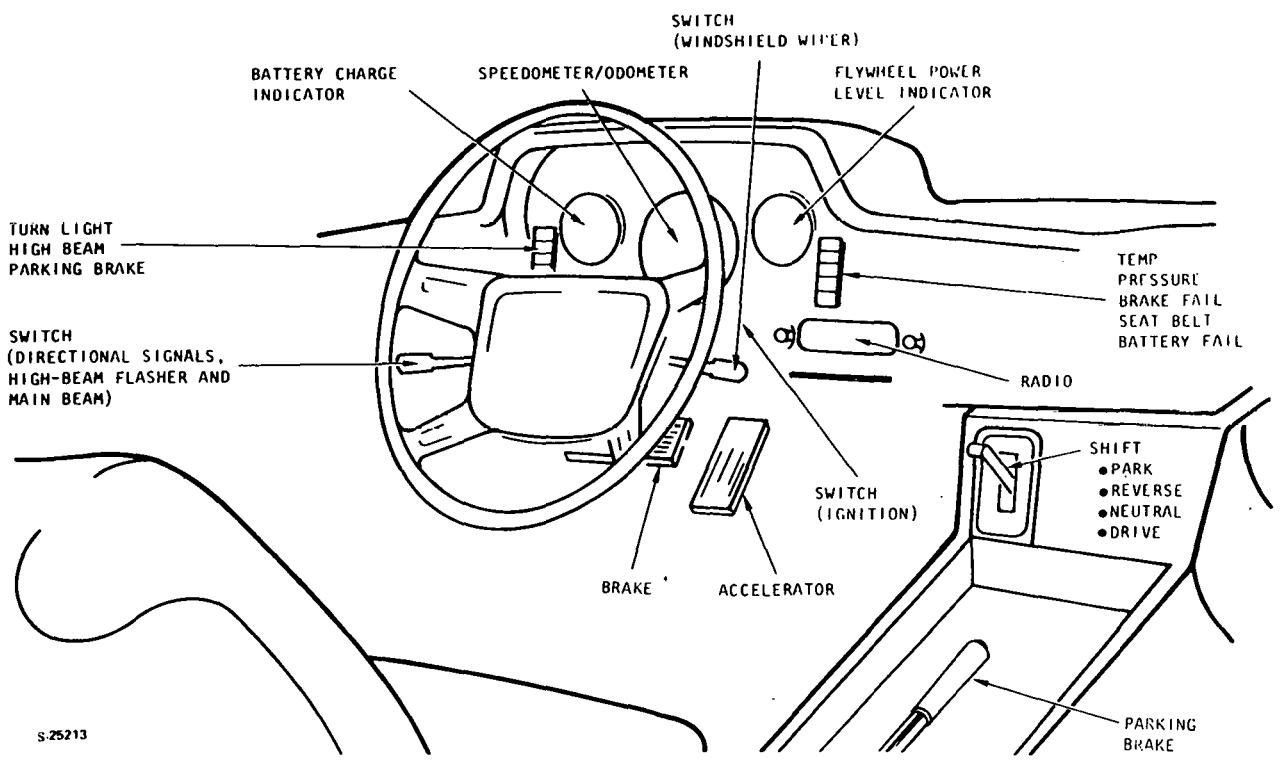


Figure 73. Instrument Panel Layout

POWER--A conventional tachometer electrically driven from the controller. It is driven as a function of flywheel speed and vehicle speed and provides the driver a general indication of the vehicle's acceleration capabilities. It allows the driver to determine the proper flywheel charge to permit safe operation of the vehicle and judge reserve power available for acceleration. The driver is encouraged to allow the flywheel speed to reach a minimum acceptable level during the startup mode (as indicated by the green region) to enhance the overall vehicle performance.

BATTERY CHARGE--Indicates the energy remaining in the battery pack. It is also electrically driven from the controller during the discharge mode and from the charger during the charge mode.

TEMP--Several temperatures in the power unit are monitored. These include motor/generator winding temperatures and the electronic power conversion unit operating temperatures. If any temperature exceeds a predetermined limit, the TEMP light is illuminated.

PRESSURE--Flywheel vacuum pressure is monitored; any flywheel vacuum out-of-tolerance condition illuminates the PRESSURE indicator light.

BRAKE FAIL--Signals loss of pressure in one portion of the hydraulic system.

SEAT BELT--Signals open seat belt.

BATTERY FAIL--Signals that one or more battery cells are out of tolerance.

The remaining displays are conventional.

## ELECTRONIC COMPONENT TESTING

The following tests have been completed:

### Power Conversion Unit

| | |
|---|---|
| Armature chopper development and motor/generator support tests | 13 hrs |
| Field choppers development and motor/generator support tests | 46 hrs |
| Accessory power supply development and system checkout | 206 hrs |

### Controller

| | |
|---|---|
| Functional check out and software development test | 108 hrs |

### Charger

| | |
|---|---|
| Battery charging | 1248 hrs |

### Cooling Fan

| | |
|---|---|
| Motor cooling | 106 hrs |

# SECTION 6

# VEHICLE DESIGN

# SECTION 6

# VEHICLE DESIGN

Renderings of the Near-Term Electric Vehicle (NTEV) are shown in Figures 74 and 75. The design was directed to satisfy these objectives:

- Safety
- Attractiveness
- Minimum weight
- Marketability

The design meets all pertinent Federal Motor Vehicle Safety Requirements (FMVSS), and many subscale tests have been conducted to verify its integrity. Wraparound glass, a thin roof section, and character lines high on the body sides and ends provide an attractive appearance. Weight has been minimized by constraining the physical size and by extensive use of fiber reinforced plastic (FRP) in place of steel. It is expected that the NTEV's attractive appearance, its practical size and weight, and its many functional and performance features will provide a marketable vehicle.

A unibody concept is used; all body panels and structure trim are fabricated from FRP. The complete suspension, steering, and brakes are from the BMW 320i to take advantage of available, proven hardware that is lightweight and efficient.

A cross section of the NTEV is shown in Figure 76. The power unit is rear mounted and the 18 batteries are contained in a tunnel that runs nearly the length of the vehicle. Though the battery does present a challenge to interior styling, it provides a reasonable weight distribution and polar moment of inertia in the pitch and yaw axes. The BMW four-wheel independent suspension integrates very well with the battery tunnel. The front portion of the battery tunnel is corrugated to provide efficient energy management in crash situations. Corrugated energy-absorbing tubes also are provided at the front and rear for crash protection.

Pertinent vehicle specifications are:

| | |
|---|---|
| Curb weight, lb | 2849 |
| Gross weight, lb | 3449 |
| Weight distribution front/rear, percent | 45/55 |
| Wheelbase, in. | 95.0 |
| Track, front/rear, in. | 60.0/59.0 |

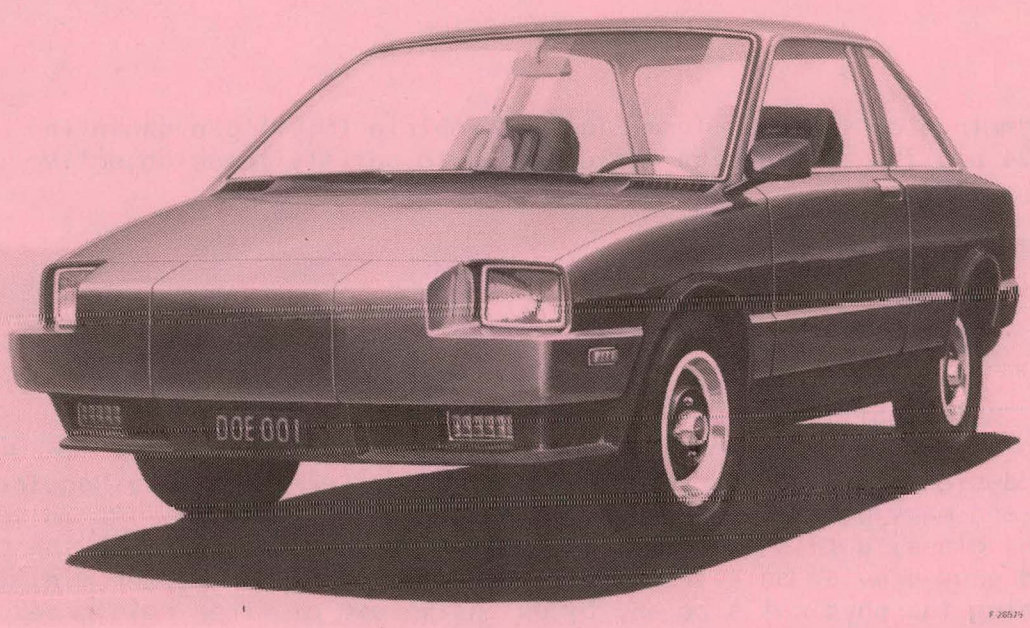


Figure 74. NTEV Three-Quarter Front View

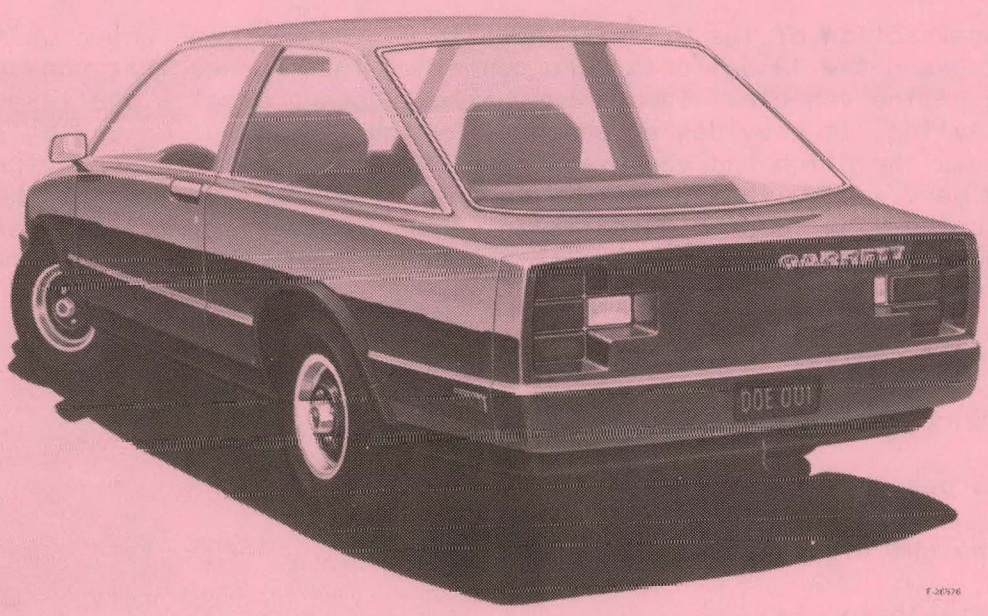


Figure 75. NTEV Three-Quarter Rear View

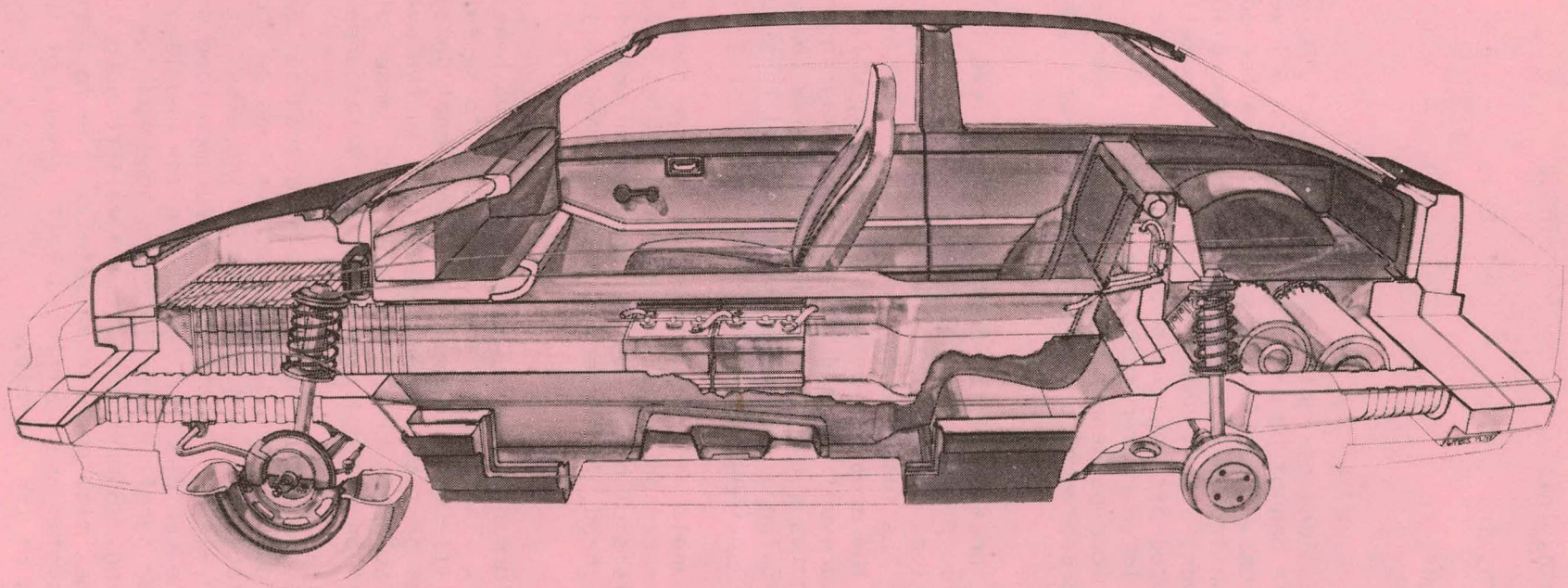

F-26580

Figure 76. NTEV Cross-Sectional View

| | |
|---|---|
| Length, in. | 165.0 |
| Width, in. | 68.0 |
| Height, in. | 54.9 |

EXTERIOR DESIGN

While many discussions of vehicle styling predict "boxy" shapes for future vehicles, this formula cannot be uniformly applied to all vehicle types or to all marketing situations. Domestic cars have been patterned after the Mercedes package; this has resulted in improved occupant accommodations and reduced vehicle weight; however, a boxy shape is not vital to excellent interior accommodations, and a squared-off vehicle shape does not provide the best occupant protection, aerodynamic characteristics, or manufacturing costs on a material basis. The proposed four-passenger NTEV styling has been kept simple and clean to optimize product acceptance, provide good aerodynamic performance, and ensure ease of manufacture.

As shown in the three-quarters front and rear views (Figures 74 and 75), the body styling reflects a lightweight-vehicle appearance. The wraparound glass, thin roof section, and character lines high on the body sides and ends enhance this effect. The tucked-under rocker panels contribute to remove "visual weight" from the area low between the wheels, while small flares have been incorporated to prevent mud and stones from damaging the body finish. The low body incorporates substantially more plan-view contouring than conventional vehicles, narrowing at the nose and tail, and thus saves material required for manufacture (and reduces weight).

The individual panels and panel separations have been minimized for quality control and ease of repair or replacement in the field. The lower body (below the greenhouse) consists of only seven primary outer mold line (OML) panels--soft nose, soft tail, hood, left door, right door, and left and right rear quarter panels.

Lightweight, deformable-bumper, facia panels have been incorporated at the vehicle nose and tail. These units are configured to sustain continued abuse at low speeds with little or no cosmetic or functional damage, and to provide substantial additional protection for pedestrians in the event of an impact. The section of soft facia has been doubled at each corner of the vehicle to allow greater deformation without damage in this vital area.

Lighting systems, both front and rear, have been set back from the bumper-impact zone to avoid damage during bumper stroke, and to protect pedestrians or cyclists from contact with hard surfaces in the event of collision. The newly approved, 200-by-142 mm, rectangular headlamps (one on each side) have been designed into the vehicle front end. The low headlamp profile and location well aft of the bumper permit a steeply raked hood and low nose for improved aerodynamics and vision. Bumper corners are well rounded to improve aerodynamic performance, and to maximize pedestrian safety. The tail light and the backup/license-plate light system are positioned well forward of the rear impact area, and away from corners of the vehicle.

During the vehicle design process, two useful aids were built and used. A one-fifth scale clay model (shown in Figures 77 and 78) was created early in the design and served as the test bed for design acceptance and proposed revisions. When the design was reasonably firm, the clay model was used as a reference for creating both the full-size loft diagram and the male styling buck.

The full-size male buck provided a final design acceptance model and also is the master tool from which the NTEV bodies will be built. The buck was built on a framework of steel and plywood, contouring was accomplished with polyurethane foam, and the final surface was several layers of fiberglass cloth with a final hard epoxy coating. The nearly finished buck is shown in Figures 79 and 80.

## INTERIOR DESIGN

The width of the car is strongly influenced by the battery tunnel, which runs up the center of the vehicle. The ample body width provides additional room between passengers and creates a general feeling of roominess. A rendering of the NTEV interior is presented in Figure 81. Every attempt has been made to have the NTEV appear and operate like a conventional internal combustion engine (ICE) car. Controls and operation are identical to those for an ICE car equipped with an automatic transmission. There is no clutch, and a remote shift selector lever is used. Instruments are conventional except for one gage indicating flywheel energy and another indicating remaining battery charge. Ample package storage is provided in the passenger dash area and on top of the battery tunnel console.

An exploded view of the NTEV interior is shown in Figure 82. Maximum use is made of available parts. The steering column, brake and throttle pedals, and hand brake are from the BMW 320i. Front seats are Stylex Grande Luxe Recliners, which are available aftermarket seats made in England. These seats are lightweight and comfortable. Window riser mechanisms are from the VW Rabbit and are efficient and lightweight.

The interior mockup is shown in Figures 83 and 84. These pictures indicate that the NTEV has adequate head room and passenger comfort. The influence of the battery tunnel is clearly evident in Figure 84, which shows the passengers seated nearer the A-posts than in conventional vehicles.

A standard passenger restraint system is used. In the front, the 3-point, continuous loop system from the '77 Mustang is used. The system uses an inertia locking retractor that is buried in the B post. A standard Type 1 lap belt is used in the rear seat. Verification of the restraint anchor points will be accomplished by static testing of structural sections and also by the 30-mph frontal barrier crash test of vehicle SN 002.

## CONTROLS AND DISPLAYS

The design objective in this area is to make the controls and displays as simple and conventional as possible. It would be a great advantage if a first-time driver could enter the NTEV and drive away with little or no instruction. The control and display arrangement is shown in Figure 85.


Figure 77. One-Fifth Scale Model - Rear

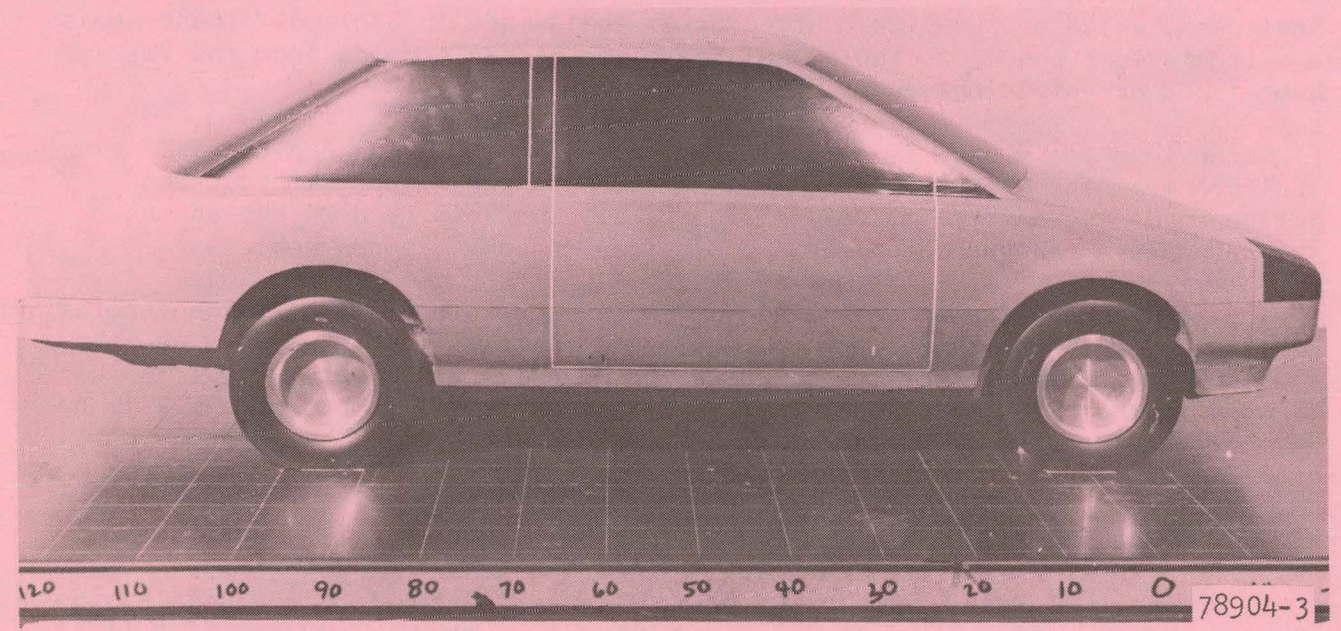


F-26049

Figure 78. One-Fifth Scale Model - Side


Figure 79. Nearly Finished Male Buck - Rear


Figure 80. Nearly Finished Male Buck - Front

F-26949

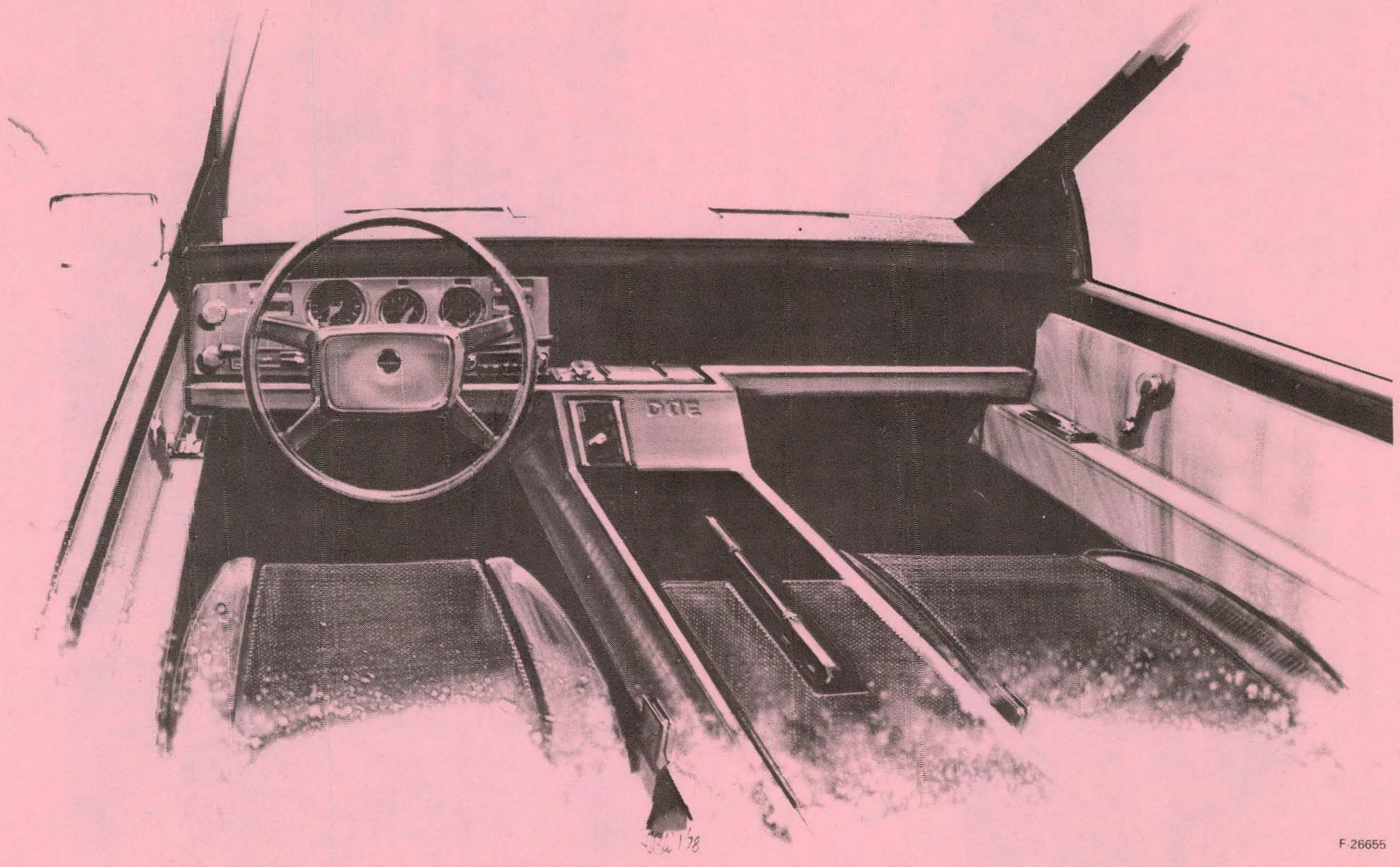


Figure 81. NTEV Interior - Artist's Concept

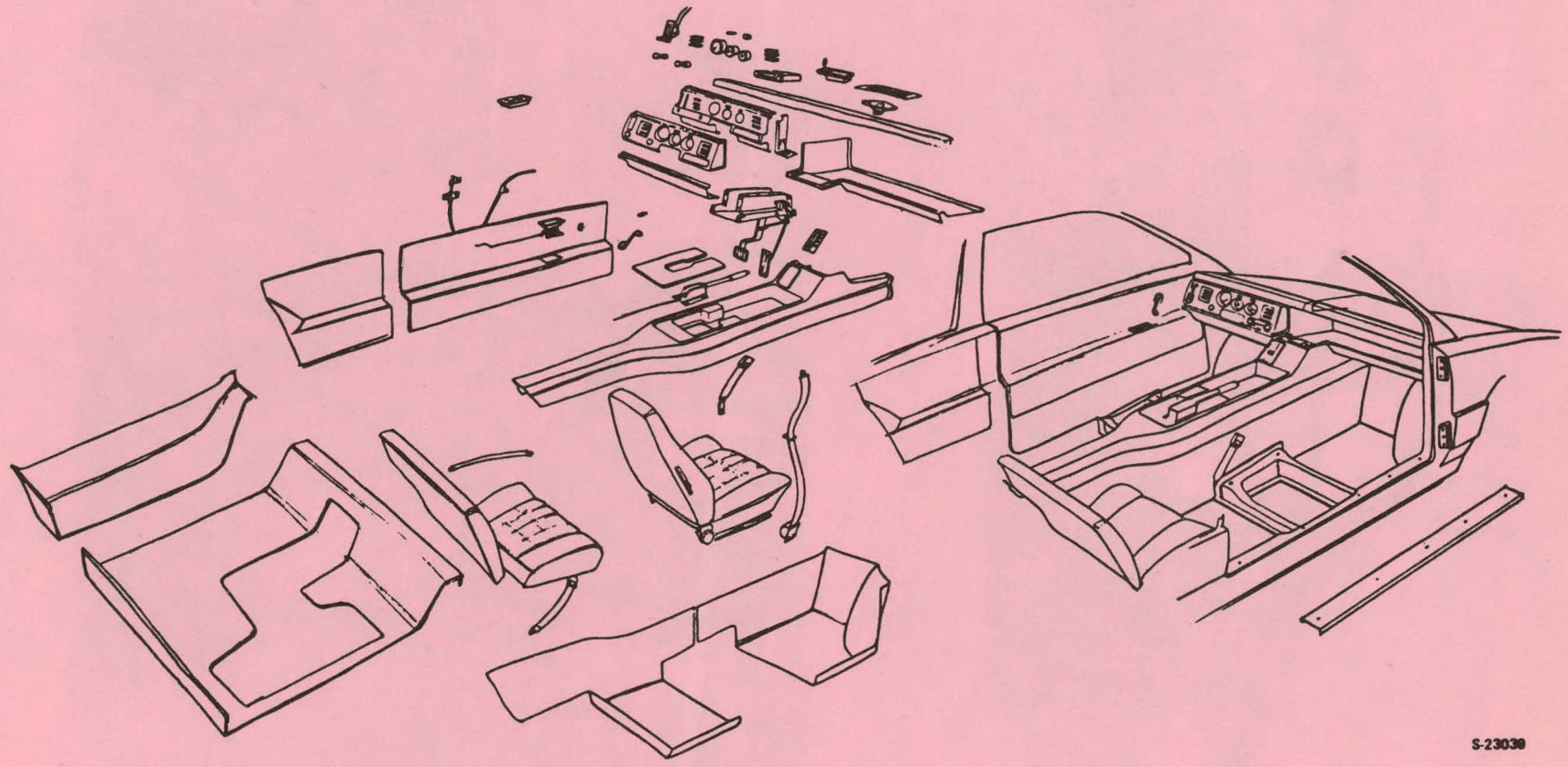


Figure 82. NTEV Interior - Exploded View

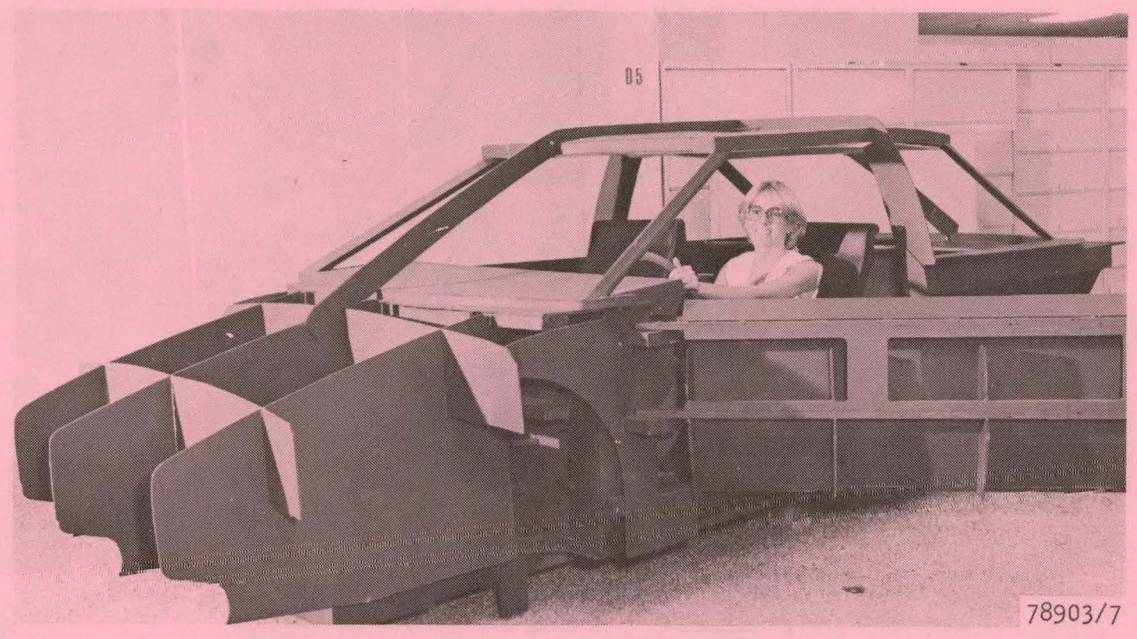


Figure 83. Full-Scale Interior Mockup


Figure 84. Wide Passenger Seating

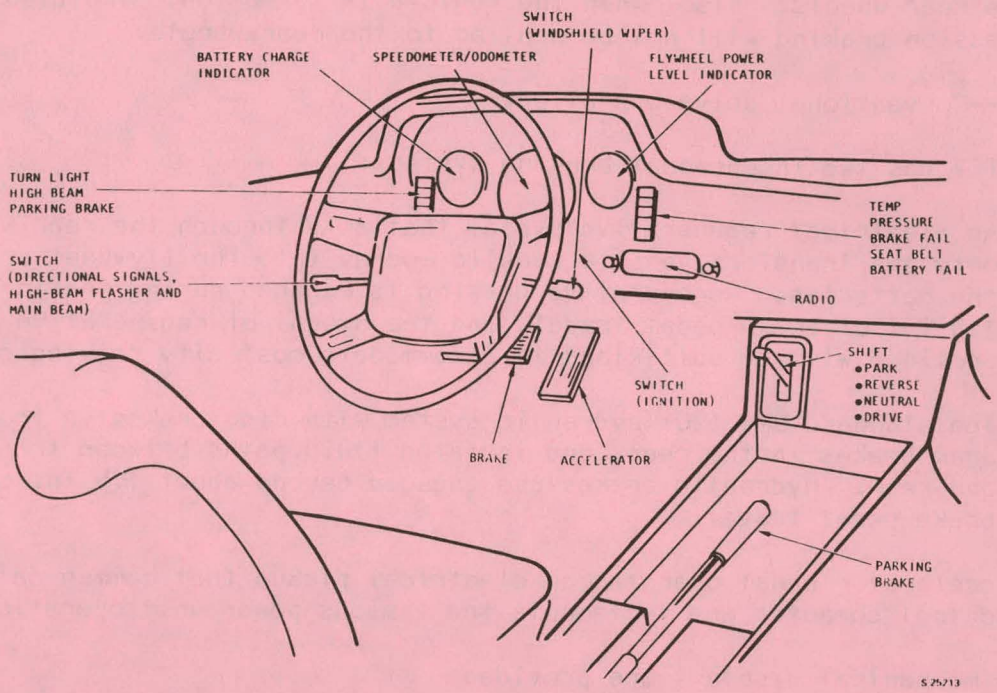


Figure 85. Dashboard Display

The NTEV operates exactly the same as a conventional ICE car with an automatic transmission. The operating controls consist of:

(a) Steering wheel

(b) Shift selector

(c) Accelerator pedal

(d) Brake pedal

The shift selector is set up exactly the same as an automatic transmission selector with the following positions and functions:

PARK--The vehicle is mechanically locked in place. At startup, with the selector in PARK and the ignition key ON, the NTEV control will bring the flywheel up to speed. The start sequence can be terminated at any time by moving the selector to another position (except NEUTRAL).

REVERSE--Conventional reverse operation.

NEUTRAL--The power unit is energized, but power will not be applied to the rear wheels. Also, when the vehicle is in motion, simulated compression braking will not be applied to the rear wheels.

DRIVE--Conventional drive operation.

The NTEV has two independent braking systems:

(a) An electrical regenerative system that acts through the rear wheels only and transfers vehicle kinetic energy into the flywheel or into the batteries. Regenerative braking is engaged during the initial 1.5 in. of brake pedal travel, and the amount of regenerative braking provided will be sufficient to accommodate most city driving cycles.

(b) The standard BMW 320i hydraulic system with disc brakes in front, drum brakes in the rear, and isolated fluid paths between front and rear. Hydraulic brakes are engaged beyond about 1.5 in. of brake pedal travel.

The accelerator pedal operates an electrical pickup that communicates with the EPPV control computer and implements the various power unit operating modes.

Three mechanical displays are provided:

Speedometer/Odometer--This is an electrically driven instrument using conventional format.

Flywheel Power Indicator--The purpose of this display is to inform the driver, in broad terms, of his vehicle's performance capability. This instrument is driven by the NTEV controller and shows three zones: (1) red for low performance, (2) orange for acceptable performance, and (3) green for design-level performance. The main parameter involved in this display is flywheel speed, and the main purpose of the display is to warn the driver against entering situations requiring higher performance when the flywheel charge is low.

Battery Charge--The NTEV computer solves a somewhat complex algorithm involving battery voltages and temperatures and displays the battery charge condition to the driver. Two warning lights are provided for power unit functions. A TEMP light warns if any lubricant or metal temperatures exceed predetermined limits and the PRESSURE light warns of low flywheel vacuum.

Remaining controls and displays are for normal vehicle functions, such as heater/defrost control, lights, turn signals, and windshield wipers.

HEAT/VENT/DEFROST SYSTEM

The NTEV airflow arrangement is shown in Figure 86. Outside air is brought in via the inlet plenum located at the base of the windshield. The air may be brought directly into the passenger compartment for ventilation or may be directed through the fuel-type heater. Flow-through vent valves are provided

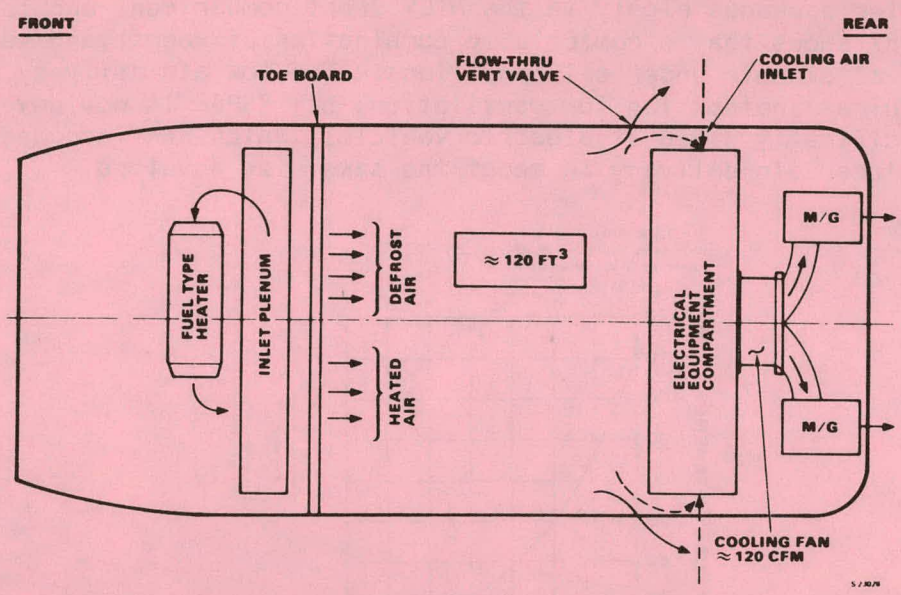


Figure 86. NTEV Airflow Arrangement

in the rear of the vehicle. A register, regulated from the driver's station, will be provided to permit air to be taken from the passenger compartment into the rear electrical equipment compartment.

The heater selected is an ESPAR X2K diesel-fueled hot-air heater. These heaters have long been in production for European air-cooled as well as water-cooled automobiles. Characteristics of the candidate heaters considered are shown in Table 18.

TABLE 18

CANDIDATE NTEV HEATERS

| Heater | Capacity, Btu/hr | Dimensions, in. (L x dia x H) | Weight, lb | Air Delivery, cfm |
|---|---|---|---|---|
| ESPAR DIL | 5,800 | 12 x 4 x 6 | 8 | 40 |
| ESPAR X2K | 8,000 | 19 x 5 10 | 9 | 45 |
| ESPAR D4LK | 15,000 | 23 x 10 x 12 | 23 | 145 |
| ESPAR, New Model | 11,400 | 15.9 x 5.3 x 5.5 | NA | 60 |
| South Wind 10603 BH | 20,000 | 15.5 x 8W x 15 | 35 | 100 |

The X2K heater packages nicely in the NTEV front compartment and is lightweight. Figure 87 shows that a comfortable combination of warmth and ventilation should be attainable under all conditions. The low air delivery of the X2K (45 cfm) requires another fan for ventilation, but ESPAR is now developing a new heater specifically aimed at electric vehicles, which has increased heating capability and higher air delivery in about the same size envelope.

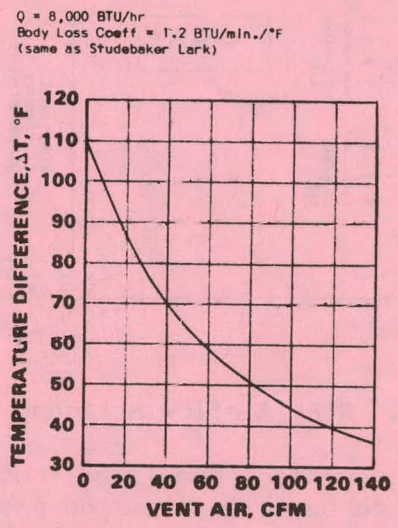


Figure 87. ESPAR X2K Heater Performance

A schematic of the heat/vent/defrost system is shown in Figure 88. Controls are conventional and provide options ranging from full heat/no ventilation to no heat/full ventilation. The temperature of defrost air also can be regulated. This arrangement should prove quite effective because the diesel heater requires no warmup and it can even be switched on during the initial flywheel charging mode to preheat the vehicle.

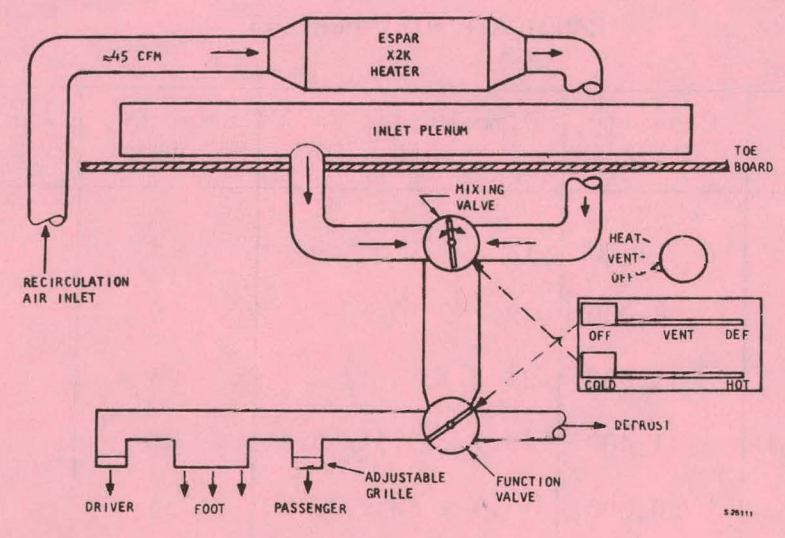


Figure 88. Heat/Vent/Defrost Schematic

GLAZING

Glass always has been the preferred glazing material for automobiles. It is hard, abrasion resistant, has good optical qualities, and is very stiff. It is also very heavy, 0.08855 lb/cu in., which is 31 percent of the density of steel. Since American car manufacturers have become weight conscious, plastics are being seriously considered for glazing. New coatings have improved abrasion resistance, optical qualities are good, and their density is half that of glass at 0.043 lb/cu in. The potential weight savings makes plastic glazing very attractive for future electric vehicles.

Plastic glazing will be used extensively in the NTEV. Coated acrylics will be used for all glazing except the windshield, which will be the conventional laminated safety glass. Characteristics of the plastic NTEV glazing are presented in Table 19. Stretched acrylic, because of its superior ductility, is used for the roll-up windows and the back light, while the as-cast material is sufficient for the fixed rear quarter-windows. Though the acrylic must be thicker than its glass counterpart because of its low bending modulus, plastic glazing offers the NTEV a 21.5-lb weight savings potential.

TABLE 19

CHARACTERISTICS OF NTEV PLASTIC GLAZING

| Glazing | Material | Thickness, in. | Weight, lb | Glass Weight, lb (Thickness, in.) | Weight Savings, lb |
|---|---|---|---|---|---|
| Driver's window | Stretched acrylic | 0.125 | 3.75 | 7.3 (0.118) | 3.5 |
| Passenger window | Stretched acrylic | 0.125 | 3.75 | 7.3 (0.118) | 3.5 |
| Rear light | Stretched acrylic | 0.250 | 15.84 | 24.7 (0.188) | 8.9 |
| Right quarter-window | As-cast acrylic | 0.125 | 2.97 | 5.8 (0.118) | 2.8 |
| Left quarter-window | As-cast acrylic | 0.125 | 2.97 | 5.8 (0.118) | 2.8 |
| | | Totals | 29.28 | 50.9 | 21.5 |

BATTERY SERVICE CONCEPT

The 18 batteries are located in a central longitudinal tunnel as shown in Figure 89. The batteries are mounted in a lightweight tray, and each battery row is strapped firmly to the tray. The tray has two runners on its bottom covered with a Teflon-like material. These runners move on tracks (also made from Teflon-like material) along the bottom of the battery tunnel. The coefficient of friction between the runners and the tracks is approximately 0.10. Thus, a 100-lb pulling force will be sufficient to slide the 1040-lb battery pack out of the vehicle.

The concept for removing and installing the battery pack is shown in Figure 89. The NTEV will be lifted at its four jacking points until the wheels are off the ground, which will ensure a fixed position for the battery tunnel during the battery-removal process. A battery cart will be specially designed for the servicing operation. The cart will have the Teflon-like tracks on its bed, and will have a hand-operated crank-ballscrew arrangement forward. The process of removing the batteries is as follows:

(a) Remove front bumper center section.

(b) Raise car using four jacks; adjust jacks so bottom of battery tunnel is level with bed of service cart.

(c) Remove bolts located beneath vehicle that secure battery tray to floor of battery tunnel.

(d) Fasten cart attaching screws to front of battery tray, and crank battery pack out of tunnel and onto service cart.

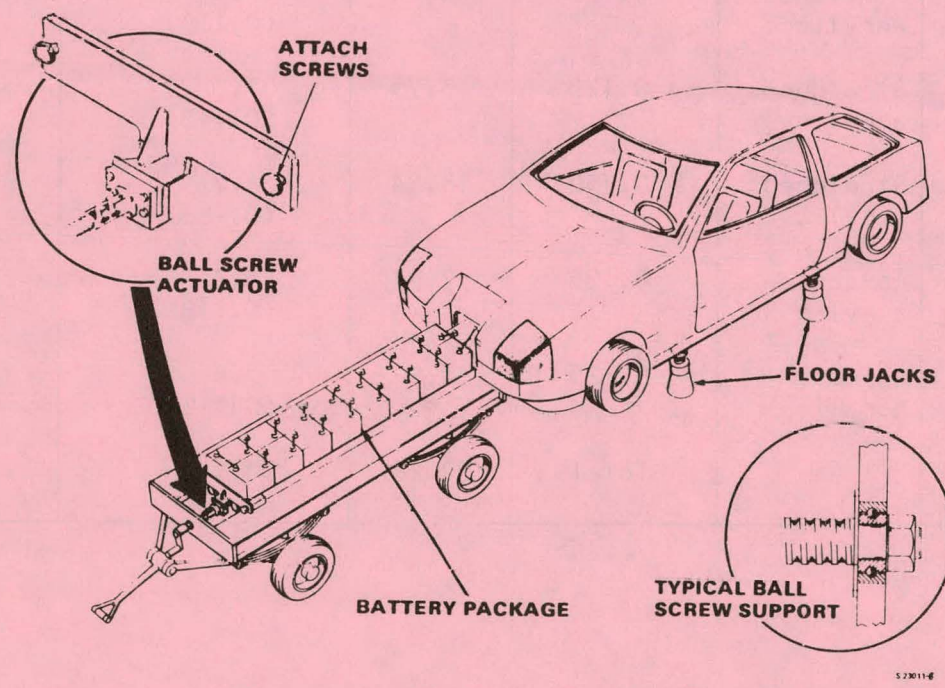


Figure 89. Battery Service Concept

For installation, the battery tray is pushed back into place by the crank-ballscrew actuator.

All battery servicing will require battery removal. Because of the antimony-free construction of the Eagle-Picher batteries, there will be a minimum of outgassing, and water depletion will be small. It is estimated that the batteries will require checking for water level at two-month intervals.

## STRUCTURE

### Structure Concept

The structure will be primarily fiber reinforced plastic (FRP). A total of 22 components will be fabricated separately, and then will be bonded together to form the total structure. An exploded view of the NTEV structure is shown in Figure 90.

A more detailed chart showing the overall body breakdown and the assembly sequence is shown in Figure 91.

The structure concept uses the battery tunnel as a primary structural member. The tunnel structure carries most of the normal running and operating loads and the front and rear suspension loads. The passenger compartment provides additional structural rigidity to meet rollover requirements and to maintain integrity under crash conditions.

The batteries are mounted in a double row and run the length of the battery tunnel. This approach locates all the batteries in a common pack, simplifies wiring, simplifies servicing, and provides desirable weight distribution. In addition, the approach offers desirable crash-energy management characteristics.

Each pair of batteries is strapped to a continuous battery support tray. The tray is attached to the structure from the underside with approximately eight bolts. These connections are designed to restrain the pack in the tunnel under loads of up to about 10 g. Under major front-end-impact conditions, the connections will fail and allow the batteries to move relative to the tunnel and absorb their own kinetic energy. The upper portion of the tunnel is integral with the floor structure to provide a continuous barrier to exclude battery acids and fumes from the passenger compartment. The bottom section is bonded into position, and is stiffened to carry the battery loads back into the side walls.

Figure 92 shows a cross-section of the NTEV body through its centerline. The flexible foam bumpers are designed to absorb the energy of a 5-mph collision and to return undamaged. In a 10-mph collision, front or rear, the fiberglass backup beam will absorb the impact and may be damaged, but the remaining structure will be totally intact. In a 30-mph collision, the structure will crush and absorb energy in a manner that limits passenger g-loading to safe levels.

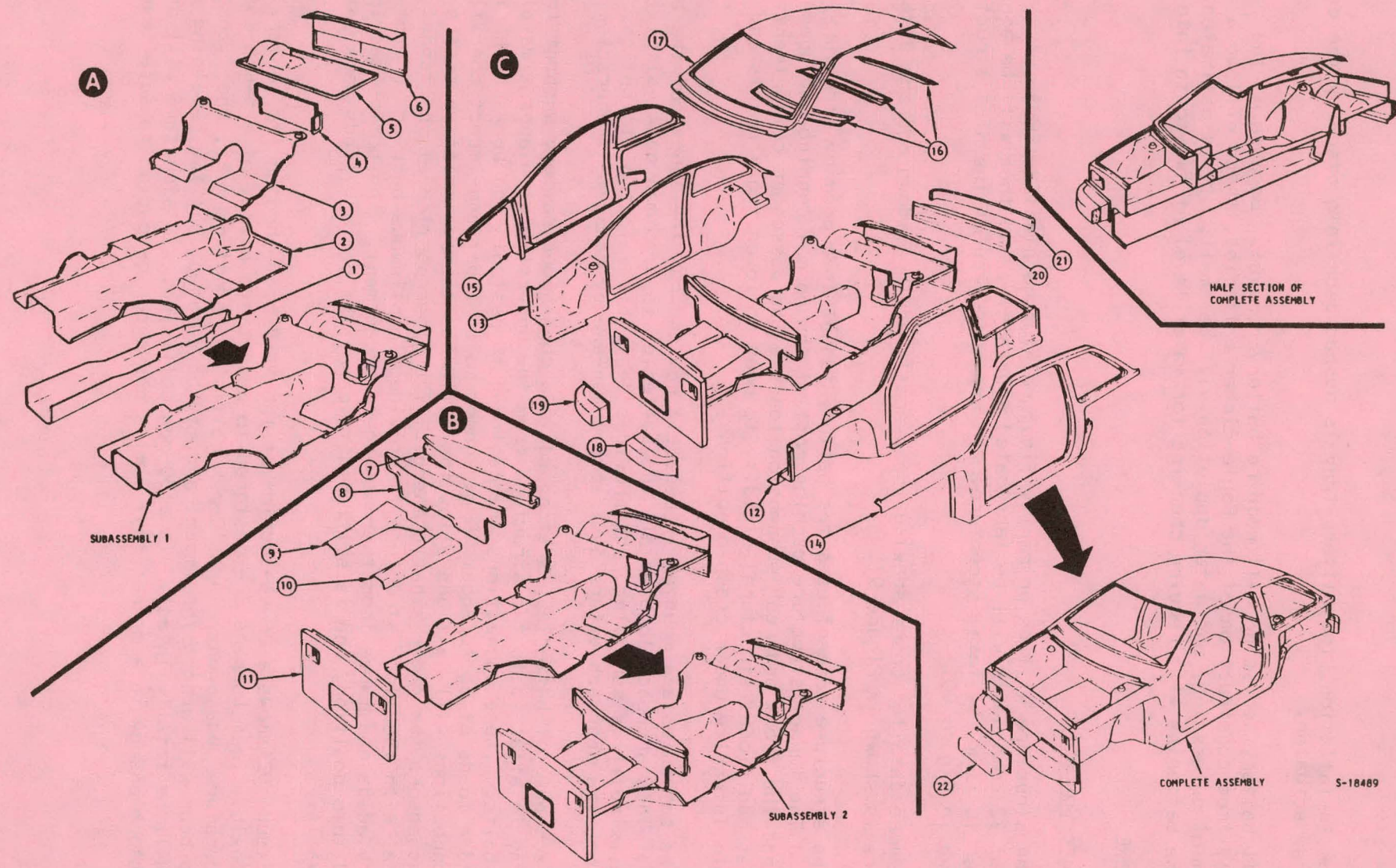


Figure 90. Body Structures

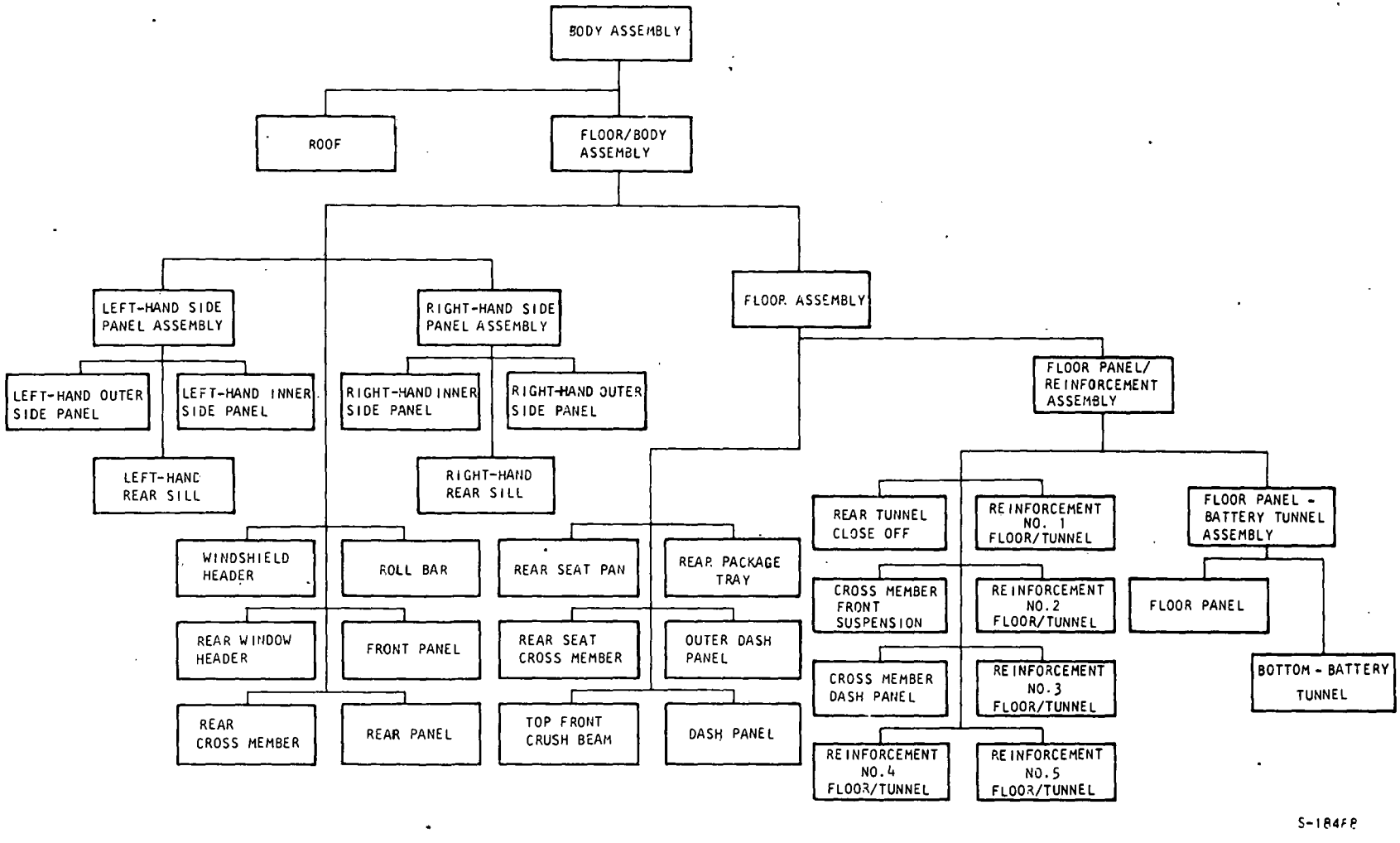


Figure 91. Body Overall Breakdown

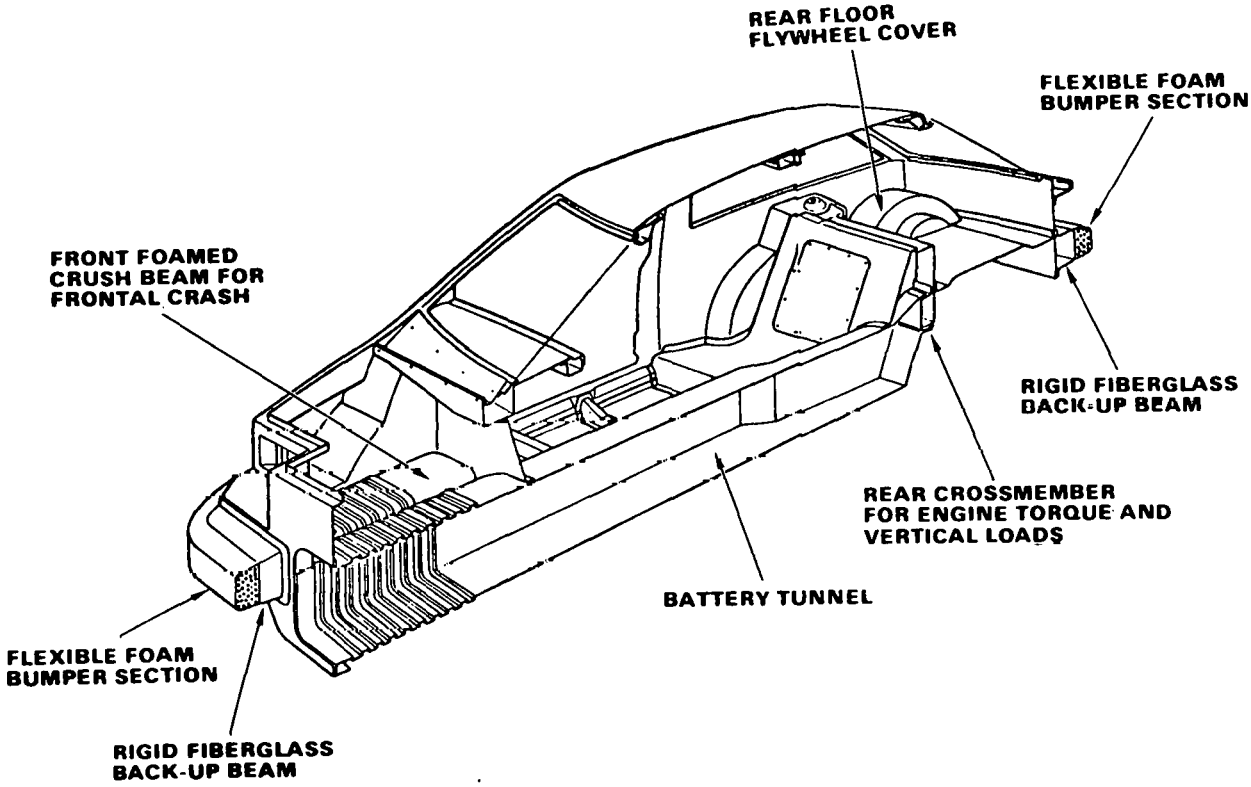


S 77788 A

Figure 92. Body Structure, Centerline Cross-Section

A section through the front axle is shown in Figure 93. The energy management front crush elements are located on each side of the battery tunnel. A metal front cross-member picks up the lower control arms and is in turn bolted to the battery tunnel.

The rear structure is shown in Figure 94. Rear crash loads are carried forward by the rear sills from the rear bumper, around the wheel wells, and into the side sills. The rear sills also contain energy-absorbing elements.

A side view of the rear sill is shown in Figure 95. The forward part of the rear sill is spoon shaped and is bonded onto the side sill. The power unit is suspended on four Barry 500 series motor mounts. These are all-angle isolators utilizing elastomers in compression. Power unit removal is accomplished by removing four motor mount bolts and lowering the power unit with a special fixture.

The door concept is shown in Figure 96. A fiberglass corrugated-type beam runs the length of the door to absorb side impact loads. Deflection tests have been conducted on this beam to verify its stiffness and strength.

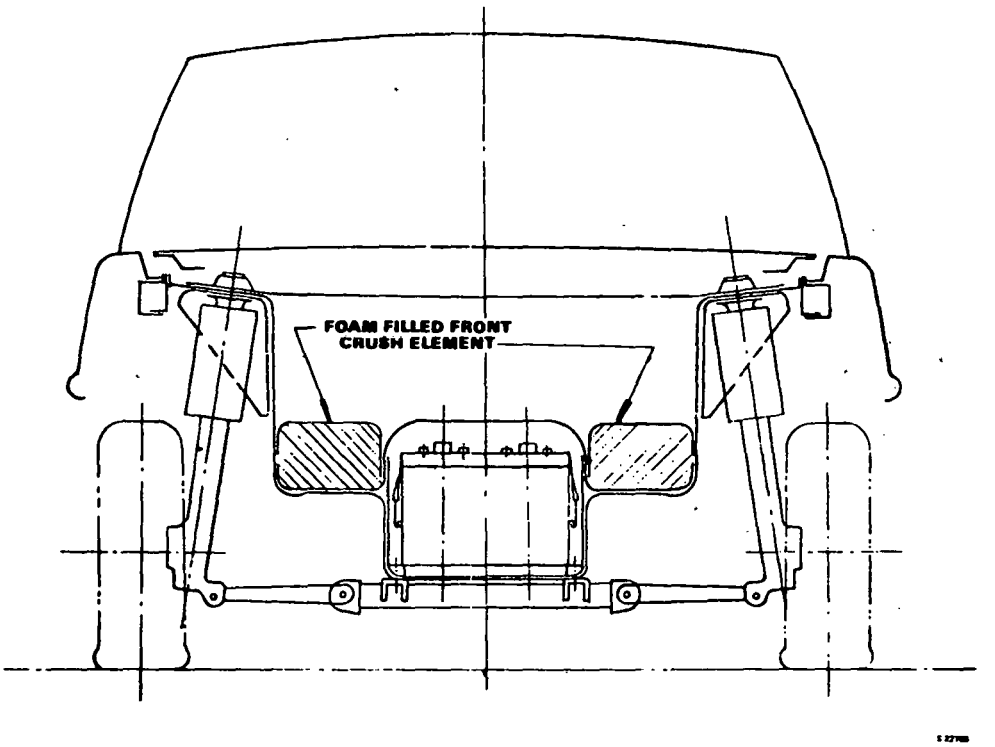


Figure 93. Body Structure, Front Axle Section

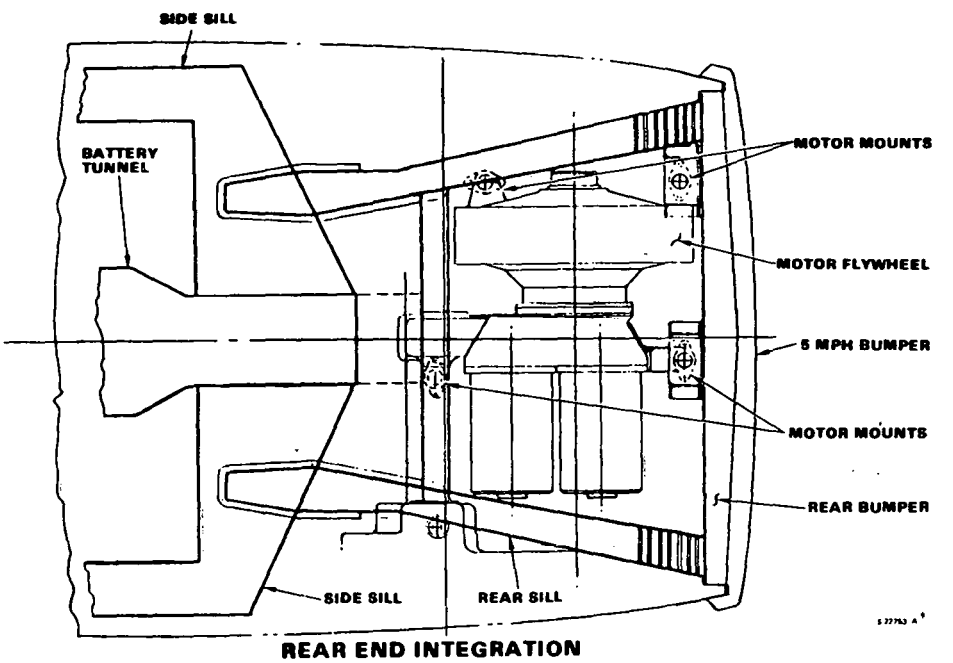


Figure 94. Body Structure, Rear, Top View

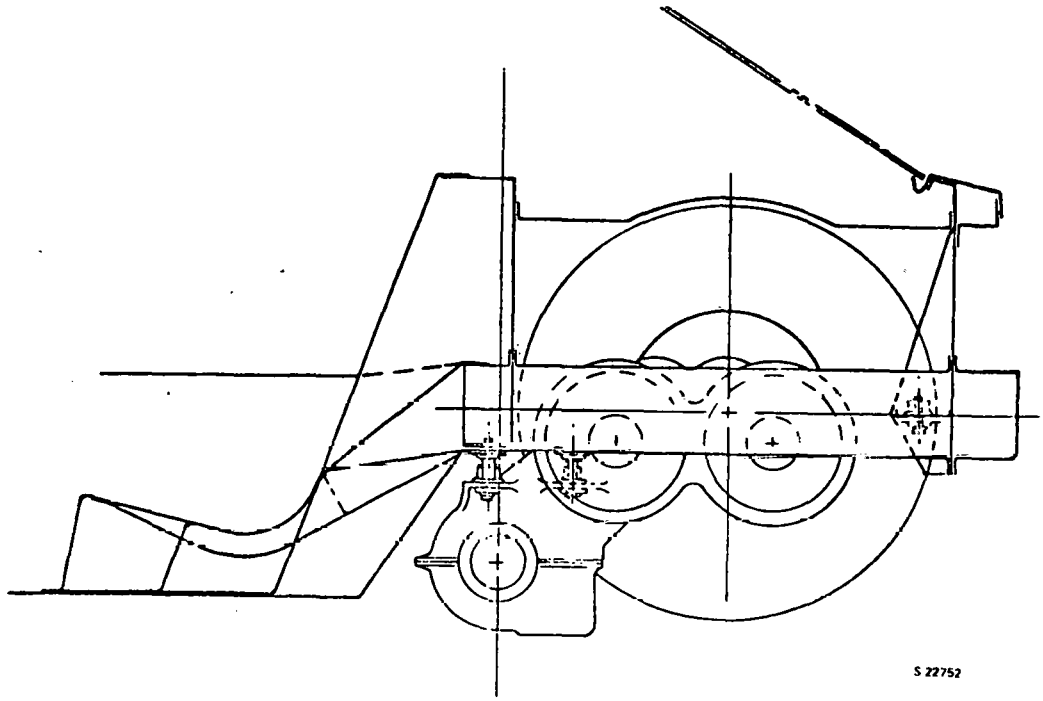


Figure 95. Body Structure, Rear, Side View

The hood concept is shown in Figure 97. It is rear-opening, two-part construction with conventional hinges and latches.

The rear hatch concept is shown in Figure 98. The hatch is a formed piece of 0.250-in. stretched acrylic. The hinges and latches are bolted directly to the acrylic.

Crash Management

In order to design the crash-energy-management system for the electric vehicle, it is necessary first to establish the overall crushing resistances required of the vehicle structure. The weight of the electric vehicle, with occupants, is approximately 3449 lb. Included in this weight is 1040 lb of batteries.

The vehicle design concept requires the batteries to be decoupled from the vehicle structure during a crash situation, so that the vehicle structure will not be forced to absorb the kinetic energy of the batteries. This concept was demonstrated in battery crash testing performed by The Budd Company.

Drop-tower tests, conducted by The Budd Company on its 30-mph test facility, have indicated that the major structural elements used in the vehicle will provide adequate crush resistance. The test results on the battery tunnel indicate an average crush force of 10,000 lb, and the two energy-absorbing

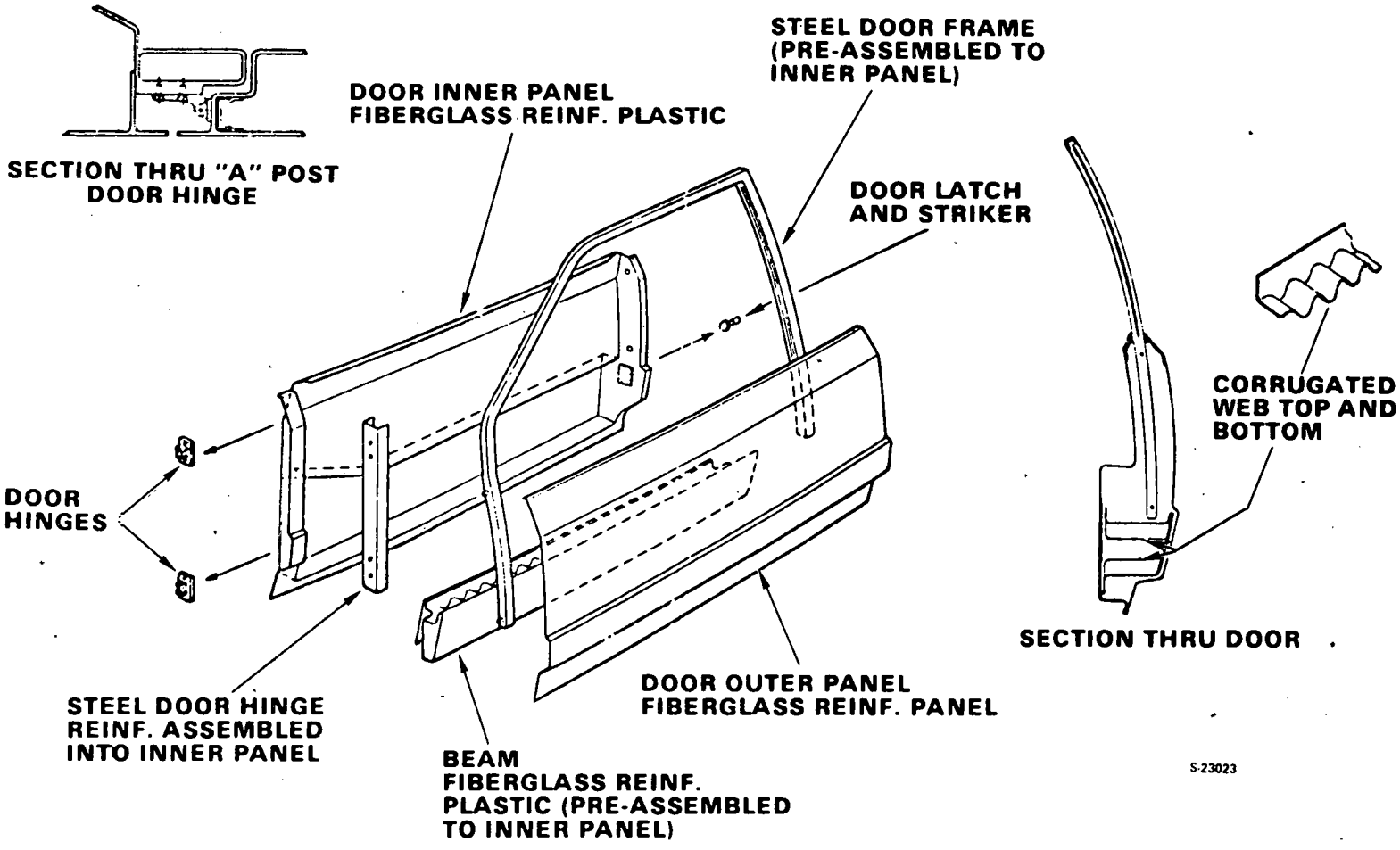


Figure 96. Door Construction

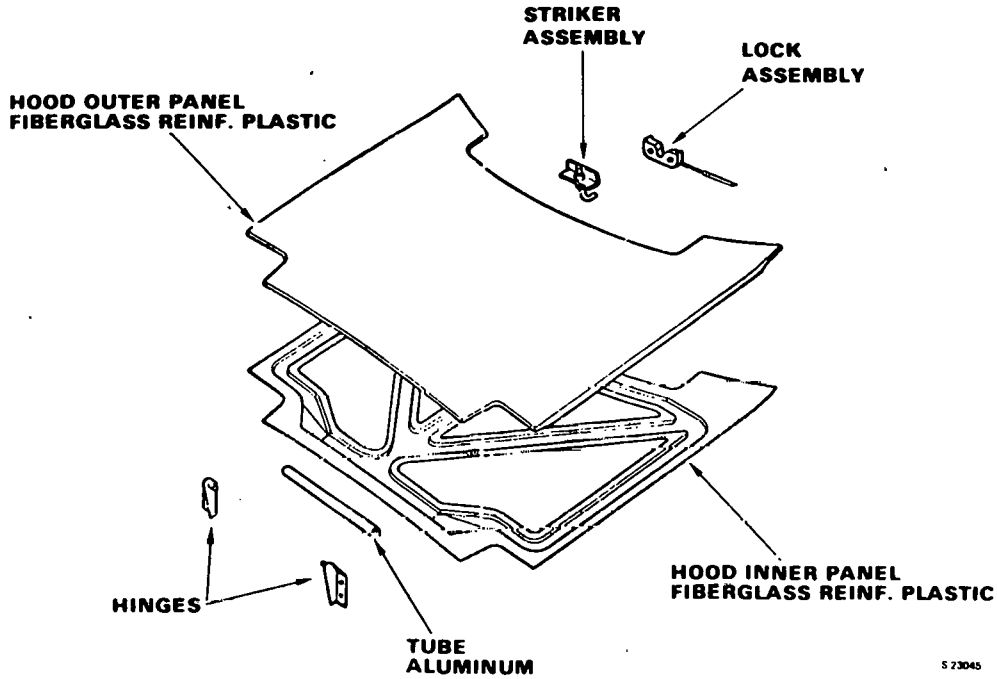


Figure 97. Hood Construction

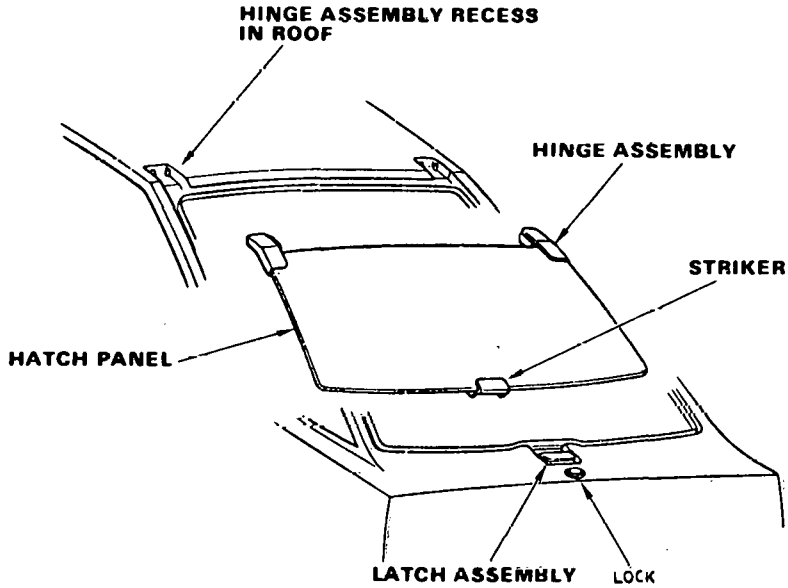


Figure 98. Hatch Construction

elements (foam-filled tubes) yield an average crush force of 29,000 lb. The combined crush resistance is 39,000 lb. Based on the 39,000-lb figure, the crush distance would be approximately 1.64 ft.

Since these crush distances are for an ideal square-wave energy absorber, additional distance should be provided to take into account the actual performance of the front-end structure. Based on past experience, approximately 36 in. of crush distance will be provided in the front-end design.

The crash-energy data are summarized in Table 20.

TABLE 20

CRASH ENERGY MANAGEMENT

| | |
|---|---|
| Vehicle kinetic energy at 30 mph less batteries and with 2 passenger, ft-lb | 63,400 |
| Average force for 2-ft crush, lb | 31,700 |
| Average force for structural elements, lb | |
| Tunnel | 10,000 |
| Absorbers | 29,000 |
| | 39,000 |

## Sectional Properties

Figure 99 presents a preliminary study of the sectional properties of the vehicle, as conceptually designed. Shown for comparison purposes on the figure are the properties for a metal vehicle structure of the same size.

The torsional rigidity of the design is shown in Table 21 and is compared with values for other vehicle designs.

## Materials

Primary body materials are predominantly fiber-reinforced polyester (FRP) with metal inserts in high-stress areas such as suspension attachment points. In most of the body structure, glass-mat-reinforced polyester with glass content of 35 percent (referred to as Class 1) will be used. In some high-stress areas, glass-cloth-reinforced polyester with glass content from 50 to 65 percent (referred to as Class 2) will be used.

Material properties (except the fatigue strengths) presented in Table 22 are test results from three or more flat-test specimens, machined from test slabs, 0.090 to 0.125 in. thick. All values presented are those at room temperature. The fatigue strengths are based on PPG published data.

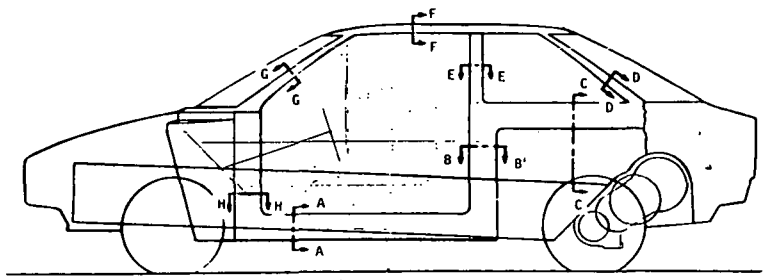


| SECTION | ELECTRIC VEHICLE | | | BUDD - SWIFT | | | $EI_X$ | | $EI_Y$ | |
|---|---|---|---|---|---|---|---|---|---|---|
| | AREA | $I_X$ | $I_Y$ | AREA | $I_X$ | $I_Y$ | E.V. | SWIFT | E.V. | SWIFT |
| A-A | 2.17 | 9.69 | 10.48 | 0.46 | 1.24 | 1.09 | 14.54 | 37.20 | 15.72 | 32.70 |
| B-B | 2.07 | 1.25 | 17.11 | 0.28 | 0.90 | 0.20 | 1.88 | 27.00 | 25.67 | 6.00 |
| C-C | 1.97 | 13.18 | 1.35 | 0.36 | 0.57 | 0.29 | 19.77 | 17.10 | 2.03 | 8.70 |
| D-D | 0.97 | 0.94 | 0.74 | 0.47 | 0.77 | 0.73 | 1.41 | 23.10 | 1.11 | 21.90 |
| E-E | 0.99 | 0.13 | 1.65 | 0.19 | 0.06 | 0.07 | 0.20 | 1.80 | 2.48 | 2.10 |
| F-F | 0.95 | 0.84 | 0.74 | 0.34 | 0.15 | 0.16 | 1.26 | 4.50 | 1.11 | 4.80 |
| G-G | 1.13 | 1.48 | 1.04 | 0.28 | 0.13 | 0.06 | 2.22 | 3.90 | 1.56 | 1.80 |
| H-H | 2.21 | 6.97 | 11.85 | 0.62 | 1.03 | 1.01 | 10.46 | 30.90 | 17.78 | 30.30 |
| TUNNEL | 6.47 | 178.81 | 305.38 | 0 | 0 | 0 | 268.22 | 0 | 458.07 | 0 |

Figure 99. Comparison of Section Properties

TABLE 21

COMPARISON OF TORSIONAL BODY STIFFNESSES

| Vehicle | Torsional Stiffness, $\frac{\text{ft-lb}}{\text{degree}}$ |
|---|---|
| Electric vehicle proposed design | 9,100 |
| Chevrolet plastic-foam body - XP-898 | 3,240 |
| Budd Company designed - Swift vehicle | 5,600 |
| British Leyland vehicle | 6,430 |
| Fiat 128 | 8,700 |

Secondary materials are glazing materials, polyurethane foam, rubber, adhesive materials, etc., which are nonstructural in nature. Suspension components are BMW 320i parts, made of high-strength steel. Table 23 lists materials uses.

TABLE 22

FRP MATERIAL PROPERTIES

| Property | Units | Values | | Test Method |
|---|---|---|---|---|
| | | Class 1 | Class 2 | |
| Tensile strength, min. | ksi | 15 | 34 | ASTM-D-638 |
| Tensile modulus, min. | msi | 1.4 | 2.2 | ASTM-D-638 |
| Flexural strength, min. | ksi | 23 | 30 | ASTM-D-790 |
| Flexural modulus, min. | msi | 1.2 | 1.0 | ASTM-D-790 |
| Compressive strength, min. | ksi | 22 | 30 | ASTM-D-695 |
| Fatigue flux (10 cycles)<br>Impact strength, min. | ksi<br>lb/in. | 3.8<br>5 | 6.1<br>6 | ASTM-D-256 |
| Specific gravity, min. | --- | 1.35 | 1.5 | ASTM-D-792 |
| Flammability, min. | --- | Pass | Pass | FMVSS 571.302 |

TABLE 23

NTEV MATERIALS USES

| Material | Use |
|---|---|
| Glass mat/reinforced polyester: | Chassis |
| 0.060 in. thick | Nonstructural |
| 0.090 in. thick | Structural |
| Glass cloth/reinforced polyester | High-stress areas |
| Glazing: | |
| Laminated glass, EZ3-eye tinted, 0.250 in. thick | Windshield |
| Abrasion-resistant acrylic, EZ-eye tinted, 0.125 in. thick | Door windows |
| 0.125 in. thick | Rear quarter windows |
| 0.250 in. thick | Rear window |
| Polyurethane foam: | |
| 2 PCF rigid | Energy absorption |
| Flexible | Cushions |
| 6 PCF, flexible | Bumpers |
| Vinyl, cloth backing | Upholstery |
| Neoprene foam, butyl rubber | Door and window seals |
| Epoxies, urethanes | Adhesives |
| Steel | Suspension components |

WEIGHT SUMMARY

The overall vehicle weight summary is shown in Table 24. Components are organized along the lines of the Universal Parts Grouping used by automobile manufacturers. Target weights for each grouping were set early in the EPPV program and will not change. Estimated weights are calculated from detail drawings as they become available and actual weights are obtained by weighing the hardware.

TABLE 24

VEHICLE WEIGHT SUMMARY

| UPG No. | Part Name | Weight, lb |
|---|---|---|
| 11 | Body assembly, final | 498.6 |
| 12 | Operating hardware | 53.7 |
| 13 | Lamps, switches, and instrument panel control | 7.2 |
| 14 | Exterior ornaments | 16.3 |
| 15 | Trim panels | 7.0 |
| 16 | Seats | 65.0 |
| 17 | Seals, weather strip, insulation | 5.5 |
| 18 | Glazing | 82.6 |
| 19 | Convenience items | 17.8 |
| 20 | Interior molding and ornaments | 0.5 |
| 21 | Instrument panel and console | 13.5 |
| 22 | Paint | 10.0 |
| 30 | Power system* | 1646.45 |
| 31 | Final drive | 26.0** |
| 33 | Suspension | 143.4** |
| 34 | Steering | 16.7** |
| 35 | Brakes | 86.1** |
| 36 | General chassis components | 128.0 |
| 37 | Chassis indirect materials | 2.5 |
| 80 | Heater | 13.0 |
| 85 | Accessory equipment | 9.2 |
| | Total | 2849 |

*Includes batteries, 1040 lb
**Denotes actual weights; other values are estimated

# SECTION 7

# SUSPENSION, BRAKES, AND STEERING

## SECTION 7

## SUSPENSION, BRAKES, AND STEERING

The design objective for suspension, brakes, and steering components was to adopt existing components to the NTEV. Following a study of candidate vehicles, the total system from the BMW 320i was selected. The 320i is about the same size and weight as the NTEV, and its four-wheel independent suspension fits the packaging requirements dictated by the central battery tunnel.

A comparison of NTEV and 320i physical characteristics is shown in Table 25. From the suspension standpoint, the only change required will be extensions on the steering links to accommodate the 5.4 in. greater track width of the NTEV. Although the NTEV is slightly heavier than the 320i, it has less weight on the front wheels. This should ensure reasonable steering effort without power steering.

TABLE 25

NTEV/320i PHYSICAL CHARACTERISTICS

| | NTEV | BMW 320i |
|---|---|---|
| Curb weight, lb | 2849 | 2605 |
| Gross weight, lb | 3449 | 3205 |
| Weight distribution front/rear, percent | 45/55 | 54/46 |
| Weight on front wheels (curb), lb | 1279 | 1406 |
| Wheelbase, in. | 95.0 | 100.9 |
| Track, front/rear, in. | 60.0/59.0 | 54.6/55.1 |
| Length, in. | 165.0 | 177.5 |
| Width, in. | 68.0 | 63.4 |
| Height, in. | 54.9 | 54.3 |

### SUSPENSION AND STEERING

Characteristics of the NTEV suspension and steering system are presented in Table 26. Views of the selected system are presented in Figures 100, 101, and 102.

TABLE 26

NTEV SUSPENSION AND STEERING DATA

| | |
|---|---|
| **Front Suspension** | |
| Upward wheel travel, in. | 3.3 |
| Downward wheel travel, in. | 4.3 |
| King-pin inclination, deg, min. | 10°, 54' |
| **Steering** | |
| Maximum wheel lock, inside wheel, deg | 40.4 |
| Maximum wheel lock, outside wheel, deg | 35.3 |
| Overall steering ratio | 21.1:1 |
| Turns lock-to-lock | 4.1 |
| **Rear Suspension** | |
| Upward wheel travel, in. | 4.0 |
| Downward wheel travel, in. | 4.8 |

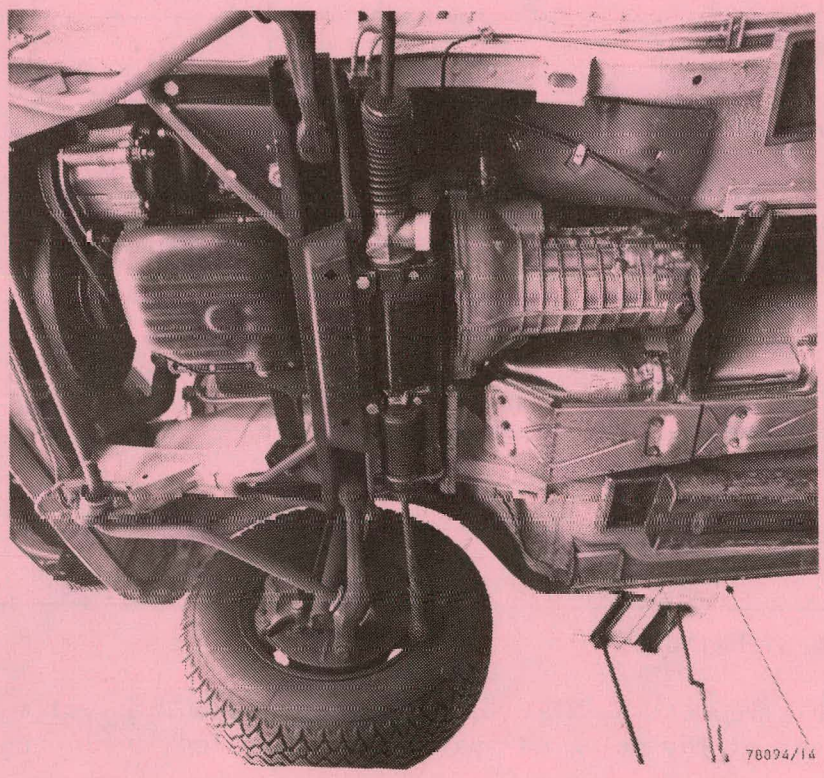


Figure 100. Front Suspension Underside View Showing Steering Components

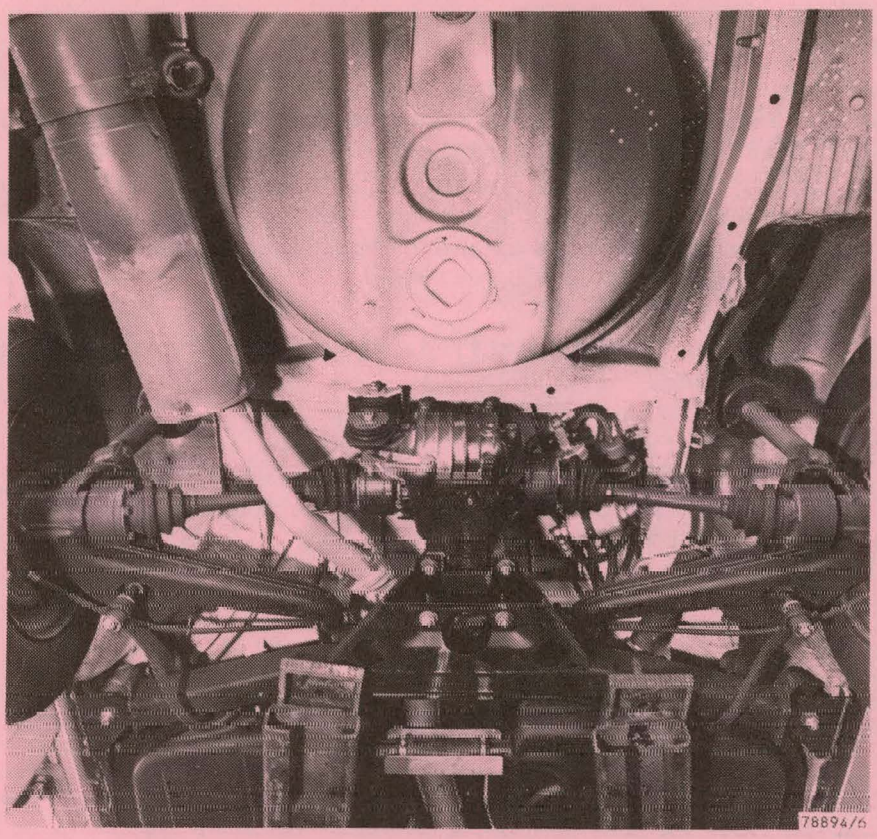


Figure 101. Rear Suspension Underside View

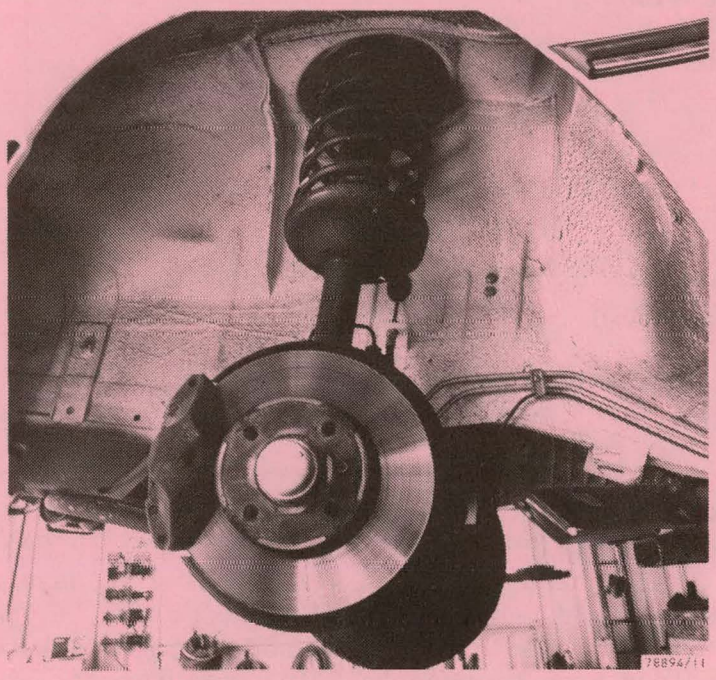


Figure 102. Front Suspension View Showing Spring and Shock Absorber Detail

An attempt was made to replace the front disc brakes in order to: (a) reduce weight, (b) reduce pedal force requirement, and (c) reduce brake drag. These are significant advantages for electric vehicles and should be explored further in the future; however, replacing the discs would have required considerable design and development and was not consistent with the NTEV objectives, so the discs were retained. Solid brake discs, which are standard on the 1978 320i, are being considered for weight savings.

The rear torsion bar will be omitted. It is also omitted on the 1978 320i as a weight-saving measure.

A weight summary of the overall suspension system is presented in Table 27. The 320i system is lightweight by comparison with American car counterparts, and little further weight reduction can be expected until composite materials are more fully developed.

TABLE 27

SUSPENSION WEIGHT PER CAR SET

| | Weight, lb |
|---|---|
| Front suspension | 87.1 |
| Front brakes | 42.2 |
| Rear suspension | 56.3 |
| Rear brakes | 33.5 |
| Steering | 16.7 |
| Master cyclinder and brake lining, etc. | 10.4 |
| Tires | 82.0 |
| Wheels (aluminum) | 40.0 |
| Axles and constant-velocity joints | 26.0 |
| Total | 394.2 |

Since the geometry relationship of the NTEV suspension will be unchanged from the 320i, measurements were made on a 320i to obtain basic suspension characteristics. These characteristics will be used to develop desired handling and to help understand and solve handling problems if they should arise. The test car and the instruments and aids used to take measurements are shown in Figure 103. Springs were removed to allow measurements at all wheel travel positions. Special discs with reference scribe lines were built and mounted in place of the wheels.

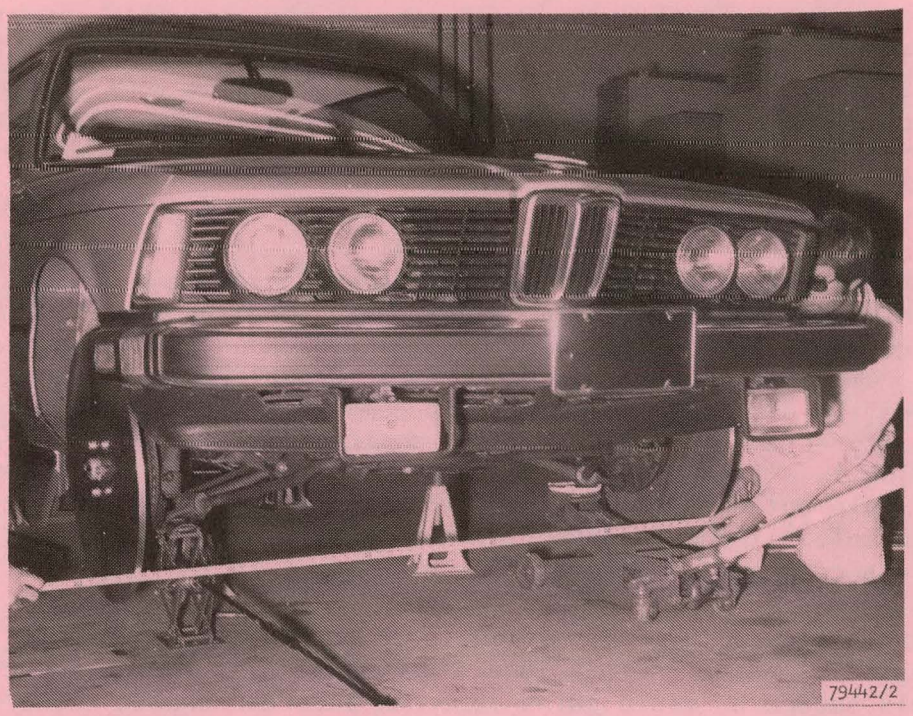


a. WHEEL TREAD

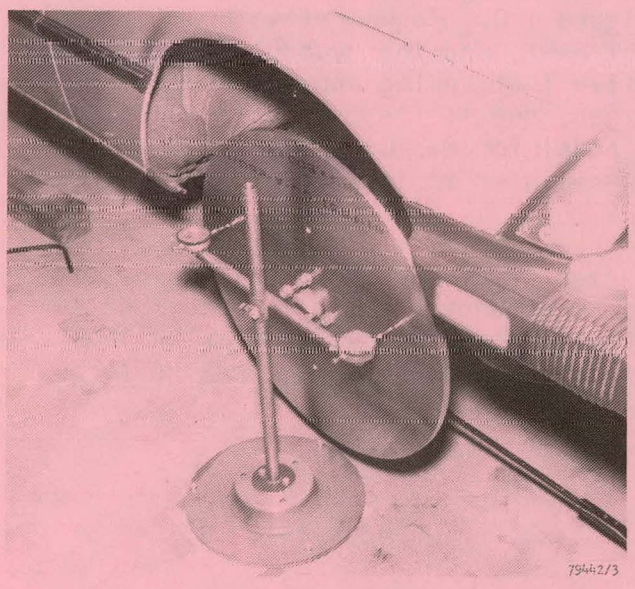


b. TOE CHANGE

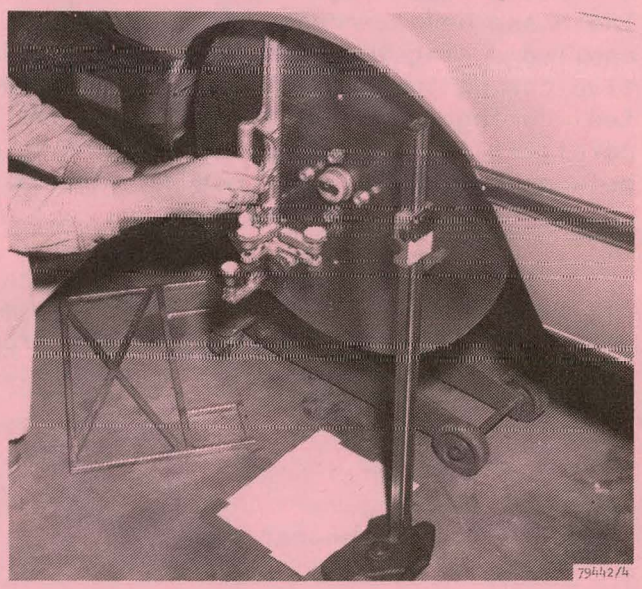


c. CASTER/CAMBER

Figure 103. BMW Test Car Suspension Geometry Measurement

Results of the measurements are presented in Figures 104, 105, 106, and 107. Probably the most significant result appears in Figure 108, which shows that the 320i and NTEV theoretical Ackermann diagrams are very similar. This indicates there should be very little tire scrubbing in the small wheel angle range where most driving is conducted.

BRAKES

The NTEV has both electrical regenerative and hydraulic brakes. A schematic of the NTEV brakes is shown in Figure 109. The regenerative and hydraulic systems are completely separate. Potentiometer pickups on the accelerator and brake pedals communicate with the controller. Signals from the accelerator pedal apply regenerative braking to simulate the compression braking experienced in the conventional ICE auto. The first 1.5 in. of brake pedal travel applies full regenerative braking in a linear manner to the NTEV rear wheels. Regenerative braking is normally implemented by transferring the vehicle's kinetic energy directly into the flywheel. If the flywheel has reached its saturation speed of 25,000 rpm, the excess current is directed to the battery.

As shown in Figure 109, the hydraulic brakes are separate and unchanged. Direct mechanical linkage from the brake pedal operates the master cylinder, which controls separated fluid paths to front and rear brakes. The parking brake operates mechanically on the rear wheels.

The front disc brakes require relatively high actuation force, and the artificial feel required during regenerative braking increases pedal pressure. The brake pedal arrangement is shown in Figure 110. Regenerative braking is applied during the first 1.5 in. of pedal travel, and the hydraulics are effective during the next 2.5 in. The regenerative feel spring applies the artificial feel during the first 1.5 in. of travel; then, due to its overcenter anchor point, it is relaxed to avoid building up pedal force. Clearance is provided between the brake pedal rod and the master cylinder to lock out the hydraulics during regenerative braking.

NTEV braking torque/pedal force characteristics are shown in Figure 111 All requirements of FMVSS 571.105 are met. Emergency braking is accommodated with 116 lb of pedal force, and the front failure emergency is met with 150 lb of pedal pressure, all within 571.105 requirements. Maximum braking torques are:

| | |
|---|---|
| Total | 2550 ft-lb |
| Regenerative | 400 ft-lb |
| Front hydraulics | 1720 ft-lb |
| Rear hydraulics | 430 ft-lb |

The most severe failure condition is with the front hydraulics inoperative, which reduces braking torque 67 percent. Because of the regenerative braking on the rear wheels, that failure case is less severe than with the standard 320i where a front hydraulics failure reduces braking capability by 80 percent.

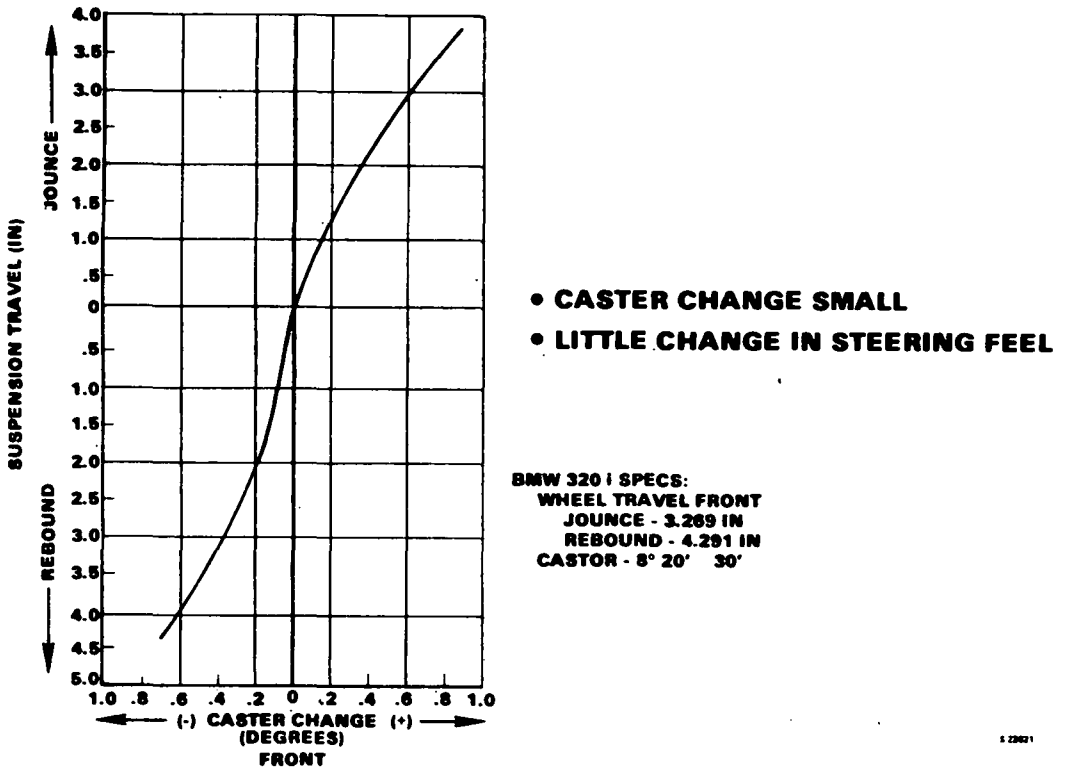


Figure 104. Caster Change with Wheel Travel

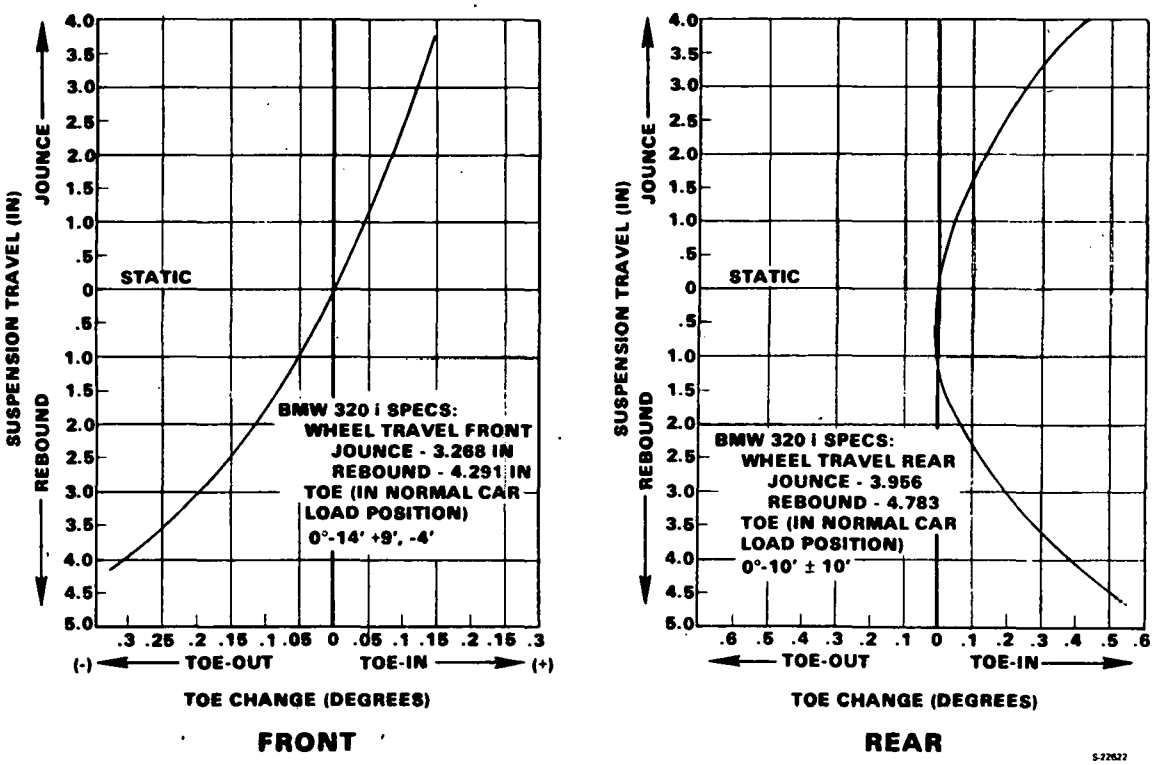


Figure 105. Toe Change with Wheel Travel

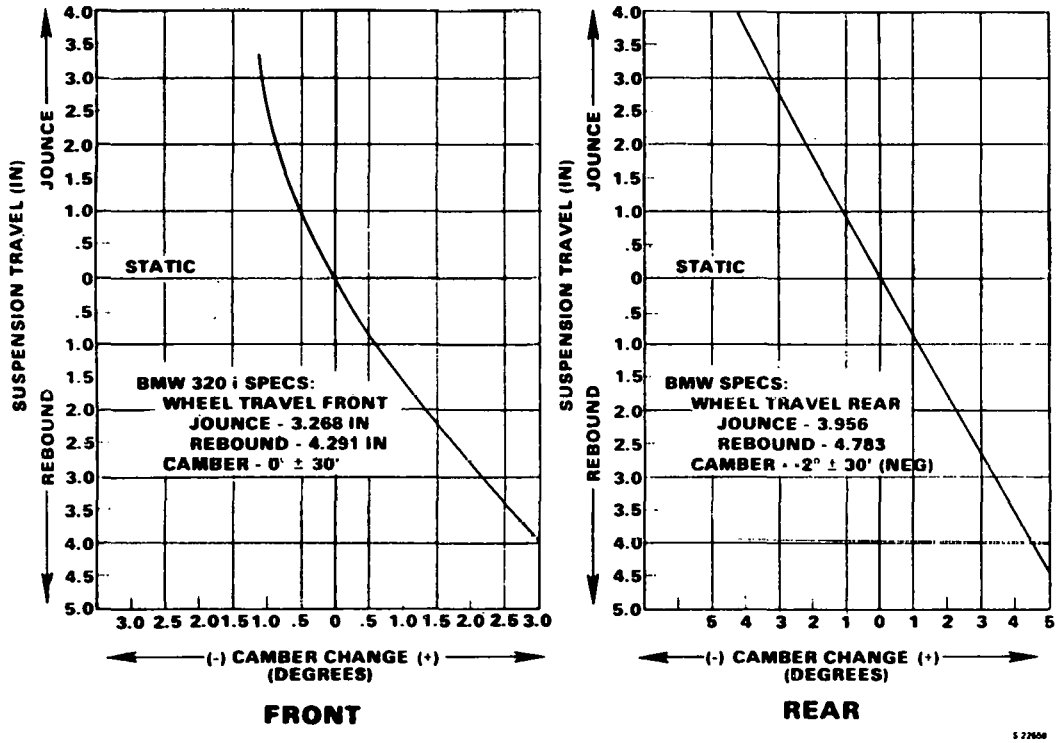


Figure 106. Camber Change with Wheel Travel

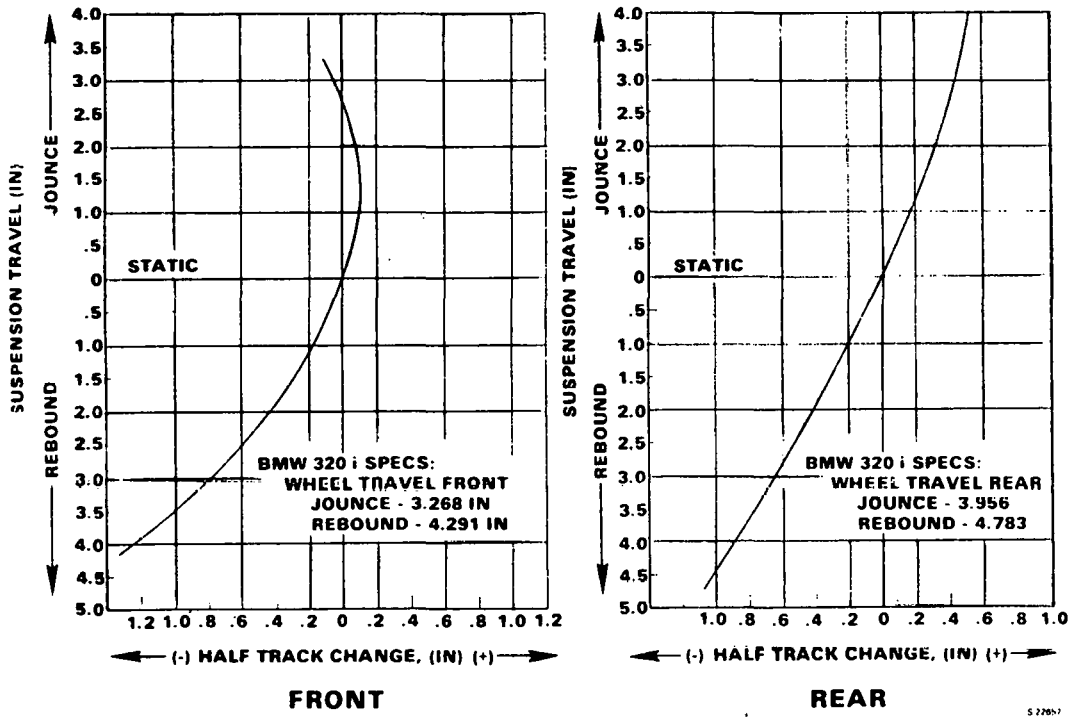


Figure 107. Tread Change with Wheel Travel

- **DATA TAKEN FROM BMW 320i**

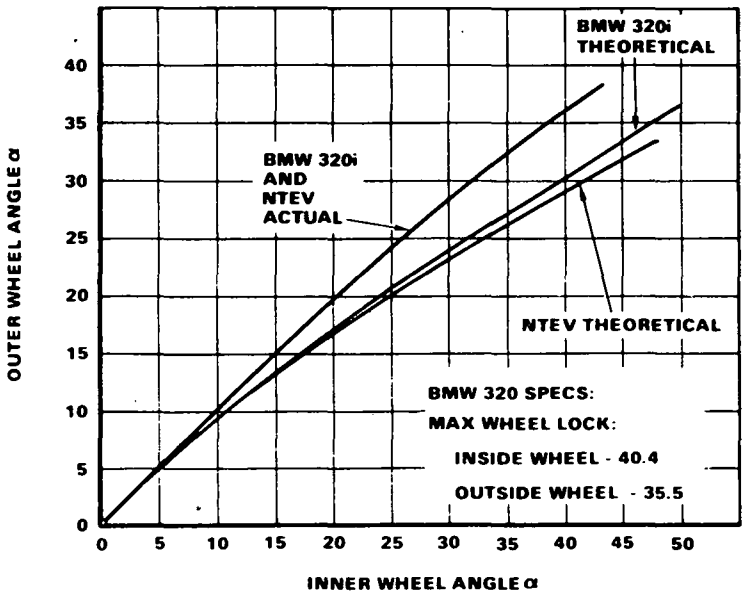


- **NO WHEEL SCRUB AT NORMAL DRIVING ANGLES**

Figure 108. Ackermann Diagram

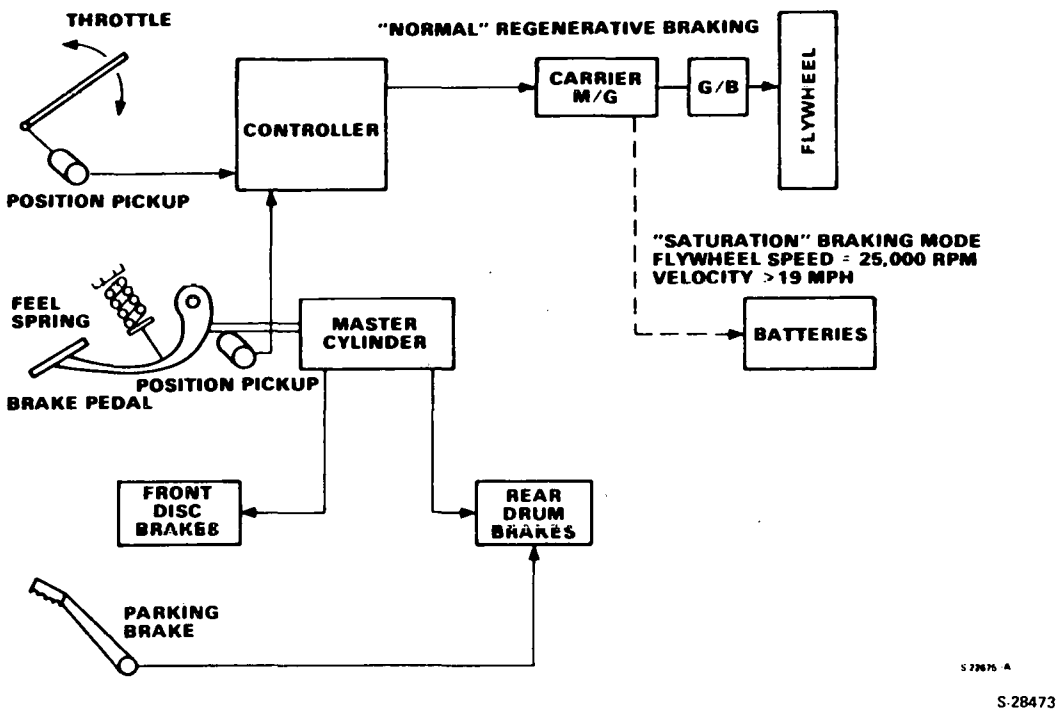


Figure 109. Brake System

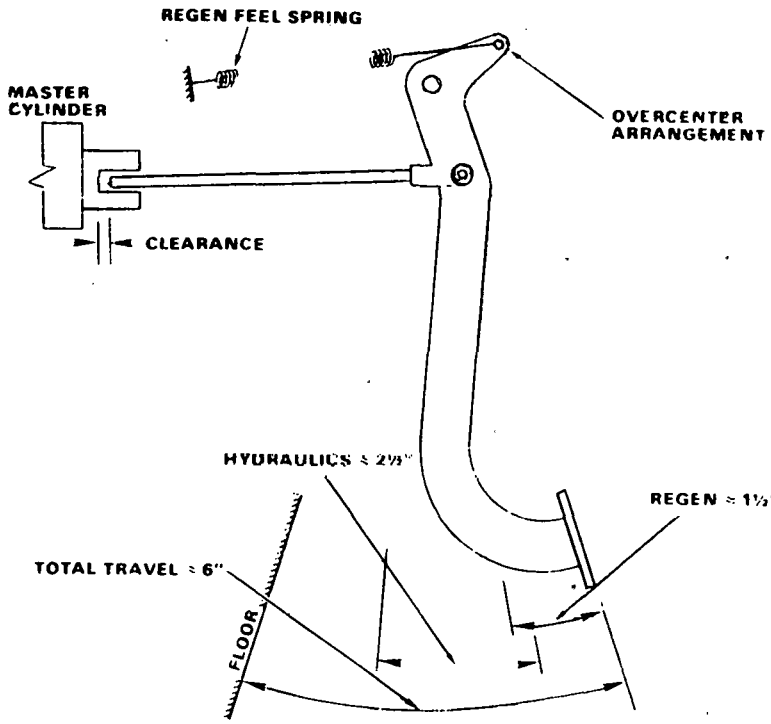


Figure 110. Brake Pedal Arrangement

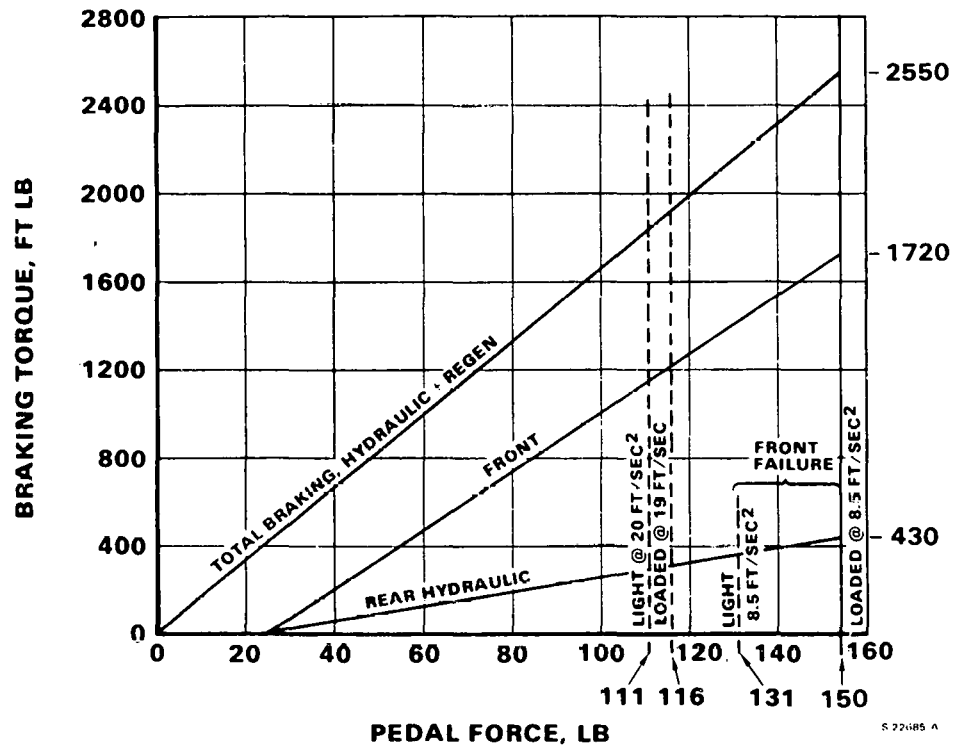


Figure 111. Brake Characteristics

In Figure 111, regenerative braking is included as a constant 400 ft-lb torque. As shown in Figure 112, maximum regenerative braking varies as a function of vehicle velocity. Peak braking is 540 ft-lb at 20 mph and it is above 400 ft-lb to beyond 60 mph. At low speeds, regenerative braking is effective to about 4 mph and it drops linearly to zero at standstill. When the flywheel is saturated and the energy is being put back into the batteries, regenerative braking is reduced by about one-half and is not effective below 30 mph.

Figure 113 shows the potential usefulness of regenerative braking. Various parameters of the Federal Urban Driving Schedule are shown. The lower curve shows the braking duty cycle required for FUDS and shows that most of the braking can be handled regeneratively.

The BMW hydraulic system will be used without change. Characteristics of the system result in applying 80 percent of the braking to the front wheels on the BMW. Figure 114 shows the overall braking on the rear wheels as a function of deceleration rate. At very low rates, when regenerative braking alone is applied, braking is 100 percent on the rear. When the hydraulics are brought in, more and more braking is placed on the front wheels.

Also shown in Figure 114 is the NTEV dynamic weight distribution. At standstill, 54 percent of the NTEV weight is on the rear wheels. The effect of deceleration is to dynamically shift more weight to the front. At low decelerations there is more braking than weight on the rear wheels and there will be a tendency to lock the rear wheels on poor road surfaces. At about 11 ft/sec the brakes and car are matched and all four wheels are equally effective. At higher deceleration rates, which include the FMVSS 571.105 emergency stops, enough braking has shifted to the front to lock the front wheels if a skid were to occur.

## TIRES AND WHEELS

The NTEV design objective in this area is to obtain lightweight wheels and tires with low rolling resistance. Aluminum wheels will be used and a minimum weight for a street-compatible wheel is about 10 lb. Two approaches will be used to reduce rolling resistance--use of oversized steel radial tires and use of the high-pressure elliptical tire.

Loaded weight of the NTEV is 3449 lb, with 1587 lb on the front wheels and 1862 lb on the rear wheels. Maximum tire load is therefore 930 lb on the rear. This could be accommodated by an AR 78-13 steel radial tire with a load rating of 980 lb at 28 psi. The baseline plan for NTEV is to increase the tire size to a CR 78-13 and operate at higher pressure. The larger size and higher pressure both reduce rolling resistance. Baseline performance data will be taken with this combination.

It is also planned to evaluate NTEV performance with the Goodyear elliptical tire. The elliptical tire requires a special wheel that must be built to accommodate the BMW 320i hubs. The tire size required is the Goodyear designation P165/65R365.

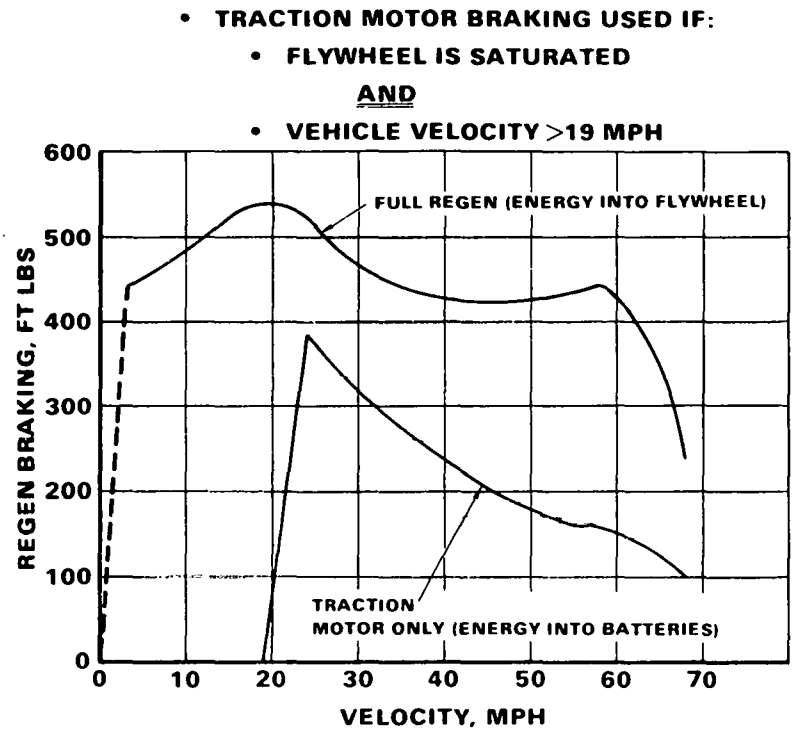


Figure 112. Flywheel Saturation Provisions

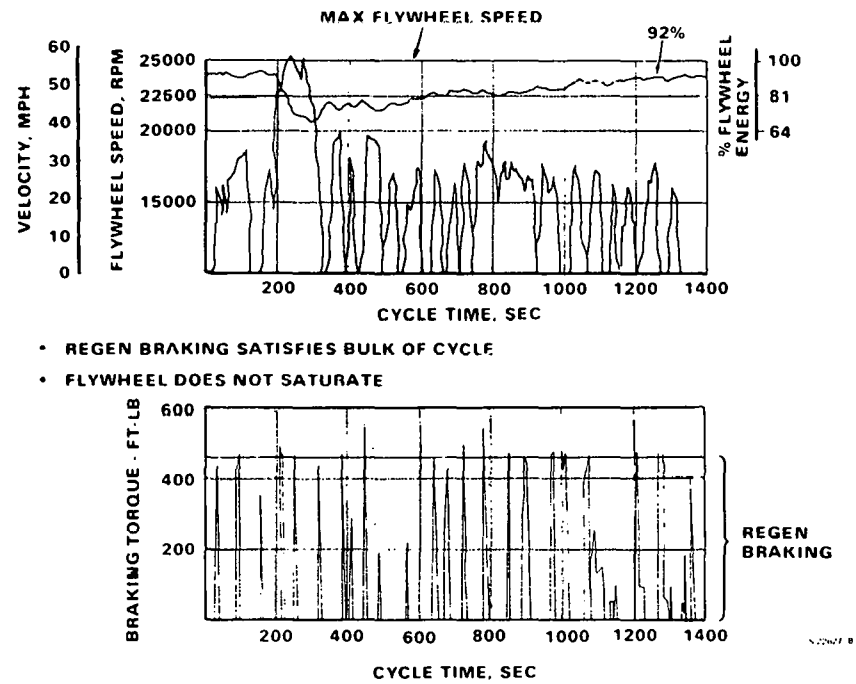


Figure 113. Brake Characteristics During Federal Urban Driving Cycle

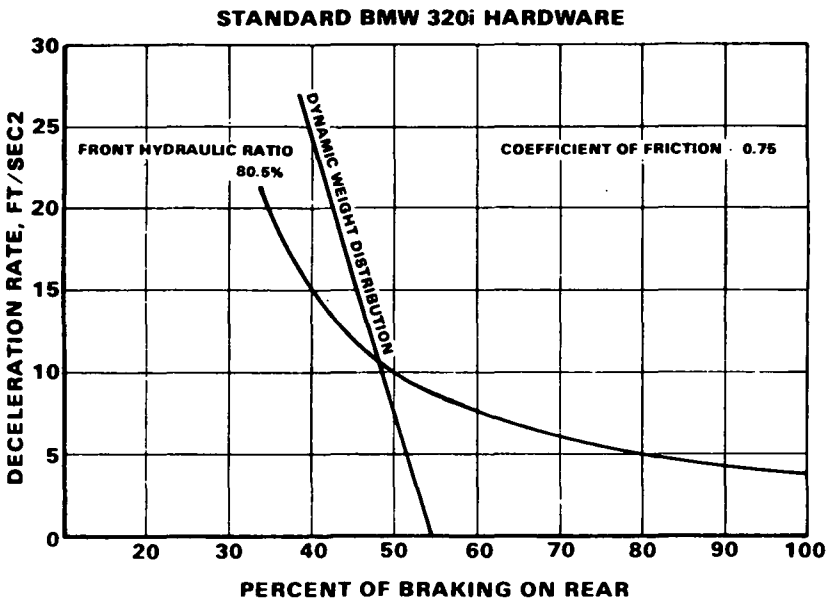


Figure 114. Braking Performance

To reduce rolling resistance it is necessary to increase tire inflation pressure. With conventional radial tires, the pressure can only be increased to about 35 psi before the ride becomes too hard. As shown in Figure 115, pressure in the elliptical tire can be increased to 44 psi without compromising the ride.

A comparison of the elliptical tire and a standard radial tire cross-section is shown in Figure 116. The elliptical tire has a lower profile and is more curved in the sidewall than current radials. This contributes to a comfortable ride at higher inflation. The rim flange is lower and canted out to conform to the elliptical shape of the tire body. Rim diameters with the elliptic are increased to complete the geometry.

Comprehensive data on the Goodyear elliptical tire are not yet available, especially in the size required for the NTEV; however, available data are encouraging. Data from tests conducted by Calspan Laboratory are presented in Table 28. At the lower inflation pressure of 38 psi, the elliptic shows promise of delivering the 0.006 coefficient on which the NTEV performance predictions are based. This table presents data for two different elliptical tires, serial numbers 8303 and 8302.

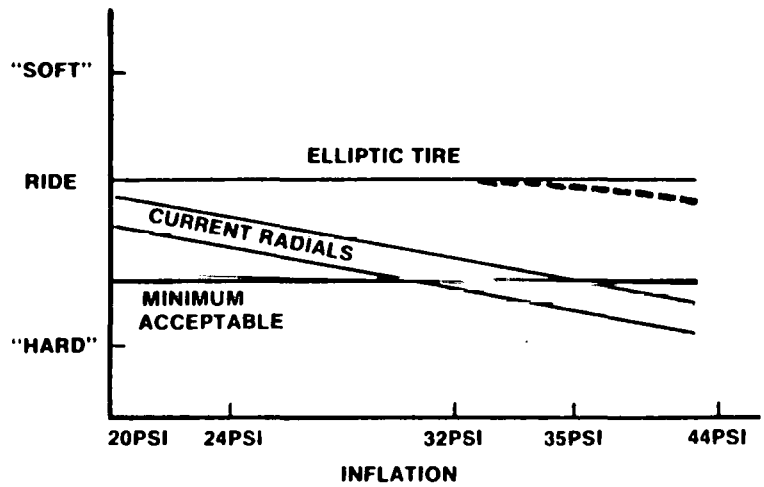


Figure 115. Inflation/Ride Characteristics

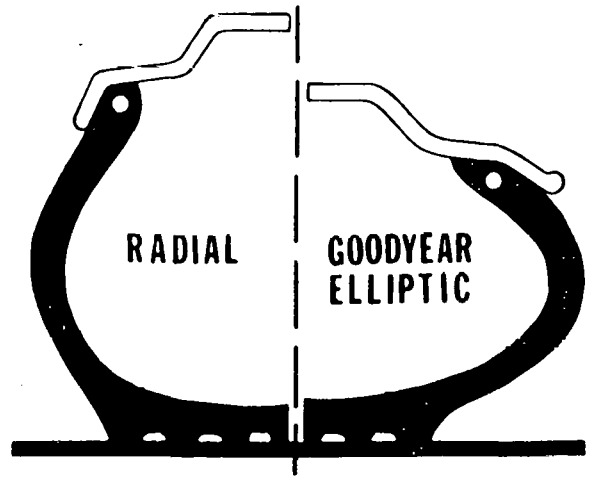


Figure 116. Elliptic Tire Section

TABLE 28

CALSPAN LABORATORY ROLLING RESISTANCE
(POUNDS OF DRAG FORCE, SPEED = 50 MPH, TIRE LOAD = 1024 LB)

| | 67-in. Drum Test | | Flat Belt Test | |
|---|---|---|---|---|
| | 30 psi | 39 psi | 30 psi | 38 psi |
| FR78-14 CPSR Control | 8.63 | 7.95 | 10.0 | 9.0 |
| P215/65E 390 7X8303 | 6.75 | 6.03 | 7.9 | 6.8 |
| P215/65E390 7X8302 | 5.801 | 5.20 | 6.6 | 6.5 |

# SECTION 8

# SCALE MODEL TESTING

# SECTION 8

# SCALE MODEL TESTING

The following tests are planned in support of the NTEV structure development:

- Battery Element Tests
- Battery Tunnel Test--Full-Scale
- Energy Absorber Element Tests
- Front-End Crash Tests--Half-Scale
- Rear-End Crash Tests--Half-Scale
- Element Fatigue Tests
- Modal Survey Tests
- Frontal Barrier Crash Test--Full-Scale

The first four tests listed above have been conducted and results are reported in this section.

## BATTERY ELEMENT TESTS

The first phase of component testing was to determine the crush characteristics of the batteries. The primary concern was to establish the ability of the 1040 lb of batteries to absorb their own energy in a crash situation. Existing plate-type batteries were used throughout the test and design program because the new tubular-plate batteries being developed specifically for this program will not be available during the structural design period. The impact and crush characteristics of the tubular type are not expected to be significantly different.

### Single Battery Static Crush Tests

The first tests performed on the batteries were static crush tests. Exide EV-106 golf-cart batteries were procured and tested in a Baldwin tensile-test machine. Tests were performed with the force applied in the direction parallel to, and then perpendicular to, the battery plates as indicated by Figure 117. Figure 118 illustrates the results of these tests in terms of force vs deflection. As shown in the figure, the battery proved to be softer in the force direction perpendicular to its plates. Figure 119 shows the battery being tested under load in the direction parallel to its plates. A cross-section of the battery after test is given in Figure 120.

### Single Battery Dynamic Crush Tests

The next tests were performed to establish the dynamic properties of single batteries. In these tests, the batteries were drop-tested on the crash-tower facility at the Budd Tech Center at speeds of 30 to 40 fps. Once again, the batteries were tested in both directions. Figure 121 shows that the battery tested in the direction perpendicular to its plates performed somewhat better, once again exhibiting lower force levels and larger deflections.

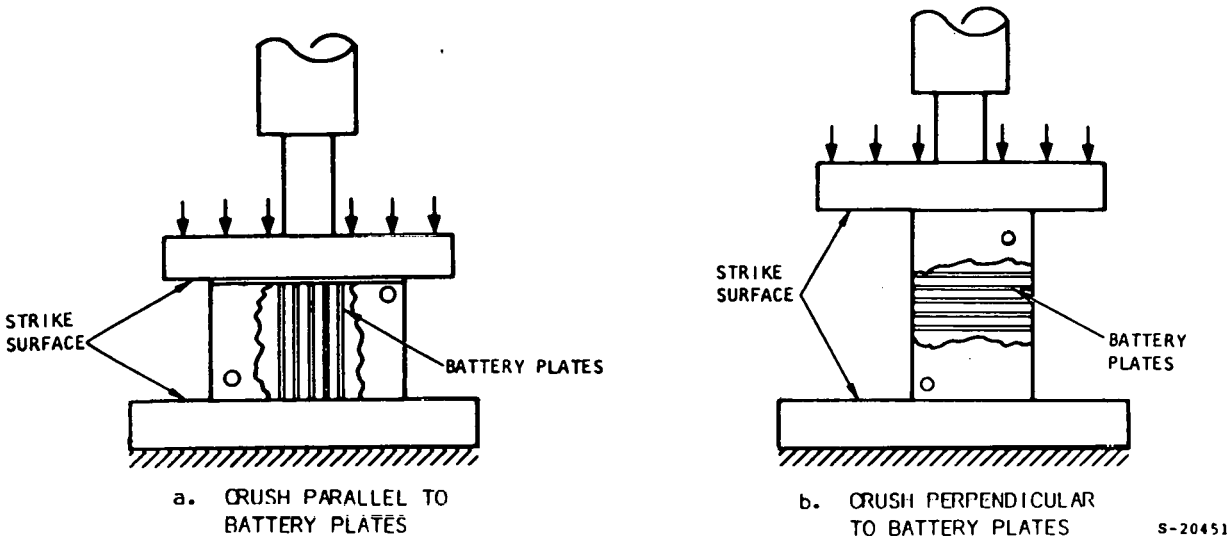


Figure 117. Battery Test Orientation

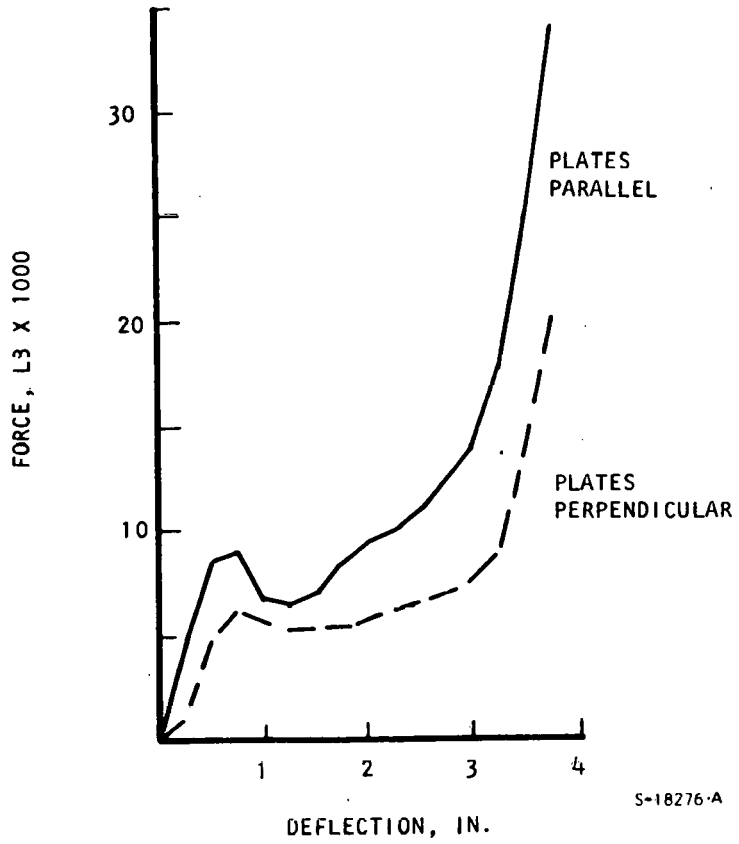


Figure 118. Single-Battery Static Crush Test Results

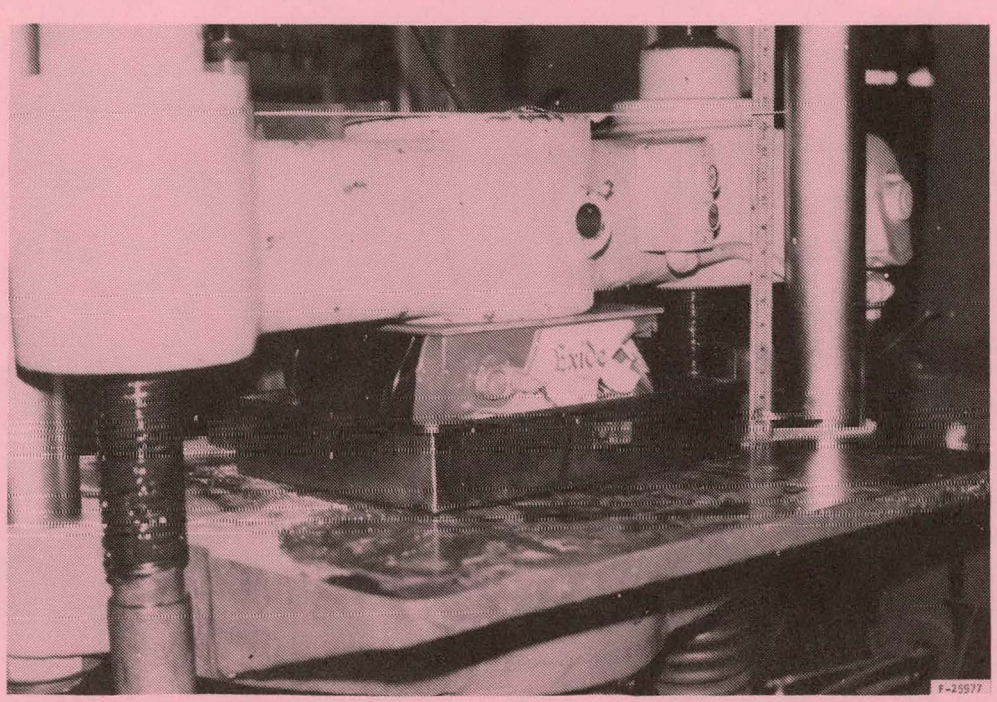

Figure 119. Static Crush Parallel to Battery Plates

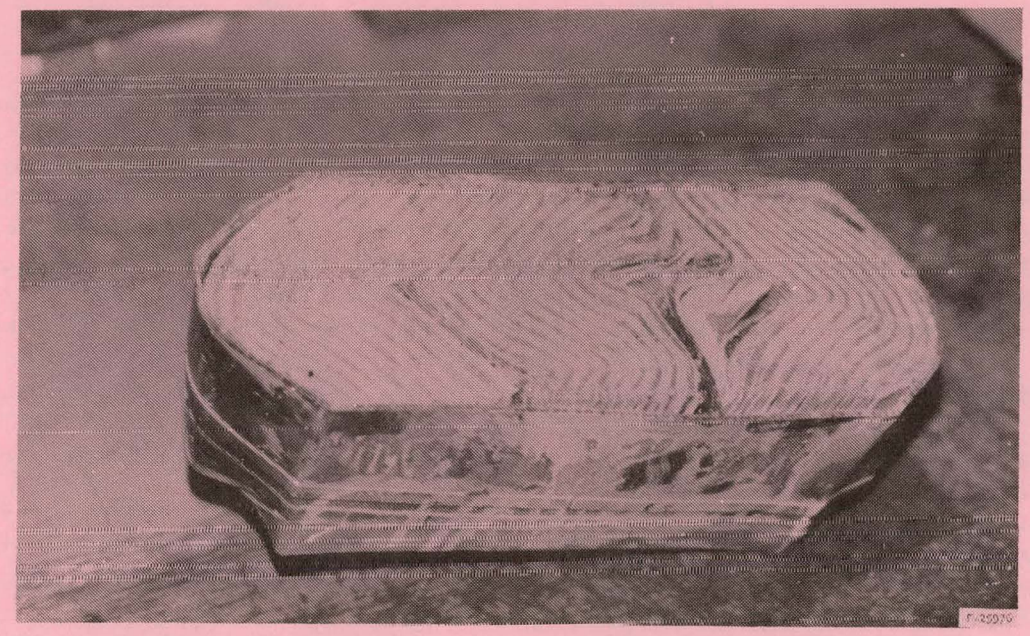

Figure 120. Test Results for Static Crush Parallel to Battery Plates

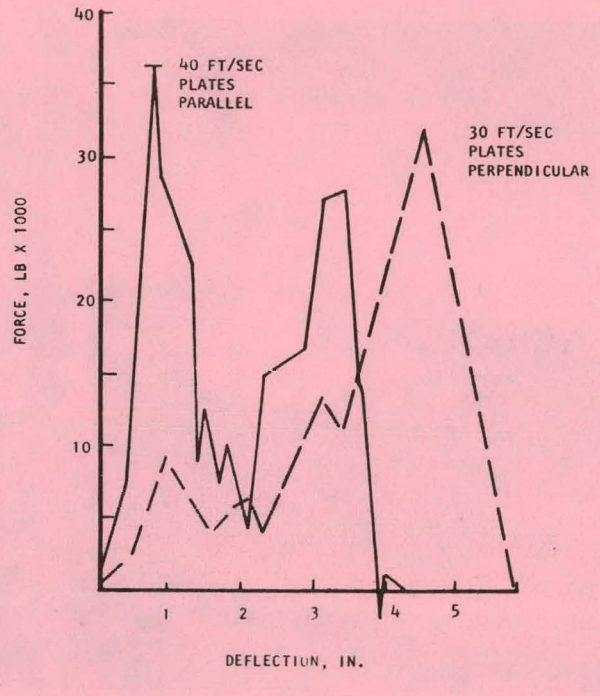


Figure 121. Single-Battery Dynamic Crush Force Characteristics

Based on these results and packaging considerations in the vehicle tunnel structure, the decision was made to orient the battery with the plates perpendicular to the frontal-barrier crash direction.

Battery Tunnel Crush Tests

The next step in battery testing was to determine what type of column effects and overall crush distances would be encountered with the long row of batteries. To accomplish this a full-scale, battery-tunnel structure was constructed of fiberglass-reinforced polyester. The tunnel was designed to accommodate a single row of 11 Exide EV-106 batteries. The batteries were filled with a water-salt solution to simulate specific gravity of the acid. The tunnel was then impact-tested on the crash-tower facility (Figure 122) at a speed of 30 mph. Figure 123 shows the tunnel after impacting. The simulated firewall was positioned 33 in. from the front of the tunnel. As shown in the figure, the tunnel structure was undamaged in the area of the passenger compartment. There would have been, therefore, no acid spillage or intrusion into that area. The battery-column crush distance was measured to be somewhat in excess of 20 in.

Upon removal of the batteries, it was noted that the first five batteries were crushed, and the next four batteries were intact. The crush-force-characteristic results are shown in Figure 124. With the exception of the high initial peak that is attributable to the battery stack, the results were approximately as anticipated, demonstrating that the battery configuration was a feasible approach from an energy-management standpoint. The aggressiveness of

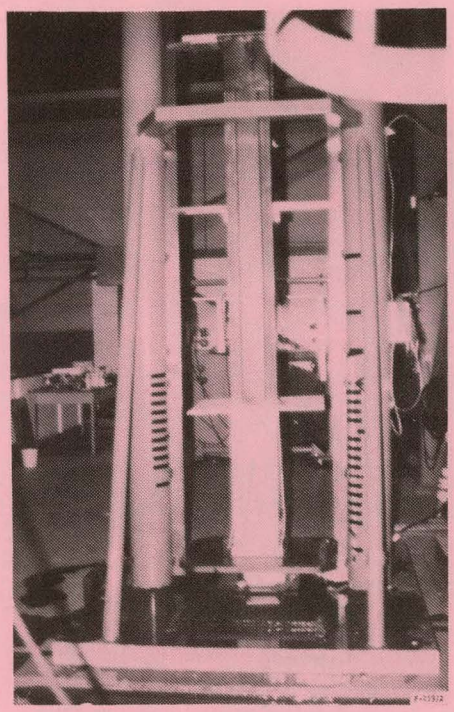

Figure 122. Battery Tunnel Crush Test

Figure 123. Battery Tunnel Crush Test Results

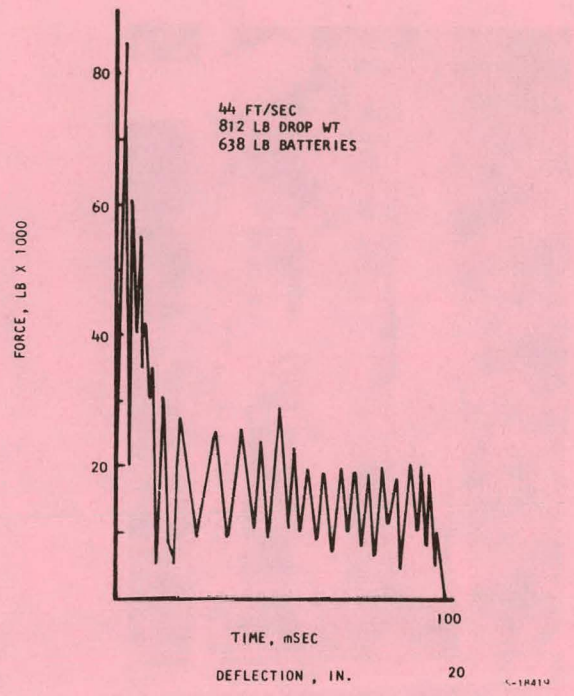


Figure 124. Battery Tunnel Crush Force Characteristics

the battery column will not exceed that of the rest of the front-end structure, and the batteries, when decoupled from the structure, will absorb their own kinetic energy.

The problem of the high peak force from the front end of the tunnel was next verified and then addressed. To verify the effect, a one-half-scale model of the tunnel front-end was constructed, as shown in Figure 125. The model was then drop-tested with the resulting peak phenomena once again observed, as shown in Figure 126.

The objective then was to provide a trigger mechanism in the forward section that would reduce the peak and provide for a controlled-crushing reaction. Three approaches were tested to obtain this effect. The first, as shown in Figure 127, was to provide lead-in slits in the front portion of the structure. This approach was unsuccessful, as illustrated in Figure 128, and can also be verified in the force-time history shown in Figure 129. The test specimen was half scale, so the average force level projected to the full-scale tunnel was 18,400 lb, as shown.

The next approach was to provide incremental slits in the stiff radius portion, as illustrated in Figure 130. The test configuration provided considerably improved results. A controlled, sequential crushing occurred at approximately the desired crush force (10,000 lb), as shown in Figure 131. While the configuration supplied the desired energy-management characteristics, concern over the performance of the slits in a fatigue environment initiated work on the third configuration.

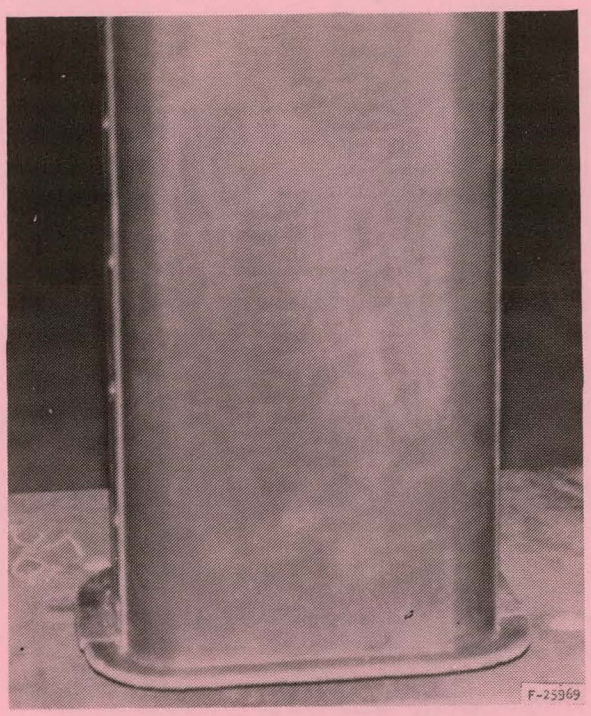


Figure 125. Half-Scale Model of Tunnel Front End

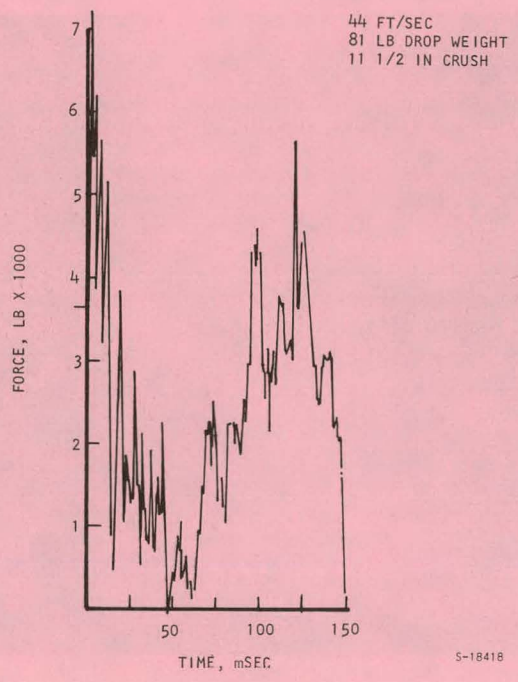


Figure 126. Half-Scale Tunnel Crush Force Characteristics

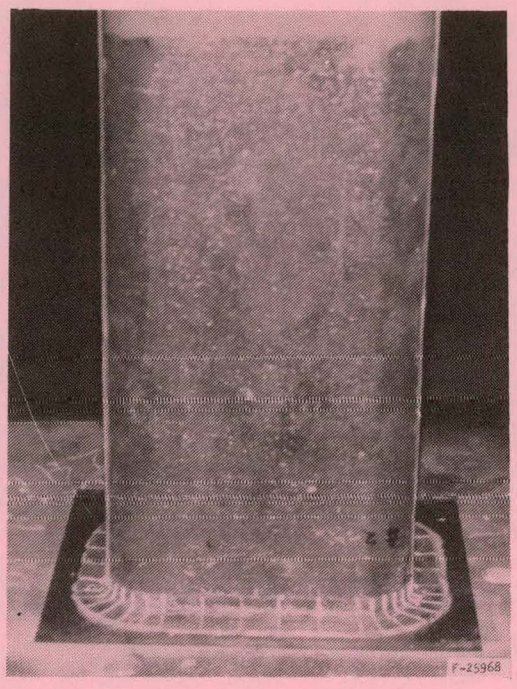


Figure 127. Battery Tunnel End-Slit Trigger Mechanism

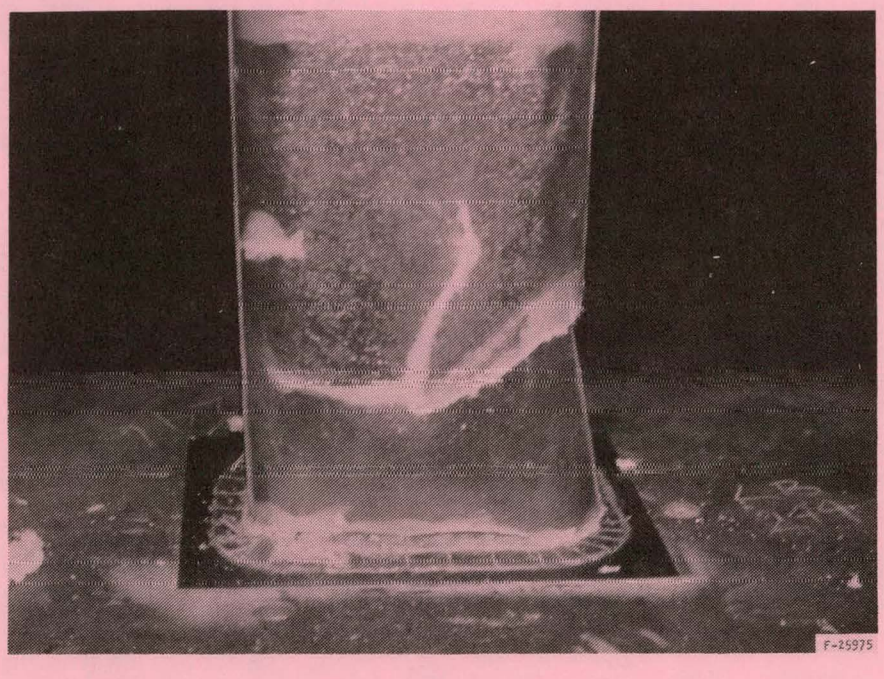


Figure 128. Battery Tunnel End-Slit Test Results

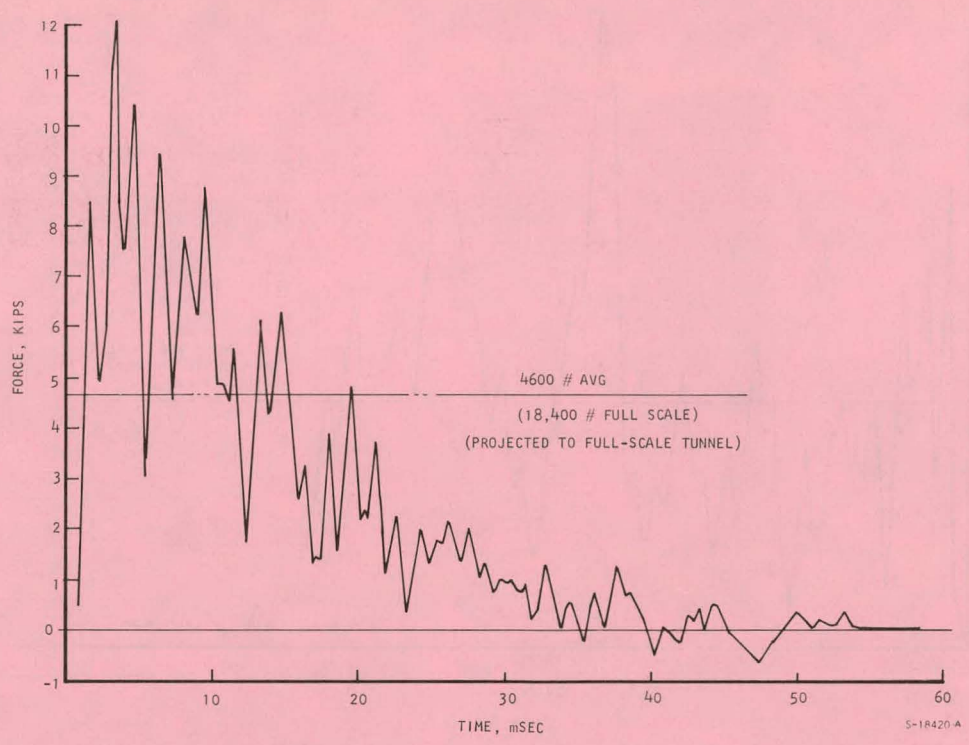


Figure 129. End-Slit Crush Force Characteristics

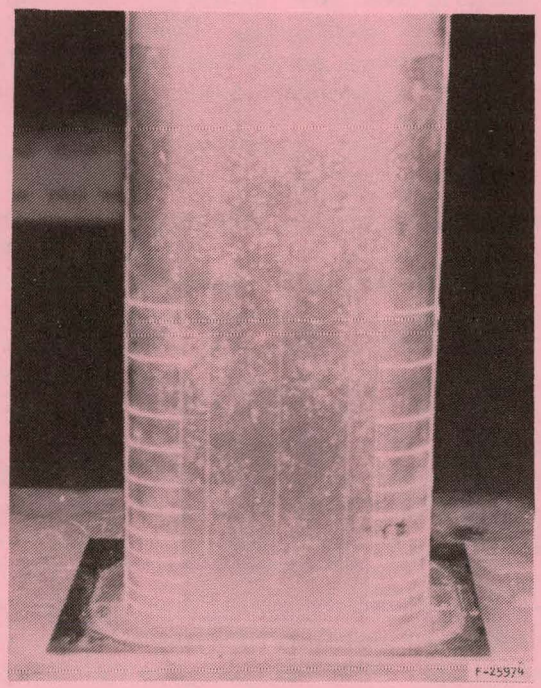


Figure 130. Trigger Mechanism - Incremental Slits

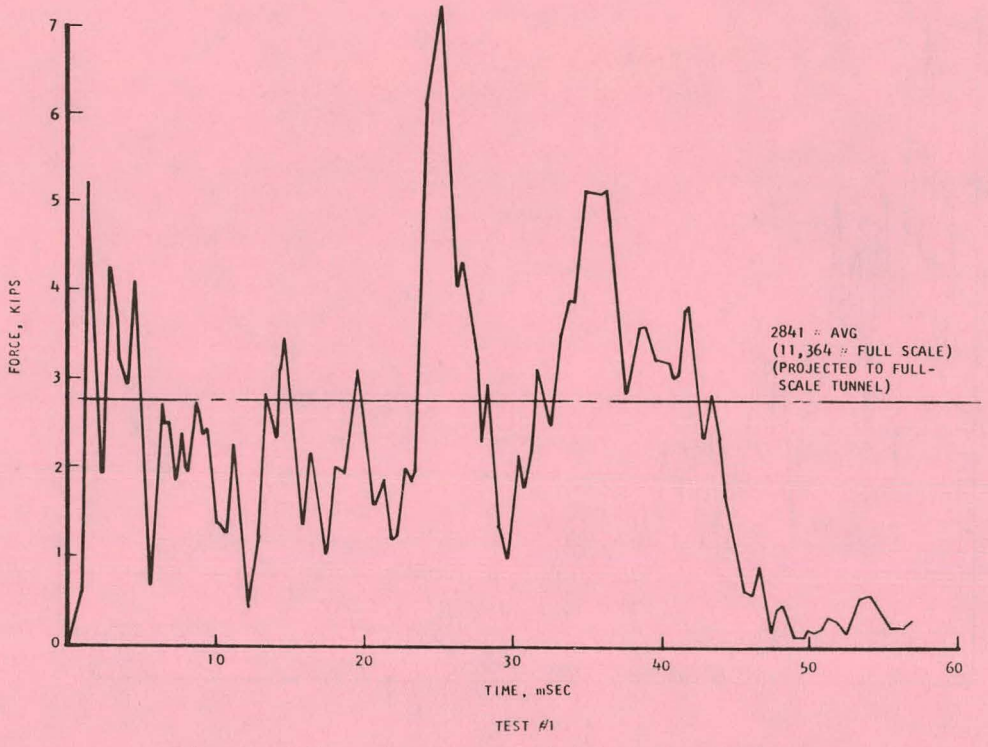


Figure 131. Incremental-Slit Crash Test

The third approach employed a corrugated front end, as illustrated in Figure 132. The test speciman was full scale. The results of the impact test on this element were also quite favorable. Controlled failure was observed once again, and the force levels were well within acceptable values. (see Figure 133). Consequently, this technique was chosen for the final design.

FRONT-END TESTS

Following the element tests on the battery tunnel and the energy absorber tubes, it was important to assemble the front-end structure and to determine how it behaved as a system. Three half-scale front-end models were built and tested. The first two front-end models were simplified and consisted of only the basic structural elements. The third model was more elaborate, including fenders, hood, cowl, A-post, toe board, and side sills.

The first model is shown in Figure 134. The model included the battery tunnel, energy-absorbing tubes, front bulkhead, and bumper system. The model also has a battery tray, shown in Figure 135, complete with motorcycle batteries and honeycomb material to simulate battery stiffness.

The initial front-end half-scale model was tested on November 4. An after-test photo of the model is shown in Figure 136. Failure was not as intended and was unsymmetrical. The battery tunnel buckled as opposed to crushing evenly. In addition, to provide the desired force/deceleration characteristics, the model should have crushed about 12 in., but as shown, it crushed only 8 in.

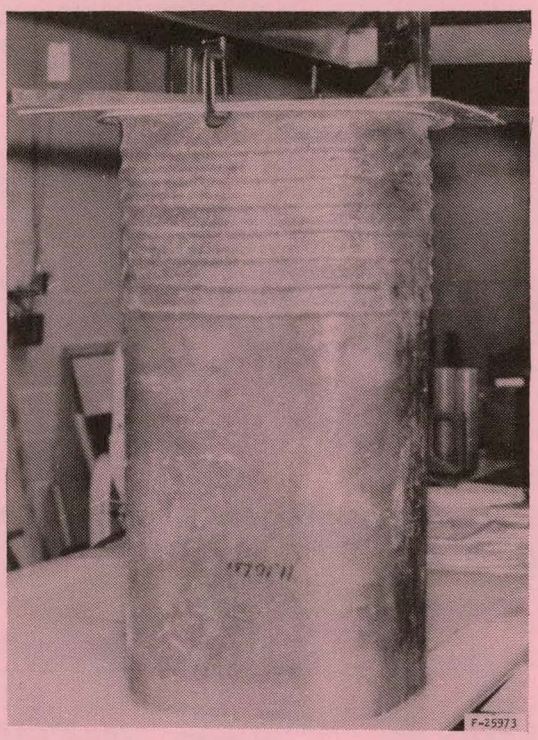


Figure 132. Corrugated End Trigger Mechanism

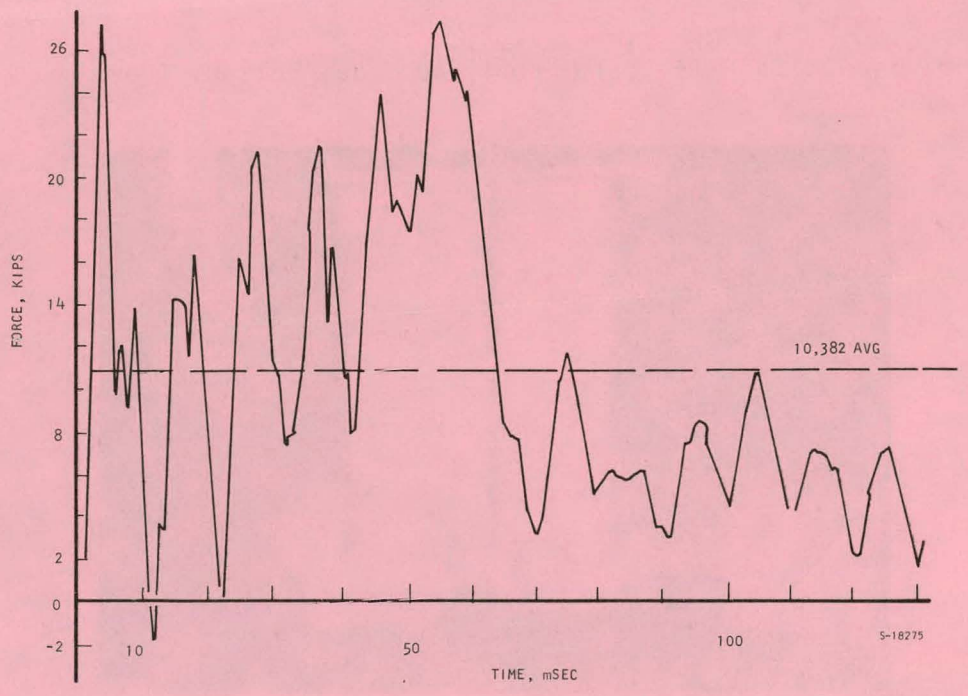


Figure 133. Corrugated End Crush Force Characteristics

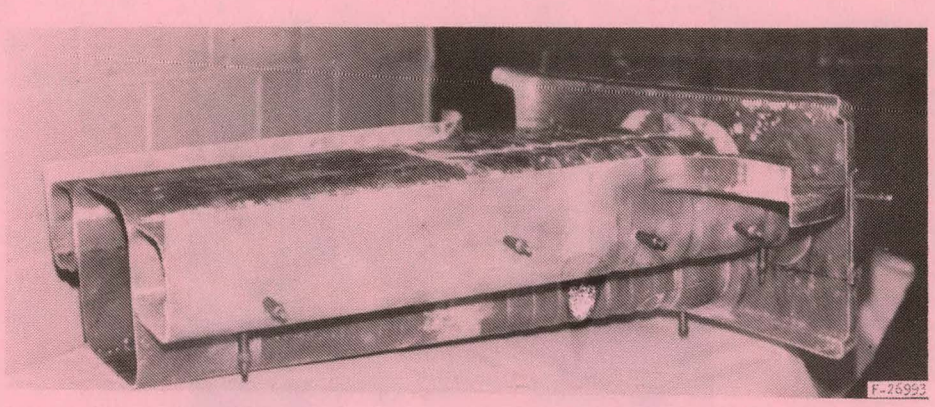

Figure 134. Half-Scale Front End Model

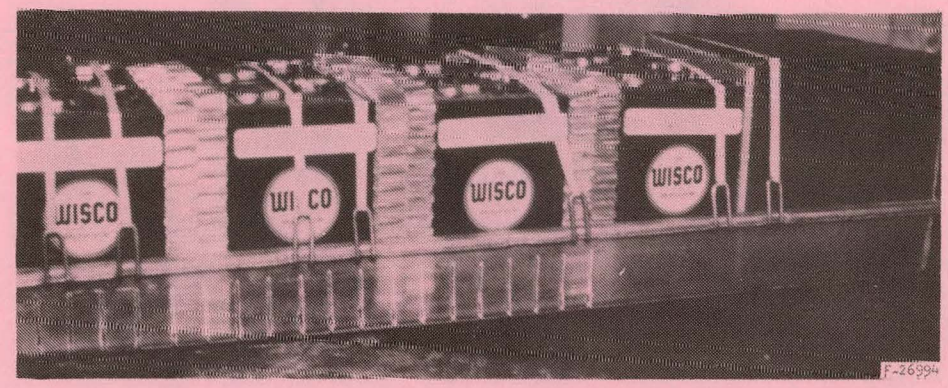


Figure 135. Half-Scale Front End Model Battery Tray

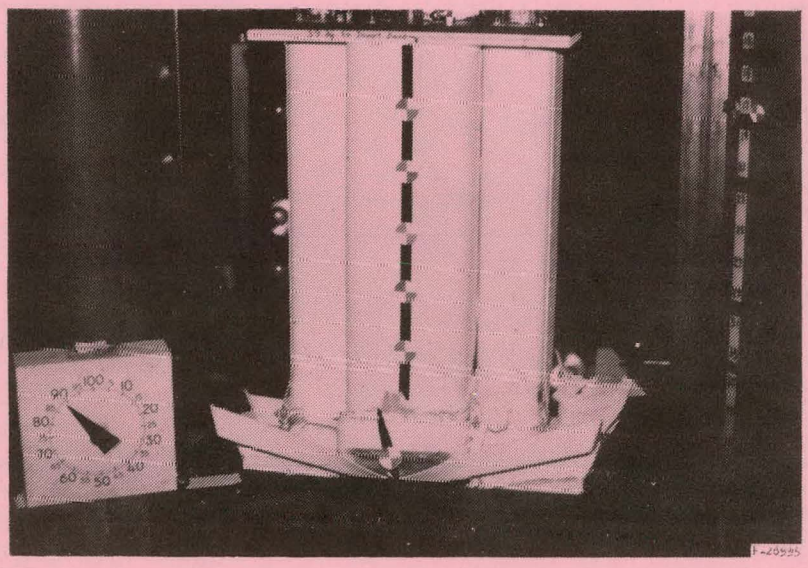

Figure 136. Half-Scale Front End Model Test Results

Examination of the test specimen and the film record after crash test revealed several reasons for the unexpected behavior. Due to the location and strength of the front bumper, the initial forces loaded the batteries and tunnel in an offset manner with respect to their centers. This applied a bending moment into the structure that is believed to have contributed significantly to the mode of failure. The off-center loading on the batteries caused them to fail in a different manner from the previously full-face loaded battery element tests. The net result was that the crush distance was greatly reduced on the battery pack, causing the structure to eventually bottom on the batteries.

In summary, from the first test model, it was learned that:

(a) The center section of front bumper beam must be a reduced-strength element such as a low-density foam with facia panel to avoid the off-center loading of the batteries.

(b) The side bumper elements must be tailored to meet the 5-mph criterion and to fail at approximately 10 mph to alleviate the off-center loading of the overall structure.

(c) The eccentricity of the corrugations in the first few inches of the frontal structure should be increased to reduce aggressiveness.

The three changes described above were incorporated into the second front-end model. A photo taken after its drop test shows that the front end crushed in a satisfactory manner; the desired crush distance was increased to over 10 in. Data taken from the test are presented in Figures 137, 138, and 139.

Peak deceleration is about 70 g; there was no bottoming of the batteries on the structure, and the force-displacement characteristics of the tunnel and the energy absorbers were as predicted. Force numbers shown have been projected to full scale.

The following numerical example shows how close test results from model 2 came to predictions.

| | |
|---|---|
| Vehicle kinetic energy at 30 mph with 2 passengers (less batteries), ft-lb | 63,400 |
| Average force for 2-ft crush, lb | 31,700 |
| Average force for structural elements, lb | |
| Tunnel | 8,944 |
| Absorbers | 23,218 |
| | 32,162 |

Thus, the test average force was only 0.5 percent higher than predicted. This does not mean that all future models and NTEVs will be within this precision, but it does indicate that the basic mechanisms and techniques used in the NTEV energy management are effective, understood, and predictable.

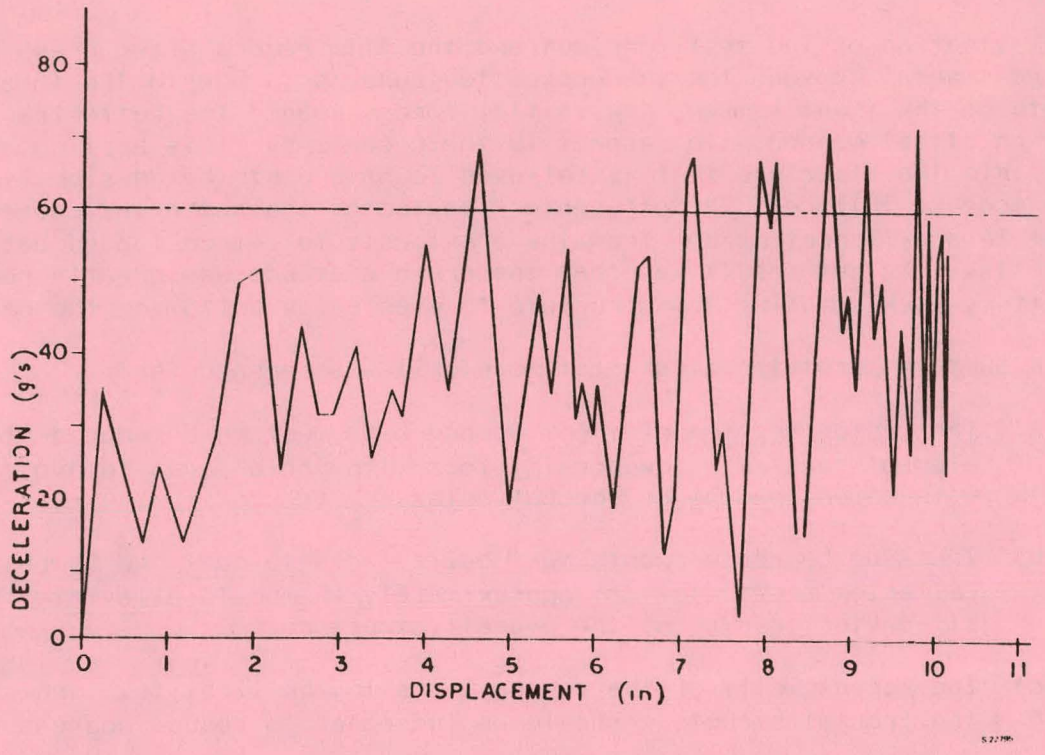


Figure 137. Half-Scale Front End Model 2 Deceleration vs Displacement

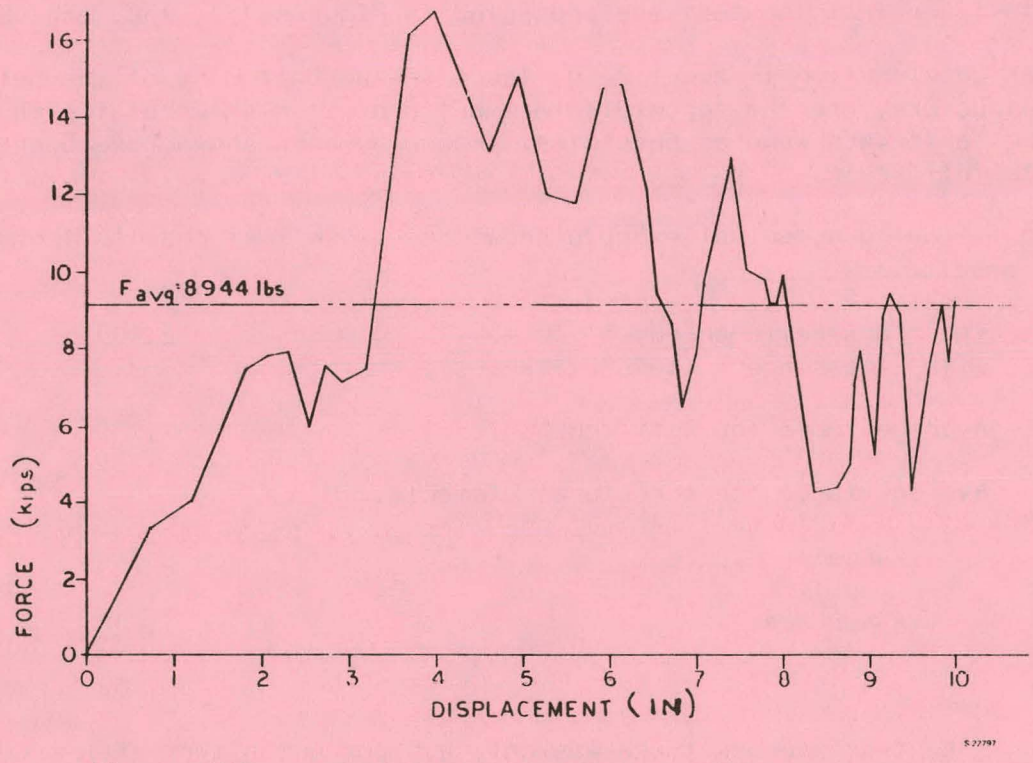


Figure 138. Half-Scale Front End Model 2 Tunnel Force vs Displacement

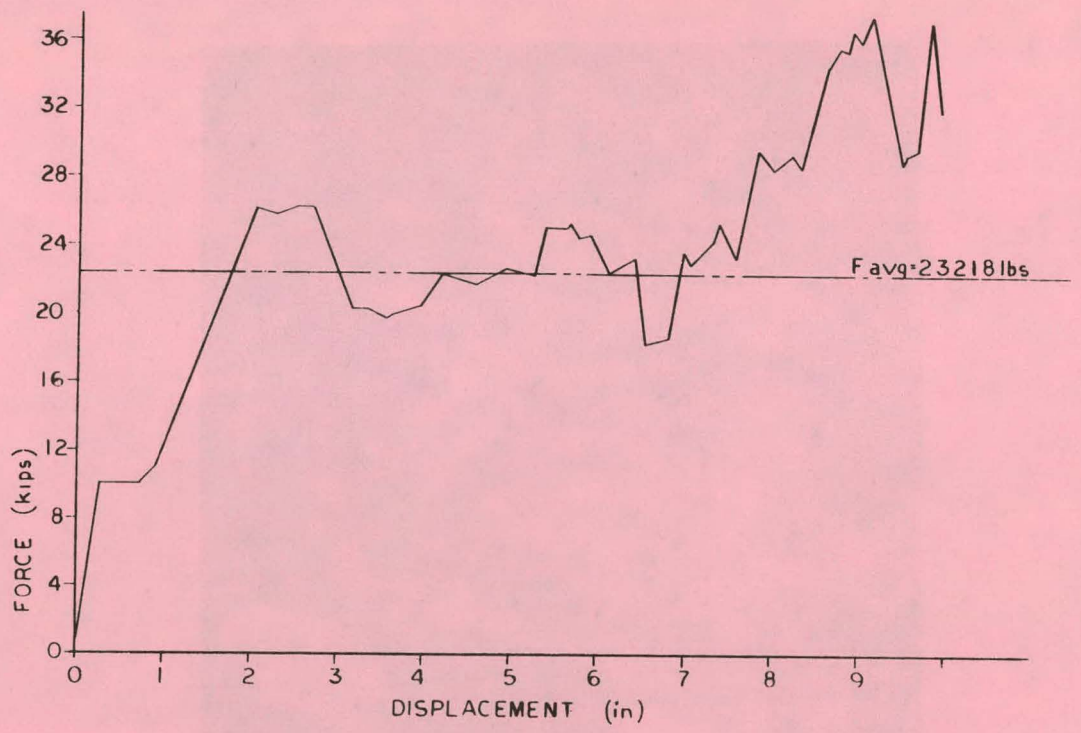


Figure 139. Half-Scale Front End Model 2 Energy Absorber Force vs Displacement

The third half-scale front-end model was much more elaborate and detailed. Figure 140 shows the front of the unit and the cowl, wheel houses, energy absorbers, and bumper system. The model has a battery tray and motorcycle batteries. Figure 141 is the interior of the model and shows the tunnel, A-posts, seat riser, and toe board.

Before-and-after test photos of model 3 are shown in Figures 142 and 143. Formal numerical results are not yet available at this writing, but the preliminary test results and the slow-motion film record indicated that the desired crush distance of 12 in. was obtained; all elements failed in a controllable manner as intended; there was no off-center loading or battery bottoming; and above all, the passenger compartment remained intact with almost no distortion and no fluid leakage. The test was a complete success and the crash management design concept was verified.

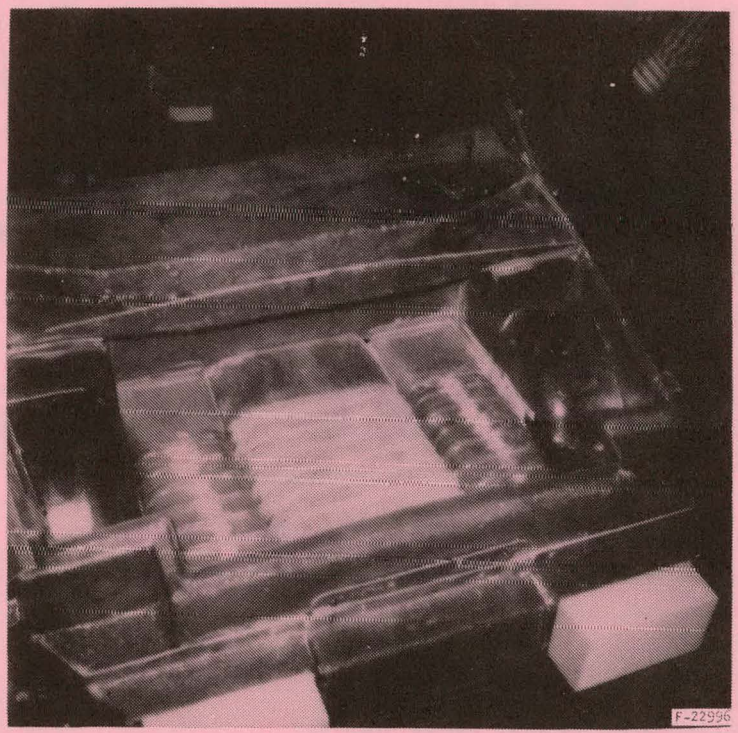


Figure 140. Half-Scale Front End Model 3 Front View

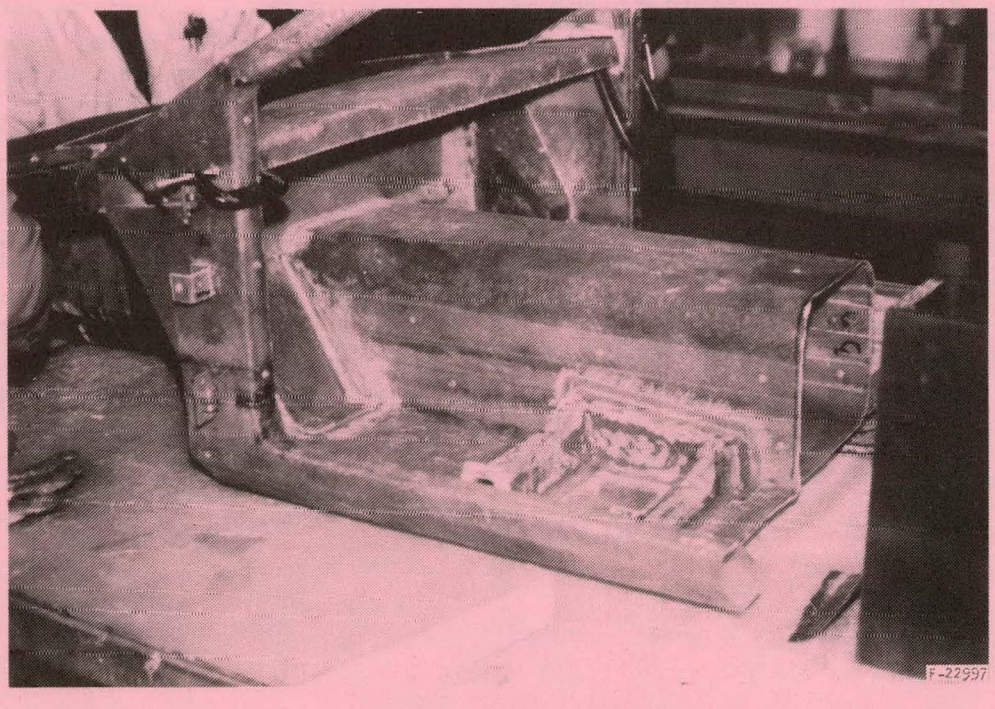


Figure 141. Half-Scale Front End Model 3 Passenger Compartment View

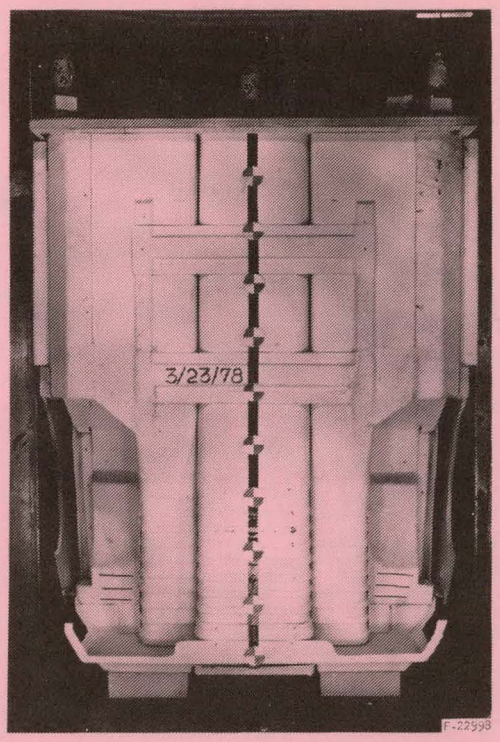


Figure 142. Half-Scale Front End Model 3 Before Crash Test

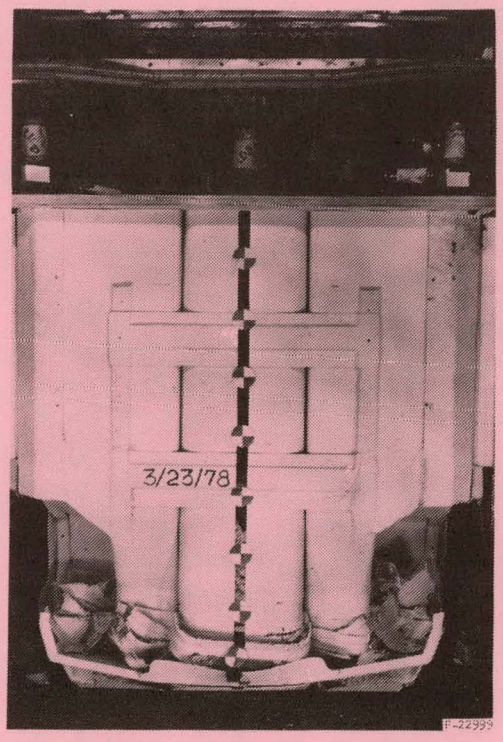


Figure 143. Half-Scale Front End Model 3 After Crash Test

# SECTION 9

# STRUCTURAL ANALYSIS

SECTION 9

# STRUCTURAL ANALYSIS

The usefulness of the finite-element method in vehicle structural design has been well established. Besides the economy of solutions and quality and quantity of results, the speed at which the various design changes can be evaluated accurately has helped to confirm the superiority of the technique. For the NTEV, finite-element analysis effort is being pursued by the Budd Company and AiResearch; static loads are being studied by the Budd Company, and dynamic-response analysis is being conducted by AiResearch.

## STATIC ANALYSIS

The structure of the electric vehicle has been modeled, using the beam and panel elements, as shown in Figure 144. Except for the location of the power unit, the vehicle is symmetrical about the longitudinal axis. Consequently, only one-half of the structure need be considered in the analysis. The effect of various bending and torsion loadings is examined by varying the boundary conditions along the plane of symmetry. The static response of the vehicle is being examined under the loading conditions discussed in the following paragraphs.

### Vertical Load

A 3.0-g vertical load, acting on the structure, has been simulated as a vertically applied loading condition. The weight of the batteries is distributed along the tunnel, and the passenger weights are applied at the front- and rear-seat locations. The weight of the power unit, acting at the rear, also has been included. The deformation of the structure under this loading condition is shown in Figure 145. For the analysis, the structure was supported at the top of the front- and rear-wheel housings. Under this loading condition, the maximum deflection of 0.091 in. occurs in the tunnel. The side sill in the door opening deflects 0.039 in. The maximum stresses occurred at the front shock tower designated as Area 3. The locations and magnitudes of these stresses are shown in Figure 146. Fatigue load is 3.0 g while 6.0 g is for the ultimate condition.

### Torsional Rigidity

The purpose of the torsional loading condition is to evalute the torsional rigidity of the vehicle. For this loading condition, the rear end of the vehicle is held rigid, while the front end is twisted. The result is shown in Figure 147.

### Front-End Crash Load

A 6.0-g end load is applied to the front energy-management area of the structure to study its deformation and determine how the load is distributed into the structure ahead of the passenger compartment.

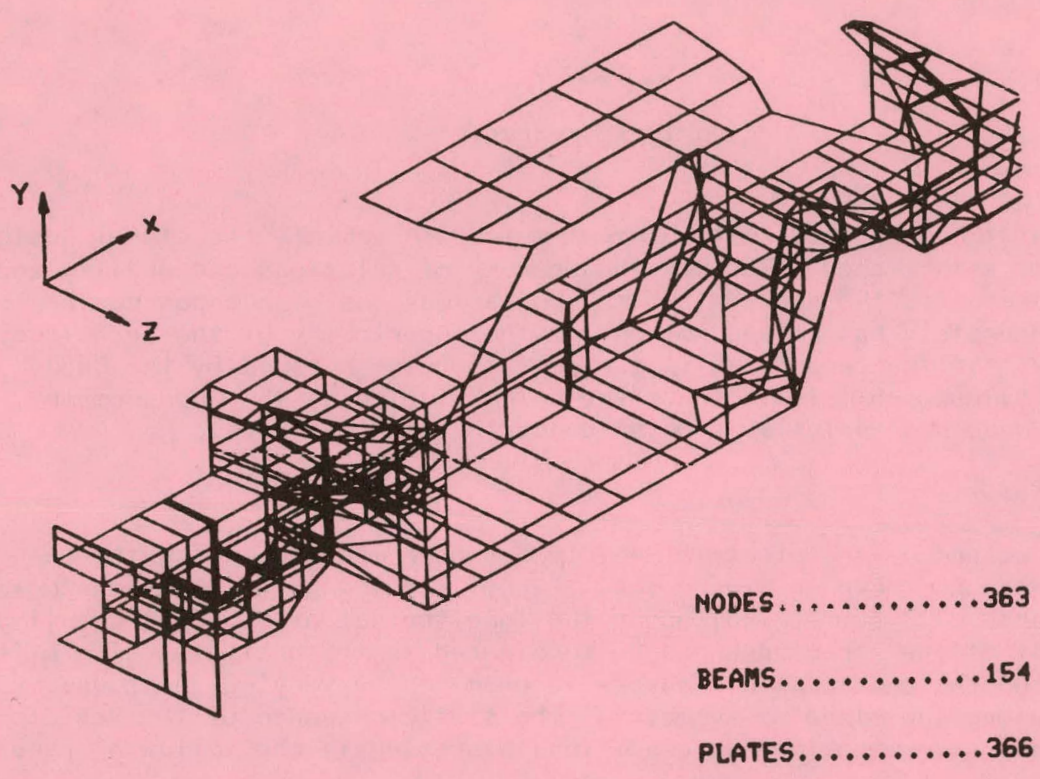


Figure 144. Finite-Element Static Analysis Model

S.22790

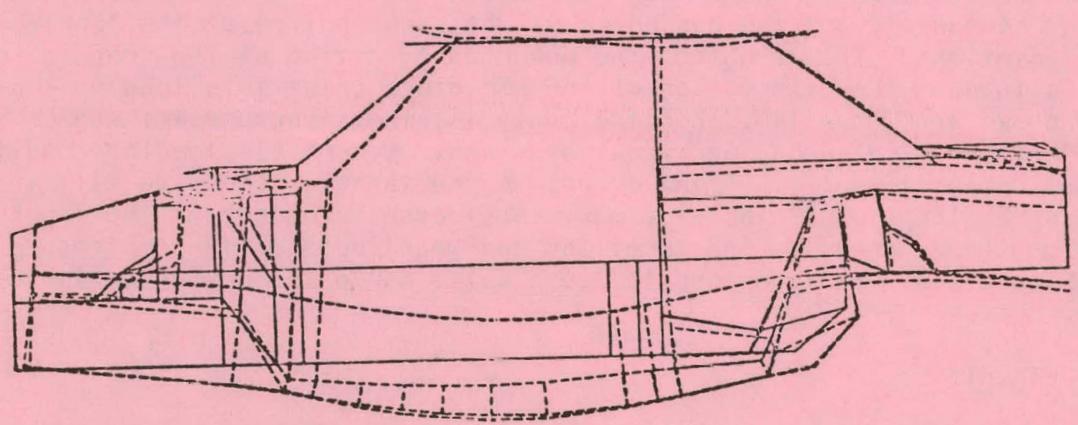

**MAXIMUM DEFLECTIONS**

| | |
|---|---|
| **SIDE SILL** | **0.039 IN.** |
| **TUNNEL** | **0.091 IN.** |
| **REAR SILL** | **0.023 IN.** |

S.23003

Figure 145. Finite-Element Static Analysis--Deflection Under 3.0-g Vertical Load

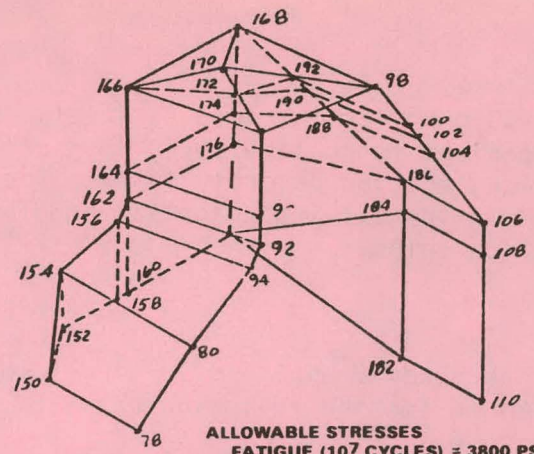


**ALLOWABLE STRESSES**
**FATIGUE ($10^7$ CYCLES) = 3800 PSI**
**ULTIMATE 25,000 PSI**

| | PANEL 164-172 | BEAM 166-170 | BEAM 88-170 | BEAM 170-98 | BEAM 170-168 |
|---|---|---|---|---|---|
| LOAD | STRESS | STRESS | STRESS | STRESS | STRESS |
| 3 G | 1040 | 2370 | 1255 | 1370 | 2225 |
| 6 G | 2080 | 4740 | 2510 | 2740 | 4450 |

S 27783

Figure 146. Finite-Element Static Analysis - Locations and Magnitudes of Maximum Stresses Due to 3.0-g and 6.0-g Vertical Loads

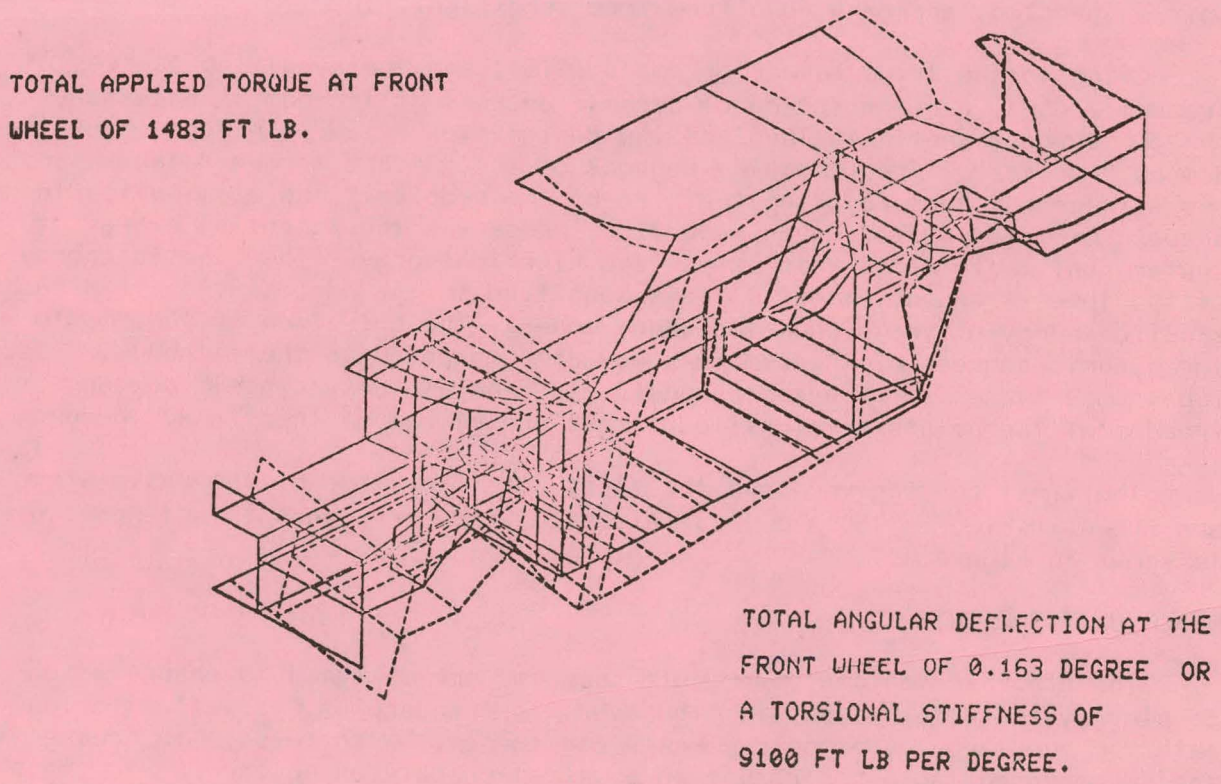


Figure 147. Electric Vehicle Static Torsional Mode

Rear-End Crash Load

The purpose of a 6.0-g horizontal load is to simulate the rear impact on the vehicle. It is important to realize that, in practice, such a peak load is of very short duration, and the severity is localized; however, the static analysis will be useful in identifying potential problems in the rear structure and load-distribution paths.

DYNAMIC ANALYSIS

The objective of the dynamic analysis is to obtain the bending and torsional modes of the vehicle for the following cases:

(a) A stripped vehicle, containing only the structural elements.

(b) A completely loaded vehicle, including doors, hood, and windshield.

The procedure of the finite-element dynamic analysis of the vehicle is outlined in Figure 148. The finite-element model used for the dynamic analysis is nearly identical to the one used for the static analysis, and is shown in Figure 149. Once again, the whole structure is assumed to be symmetrical about the center-plane, and the analysis is divided into a symmetric and antisymmetric case of the half-structure. The battery weights are distributed as lumped masses along the length of the tunnel. The weights of the passengers and the power unit are also included in the model as lumped masses, attached at appropriate locations. The dynamic model of the vehicle is supported on a soft suspension, approaching a free-free condition.

Owing to the large number of nodes (276), and the resulting degrees of freedom (1656), a condensation of dynamic degrees of freedom is necessary. The procedure essentially involves the designation of certain degrees of freedom as "masters". The remaining degrees of freedom are termed "slaves" and are eliminated, thus reducing the size of the problem. The elimination technique, sometimes called Guyan reduction, preserves the potential energy of the system, but modifies to some extent the kinetic energy. The kinetic energy of the lower-frequency modes is less sensitive to the condensation than the kinetic energy of the higher-frequency modes. The selection of the "masters" for dynamic degrees of freedom is somewhat comparable to the method of selecting lumped masses for a dynamic model. In general, only dynamic degrees of freedom at the points of significant mass and moment of inertia are needed.

The first bending mode and the first torsional mode of the basic structure are shown in Figures 150 and 151. A vehicle body frequency interference diagram is shown in Figure 152.

POWER UNIT SUPPORTS

The electric vehicle power unit supports are designed to ensure an uncoupled system with respect to other vehicle frequencies, as well as a load path for the large gyroscopic moments and forces. With respect to frequencies, the recommended isolators result in a vibration between 10 and 20 Hz. This avoids coupling with the vehicle suspension (2 to 3 Hz) and the anticipated

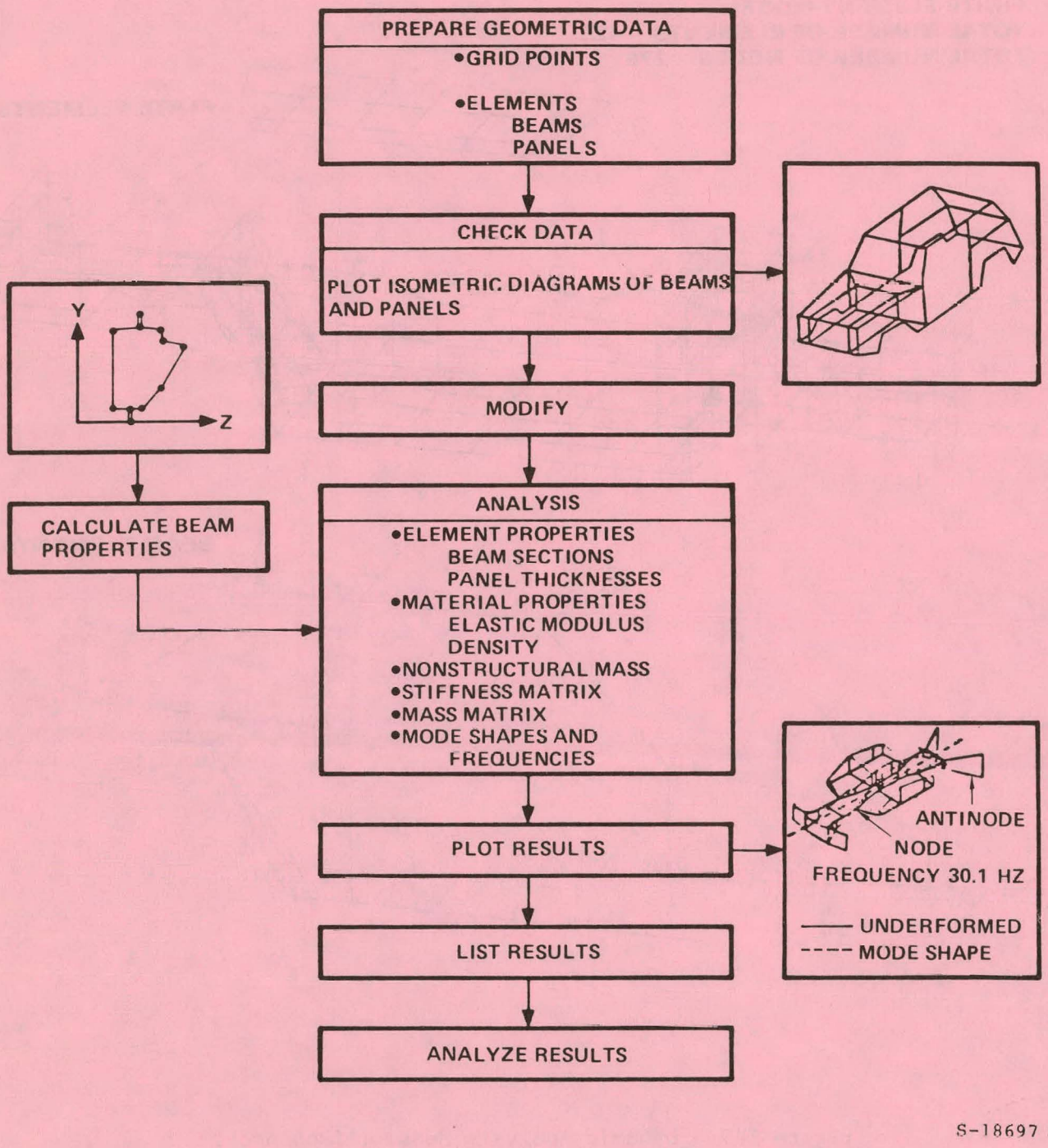


Figure 148. Flow Diagram - Finite Element Dynamic Analysis

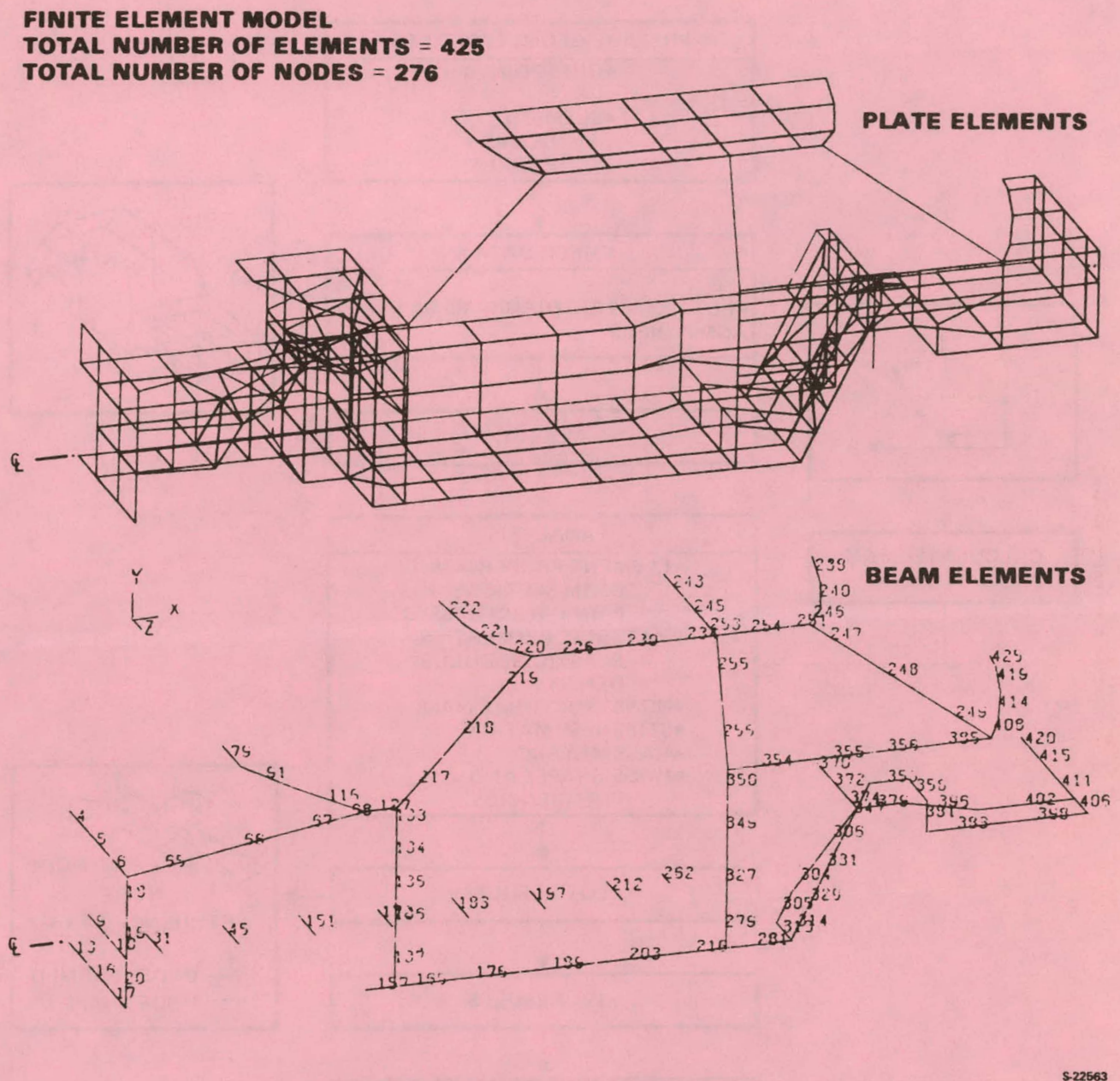


Figure 149. Dynamic Analysis Model (AiResearch)

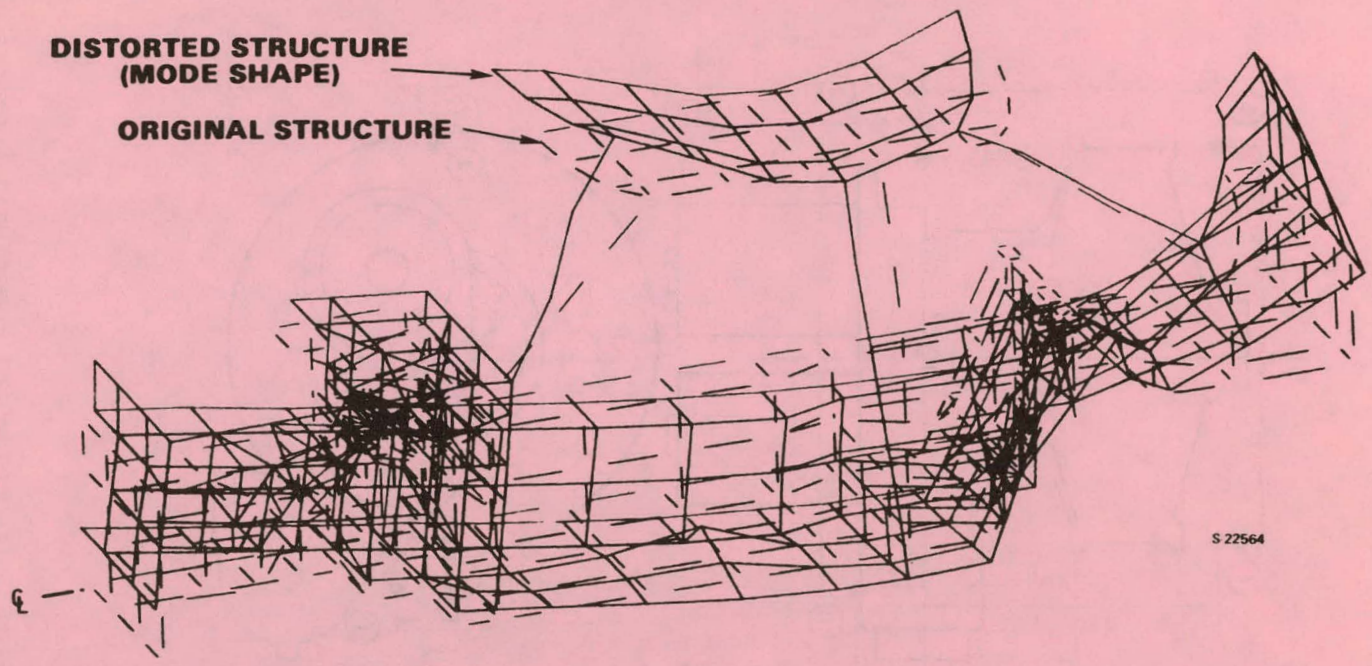


Figure 150. Dynamic Results--First Bending Mode
(Frequency = 16.077 Hz)

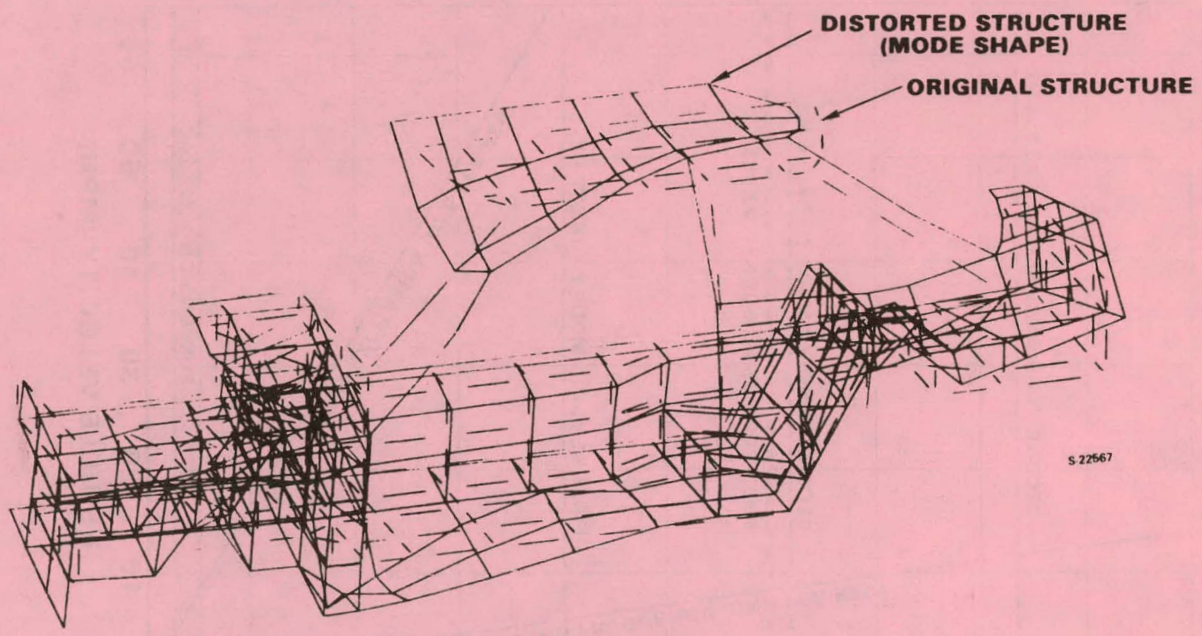


Figure 151. Dynamic Results--First Torsion Mode
(Frequency = 23.893 Hz)

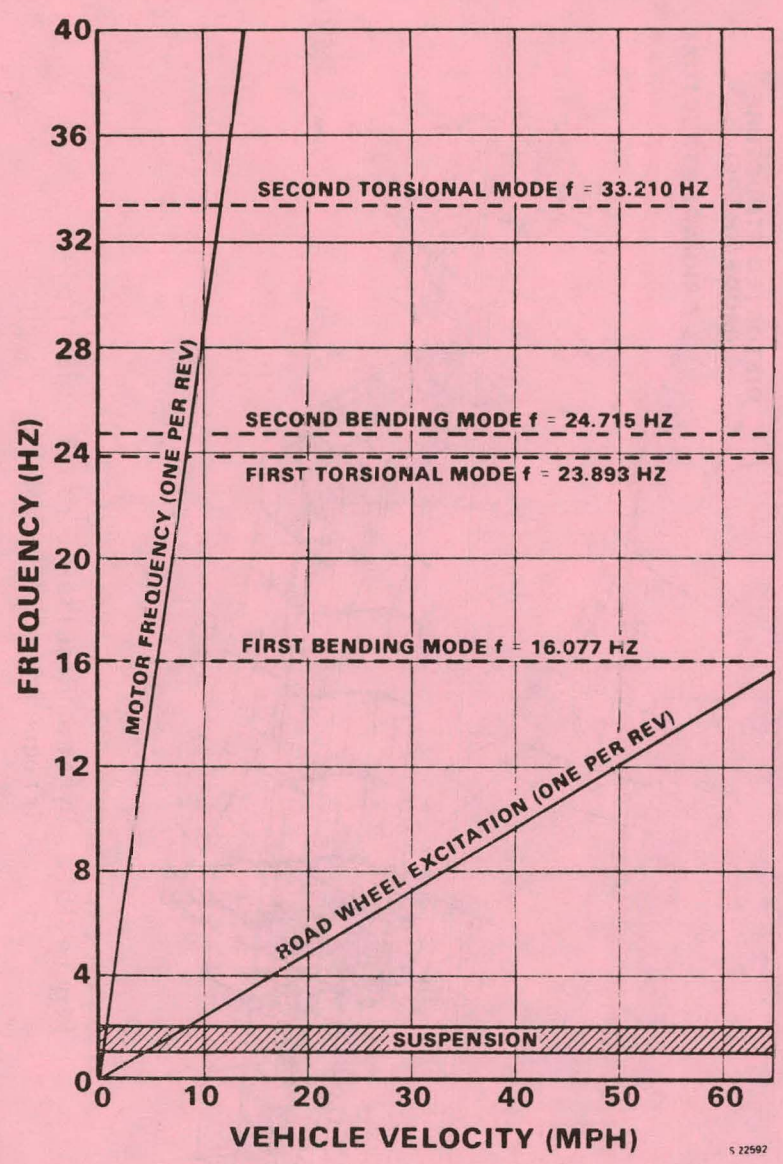


Figure 152. Vehicle Body Frequency Interference Diagram

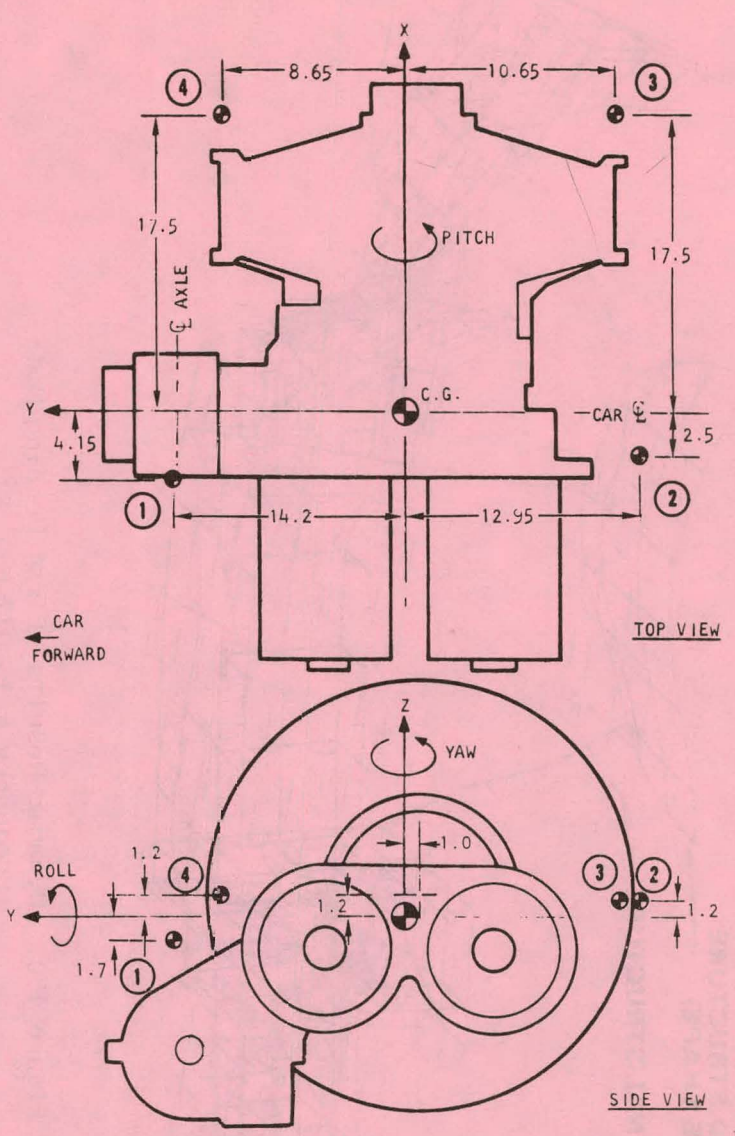


Figure 153. Location of Power Unit Supports

vehicle local mount structure first-mode frequency of 30 Hz. Large loads and deflections are minimized by locating the supports as far away from the power unit center of gravity as possible. The present locations result in a maximum load of 1057 lb and an un-snubbed displacement of 0.876 in. for the limit-load condition of 1.42 radians per second yaw. The snubbing effect of the mounts will limit this deflection to less than 0.5 in.

Support Geometry

The locations of the supports (numbered 1 through 4) are shown in Figure 153. The center of gravity of the unit is assumed as the coordinate system origin, and it lies on the centerline of the vehicle; however, the center of gravity does not lie on the rotational axis of the flywheel, being slightly forward and below. Also shown in the figure are the pitch, roll, and yaw axes with respect to the vehicle body.

Loads

The loads shown in Table 29 are given with respect to the power unit's coordinate system. The limit load condition was used to determine reaction for this analysis.

TABLE 29

POWER UNIT PRELIMINARY LOAD FACTORS

| Load | Y g | X g | Z g | Roll rad/sec | Pitch rad/sec | Yaw rad/sec |
|---|---|---|---|---|---|---|
| Design | 1.0 | 0.7 | 2.0 | 0.3 | 0.3 | 0.5 |
| Limit | 6.0 | 2.5 | 3.0 | 0.6 | 0.6 | 1.42 |
| Crash | 10. | 10. | 10. | 6.0 | - | 6.0 |

NOTE 1. All loads and rates assumed to be applied independently for preliminary analysis.

2. An additional lg vertical, static, downward load was applied in all above cases.

$M_{GYRO} = 2030\ \Omega$ ft-lb

where $\Omega$ is the roll or yaw angular velocity in rad/sec

Isolators

The isolators considered for this application are Barry Mount series 507. These meet the stiffness and load requirements and are available as off-the-shel

items. They are also available with snubber washers which minimize the deflection. The isolator characteristics are as follows:

| Mount Number | Stiffness KX = KY = KZ, lb/in. |
|---|---|
| 1 and 2 | 2300 |
| 3 and 4 | 1000 |

Method of Analysis

To eliminate strong model coupling, a computer program was developed to compute the required isolator stiffness for an uncoupled system, given a specific set of support locations. Standard isolators, which closely resemble the required stiffness, were used in a computer program developed to compute support loads and natural frequencies of a rigid body mounted on a redundant spring suspension. The program includes the gyroscopic effect of the flywheel in computing the support reactions, but it does not include the gyroscopic stiffening in computing the natural frequencies. The gyroscopic effects on the natural frequencies have been calculated and added to the frequency summary.

Natural Frequencies

Table 30 summarizes the natural frequencies and mode shapes. It should be noted that the gyroscopic effects are calculated from an equation that assumes an uncoupled system. The mode shapes indicate coupling in the YY and ZZ directions. Thus the values representing the gyroscopic effect are an upper limit. The actual frequency is somewhere between the two.

TABLE 30

FREQUENCY SUMMARY

| Natural Frequency (Hz) | | 8.7 | 11.3 | 11.8 | 12.5 | 15.5 | 18.4 |
|---|---|---|---|---|---|---|---|
| With Gyro Effects | | 23.0 | -- | -- | -- | 26.0 | -- |
| Mode shape (Motion of CG) | X | 0.006 | 0.038 | 0.997 | 0.067 | 0.036 | 0.013 |
| | Y | 0.087 | 0.994 | 0.044 | 0.094 | 0.963 | 0.260 |
| | Z | 0.982 | 0.095 | 0.063 | 0.992 | 0.104 | 0.018 |
| | XY | 0.020 | 0.0 | 0.0 | 0.007 | 0.038 | 0.962 |
| | YY | 0.151 | 0.002 | 0.0 | 0.043 | 0.028 | 0.051 |
| | ZZ | 0.015 | 0.026 | 0.0 | 0.005 | 0.241 | 0.063 |

## Deflections of Supports

The deflections at the supports are due to the limit load condition. Limit load displacements are tabulated in Table 31. No consideration has been given to snubbing, which is available on the isolators. The installation will include deflection-limiting devices.

## Support Reactions

The support reactions are based on the limit load condition. Gyroscopic effects of the flywheel due to vehicle motions have been included. The limit load reactions are tabulated in Table 32.

## CRASHWORTHINESS ANALYSIS

The vehicle structure is being designed to meet the current Federal Motor Vehicle Safety Standards. Applicable standards, related to structures, are tabulated below.

FMVSS 204, Steering column rearward displacement

FMVSS 208, Occupant protection

FMVSS 214, Sidedoor strength

FMVSS 215, Exterior protection

FMVSS 216, Roof crush resistance

FMVSS 301, Fuel system integrity

A computer-simulation study was performed in the preliminary design phase to provide design guidance in occupant and structural crashworthiness for the electric vehicle. The study determines load paths and stiffness capable of absorbing the energy of a 30-mph, flat-barrier, front impact. Side impact and rear impact have also been investigated. The initial curb weight of 2386 lb was used in the study.

A lumped-parameter, nonlinear-spring, planar, computer code was developed to obtain the structural dynamic response of a modeled representation of the vehicle. The mathematical idealization of the front, side, and rear-impact models is illustrated in Figures 154, 155, and 156. The batteries are located along the vehicle centerline, and are decoupled from the vehicle structure longitudinally.

Motion is limited to the planar attitude only. Springs have nonlinear characteristics, reversal, hysteresis, and viscous damping characteristics. Damping is assumed to be zero in the present simulations. Based on the classical rigid-body-dynamics theory, the equations of motion are generated internally in the computer program through input descriptions. The program then integrates the equations of motion by an Adams-Moulton, variable-step, corrector-predictor routine.

TABLE 31

LIMIT LOAD DISPLACEMENTS

| Mount Number | Load Direction and Magnitude | Displacement in Inches (Unsnubbed) | | |
|---|---|---|---|---|
| | | X | Y | Z |
| 1 | Fx = 2.5 g | 0.175 | 0.001 | 0.002 |
| | Fy = 6.0 g | 0.070 | 0.459 | 0.008 |
| | Fz = 2.0 g | 0.005 | 0.001 | 0.166 |
| | Roll $\dot{\theta}y$ = 0.6 rad/sec | 0.124 | 0.063 | 0.003 |
| | Yaw $\dot{\psi}z$ = 1.42 rad/sec | 0.060 | 0.014 | 0.330 |
| | Torque Mx = 4000 in.-lb | 0.001 | 0.006 | 0.050 |
| 2 | Fx | 0.177 | 0.001 | 0.003 |
| | Fy | 0.066 | 0.450 | 0.001 |
| | Fz | 0.001 | 0.002 | 0.174 |
| | Roll | 0.116 | 0.050 | 0.015 |
| | Yaw | 0.013 | 0.024 | 0.386 |
| | Torque | 0.001 | 0.005 | 0.054 |
| 3 | Fx | 0.177 | 0.002 | 0.005 |
| | Fy | 0.054 | 0.349 | 0.013 |
| | Fz | 0.002 | 0.003 | 0.080 |
| | Roll | 0.095 | 0.130 | 0.015 |
| | Yaw | 0.021 | 0.044 | 0.770 |
| | Torque | 0.001 | 0.002 | 0.033 |
| 4 | Fx | 0.175 | 0.002 | 0.006 |
| | Fy | 0.044 | 0.349 | 0.009 |
| | Fz | 0.007 | 0.003 | 0.069 |
| | Roll | 0.078 | 0.130 | 0.026 |
| | Yaw | 0.087 | 0.044 | 0.876 |
| | Torque | 0.002 | 0.002 | 0.042 |

TABLE 32

LIMIT LOAD REACTIONS

| Mount Number | Load Direction and Magnitude | Reactions in Pounds | | |
|---|---|---|---|---|
| | | X | Y | Z |
| 1 | Fx = 2.5 g | 403 | 2 | 5 |
| | Fy = 6.0 g | 162 | 1057 | 19 |
| | Fz = 2.0 g | 11 | 2 | 381 |
| | Roll $\dot{\theta}y$ = 0.6 rad/sec | 284 | 145 | 6 |
| | Yaw $\psi z$ = 1.42 rad/sec | 138 | 32 | 759 |
| | Torque Mx = 4000 in.-lb | 2 | 14 | 115 |
| 2 | Fx | 408 | 1 | 6 |
| | Fy | 152 | 1036 | 3 |
| | Fz | 2 | 5 | 399 |
| | Roll | 267 | 114 | 34 |
| | Yaw | 30 | 56 | 887 |
| | Torque | 3 | 11 | 125 |
| 3 | Fx | 177 | 2 | 5 |
| | Fy | 54 | 348 | 13 |
| | Fz | 2 | 3 | 80 |
| | Roll | 95 | 130 | 15 |
| | Yaw | 21 | 44 | 770 |
| | Torque | 1 | 2 | 32 |
| 4 | Fx | 175 | 2 | 6 |
| | Fy | 44 | 348 | 9 |
| | Fz | 7 | 3 | 69 |
| | Roll | 78 | 130 | 25 |
| | Yaw | 87 | 44 | 876 |
| | Torque | 2 | 2 | 42 |

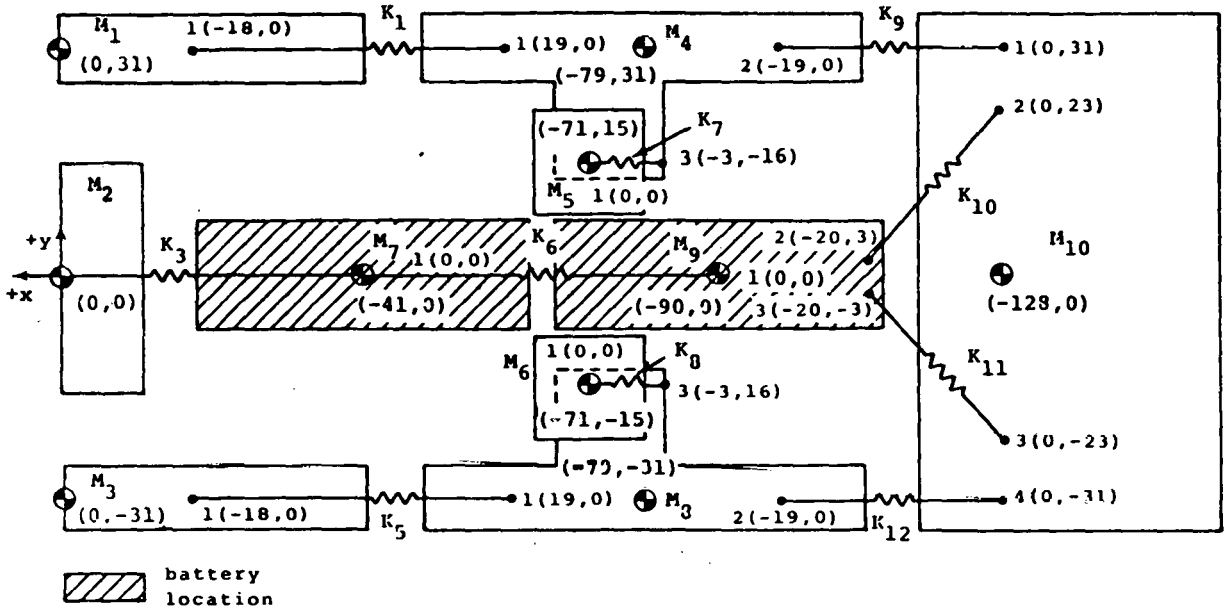


Figure 154. Frontal Impact Model

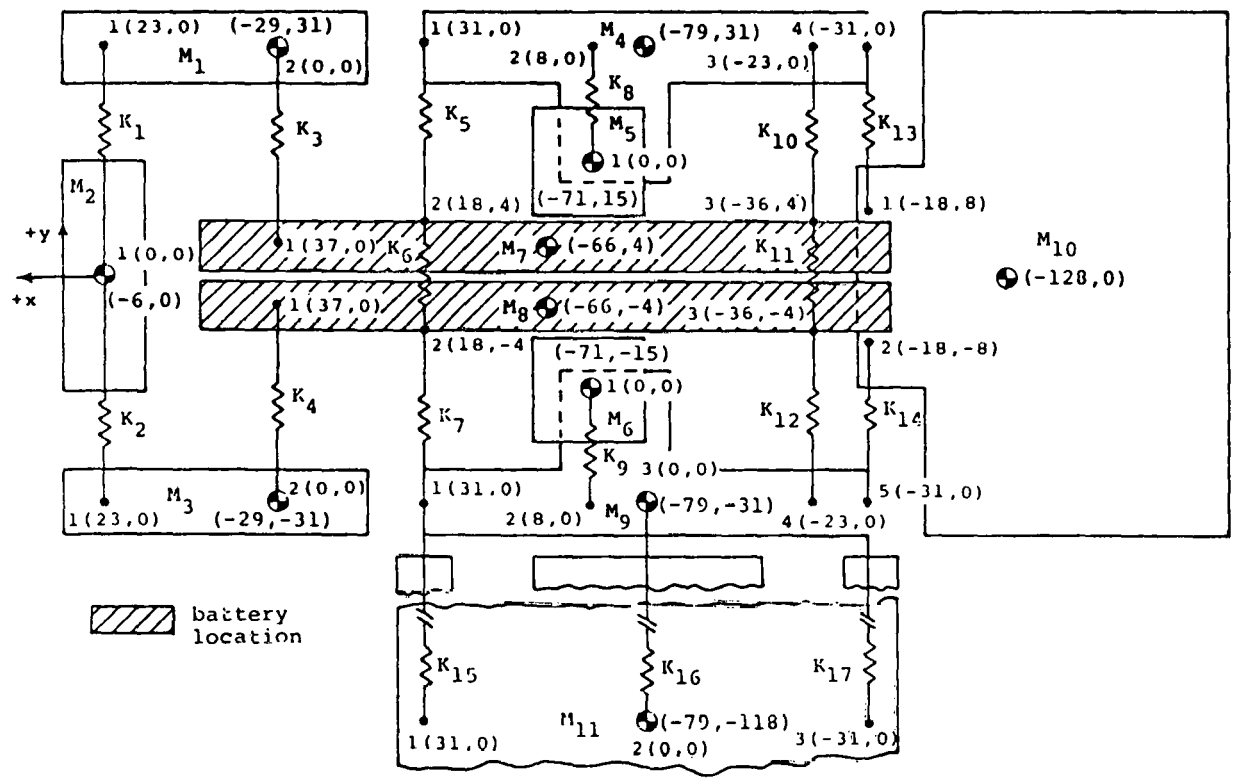


Figure 155. Lateral Impact Model

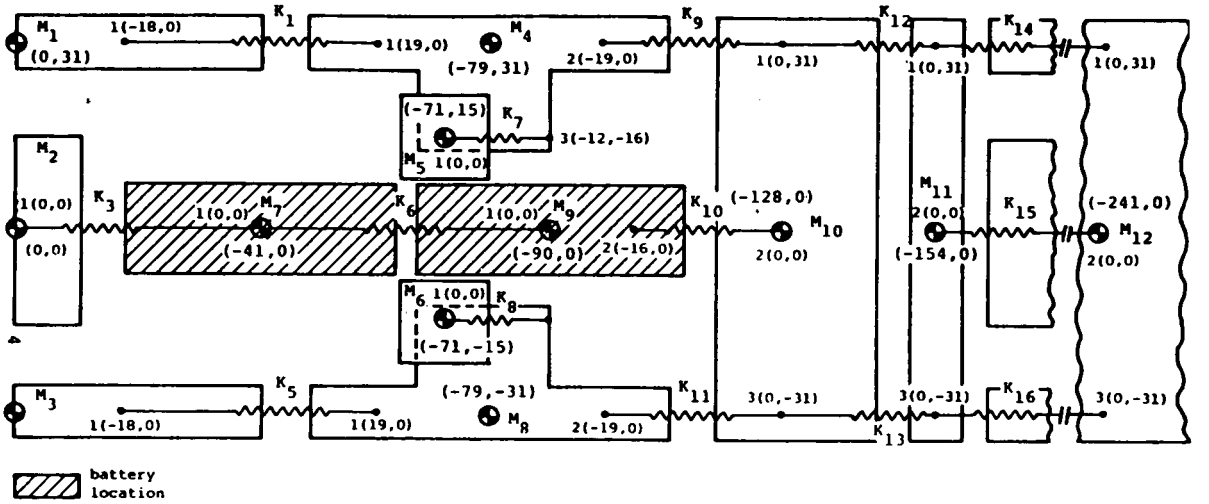


Figure 156. Rear Impact Model

Program outputs are specified through input descriptions and contain the following:

- Displacement time histories
- Velocity time histories
- Acceleration time histories
- Spring force time histories
- Spring deformation time histories
- Energy balance time histories

## PARAMETRIC STUDIES AND SUMMARY RESULTS

The mass distribution of each model is sized and located to best reflect the current vehicle geometry and location of major substructures, and to provide simulation output at desired specific locations within the model. The numerical values for the front- and side-impact models are given in Table 33, while those of the rear-impact model are given in Table 34. The load paths within the model are represented by the spring locations and directions. The baseline load-deflection characteristics are estimated values, based on past experience. The characteristics are then scaled ±25 percent to obtain the "stiff" and the "soft" cases to complete one series of cases. Based on the results, certain load-deflection characteristics are then further modified for the next series of cases to improve the vehicle crashworthiness. A total of eight series, consisting of more than 60 cases, was investigated. The latest results of the front impact are summarized in Table 35.

TABLE 33

WEIGHT DISTRIBUTION FOR FRONT AND LATERAL IMPACT MODELS

| Mass | Component | Component Weight, lb | Total Mass per Car, lb |
|---|---|---|---|
| $M_1$, $M_3$ | Wheel | 11 | |
| | Tire | 25 | |
| | Suspension | 30 | |
| | Brake | 25 | |
| | Frame and body | 50 | 282 |
| $M_2$ | Frame and body | 30 | |
| | Steering | 30 | 60 |
| $M_4$, $M_8$ | Door | 117.5 | |
| | Frame and body | 25 | 285 |
| $M_5$, $M_6$ | Seat (body) | 25 | |
| | Restraint | 3 | |
| | Driver/pass. | 150 | 356 |
| $M_7$, $M_9$ | Frame and body | 105 | |
| | 9 Batteries | 520 | 1250 |
| $M_{10}$ | Wheels | 22 | |
| | Tires | 50 | |
| | Brakes | 50 | |
| | Suspension | 60 | |
| | Frame and body | 118.75 | |
| | Propulsion | 353.5 | 654.25 |
| (Includes 300 lb of occupants) | TOTAL WEIGHT | | 2887.25 |

TABLE 34

WEIGHT-DISTRIBUTION FOR REAR IMPACT MODEL

| Mass | Component | Component Weight, lb | Total Mass per Car, lb |
|---|---|---|---|
| $M_1$, $M_3$ | Wheel | 11 | |
| | Tire | 25 | |
| | Suspension | 30 | |
| | Brake | 25 | |
| | Frame and body | 50 | 282 |
| $M_3$ | Frame and body | 30 | |
| | Steering | 30 | 60 |
| $M_4$, $M_8$ | Door | 117.5 | |
| | Frame and body | 25 | 285 |
| $M_5$, $M_6$ | Seat (body) | 25 | |
| | Restraint | 3 | |
| | Driver/pass. | 150 | 356 |
| $M_7$, $M_9$ | Frame and body | 105 | 1250 |
| $M_{10}$ | Wheels | 22 | |
| | Tires | 50 | |
| | Brakes | 50 | |
| | Suspension | 60 | |
| | Frame and body | 78.75 | |
| | Propulsion | 353.5 | 614.25 |
| $M_{11}$ | Rear frame and body | 20 | |
| | Rear bumper | 20 | 40 |
| $M_{12}$ | Moving Barrier | | 2886.75 |
| Total (includes 300 lb of occupants) | | | 2887.25 |

TABLE 35

SUMMARY OF FRONT IMPACT ANALYSIS
FOR 500, 600, AND 700 SERIES CASES

| Case | Driver Accel. 1st/2nd Peaks, g | Front Deformation, in. | % Energy Absorbed by Batteries (1) | % Energy Absorbed by Front Side Structure (2) | %Energy Absorbed by Front and Rear Side Structure (3) |
|---|---|---|---|---|---|
| 500 | 66.6/52.3 | 20.1 | 30.0 | 28.5 | 41.0 |
| 501 | 66.6/52.4 | 20.1 | 33.0 | 28.5 | 41.1 |
| 502 | 68.4/53.7 | 18.0 | 29.1 | 22.6 | 40.5 |
| 503 | 68.4/74.4 | 18.0 | 32.0 | 23.5 | 41.3 |
| 504 | 69.4/75.7 | 16.4 | 26.9 | 31.7 | 57.8 |
| 505 | 69.5/76.9 | 16.4 | 30.2 | 33.6 | 58.4 |
| 600 | 45.2/53.0 | 25.8 | 33.1 | 32.6 | 39.8 |
| 601 | 60.2/56.1 | 22.6 | 32.5 | 36.0 | 51.3 |
| 602 | 50.6/64.9 | 26.9 | 32.6 | 37.1 | 51.3 |
| 700 | 44.9/52.2 | 25.9 | 31.7 | 33.0 | 39.5 |
| 701 | 45.0/52.7 | 25.9 | 32.9 | 32.8 | 39.7 |
| 702 | 44.9/52.2 | 25.9 | 31.7 | 33.0 | 39.5 |

Notes:
1) Represented by $K_3$ and $K_6$ - % of initial total kinetic energy.
2) Represented by $K_1$ and $K_5$ - % of initial total kinetic energy.
3) Represented by $K_1$, $K_5$, $K_9$, and $K_{12}$ - % of initial total kinetic energy.

The stiffness requirements for the 600 series are similar to those proposed by the Budd Company. Further modifications of the load-deflection characteristics do not significantly improve the crashworthiness, as seen by results of 700 series. Even though the drive accelerations of 45.2/53.0 g are on the high side, they are considered acceptable at present, because of lack of exact load-deflection characteristics of fiberglass vehicle components. The structure and the passenger crashworthiness will be verified later in the half-scale model tests.

# SECTION 10

# VEHICLE DYNAMICS ANALYSIS

## SECTION 10

## VEHICLE DYNAMICS ANALYSIS

### HANDLING ANALYSIS

A unique feature of the NTEV is the flywheel, mounted at the rear-right of the car, with its spinning axis parallel to the axle, and rotating in the opposite direction. This configuration was selected because:

(a) Vehicle pitch occurs more frequently, and generally with higher rate, than vehicle roll and yaw. Thus, the gyro-moment produced by pitch could be largest. To eliminate this moment, the flywheel axis must be parallel to the pitch axis.

(b) After the flywheel axis is selected, the flywheel rotation can be either the same as or opposite to axle rotation. Vehicle yaw rate is generally higher than roll rate, such as in accident-avoidance maneuvers. It was decided to rotate the flywheel in the opposite direction of the axle, so that gyro-moment might offset the centrifugal force to some extent.

Figure 157 shows a simplified vehicle model, subjected to the gyro-moment and the centrifugal force. The moment produced by the flywheel is given by

$$Mg = I_f \omega \Omega$$

where $Mg$ = gyro-moment, ft-lb

$I_f$ = flywheel inertia = 0.772 ft-lb-sec$^2$

$\omega$ = flywheel rotating speed (= 25000 rpm = 2618 rad/sec)

$\Omega$ = precession (yaw) rate in rad/sec

Sustitution yields

$$Mg = 2021\Omega \text{ ft-lb}$$

The moment produced by the centrifugal force is given by

$$M_C = \frac{W}{g} R\Omega^2 H$$

where $M_C$ = moment caused by centrifugal force in ft-lb

$W$ = sprung weight = 2700 lb

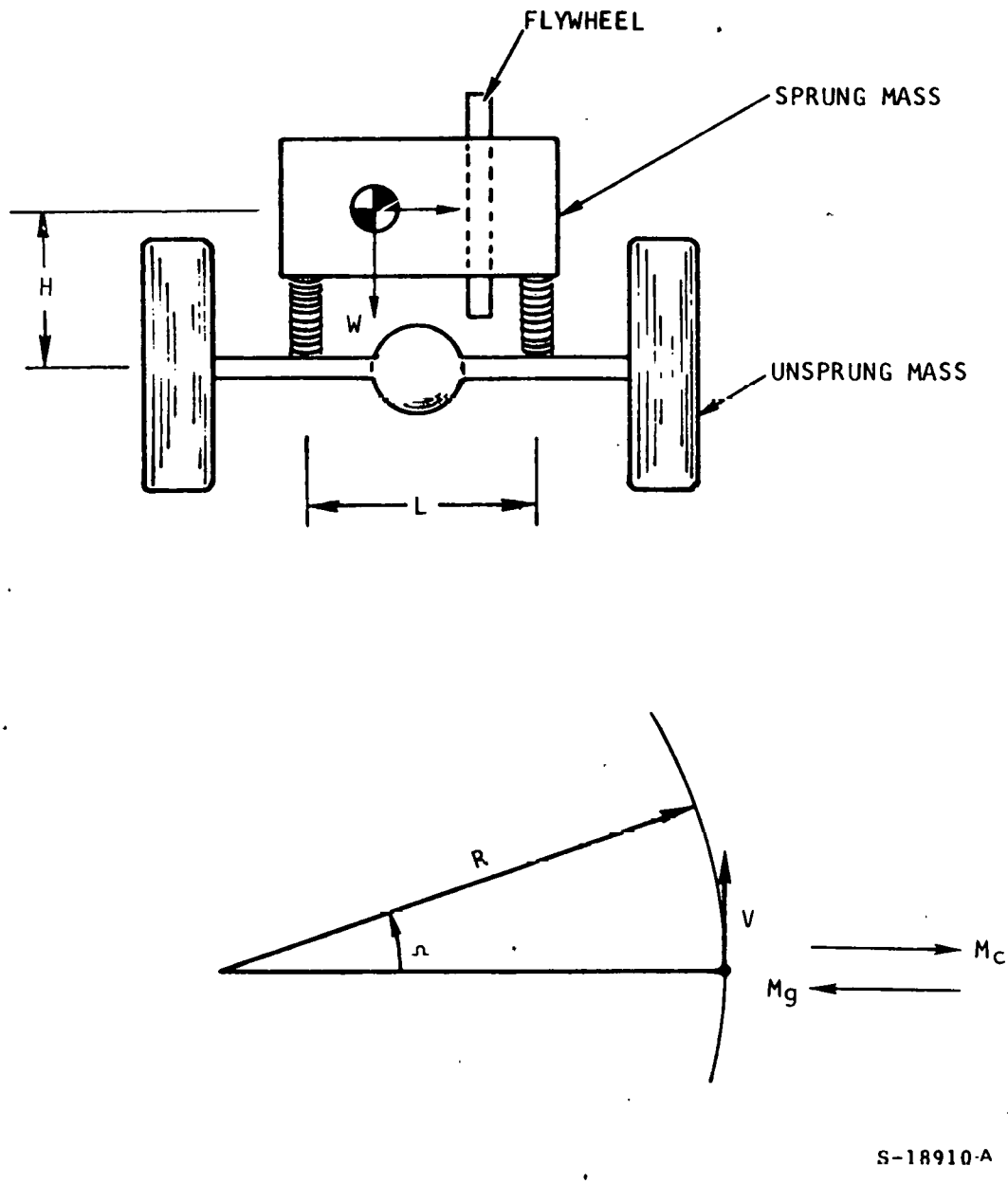


Figure 157. Vehicle Model on a Curve

R = turning radius, ft

H = distance between the c.g. and rolling center = 1.3 ft

$\Omega$ = yaw rate in rad/sec

Substitution yields

$$M_C = 109.01 \; R \; \Omega^2$$

Figure 158 shows the stabilizing effect of the gyroscopic moment as a function of vehicle speed and rate of turning. Also shown for comparison are values of the rolling moments without the gyro effect; i.e., the moments encountered in the conventional vehicle without the flywheel stabilizing effect. The data show that the tendency of the vehicle to roll or lean during all speeds and all possible turning rates is significantly reduced, particularly at the lower speeds. At freeway speeds of 50 mph, the rolling tendency is reduced by 25 percent and at 20 mph the tendency is reduced by over 60 percent. At still lower speeds, the rollover tendency is almost completely eliminated, even at turning rates at the limit of tire adhesion.

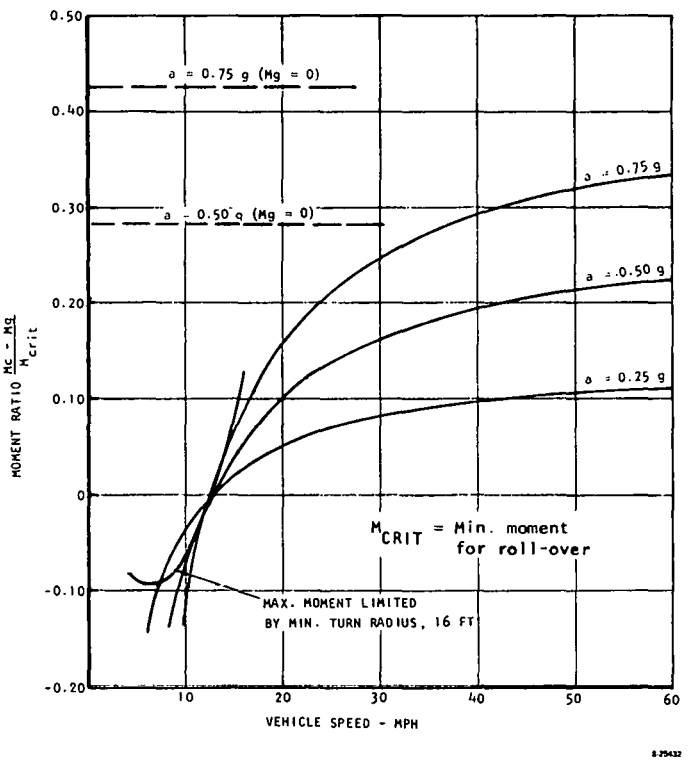


Figure 158. Gyro Stabilizing Effect

The effect of the flywheel-gyro forces on vehicle-handling response was investigated. Steady-state and transient yaw responses are used as measures of the vehicle lateral-directional response. The yaw response requirements, based on the Research Safety Vehicle Specification, specify that in response

to a steering input for which the lateral acceleration is 0.4 g (+0.02), the vehicle must:

(a) Maintain a steady-state yaw response at forward velocities of 36.7 ft/sec (25 mph), 73.3 ft/sec (50 mph), and 102.7 ft/sec (70 mph) within the envelope defined by Figure 159.

(b) Within this envelope, the specific vehicle-response curve must be concave downward at all points. Similar response curves, obtained with different lateral accelerations, shall exhibit the same characteristic shapes. In relation to the 0.4-g yaw-response curve on Figure 159 coordinates, as lateral acceleration increases from 0.4 g, the yaw-response curve shall progressively move downward; as lateral acceleration decreases from 0.4-g, the yaw-response curve shall progressively move upward.

(c) With a steering input applied at a rate no less than 500 deg/sec, and held constant at a value that produces 0.4-g steady-state, lateral acceleration with test velocities of 25 and 70 mph, the transient yaw response shall be as described for Figure 160. The initial time is the time at which one-half the steering-wheel input is complete. In this figure, the upper curve is the upper limit for a test speed of 70 mph, while the lower curve is a lower limit for a test speed of 25 mph, and does not apply to the 70-mph test.

VEHICLE MODEL

A vehicle handling model for the electric vehicle was established. Figure 161 presents a schematic representation of the mathematical model.

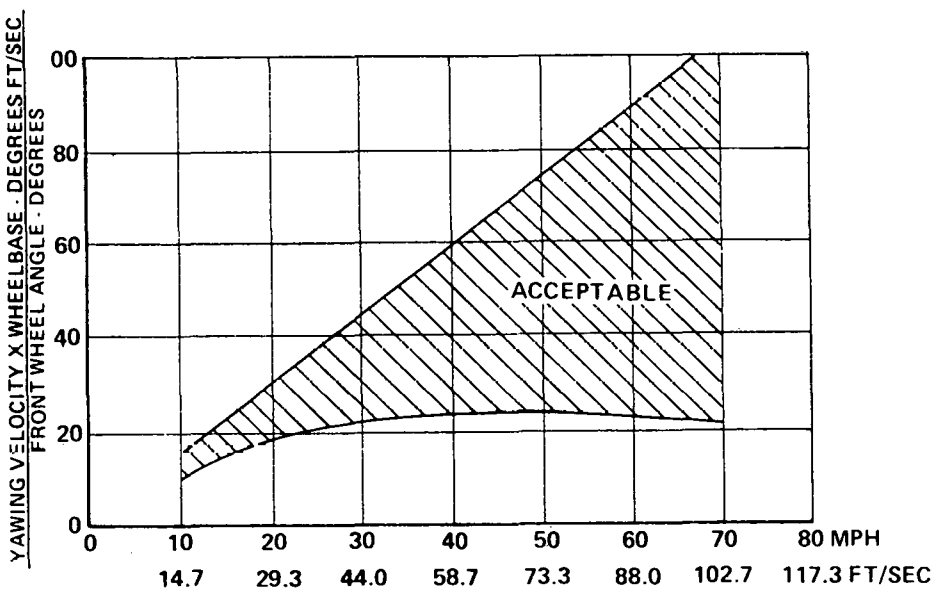


Figure 159. Steady-State Yaw Response Versus Tangential Velocity

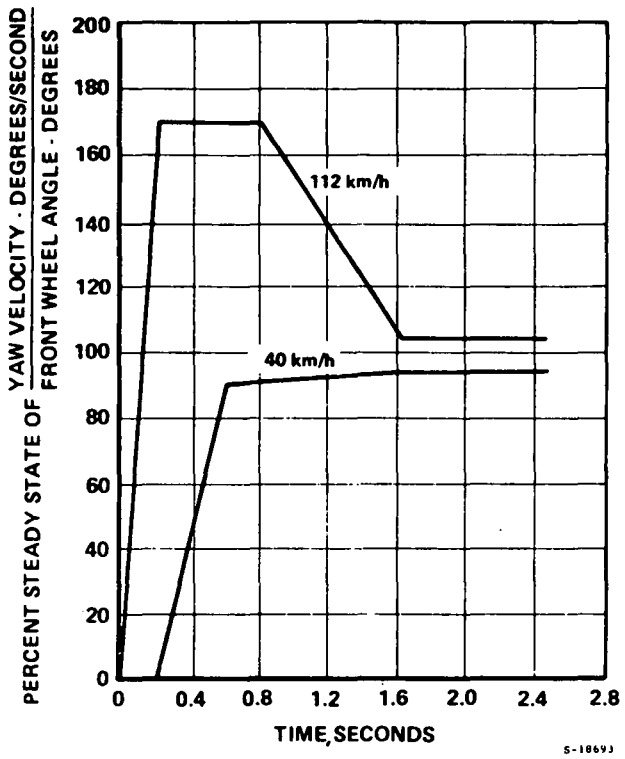


Figure 160. Transient Yaw Response Versus Time

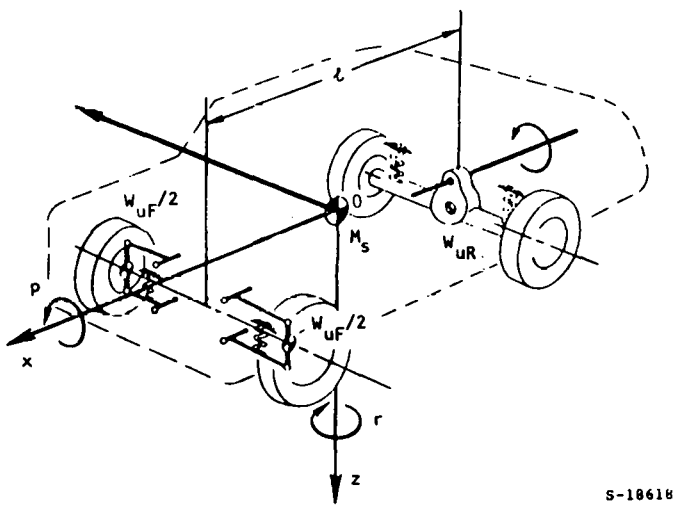


Figure 161. Analytical Representation of Vehicle

The model has the following characteristics:

(a) 3 degrees-of-freedom for the sprung mass (roll, yaw, and sideslip)

(b) The flywheel gyro forces are applied as D'Alembert Forces on the vehicle body.

Certain assumptions are inherent in this model. These include:

(a) Constant vehicle speed during a maneuver

(b) No significant pitching of the vehicle

(c) Weight shift is proportional to lateral acceleration

(d) Small angles

(e) Rigid spring mass

A Dynamic Science Inc. computer program was modified to include the effect of the flywheel gyro forces.

Table 36 presents the data input parameters and the values used for the electric vehicle. The values for $I_E$ (flywheel inertia) and $W_E$ (flywheel angular velocity) are input values for the spinning gyro. These two parameters are set equal to zero for the case of a vehicle without a flywheel.

Handling Analysis Conditions

Conditions used to evaluate the effect of the flywheel gyro forces are derived from the Research Safety Vehicle (RSV) Specification for yaw response. Two criteria were used for evaluation:

> The predicted yaw responses should be within the boundaries of Figures 159 and 160.
>
> The response parameter values for the NTEV, with and without a rotating flywheel, would be compared to evaluate the effect of the flywheel.

In essence, the transient-yaw-response condition used the vehicle's steering gain (yaw velocity divided by front-wheel angle) to evaluate vehicle turning performance. The steering gain represents the ratio of how much the vehicle turns to how much steering input is required. The larger the steering gain, the tighter the vehicle turns (has more oversteer) for a given steering input.

Analysis Results

The results for the NTEV analysis are presented in Figures 162 through 164. Figure 162 illustrates that the steady-state yaw response is within the acceptable boundary, and that there is no significant difference in response, with or without the flywheel.

# TABLE 36.

## DATA INPUT FOR NTEV

| Variable | Definition | Units |
|---|---|---|
| Card 1: | | |
| $W_f$ = 1571 | Total weight on front wheels of the vehicle (with 4 occupants) | lb |
| $W_r$ = 1885 | Total weight on rear wheels of the vehicle (with 4 occupants) | lb |
| $W_{uf}$ = 150 | Front unsprung weight | lb |
| $W_{ur}$ = 160 | Rear unsprung weight | lb |
| $\ell$ = 95.0 | Wheelbase | in. |
| $h_f$ = 1.04 | Front roll center height above road plane | in. |
| $h_r$ = 5.65 | Rear roll center height above road plane | in. |
| $h_{uf}$ = 11.30 | Front unsprung weight cg height above road plane | in. |
| $h_{ur}$ = 11.30 | Rear unsprung weight cg height above road plane | in. |
| $h_t$ = 18.41 | Total vehicle cg height above road plane (with 4 occupants) | in. |
| $I^s_{xx}$ = 469.0 | Sprung mass roll inertia about origin on roll axis below cg of total vehicle | lb-sec$^2$-ft |
| $I^s_{zz}$ = 2261.0 | Sprung mass yaw inertia about origin on roll axis below cg of total vehicle | lb-sec$^2$-ft |
| $I^u_{zz}$ = 247.6 | Unsprung mass yaw vehicle about origin on roll axis below cg of total vehicle | lb-sec$^2$-ft |
| $I^s_{xz}$ = -10.59 | Sprung mass product of inertia about origin of roll axis below cg of total vehicle | lb-sec$^2$-ft |
| $D_f$ = 1.91 | Front roll damping coefficient | ft-lb-sec/deg |
| $D_r$ = 3.48 | Rear roll damping coefficient | ft-lb-sec/deg |
| $K_f$ = 993 | Front roll stiffness | ft-lb/deg |
| $K_r$ = 558 | Rear roll stiffness | ft-lb/deg |
| $\Gamma_{\phi f}$ = 0.725 | Front roll camber coefficient (+ understeer) | |
| $\Gamma'_{\phi r}$ = 0.0 | Rear roll camber coefficient (+ understeer) | |
| $E_{\phi f}$ = 0.10 | Front roll steer coefficient (+ understeer) | |
| $E'_{\phi f}$ = -0.09 | Rear roll steer coefficient (+ understeer) | |
| Card 2: | | |
| $E_{Nf}$ = 0.016 | Front aligning torque deflection steer per wheel (+ understeer) | deg/ft-lb |
| $E_{Yf}$ = 0.0007 | Front lateral force deflection steer per wheel (+ understeer) | deg/lb |
| $\Gamma_{Nf}$ = -0.0002 | Front aligning torque deflection camber per wheel (+ understeer) | deg/ft-lb |

TABLE 36. (Continued)

| Variable | Definition | Units |
|---|---|---|
| $\Gamma_{Yf}$ = 0.0022 | Front lateral force deflection camber per wheel (+ understeer) | deg/deg/lb |
| $E'_{Nr}$ = -0.002 | Rear aligning torque deflection steer per wheel (+ understeer) | deg/ft-lb |
| $E'_{Yr}$ = -0.0003 | Rear lateral force deflection steer per wheel (+ understeer) | deg/lb |
| $\Gamma'_{Nr}$ = 0.0001 | Rear aligning torque deflection camber per wheel (+ understeer) | deg/ft-lb |
| $\Gamma'_{Yr}$ = -0.0019 | Rear lateral force deflection camber per wheel (+ understeer) | deg/lb |
| $C_{\alpha f}$ = 109.4 | Front tire cornering stiffness for one tire (always positive) | lb/deg |
| $C_{\alpha r}$ = 113.6 | Rear tire cornering stiffness for one tire (always positive) | lb/deg |
| $C_{\gamma f}$ = 4.8 | Front tire camber stiffness for one tire (positive) | lb/deg |
| $C_{\gamma r}$ = 5.4 | Rear tire camber stiffness for one tire (positive) | lb/deg |
| Card 3: | | |
| $N_{\alpha f}$ = 12.2 | Aligning torque per unit slip angle for one front tire (positive) | ft-lb/deg |
| $N_{\alpha r}$ = 13.4 | Aligning torque per unit slip angle for one rear tire (positive) | ft-lb/deg |
| $N_{\gamma f}$ = 0.81 | Aligning torque per unit camber angle for one front tire (positive) | ft-lb/deg |
| $N_{\gamma r}$ = 0.90 | Aligning torque per unit camber angle for one rear tire (positive) | ft-lb/deg |
| $I_E$ = 0.7754 | Flywheel inertia | lb-sec$^2$-ft |
| $\omega_E$ = 2618* | Flywheel angular velocity | rad/sec |
| $A_{Yss}$ = ** | Steady state lateral acceleration selected by user | ft/sec$^2$ |
| x = 51.81 | Distance from front wheel center to lateral acceleration measurement point (positive for points behind wheel center) (with 4 occupants) | in. |
| z = 18.45 | Distance from road plane to lateral acceleration measurement point (positive for points above road plane) (with 4 occupants) | in. |
| u = *** | Forward velocity | mph |
| $\Delta t$ = .10 | Printing time increment for transient response (not to exceed 0.1 sec) | sec |
| $t_{max}$ = 5.0 | Total time interval for transient response | sec |

*0.0 for cases with flywheel stationary.
**Steady state lateral accelerations to be used include 0.2 g (6.44 ft/sec$^2$), 0.4 g (12.88 ft/sec2), and 0.7 g (22.54 ft/sec$^2$).
***Vehicle forward velocities to be used include 25, 40, 50, 60, and 70 mph.

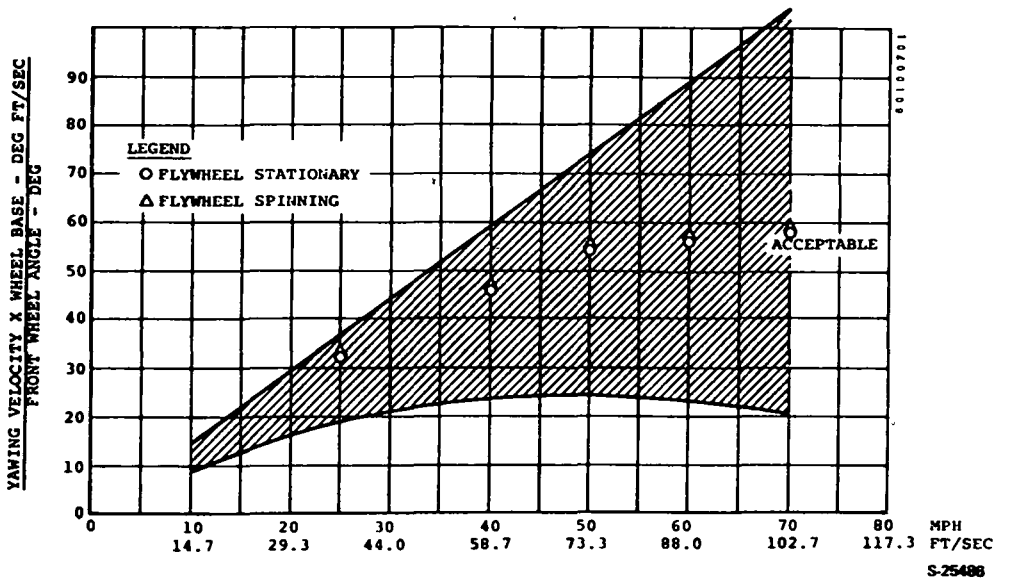


Figure 162. Electric Vehicle Steady-State Condition at 0.4 g

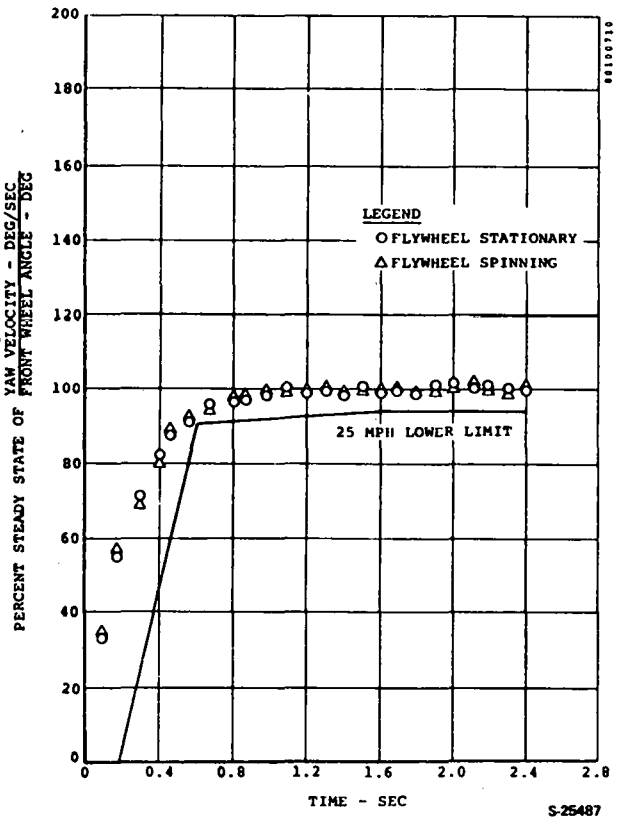


Figure 163. Electric Vehicle Transient Yaw, 25 mph at 0.4 g

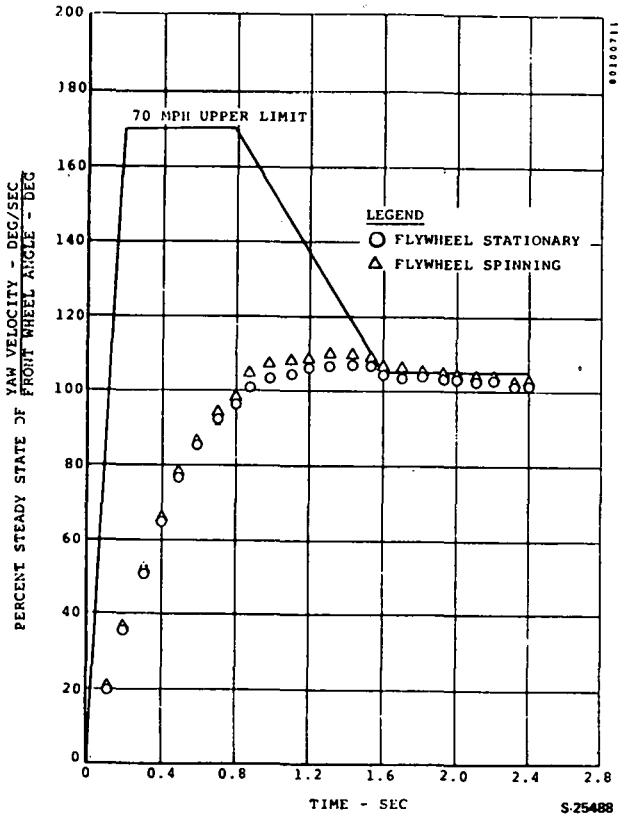


Figure 164. Electric Vehicle Transient Yaw, 70 mph at 0.4 g

Figure 163 illustrates that the transient-yaw response at 25 mph is well above the required lower limit. This figure also shows no significant difference in transient-yaw response, with or without the flywheel.

Figure 164 illustrates that the transient response at 70 mph is within the required upper boundary, except for a small time period around the 1.6-sec point. The response for the spinning-flywheel case is slightly worse than the response for the stationary-flywheel case.

These results at 70 mph should not be construed to mean that the electric-vehicle steering performance is unacceptable; however, the pertinent vehicle-design parameters will be reviewed, with the objective of providing a somewhat quicker yaw response for the vehicle system.

Table 37 presents a comparison of selected response parameters for cases with and without a rotating flywheel. Table 38 provides a glossary of the response parameters. The effects of the spinning flywheel are as follows:

(a) Yaw velocity

The peak yaw velocity is slightly larger and occurs earlier

TABLE 37

COMPARISON OF SELECTED RESPONSE PARAMETERS AT 0.4 G

| Response Parameter | 25 mph | | 40 mph | | 50 mph | | 60 mph | | 70 mph | |
|---|---|---|---|---|---|---|---|---|---|---|
| | Spinning | Stationary | Spinning | Stationary | Spinning | Stationary | Spinning | Stationary | Spinning | Stationary |
| Yaw velocity, deg/sec | 20.152 | 20.128 | 12.688 | 12.617 | 10.365 | 10.210 | 8.908 | 8.696 | 7.947 | 7.690 |
| Sideslip angle, deg | -1.547 | -1.582 | -2.765 | -2.783 | -3.069 | -3.071 | -3.263 | -3.244 | -3.415 | -3.370 |
| Roll angle, deg | -0.701 | -1.177 | -0.846 | -1.146 | -0.910 | -1.147 | -0.959 | -1.152 | -1.003 | -1.161 |
| Lateral acceleration, ft/sec | 12.930 | 12.913 | 12.922 | 12.890 | 12.979 | 12.927 | 13.136 | 13.003 | 13.337 | 13.125 |
| Yaw velocity response time, sec | 0.521 | 0.553 | 0.677 | 0.695 | 0.693 | 0.716 | 0.672 | 0.702 | 0.635 | 0.671 |
| Lateral acceleration response time, sec | 0.850 | 0.857 | 1.075 | 1.123 | 1.217 | 1.266 | 1.275 | 1.337 | 1.307 | 1.380 |
| Sideslip response time, sec | 0.948 | 0.966 | 1.202 | 1.240 | 1.270 | 1.321 | 1.313 | 1.380 | 1.337 | 1.416 |
| Steady-state yaw velocity, deg/sec | 20.126 | 20.126 | 12.579 | 12.579 | 10.063 | 10.063 | 8.386 | 8.386 | 7.186 | 7.186 |
| Steady-state sideslip, deg | -1.533 | -1.576 | -2.752 | -2.779 | -3.035 | -3.057 | -3.189 | -3.207 | -3.281 | -3.297 |
| Reference steer angle, deg | 4.729 | 4.758 | 2.092 | 2.110 | 1.484 | 1.499 | 1.155 | 1.167 | 0.951 | 0.967 |
| Roll gain, deg/g | -1.619 | -2.823 | -2.071 | -2.823 | -2.221 | -2.823 | -2.321 | -2.823 | -2.393 | -2.823 |
| Sideslip gain, deg/g | -3.829 | -3.936 | -6.875 | -6.942 | -7.503 | -7.636 | -7.968 | -8.013 | -8.202 | -8.240 |
| Control sensitivity, $ft/sec^2/deg$ | 2.724 | 2.707 | 6.157 | 6.104 | 8.676 | 8.593 | 11.152 | 11.037 | 13.466 | 13.322 |

TABLE 38

GLOSSARY OF RESPONSE PARAMETER TERMS

| Terms | Definitions |
|---|---|
| Yaw velocity | The angular velocity about the z-axis (deg/sec) |
| Sideslip angle | The angle between the traces on the x-y plane of the vehicle x-axis and the vehicle velocity vector at some specified point in the vehicle (deg) |
| Roll angle | The angle between the vehicle y-axis and the ground plane (deg) |
| Lateral acceleration | The component of the vector acceleration of a point in the vehicle perpendicular to the vehicle x-axis and parallel to the road plane ($ft/sec^2$) |
| Yaw velocity response time | The time required for the vehicle's yaw velocity to reach at least 90 percent of the steady-state yaw velocity (sec) |
| Lateral acceleration response time | The time required for the vehicle's lateral acceleration to reach at least 90 percent of the steady-state lateral acceleration (sec) |
| Sideslip response time | The time required for the vehicle's sideslip angle to reach at least 90 percent of the steady-state sideslip angle (sec) |
| Steady-state yaw velocity | The final yaw velocity obtained that remains relatively constant over a long period of time (deg/sec) |
| Steady-state sideslip angle | The final sideslip angle obtained that remains relatively constant over a long period of time (deg) |
| Reference steer angle | The steer angle required to obtain a given lateral acceleration based on a known velocity and turning radius (deg) |
| Roll gain | The rate of change in vehicle roll angle with respect to change in steady-state lateral acceleration on a level road at a given trim* and test conditions (deg/g) |
| Sideslip gain | The rate of change in vehicle sideslip angle with respect to change in steady-state lateral acceleration on a level road at a given trim and test conditions (deg/g) |
| Control sensitivity | The change in steady-state lateral acceleration on a level road with respect to change in steering wheel angle at a given trim and test conditions ($ft/sec^2$/deg) |

*Trim may be defined as the steady-state condition of the vehicle with constant input that is used as the reference point for analysis of dynamic vehicle stability and control characteristics.

The difference between a spinning and stationary flywheel increases with vehicle speed

The steady-state yaw velocity is independent of flywheel-spinning conditions

(b) Roll Angle

The peak roll angle is considerably less at the lower vehicle speeds, and slightly less at the higher vehicle speeds.

(c) Sideslip Angle

The peak sideslip angle is slightly less at lower vehicle speeds, but slightly more at higher vehicle speeds.

(d) Steering Input

Less steering input is required to achieve the same lateral-acceleration turn.

In summary, the effect of the spinning flywheel is:

A slightly quicker response to the turn

A slightly more overshoot of the turn

A slightly increased oversteer response

An improved roll response during the turn

RIDE ANALYSIS

The main factors that affect the ride of a vehicle are front suspension, rear suspension, seat suspension, weight distribution, structural stiffness, and tire characteristics (Figure 165). In the following discussion, the term "suspension system" will be used in a broad sense to include all these factors.

In designing the suspension system, the objective is to minimize the acceleration levels transmitted to the car floor and to the driver and passengers. Acceleration levels primarily indicate the ride comfort of the vehicle. These criteria are given in Figure 166, and are recommended by the International Standards Organization. Because of the range limitation of the NTEV, the 2.5-hr curve, shown in Figure 166, will be used for the design goal.

The motion of a vehicle in a path is treated as a system that consists of mass points interconnected by springs and dashpots. Since the large number of degrees of freedom makes the computer simulation complicated and time consuming, the vehicle model generally adopted by analysts is to treat the car-body weight as having six degrees of freedom. Also, the bending mode of

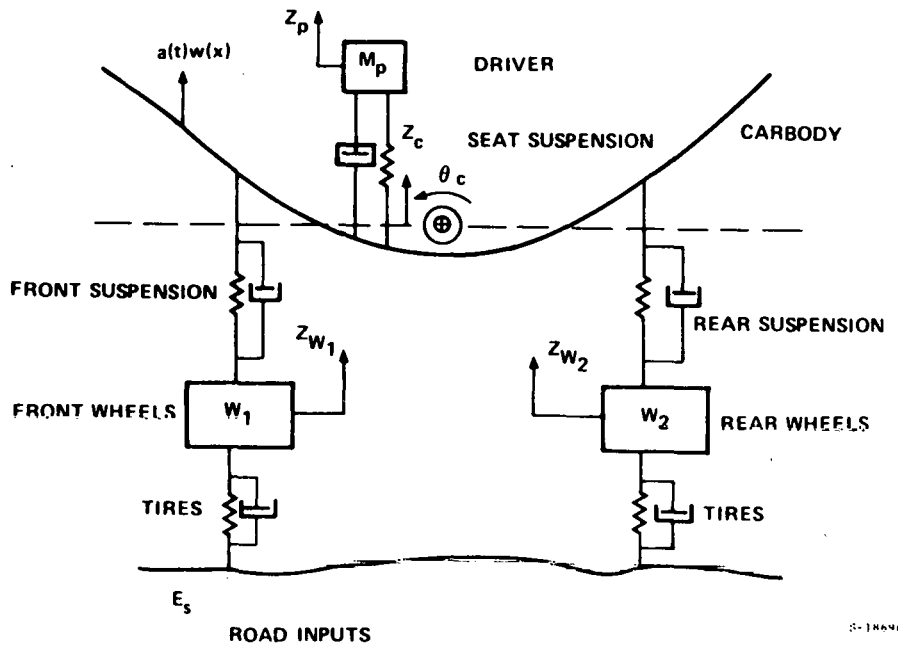


Figure 165. Vehicle Model With Vertical Plane of Symmetry

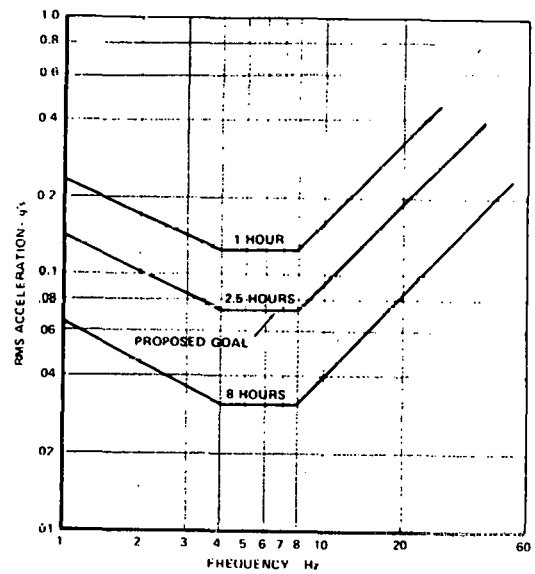


Figure 166. Vertical Ride Quality, ISO Proposed Recommendation

the car may be significant, because of the heavy battery load. For a majority of highway-travel conditions, a vehicle is travelling on a relatively flat and straight road at a constant forward speed. The excitation of the road profile causes vertical motion of the axles, and consequently, pitch and bounce of the vehicle. Assume that the waviness is equal in the left and right tracks, and that the vehicle and rotational modes are not coupled to the lifting and pitching oscillations. A ride-analysis model can be constructed as shown in

Figure 165, showing the individual components that are important in vibration investigations.

The car is treated as a flexible member. Each wheel with a pneumatic tire is modelled as an unsprung mass, plus a spring and dashpot. A suspension system, with springs and shock absorbers, connects the wheels and the spring mass. It should be noted here that the spring rates and the damping characteristics can be linear or non-linear, such as friction and hysteresis. The model has a total of six degrees of freedom. The various road excitations can be thought of as inputs, or forcing functions, to the system.

The BMW 320i suspension has been selected for the NTEV; however, specific components, such as the springs and shocks, are yet to be determined. Typical bounce frequencies for the BMW 320i system are 1.0 to 1.5 Hz in the front, and 1.3 to 1.8 Hz in the rear. Ride-analysis results have not yet been completed.

NOISE ANALYSIS

The interior and exterior noise levels of the NTEV must be controlled to produce a vehicle that will be publicly acceptable. The criteria for allowable noise inside the passenger automobiles are not standardized, because "quietness" is an important factor in competition among manufacturers. Therefore, interference with speech becomes an important consideration. Figure 167 shows the speech-interference levels in decibels at which reliable speed communication is barely possible between persons at the distances and voice efforts shown. Based on these data, the preliminary interior noise level objective is set at 70 dBA. Both the speech interference problem, as well as the feasibility of achieving this level, were considered in setting this goal. Criteria for exterior noise are regulated by federal, state, and local governments. Although the data below may not be up to date, it nevertheless provides a reasonable guideline. A search is being made to find existing noise regulations that can be used to help establish exterior noise goals. At present, the exterior noise level goals at a distance of 50 ft from the centerline of the traffic lane are shown below:

| Location | Less than 35 mph | Greater than 35 mph | Maximum |
|---|---|---|---|
| Federal | -- | 82 dBA | -- |
| California | 76 dBA | 82 dBA | -- |
| Chicago (SAE) | -- | -- | 80 dBA<br>75 dBA (after 1980) |

A common impression is that an electric-powered vehicle should be quieter than the ordinary internal-combustion-engined (ICE) vehicle. In order to obtain more quantitative noise data, the interior-noise levels were surveyed on various ICE vehicles, and on the Copper Development Association (CDA) electric car. The measurements are summarized below for 55 mph on the freeway, measured at passenger car height:

| Vehicle | Window Closed | Window Open | Remarks |
|---|---|---|---|
| CDA | 77 dBA | 81.5 dBA | -- |
| VW Bug | 73 | 73.5 | With bad window seal - 1969 |
| VW Bug | 71 | -- | 1977 Model |
| Cordoba | 64 | 68.5 | A/C on, 1977 |
| Granada | 63 | -- | 1977 Model |

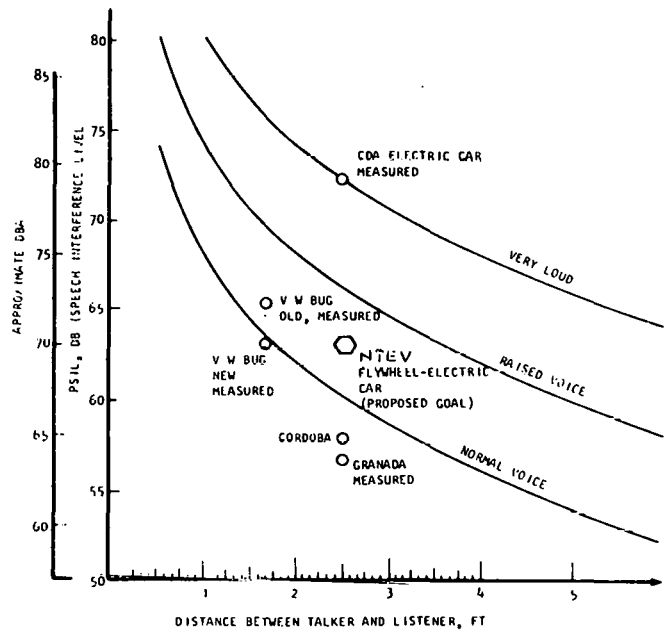


Figure 167. Interior Noise Goals

The CDA electric car was found to be noisier than the ICE cars, the major noise source being the power system.

The Cordoba and Granada had good muffler attenuation, low engine-radiated noise because of water cooling, and low car-body radiated noise because of their weight.

The VW Bug had moderate acoustic treatment for its power system, and had a high car-body radiated noise because of its light weight. The CDA electric vehicle, also, had no special acoustic treatment for its power system, and the high car-body radiated noise was due to its light weight.

The sum of the tire noise and the aerodynamic wind noise of the Cordoba was 68.5 dBA at the passenger-ear location. The car-body attenuation, that

is, with window open-window closed, for the Cordoba and for the CDA electric car was 4.5 dBA, while for the VW Bug it was 2.5 dBA. The loss of 2 dBA attenuation for the case of the VW Bug was due to radiated noise from both the engine and the car body.

## Noise Transmission and Control

The major sources, and their respective transmission paths in the NTEV, are shown in Figure 168. The levels of aerodynamic noise and tire noise cannot be reduced significantly, and therefore, these factors set the minimum exterior-noise level that can be achieved. The transmission loss of the car body defines the minimum-possible noise level that can be achieved in the interior of the car for these two noise sources. The major noise source for the NTEV will be the power unit, which generates both airborne and structure-borne noises. By careful design, these noise sources can be reduced without acoustic treatment. All mounts of the power unit and the mounts of the suspension system are resilient. A very complex theory is required to account for the differences in mechanical impedances of the supporting structure from point to point. As a result, empirical methods are employed. Some noise-control considerations at the preliminary-design stage are listed below.

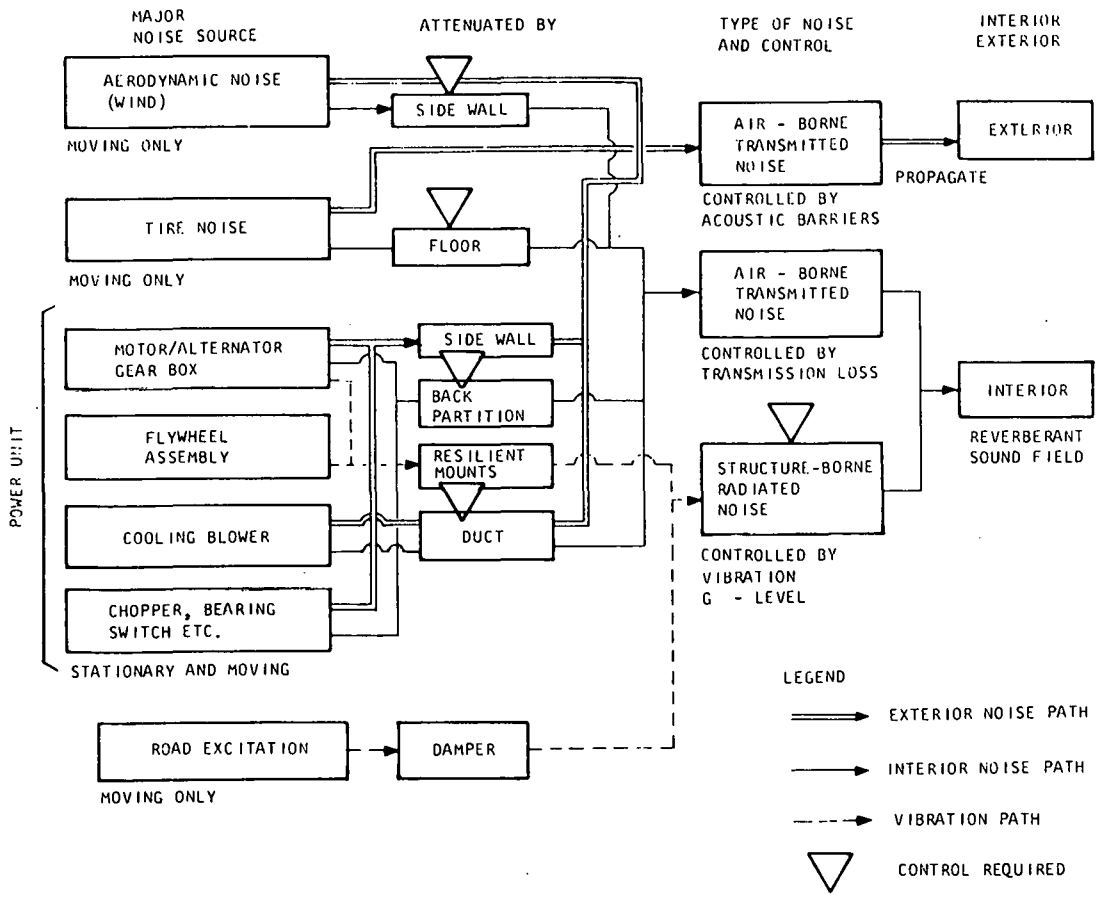


Figure 168. Noise Sources and Their Transmission Paths

Radiated noise can be minimized by eliminating the structural resonances of the power unit. This analysis is being performed.

Balancing the rotating machinery of the power unit will minimize the strength of the excitation sources.

Isolating the power unit from the car-body structure, using soft power-unit mount (10 to 12 Hz translational natural frequencies), will attenuate noise transmission, while the car-body structure must be maintained as stiff as possible at the mounting points to achieve good isolation.

The tire-tread pattern with the lowest noise must be selected, a tread pattern such as that which staggers a random tread with the center rib.

Wind noise is minimized by smoothing the exterior lines of the body, and by eliminating leakage through sealing around all openings.

The cooling fan must have a low air-flow speed and a prime number of blades.

High-precision gears and bearings are being used. Helical gears are used in the design where practical to reduce noise.

Solid-state chopper noise will be minimized. The varying electromagnetic field in the chopper excites adjacent structures. This structural noise will be minimized by appropriate design.

Testing

A noise test will be conducted as soon as the first power unit is available. The results from this test will identify problems in terms of the criteria above. Detailed test procedures for noise will be integrated with the power-unit test procedures. A noise test of the entire vehicle will be conducted during that series of tests to evaluate the overall performance. The test setup and data acquisition system will follow the requirements of the SAE J986A Standard.

☆ U.S. GOVERNMENT PRINTING OFFICE : 1978—O-273-484